Université de Strasbourg

Ecole doctorale des sciences de la vie et de la santé de Strasbourg (ED414)

Laboratoire de Neurosciences Cognitives et Adaptatives (LNCA - UMR 7364)

THÈSE présentée par

Christopher BORCUK

Soutenue le 20 Avril 2021

Pour obtenir le grade de: **Docteur de l'Université de Strasbourg**

Discipline / spécialité: **Biologie / Neurosciences**

Déficits précoces de la cognition et de la connectivité cérébrale chez la Souris *App*$^{NL-F}$*/MAPT*: modélisation du stade prodromal de la maladie d'Alzheimer

THÈSE dirigée par:

Mme. MATHIS Chantal	Directeur de Recherche CNRS, Université de Strasbourg

RAPORTEURS:

M. DELATOUR Benoit	Chargé de Recherche-HDR, Sorbonne Universités
Mme. SCHUMANN-BARD Pascale	Professeur des Universités- Université Caen Basse Normandie

AUTRE MEMBRE DU JURY:

M. MENSAH-NYAGAN Ayikoé	Professeur, Université de Strasbourg

MEMBRES INVITÉS:

M. GOUTAGNY Romain	Chargé de Recherche CNRS, Université de Strasbourg
Mme. HÉRAUD Céline	Maître de Conférence, Université de Strasbourg

Acknowledgements

Many thanks to…

The jury members, Dr. Benoit Delatour, Prof. Pascale Schumann-Bard, and Prof. Ayikoé Mensah-Nyagan for taking part of their precious time to review and evaluate my thesis work.

Dr. Chantal Mathis for her unwavering guidance and presence.

Dr. Celine Heraud for her support and consistent air of positivity.

Dr. Romain Goutagny for his encouragement of my work.

Dr. Demian Battaglia for his enthusiasm and invaluable input.

Karine Herbeaux for all her methodological help, always with a smile.

Prof. Jean-Christophe Cassel for welcoming me to the LNCA.

Catherine Kreiger for administrative help.

All of the LNCA for contributing to a friendly and lively atmosphere.

Vincent, Belle and Lucas for the board game afternoons.

Eva and Pista for their hospitality and delicious cuisine.

Thomas for bringing spice to life.

Julie for many things.

Caroline, Gaelle, Isabel, Iris, Laura D, Laura T and Theo, Rafael, Romain B, Wilf, Yann for the soirées, trips, work out sessions in the park, beers, loup garou, lindy hop. Thank you for making my time in Strasbourg wonderful and never without a dull moment.

My family, Jim, Alma, Raena, Steve, Kris, Shauntee and everyone else, for rooting me on from afar.

CHRISTOPHER BORCUK

christopher.borcuk@etu.unistra.fr
50 rue Saint Aloise
67100 Strasbourg FR
+33 7 83 79 70 73

CURRENT POSITION

Laboratoire de Neurosciences Cognitives et Adaptatives (LNCA) **Strasbourg, FR**
PhD Candidate, obtained an MESRI grant at the ED414 competition in 2017 **2017-Present**

EDUCATION

Université de Strasbourg, University of Freiburg **Strasbourg, FR**
Joint Masters in Neuroscience, mention *bien* **2015 - 2017**

California State Polytechnic University, Pomona **Pomona, CA, USA**
BS, *magna cum laude,* Biotechnology **2011 - 2015**

APPOINTMENTS

Laboratoire des Neurosciences Cognitives et Adaptatives (LNCA) **Strasbourg, FR**
Graduate Researcher **2017-Present**

- Object recognition testing of a novel mouse model of Alzheimer's disease
- Analysis of task-dependent functional networks through graph theory
- Use of a molecular biology, ex-vivo imaging, and electrophysiology techniques

Interdisciplinary Institute for Neuroscience **Bordeaux, FR**
Masters Research Internship **2017**

- Maintained and transfected neuronal banker cultures.
- Used TIRF microscopy to image exocytositic events with pH and glutamate sensitive markers.
- Using Matlab, programmed applications to detect and analyse single vesicle release.

Laboratoire de Neurosciences Cognitives et Adaptives **Strasbourg, FR**
Masters Technical Internship **Spring 2016**

- Performed various behavioral techniques with rats, such as the morris water maze, elevated plus maze, beam walking test, open field.
- Carried out statistical analysis of experimental data.

Loma Linda University Medical Center **Loma Linda, CA, USA**
Research Intern **Summer 2015**

- Utilized western immune-blotting for immune-specific targeting of biomarkers of traumatic brain

injury.
- Used NICOMP and acetylcholinesterase assays for analysis of exosomes.

Western University of Health Sciences **Pomona, CA, USA**
Research Volunteer **Spring 2015**
- Studied the effects of particulate matter on cells of the central nervous system
- Performed various assays including quantitative PCR, cell counting, and immunocytochemistry assays

PROFESSIONAL TRAINING

Université de Strasbourg **Strasbourg, FR**
Participant, Conception of Projects Using Animal Experimentation **2017**
- Principles for ethical animal experimentation

Bordeaux School of Neuroscience **Bordeaux, FR**
Participant, CAJAL School Linking Neural Circuits and Behaviour **2018**
- Techniques involving calcium imaging and electrophysiology in vivo

Université de Strasbourg **Strasbourg, FR**
Participant, Surgery of Rodents **2019**
- Principles and techniques for performing ethical and humane surgery on rodents

Université de Strasbourg **Strasbourg, FR**
Participant, Start programming with Python **2020**
- Beginner's principles of the python programming language

PRESENTATIONS AT MEETINGS

Borcuk, C., Diaz, J., Moyron, R., Gonda, A., and Wall N.R. Analyzing trauma from blood via biomarkers stored in exosomes. Poster presentation delivered at the Loma Linda Undergraduate Research Symposium, Loma Linda, CA, USA, June, 2015

Borcuk, C., Perreira-Vasconcelos, A., and Cassel JC. Phenotypic characterisation of rats lacking the amyloid precursor protein. Poster presentation at the Joint Masters in Neuroscience Technical Internship Symposium, Strasbourg, FR, April, 2016

Borcuk, C., Pistono, C., Saito, T., Hashimoto, S., Saido, T.C., Heraud, C., and Mathis C. Subtle memory deficits at early ages in a new double knock-in mouse model of Alzheimer's disease. Poster Presentation delivered at the CAJAL School Linking Neural Circuits and Behaviour, Bordeaux, FR, October, 2018

Borcuk, C., Pistono, C., Saito, T., Hashimoto, S., Saido, T.C., Heraud, C., and Mathis C. Phenotyping a novel mouse model of Alzheimer's disease. Poster Presentation delivered at the NeuroFrance Conference of the French Society of Neuroscience, Marseille, FR, May, 2019

Borcuk, C., Pistono, C., Saito, T., Hashimoto, S., Saido, T.C., Heraud, C., and Mathis C. In search of earliest memory deficits in a novel mouse model of Alzheimer's disease. Blitz oral presentation given at the Neuropole Conference 2020, Strasbourg, FR, January, 2020

SCHOLARSHIPS AND AWARDS

MESRI grant given at the Université de Strasbourg Doctoral School 414 competition **2017**

Neuropole travel grant for attending the Neurofrance 2019 conference **2019**

Société des Neurosciences grant for attending the FENS 2020 conference **2020**

Federation of European Neuroscience Societies (FENS) grant for attending the FENS 2020 conference **2020**

TEACHING EXPERIENCE

Université de Strasbourg **Strasbourg, FR**
Teaching Assistant, Cell Division **Fall 2018**
Teaching Assistant, Genetics and Human Embryology **Winter 2018**

Fete de la Science **Strasbourg, FR**
Neuroscience booth operator, taught concepts of memory to the public **Fall 2019**

SKILLS AND TECHNIQUES

Programming Languages
- R, Matlab, Python, ImageJ

Statistics
- Graph theory – igraph, braingraph packages on R
- Bootstrap, permutation testing
- Task-PLS – caret package on R

Cell Biology
- PCR
- Western blot
- Immunohistochemistry
- Maintenance of neuronal banker cultures
- TIRF imaging of banker neuronal cultures

Behavioural Testing
- Spontaneous Object Exploration
- Morris Water Maze
- Elevated Plus Maze
- Light Dark
- Actigraphy
- Barnes Maze

LANGUAGES

English	**French**
Native	Fluent

Table of Contents

Abbreviations

ACC – anterior cingulate cortex

AD – Alzheimer's disease

AICD - APP intracellular fragment

aMCI – amnestic mild cognitive impairment

APOE - Apolipoprotein E

APP – amyloid precursor protein

App^{NL-F} – single knock-in mouse with humanized FAD mutated *App*$^{NL-F}$

Aβ – Amyloid-β peptide

CDR – clinical dementia rating sum of boxes

CLA – claustrum

CTF –carboxy-terminal fragment (of APP)

DG – dentate gyrus

DH – dorsal hippocampus

dKI - *App*$^{NL-F}$*xMAPT* double knock-in

DMN – default mode network

EI – exploration index

EPM - elevated plus maze

FAD – familial Alzheimer's disease

FC – functional connectivity

FDOL5' – fine discrimination object location with a 5-minute ITI

FDOR5' – fine discrimination object recognition with a 5-minute ITI

fMRI – functional magnetic resonance imaging

IL – infralimbic cortex

ITI – inter-trial interval

KI – knock-in

LEC – lateral entorhinal cortex

MAPT – microtubule associated protein tau *gene* (also name for humanized *MAPT* KI mouse)

MCI – mild cognitive impairment

MEC – medial entorhinal cortex

MI – memory index

ME/EI – memory index divided by the exploration index

MMSE - Folstein's Mini Mental State Examination

mPFC – medial prefrontal cortex

MTC – medial temporal cortex

MTL – medial temporal lobe

MWM – Morris water maze

NFTs – neurofibrillary tangles

OiC24 – object-in-context with a 24-hour ITI

OL5' – object location with a 5-minute ITI

OP5'- object-in-place with a 5-minute ITI

OR24 – object recognition with a 24-hour ITI

OR5' – object recognition with a 5-minute ITI

PCC – posterior cingulate cortex

PET – positron emission tomography

PHC – postrhinal cortex in rodents (parahippocampal cortex in humans)

PHF – paired helical fragments

PMC – posterior medial cortex

POC – postrhinal cortex in rodents (parahippocampal cortex in humans)

PRC – perirhinal cortex

PRL – prelimbic cortex

PS1 or PS2 – proteins presenilin 1 or 2

PSEN1 or *PSEN2* – genes that code for presenilin 1 or 2

ptau – phosphorylated tau

RSC – retrosplenial cortex

sAPP – soluble APP

SCD – subjective cognitive decline

sMRI – structural magnetic resonance imaging

Introduction

1. Dementia and Alzheimer's disease

A. The 18th Richest Country in the World

Dementia is a syndrome caused by a variety of brain diseases, characterized by a decline in memory, language, and/or other cognitive skills that affect a person's ability to perform everyday tasks. It is estimated to affect over 45 million people worldwide (Nichols et al., 2019) and is predicted to triple by 2050 as average life expectancy increases (An Aging World : 2015, NIH, 2016), especially in the developing world (World Alzheimer Report 2010). In 2015, the worldwide cost of dementia was estimated at 818 billion dollars, exceeding the gross domestic product of countries such as Indonesia and the Netherlands, making dementia the "18th richest country" in the world. These include costs for informal care from family members and others, social care from care professionals and residential homes, and medical care (World Alzheimer Report 2015). Given its overwhelming and ever increasing global impact, it is vital to take an active stance in combatting dementia and promoting research for cures and therapies against the diseases that cause it. Until breakthroughs are made, dementia will constitute an increasing challenge to health-care systems across the globe.

B. Alzheimer's Disease

The predominant cause of dementia is Alzheimer's disease (AD), accounting for around 70% of dementia cases worldwide (Nichols et al., 2019). The disease is named after the German psychiatrist, Alois Alzheimer. In 1907, Alzheimer published a case report detailing a 55 year old female patient who was described as "completely deeply disoriented in time and place", and who "had completely lost the ability to retain information" (Alzheimer, 1895; Strassig and Ganguli, 2005). Using a silver staining histology technique, her brain biopsy presented unusually intensely stained "neurofibrils" within cortical cells. These lesions are now called "neurofibrillary tangles" (NFTs), the hallmark of tau pathology. Alzheimer also found seed like protein lesions scattered throughout the cortex, though these had already been described years before by Czech contempary Oskar Fischer. These lesions are now called "amyloid plaques", the hallmark of amyloid pathology. Over the next couple of years, he would describe more cases exhibiting similar neural pathology and cognitive troubles. In 1910, these cases would be detailed in a

psychiatry textbook by Alzheimer's colleague, and would be coined as "Alzheimer's disease" (AD).

2. Symptomatology of AD

Initial symptoms of AD mainly involve brief recognition memory lapses where the sufferer may sometimes forget recent events, taxing episodic memory. Episodic memory is necessary to remember personally relevant events with complex and context-rich details (recollection process). This form of memory is often evaluated in recognition paradigms using the remember/know procedure (Tulving, 1985). Instructions are adapted to differentiate the episodic process of recollection from the arguably non-episodic process of familiarity (see Yonelinas, 2002; Rugg and Yonelinas, 2003; Vilberg and Rugg, 2008 for a discussion of the dual processes account of recognition memory). They will also show lapses in spatial memory where they first have trouble remembering where they have placed objects and spatial orientation difficulties, especially in learning a new route. In advanced stages, AD patients will progressively lose their ability to navigating to and from familiar places. Moreover, executive function is affected as the sufferer will find it harder to make decisions (decision making deficits), change their habits (loss of cognitive flexibility) or show some difficulty retaining simple information necessary in routine multi-step tasks such as following a new recipe. The later task typically depends on working memory. The prodromal stage of AD characterized by light cognitive troubles that do not severely affect everyday function, and corresponds to a cognitive state termed Mild Cognitive Impairment (MCI; Petersen et al., 2001). As the disease develops the problems with memory and executive function worsen. Eventually, the symptoms are severe enough as to necessitate everyday support, signaling the transition from MCI to dementia. They will struggle to recognize family and friends. Their personality may also change with increasing anxiety and agitation. As they become more disoriented, they will start to wander, especially during sleep time, and forget which day it is or where they are. Their anxiety may divulge further, with some patients developing severe depression. Many will experience delusions and paranoia. Completely new symptoms will start to develop such as disturbed sleep architecture, and aphasia (loss of spoken language). Sleep disturbances are frequent in AD, affecting up to 45% of AD patients (Moran et al., 2005; McCurry et al., 2000). Sleep disorders are particularly important in regard to

AD's symptomatology as sleep plays a crucial role in memory formation and other cognitive functions (Mander et al., 2016). In the final stage of the disease the patient may develop physical symptoms including severe weight loss, and difficulties in moving or eating.

AD diagnosis first relies on a qualitative behavioral examination by a doctor which consists in an interview of the patient and its relatives. Cognitive impairments are then assessed more quantitatively using scoring in cognitive tests. The most common of these is the Folstein's Mini Mental State Examination (MMSE) (Folstein and Whitehouse, 1983). This test provides a global cognitive exploration of the patient using thirty questions. It provides information on the patient's spatio-temporal orientation, short and medium-term memory, mental calculation, attention, language, comprehension and constructive practices. Additional biological exams evaluating the neuropathological state are always necessary to confirm the diagnosis. In the past, final AD diagnosis could only be delivered after post-mortem examination of the brain confirming the presence of the two AD hallmarks, namely the amyloid plaques and NFTs.

A. The hallmark aggregates

Amyloid plaques, the seed like protein lesions as described by Alzheimer and Fischer, are formed by the extracellular accumulation of an amyloid peptide (Aβ). Aβ results from the processing of amyloid precursor protein (APP). Accumulation in the brain can result from an altered imbalance in the production and clearance pathways in the case of sporadic AD, or overproduction of Aβ due to genetic mutations in familial AD (FAD) (Selkoe and Hardy, 2016). Aβ peptides fold into beta-pleated sheet structures that are highly fibrillogenic, and aggregate to form oligomers, then filaments and finally amyloid plaques (Rozemuller et al., 1989). There are two main subtypes of Aβ, $A\beta_{40}$ and $A\beta_{42}$. $A\beta_{42}$ more readily aggregates and is found in higher abundance in amyloid plaques. Evaluating decreases in $A\beta_{42}$ levels in cerebral spinal fluid (CSF) is a reliable way of predicting augmented brain amyloid deposition and it is routinely performed to confirm AD diagnosis. It must be noted that in healthy conditions, the amyloidogenic processing of APP is secondary compared to the non-amyloidogenic processing which involves an α-secretase acting within the Aβ sequence thereby releasing the highly neurotrophic and neuroprotective secreted form of APP (Dodart et al., 2000).

There are two main forms of plaques, diffuse and dense-core (***Figure 1***). Diffuse plaques, the earliest subtype, have an amorphous structure (Yamaguchi et al., 1988) and are stained weakly by thioflavin S (a compound used for staining protein aggregates) and amyloid binding dyes such as Congo red. Dense core plaques have a compact core consisting of densely packed amyloid fibrils (Kidd, 1964), and are intensely positive with thioflavin S and Congo red (Dickson et al., 1997). A subset of dense core plaques, termed neuritic plaques, contain degenerative neuronal processes (neurites) surrounded by reactive glia and synaptic loss (Thal et al., 2006; Yasuhara et al, 1997).

NFTs, the neurofibrils described by Alzheimer, are aggregates of filamentous tau protein (Goedert et al., 1988). Tau is a protein that normally functions to stabilize and organize axonal microtubules (Weingarten et al., 1975). Abnormal phosphorylation of tau leads to loss of function and subsequent aggregation, first into oligomers (Maeda et al., 2006), then filaments (Goedert et al., 2018), and finally NFTs. The most common tau filaments have a twisted double-helical structure and are thus called paired helical filaments (PHF), though straight helical filaments (SH) also exist.

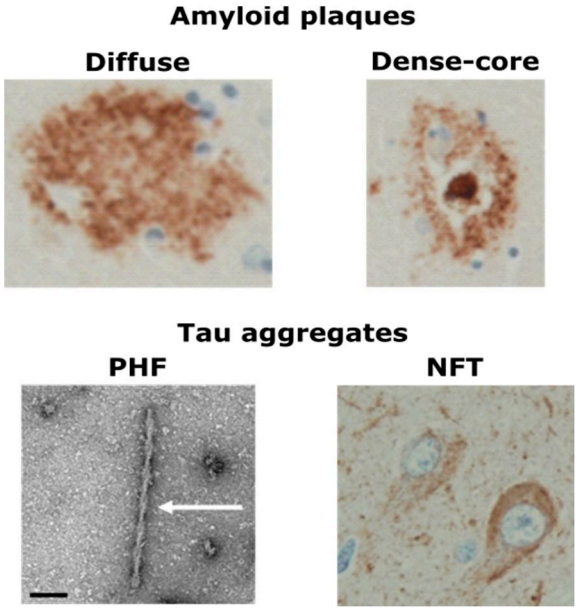

Figure 1. *The two AD hallmarks. NFT : neurofibrillary tangles. PHF : paired helical fragment. Adapted from Deture and Dickson 2019*

B. From treatment to prevention

The most common available method for diagnosing AD is through a qualitative examination of a patient's mental state as evoked previously. Nowadays, biological exams consist in CSF testing and eventually neuroimaging investigations to verify the presence of both amyloid and tau pathologies. As it stands this diagnosis pipeline is able to efficiently detect mild to moderate stages of AD. Clinical trials have mostly been conducted at this stage of AD, including those testing anti-bodies targeting Aβ (solanezumab, bapineuzumab) and inhibitors of β (verubecestat) and γ (semagacestat) secretases. Unfortunately, so far these treatments have failed to significantly slow cognitive and functional decline (Doody et al., 2013, 2014). This is largely due to the fact that these treatments occur too late, after physiological changes such as atrophy have reached a potentially irreversible state. It is essential that we increase our understanding of much earlier stages of AD, so that more pro-active therapies or detection methods can be established. Throughout the rest of this text, I will focus on the physiological and cognitive perturbations that underlie the very earliest stages of AD.

3. Genetic factors and risk factors of AD

A. Sporadic AD and its risk factors

The vast majority of AD patients (95%) have the late onset sporadic form of AD. Among major non-modifiable risk factors, age is the most fundamental and well known factor. Around two third of AD patients are women in the United States or in France, as in most European countries. This was initially attributed to the fact that women aged better than men, so this unbalanced proportion only reflected a sex biased survival. However, gender has been more recently identified as a very serious risk factor in AD (Ferretti et al, 2018). The higher risk to develop AD has been partly related to an increased vulnerability of the female brain during and after menopause (Mosconi et al., 2017). In addition, many other modifiable risk factors for AD have a higher impact on female sex and gender, such as depression, sleep disorders, and caregiver burden (Rahman et al., 2019). On the other hand, research on specific environmental risk factors has gathered relatively poor evidence concerning most metals and occupational exposure (lead, paints, fuels). However, the systematic review published by Killin et al. (2016) still ends up with

a short list which includes air pollution, aluminium and pesticides showing moderate evidence as dementia risk factors that merits further investigation.

In sporadic AD, there are several common genetic polymorphisms with a low effect size that account for a significant portion of AD heritability. Rather than directly increasing production of Aβ, most of these risk genes indirectly increase the presence or the metabolism of APP or tau and/or adversely affect Aβ clearance. One of the major genetic risk factor is related to the *APOE* gene, which codes for the apoliprotein E (apoE), a protein involved in lipid transport. There are three *APOE* alleles, ε2, ε3 and ε4, giving rise to apoE2, apoE3 and apoE4 isoforms respectively. *APOE ε4* leads to a greater risk of developing AD, its heterozygous presence leading to a 3-fold increase in risk, and homozygous a 12-fold. It is estimated to be present in 15 to 20% of the population and in more than 50% of MCI patients (Silva et al., 2019). Asymptomatic carriers of *APOE ε4* are among the most commonly evaluated representations of preclinical-AD, and will be referenced throughout this text. The negative impact of *APOE ε4* in the development of AD has been related to its deleterious effects at several levels of Aβ-driven pathology as well as Aβ-independent effects on synaptic plasticity, neuronal repair or cerebrovascular functions (Yamazaki et al., 2019). Moreover, a recent study also suggests that this allele increases tau pathology (Therriault et al., 2020). There are many other genetic risk factors other than the *APOE ε4* gene. Recent state of the art Genome-wide-association-studies, have been able to screen 100s of thousands of AD cases to identify new genetic risk variants. These meta-analyses have identified over 40 disease-associated genomic loci, which may implicate over 200 potential risk genes (Lambert et al,. 2013; Jansen et al,. 2019).

B. Familial AD (FAD)

Around 1 % of AD cases are of the autosomal dominant familial form (FAD), meaning that they are linked to a single gene mutation(s) that leads to a 100% risk of developing early-onset AD. Dominant mutations are found in three genes, *App*, *PSEN1* and *PSEN2*. *App* encodes for the amyloid precursor protein (APP), a protein that is cleaved to form the amyloid peptide (Aβ). *PSEN1* and *PSEN2* encode for presenilins 1 and 2 respectively, the catalytic subunits of the γ-secretase complex that cleaves APP and contributes to the formation of Aβ. Mutations to these genes therefore promote Aβ production by augmenting amyloidogenic specific cleavage of APP,

or increasing $A\beta_{42}/A\beta_{40}$ ratio. Asymptomatic individuals with FAD represent the most robust way of tracking pathological trajectories of AD patients, and were instrumental in first defining the preclinical progression of AD staging.

Neuropathological changes in AD occur decades before cognitive decline (Selkoe, 2012). Assessment of FAD patients shows that $A\beta_{42}$ levels in CSF begins to decline as early as 25 years before expected symptom onset (Bateman et al., 2012). Then, amyloid deposits, and progressive brain atrophy is detected through neuroimaging techniques (amyloid plaque positron emission tomography (amyloid-PET) imaging and structural magnetic resonance imaging (sMRI)), shortly followed by increased levels of total tau and phosphorylated tau (ptau) in CSF appear roughly 15 years before expected symptom onset (Bateman et al., 2012; Fleisher et al., 2015). It must be noted that cognitive impairments in the MMSE and Clinical Dementia Rating scale are detected only 5 years before the diagnostic of dementia. CSF contents in total tau and ptau are now routinely evaluated to confirm clinical diagnosis of AD. Tau deposits are seen with PET imaging 6 years before expected symptom onset, and are well correlated with MMSE performance (Quiroz et al., 2018). This time course is generally retained in complementary cross-sectional evaluation of sporadic AD (see ***Figure 2***, and Jack et al., 2010).

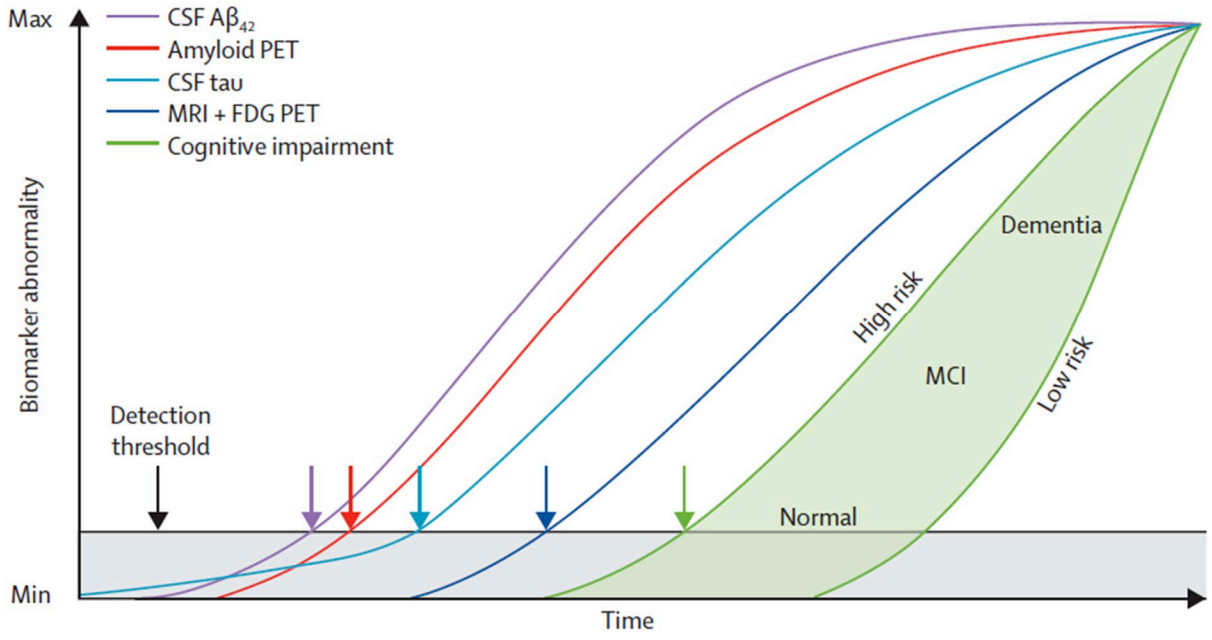

Figure 2. *Progression of Alzheimer's disease. Evolution of the biomarkers currently used for AD diagnosis as a function of time. Reproduced from Jack et al 2013.*

4. Detecting early stages of AD

A. Mild Cognitive impairment

Mild cognitive impairment (MCI) is a syndrome defined by cognitive decline that is greater than normal for an individual's age but not bad enough to severely interfere with daily life (Gauthier et al,. 2006). The prevalence of MCI in adults over 65 years is 10 to 20% (Langa et al., 2014). MCI can be diagnosed based on anecdotal evidence, or through neuropsychological tests such as the Short Test of Mental Status and the Montreal Cognitive Assessment (Tang-Wai et al., 2003; Nasreddine et al., 2005). There are two subtypes of MCI, amnestic and nonamnestic. Amnestic MCI (aMCI) concerns noticeable episodic memory impairments, with other capacities such as executive function remaining more or less unaffected. Nonamnestic MCI is conversely characterized by a subtle decline in separate functions such as executive function, language, and visuospatial skills. People with aMCI have a greater chance of transitioning into AD, with the rate of progression of at least 10% per year versus the 2% in normal elderly (Campbell et al., 2013; Roberts et al., 2014), so it is considered as a prodromal stage of AD (***Figure 3***). However, it is important to keep in mind that MCI only describes a set of symptoms, not a specific disease. MCI patients are not necessarily developing an early phase of AD because the MCI population also includes other etiologies for such as depression and other neurodegenerative diseases that affect the cognitive sphere.

B. Preclinical and Subjective cognitive decline

After three decades of intense research, clinical trial failures and data collected in presymptomatic FAD and sporadic AD patients in the early 2010s (Jack et al. 2010; Bateman et al., 2012), the worldwide community of AD researchers understood that early intervention would offer better therapeutic success. Therefore, the development of effective prevention and treatment would depend on increasing knowledge on initial steps of the disease (Selkoe, 2012). In the meantime, extensive research and clinical trials has been conducted… and there is still no efficient treatment in our hands (Yiannopoulou and Papageorgiou, 2020). This lack of progress in therapeutic approaches has greatly stimulated research on earlier stages than MCI as illustrated by the steep increase in publications on preclinical, subjective cognitive decline and

"cognitively healthy" middle-aged and elderly with amyloid deposits. The present work is part of this general effort to focus on preclinical stage. This led us to search a definition of this "preclinical stage". Sperling and colleagues (2011) proposed a 3-stage framework for preclinical AD based on currently used clinical biomarkers. The first asymptomatic amyloidosis stage is characterized by high PET amyloid tracer retention and low CSF Aβ42, the second one adds neurodegeneration with neuronal dysfunction on 18F-fluorodeoxyglucose-PET (FDG-PET) or functional MRI (fMRI), high CSF tau/ptau and cortical thinning/hippocampal atrophy in sMRI, and finally the third stage adds subtle cognitive decline with evidence of changes from baseline level of cognition, poor performance on more challenging cognitive tests without meeting criteria for MCI (According to Dubois et al., 2016, "*preclinical AD would theoretically span from the first neuropathologic brain lesions to the onset of the first clinical symptoms of AD*"). However, they evoke the difficulty to set the boundaries of what should be considered as the first neuropathological sign and what should be considered as the first clinical symptom of AD. Indeed, a new stage of preclinical AD called subjective cognitive decline (SCD) has been recently considered as the first clinical manifestation of AD. SCD is based on self-reported decline in cognitive functions without any impairment in the classical diagnostic battery. Neuroimaging studies of SCD found abnormal amyloid and tau aggregates, regional atrophy and white matter alterations (Wang et al, 2020). These characteristics are relatively close to those listed for the third stage proposed by Sperling et al. (2011). An overview of the different stages of AD can be seen in ***Figure 3***.

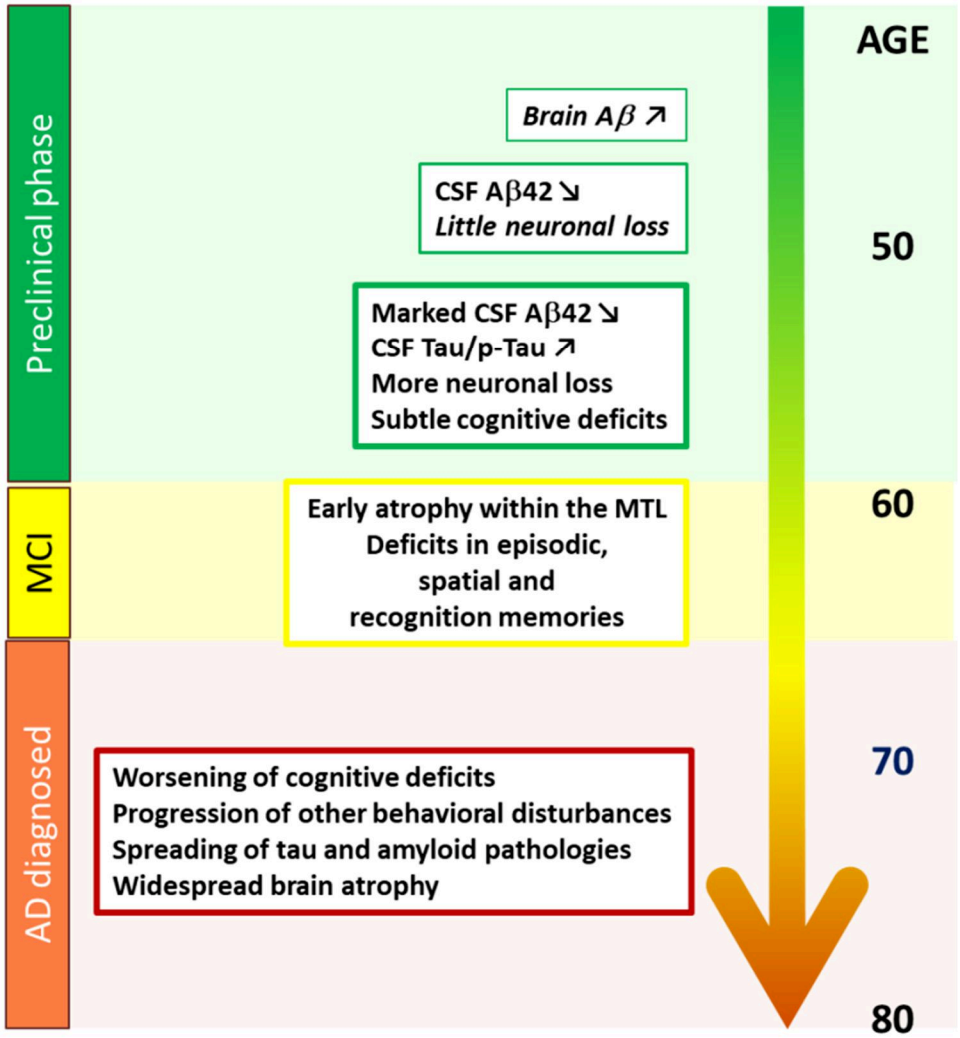

Figure 3. *Staging of AD with cognitive and biological markers. Inspired by Selkoe, 2012 and Bateman et al., 2012.*

C. Neuropathological staging of AD

Protein accumulation affects different regions of the brain at different time points, making it possible to characterize deposition in an AD staging system. The first staging systems were developed using postmortem neuropathologic studies of the brain, detailed in seminal research by the teams of Heiko Braak and his student Dietmar Thal. Braak and Thal described a descendent progression of amyloid deposition, described in the "Thal stages": stage 1 in the neocortex, stages 2 and 3 in the allocortex (medial temporal and insular cortex) and limbic system, and stages 4 and 5 in subcortical region. Braak described tau progression with the "Braak stages", stages 1 and 2 starting in the medial temporal lobe, stages 3 and 4 in the limbic

system, and finally stages 5 and 6 in the neocortex. These Braak and Thal staging patterns are illustrated in ***Figure 4A***.

With the recent development of functional imaging techniques, we have obtained a more precise look at AD deposition and concurrent changes in brain physiology (Jagust et al., 2018) (***Figure 4B***). Positron emission tomography (PET) is a technique that uses radioactive substances known as radiotracers to visualize changes in brain physiology (Ametamey et al., 2008). Some radiotracers have been verified in postmortem brains to label amyloid plaques and fibrils (Klunk et al., 2004; Clark et al., 2012; Sabri et al., 2015; Curtis et al., 2015) as well as tau PHFs and NFTs (Xia et al., 2013; Marquié et al., 2015; Schonhaut et al., 2017). These can be coupled with other neuroimaging techniques to evaluate concurrent changes in brain physiology. The radiotracer glucose analogue 18F-fluorodeoxyglucose used in FDG-PET can map brain glucose metabolism. The cellular relevance of this technique is somewhat ambiguous, but the recorded signal is likely linked to synaptic or glial dysfunction. Magnetic resonance imaging techniques such as sMRI and fMRI measure brain volume (through detection of random water movement in tissues) and brain activity (through detection of blood oxygen levels) respectively. Finally, physiological measures have been evaluated in tandem with standardized assessments of cognitive function, quantified with testing protocols including the Mini-Mental State Examination (MMSE), and the Clinical Dementia Rating Scale Sum of Boxes (CDR).

Amyloid-PET reveals more detail into what is essentially Thal stage 1. Earliest amyloid deposits are seen in medial prefrontal (mPFC) and posterior medial cortex (PMC) (including the posterior cingulate, retrosplenial, precuneus) (Palmqvist et al., 2017). Amyloid deposition then progresses to the other neocortical areas described in Thal stage 1 (Mattson et al., 2019). Correspondence of amyloid-PET with hypometabolism or atrophy is not clear. Many studies report no correspondence (Furst et al., 2012, Lehmann et al., 2013). In MCI, increased amyloid deposition in the PMC was associated with atrophy in medial temporal regions, and this may reflect an indirect association through tau staging (Tosun et al., 2011). Others have reported an association between amyloid and atrophy only during the preclinical stage SCD, suggesting that initial Aβ may induce subtle atrophy early on before this dependence is muddled by the appearance of other atrophic processes (Chételat et al., 2010). Amyloid staging presents itself decades before dementia, and is even found in abundance in the cognitively healthy elderly (Villeneuve et al.

2015). Most cognitively healthy individuals show less association of atrophy and hypometabolism to Aβ, indicating Aβ resistance as a potential mechanism for maintained cognition (Ewers et al., 2012).

Tau-PET largely recapitulates Braak staging (Schwarz et al., 2016; Schöll et al., 2016). Tau deposition appears after amyloid deposition, but increased tau is associated with increased amyloid (Johnson et al., 2016; Tosun et al., 2017). Even in the cognitively normal, very slight increases in cortical amyloid, regardless of localization, associate with increases of tau in the MTL (Tosun et al., 2017, Leal et al., 2018). There is a strong correlation between the topography of tau deposition and atrophy (Wang and Mandelkow, 2016). Tau deposition and accompanying atrophy in the MTL strongly correlates with decreased cognitive function as measured by MMSE and CDR (Brier et al., 2016; Pontecorvo et al., 2017; Quiroz et al., 2018).

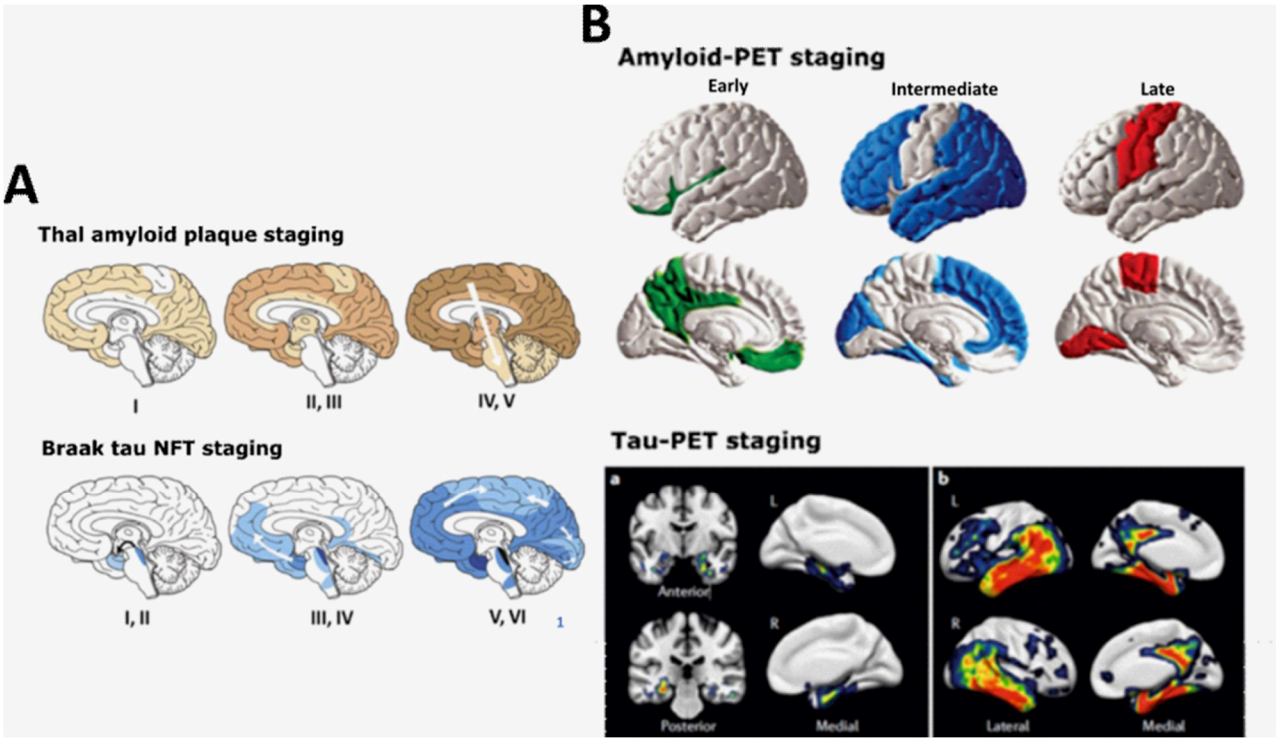

Figure 4. Staging of aggregate formation based on (A) evaluation of post mortem brains and (B) PET. Adapted from Jouanne et al., 2017; Mattson et al., 2019; Maass et al., 2017.

5. Anatomical architecture and connectivity of AD sensitive brain areas

Here I will describe the cytoarchitecture and structural connectivity of regions sensitive to early AD deposition. This will mostly evoke results arising from studies on macaques and rodents, which are required to provide an appropriately detailed understanding of anatomical connectivity. All observations are generally conserved between primates and rodents.

A. Medial Temporal Lobe (Tau)

i. Hippocampus

The hippocampus is made up of two principal parts: the cornu Ammonis (CA), which emerges into the dentate gyrus (DG) (***Figure 5***). The cornu Ammonis, is sometimes considered on its own as the hippocampus proper, and is composed of 4 sections that each reaches closer to the DG: the CA1, CA2, CA3 and CA4. It has stratified brain structure. Its most superficial stratum is called the stratum oriens. This stratum rests on the pyramidal stratum which takes its name from the glutamatergic pyramidal cells that compose it. The basal dendrites of these pyramidal cells are located within the stratum oriens. Their apical dendrites, on the other hand, first go into the stratum radiatum, located just below the pyramidal stratum, then sink into the stratum lacunosum-moleculare, the deepest layer of the hippocampus proper. The axons of the pyramidal cells form the Schaffer collaterals that innervate the CA1 and CA3 fields.

The DG contains a granular layer, the hilum, and the molecular layer. The granular layer contains granular cells. These neurons are characterized by a rounded soma, a dense apical dendrite and scattered basal dendrites. The granular layer surrounds the hilus, which contains the axons of granular cells called mossy fibers. Above the upper granular layer is the molecular layer that contains the apical dendrites of the granular cells and their afferents (Amaral et al., 2007).

The subiculum is the main output of hippocampal information and is composed of three layers: a molecular layer, continuous with strata lacunosum-moleculare and radiatum of the adjacent CA1 field, and a polymorphic layer.

The hippocampus is widely considered as essential in episodic memory, spatial memory and cognitive flexibility (Eichenbaum, 2017, Tulving and Markowitsch, 1998).

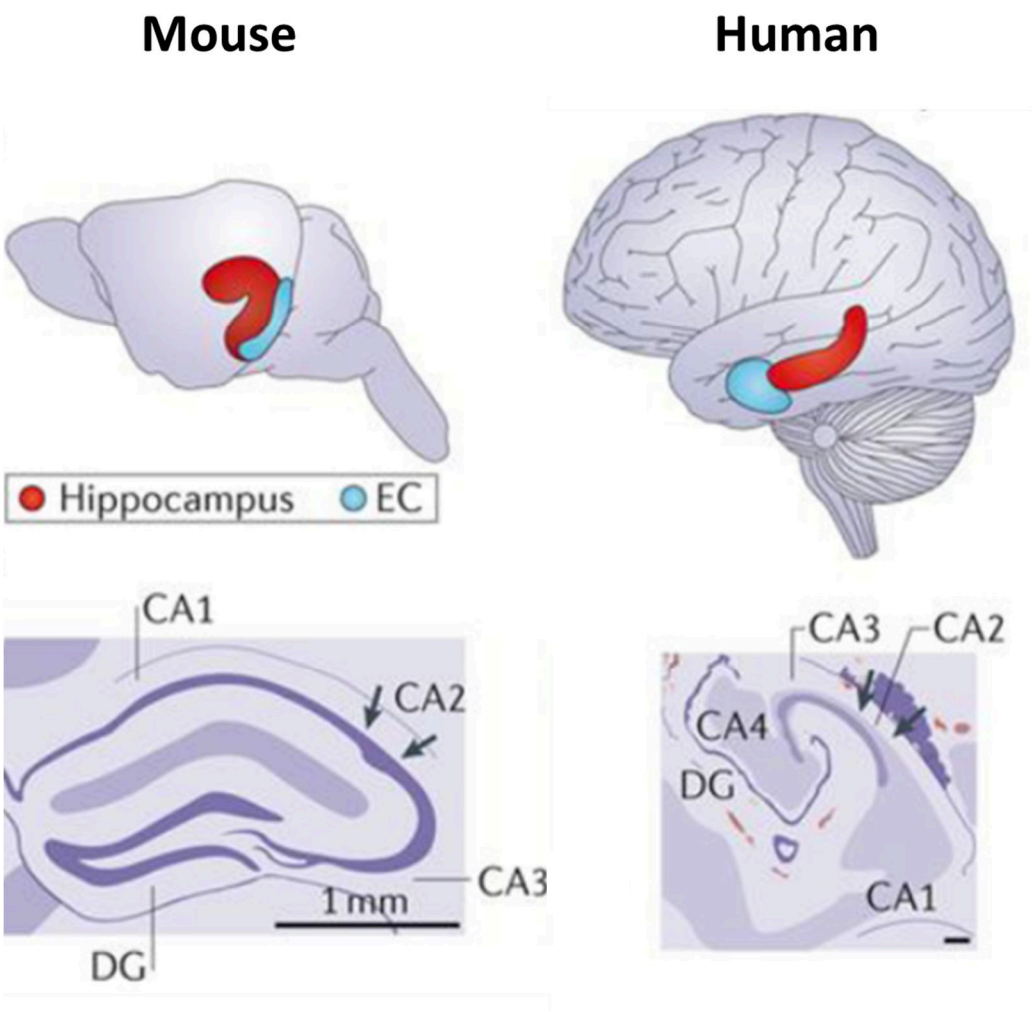

Figure 5. *Organisation of the hippocampus in rodents and humans. CA: CA fields of the hippocampus; Dist: distal; DG: dentate gyrus; EC: entorhinal cortex. Adapted from Strange et al., 2014.*

ii. Entorhinal Cortex

The entorhinal cortex (EC; Brodmann 28 area) is the main relay of information between the neocortex and the hippocampus (Muñoz and Insausti, 2005) (***Figure 6***). This cerebral structure plays a central role in the integration of sensory information of different natures into more elaborate memory representations (Eichenbaum et al., 2007; Tsao et al., 2013). It exhibits cytoarchitecture and laminar structure similar to the neocortex. Layers I and IV are relatively devoid of neurons. The main efferent neurons are the glutamatergic pyramidal cells from layers

I, II and III (Canto et al., 2008). These are accompanied by GABAergic inhibitory interneurons that build local intrinsic connections and aid in homeostatic control of the EC.

The EC is divided into two sub-regions: the lateral entorhinal cortex (LEC) and the medial entorhinal cortex (MEC) (Kerr et al., 2007; Canto et al., 2008). The LEC is located in the anterior lateral EC, while the MEC is located in the posterior medial EC (van Strien et al., 2009). The subregions differ in terms of cytoarchitecture, interregional connectivity, and functionality (Witter et al., 2000a, 2000b). The LEC is connected to the perirhinal (PRC), olfactory, and insular cortex and the amygdala. The MEC is connected to the postrhinal cortex (POC), the presubiculum and the occipital and retrosplenial visual associative cortex. The two subregions are also connected differently with the hippocampus. While both subregions target the same neurons of the dentate gyrus and the CA3 ammonic field of the hippocampus, they connect reciprocally to different cell groups of CA1 and the subiculum.

Layer II neurons primarily project to the dentate gyrus and the CA3 ammonic field of the hippocampus, while Layer III neurons distribute their axons to the CA1 field and the subiculum. Cortical inputs primarily target neurons in layers II and III. Cholinergic and monoaminergic subcortical inputs from the amygdala, septum, thalamus and brainstem have a diffuse distribution over the EC. The claustrum also sends strong projections. The CA1 field, the subiculum, the mPFC and retrosplenial cortex (RSC), and in primates the posterior cingulate cortex (PCC), target layers V and VI. In turn, the EC sends reciprocal cortical and subcortical projections towards the amygdala, septum, striatum and thalamus (Witter et al., 2000a, 2000b).

The EC is widely considered as essential in episodic and spatial memory (Sugar and Moser, 2019; Murray and Richmond, 2001).

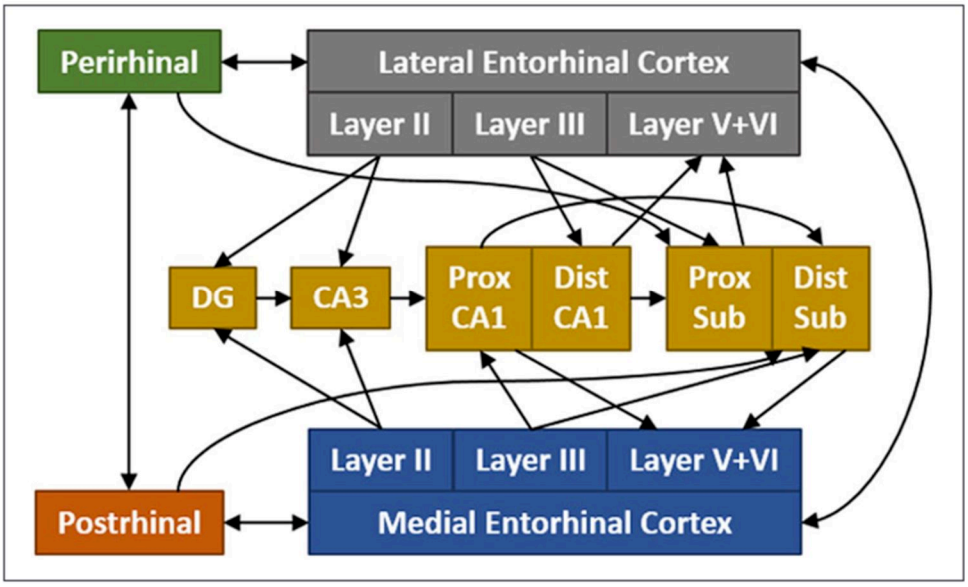

Figure 6. *Schematic representation of hippocampal–parahippocampal interactions in the rodent brain. CA: CA fields of the hippocampus; Dist: distal; DG: dentate gyrus; Prox: proximal; Sub: subiculum. Adapted from Bubb et al., 2017.*

iii. Perirhinal and Postrhinal Cortex

The cortical regions adjacent to the EC (laterally in primates, dorsally in rodents), are an anterior region, the PRC, and a posterior region, the parahippocampal cortex (postrhinal cortex in rodents) (POC). The PRC itself splits into two subregions, Area35 and Area36. The PRC is more strongly connected with the LEC, and the POC with the MEC. The PRC and POC make up the primary relay for the EC to sensory and association cortices.

Neocortical afferents from association, somatosensory, auditory, and visual areas, targets area 36 of the PRC, which then projects to area 35. These are topographically organized: somatosensory, auditory, and visual areas preferentially target anterior, mid-rostrocaudal, and caudal area 36, respectively (Burwell, 2001). Area 35 also receives substantial input from the LEC, piriform cortex, and insular areas. The POC is heavily innervated by visual association and visuospatial areas, including the RSC and parietal cortices. Cortical efferents are similarly segregated, with POC targeting mainly visual and visuospatial regions and the PRC targeting all sensory modalities. Even direct cortical connections to the EC (mPFC, RSC, PCC) mainly target areas of the EC bordering the PRC/POC (Agster and Burwell, 2009). Strong subcortical projections to the

PRC arise from the claustrum, olfactory regions, amygdala and the dorsal thalamus. The POC receives predominantly projections from the dorsal thalamus and claustrum (Pereira et al., 2016). An overview of interactions between the hippocampus, entorhinal cortex and peri/postrhinal cortices can be seen in ***Figure 6***.

The PRC is widely considered as essential in object recognition memory (Brown and Aggleton, 2001; Murray and Richmond, 2001), and the POC appears to be important for spatial contextual memory (Aminoff et al., 2013, Norman and Eacott, 2005).

B. Anterior and posterior midline cortices (Amyloid)

i. Medial Prefrontal Cortex

The medial prefrontal cortex (mPFC) covers the anterior portion of the midline cortex. In humans is composed mainly of the anterior cingulate cortex (ACC), including the anterior midcingulate cortex (BA24), the pregenual ACC (BA32) and the subgenual ACC (BA25) (***Figure 7***). The dorsal areas (BA24 and the dorsal portion of BA32) are heavily connected with sensorimotor and association neocortical areas (RSC), while the ventral areas (BA24 and the ventral portion of BA32) have connections with the amygdala and temporal, limbic association cortices. In rodents there are equivalents to the anterior midcingulate cortex (classically termed the cingulate cortex 1 and 2 (Cg1, Cg2)), the pregenual ACC (classically termed the prelimbic cortex (PRL) and the subgenual ACC (classically termed the infralimbic cortex (IL)) (Vogt and Paxinos, 2012).

The mPFC is widely considered as essential in working memory, cognitive flexibility and memory consolidation in interaction with the hippocampus (Miller and Cohen., 2001; Euston et al., 2012; Funahashi, 2017).

ii. Posterior Medial Cortex

The posterior medial cortex (PMC) makes up the posterior extension of the midline cortex. In humans and non-human primates is composed of the precuneus, the PCC, and the RSC (The PCC and RSC are depicted in ***Figure 7***). The PCC and precuneus are reciprocally connected to many cortical regions not present in the rodent, including other parts of the parietal lobe (Parvizi

et al., 2006), the lateral prefrontal cortex (BA46), and the frontal poles (BA10/11). The PCC and RSC are highly connected to other paralimbic, limbic and dorsal thalamic structure. Reciprocal connections to the medial temporal lobe and the mPFC are seen with the ventral PCC and RSC (Kobayashi and Amaral, 2007; Kobayashi and Amaral, 2003).

The posterior portion of the midline cortex in rodents is most akin to the human RSC, according to indices of cytoarchitecture and structural connectivity (***Figure 7***). However, as discussed above, the RSC shares a very similar structural connectivity profile to the ventral PCC, with both exhibiting strong reciprocal connections with the MTL and the mPFC. Many of the functional properties of the human PCC is retained in the rodent RSC, especially in regards to their position as central hubs for resting state functional networks (Lu et al., 2012, Stafford et al., 2014). The PMC also heavily contributes to associative and episodic memory (Ritchey and Cooper, 2020).

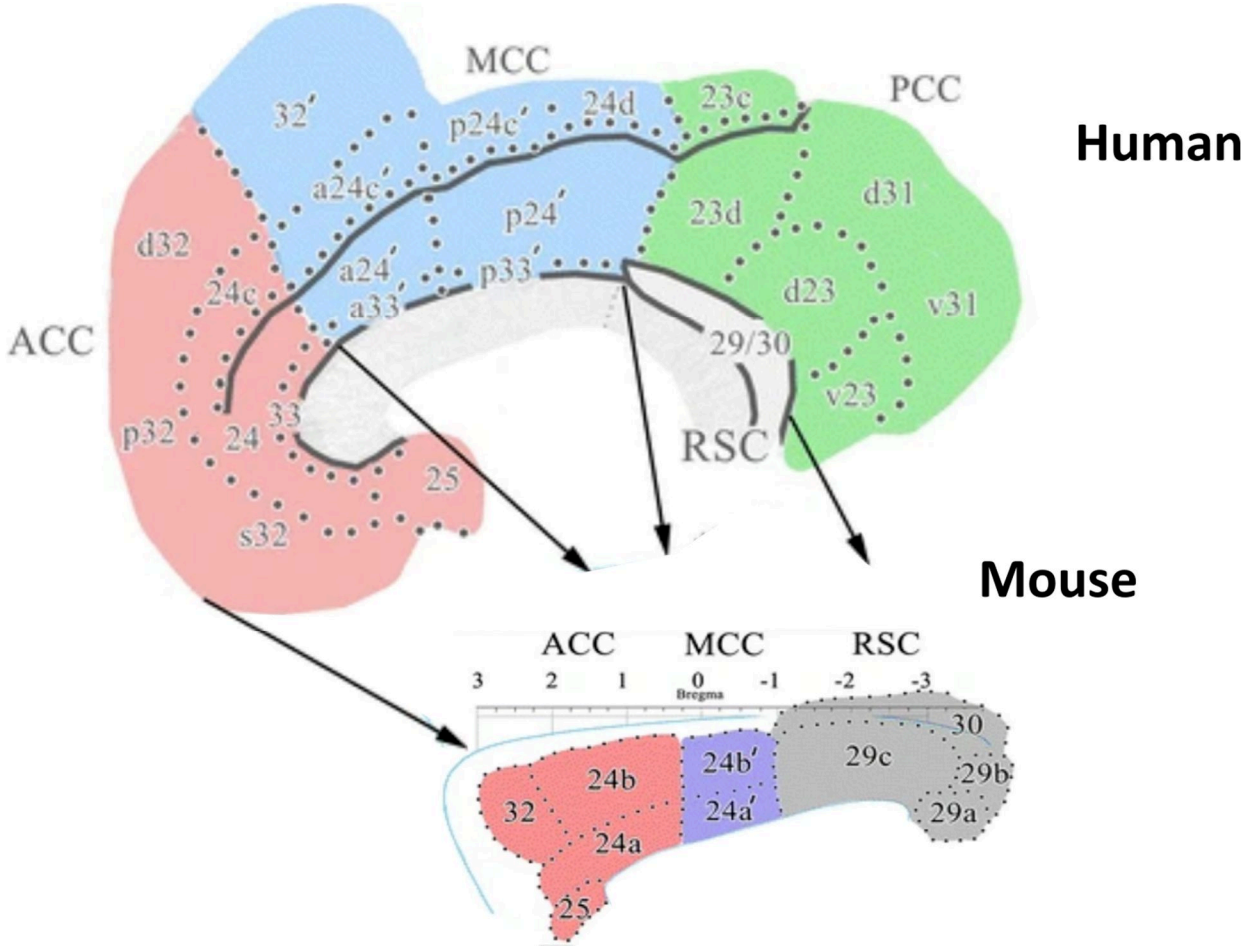

Figure 7. *Anteriour-posterior extent of the midline cingulate cortex in humans and mice, with Brodmann's areas indicated. ACC: anterior cingulate cortex; MCC: middle cingulate cortex; PCC: posterior cingulate cortex; RSC: retrosplenial cortex. Adapted from Vogt and Paxinos, 2014.*

6. Functional perturbations of early AD

A. Hyper-activity in the MTL

Using fMRI and FDG-PET in patients of MCI, several studies have reported hyper-activity in the basal forebrain (Kim et al., 2012) and most prevalently in the MTL (Johnson et al., 2006a; Hämäläinen et al., 2007; Huijbers et al., 2015). Hyper-activity of the MTL is also observed in asymptomatic preclinical individuals at genetic risk for developing AD, including carriers of FAD mutations (Quiroz et al., 2010; 2015; Reiman et al., 2012) and in carriers of APOE ε4 at increased risk for sporadic AD (Bookheimer et al., 2000; Johnson et al., 2006b; Tran et al., 2017). Reduction of MTL hyperactivity improves cognition in aMCI (Bakker et al., 2012). There is a clear link between increased tau and MTL hyper-activity in cognitively healthy individuals, as assessed with Tau-PET (Marks et al., 2017; Huijbers et al., 2019), and CSF tau levels (Berron et al., 2019). Hyper-activity also correlates well with atrophy and cortical thinning (Putcha et al., 2011, Hämäläinen et al., 2007). Given its prominence in asymptomatic individuals, hyper-activity was hypothesized to be part of a compensation mechanism counteracting the first AD-associated neuropathologic alterations. Indeed, studies have shown that hippocampal hyper-activity during encoding (Kircher et al., 2007) can transiently correlate positively with better performances during a memory task. However, we will see later that MTL hyper-activity may adversely affect specific subtle forms of memory, which as of yet go largely undetected in preclinical individuals.

B. Default Mode Network

i. Overview

The default mode network (DMN) is most simply described as a set of brain regions that co-activate in time (in other words they exhibit functional connectivity) during rest or passive task states (Buckner et al., 2008). These include primarily regions of the the mPFC, the PMC and the temporal lobe. However, the DMN can be more aptly described as a set of subsystems that converge onto midline hubs. There are two principle subsystems which converge onto the hubs of the anterior mPFC (amPFC) and PMC: the “medial temporal subsystem” containing the

hippocampal formation/MTL, the RSC and the ventral mPFC (vmPFC), and a "dorsal medial subsystem" containing the dorsal mPFC (dmPFC), the inferior parietal lobe and the lateral temporal cortex (Andrews-Hanna et al., 2010). These subsystems are functionally divergent, each supporting distinct processes supporting autobiographical thought. The medial temporal subsystem is more involved in episodic memory retrieval, whereas the dorsal medial subsystem is more involved with mentation (ability to represent the feeling and emotions of one's self and others) (Andrews-Hanna et al., 2014) (***Figure 8***). With more advanced analysis techniques, many other subsystems and individual networks contributing to the global DMN have been identified, such as the posterior DMN (pDMN) and the anterior DMN (aDMN), which have higher involvement of the PMC and mPFC respectively. (Jones et al., 2012; Buckner and DiNicola, 2019)

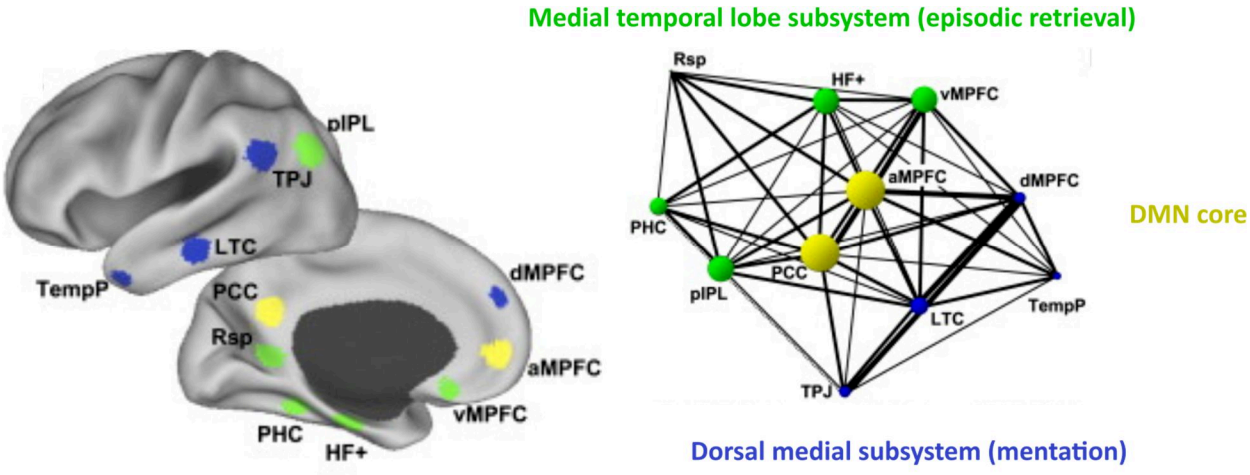

Figure 8. *The default mode network and its primary subsystems which contribute to different aspects of autobiographical memory. The dorsal medial subsystem is required for mentation and includes the dorsal medial prefrontal cortex (dMPFC), temporoparietal junction (TPJ), lateral temporal cortex (LTC), and temporal pole (TempP). Medial temporal lobe (MTL) subsystem is required for episodic retrieval and includes the ventral medial prefrontal cotrex (vMPFC), posterior inferior parietal lobule (pIPL), retrosplenial cortex (Rsp), parahippocampal cortex (PHC), and hippocampal formation (HF+). These subsystems overlap in the DMN through midline core regions of the posterior cingulate cortex (PCC) and the anterior medial prefrontal cortex (amPFC). Adapted from Andrews-Hanna et al., 2010.*

ii. In early AD

One may have noticed that the primary hubs supporting the DMN are those that are initially affected by early amyloid deposition, the mPFC and the PMC. Even preceding the development of amyloid-PET, it was noted through FTG-PET that the mPFC and PMC showed reduced

resting state glucose metabolism and hypo-activity in asymptomatic carriers of APOE ε4 (Reiman et al., 1996, 2004). It is valid hypothesis then that the default mode network may be particularly sensitive in preclinical AD.

The strength/integrity of a functional network, or between functional networks or subsystems, can be defined by how strongly their regions co-activate together in time. Evaluations of asymptomatic individuals consistently link early AD biomarkers (increased amyloid-PET, decreased $A\beta_{42}$ and increased ptau181 in CSF) to reduced connectivity of the DMN to the PMC (Hedden et al., 2009; Sheline et al., 2010; Wang et al., 2013a). Jones and colleagues showed that in asymptomatic carriers of APOE ε4, the DMN subsystem involving primarily the PMC, the pDMN, exhibits decreased within-system functional connectivity before the appearance of plaques (Jones et al., 2016). This study was coupled to a cross-sectional analysis, which revealed that with high amyloid burden and severe hippocampal atrophy in early AD and late MCI, the connectivity of this PMC subsystem continues to decrease substantially, but at the same time the connectivity between the pDMN and other DMN subsystems actually increases. In AD stages with absent or low amyloid burden (in CN, SCD or early MCI) the relationship between amyloid load and connectivity strength are not so clear. This may indicate that this intermediate point of AD pathology, generally between pre-plaque and post-plaque stages, accompanies a dynamic mixture of connectivity profiles (from PMC *hypo*-connectivity to global DMN *hyper*-connectivity) that cannot be easily characterized. The dynamic nature of DMN perturbation in prodromal AD poses a problem for evaluations of aMCI, which should encompass a mixture of AD proteopathic states. A review of resting state functional connectivity assessments in aMCI across 22 studies shows that DMN connectivity to the PMC is consistently affected but the direction of the perturbation (hyper vs. hypo connectivity) varies. However, they do find a trend towards PMC-DMN hyper-connectivity (Badhwar et al., 2017), suggesting a greater representation of late stage MCI, with an already high level of amyloid burden and hippocampal atrophy. In SCD, a similar inconsistency is found; some studies report increased connectivity within the DMN (Wang et al., 2013b), or between the PMC the rest of the DMN (Verfaillie et al.; 2018). In contrast, others have reported decreased connectivity between the pDMN and other DMN subsystems (Dillen et al., 2017; Yasuno et al., 2015).

iii. Graph theoretical analyses

To obtain a more informed understanding of information flow in a functional network, we may evaluate its topology using graph theory. With graph theory, a functional network can be represented as *graph* with *nodes* (regions) that are inter-connected by *edges* (connections), which exist if two regions significantly co-activate together in time (***Figure 9A***). Efficient networks are those that are able to effectively transfer information between any two regions. This is commonly measured as a network's *global efficiency*. Network global efficiency is shown to scale with cognitive performance, and is heavily dependent on the presence of hub regions (such as the PMC in the DMN) to act as information relays (Toussaint et al., 2014). Hub regions are most commonly and simply detected as the regions with the greatest number of connections. The number of connections a region has is measured as its *degree*, and regions with higher degree can be said to have higher hub strength (***Figure 9B***). Finally, one can also evaluate to what extent the network segregates into separate clusters or communities/modules (***Figure 9C***), as measured through the *clustering coefficient* or *modularity*. The supported theory of neural networks posits that healthy cognition should require small world topology, combining local segregation between anatomically and functionally similar regions (e.g. for the precise processing of specific modalities), and good integration between distant regions (e.g. for the association of different modalities), as facilitated by hubs.

Small world parameters have been evaluated in resting state networks related to aMCI. Drzezga and colleagues directly linked decreased resting state hub strength of the PCC/RSC to increased amyloid burden in the cognitively healthy (Drzezga et al., 2011). Studies evaluating aMCI have often reported a decrease in network efficiency and segregation in resting state networks (Wang et al., 2013c; Bai et al., 2013; Lin et al., 2017). In theory, network efficiency is a more informed measure of information transfer than global network functional connectivity strength, because it takes into account the importance of hubs for relaying information between otherwise disconnected regions. Indeed, Wang and colleagues showed that reduced resting state network efficiency along with decreased strength of parietal and temporal hubs, but not reduced global network strength, correlated with recognition memory decline (but not other cognitive measures) in aMCI (Wang et al., 2013c). Still, graph theory does not remove the inconsistency of evaluating the DMN in aMCI. For example, another study of SCD reported increased temporal

lobe hub strength in aMCI (Liang et al., 2020), which has a detrimental effect on MMSE performance. The inconsistency of these findings reflects the heterogeneity of SCD and MCI in relation to their diagnosis, underlying pathologies, or AD proteopathic staging.

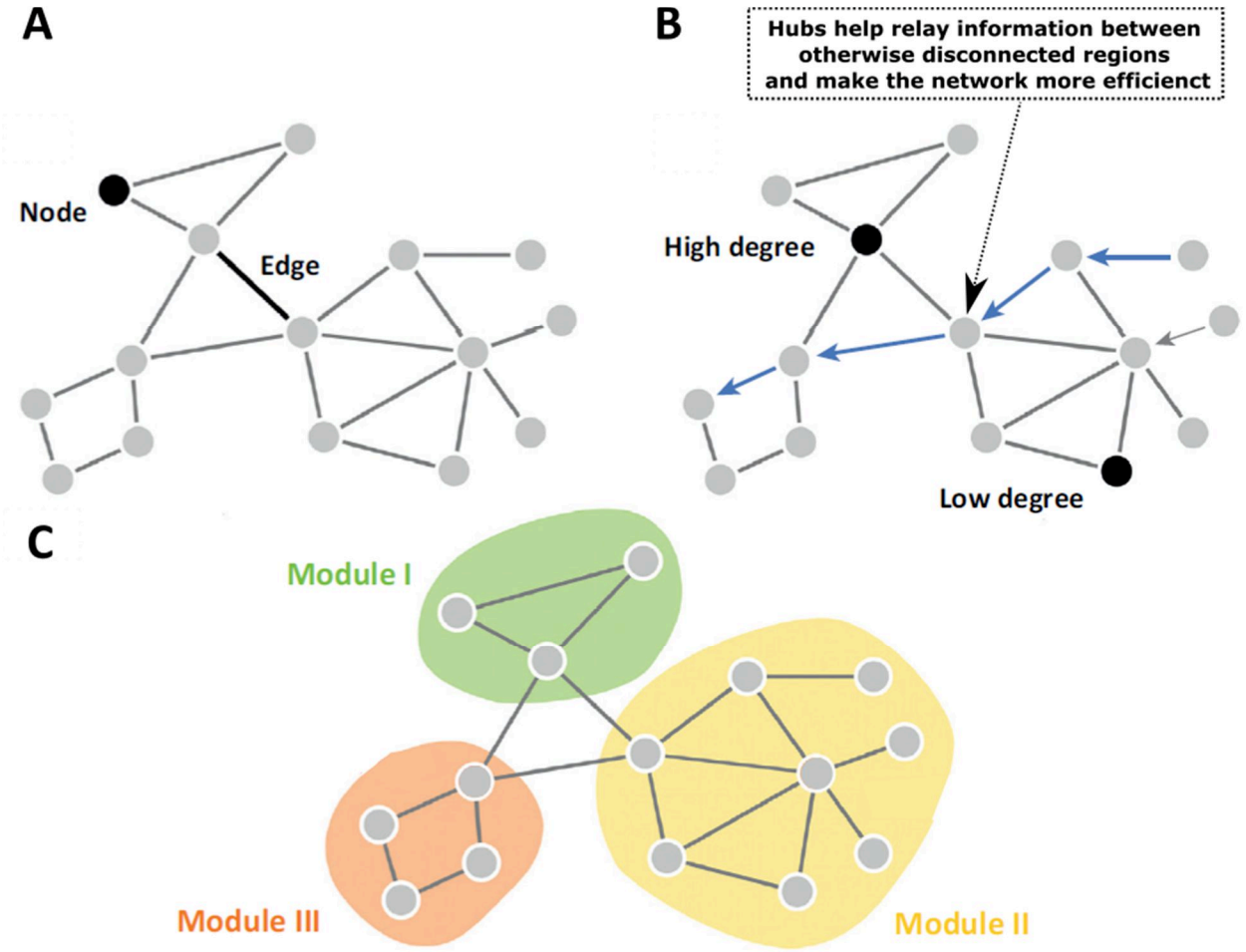

Figure 9. *Graph theoretical basic properties. (A) Nodes represent regions and edges represent significant functional connections. (B) Hub regions typically have a high degree (number of connections), and help relay information between peripheral regions. A network with a greater number of hub regions should be more efficient at integrating distant regions. (C) Networks can often be further split into communities (modules) of regions that are more strongly connected with each other than the rest of the network. Adapted from van den Heuvel and Sporns, 2013.*

7. Subtle memory loss in preclinical AD

I have so far highlighted the problematic heterogeneity of SCD and MCI in representing preclinical and prodromal AD stages, respectively. The standardized methods for evaluating cognitive decline (MMSE) are good for evaluating general onsets of dementia/aMCI but are too broad and should expectedly capture a mixture of underlying pathologies and AD proteomic stages. Moreover, these mostly represent the prodromal stage of AD that already presents potentially irreversible deficits such as aberrant connectivity perturbations or hippocampal atrophy. To address this, we need more specific behavioral evaluations to target regionally specific perturbations related to the earliest preclinical stages. The most consistent functional perturbations associated with preclinical AD are hyper-activity of the MTL, and hypo-activity/hypo-connectivity of the PMC-DMN. Cognitive tasks that require precise functioning of these brain areas are more likely to reveal preclinical AD specific decline. Such tasks include sensitive recognition or spatial memory paradigms that require the precise functioning within and between MTL regions, or associative memory paradigms that require association cortices of the PMC and mPFC. In the following section, I will discuss potential tasks for evaluating subtle cognitive deficits in preclinical AD.

A. Mnemonic Discrimination (Pattern Separation)

In the mnemonic fine discrimination task, also called the behavioral pattern separation task, one has to detect very slight changes in the identity or location of objects. This type of memory is considered to depend on the pattern separation computational process needed to separate overlapping patterns, which can represent overlapping representations of memory, or overlapping cell assemblies. This memory task is shown to heavily tax the hippocampus, especially the DG and CA3, in fMRI evaluation of the task (Bakker et al., 2008). In mice, the DG was shown to have varying cell assemblies and the CA3 varying activity profiles in reaction to very slight changes in environment, depicting a clear physiological mechanism of pattern separation (Leutgeb et al., 2007). A similar phenomenon was later verified in humans using high resolution fMRI (Berron et al., 2016). Pattern separation tasks also involve communication between all regions of the MTL, though separate interactions are involved if object or spatial

modalities are tested. Object pattern separation involves communication between the hippocampus and the anterior MTL (LEC, PRC), whereas the spatial requires preferentially hippocampal communication with the posterior MTL (MEC, POC) (Reagh and Yassa; 2014; Leal and Yassa, 2018).

The precise nature of the pattern separation computational process should make it susceptible to the hippocampal hyper-activity present in the preclinical stages of AD. This hyper-activity could theoretically blur the lines between the "patterns" physiologically represented in the hippocampus. Pattern separation is shown to be affected in aMCI (Yassa et al., 2010) and even in cognitively healthy elderly (Reagh et al., 2016). In cognitively healthy elderly, the intra-MTL communication is largely reduced, and accompanied by hypo-activity in the LEC and hyper-activity in the DG and CA3. Asymptomatic APOE ε4 carriers also showed significant deficits in pattern separation with hippocampal hyper-activity (Sinha et al., 2018). Another study found that object pattern separation was accompanied by increases in CSF pTau, and accompanying hyper-activity in the MTL (Berron et al., 2019). Interestingly however, deficits in spatial pattern separation were accompanied by decreases in CSF $A\beta_{42}$ (Wesnes et al., 2014), but not increases in CSF ptau. Deficits in spatial pattern separation also correlate with increased amyloid-PET burden (Webb et al., 2020). This dichotomy between the object and spatial pattern separation in relation to tau and amyloid respectively may reflect the separate impact of these proteiniopathies on different brain regions. In line with this hypothesis, object specific separation loss was associated to tau-PET in temporal lobe, but scene/context based pattern separation loss was associated to amyloid-PET in the PMC (Maass et al., 2019). This reflects the PMC's important role in associating features for scene construction related to episodic memory, a quality that is evaluated in the next memory task.

B. Associative Memory

We previously highlighted the medial temporal subsystem of the DMN involving the mPFC, the PMC and the MTL, and its involvement in episodic memory recollection (Andrews–Hanna et al., 2014; Bellana et al., 2016). When looking at this network, it is useful to consider the cognitive operations that constitute episodic thought. At the core of episodic thought is the set of features defining a unique event, which includes the people, objects, places, and other contextual details

associated with the event. These event features must be embedded within a coherent relational framework that represents the associations among them, producing a unified personal experience. As discussed before, and in relation to pattern separation, the medial temporal lobe regions are required for providing precise detail to object (HIP/LEC/PRC) or spatial (HIP/MEC/POC) features. In contrast, the binding of features and the multi-dimensionality of event representations appear to be dependent on the complex interactions between the MTL, the parietal lobe and mPFC, where the PMC, especially the RSC, acts as an important anatomical and functional hub (***Figure 10***) (Andrews-Hanna et al., 2010; Rugg and Vilberg, 2013; Kaboodvand et al., 2018; Cooper and Ritchey, 2019; Ritchey and Cooper; 2020).

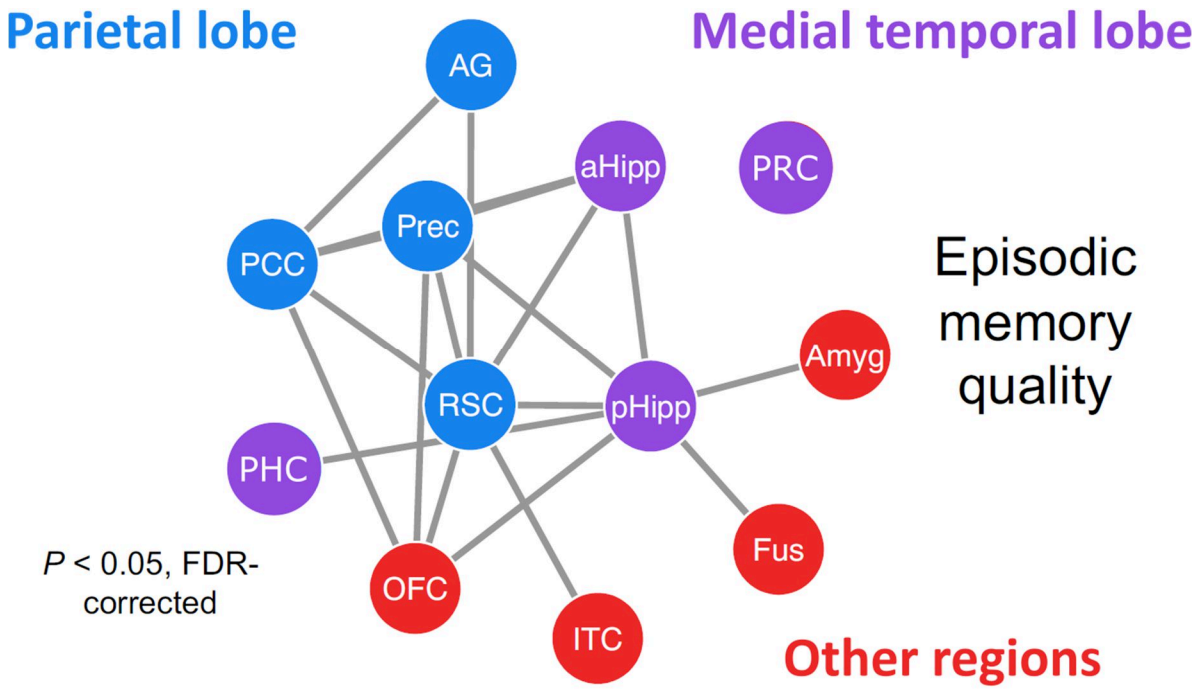

Figure 10. *Interregional functional connections whose connectivity strength positively tracks the quality (total amount and precision of detail) of episodic retrieval. This was determined through a series of independent seed-to-target psychophysiological interaction (PPI) analyses in an analysis by Cooper and Ritchey, 2019. AG: angular gyrus; prec: precuneus; PCC: posterior cingulate cortex; RSC: retrosplenial cortex; pHipp: posterior hippocampus; aHipp: anterior hippocampus; PRC: perirhinal cortex; PHC: parahippocampal cortex; fus: fusiform gyrus; ITC: inferior temporal cortex; OFC: orbital frontal cortex; amyg: amygdala. Adapted from Ritchey and Cooper, 2020.*

Thus, paradigms that tax the ability to associate independent features may be susceptible to the reduced connectivity of the PMC, as seen in resting state evaluations of preclinical AD. This specific susceptibility of associative memory was robustly identified by one study that performed a neuropsychological battery testing of associative and non-associative memory, attention, language, visuospatial and executive functions. They showed that asymptomatic carriers of FAD mutations performed significantly worse than healthy controls in the feature binding condition only (Parra et al., 2010).

One common and simple associative memory task is the "face-cued word recall", where a person has to remember an association of a face to a random word (like "pencil" or "beach"). This task is shown to be heavily reliant on PMC-MTL communication, as transcranial stimulation of the parietal lobe increases functional connectivity of these regions which correlates improved task performance (Wang et al., 2014, Warren et al., 2019). A similar task to the "face-cued word recall" task is the "face-name" task, where the person must associate a face to a name rather than any random word. This task is favored because it is less sensitive to increases in cognitive reserve. This is because a name comes with fewer a priori connections than a random word (***pencil*** - wood, school, writing vs. ***Tanya*** - who?) that may help strengthen remembering in those who have a greater semantic knowledge. This theory is supported by research that showed it easier to remember "Baker" when it is presented as a profession than when it is presented as a proper name (James et al., 2008). Indeed decreased performance in the face-name task correlated with increased amyloid load in the PMC, and frontal cortex in cognitively healthy individuals (Rentz et al., 2011) and correlated specifically with increased PCC amyloid in individuals with SCD (Sanabria et al., 2018). In both cases, the face-name task performed better than a face-occupation (associating a face to an occupation, e.g."teacher"), and better than word list learning paradigms (tasks semantic verbal memory and are more reliant on prefrontal and lateral temporal communication) at predicting amyloid load. These studies highlight associative memory loss as an effective cognitive marker for preclinical AD.

8. Pre-aggregate effects of AD soluble proteins

Thus far I have described functional and behavioral markers of preclinical-AD that associate with early biomarkers according to PET or CSF. However even these biomarkers represent a relatively late stage of preclinical AD, appearing after decades of preceding soluble protein form based pathologies. Research in rodents has shown that soluble protein forms preceding aggregate formation impact cognitive processing and have an even more detrimental effect on brain physiology. In the following section, I will highlight the advances made in the understanding of the physiological effects of soluble amyloid and tau pathologies which are most probably involved in the initial alteration of brain functions during preclinical stages of AD. This knowledge was mainly obtained in cell cultures and in mouse models of AD using genetic manipulations to express human mutated forms of APP and/or tau proteins. Mouse models of AD will be presented more in depth after this section.

A. Amyloid precursor protein and non-amyloidogenic processing

i. The amyloid precursor protein (APP)

The *App* gene coding for APP is on the human chromosome 21 and the mouse chromosome 16. Full length APP is a transmembrane glycoprotein with its amino terminus within the lumen/extracellular space and its carboxyl terminus within the cytosol (Haass et al., 2012). As shown in ***Figure 11***, this large protein has the characteristics of a cell surface receptor that interacts with extracellular matrix proteins (Beher et al., 1996; Cáceres and Brandan, 1997) and cell surface proteins, including Reelin (Hoe et al. 2009), Notch2 (Chen et al. 2006), and Netrin (Lourenco et al. 2009). This makes APP an important component of cell migration and synapse formation, and thus essential for CNS development (Löffler and Huber, 1992; Young-Pearse et al., 2007; Tyan et al., 2012). The APP carboxyl terminus interacts with a variety of intracellular proteins, with functional implications including signal transduction, axonal transport and cytoskeletal formation (van der Kant and Galdstein, 2015). APP is part of the APP family of proteins, which also includes APP-like proteins 1 and 2 (APLP1 and APLP2) (Shariati and De Strooper, 2013). Despite the apparent functional importance of APP, APP KO mice are viable

and fertile thanks to the compensatory effects of APLP1 and APLP2 (Zheng and Koo, 2006). Indeed, KO mice for both APP, APLP1 and APLP2 die early after birth (Heber et al., 2000).

Extracellular

name	location
Alcadein	Cell Surface
F-spondin	Cell Surface
Reelin	Cell Surface
LRP1	Cell Surface
sorL1/LR11	Cell Surface
Nogo-66 receptor	Cell Surface
Notch2	Cell Surface
Netrin	Cell Surface
collagen	Extracellular Matrix
laminin	Extracellular Matrix
heparin sulfate proteoglycans	Extracellular Matrix
pancortin glycoproteins	Extracellular Matrix

Intracellular

name	function
Pin1	APP C-terminal conformation
Go-protein	neuronal migration
GRB2	signal transduction
ShcA	signal transduction
FE65	neuronal migration
DAB1	neuronal migration
X11/Mint	sorting
Jip1b and Jip2	transport
AP-4 complex	sorting
Kinesin	transport
Dynein	transport
Myosin	transport
Wnt/PCP recep.	signal transduction

Figure 11. *APP interactomics showing its main interaction with extracellular and intracellular proteins. Adapted from van der Kant and Galdstein., 2015.*

ii. APP metabolism

APP has multiple sites for cleavage by different secretases, including α, β, γ, and η secretases. APP thus has many downstream metabolites, with vast and varying impacts to physiology. There are three main metabolic pathways which occur in tandem under normal conditions, the non-amyloidogenic α-secretase and η-secretase pathways and the amyloidogenic β-secretase pathway (***Figure 12***). In the following section, I will discuss their impacts on cellular function.

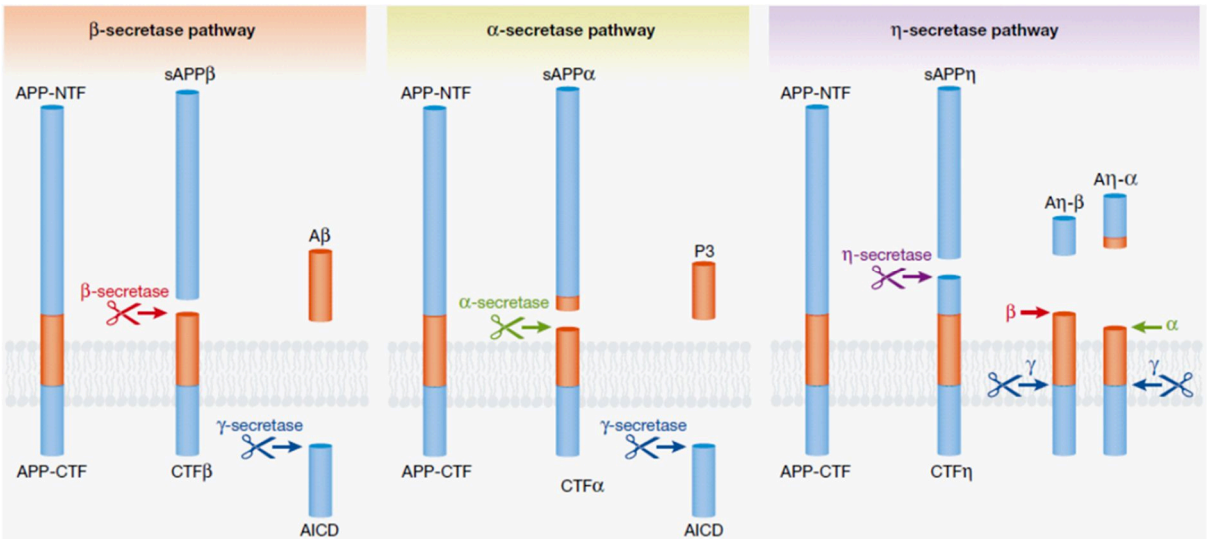

Figure 12. *Metabolic pathways of APP. Full length APP is processed through three main naturally occurring pathways which depend on the interplay of four identified secretases: the α-secretase, the β-secretase, the γ-secretase and/or the η-secretase. There is one amyloidogenic pathway producing Aβ peptides and two non-amyloidogenic pathways excluding the production of Aβ peptides. Reproduced from Sasaguri et al., 2017.*

iii. Non-amyloidogenic cleavage of APP

Cleavage of APP by α-secretase leads to the release of an extracellular soluble APPα fragment (sAPPα), and a transmembrane fragment called the α-terminal carboxy fragment (α-CTF). The α-CTF is then cleaved in its transmembrane domain by the γ-secretase complex consisting mainly of four proteins: presenilin 1 or 2 (PS1 or PS2) which carries the catalytic activity, APH-1 (Anterior Pharynx-Defective 1) necessary for proteolytic activity, nicastrin which intervenes in intracellular trafficking and stabilizes the complex, and PEN-2 (Presenilin Enhancer 2) also necessary for the stabilization of the enzyme complex (Wolfe, 2011). Cleavage of α-CTF by γ-secretase gives rise to the extracellular p3 peptide and an APP intracellular domain (AICD).

Given that it interacts with several extracellular proteins in common with full-length APP, sAPPα has similar important role in CNS development: it acts as a growth factor (Herzog et al., 2004), and regulates cell proliferation (Guillot-Sestier et al., 2012), neurite growth and synaptogenesis (Milward et al., 1992; Mattson, 1997; Gakhar-Koppole et al., 2008). sAPPα is also involved in synaptic signaling as it facilitates long-term potentiation (LTP) (Ishida et al., 1997) and regulates synaptic activity (Furukawa et al., 1996) through combined interactions with NMDA (Taylor et al., 2008), $GABA_BR1a$ (Rice et al., 2019) and K^+ synaptic receptors

(Furukawa et al., 1996). With this role in synaptic plasticity, it is no surprise that sAPPα also contributes strongly to learning and memory (Meziane et al, 1998; Xiong et al., 2017; Taylor et al., 2008). It is suggested that sAPPα may play a central role as part of an activity-dependent negative-feedback loop to suppress synaptic release and maintain proper homeostatic control of neural circuits (Mattson et al., 1993), a possible mechanism for the neuroprotective effect of sAPPα against excitotoxicity. Indeed, the neuroprotective property of sAPPα is found against many forms of cellular stress including proteasomal stress (Copanaki et al., 2010), oxidative stress (Goodman and Mattson, 1994) and ischemic injury (Smith-Swintosky et al., 1994). In APP deficient mice, application of sAPPα was sufficient to rescue synaptic defects and reduced spine density (Weyer et al., 2007), long-term potentiation (LTP; a form of synaptic plasticity contributing to learning and memory) (Hick et al., 2015), and spatial learning (Ring et al., 2007), indicating that the extracellular domain of APP drives many of these functions. Interestingly, sAPPα has been shown to directly combat AD pathology. It inhibits the activity of cyclin-dependent protein kinase 5 (Cdk5), which is partly responsible for the abnormal hyperphosphorylation of tau (Han et al., 2005). It is also a direct inhibitor of β-secretase, and thus regulates the production of Aβ (Peters-Libeu et al., 2015). In a transgenic mouse model of AD, inhibition of the activity of sAPPα promotes the amyloidogenic cleavage of APP, further suggesting that inadequate levels of sAPPα may increase susceptibility to amyloid pathology (Obregon et al., 2012).

Besides the Aβ peptide, the p3 peptide also exhibits some neurotoxic effects. It is a major constituent of diffuse amyloid deposits present in the brain of AD patients (Gowing et al., 1994). In cell culture, p3 induces apoptosis, although this neurotoxicity is less than that of the peptide Aβ (Wei et al., 2002). In addition, this peptide promotes inflammatory responses in several cell types by producing pro-inflammatory cytokines and chemokines (Szczepanik et al., 2001). However, since the p3 peptide does not contain the entire sequence of Aβ and its oligomers are unstable, it is generally considered as a relatively harmless fragment (Dulin et al., 2008). The physiological roles of the α-CTF are poorly known to date.

The AICD intracellular fragment is known to be involved in nuclear signaling (Gao and Pimplikar, 2001), transcriptional regulation (Hebert et al., 2006), cell death (Nakayama et al., 2008, Ohkawara et al., 2011), and DNA repair (Minopoli et al., 2007). The protein is quickly

degraded (Pardossi-Piquard and Checler, 2012), though its stability can be enhanced through protein interactions (Kimberly et al., 2001) or through site dependent phosphorylation (Farris et al., 2003). Site dependent phosphorylation also affects its interaction with other signaling proteins and downstream function (Tamayev et al., 2009).

Recently a new η-secretase proteolytic pathway was discovered that cleaves APP into η-CTF and sAPPη. Cleavage of η-CTF by α-secretase forms a short extracellular Aη-α fragment which reduces long-term potentiation and attenuates neuronal activity (Willem et al., 2015).

B. Amyloidopathy and peripheral effects

i. Amyloidogenic cleavage of APP

The amyloidogenic proteolytic pathway is initiated through cleavage by the β-secretase, the most common being the beta-site APP cleaving enzyme 1 (BACE1). This leads to formation of the sAPPβ and the β-CTF proteins. Cleavage of β-CTF by γ-secretase releases AICD (identical to the non-amyloidogenic product) and Aβ.

The soluble fragment sAPPβ shares the same sequence as the fragment sAPPα, except it does not contain last 16 amino acids of the C-terminal (Chasseigneaux and Allinquant, 2012). Interestingly, many of the neuroprotective and synaptoplastic properties of sAPPα are not conserved in sAPPβ, suggesting a particular importance to these 16 absent residues. For example, sAPPβ is 50 to 100 times less powerful than sAPPα in combatting excitotoxicity and Aβ induced toxicity (Furukawa et al., 1996; Barger and Harmon, 1997). In addition, at similar doses to sAPPα it is not neuroprotective against proteasomal stress (Copanaki et al., 2010) and does not facilitate hippocampal LTP (Taylor et al., 2008, Hick et al., 2015). This functional divergence of sAPPα and sAPPβ suggests a possible loss of function of sAPPα which could play a role in AD deficits. In certain cases sAPPβ is even shown to be neurotoxic: sAPPβ can be cleaved to generate a cytotoxic derivative interacting with the death receptor 6 (DR6) that activates caspase 6 responsible for cell death (Nikolaev et al., 2009). On the other hand, sAPPβ does support developmental processes, such as neurite growth (Chasseigneaux et al., 2011) and cellular proliferation (Freude et al., 2011).

The β-CTF, the direct precursor to Aβ, is considered to be neurotoxic and may initiate early deficits in AD. In transgenic mice, intraneuronal staining of β-CTF occurs before accumulation of Aβ, and coincides with decreases in LTP (Lauritzen et al., 2012) and increased inflammatory responses (Lauritzen et al., 2016). β-CTF affects calcium homeostasis by forming pores and ion channels in the cell membrane (Fraser et al., 1997), increasing excitotoxicity (Kim et al., 2000). It also migrates towards the cell nucleus influence the transcription of genes such as glycogen synthase kinase-3β (GSK-3β) which promotes the production of DNFs (Lauritzen et al., 2016). In addition, it is involved in mitochondrial alteration that results in the release of cytochrome C and activation of caspase 3 responsible for apoptosis (Chang and Suh, 2005). Early *in vitro* studies showed that β-CTF application was generally more neurotoxic than Aβ in terms of free radical generation (Rah et al., 2001), and triggering inflammation (Chong et al., 2001). The toxicity of β-CTF has implications when considering therapies targeted at γ-secretase. Treatment with γ-secretase inhibitors induces β-CTF accumulation along with synaptic and memory deficits in mice (Mitani et al., 2012; Tamayev and D'Adamio, 2012), and accelerates cognitive decline in humans (Doody et al., 2013). The many deleterious effects of β-CTF are summarized in ***Figure 13***.

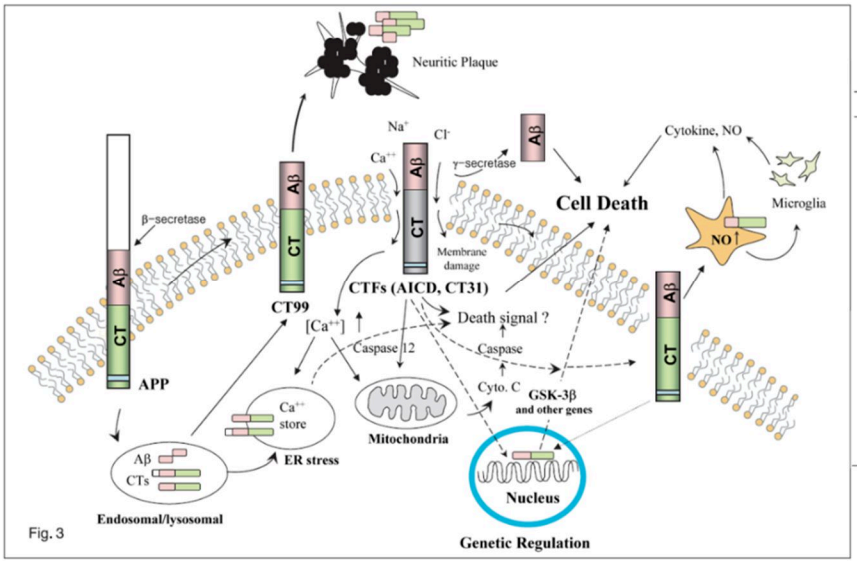

Table 1. Summary of various effects of Aβ and CTF

	Aβ	CTF
Neurotoxicity		
Cultured cells	+	+10
in vivo i.c.v.	+	++++
Neuritic plaques of transgenic mice	+++	+++
Channel effect		
Xenopus oocytes	–	+++
Purkinje cells	–	+++
Lipid bilayer	+	++
Intracellular Ca^{2+}	+	+++
Free radical generation		
NO generation	+	+++
MAPK signaling	+	+++
NF-κB	+	+++
Nuclear translocation	–	+++
Inflammatory cytokines & chemokines	+	+++
Gliosis & astrocytosis	+	+++

Figure 13. *Deleterious effects of the β-CTF fragment. β-CTF can lead to endoplasmic reticulum (ER) stress, increased neuritic plaques, altered mitochondrial function, cell death and microglia activation through nitic oxide (NO) production. Reproduced from Chang and Suh, 2005.*

ii. Amyloid hypothesis

Before moving on to the next section devoted to the Aβ peptide, it seems necessary to evoke the amyloid hypothesis (or so-called amyloid cascade hypothesis) that dominated the research on AD for more over 25 years. It was first proposed by Hardy and Allsop (1991) and clearly named as so by Hardy and Higgins (1992). This hypothesis posits that Aβ deposition plays a central role in the pathogenesis and is responsible of memory deficits in AD. The discovery of the FAD mutation strongly supported this hypothesis because their main effect was to increase dramatically the production of Aβ. It was further reinforced by the fact that Down's syndrome characterised by trisomy 21 (associated to three exemplars of the *App* gene) also showed Aβ deposition (Kolata, 1985). The hypothesis was slightly adapted later (Selkoe and Hardy, 2016), integrating the role of soluble forms of Aβ when it became quite evident that amyloid plaques were probably not the most toxic form of Aβ (see below). In addition, other products of the amyloidogenic pathways such as C-terminal fragments also showed neurotoxic properties, facilitates pathogenesis in sporadic AD and FAD, and could even induced their own deleterious effects of memory (Svedružić et al, 2015; Hamm et al., 2017). Moreover, neuronal loss and amyloid deposition seem to be unrelated (Chételat, 2013). These findings and many others call into question the amyloid hypothesis, sometimes into favor of an even older cholinergic hypothesis (Daly et al., 2020).

iii. Aβ monomers

The Aβ peptide is an extracellular cleavage product of the amyloid precursor protein (APP). Aβ is produced inside and, to a lesser extent, outside the CNS. It is present in CSF and blood (Seubert et al., 1993). Normally, Aβ is found at picomolar concentrations. As the concentration levels of the peptide increase to above 0.1 micromolar, it will aggregate to form soluble oligomers (Novo et al., 2018), then fibrils and finally amyloid plaques. Post-translational modifications of Aβ, such as phosphorylation and nitritation, can also increase aggregation (Kumar et al., 2011; Kummer et al., 2011).

At physiologically normal picomolar concentrations, Aβ positively modulates synaptic plasticity and memory by facilitating LTP (Puzzo et al., 2008), and increasing synaptic vesicle recycling (Lazerevic et al., 2017). Inhibition of Aβ production induces deficits in memory acquisition and consolidation which can be rescued through application of picomolar levels of exogenous Aβ

(Garcia-Osta and Alberini, 2009). These neuroplastic effects are largely mediated through the strong interaction of Aβ with the α7 nicotinic acetylcholine receptor (α7nAChR) receptor (Wang et al., 2000, Puzzo et al., 2011), which provides one explanation to the particular susceptibility of the cholinergic system in AD. Aβ also positively regulates neuronal activity, where even small 2-fold increases in physiological concentrations positively regulate presynaptic release probability and induce hyper-activity in hippocampal slices (Abramov et al., 2009). At higher nanomolar concentrations, Aβ inhibits LTP through increased internalization or desensitization of postsynaptic glutamate receptors (Walsh et al, 2002), and perturbation of presynaptic vesicle trafficking (Park et al., 2013). However, at nanomolar concentrations Aβ begins to aggregate (Novo et al., 2018), making these deleterious effects likely oligomer- rather than monomer-dependent (***Figure 14***).

The size of Aβ can range from 39–43 residues long, but it is most present in two major forms in the brain: $A\beta_{40}$ and $A\beta_{42}$. These 2 differentiating amino acids are found on the "gamma side" of Aβ, and the resulting form depends largely on γ-secretase activity (DeStrooper et al., 2012). In non-pathological basal conditions, 90% are of the $A\beta_{40}$ type, and 10% of the $A\beta_{42}$ type. $A\beta_{42}$ more readily aggregates, likely due to its increased hydrophobicity (Burdick et al., 1992; Pike et al., 1995; Selkoe, 2001), and is the predominant component of amyloid plaques in AD (Cummings et al., 1996). In fact, $A\beta_{40}$ is capable of inhibiting the oligomerization of $A\beta_{42}$ (Murray et al., 2009) and can reduce amyloid deposition (Kim et al., 2007). It follows that the total $A\beta_{42}/A\beta_{40}$ ratio in CSF or plasma is a reliable clinical predictor of amyloid deposition (Fandos et al., 2017; Doecke et al., 2020). In cell cultures, specifically $A\beta_{40}$ is shown to contribute to neuronal development; even at high micromolar levels it promotes neurogenesis of neuronal progenitor cells (Chen and Dong, 2009) and interacts with components of the extracellular matrix to promote neurite proliferation (Koo et al., 1993).

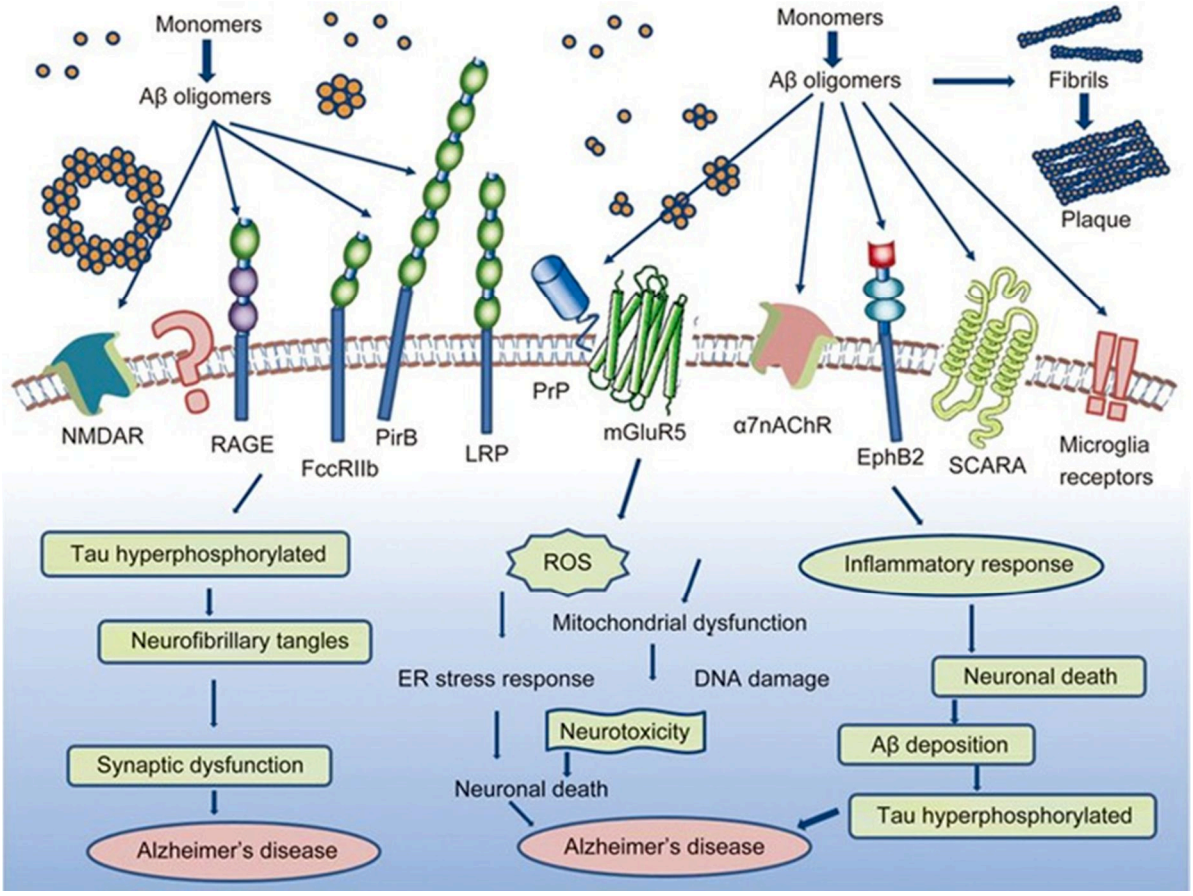

Figure 14. *The many cell surface interactors with Aβ oligomers. These activate downstream pathways to generate reactive oxygen species, hyperphosphorylate Tau protein, cause inflammatory responses, leading to increased neurotoxicity and potentially cell death. Reproduced from Chen et al., 2017.*

iv. Aβ oligomers

Soluble oligomeric forms of Aβ are generally considered to be its most toxic state (Walsh and Selkoe, 2007; Crews and Masliah, 2010; Lublin and Gandy, 2010). The severity of the cognitive deficits encountered in AD correlates with the level of oligomers in the brain, and not amyloid load (Lue et al., 1999; McLean et al., 1999). Aβ oligomers are shown to interact with a variety of cell surface receptors (Chen et al., 2017), with downstream impacts on cell death (Mark et al., 1995), neuroinflammation (Perini et al., 2002), oxidative stress (White et al., 2005), and vascular stress (Zlokovic et al., 2005) (***Figure 14***). On brain slice preparations, the dimeric and trimeric forms of $A\beta_{42}$ are synaptotoxic (Walsh et al., 2002; Klyubin et al., 2008). Treatment with dimers

of $A\beta_{42}$ inhibits LTP, increases long-term depression (LTD) and reduces the density of dendritic spines in rodent hippocampal neurons (Shankar et al., 2008). Oligomers of $A\beta_{42}$ can increase the permeability of the plasma membrane, by altering ion channels and by forming pores (Demuro et al., 2005, 2011). In terms of neuroinflammation and oxidative stress, oligomers, but not fibrillar Abeta, induce high levels of iNOS, NO, and TNF-alpha (White et al., 2005). Moreover, oligomeric dependent increases in oxidative stress lead to capillary constriction, resulting in reduced blood flow and neuronal damage (Nortley et al., 2019). With all these damaging effects, Aβ oligomers are currently considered as one of the most detrimental amyloid-related species.

v. Aβ clearance

In sporadic forms of AD, the development of amyloid pathology is thought to be related to Aβ accumulation in the brain. The increase in amyloid load could be related to a decrease in the mechanisms of Aβ degradation and clearance. Although we focused on brain Aβ up to now, there is also a circulating pool of Aβ produced by peripheral tissues. Its concentration in the brain is about six times higher than in the plasma (Bates et al, 2009). This suggests that there is an active regulation of brain Aβ concentration at the level of the blood brain barrier. For example, the Receptor for Advanced Glycation End products (RAGE) is involved in Aβ influx whereas the low-density Lipoprotein Receptor-related Protein-1 (LRP-1) is involved in Aβ efflux (Bates et al, 2009). Thus, RAGE could participate to the development of amyloid pathology through a vicious circle because the presence of Aβ increases RAGE's activity which induces oxidative stress, cell death, microglial activation and increased Aβ production as well as other AD-like pathological events such as tau hyperphosphorylation and LTP impairment (Lue et al., 2001). LRP-1 may have a dual involvement in AD pathology as it is more efficient in removing $A\beta_{40}$ than $A\beta_{42}$ through the blood brain barrier (Shibata et al, 2000; Monro et al., 2002). Among many other Aβ-binding proteins, Apolipoproteins E and J also participate in the clearance of Aβ, especially the most toxic form $A\beta_{42}$. Among the three APOE alleles, the AD risk factor APOE ε4 was shown to decrease the clearance of $A\beta_{42}$. Recent genome wide association studies have identified additional risk loci that involve lipid processes similar to APOE ε4. Within the brain, several proteases participate to the enzymatic clearance of Aβ such as neprilysin (NEP) and insulin-degrading enzyme (IDE) (Yoon et al, 2012). As an exemple, deletion of NEP gene and brain infusion of NEP inhibitors increase brain contents in Aβ and affect memory performance in

mouse models of AD (Klein et al., 2018; Huang et al., 2006). Moreover, introduction of a human NEP gene in such models improve spatial memory performance and reduces amyloid load, oxidative stress and neuroinflammation (Marr et al., 2004; El-Amouri et al., 2008). The mechanisms of Aβ clearance and degradation have stimulated much interest with the hope of finding a new avenue for the treatment of AD.

C. Tauopathy

i. Tau

Tau is coded by the microtubule-associated protein tau gene, named *MAPT*, which is located on chromosome 17 in humans and chromosome 11 in mice. The tau protein contains an acidic N-terminal domain, a basic mid-domain rich in proline (P), and repetitive regions on its C-terminal side (***Figure 15***). Tau can bind microtubules through these repetitive regions, making them part of the microtubule associated protein (MAP) family. Tau proteins promote microtubule assembly through tubulin polymerization (Cleveland et al., 1977), and are involved in neurite growth (Kosik and McConlogue, 1994), establishment of cell polarity (Drewes et al., 1998) and axonal growth in adult neurogenesis (Llorens-Martin et al., 2012), especially in the hippocampus (Hong et al., 2010). The size of the N-terminal domain of MAPs regulates the spacing between microtubules. For tau, this domain is relatively small and allows for tight binding of microtubules (Felgner et al., 1997). Transgenic mice that do not express tau do not show major deficits, possibly due to compensation by other MAPs (Harada et al., 1994).

In the human CNS, there are 6 isoforms of tau, depending on the number of inserts at the N-terminal part (either 0N, 1N, or 2N), and the number of repetitive regions (R) at the C-terminal part (either 3R, or 4R) (***Figure 15***). 4R isoforms are more efficient at promoting microtubule assembly (Goedert et al., 1990), and have faster turnover rates (Sato et al., 2018). The 2N isoforms may trigger toxic mechanisms that impair axonal sorting and facilitate neuronal dysfunction and death (Liu et al., 2016).

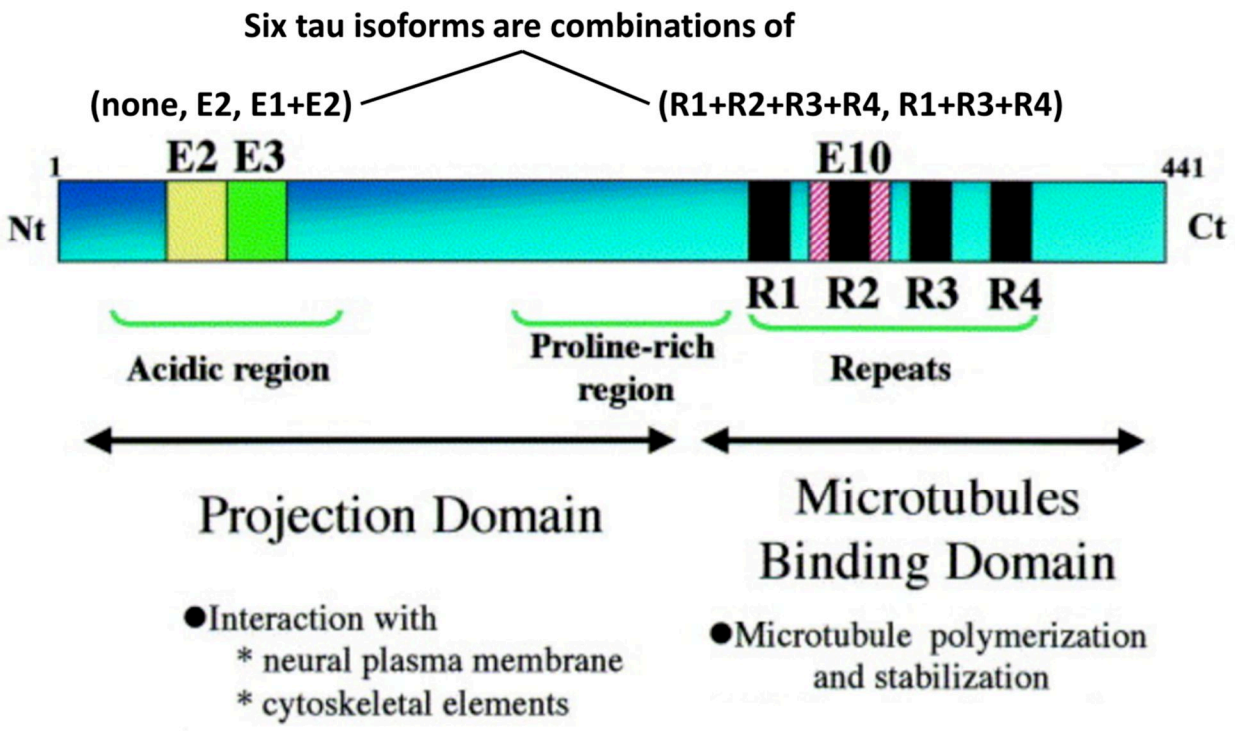

Figure 15. *Subdomains of the tau protein. The N-terminal projection domain plays a role in signal transduction and the C-terminal microtubule binding domain is needed for microtubule polymerization and stabilization. Adapted from Buée et al.,2000.*

ii. Hyperphosphorylation of tau

Under normal condition, tau undergoes a regulated balance of phosphorylation by kinases (such as glycogen synthase kinase-3β: GSK3β) and de-phosphorylation by phosphatases (Maccioni, 2011). In pathological conditions, this balance is perturbed and tau becomes hyperphosphorylated (ptau). Overexpression of tau can lead to neurodegeneration, behavioral abnormalities and synaptic dysfunction before NFT formation (Wittmann et al., 2001; Yoshiyama et al., 2007; Cowan et al., 2010), indicating the hyperphosphorylated soluble forms of tau have a direct effect on the observed dysfunction. Tau contains 85 potential serine (S), threonine (T), and tyrosine (Y) phosphorylation sites. Many of the phosphorylated residues are found in the proline-rich domain, flanking the microtubule-binding domain. Phosphorylation is thus often found to have a disruptive effect on microtubule binding (Mandelkow et al., 1995a; Trojanowski and Lee, 1995; Delacourte and Buée, 1997). $A\beta_{42}$ first induces phosphorylation of tau at few specific sites: Ser396, Ser404, Thr231, and Ser235 (Montdragon-Rodriguez et al.,

2012). The Ser396/Ser404 and Thr231 sites sites were both reported as some of the earliest phosphorylation events during AD development. $A\beta_{42}$ induced phosphorylation of tau is mediated by activation of GSK3β which leads to caspase cleavage, followed by increased aggregation of tau (Cho and Johnson, 2004). Restoration of basal activity of GSK-3β reduces abnormal tau hyperphosphorylation, reactive gliosis and neuronal death, and restores spatial memory deficits in mice (Engel et al., 2006). Therefore, GSK3β seems to play a key role in the $A\beta_{42}$ related neurotoxicity (Mondragón-Rodríguez et al., 2020). This is also in agreement with early studies showing that elevated Aβ increases the severity of tau pathology (Gotz et al., 2001, Lewis et al., 2001). Abnormal activation of the kinase cdk5 is associated with neurodegeneration of hippocampal cells (Alvarez et al., 2001). Because phosphorylation of tau by cdk5 potentiates the phosphorylation of tau by GSK-3β, this could represent a vicious cycle involved in the build-up of tau pathology (Sengupta et al., 1997).

iii. Tau oligomers

When hyperphosphorylated tau aggregates, it first forms soluble oligomers. Onset of clinical symptoms in AD correlate with elevated levels of tau oligomer (Maeda et al., 2006; Lasagna-Reeves et al., 2012), and sporadic formation of tau oligomers potentiate neuronal damage in traumatic brain injury (Gerson et al., 2016). When tau oligomers, rather than tau monomers or fibrils, are injected into the brain of wild-type mice, cognitive, synaptic, and mitochondrial abnormalities follow (Lasagna-Reeves et al., 2011; Castillo-Carranza et al., 2014b).

Tau oligomers inhibit anterograde fast axonal transport (Kanaan et al., 2011, Patterson et al., 2011), induce mitochondrial damage (Lasagna-Reeves et al., 2011), and reduce membrane integrity (Flach et al ., 2012). Extracellular tau monomers and oligomers, but not PHFs, act on M1 and M2 muscarinic receptors to increase intracellular calcium levels and induce cell death in neurons (Gómez-Ramos et al., 2006; Gómez-Ramos et al., 2008). Tau oligomers also show the capacity to seed the spreading of tau pathology in the brains of mice expressing human tau (Gerson et al., 2016). This leads me to expose in the next paragraph an emerging hypothesis for the spreading of AD neuropathology in the brain.

D. The prion-like hypothesis for neurodegenerative disease

The concept of the "prion paradigm" suggests that most neurodegenerative diseases are so-called proteinopathies. Such diseases are characterized by the aggregation of proteins seem to arise from misfolded proteins that corrupt and impose their anomalous structure to naive proteins which favors aggregation and self propagation of misfolded species (Jucker and Walker, 2013). Such a Prion-like mechanism has been proposed for amyloid deposits, NFTs and α-synuclein inclusion in Parkinson's disease and Lewy body dementia. This proposition was supported by the induction of amyloid deposition by injecting Aβ aggregates or AD brain extracts to rodents expressing human Aβ (Kane et al., 2000; Meyer-Luehmann et al., 2006). Moreover, deposits can eventually appear in axonally coupled regions as time passes (Hamaguchi et al., 2012). This phenomenon could explain the progressive spreading-like appearance of brain lesions which seem to propagate through connected regions. Such a mechanism has also been proposed for tau pathology (Mohamed et al, 2013), and supported by similar experiences using brain extracts injections or human tau expression in the brains of rodents (Clavaguera et al., 2009; Liu et al., 2017). Interestingly, tau pathology induced by pre-aggregated Aβ injections was shown to spread to functionally connected brain areas which suggests a mechanism for Aβ-induced propagation of tau pathology (Vasconcelos et al., 2016). The prion-like hypothesis has gained credibility over years of researches and the concept of self-propagation is now considered as a key process in the progression of AD neuropathology.

9. Animal Models of AD

A. Before Transgenic mice

In the early 1980's, the first mouse models of AD were developed. Before gene editing techniques were commonplace, rodent models were produced pharmacologically through the modulation of neurotranmitter systems or the stereotaxic lesioning of brain structures. The initial rodent models of AD were based primarily on the cholinergic hypothesis, and were developed through the pharmacological reduction of cholinergic system activity (Bartus et al. 1982). These would play an integral role in the advancement of cholinometics based drugs, which are still in use today for treating symptomatic features of AD. These initial AD models would prove invaluable in elucidating the underpinnings of the symptomatic changes seen in AD. Nonetheless, further breakthroughs were needed to untangle the origin of the disease and understand the impact of its amyloid and tau proteinopathies.

In the meantime, in 1982 it was shown for the first time that through the pronuclear injection of modified DNA into fertilized zygotes one could develop mice to specifically express proteins of interest (Palmiter et al., 1982, Gurumurthy and Lloyd, 2019). This would be the first instance of the transgenic mouse, a technological innovation that would revolutionize animal research.

B. Transgenic Mouse Models

i. Single transgenic APP

Over a decade later, the first transgenic mouse models for AD would come to fruition. This initial set of transgenic mice overexpressed humanized APP with single or multiple FAD mutation(s) found in early onset AD. The two FAD mutations most commonly used are the Indiana mutation (V717F) and the Swedish double mutation (KM670/671NL). The Indiana mutation is found at the γ cleavage site of APP and leads to an elevated $A\beta_{42}/A\beta_{40}$ ratio (Suzuki et al., 1994; Tamaoka et al., 1994). The Swedish mutation is found at the β cleavage site and leads to an overall increased production of Aβ (Citron et al., 1992).

The first transgenic model of AD is the PDAPP mouse, which expresses humanized APP with the Indiana (V717F) mutation. It presents amyloid deposition as soon as 6 months in the

neocortex and hippocampus, along with associated gliosis (Games et al., 1995). There are two early transgenic models that express humanized APP with the Swedish double mutation (KM670/671NL), but under different promoters and with different backgrounds. These are the APP23 (under the Thy-1.2 promoter on the C57BL/6 background) and the Tg2576 (under the hamster prion promoter on the B6; SJL mixed background) lines. APP23 mice display a similar neuropathological timeline to PDAPP mice, developing neocortical and hippocampal amyloid deposits as soon as 6 months (Sturchler-Pierrat et al., 1997; Dodart et al., 2000). Tg2576 mice, the most commonly used AD mouse model, display a less severe phenotype with amyloid deposition at only around 9 months preceded by gliosis at 8 months (Hsiao et al., 1996). This late onset of AD pathology and the absence of some critical hallmarks of AD such as extensive neuronal loss and absences of NFTs led to the creation of new mouse models cumulating different FAD mutations.

ii. Multiple transgenic APP

Multiple FAD mutations were combined to obtain a more aggressive phenotype. The TgCRND8 model combines the expression of both the Swedish and the Indiana mutations on a humanized APP. Understandably, this leads to an accelerated neuropathology, with amyloid deposits appearing as soon as 3 months in the subiculum, amygdala and frontal cortex, and is accompanied by reactive gliosis (Chishti et al. 2001). These mice also show hyperphosphorylation of tau and the formation of tau oligomers in the hippocampus and the neocortex, but no NFTs (Belluci et al., 2007).

FAD mutations found in the *PSEN1* or *PSEN2* genes affect γ-secretase activity and increase the $A\beta_{42}/A\beta_{40}$ ratio. When expressed alone in mice they increase levels of $A\beta_{42}$ but do not lead to amyloid deposition and the phenotype is quite subtle (Duff et al., 1996; Borchelt et al. 1996). The $APP_{SWE}/PS1_{dE9}$ mouse model combines the Swedish mutation on APP with mutated PSEN1 and presents amyloid pathology at 6 months of age (Jankowsky et al., 2004). Among the early onset models, this mouse line is now at least as popular as the Tg2576 model. In the 5xFAD mouse model many different FAD mutations are combined, with 3 separate mutations on APP and 2 mutations on PSEN1. It displays a very aggressive neuropathology with amyloid deposits appearing in the subiculum and cortex as early as 2 months (Oakley et al., 2006).

iii. Transgenic Tau

Unlike in the human condition, mouse models only expressing FAD mutations do not develop NFTs, although they do sometimes display increased levels of ptau. This is likely due to the limited expression of only the three 4R isoforms of tau in mouse rather than a complete set of six isoforms (three 3R and three 4R) found in humans. In order to induce NFT formation, new transgenic mice expressing mutated forms of humanized tau were developed. The most prevalent mutation of tau used to induce NFTs is the tau_{P301L} mutation found in frontal temporal lobe dementia, but not in AD. Tau P301L mice expressing this mutation display tangle formation anatomically dissimilar to the Braak stages seen in AD, with NFTs first appearing in the hindbrain and spinal cord at 8 months instead of the entorhinal region, preceded by gliosis at 7 months (Lewis et al., 2000). Several years later, the Thy-Tau22 mouse model was engineered to express human 4-repeat tau mutated at sites G272V and P301S under a Thy1.2-promoter with no motor dysfunction (Schindowski et al, 2005). It shows hyperphosphorylation at AD-relevant epitopes (including Ser396, Ser202/Thr205 and Thr212/Ser214) and NFTs at an early stage around 3-6 months, as well as a decrease in synaptic transmission and neurodegeneration in the hippocampus around 10 months when Thy-Tau22 mice show spatial memory deficits in the Morris water maze task. Interestingly, Thy-Tau22 mice show an important loss of medial septum cholinergic neurons, an AD characteristic rarely observed in mouse models of AD (Belarbi et al., 2011).

The hTau transgenic mouse, which overexpresses all 6 isoforms of non-mutated tau without the presence of mouse endogenous tau, is much less common but nonetheless interesting. Since it contains no tau mutations, it represents a closer neuropathological profile to human AD. hTau mice display CP13 positive ptau in the soma of hippocampal pyramidal cells at 3 months followed by NFTs at 8 months, similar to Braak stage development (Andorfer et al., 2003). Still, this contrasts with the human condition where NFTs do not normally form without tau mutations or accompanying amyloid pathology. This can be largely explained by tau overexpression and by the imbalanced ratio of tau isoforms, with protein levels of the common species 3R isoforms significantly exceeding that of the human 4R isoforms in hTau mice. When the 3R to 4R ratio is rectified using in-vivo trans-splicing of the transgene, the number of pyramidal cells displaying NFTs is significantly reduced (Espindola et al., 2018). Moreover, hTau mice that co-express

endogenous mouse tau, and thus overexpress vast amounts of 4R tau and inverse the 3R/4R ratio, do not form NFTs (Duff et al., 2000).

iv. Combining Transgenic APP and Tau

In order to produce a more complete model of AD, with concurrent amyloid and tau pathologies, mouse lines were developed to overexpress humanized APP with FAD mutations along with mutated humanized tau. The 3xTg mouse model is one of the most commonly used mouse models of AD, and combines the Swedish mutation of APP, the $PS1_{M146V}$ and tau_{P301L} mutations. 3xTg mice display amyloid deposits at 6 months in the frontal cortex and tangle formation more similar to Braak stage development, with hyperphosphorylated tau aggregates appearing as soon as 6 months in the hippocampus (Oddo et al., 2004) followed by NFTs at 12 months (Oddo et al., 2003) .

10. Evaluating memory in rodents

In the following section, I will discuss a variety of memory forms as evaluated in rodents. Each will be discussed in two parts. The first part will overview the structural networks required for the task. The second will report deficits seen in AD mice and how they may relate to pathophysiological changes previously mentioned. Most of the memory tasks presented are derived from the spontaneous object exploration paradigm. These tasks are depicted in ***Figure 16***, which will be referenced throughout this section.

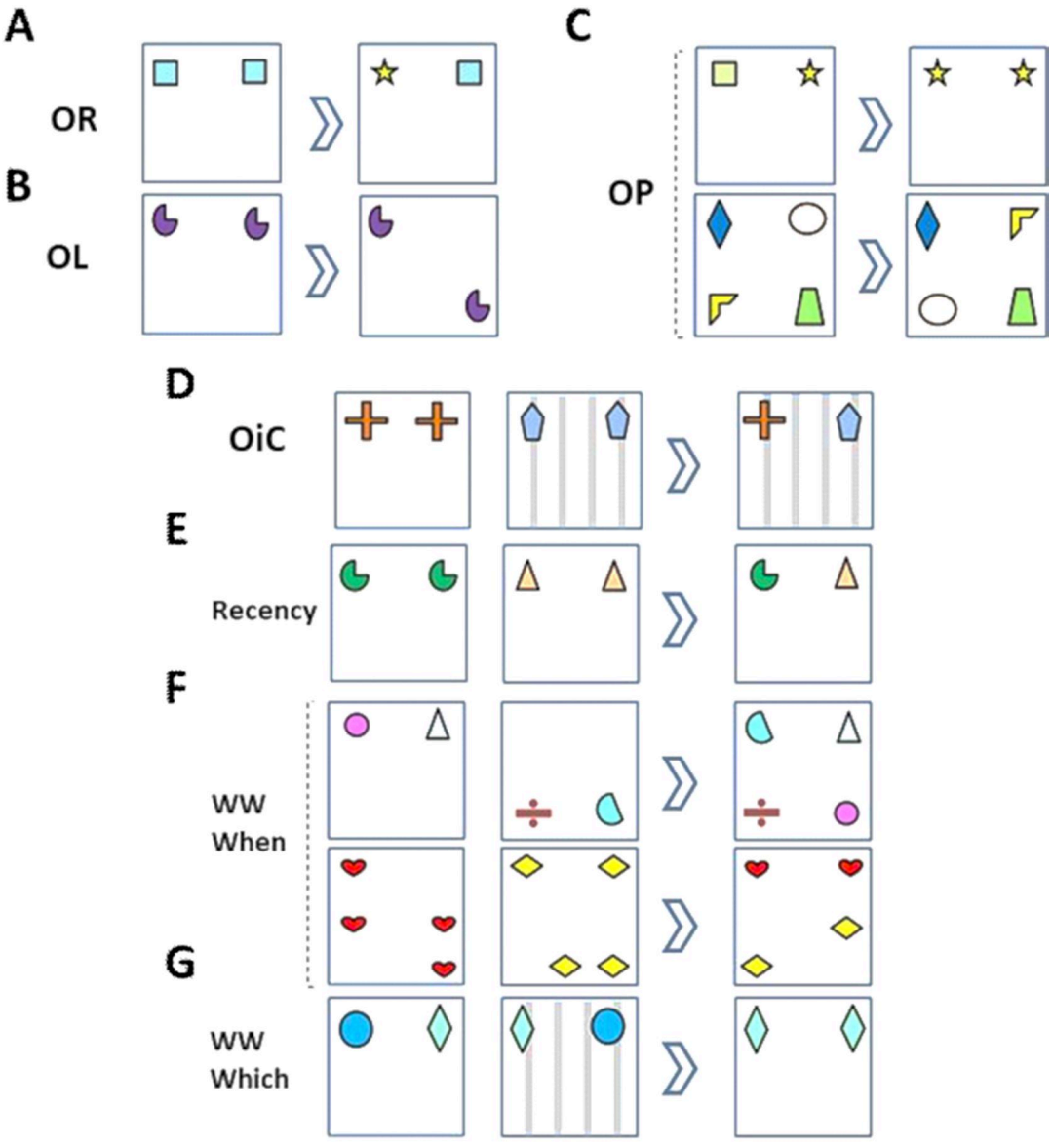

Figure 16. *Spontaneous object exploration tasks. OR : object recognition, OL : object location, OP: object-in-place, OiC: object-in-context, WWWhen: what where when, WWWhich : what where which. Adapted from Chantal Mathis.*

A. Recognition Memory

i. Background and anatomy

Mice are innately curious. The spontaneous object recognition paradigm, first described by Ennaceur and Delacour in 1988, makes use of this trait by using increases in novelty exploration as a measure of memory retention. It consists first of an acquisition phase, where a mouse is placed in an open field to explore a set of two identical objects. This is followed by the inter-trial-interval (ITI) phase, where the mouse is left for a defined amount of time in its home cage away from the aforementioned objects and open field. Finally, testing ends with the retention phase where the mouse is shown a new set of objects, one copy of the familiar object and a new object (***Figure 16A***). The experimenter may then evaluate novel object recognition as an increase in exploration of the novel object as compared to the unchanged object. Short- and long-term recognition memory can be evaluated by varying the length of the ITI from several minutes to hours or even days.

The most consistent region implicated with OR at any length of ITI is the PRC. The PRC, especially its most caudal part, was shown to play a key role in OR performance for ITIs of 5 min to 24 h using various experimental approaches (Ennaceur et al. 1996; Wan et al. 1999; Norman and Eacott, 2004; Winters et al. 2004; Barker et al. 2007; Albasser at al, 2010). It must be noted that the contribution of PRC may also be influenced by object complexity given its involvement in the processing of perceptual properties of objects (Norman and Eacott, 2005; Bartko et al. 2007).

Many studies have reported spared OR on a wide range of retention delays in hippocampal lesioned rats and mice (Mumby et al. 2002; Save et al. 1992; Winters et al. 2004; Oliveira et al. 2010; Barker and Warburton, 2011; Sannino et al. 2012). In some cases, the involvement of the hippocampus was shown to depend on lesion size, access to spatial cues (i.e., transparent walls), mutliple trials for arena habituation or sampling, or a large number of objects (Broadbent et al. 2004; Ainge et al. 2006; Oliveira et al. 2010; Dees and Kesner, 2013; Sannino et al. 2012). Modulating hippocampal activity by local infusion of pharmacological treatments could either improve or reduce long-term OR memory (Hammond et al. 2004; Oliveira et al. 2010; Melichercik et al. 2012; Cohen et al. 2013). Therefore, one might propose that the contribution

of hippocampus may depend on whether performance efficiency in a given task requires the establishment and recall of specific spatial representations or complex item binding, and/or the formation of an enduring memory trace. This contribution to long-term OR memory is known to depend crucially on the interplay between the PFC and the hippocampus (Preston and Eichenbaum, 2013).

The mPFC and the RSC appear to be important for sustaining long-term consolidation of OR memory (Warburton and Brown, 2015), as disrupting either is shown to specifically perturb OR performance after a 24-h ITI (Akirav and Maroun, 2006, de Landeta et al., 2020). The involvement of the LEC and the MEC does not seem to be essential for OR memory (Wilson et al., 2013a; Rodo et al., 2017)

ii. In AD mouse models

Single transgenic APP-Tg (PDAPP, APP23 and Tg2576) and $APP_{SWE}/PS1_{dE9}$ mice exhibit initial deficits in OR at around 6 months with ITIs ranging from 1h to 48h (Dodart et al., 1999; Huang et al., 2006; Mouri et al., 2007; Frye and Walf., 2008). Multiple transgenic APP-Tg mice (TgCRND8, 5xFAD) display an accelerated progression with initial deficits appearing around 4 months with shorter ITIs from 5 minutes to 24 hours (Tohda et al., 2012; Richter et al., 2008). When multiple ITIs are tested in the same study, performances on longer retention delays tend to be affected before those on shorter delays (Kubota et al., 2016; Sierksma et al., 2014). In other words, long-term memory seems highly sensitive to AD pathology.

Induction of tauopathy appears to have a less severe impact on recognition memory. hTau mice display deficits with a 24hour ITI at 12 months but not 4 months (Polydoro et al., 2009), but are cognitively normal when the 3R/4R imbalance is rectified (Espindola et al., 2018). Tau P301L mice display no OR deficits even at 17 months (Kent et al., 2017). In fact, 9 week old Tau P301L mice present improved OR performance with a 3.5h ITI, which was attributed to improved long-term potentiation in the hippocampus precluding tau hyper-phosphorylation (Boekhoorn et al., 2006). The 3xTg-AD mice are impaired in the OR task from the age of 6 months onwards with ITIs ranging from 15 min to 24 h.

The interpretation of OR deficits in App-Tg mice is quite complicated by the fact that one of the key region involved in encoding object identity is the PRC which is nearly never explored for

neuropathology or neuronal activity. When long-term OR performance are selectively affected, then it is possible that functional disturbance in the hippocampus could have been involved in this deficit given its role in OR consolidation.

B. Spatial Memory

i. Background and anatomy

The spontaneous object exploration paradigm can be adjusted to evaluate spatial recognition memory, by displacing an object instead of changing it you get an object location (OL) task (***Figure 16B***). This task is highly dependent on the hippocampus as almost all spatial memory tasks. Thus, in this section I will relate findings from OL to those found using the most common techniques for evaluating spatial navigation learning and memory. The Morris Water Maze, developed by Richard Morris (Morris, 1981), is very popular. It usually involves a 1-meter diameter circular tub filled with non-transparent water, with a hidden platform located under the water somewhere in the maze. When a mouse or rat is placed in the water it is naturally inclined to search for the platform due to its aversion to water (mice) or cold water (rats). Through several days of swimming and searching, and trial and error, the animal learns the location of the platform. Memory retention can be tested after training by giving the animal a probe trial, where the platform is removed and the experimenter records how much time the animal spends in the correct quadrant of the maze where the platform was previously located. The probe trial can be given just after or from several hours to several weeks after training, to test short-term, long-term and even remote memory, respectively. The task is robust and reliable, but induces high levels of stress in mice their natural tendency to avoid water as opposed to rats. For this reason, the task is more readily used in rats, who are natural swimmers.

In its classical form, the animal is placed in different locations of the maze to start each training session, meaning that it has to process and orient itself according to the arrangement of distal spatial cues for spatial navigation. This type of spatial processing is termed allocentric and is dependent on the hippocampus. In contrast, egocentric processing requires the animal to find it way in relation to its own position, irrespective of spatial cues. For goal directed tasks, this is connected to procedural memory where the mouse can find its goal by always taking the same

path ("turn left then turn right"). Egocentric spatial navigation can be acquired by always placing the animal in the same location for each trial so that they learn to take an identical path to the goal (always "turn left then turn right").

The Y-maze spontaneous alternation task is another spatial memory task closer to the OL task because it relies on the animal's innate curiosity and inclination to visit areas (arms) that has not been recently visited. This task can require both allocentric (if walls are transparent and distal spatial cues are present) and egocentric spatial processing (if walls are opaque and no spatial cues available). More importantly, this task relies on working memory which relies on the capacity of the animal to retain and use information gathered during the trial (i.e., which arm was most recently visited).

The hippocampus is the most consistent region to be implicated in allocentric spatial navigation, working memory and detection of spatial novelty. Interfering with hippocampal function through a variety of methods leads to severe learning deficits in spatial navigation task, in the MWM for example (Morris et al., 1982; Morris et al., 1990; McDonald and White, 1994). Performance is also affected in a working memory tasks such as the Y-maze spontaneous alternation task. Moreover, there is also a general agreement on the critical involvement of hippocampus in spatial object recognition task, OL, on a wide range of ITIs (Save et al. 1992; Wan et al. 1999; Mumby et al. 2002; Assini et al. 2009; Oliveira et al. 2010; Burke et al. 2011). The importance of the hippocampus in spatial learning and memory is unsurprising, given the abundance of place cells in the CA1 and CA3, where each place cell will fire preferentially at a specific location in the open field (Manns and Eichenbaum, 2009).

The MEC is another putative region, given the presence of grid cells, whose firing pattern generates virtual maps of the surroundings that resemble grids of repeating triangles (Weber and Sprekeler, 2018). The MEC-hippocampus network is critical for spatial navigation as grid cells are involved in processing self-motion information and maintaining stable hippocampal place-cell mapping (Jacob et al, 2020). Lesioning the MEC leads to stark spatial learning and retention deficits in the MWM close to those resulting from a hippocampal lesion (Van Cauter et al., 2013; Hales et al., 2014). Interestingly, these two studies found contradicting results with parallel OL experiments. Hales and colleagues found no deficit, while Van Cauter and colleagues did. Thus, spatial navigation and spatial novelty detection may not necessarily rely on the same entorhinal-

hippocampal subnetworks. In a complementary work of the Save group (Rodo et al., 2017) showed that the involvement of the MEC in OL memory increased with the complexity of the environment (object number and diversity). Interestingly, the same relationship was true for the involvement of the LEC in the object recognition task. The MEC and the LEC are not connected exactly to the same hippocampal subregions and each of their layers have preferential interactions with different hippocampal areas. This strongly suggests that the entorhinal-hippocampal system is able to process a wide variety of information, each one being conveyed by one of these specific routes.

Concerning the LEC and the MEC, electrophysiological and lesion data suggest that there is a graded involvement of both structures in object and spatial information, with preferential object-related processing in the lateral region and contextual/spatial processing in the medial region (Deshmukh and Knierim, 2011; Hunsaker et al. 2013). Thus, lateral entorhinal cortex seems to integrate some spatial information to the purely nonspatial representations elaborated in the PRC (Deshmukh et al. 2012; Tsao et al. 2013). On the other hand, the POC (parahippocampal cortex in primates) is considered as part of the spatial/contextual information processing pathway (Aminoff et al., 2013, Norman and Eacott, 2005).

The RSC, primarily the dysgranular part, contains a variety of spatial orientation cells, including place cells similar to those of the hippocampus, and local landmark dependent head direction cells (Mao et al., 2017, Jacob et al., 2017). Lesioning the RSC leads to deficits in allocentric spatial processing, particularly when visual cues are needed for orientation (Mitchell et al., 2018), as tested with the MWM (Sutherland et al., 1988; Whishaw et al., 2001). The RSC is not needed for egocentric processing (Vann and Aggleton, 2002) and unlike the hippocampus, is not needed for intact Y-maze performance (Nelson et al., 2015). The anterior thalamic nucleus exhibits strong connections to the RSC, the mPFC and the subiculum, and also contains place, head direction, and border cells. Lesioning this region leads to deficits in a multitude tasks related to allocentric spatial memory processing, such as in the MWM and the radial arm maze (Aggleton and Nelson, 2015).

The dorsal striatum is shown to be essential for egocentric but not allocentric spatial memory (Cook and Kesner, 1988). Integrity of other medial temporal lobe regions, such as the PRC or the

LEC, does not seem to be necessary for spatial learning in the MWM or OL (Barker et al. 2007, Wilson et al., 2013a; Van Cauter et al., 2013).

ii. In AD mouse models

A longitudinal analysis of over 250 mice revealed that Tg2576 mice have deficits in the MWM within 6-11 months (Reed et al., 2010). In multiple APP-Tg mice, MWM deficits appear sooner, by around 4 months (Chishti et al., 2001). Tau pathology also affects spatial memory as hTau mice show deficits at 12 months but not 4 months (Polydoro et al., 2009). 3xTg-AD mice also show deficits in spatial memory at 4 months (Billings et al., 2005). Interestingly, results are similar in the OL task, with deficits seen in Tg2576 and APP23 at 7-8 months (Ognibene et al., 2005; Middei et al., 2006; Yassine et al., 2013), in TgCRND8 mice at 2 months (Hamm et al., 2017), and in 5xFAD at 5 months (Park et al., 2016).

Contrarily to the PRC poorly investigated in mouse models of AD, the hippocampus has always been under the spotlight throughout the transgenic adventure. Therefore, it is well known that the hippocampus was systematically shown to be one of the first regions affected by AD-like neuropathology in all these models. Given the clear involvement of the hippocampus in spatial navigation and OL tasks, deficits were clearly expected and generally obtained in these tasks whatever the model, at least at advanced stages of their pathology.

C. Fine mnemonic discrimination (pattern separation)

i. Background and anatomy

Fine mnemonic discrimination tasks used in humans has been translated to the spontaneous object exploration paradigm in mice (Bolz et al., 2015; Cès et al., 2018). In the fine discrimination object recognition task, small changes in object identity can be controlled through the use of lego objects, where the only change is pattern of the legos used to construct the changed object (only the pattern of the blocks changes, not the shape or the composition). In the fine discrimination object location task, small changes in object location are induced by displacing the object a smaller distance (20 cm vs 50 cm). Both tasks could detect deficits in old but not young mice, and in the absence of deficits from the traditional OR and OL tasks (Cès et

al., 2018). This deficit could be rescued by D-serine treatment, which increased neurogenesis in the dentate gyrus, illustrating a possible link of an age dependent reduction in dentate gyrus neurogenesis to disrupted pattern separation. These results confirm the hypothesis of an involvement of DG neurogenesis in pattern separation function (Bolz et al., 2015; Clelland et al., 2009).

ii. In AD mouse models

Very surprisingly, despite many reports on fine discrimination deficits in MCI and AD patients, not much has been done in AD mouse models. There is an elegant study from Zhu and colleagues (2017) showing spatial fine discrimination deficits in Tg2576 mice. This deficit was related to degeneration of the cholinergic input to the DG and associated reduction in local neurogenesis (Zhu et al., 2017). Within our team, we showed that this deficit appears at the age of 4 month in this mouse line, in the absence of deficits in other recognition tasks (manuscript in preparation).

D. Associative Memory

i. Background and anatomy

Several variants of the object exploration paradigm were designed to evaluate different forms of associative memory. The first variant, often called the object-in-place (OP) task (***Figure 16C***), tests the ability of the animal to detect the intrusion of a *familiar* object in the *position* previously occupied by a different *familiar* object (Dix and Aggleton, 1999). In other words, this task probes the specific association of object identity and place. Intact PRC, mPFC, RSC, anterior thalamic nucleus and hippocampus as well as the dual interactions PRC-hippocampus, PRC-mPFC are necessary to perform the 4-object version of the OP task (Nelson and Vann., 2014; Parron and Save., 2004; Barker et al., 2007; Barker and Warburton, 2015; DeVito and Eichenbaum, 2010). Only a few studies have evaluated the simple two-object version of the task, and have shown the involvement of the LEC and the LEC-mPFC pathway up to now (Wilson et al., 2013a; Chao et al., 2016). The network underlying novelty detection in the OP task may vary with the number of object and/or access to an allocentric (versus egocentric) spatial frame. Indeed, “allocentric” 2-object OP tasks seemed to rely mainly on the LEC and the hippocampus,

but not PRC and POC (Eacott and Norman, 2004; Langston and Wood, 2010; Wilson et al., 2013a)

The object-in-context (OiC) task was designed to test the ability of the animal to detect, which *familiar* object has never been presented in a *specific, familiar context* (Dix and Aggleton, 1999). The integrity of POC and its interaction with the PRC are mandatory in sustaining context-guided object recognition performance in the OiC task (*Figure 16D*) (Norman and Eacott, 2005; Heimer-McGinn et al., 2017). It was proposed that a spatial layout of objects was first integrated in the POC through its reciprocal connections with the PRC (Furtak et al., 2012). Downstream, an intact LEC and its interaction with mPFC are also necessary for OiC performance (Wilson et al., 2013b; Chao et al., 2016). Additionally, the LEC extends its involvement to the detection of mismatches in place to context and OP to context combinations (tasks not shown), which suggests that this structure is necessary for further integration of object locations and/or to add OP associations to the contextual layout (Wilson et al., 2013b). Note that one or the other role could be held by other(s) region(s), such as the hippocampus (Hunsaker et al., 2013; but see Langston and Wood, 2010).

While the existence of episodic memory in animals is still an open question, recognition tasks based on the object exploration paradigm are frequently considered as evaluating "episodic-like" memory in rodents. This is most probably related to the poor knowledge in the critical difference between familiarity guided recognition ("non contextual feeling that") and recollection guided recognition (contextually remembering the whole event) (see Ennaceur, 2010). In most tasks evoked above, the animal may simply detect that he is more familiar with one object than another one (OR tasks) or one position previously occupied or not (OL tasks). OP and OiC tasks are taxing associative memory binding two environmental stimuli, but successful performance does not ensure that the rodent proceeded through complete remembrance of the past event where it first encountered the objects. In other word, he might express familiarity but not necessarily remembered what happened where and when. This recollection/familiarity debate is still a main issue in the domain of recognition memory research. Thus, two tasks were designed to evaluate some form of recollection of past experience which is based on an associative memory of i) *what* happened, *where* and *when* (***Figure 16F***) (WWWhere task; Dere et al., 2005) or ii) *what* happened, *where* in *which* context (***Figure 16G***) (WWWhich; Eacott and Norman,

2004). As expected from the role of the hippocampus in context-rich memories, the ability to perform successfully WWWhen and WWWhich tasks on all three components requires an intact hippocampus, but not necessarily the integrity of other individual regions of medial temporal lobe such as the PRC or the POC (Eacott and Norman, 2004; Langston and Wood, 2010; De Vito and Eichenbaum, 2010). Similarly to the OP and OiC tasks, an intact interaction between LEC and mPFC is necessary to succeed in the WWWhen task (Chao et al., 2016). When considering the memory for temporal order separately within these tasks or in a dedicated task, it is noteworthy that the hippocampus, the PRC, the RSC and the mPFC have all been reported to play a role in detecting object recency (***Figure 16E***) (Mitchell and Laiacona, 1998; Barker et al., 2007; DeVito and Eichenbaum, 2010; Powell et al., 2017).

ii. In AD mouse models

Tg2576 mice are deeply impaired OL component of a WWWhere task from the age of 4 months (Lanté et al., 2013). This single-domain deficit may question the episodic-like nature of their deficits. $APP_{SWE}/PS1_{dE9}$ mice showed deficits in the WWWhere task at the age of 3 months, in the absence of thioflavin stained plaques (Ramos-Rodriguez et al., 2013). Another study found deficits in the 4-object version of OP task at the age of 5 months with no concurrent deficits in OR or object recency, but concurrent $A\beta_{42}$ stained plaque formation (Bonardi et al., 2016). Two-month old TgCRND8 mice also showed deficits in the allocentric 2-object version of the OP task along with deficits in the OL task but not the OR task, and in the absence of plaques (Hamm et al., 2017). Their early deficit in OP was rescued by inhibiting β- but not γ-cleavage, indicating that it was not caused by an increase in Aβ, but rather by an increase in toxic β-CTF or a decrease in neuroprotective sAPPα.

All these 2- to 3-domain associative tasks depend on the integrity of the hippocampus. Thus, as suggested for spatial memory, it is not surprising that nearly all classical models have been tested in these task and showed performance deficits. This is also in accordance with the crucial role of the hippocampus in human episodic memory. Associative memory also requires communication between the LEC and the PFC (Wilson et al., 2013a; Chao et al., 2016). This is particularly interesting as there is increasing evidence for specific and early pathological alterations in the frontal cortex and LEC in many of these mouse models (Zhuo et al., 2008; Xu et al., 2015).

11. Drawbacks of Transgenic Mouse Models

For the past 20 years, transgenic mouse models allowed us to understand the physiological impact of amyloid and tau pathologies in a more precise manner than what could have been achieved in the clinic. However, these models do come with a series of drawbacks that contribute to artificial phenotypes and limit the capacity of these models to represent the disease.

First, transgenes are overexpressed, as they are controlled through artificial promoters and often have multiple insertion sites (***Figure 17A***). Overexpression is especially critical for APP, with its many proteolytic fragments encompassing a vast array of biological functions (Muller et al., 2017), such as APP in CNS development (Nicolas et al., 2014), sAPP in cell signaling (Rice et al., 2019), AICD in transcription regulation (Konietzko et al., 2012) to name a few. Not surprisingly, several studies indicate that overproduced APP and non-Aβ APP fragments altered brain region development (Dodart et al., 2000) and may function unphysiologically within cellular processes (Willem et al., 2015; Kerridge et al., 2015; Nahn et al., 2015). This makes it difficult to determine if the origin of deficits seen in APP-Tg mice are only related to the accumulation of Aβ or augmented amyloidogenic processing.

Second, transgenic mice co-express the murine version of the transgene (***Figure 17B***), unless they are crossed with a knock-out model. Note that even in this case the endogenous promoter of the homologous gene does not control the inserted gene (e.g., *App* or *MAPT*). Co-expressed endogenous proteins may interfere with pathological processes induced by AD proteins. This is exemplified by the impact of endogenous tau co-expression in hTau mice, which completely halters tangle formation (Andorfer et al., 2003). Certain APP fragments are shown to have a beneficial effect on synaptic plasticity and cognition, including sAPPα (Meziane et al., 1998, Ishida et al., 1997) which would be deregulated by increases in β cleavage. Loss of function effects that may arise from elevated amyloidogenic cleavage may therefore be compensated for by endogenous co-expression.

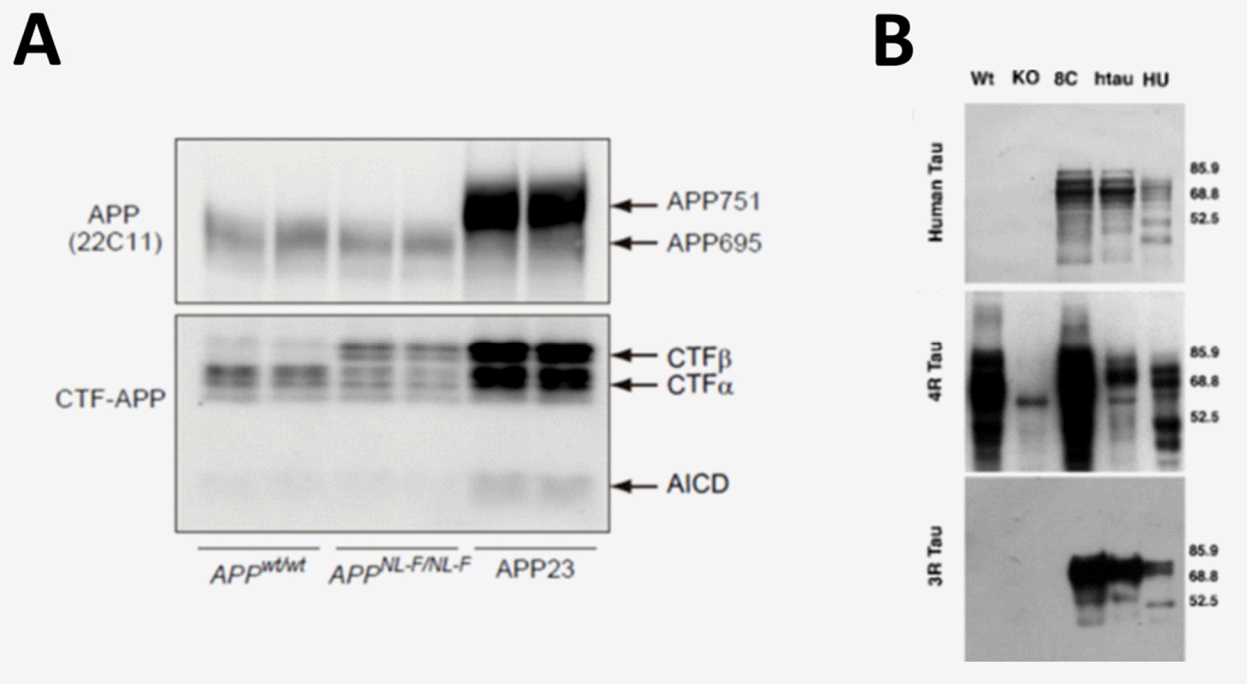

Figure 17. *Examples of protein co-expression or overexpression in transgenic mice. (A) Overexpression of APP-derived fragments in transgenic (APP23) mice compared to wt and knock-in mice. (B) Co-expression of endogenous 4R tau in WT and the transgenic model 8C (hTau without the endogenous MAPT gene knocked out). Adapted from Andorfer et al., 2003 and Saito et al., 2014.*

Third, variability arises from the random nature in which transgenes are inserted, and the use of different artificial promoters. This is underlined with a recent study that presents differences in expression level and brain regional patterning of exogenous APP among different APP-Tg mouse lines (Höfling et al., 2016). Depending on the insertion location of the transgene, endogenous loci can be severely disrupted or destroyed (Verret et al., 2012; Saito et al., 2016). Artificial promoters compete with endogenous promoters for transcription factors, and can lead to expression of the transgene in cell types that do not normally express it.

12.Knock In Mouse Models

The drawbacks seen in transgenic mice can be largely accounted for by using knock-in (KI) technology. Knocked in genes are directly inserted under the mouse locus, replacing endogenous gene expression. As a result, the inserted gene is not over-expressed nor is there co-expression of the endogenous mouse gene. Since the gene insertion is targeted, there should be no disruption of other endogenous loci. Any problems that arise from artificial promoter insertion, such erroneous cell type expression, are bypassed.

In 2014, Saito and colleagues presented a novel set of homozygous KI mice expressing humanized Aβ with FAD mutations (Saito et al., 2014). Three KI models were created: the App^{NL} with the Swedish mutation (KM670/671**NL**), the App^{NL-F} with both the Swedish and the Beyreuther/Iberian (I716**F**) mutations, and the App^{NL-G-F} with the Swedish, the Beyreuther/Iberian and the Arctic (E693**G**) mutations (***Figure 18A***). The Swedish mutation has been described previously, it affects β cleavage of APP increasing the overall production of Aβ. The Beyreuther/Iberian mutation works like the Indiana mutation, it affects γ cleavage elevating the $A\beta_{42}/A\beta_{40}$ ratio (***Figure 18B***) (Guardia-Laguarta et al., 2010). The Arctic mutation is found in the middle of the Aβ sequence and is shown to increase the Aβ aggregation rate and the quantity of large Aβ oligomers (Nilsberth et al., 2001).

The App^{NL} mice do not accumulate any amyloid deposits, but show minor microgliosis in the hippocampus (Masuda et al., 2016). App^{NL-F} mice display initial sparse hippocampal and cortical amyloid deposits at 6 months along with reactive gliosis. In App^{NL-G-F} mice amyloid deposition is accelerated, with initial deposits appearing at 2 months in the cortex. As expected none of the KI models form NFTs, but App^{NL-F} and App^{NL-G-F} mice do present elevated levels of ptau in dystrophic dendrites surrounding plaques (Saito et al., 2014).

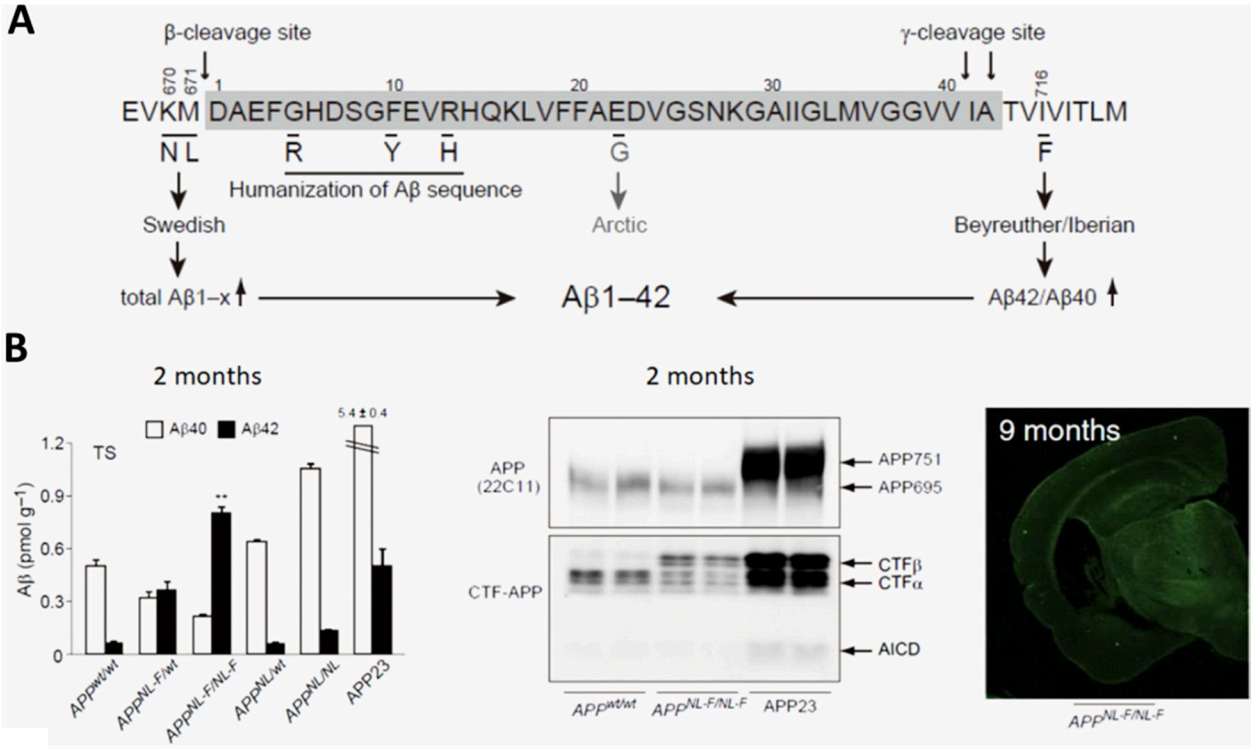

Figure 18. *Knock in mice created by Saito and colleagues (2014). (A) Humanized Aβ sequence with inserted FAD mutations. (B) Focus on the App^{NL-F} mouse. Left: compared to other models, the homozygous App^{NL-F} mouse shows an increase in $A\beta_{42}/A\beta_{40}$ as a primary neuropathological marker induced by the F mutation. Middle: It also shows an increase in β-CTF, and a decrease in α-CTF, due to the increase in β cleavage as induced by the NL mutation. Both figures highlight the lack of overexpression as compared to the transgenic APP23 mouse model. Right: Initial plaque formation is reported to start at 6 months, though even at 9 months plaques are still very sparse. Adapted from Saito et al., 2014.*

From now on, I will mainly focus on the homozygous *App*$^{NL-F}$ mouse because it was used as a parental mouse line to produce the model of my thesis work. *App*$^{NL-F}$ mice showed impaired performance at the age of 18 months in the Y-maze spontaneous alternation task, but not in the Morris water maze spatial memory task (Saito et al., 2014). In another study (Shah et al., 2018), intact spatial navigation learning was confirmed at earlier ages (3 and 7 months). Interestingly, the 3-month old mice demonstrated impaired cognitive flexibility in reversal learning which accompanied resting state hippocampal-PFC and hippocampal–RSC functional connectivity alterations. At the same time, a pharmacological study reported that *App*$^{NL-F}$ mice display deficits at 12 months, but not 9 months, in a long-term OR task (Izumi et al., 2018). This is also reminiscent of impaired dialog between the hippocampus and the PFC. These results prompted us to integrate the 24h retention delay OR task in our battery of recognition tasks.

Saito and his team also developed a novel KI mouse model for humanized *MAPT*, the gene that expresses tau (Saito et al., 2019; Hashimoto et al., 2019). The *MAPT* KI mice express all 6 isoforms of tau (***Figure 19A***), with the level of 4R mRNA approximately 70 percent that of 3R mRNA (***Figure 19B***). They do not form NFTs, but did show an accelerated propagation of pathological tau (AT8-immunoreactive) species after AD-derived tau was injected into the mouse brain. The *MAPT* KI mouse has been crossed with the App^{NL-F} and the App^{NL-G-F} mice to create the $App^{NL-F}xMAPT$ and the $App^{NL-G-F}xMAPT$ double knock in (dKI) mouse lines respectively. These dKI mice do not show any overt changes from the original single KI mice. Neither dKI displays NFTs but they do show increased levels of ptau compared to the single KI *MAPT* (Saito et al., 2019) (***Figure 19C***). To the best of our present knowledge, the $App^{NL-F}xMAPT$ dKI mouse line has never been evaluated in behavioral tasks.

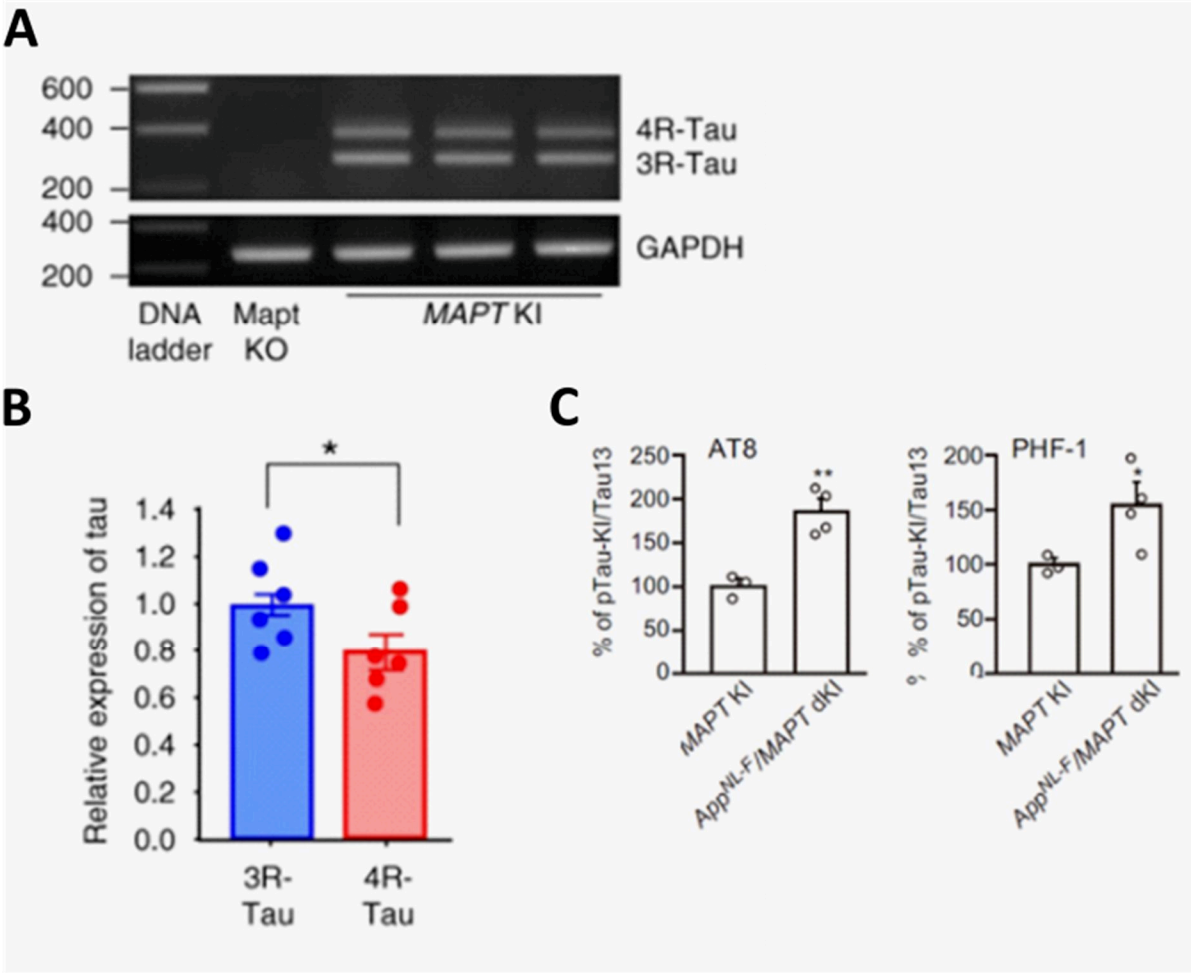

Figure 19: *Tau pathology in MAPT and $App^{NL-F}xMAPT$ dKI mice. (A) Representative PCR electrophoresis gel performed to B) compare levels of 4R-tau and 3R-tau in MAPT KI mice. C) Crossing the MAPT KI with App^{NL-F} KI increases the amount of ptau at 24 months of age. Adapted from Hashimoto et al., 2019 and Saito et al., 2019.*

13. My project

The main goal of my project was to detect the first impairment of recognition memory in dKI mice and then unravel the origin of this early memory disorder in the dKI model. My first aim was to characterize extensively recognition memory performances in search of the most precocious deficit using a battery of tasks based on the object exploration paradigm. The second aim was to perform task-related ex vivo imaging of neuronal activation in WT and dKI mice in order to identify the earliest region affected in dKI mice. Witht the help of Demian Battaglia, regional activity levels and functional networks were evaluated to assess perturbations well described in human studies of preclinical AD. The third aim was to decipher the origin of the functional disturbances in this cerebral region. To achieve this aim, we planned to use two approaches. In collaboration with Céline Héraud, I would first determine the relative importance of amyloid and tau pathologies using western blot focusing on a set of brain regions potentially involved in the impaired memory task, including the region of interest. This region was expected to show exacerbated pathology. Finally, functional perturbations of the affected regions would be more precisely evaluated using electrophysiological techniques with the aid of Romain Goutagny.

Materials and Methods

1. Animals

My thesis work consists in characterizing a new, doubly humanized model resulting from the cross of two knock-in (KI) mouse lines for the *App*$^{NL-F}$ (Beyreuther/Iberian and Swedish FAD APP mutations, Saito et al., 2014)) and for the *MAPT* (Hashimoto et al, 2019) which were both produced by T Saido and T Saito (RIKEN Brain Science Institute, JAPAN) and sent to us by the RIKEN BioResource Center. The *App*$^{NL-F}$ KI mouse has mutations on the β and γ cleavage sites of APP, which lead to a direct increase in production of $A\beta_{42}$, without the overexpression of APP. The *MAPT* KI mouse expresses all 6 isoforms of tau under physiologically normal levels (Hashimoto et al., 2019). Through combining the mouse promoter-controlled expression of APP with two FAD mutations and of all normal human tau isoforms in absence of their equivalent murine proteins, the *App*$^{NL-F}$*/MAPT* double knock in (dKI) model should favor the development of AD-like pathology closer to the human condition. All experiments were performed on male dKI and wild type (WT) mice.

For a separate aging study, 3-month and 18-month old C57BL/6J mice were obtained from Charles River Laboratories (France). These mice were maintained in the same conditions than dKI and wt mice and they were aged in our laboratory.

Procedures were in compliance with rules of the European Community Council Directive 2010-63 and French Department of Agriculture Directive 2013-118 and approved by the local review board (CREMEAS) and authorized by the "*Ministère de l'Education Nationale, de l'Enseignement Supérieur et de la Recherche*" (APAFIS #9848 and APAFIS #21562 for dKI and WT mice; APAFiS #2154 for comparing young and old mice). Animal facilities at the LNCA were approved for animal experimentation (H 67-482-13). Mice were group-housed with food and water ad libitum, nesting material, and additional food pellets on bedding to promote natural behavioral patterns. The animal room was under controlled temperature (23 °C ± 1 °C) and a 12/12-hour light/dark cycle (lights on at 8.00 AM). Behavioral testing took place during the light phase.

2. The dKI breeding strategy

The *App* and *MAPT* genes are located on different autosomal chromosomes, 16 and 11, respectively. This led to a complicated breeding strategy to obtain dKI mice and their WT controls, to maintain these mice on an acceptable C57BL/6J derived background and to produce experimental groups. Parental App^{NL-F} KI and *MAPT* KI mice obtained from the RIKEN BioResource Center were heterozygous for their KI insertion. Thus, the first step (step1) upon arrival was to produce sufficient homozygous KI mice and WT mice to reach a second step (step2) to create the dKI mice (***Figure 20***). It consisted in crossing homozygous App^{NL-F} KI or *MAPT* KI mice in order to produce double heterozygous mice (heterozygous for App^{NL-F} KI AND the *MAPT* KI). The third step (step 3) consisted in crossing these mice to produce a large number of mice because only a limited number would bear interesting genotypes, i.e., 1/16 of WT mice, homozygous single KI for the App^{NL-F} KI or the *MAPT* KI, and homozygous dKI mice. Two types of breeding was used to produce enough founders of each mouse line: step 4a was the main one, used to produce founders and then maintain each mouse line, and step 4b only used to produce more founders using as much as possible the numerous animals produced in step 3 (comply to the "reduction" rule and avoid one more breeding step). The great advantage of this breeding strategy was that founders of the WT and the KI lines were littermates, thereby ensuring as much as possible similar genetic background to all mouse lines. Mouse lines were maintained with homozygous breeding for only 3 generations to avoid a genetic drift which would hamper the use of the "WT" line as a control for KI lines. After 3 generations WT and dKI mouse lines were each backcrossed to male and female C57BL/6J mice (Janvier Labs, Le Genest St Isle, France) to produce again double heterozygous mice and these mice were bred following step 3 to found new backcrossed WT and dKI mouse lines. Note that single KI lines were only maintained for 1 generation as these mice were not used much in the present work. Mice were genotyped at least once at each breeding step.

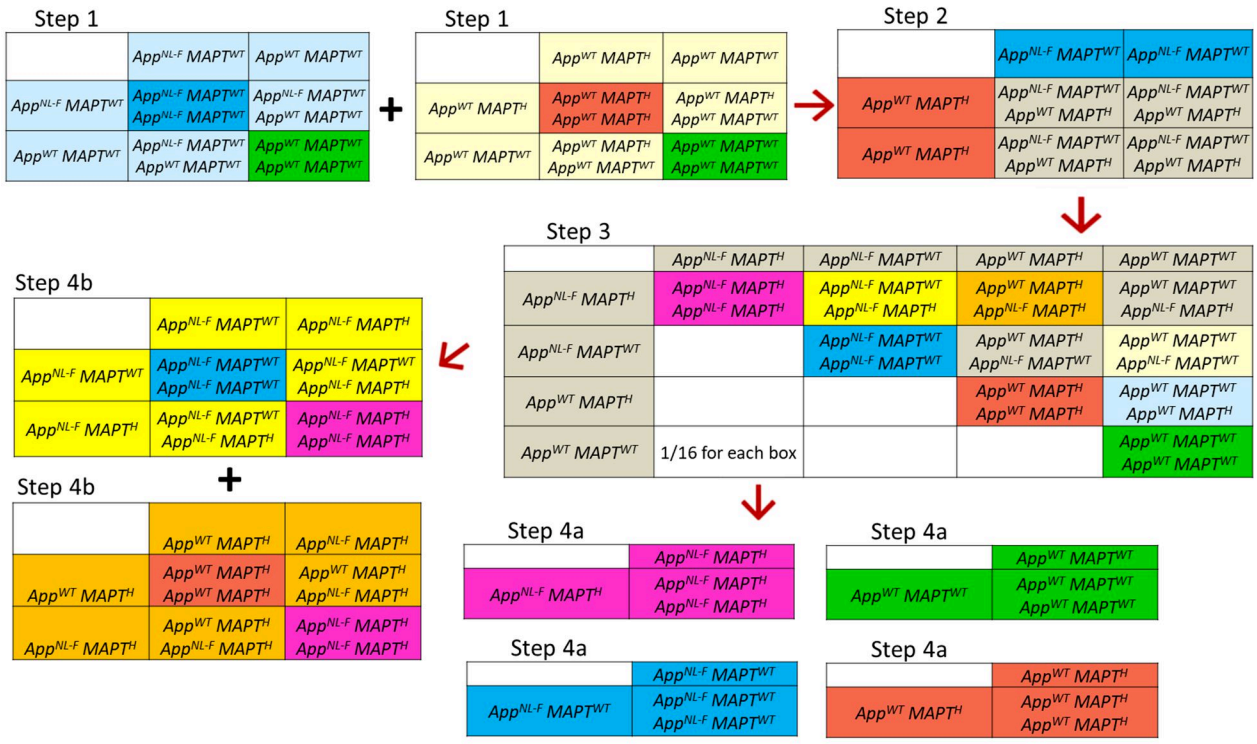

Figure 20. *Breeding strategies to produce homozygous App^{NL-F}xMAPT (dKI) mice. Color code: magenta for homozygous dKI, green for WT, dark blue for homozygous App^{NL-F}, red for homozygous humanized MAPT (termed MAPT^{H} here), light brown for double heterozygous KI, light beige for heterozygous App^{NL-F} KI, light blue for heterozygous MAPT KI, yellow for homozygous App^{NL-F} KI/ heterozygous MAPT KI, and orange homozygous MAPT KI/ heterozygous App^{NL-F} KI. For details on each step, see the text.*

3. Actigraphy

A. Purpose

Animals follow a circadian rhythm where they organize their behavior over a 24 hour day/night cycle in a regular and constant fashion especially in our animal facility set on a 12/12-hour light/dark cycle. Mice are mainly active during the dark phase. Though the most obvious resulting behavior is the regulation of animal's activity, the circadian rhythm has implications with physiological indices such as core body temperature, brain oscillatory activity, cardiovascular and respiratory function, and immunity (Logan and McClung, 2019). Alzheimer's disease is largely shown to affect and/or be affected by changes in the circadian rhythm. Numerous studies have shown that sleep-wake activity is disturbed in individuals with dementia due to AD (Lim et al., 2014). Moreover, levels of Aβ and ptau can be exacerbated with

decreased sleep due to lowered metabolism and clearance processes (Homolak et al., 2018). Recent studies coupling PET imaging and EEG have shown that AD protein deposition can correlate with abnormal sleep brain wave activity, such as an increase of tau-PET correlating to decreases in non rapid eye movement (non-REM) sleep (Lucey et al., 2019). In their recent review, Wang and Holtzman (2020) state that sleep disturbance appears in early stages of AD and that there is a "bidirectional relationship" between sleep/wake rhythms and both Aβ pathologies.

B. Protocol

Given its connection to AD, and evidence for early circadian disturbances in AD pathology, we decided to test the circadian activity in dKI mice. This was accomplished using an actigraphy setup. The mice were placed into 11.5cmx29.5cmx13cm cage with a small amount of litter. Two infrared light beams coupled to photocells passed through the opposite ends of each cage (***Figure 21***). The home made actigraphy software counted a cage crossing for each time a mouse crossed both lasers consecutively. The mice were left in the actigraphy undisturbed for 3 nights starting on Friday evening. Testing during the weekend permitted the least amount of disturbance. The number of cage crossings was considered as a measure of locomotor activity counted every 15 minutes.

Figure 21. *Actigraphy set up. Cage and location of two lasers at each end.*

4. Recognition Memory Tasks

A. Purpose

Recognition memory dysfunction is one of the earliest behavioral changes seen in AD. Human studies have shown that some tasks evaluating subtle forms of recognition memory, such as object-place associative memory and fine discrimination abilities, are able to detect impairments during early cognitively normal preclinical stages of the disease during and even preceding the aMCI condition (Stark et al., 2013; Yeung et al., 2019).

Mice are innately curious. They show a spontaneous tendency to explore a new object or an object that moved to a new position. The two-trial object exploration paradigm, first described by Ennaceur and Delacour in 1988, makes use of this trait by taking increases in novelty exploration as a measure of memory retention. The object exploration paradigm has proven flexible, allowing the experimenter to evaluate various types of recognition memory simply by manipulating the environment or the testing protocol. As an example, one can test object recognition memory by changing the identity of the object, or spatial memory by changing the location of an object. To increase the difficulty of the task, the inter-trial-interval (ITI) may be increased to test the more difficult long-term memory (ITI = several hours) or the less difficult short-term memory (ITI = a few minutes; Dodart et al, 1997, Bour et al, 2004). The SOR task can be made more sensitive by increasing the subtlety of the changes. Small changes in the object's features or location evaluate fine discrimination object recognition and spatial recognition respectively. These tasks are able to detect memory impairments that would not be detected by the more traditional tasks. Aged mice are shown to be deficient in fine discrimination memory (Ces et al., 2018), while they show no deficits in the more traditional OR and OL tasks. The tg2576 (or APP_{SWE}) AD mouse model also shows specific fine discrimination deficits as soon as 4 months of age (manuscript in preparation; Zhu et al, 2017).

Another way to increase the difficulty of the task is to test associative memory. The task that probes for "what and where" associative memory is termed the object-in-place (OP) task. In the two-object version of this task, the mouse is shown two different objects during the acquisition phase. During the retention phase the mouse is shown two identical objects in the same positions as during acquisition, where one of the previous objects has been replaced by a copy of the other.

Here, it is not the identity of the object that is novel, nor is it the position within the open field, but the association of that specific object to its position. Using this task with a 3 hour delay, CRND8 mice were shown to have memory deficits as soon as 2 months of age (Hamm et al., 2017).

B. Optimization with single KI mice

Behavioral protocols were optimized with single KI mice (WT n = 7, *MAPT* n = 8, App^{NL-F} n = 7) before the dKI mice had been developed. For this many different protocols (test order, object identity/location per task, luminosity) were used and optimized based on the results. Some essential optimizations consisted in limiting the number of consecutive testing days to 4 (to reduce stress), and transferring the mice into a quiet room next to the testing room at least one week before testing and for the whole duration of the testing period. The OP protocol was massively optimized with essential parameters including finding the right objects, placing them on the diagonal further apart to accentuate their "place", and increasing the luminosity to 15 lux so that mice can more easily see distal spatial cues. Initially, we intended to test the mice every two months until the first deficits would appear. However, we noticed quite rapidly that with only two months between testing periods, results of the third period were not satisfactory. Thus from that moment, each mouse was only tested twice and we balanced as much as possible the three testing periods (2-4, 2-6 and 4-6 months) for each cohort of 6 to 12 mice.

C. Set Up and General Testing Protocol

The mice were tested in a 100cmx100cmx50cm open field with dark grey plexiglass walls and a metal floor (Ugo Basile, Italy). The open field was homogeneously lit by 3 fluorescent lamps evenly distributed in the room. The luminosity was set to 13-15 lux in the center of the open field and around 6-8 lux in the corners. The background noise was set to 48±2 dB from the center of the open field, as adjusted from a radio situated near a corner of the open field.

Before each test the mouse was left in the testing room for at least 15 minutes. Each test consisted of an acquisition phase, the ITI phase and the retention phase. Before each trial, the objects were cleaned with 35% alcohol and the open field was wiped with a water soaked paper towel. During OL and fine discrimination OL the objects were not cleaned with alcohol to limit novelty to the location of the object.

D. Isolation

Fighting between male C57BL/6J mice, especially during adverse and novel conditions, is well documented and can lead to variations in brain function and behavior (e.g., Greenberg et al., 2014). In addition, ex vivo brain activity imaging was already planned as the next step of the thesis project, so keeping each mouse alone to minimize external stimulation would then be an absolute necessity. Therefore, mice were isolated two weeks before the start of testing. The mice were then placed into a room situated between the testing room and the corridor, termed the sas. The sas was lit by a halogen lamp, which was set to a luminosity of 15 lux as measured from the mouse cages. The volume was set to around 47 decibels, as adjusted through a radio situated in the corner of the room.

E. Habituation to Tubes

During testing, tubes were used to facilitate transportation of the mice between their homecage and the open field (Gouveia and Hurst, 2013). A semi-opaque garden hose (4-cm Ø) was sectioned in 15-cm long tubes. A tube was present in the cage since the mice were singly housed. One week after isolation the mice were habituated to being moved in and out of their home cage with the tube. This consisted of placing a mouse into an empty cage for 2 minutes, after which a tube was placed against a wall of the cage until the mouse entered it. The mouse was then transported smoothly in the tube back to its home cage. This process was repeated once more at least 30 minutes later. The whole process was repeated again two days later.

F. Memory index

Memory retention is evaluated using the memory index, the ratio of time a mouse spends exploring the novel object more than the fixed object. The memory index is 0 at chance level, when a mouse explores both objects equally. Mice that explored less than 2 seconds were removed from the analysis in comparing memory index between groups.

$$\text{Memory index} = \frac{\text{Time at novel object}}{\text{Time at both objects}} - .5$$

5. Detecting Earliest Object Recognition Deficits

A. Purpose

We expected that the dKI mouse model would have a slowly evolving neuropathology based on the initial characterization of the single App^{NL-F} mice (Saito et al., 2014). Thus, we decided to begin the phenotyping at the age of 2 months and to first evaluate them using tasks that are able to detect subtle deficits. The dKI mice were therefore tested with a barrage of especially sensitive object exploration tasks. The testing consisted of long-term object recognition with a 24 hour ITI (OR24), fine discrimination object recognition (FDOR5'), fine discrimination object location (FDOL5') and finally object in place (OP5'). By determining which task reveals initial deficits we would have a clue as to which structural networks are affected first in the dKI mice. Different cohorts of mice ended up being tested at two of 3 different ages, 2 (WT n = 10, dKI n = 10), 4 (WT n = 12, dKI n = 9) and 6 (WT n = 8, dKI n =11) months, and not at later ages since the first deficits were found as early as 4 months in the first cohorts of male mice.

There was no habituation day for this initial set, since previous experiments showed that 6 days of testing was too stressful for the mice. Testing started gently with the OR24 task which is quite robust and requires limited manipulations with one trial per day instead of two for subsequent tasks (see ***Figure 22***).

B. Day 1 and 2 – Long-term Object Recognition (OR24)

This test evaluates long-term recognition memory (Ennaceur and Delacour, 1988). For the acquisition phase, the mice were first placed into the open field containing two identical objects, and are left to explore for 10'. The mice were then transported back to their home cage and left in the sas overnight for an ITI of 24 hours. During the retention phase, one of the objects was replaced by another object of different shape, color and material in sharp contrast with the familiar object and mice were left to explore for 8'. The mice were then placed back into their homecage and placed back into the sas as each time a mouse completed a daily session.

Two sets of very different objects were selected after preliminary experiments to ensure that 1) control animals displayed high levels of OR performances after 24h, and that the two objects were equally attractive to the mice. To minimize any possible bias, the role of familiar and new

object and the position of the new object were pseudorandomly distributed among genotypes and time of the day. Similar precautions were taken for all following tasks dealing with object identity.

C. Day 3 - Fine Discrimination Short-term Object Recognition (FDOR5')

This test evaluates recognition memory for subtle changes in object identity (Cès et al, 2018). The set of objects are made of legos. Each different object within the set is made of the same set of lego block colors but the organization of the blocks changes. The objects were made to have a very different composition, giving normal object recognition, or very similar composition, giving fine discrimination object recognition. The very similar compositions were previously tested with older mice of 18 months, who were unable detect a change in the very similar composition of these objects after a 5'delay. The protocol was identical to that of the OR above, except an ITI of 5'.

D. Day 4 - Fine Discrimination Short-term Object Location (FDOL5')

This test evaluates fine discrimination spatial memory (Cès et al., 2018). During the retention phase an object is displaced a distance of 20 cm instead of the more evident displacement of 40 cm used in the normal object location task. The displacement of 20 cm revealed fine discrimination deficits in 18 month old mice that were still able to detect a 40cm change.

For the acquisition phase, the mice were first placed into the open field containing two identical objects, and were left to explore for as long as 12 minutes because this task is particularly difficult. The mice were then transported back to their home cage and left for and ITI of 5 minutes. During the retention phase, one of the objects was displaced 20 cm and mice were left to explore for 8 minutes.

E. Day 5 – Short-term Object in Place (OP5')

This test evaluates object in place associative memory (Wilson et al., 2013a). For the acquisition phase, the mice were first placed into the open field containing two different objects, and were left to explore for 10'. The mice were then transported back to their home cage and left for and ITI of 5'. During the retention phase one of the objects was replaced by a copy of the other object and mice were left in to explore for 8'.

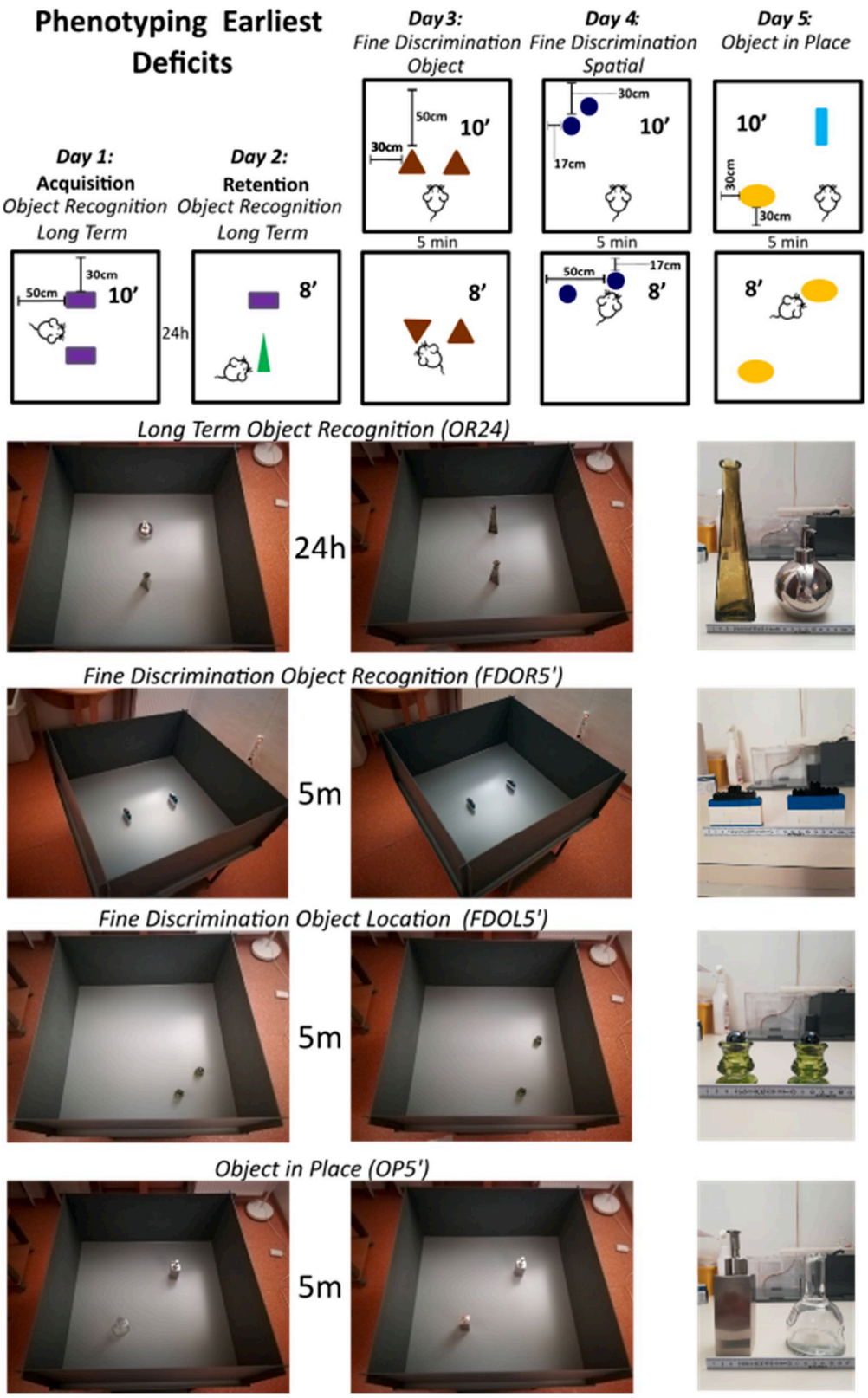

Figure 22. *Phenotyping earliest deficits in young 2, 4 and 6 month old dKI mice.*

6. Short-term Object in Place for Ex-Vivo c-Fos Imaging

A. Purpose

It was determined that the earliest and most pronounced deficit in male dKI mice was found as soon as 4 months of age in the OP5' task. To elucidate the physiological underpinnings of this deficit we aimed to assess which brain regions showed altered activity during the task. Here we adopted one of the most widely used ex-vivo imaging technique based on c-Fos expression which has been successfully applied to object recognition tasks (Belblidia et al., 2018; Kinnavane et al., 2015). The protein c-Fos is coded by the immediate early gene *c-fos*. The expression of *c-fos* and its c-Fos protein product is triggered by the calcium signal transduction cascades associated to neuronal activation. The peak expression of c-Fos occurs from 60 to 90 minutes after neuronal activation. In order to have a snapshot of neuronal activation elicited by object in place memory, the mouse brains were perfused 90 minutes after the mice had finished the retention phase of the task (WT n = 11, dKI n = 11). Under the supervision of Céline Héraud, brains were sectioned and marked for c-Fos using immunohistochemistry techniques, and marked sections were subsequently analysed to determine which brain regions show differential c-Fos expression. The whole process from brain harvesting to quantification of c-Fos expression will be explained in further detail in the Immunohistochemistry section. Across-subjects correlations of activity regulated immediate early genes (IEG; *c-fos, Egr1*) levels have been successful exploring functional networks directly related to memory (Tanimizu et al., 2017; Wheeler et al., 2013; Vetere et al., 2017). Thus, this analytical approach was also carried out on c-Fos expression data of this study.

To insure the cleanest performances in the difficult object in place task, we wanted to give the mice 3 days of habituation to the open field and objects. Moreover we also wanted to test the mice in more traditional OR and OL tasks to verify that at 4 months of age the dKI mice did not show deficits in more easy recognition tasks. We therefore chose to use a 4 day protocol consisting of a habituation, OR5', OL5' and finally the OP5' task, in that order. The OR and OL testing days served not only as additional reinforcing habituation to testing conditions but also as controls to verify the conservation of simple object recognition and spatial memory in dKI mice (see ***Figure 23***).

A. Day 1 - Habituation

The mice were tested in a 100cmx100cmx50cm open field with dark grey plexiglass walls and a metal floor. The luminosity was set to 13-15 lux in the center and around 6-8 lux in the corners. The volume was set to 47 decibels from the center of the openfield. Behavioral testing took place on 4 consecutive days. Before each test the mouse was left in the room on the table for at least 15 minutes prior to testing. On the first day of testing the mouse was habituated to the open field and objects. This consisted of placing the mouse into the open field containing two identical objects and allowing the mouse to explore for 10 minutes. The mice were then transported back into their homecage using the tube and placed back into the sas. This first day of testing also played an important role in habituating the mouse to being transported to and from the open field with the tube.

B. Day 2 – Short-term Object Recognition (OR5')

This test evaluates short-term recognition memory. It follows mostly the same procedure as the *Day 1 and 2 – Long-term Object Recognition* under the *Detecting Earliest Object Recognition Deficits* experiment. The only change is during the ITI phase were the mice are left for an ITI of 5 minutes in the testing room instead of 24 hours in the sas.

C. Day 3 – Short-term Object Location (OL5')

This test evaluates short-term spatial memory. It follows mostly the same procedure as the *Day 4 - Fine Discrimination Short-term Object Location* under the *Detecting Earliest Object Recognition Deficits* experiment. The only change is during the retention phase, where the displaced object is moved 40 cm rather than 20 cm.

D. Day 4- Short-term Object in Place (OP5')

This test follows the same procedure as explained in the *Day 5-Short-term Object in Place* under the *Detecting Earliest Object Recognition Deficits* experiment. After the retention phase mice were placed into the quiet sas. After 90 minutes they were taken for perfusion.

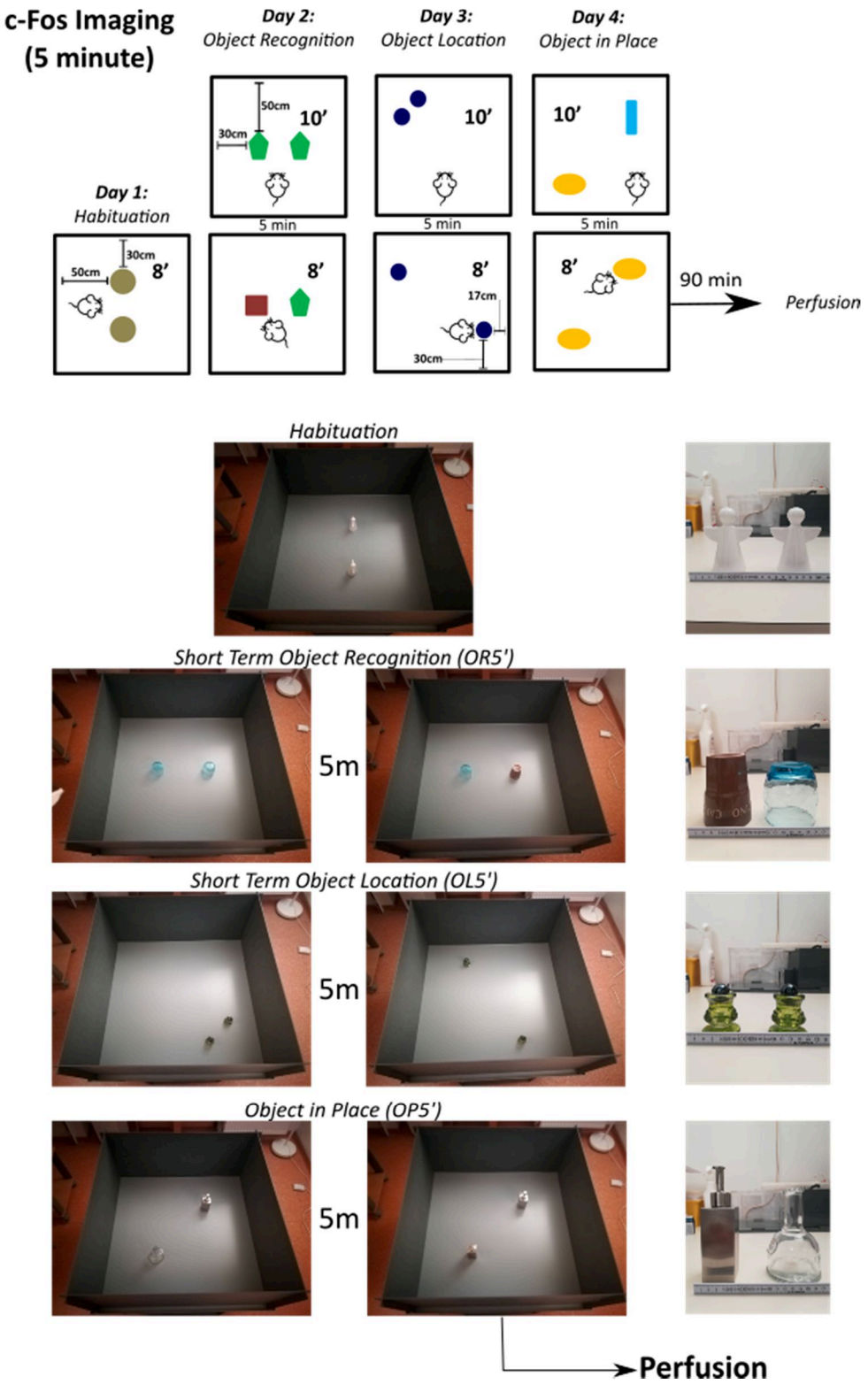

Figure 23. *Evaluating c-Fos expression in the OP5'task while also assessing performance in OR5' and OL'5 tasks.*

7. Three-hour delay Object in Place for Ex-Vivo Imaging

A. Purpose

In the previous experiment, brain activation measured through c-Fos expression resulted from a combined effect of the acquisition phase, the ITI and the retention phase. Although were able to detect genotype dependent changes, the interpretation of the results in respect to the phasing of OP memory was unclear. Moreover as our interest in functional connectivity had increased, we realized that the mixture of both test-phases in the c-Fos signal brought along some detrimental drawbacks in terms of interpreting functional connectivity. These will be discussed in the results of OP5' (Study n°2). In order to remedy this, we decided to increase the ITI to 3h, the shortest ITI delay that would ensure good OP3h performance in WT mice and proper isolation between the acquisition and retention phases in respect to c-Fos expression. This protocol would allow us to detect genotype dependent changes in brain activity with respect to each phase, acquisition (WT n = 12, dKI n = 12) and retention (WT n = 14, dKI n = 14). A 3-hour ITI object location task (OL3h) was included the day before the OP3h task. This preliminary task served not only as additional reinforcing habituation to testing conditions but also as a control to verify the conservation of simple spatial recognition with a 3-hour ITI. This control is necessary to ensure that the OP3h deficit is purely due to associative dysfunction (see ***Figure 24***).

B. Day 1 - Habituation

This follows the same procedure as explained in the *Day 1 - Habituation* under the *Short-term Object in Place for Ex-Vivo c-Fos Imaging* experiment.

C. Day 2 – Three-hour delay Object Location (OL3h)

This test evaluates 3-h spatial memory. This follows mostly the same procedure as the *Day 3 – Short-term Object Location* under the *Short-term Object in Place for Ex-Vivo c-Fos Imaging* experiment. The only change is during the ITI phase were the mice are left for an ITI of 3 hours in the sas instead of 5 minutes in the testing room.

D. Day 3 – Three-hour delay Object in Place (OP3h)

This test follows mostly the same procedure as the *Day 5 – Short-term Object in Place* under the *Detecting Earliest Object Recognition Deficits* experiment. The only change is during the ITI

phase were the mice are left for an ITI of 3 hours in the sas instead of 5 minutes in the testing room. One cohort was only tested in the acquisition phase (WT n = 12, dKI n = 12), and the other for both phases including retention (WT n = 14, dKI n = 14). After the task was finished, mice were placed into the sas. After 90 minutes they were taken for perfusion.

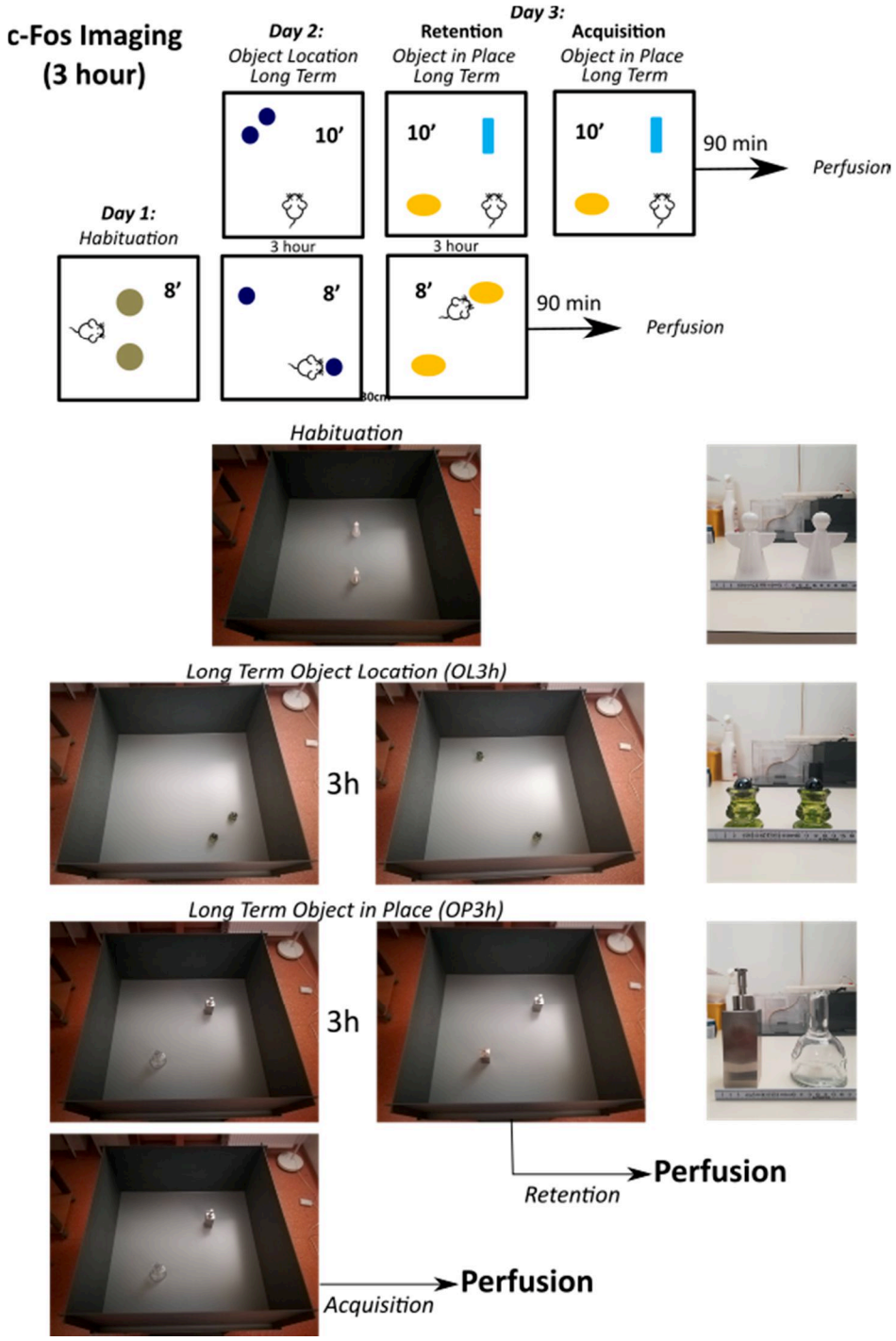

Figure 24. *Evaluating c-Fos expression in the OP3h task while also assessing performance in the OL3h task.*

8. Object in Context

A. Purpose

Considering their specific deficit in OP task, we were interested in evaluating dKI mice with a similar form of associative memory in the object in context (OiC) task (Dix and Aggleton, 1999). The mouse has to associate an object with a context (incorporating changes in smell, feel, color, a completely different environment) rather than a place. Although I did not test the dKI mice, I developed and set up the initial protocol, and evaluated it on WT mice (n = 10, 4 months of age) with the help of an M1 student, Julien Caillette. This student was also involved in helping in c-Fos imaging analysis during his internship with me. The results highlighted some important considerations involving temporal aspects of the task.

B. Object in Context (OiC24)

In this test the mice have to remember the association of an object to a context. The two contexts used were two different open fields, Context A and Context B (***Figure 25***). Context A was a 52x52x40 cm open field with black walls covered with big, white (Christmas) stickers, and a white floor. Context B was a 50x30x35 cm plastic tub with clear green walls covered with smaller (Christmas) stickers and a dark burgundy floor. One the first day, the mice are given an 8-minute habituation trial to each context, separated by a 5-minute delay. On the second day, they are given two acquisition trials, separated by a 5-minute delay. During the first acquisition trial, the mice left to explore two identical objects in one context for 8 minutes. Then for the second acquisition trial, they were placed into the other context containing a different set of two identical objects, again for 8 minutes. On the third day after a 24-hour ITI, during the retention phase, the mice were placed in one of the contexts (A or B) containing a set of two different objects, again for 8 minutes. The mice should show increased exploration of the object that has not already appeared in the given context. The two contexts were presented in the same order on the first and second day. Each of the four possible order of context presentation over the 3 days (e.g., AB, AB, A; BA, BA, A; AB, AB, B; BA, BA, B) were balance among groups.

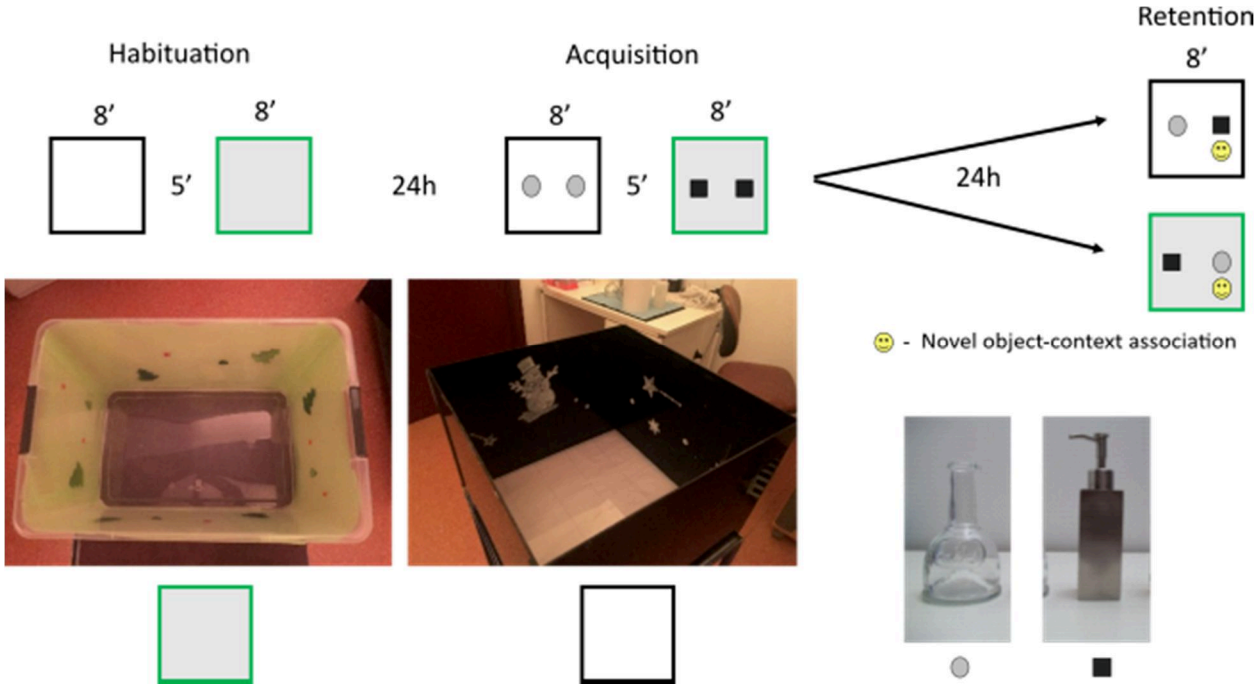

Figure 25. *Long-term object in context task (OiC24) (the second presentation is the reverse order)*

9. Light Dark

A. Purpose

Many of the behavioral tests used in my thesis can be affected by anxiety in mice (Bourin and Hascoët, 2003). During the object recognition tasks for example, anxious mice may exhibit neophobia which could reduce exploration of the novel object. The implications of anxiety on these tests necessitated testing anxiety levels of the dKI mice using the light dark test.

As they are nocturnal animals, mice avoid bright light and are naturally more at ease resting in the dark spaces, where they are able to avoid the eyes of predators. At the same time they are also curious foraging animals who benefit from exploring new environments. These two contrasting behaviors may balance differently in individual mice based on their anxiety level, and this balance can be tested using the light dark test.

In the light dark test the mouse is placed in an environment consisting of a completely dark box that is connected to a brightly lit box. Mice with anxiogenic tendencies will be more hesitant to enter and explore the light box.

B. Protocol

The light dark test was evaluated on female and male WT (n = 8 per sex) and dKI (n = 8 per sex) mice of 4 months of age. The set up used consisted of two 19x19x14.5cm covered plexiglass cages connected by a 7x5x10cm corridor. The “light box” was a cage with transparent walls and cover, and was brightly lit to 1200 lux by an incandescent bulb situated 15 cm above the cover. The “dark box” had dark gray non-transparent walls and cover. At the start of the test the mice were placed into the dark box and left to explore both cages for 5’. The latency to enter the light box, the number of passages between the light and dark boxes and the total time spent in the light box were recorded. Between each trial, the cages were wiped with 35% alcohol, and cleaned of urine and excrement.

10. Western blotting for neuropathology

Four-month-old male mice were sacrificed by cervical dislocation (n = 8 per group), and their brains were carefully dissected on ice. Hippocampi and medial temporal cortex were quickly removed, frozen in liquid nitrogen and then stored at −80°C until their use. Tissues were homogenized in 10 volumes of ice-cold radioimmunoprecipitation assay buffer containing protease inhibitor cocktail (Sigma-Aldrich), phosphatase inhibitor cocktail (PhosStop, Roche Life Science), and 1 mM phenylmethylsulfonyl fluoride (Sigma-Aldrich). After centrifugation at 20,000g for 20 min at 4°C, supernatants were aliquoted for immunoblot analysis. Brains extracts of Tg2576 and Thy-tau22 mice were homogeneized and separated in parallel to our samples as a positive control for APP proteins and cleaved fragments and for tau proteins, respectively. Protein concentration was measured using the Bio-Rad Protein Assay (Bio-Rad). Thirty or 20 microgramms were respectively loaded on 4-20% precast gel (Mini-Protean TGX precast gels, Bio-Rad) for APP and tau proteins. After electrophoresis and transfer to nitrocellulose membranes using the Trans-Blot Turbo System (Bio-Rad), membranes were incubated with 5% skimmed milk for 1 hour at room temperature and then with primary antibodies diluted in 2% bovine serum albumin (Sigma) in tris-buffered saline 0.05% Tween 20 (Sigma-Aldrich) overnight at 4°C. After washes, membranes were incubated with anti-mouse or anti-rabbit immunoglobulins conjugated to horseradish peroxidase (Jackson Immunoresearch) for development with enhanced ECL chemiluminescence detection kit (Thermo Fisher Scientific). After detection, all membranes were reprobed with anti-actin antibody for normalization of total protein. The primary antibodies used were the rabbit polyclonal anti-APP, C terminus (Sigma-Aldrich), the rabbit polyclonal anti-tau (B19, generously gifted by JP Brion, ULB, Belgium), the mouse monoclonal anti-phopho-Tau Thr181 (AT270, ThermoScientific), the mouse monoclonal anti-actin (Sigma-Aldrich) and the rabbit polyclonal anti-actin (Sigma-Aldrich). The secondary antibodies used were the peroxidase-conjugated AffiniPure goat anti-mouse and goat anti-rabbit (Jackson Immunoresearch). The quantification of the band intensity acquired with the ChemiDoc Imaging system (Bio-Rad) was performed by densitometry analysis using the ImageJ program. For each mouse, the phosphorylation degree was calculated as the ratio of total phosphorylated Thr181 tau proteins on total tau proteins. The ratio of APP-cleaved fragments was calculated as the total of APP β-CTF on α-CTF fragments.

11.Immunohistochemistry for Ex-Vivo c-Fos Imaging

A. Protocol optimization with young and aged mice

The protocols, from brain sectioning to c-Fos quantification, was optimized using brains from 3 month old and 18 month old C57BL/6J male mice that were previously Behaviorly tested and perfused. Groups of 8 animal per age, except one of 9 youngs, were each tested in one of the following tests by Anaïs Robert, a Master 1 student supervised by Chantal Mathis: OR5' (young n = 9, old n = 7), OL5' (young n = 8, old n = 8), FDOR5' (young n = 6, old n = 8), FDOL5' (young n = 5, old n = 6), and OP5' (young n = 7, old n = 8). Performances of some animals were ruined by maintenance-related noisy works, especially during testing of the FDOL5' groups. Nevertheless, Anaïs Robert showed that aged mice were significantly impaired compared to young ones only in the FDOR5' task as reported by Cès et al. (2018). While I was waiting for experimental dKI mice to be produced by the complex breeding protocol, I cut many brains from this study and then focused my efforts on those tested in the OP5' task. The results of these preliminary analyses will be presented in Study n°2. This experiment informed me for the optimization of many experimental parameters. Some of the most essential insights include increasing the sample size for future c-Fos experiments, improving testing conditions to minimize environmental interference (i.e., use the quiet sas next to the testing room), developing the most effective c-Fos quantification method and taking several Z-planes per NanoZoomer scan.

B. Perfusion

Ninety minutes after the end of testing the mice were taken for transcardial perfusion. The cages were covered with a dark towel during transportation to the surgery room to prevent visual stimuli. To induce anesthesia, the mice were first injected IP with 364.6 mg/kg/ml of euthasol (pentobarbital) in 0.9% NaCl and left for around 3 minutes. After ensuring that the mice showed no pupil response and no response to a foot pinch, they were placed for dissection. The mice were transcardially perfused with PBS containing 0.1% heparin for 5 minutes in order to purge the body of blood. This was followed by a 10 minute perfusion with 4% paraformaldehyde in 0.1 M of phosphate buffer for brain fixation. The brains underwent post-fixation in 4% paraformaldehyde for 24 hours. They were then left in 20% sucrose in 0.1 M of phosphate buffer

for 48 hours. Finally they were frozen by being immersed in isopentane at -37°C for one minute. The frozen brains were stored in a freezer at -80°C.

C. Sectioning

The brains were sectioned at -20°C using a Thermo Scientific Microm HM 560 cryostat. The sections of 40 µm thickness were taken on the coronal plane and stored in a cryoprotectant solution at -20°C until use. At least 3 sections were taken per region.

D. c-Fos immunohistochemistry

The brain sections were transferred from the cryoprotectant to a petri dish containing PBS before being placed into the immunohistochemistry plate containing PBS. The sections were placed into the plate in a manner which the dKI mice and WT mice were equally distributed. The sections were first given three 10-minute washes in PBS, followed by an incubation in 3% H2O2 for 30 minutes at room temperature in order to neutralize endogenous peroxidases that could react with 3,3-diaminobenzidine (DAB). They were washed for 5 minutes with ultra-pure water and again two times for 10 min in PBS to remove residual H2O2. This was followed by a 1-hour blocking incubation in a solution containing 5% normal goat serum (NGS) diluted in a "diluant" solution consisting of 1M PBS, and 0.5% Triton X100. The sections were then incubated at room temperature for 24 hours in a 1/1500 dilution of a polyclonal rabbit-anti-cFos primary antibody (Synaptic System) in diluant containing 2% NGS. The following day the sections were first given three 10-minute washes in PBS, and then incubated for 2 hours at room temperature in a 1/500 dilution of biotinylated goat-anti-rabbit (Vector) secondary antibody solution in diluant containing 2% NGS. Just before the end of secondary antibody incubation, avidin and biotin (ABC kit) were diluted 1/500 each in diluant and the solution was left to incubate for at least 30 minutes at 4°c. Following the secondary antibody incubation, the sections were given three 10-minute washes in PBS, followed by a 45-minute incubation in the avidin/biotin solution at room temperature. After the avidin/biotin incubation the sections were washed with two 10-minute washes in PBS and a 10-minute wash in Tris buffer. The sections were finally reveled with DAB (Vector Labs) for 9 minutes while being closely observed under a light microscope. The revelation was quenched with three 10-minute PBS washes. The sections were mounted on gelatin covered slides and left overnight to dry. A table of all antibodies used is shown in *Table I*.

The slides were mounted with coverslips which first consisted of giving the slides consecutive one minute washes in 70%, 95%, 95%, 100% and 100% alcohol. These were followed by an incubation in Clearify Clearsolv Clearing Agent for 5 minutes. Excess Clearify solution was removed and the slides were mounted with coverslips using diamount and left overnight to dry. The slides were wiped clean with 70% alcohol.

Antigen	Host species	Dilution	Supplier
c-Fos (Aging)	Rabbit (polyclonal)	1/20000	Synaptic systems ref:2260003 lot:226003/16
c-Fos (OP5')	Rabbit (polyclonal)	1/15000	Synaptic systems ref:2260003 lot:226003/16
c-Fos (OP 3h)	Rabbit (polyclonal)	1/15000	Synaptic systems ref:2260003 lot:226003/466
Rabbit immunoglobins (Aging, OP5')	Goat	1/500	Vector Labs ref: BA1000 lot: ZA 520
Rabbit immunoglobins (OP 3h)	Goat	1/500	Vector Labs ref: BA1000 lot: ZB 1007
Tau (B19)	Rabbit (polyclonal)	1/30000	gifted by JP Brion, ULB, Belgium
phopho-Tau Thr181	Mouse (monoclonal)	1/2000	ThermoScientific MN1050
APP, C terminus	Rabbit (polyclonal)	1/4000	Sigma-Aldrich ref : A8717 lot: 081M4870
Actin	Rabbit (polyclonal)	1/10000	Sigma-Aldrich ref: A3853 lot: 102M4771
Actin	Mouse (polyclonal)	1/10000	Sigma-Aldrich ref: A2066 lot: 118K846
Rabbit immunoglobins	Goat (horse raddish Peroxidase-conjuagated)	1/5000	Jackson Immunoresearch ref: 111-035-003 lot: 101844
Mouse immunogobins	Goat (horse raddish Peroxidase-conjuagated)	1/5000	Jackson Immunoresearch ref: 115-035-003 lot: 101698

Table I. *.Antibodies used for western blotting and c-Fos immunohistochemistry.*

E. Nanozoomer

Whole slides were imaged at 20x using a NanoZoomer S60 Digital slide scanner (Hamamatsu photonics) (***Figure 26***). At least 6 focus points were used per section for the Nanozoomer to detect the focus plane. Three different images were taken at three different focus planes, one image at the detected focus plane, one image 4 µm above the detected focus plane and the final image 8 µm above the detected focus plane. This image organization was chosen because the NanoZoomer focus errors tended to bias towards the slide, downwards rather than upwards. This was likely due to some focus points being placed close to ventricles, such as for the hippocampus, or close to the exterior, as for the cortex.

The .ndp files from the NanoZoomer contained the three whole slide images that could only be accessed with the NDPView program. In order to use ImageJ for image processing, smaller images of the individual sections needed to be extracted. To achieve this, individual brain sections were extracted at 20x resolution, where the image from the sharpest focus plane was taken. Individual brain section images were saved into .jpg format and the filenames contained the experiment name, the date of image extraction, the mouse ID, the Region set, and the anterior posterior absolute position in relation to bregma removing the decimal (-1.8 from bregma would be represented as 18), e.g. “19-02-13 OPdKI4momale m13 DH 18”.

Figure 26. NanoZoomer S60 Digital slide scanner. (Hamamatsu photonics).

F. c-Fos quantification

The c-Fos expression was analyzed in 22 regions of interest (ROIs), including sub-regions of the medial prefrontal cortex, claustrum, dorsal hippocampus, retrosplenial cortex, perirhinal/postrhinal cortex, and the entorhinal cortex. Image processing was done using ImageJ (National Institute of Health, Bethesda, MD). ROIs were anatomically defined according to the atlas of Paxinos and Franklin (2019). For c-Fos quantification, the images were transformed into 8-bit grayscale. A grayscale threshold for was set at a consistent level for each region by an experimenter blind to group condition. Only c-Fos positive nuclei with a grayscale intensity below the threshold and an area between 25–300 μm^2 were counted.

G. Additional information about ROI selection

Regions relevant to recognition memory and/or early AD pathology were chosen for c-Fos quantification. The medial temporal lobe regions, including the dorsal hippocampal (DH) and para-hippocampal regions, were chosen given their prominence in the early stages of AD in relation to eary tau, as well as their importance towards a variety of memory modalities according to Mathis (2018), including object recognition (perirhinal cortex: PRC), associative and spatial memory (dentate gyrus: DG, CA1, CA3, regions of the DH, medial entorhinal cortex: MEC, postrhinal cortex: POC), and object-in-place association (lateral entorhinal cortex: LEC). The prefrontal cortex (PFC) was evaluated due to its association to early amyloid staging, as well as its documented role in associative memory (Barker et al., 2007; Chao et al., 2016). The retrosplenial cortex (RSC) was chosen due to its association to early amyloid staging, and its importance in spatial and associative memory (Parron and Save, 2004; Poirier et al., 2011). Since many cortical regions across the rostral-caudal axis were to be quantified, we chose to also evaluate the claustrum (CLA), a region that exhibits ubiquitous cortical connectivity. Regions were further split into anatomically relevant sub-regions along the dorsal-ventral or rostral-caudal axis. Regions were anatomically defined according to the atlas of Paxinos and Franklin (2019).

i. Prefrontal Cortex

The medial prefrontal cortex (mPFC) was separated into anterior cingulate (CG1, A24b in Paxinos and Franklin., 2019), prelimbic (PRL, A32 in Paxinos and Franklin., 2019), and infralimbic (IL, A25 in Paxinos and Franklin., 2019) (from AP +2.4 to +1.3 in relation to bregma).

ii. Claustrum

Early tracing studies showed the claustrum (CLA) to have a highly topographical organization of cortical connectivity along the rostral-caudal axis, with the more caudal claustrum connecting more strongly with the caudal cortical structures (Kitanishi and Matsuo, 2017). The claustrum was thus separated in half along the raustral–caudal axis, into the rCLA (from AP 1.53 to 0.87) and the cCLA (from AP 0.87 to 0.01).

iii. Dorsal Hippocampus

The dorsal hippocampus (DH) was separated into CA1, CA3 and dentate gyrus (DG) (from AP -1.3 to -2.1). The DG was separated into suprapyramidal (DG_sp) and infrapyramidal (DG_ip) blades.

iv. Perirhinal/Postrhinal Cortex

The perirhinal cortex (PRC) was considered as a potential hub region between the rostral PFC/DH and the caudal medial temporal cortex (MTC). It was therefore separated along the rostral-caudal axis into an rPRC (from AP -2.3 to -2.9) and cPRC (from AP -2.9 to -3.9). The rPRC lies at the intersection between the PFC/DH and the MTC, while the cPRC appears with the LEC and thus the MTC. This repartition is shown to have functional importance in regard to novel object detection. It was shown that in the caudal portion of the PRC there is increased activation when encountering novel objects, but not in the rostral portion (Albasser et al., 2010). We were largely interested in how the PFC and DH would differentially correlate with the PRC and thus wanted to remove any same section bias that may occur in the PRC-DH but not the PRC-PFC. For this reason, only the rPRC that appears after the DH along the rostral-caudal axis is considered. The PRC was further divided into dorsal (dPRC, “Area 36” Ect in Paxinos and Franklin., 2019) and ventral parts (vPRC, “Area 35” PRh in Paxinos and Franklin, 2019). The postrhinal cortex (POC, Ect/Prh in Paxinos and Franklin, 2019) is the very caudal extension of

the PRC after AP -4.3 (from AP -4.3 to -4.7). The PRC/POC cutoff and the demarcation of the PRC/POC in general was aided based on indications from Beaudin et al. (2013).

v. Retrosplenial Cortex

Like the PRC, the retrosplenial cortex (RSC) was considered as a potential hub region between the rostral PFC/DH and the caudal MTC. It was therefore separated along the rostral-caudal axis into an rRSC (from AP -2.3 to -2.9) and cRSC (from AP -2.9 to -3.9). Moreover, this repartition may hold functional relevance. For example, lesioning only the rostral portion of RSC was sufficient enough to affect long-term object recognition in rats (de Landeta et al., 2020). For the same reason as for PRC, only rRSC that appears after the DH was considered. The RSC was further separated into dysgranular (RSCd) and granular (RSCg) parts.

vi. Lateral Entorhinal Cortex

The lateral entorhinal cortex (LEC) was separated along the rostral-caudal into the rLEC (from AP -2.9 to -3.8), and cLEC (from AP -3.8 to -4.4) which follows the appearance of the MEC. A similar repartition has been used previously to evaluate functional differences between the rLEC and cLEC for novel object recognition (Kinnavane et al., 2016).

vii. Medial Entorhinal Cortex

The medial entorhinal cortex was separated into the medial entorhinal cortex proper (MEC, MEnt in Paxinos and Franklin., 2019) (from AP -3.9 to -4.8), and the caudal medial entorhinal cortex (CMEC, CEnt in Paxinos and Franklin., 2019) (from AP -4.2 to -5.1) according to borders described in the atlas of Paxinos and Franklin (2019). Functional differences between the MEC subregions have been suggested, with some studies indicating a more involved role of the CMEC in recognition memory without a spatial component (Sauvage et al., 2010).

12. c-Fos density

Mean c-Fos density was calculated for each ROI as the quantity of c-Fos marked nuclei per mm^2, normalized to the WT-Acquisition group. For Study n°2 the c-Fos density values were not normalized. The cell density was defined by the total number of c-Fos marked nuclei divided by the total area across all sections of the region. The cell density for each region was compared between genotypes. ROIs were grouped into region subfields whenever anatomically and functionally justified. These groupings reduced the number of comparisons and, thereby, restricted Type 1 errors. Three-way ANOVAs compared test-phases (acquisition or retention), genotypes (WT or dKI) and subregions for each subfield. When an interaction was significant, the simple effects were examined.

13. Functional Connectivity

A. Preamble

Many of the methods presented here were developed on the latest OP3h study with the arrival and help of Demian Battaglia. On the two preceding c-Fos experiments, the aging experiment and the OP5' experiment; I had developed my own functional connectivity analyses inspired by the study of Tanimizu et al., 2017. These simpler, more straight-forward analytical methods will be presented in tandem with the results of those experiments under Study n°2. There, I will also describe some problems concerning these methods and why we felt they needed to be changed in favor of those that will be described here, when it came to the OP3h study. Moreover, we have chosen not to carry out the updated analysis on the aging or OP5' c-Fos data due to some problematic considerations related to the 5-minute ITI and c-Fos derived functional connectivity. This will also be discussed under Study n°2.

B. Generating functional networks as fully connected weighted graphs

From the c-Fos signals, functional connectivity was assessed by computing the across mice inter-regional Spearman correlations (see ***Figure 27A***) (Wheeler et al., 2013) for each Genotype-Phase group. Spearman correlations, rather than Pearson correlations, were used to account for potential outlier effects and the relatively small sample sizes. Correlation matrices were used to visualize all possible pairwise inter-regional correlations within each group. To assess global

functional connectivity strength, the mean r value was computed from each matrix. This was computed from matrices with conserved negative correlation coefficients, near-zeroed negative correlation coefficients and absolute correlation coefficients. In the near-zeroed case, the negative correlations were transformed into a value of .006 the smallest positive value observed. This interprets negative correlations as very weak but possible avenues for information transfer.

From each correlation matrix, a functional network was generated as a fully connected weighted graph. The edge weights of the graph reflect inter-regional correlation strengths and the nodes reflect regions. Negative correlations can be interesting, but are unfortunately very difficult to interpret and implement with many graph theory analyses. For our analysis, negative correlations were interpreted as open but difficult paths for information transfer, in essence similar to a very weak positive correlation. Therefore, in the construction of functional networks, all negative correlations were given a small edge weight of .006, the smallest positive correlation that was observed. All graph construction and graph analysis was done through the igraph (Csardi G and Nepusz T, 2006) package on R (R Core Team, 2017), unless otherwise noted.

C. Bootstrapping confidence intervals

For all network metrics, 95 % confidence intervals were computed by bootstrapping (***Figure 27A***) (Wheeler et al., 2013, Epskamp et al., 2017). Bootstrapping involves resampling subjects with replacement 10000 times and each time regenerating a functional network, then recalculating the measure of interest. Confidence intervals for the differences between network metrics were also bootstrapped to evaluate differences between groups. Groups were considered different to a $P<.05$ if the 95 % confidence interval for the difference ≥ 0, and to a $P<.01$ if the 99 % confidence interval for the difference ≥ 0. The bootstrapping workflow is demonstrated in ***Figure 27B***.

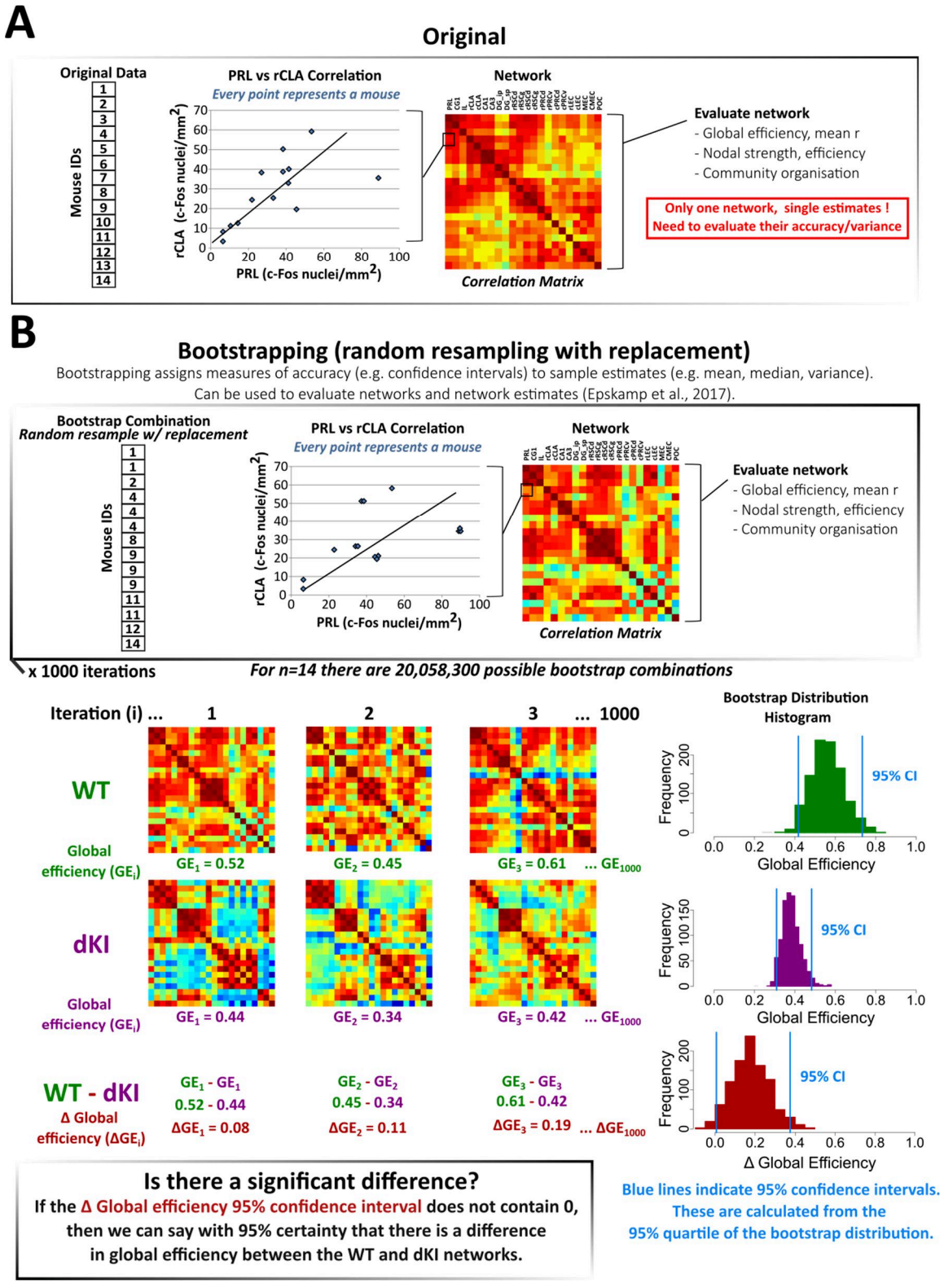

Figure 27. Bootstrapping functional networks. (A) Generate a functional network through across-mice inter-regional correlations. (B) Evaluate the accuracy of network estimates based on variance across mice through bootstrapping.

D. Community Analysis

Communities were detected through modularity maximization across all possible community partitions. Networks with high modularity have strong connections between the nodes within communities and relatively weaker connections between nodes in different communities. Allegiance matrices were used to assess community stability across bootstraps, by depicting the percentage of bootstraps that contain any given pair of regions within the same community.

E. Information Flow Concepts

Functional networks may be viewed as models of information flow between and across regions. We can consider information flow across the network at large, in essence how efficiently can information from any random point of the network reach any other point. This can be computed as a network's global efficiency. It is important to note that even if a network has reduced global functional connectivity strength (as computed from mean r), its global efficiency may rest un-affected if there are well placed "hub" regions to facilitate indirect communication.

To evaluate information flow at the regional level, node strength and nodal efficiency metrics may be used. Node strength measures the degree to which a region can exchange information directly with all other regions of the network. A region with low strength may still be able to communicate with its network indirectly, again through hub regions. This indirect communication can be measured using nodal efficiency. Organization of information flow in a network can be examined through strength and efficiency distributions. Regions with higher strength and efficiency can be considered to contribute more to their network. High strength is also shown to describe potential hub regions (Vetere et al., 2017) which, as we have described, are needed to facilitate indirect information flow and maintain global efficiency. These concepts are visualized in ***Figure 28***.

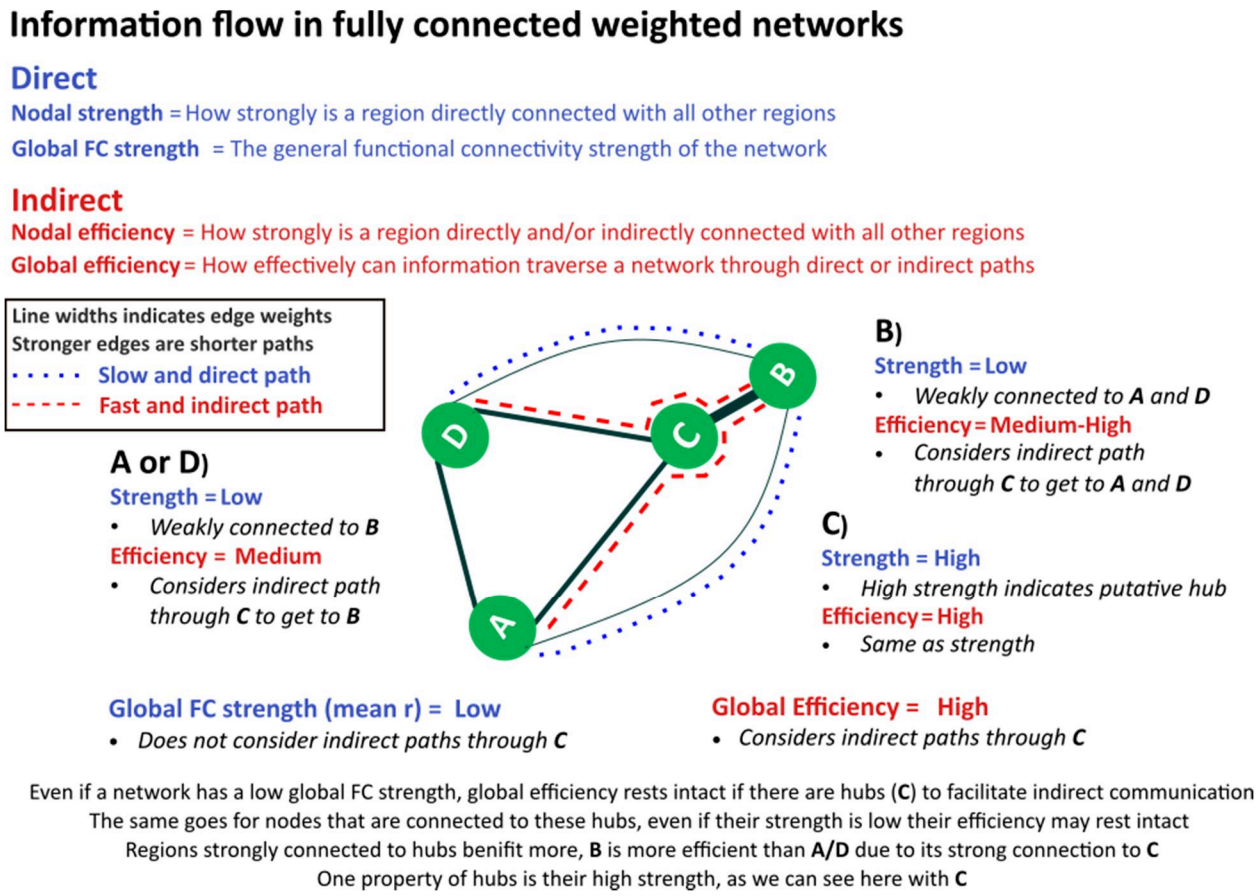

Figure 28. *Information flow in a fully connected network. FC: functional connectivity*

F. Information Flow Quantification

Global efficiency was calculated as the average inverse shortest path length. Edge lengths were calculated as the inversed edge weights. Node strength measures the degree to which a region is directly connected to all other regions of the network. This is traditionally calculated as the sum of its edge weights. In a fully connected graph this is directly proportional to the mean of its edge weights. The mean was used in our case for better comparison with nodal efficiency. Nodal efficiency measures the ease of information exchange between a region and its network, whether through direct or indirect routes. It is calculated as the average inverse shortest path length between the region and all other regions of the network. These calculations are visualized in ***Figure 29***.

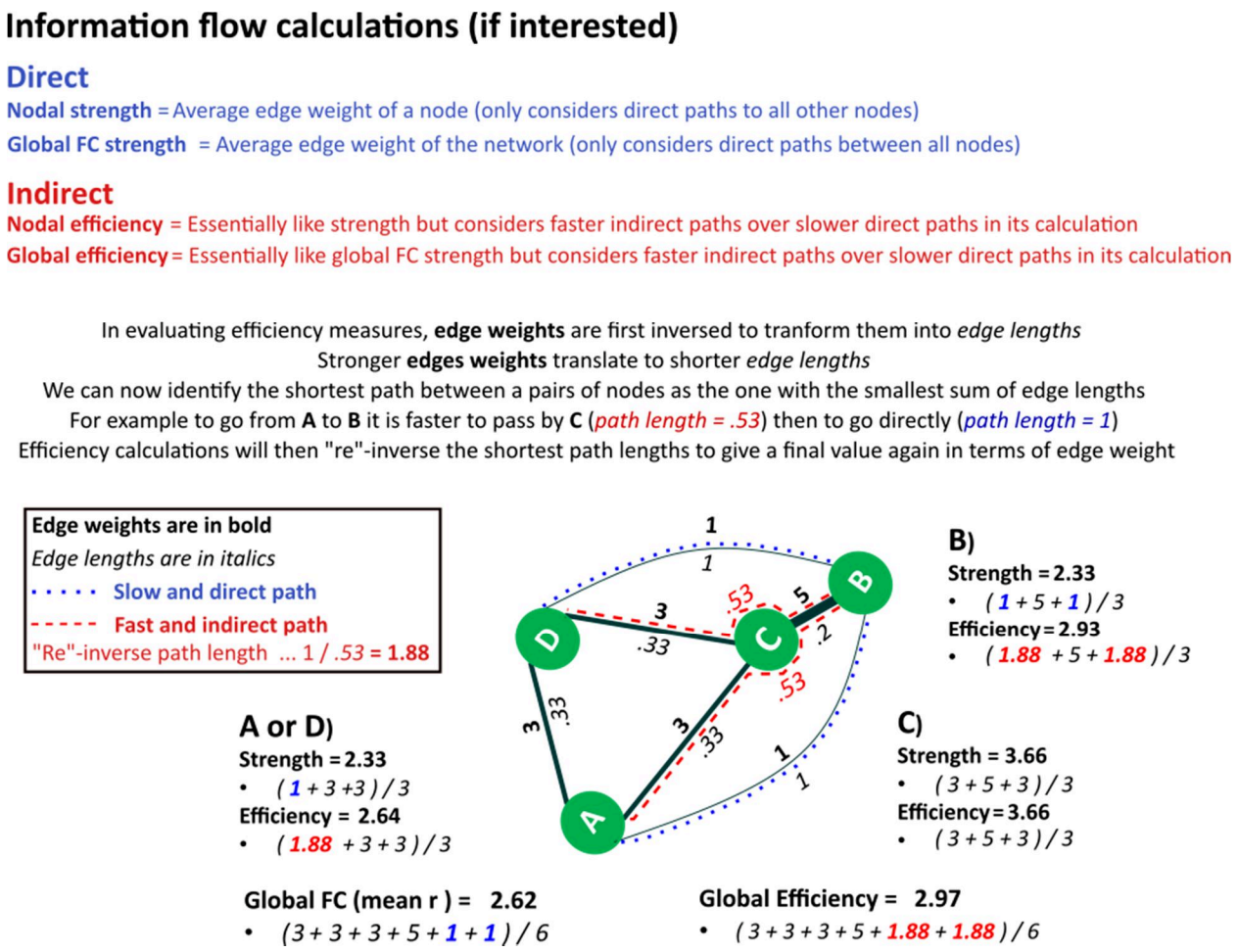

Figure 29. *Information flow calculations. FC: functional connectivity*

G. Assessing the impact of network efficiency on memory deficits

Finally, we were curious if a reduction in network efficiency could directly account for the reduction of OP memory performance in dKI mice. Our aim was thus to determine if a relationship could be found between global efficiency and memory index in the WT and be used to predict dKI memory loss. This relationship was assessed through correlation testing across sub-sampled WT populations, where each sub-sample corresponded to the removal of one mouse. Sub-samples were generated from each retention group by resampling n-1 mice without replacement (***Figure 30***). This procedure generates a set of sub-samples of size n-1, where the number of sub-samples equals the number of mice. From each subsample, the average memory index and the resulting network global efficiency were computed. Correlation significance between memory index and global efficiency was computed through both Pearson and Spearman correlation coefficients.

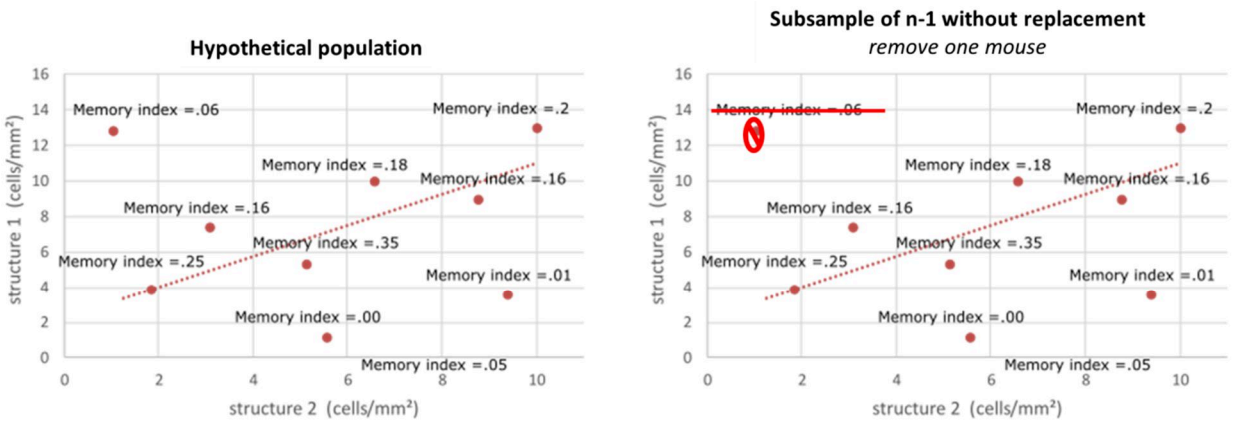

In this hypothetical population, we see that the mice with higher memory indices lie closer to the line of best fit. They contribute more to this correlation and may contribute more to the functional network at large.

In order to evaluate the contribution of memory index to FC, we remove one mouse. We calculate the average memory index and global efficiency from the resulting subsample. Then we assess the relationship between the memory index and global efficiency across all possible n-1 sized subsamples.

Figure 30. *Assessing the relationship between network efficiency and memory through n-1 subsampling.*

Later, we noticed that maybe an object exploration dependent disruptive effect exists on memory driven network efficiency. To evaluate this, we computed an exploration adjusted memory index. To compute the exploration adjusted memory index, first the exploration index was computed for each mouse as total time exploring both objects normalized to the group average.

$$\text{Exploration Index (EI)} = \frac{\text{Time exploring both objects}}{\text{Average time exploring both objects}}$$

The exploration adjusted memory index was then defined as the memory index divided by the exploration index.

$$\text{Exploration adjusted memory index (MI/EI)} = \frac{\text{Memory Index (MI)}}{\text{Exploration Index (EI)}}$$

To assess the significance of the intersection of the WT linear fit with the dKI subsample population, 1000 randomly fit linear models to the WT were generated by permuting the y labels of the WT subsample population and recalculating the best fit line each time. The mean absolute error to the dKI subsamples was calculated for each random model and their distribution is presented as a histogram. The bias corrected and accelerated confidence interval (DiCiccio et al., 1996) was computed from this distribution, and compared to the dKI mean absolute error to the original WT fit.

14. Electrophysiological interrogation of CLA->PFC projections

A. Purpose

Across both OP c-Fos studies, Study n°2 with the 5-minute ITI and Study n°3 and 3-hour ITI, we detected hyper-activity in the CLA. Another consistent result across the two OP c-Fos studies is the functional perturbation of the mPFC (hyperconnective in OP5', hypoconnective in the OP3h retention phase). The consistent functional perturbation of this region pair led us to consider evaluating the CLA->mPFC connection more closely. The CLA induces feed forward inhibition on the mPFC through direct glutamatergic action on mPFC interneurons (Jackson et al., 2017). Early stage network abnormalities in AD are shown to be linked to interneuron dysfunction (Palop and Mucke., 2016). Through investigating the CLA to PFC circuit we may also investigate how interneruron dysfunction directly affects interregional communication in early AD. We decided to interrogate the CLA->mPFC circuit using viral targeting and in-vivo electrophysiological recording of anesthetized mice. Male and female dKI and WT mice were tested in order to evaluate genotype and gender effects.

B. Viral Injections

Anesthesia was induced in mice with 3' of 4% isofluorane exposure. The mice were attached to the stereological apparatus and anesthesia was maintained with isofluorane exposure held between 1 and 1.5%. The head was shaved with scissors and the scalp was wiped with 70% alcohol. The scalp was injected subcutaneaously with 2mg/kg of lurocaine to induce local anesthesia, and subcutaneously with 0.5mg/ml-0.07ml per mouse metacam to reduce inflammatory responses. The eyes were covered with a Dulcis cream (vitamin A) to keep them hydrated. The skin was incised with a sterile scalpel and the skull was wiped with 70% alcohol, and then 0.9% NaCl solution.

The CLA->mPFC circuit was targeted through the injection of two viruses. The viruses were injected using Hamilton syringes (Hamilton syringe 85 RN) with a 33 gauge needle (.21 mm diameter). An AAVretro-syn-Cre was injected into the PFC at coordinates (AP: +1.75mm, ML: +0.50, DV: 0.70 in respect to bregma). A pAAV5-Ef1a-DIO-ChETA-EYFP was injected into the CLA at coordinates (AP: +1.25mm, ML: +2.50, DV: 2.50 in respect to bregma).

C. Electrophysiological Recordings

All steps leading up to incision of scalp were identical to those of the viral injections. A four shank silicon probe (NeuroNexus, model A4x4.3mm-50-125-177) was lowered to 0.25mm above the injection site of the PFC (AP : +1.75mm , ML : +0.50, DV : 0.50 in respect to bregma) and the optical fiber (specs, diameter power) was lowered to 0.10mm above the injection site of the CLA (AP : +1.25mm , ML : +2.50, DV : 2.40 in respect to bregma). After the probe and optical probe were in place the isofluorane flow was reduced to .9%. During a light pulse train (473 nm) the CLA was stimulated with 5ms long light pulses every 5 seconds for 200 seconds (protocol adapted from the study of Jackson et al., 2017), during which the mPFC was recorded at 20 kHz sampling rate. After each light pulse train the electrical probe was descended another 0.3 to 0.5 mm or until more active neurons were detected, and another pulse train was recorded. The PFC was recorded between DV 0.50mm and 1.70mm from bregma, corresponding to the anterior cingulate cortex, prelimbic cortex and infralimbic cortex. If neuronal activity was sparce the probe was removed and its position was changed along the anterior-posterior and/or medial-lateral axis.

Experimental Contributions

Study n°1

Behavioral phenotyping of the *App^{NL-F}xMAPT* double knock in mouse model of Alzheimer's disease and its single KI derivatives

Christopher Borcuk[1], Céline Héraud[1], Karine Herbeaux[1], Julien Caillette[1], Saito T[2], Hashimoto S[2], Saido T[2], Romain Goutagny[1], Chantal Mathis[1]

1 - Laboratoire de Neurosciences Cognitives et Adaptatives (LNCA), Université de Strasbourg, Faculté de Psychologie, 12 rue Goethe, F-67000 Strasbourg, France.

2 - Laboratory for Proteolytic Neuroscience, RIKEN Center for Brain Science, 2-1 Hirosawa, Wako-city, Saitama 351-0198, Japan

Complementary study

1. Scientific context and objectives

Fine mnemonic discrimination (pattern separation) and associative memories, are shown to be affected during preclinical stages of AD (Parra et al., 2010; Sinha et al., 2018), and occur in tandem with the early apparition of amyloid and tau biomarkers (Rentz et al., 2011, Sanabria et al., 2018; Berron et al., 2019; Maass et al., 2019).

The first objective of my thesis was to characterize early recognition memory loss in the dKI mouse model of AD. This mouse model expresses humanized FAD mutated App^{NL-F} and humanized *MAPT* genes under endogenous promoters. These gene inserts lead to an increased $A\beta_{42}/A\beta_{40}$ ratio and the expression of all six human isoforms of tau, respectively. Sensitive recognition memory performance was assessed in mice using versions of the spontaneous object exploration paradigm. Before the dKI had been developed, a rough characterization of a limited number of 6 and 10 month old mice from the App^{NL-F} and *MAPT* single KI lines was carried out to detect potential memory decline specific to isolated amyloid or tau pathologies. These animals were the surplus produced at different steps during the breeding process to obtain the dKI mice (see Material and Methods, ***Figure 20***). A preliminary phenotyping of dKI mice was carried out across 3 ages (2, 4, and 6 months) and across 4 different sensitive recognition memory tasks (long-term object recognition 24h ITI, fine discrimination object recognition 5-minute ITI, object-place association 5-minute ITI, fine discrimination object location 5-minute ITI). The earliest and most robust deficit (combination of age and task) was then validated with a second cohort. This second cohort was also perfused for c-Fos immunohistochemical staining to evaluate task-dependent changes in neural activity. This c-Fos analysis will be presented in Study n°2. Finally a third cohort was tested at the same age and in the same task, except with a 3-hour ITI. This was done to increase the specificity of c-Fos imaging for a more careful assessment of test-phase specific changes in neural activity and functional connectivity. This last c-Fos analysis will be presented in Study n°3.

In addition to recognition memory, dKI mice were also tested with actigraphy and the light-dark box, to assess locomotor/sleep-wake activity which is known to be affected in AD (Wang and Holtzman, 2020) and anxiety like behaviors which can interfere with object exploration, respectively. Finally, an object in context task taxing another form of associative memory was developed and validated on WT mice for future behavioral assessment with the dKI mice.

A. Phenotyping of single KI mice wih sensitive recognition memory tasks

WT, *App*$^{NL-F}$ and *MAPT* single KI mice were tested at 6 months in the object recognition task (OR5'), the fine discrimination object recognition (FDOR5'), the object-place task (OP5'), the object location task (OL5') and the fine discrimination object location (FDOR5') task across two cohorts. When both objects were explored less than 2 seconds during the test trial, data were removed from the analysis because duration of exploration for each object was considered to small to be relevant (*see* ***Table II***). At 6 months of age, WT mice did not have a good performance in the OR task (not significantly different from chance level). In both spatial tasks, OL and FDOL, neither single KI line explored above chance level, but they had highly variable performance (***Figure 31A***) (one sample t-test, against chance (0): WT-OR5' $t(6) = 2.03$, $P = 0.09$; *MAPT*-OL5' $t(7) = 1.457$, $P = 0.19$; *App*$^{NL-F}$-OL5' $t(6)=1.511$, $P = 0.18$; *MAPT*- FDOL5' $t(7)=2.079$, $P = 0.08$; *App*$^{NL-F}$- FDOL5' $t(6)=0.3885$, $P = 0.71$). At 10 months of age, the number of tasks was reduced as we noticed that the mice became stressed after too many testing days. Only the FDOR5', OP5', and a new long-term object recognition with a 24-h delay (OR24) tasks were performed on both cohorts. The *App*$^{NL-F}$ presented a consistent deficit, not exploring above chance level on any of the three tasks (***Figure 31B***) (one sample t-test, against chance (0): *App*$^{NL-F}$-FDOR5' $t(6)=1.151$, $P = 0.29$; *App*$^{NL-F}$-OP5' $t(6)=1.664$, $P = 0.15$*App*$^{NL-F}$-OR24 $t(6)=1.831$, $P = 0.12$). Significance was assessed without taking into account multiple comparisons corrections. No between group differences were detected with one way ANOVAs.

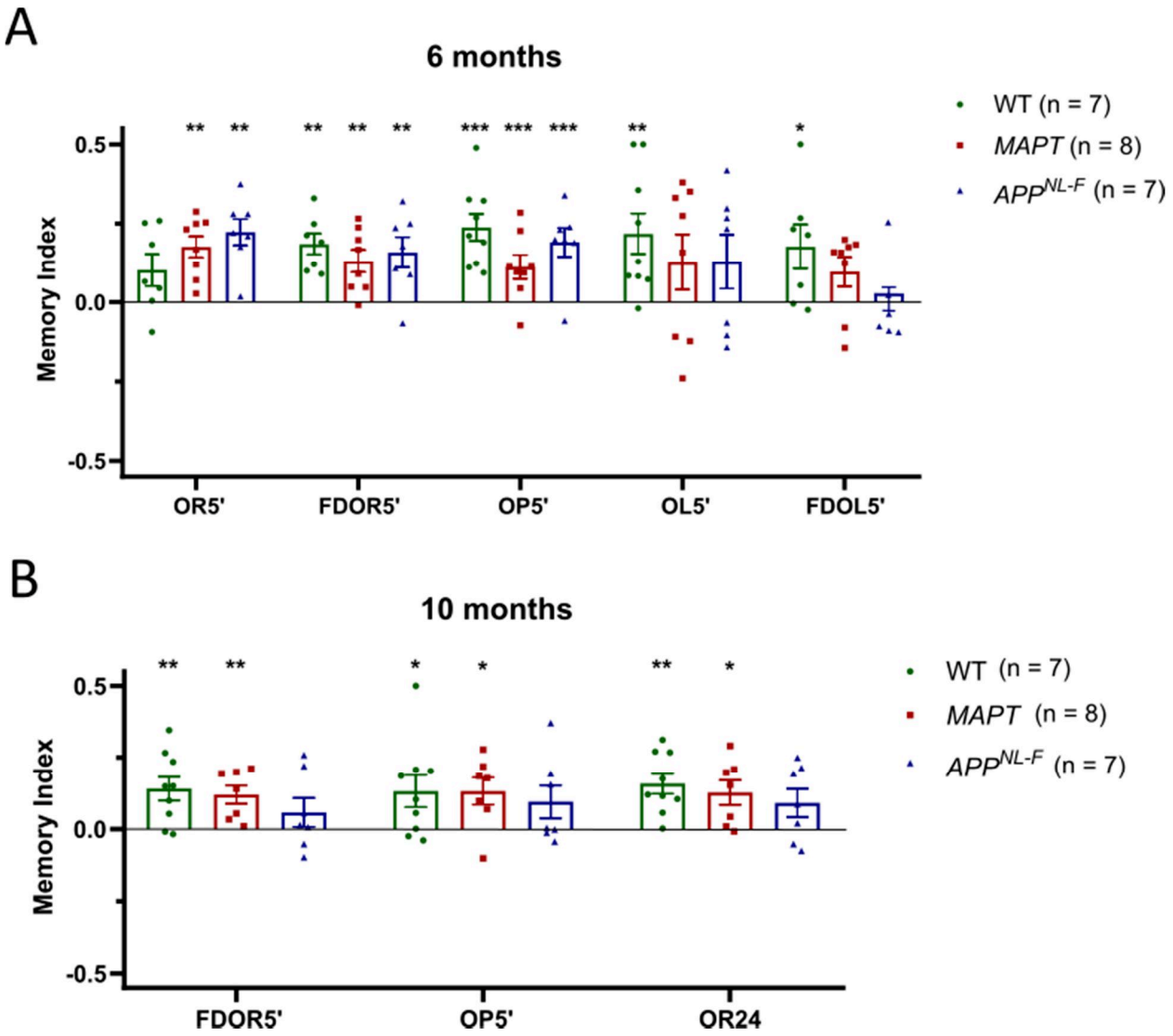

Figure 31. *Phenotyping of single KI mice at (A) 6 and (B) 10 months in the object recognition (OR5'), fine discrimination object recognition (FDOR5'), object place association (OP5'), fine discrimination object location (FDOL5'), and long-term object recognition (OR24) tasks. Bar graphs represent the mean (± SEM). * p<0.05, ** p<0.01, *** p<0.001 (one sample t-test against 0, no multiple comparisons corrections).*

Cohort	Geno	Age (mo)	Souris	OR5'	FDOR5'	OP5'	OL5'	FDOL5'	OR24
1	WT	6	4001	NA	NA	0.3221437	0.08482143	NA	NA
1	WT	6	2008	0.0663105	0.12021858	0.48897994	0.5	0.26715686	NA
1	WT	6	4006	0.25882705	NA	0.09430605	0.25241158	0.23245614	NA
1	WT	6	4015	NA	0.32969432	0.26899696	0.5	0.5	NA
1	WT	6	37	0.18264014	0.21268657	0.11125541	0.12882096	-0.02397661	NA
1	*MAPT*	6	2001	0.0279299	0.04796512	0.22691934	-0.10902256	-0.144081	NA
1	*MAPT*	6	4020	0.25290897	0.04957905	0.0959596	0.33151635	0.17509728	NA
1	*MAPT*	6	4021	0.16695577	0.1981383	-0.07295374	0.37990762	-0.07962697	NA
1	*APP*$^{NL-F}$	6	4004	0.20938023	0.31990521	0.19824163	0.232665	-0.0995	NA
1	*APP*$^{NL-F}$	6	4000	0.37381703	0.24887892	-0.05882353	0.2979798	NA	NA
1	WT	10	4001	0.5	0.14984227	0.5	0.08198381	0.17281106	0.10520095
1	WT	10	2008	0.23934426	0.05403868	0.05625	0.18310727	0.24010327	0.26853933
1	WT	10	4006	0.13839286	0.0997807	0.10402685	0.3940754	0.31980602	0.27104606
1	WT	10	4015	0.12365591	-0.01714286	0.18654646	0.24846626	-0.06587615	0.05715219
1	WT	10	37	0.09843546	0.15065502	0.2029703	0.19338959	0.33297414	0.31199539
1	*MAPT*	10	2001	0.26201244	0.19933185	0.17874016	0.15716487	-0.23340708	0.19798658
1	*MAPT*	10	4020	0.27287066	0.01051304	0.06981407	0.25747283	-0.00979592	0.15491302
1	*MAPT*	10	4021	0.20819672	0.05445545	0.27798742	0.08671171	0.18831169	-0.0078219
1	*APP*$^{NL-F}$	10	4004	0.29324895	0.00706215	0.15661861	-0.03478964	0.1961367	0.02064516
1	*APP*$^{NL-F}$	10	4000	0.18514056	0.01420176	-0.04392971	0.0503212	0.05947955	0.19350474
2	WT	6	4172	0.00520548	0.24871355	0.32571732	-0.01932203	0.05416013	NA
2	WT	6	4175	0.25197722	0.09011628	0.2112069	0.08294931	NA	NA
2	WT	6	4195	0.04482531	0.1904918	0.12325863	0.07295374	-0.00460405	NA
2	WT	6	4197	-0.09431138	0.1	0.19007804	0.35514834	0.21341463	NA
2	*MAPT*	6	4172	0.07081729	0.26590909	0.04492415	0.27388535	0.15901361	NA
2	*MAPT*	6	4175	0.2495919	0.16749073	0.11266447	-0.12249208	0.15806452	NA
2	*MAPT*	6	4195	0.23143351	-0.00928793	0.28461538	0.35096154	0.12448133	NA
2	*MAPT*	6	4197	0.28745098	0.23732252	0.09423077	-0.2397351	0.19892473	NA
2	*MAPT*	6	4198	0.12004405	0.09020852	0.11367089	0.15764448	0.18292683	NA
2	*APP*$^{NL-F}$	6	4129	0.27990654	0.08858414	0.18944724	-0.06418384	-0.07638889	NA
2	*APP*$^{NL-F}$	6	4159	0.17589679	0.1772451	0.33866995	0.41794872	0.1173913	NA
2	*APP*$^{NL-F}$	6	4162	0.22047108	0.10836084	0.23076923	0.2672956	-0.09	NA
2	*APP*$^{NL-F}$	6	4208	0.01851852	-0.06708861	0.19729454	-0.14273601	0.34751204	NA
2	*APP*$^{NL-F}$	6	4226	0.28	0.23634812	0.23831776	-0.10423453	-0.03672986	NA
2	WT	10	4127	NA	0.26658906	0.20723307	NA	NA	0.12043344
2	WT	10	4134	NA	-0.0083089	-0.02427184	NA	NA	0.00193611
2	WT	10	4171	NA	0.2349481	-0.03887114	NA	NA	0.11632948
2	WT	10	4205	NA	0.34574231	0.00165798	NA	NA	0.17653352
2	*MAPT*	10	4172	NA	0.03435732	0.09861407	NA	NA	0.29136691
2	*MAPT*	10	4195	NA	0.21109083	0.21847247	NA	NA	0.04354047
2	*MAPT*	10	4197	NA	0.19383416	0.18596352	NA	NA	0.00921659
2	*MAPT*	10	4198	NA	0.14032567	-0.10099133	NA	NA	0.2080854
2	*APP*$^{NL-F}$	10	4129	NA	0.05621845	0.00455063	NA	NA	-0.0758226
2	*APP*$^{NL-F}$	10	4159	NA	-0.09758551	-0.00135062	NA	NA	0.24982382
2	*APP*$^{NL-F}$	10	4162	NA	0.22020725	0.37118084	NA	NA	0.21398155
2	*APP*$^{NL-F}$	10	4208	NA	-0.05154251	-0.01275168	NA	NA	-0.05154251
2	*APP*$^{NL-F}$	10	4226	NA	0.25916749	0.19430625	NA	NA	0.08706697

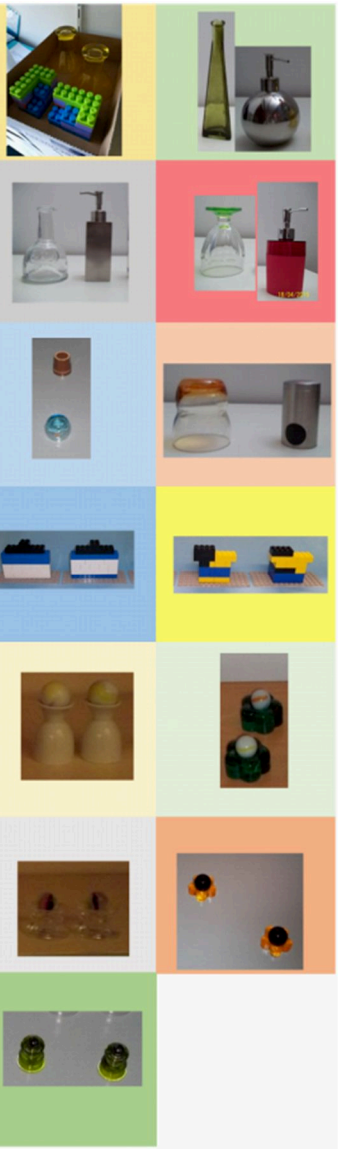

Table II. *Identities of single KI mice that were tested at 6 months and 10 months in the object recognition (OR5'), fine discrimination object recognition (FDOR5'), object place association (OP5'), fine discrimination object location (FDOL5'), and long-term object recognition (OR24) tasks across two cohorts. The numbers indicated in the task columns are the memory indices for each mouse. The various objects that were tested for different paradigms are indicated by the color code. The 10 month old mice in the second cohort were only tested on 3 tasks as we noticed that too many tasks was stressful to the mice. Mice that explored both objects less than 2 seconds during the retention trial were excluded from the analysis.*

B. Preliminary phenotyping of the dKI with sensitive recognition memory tasks

Sensitive object recognition paradigms were carried out at 2 months (WT n = 11, dKI N = 10), at 4 months (WT n = 12, dKI n = 9) and at 6 months (WT n = 8, dKI n = 11). Mice were removed from the analysis if they explored both objects less than 2 seconds. In the OR24 task, dKI mice showed no deficits (***Figure 32A***). In the FDOR5' task the dKI mice were highly variable making it so that they were not significant against chance at any age (one sample *t*-test, against chance: all dKI ts<.996, ps>0.055) (***Figure 32B***). However, between group significance was only obtained at 6 months of age (WT vs. dKI: t(17) = 2.364, P = 0.03). This variability may represent a variety of factors including perhaps affected DG neurogenesis (Scopa et al., 2020). The earliest significant deficit in dKI mice appeared at 4 months in the OP5' task (two sample *t*-test, WT_4mo vs. dKI_4mo: t(20) = 2.325, P = 0.03; one sample *t*-test, against chance: dKI t(8) = 0.2086, P = 0.84) (***Figure 32C***). This deficit which was conserved at 6 months (two sample *t*-test, WT_6mo vs. dKI_6mo: t(17) = 2.132, P = 0.047; one sample *t*-test, against chance: dKI t(10) = 0.7196, P = 0.49). Although the reduced performance of dKI mice in the FDOR may be interesting, dKI's performance showed too much variability. Therefore, we chose to continue our study with the more robust OP5' deficit. As shown in ***Figure 32D***, all groups including WT's were highly variable in the FDOL5', and the results were largely inconclusive with only the 2 month old WT mice exploring above chance level (one sample *t*-test no multiple comparisons correction, against chance (0): WT-2mo t(9)=2.608, P = 0.028).

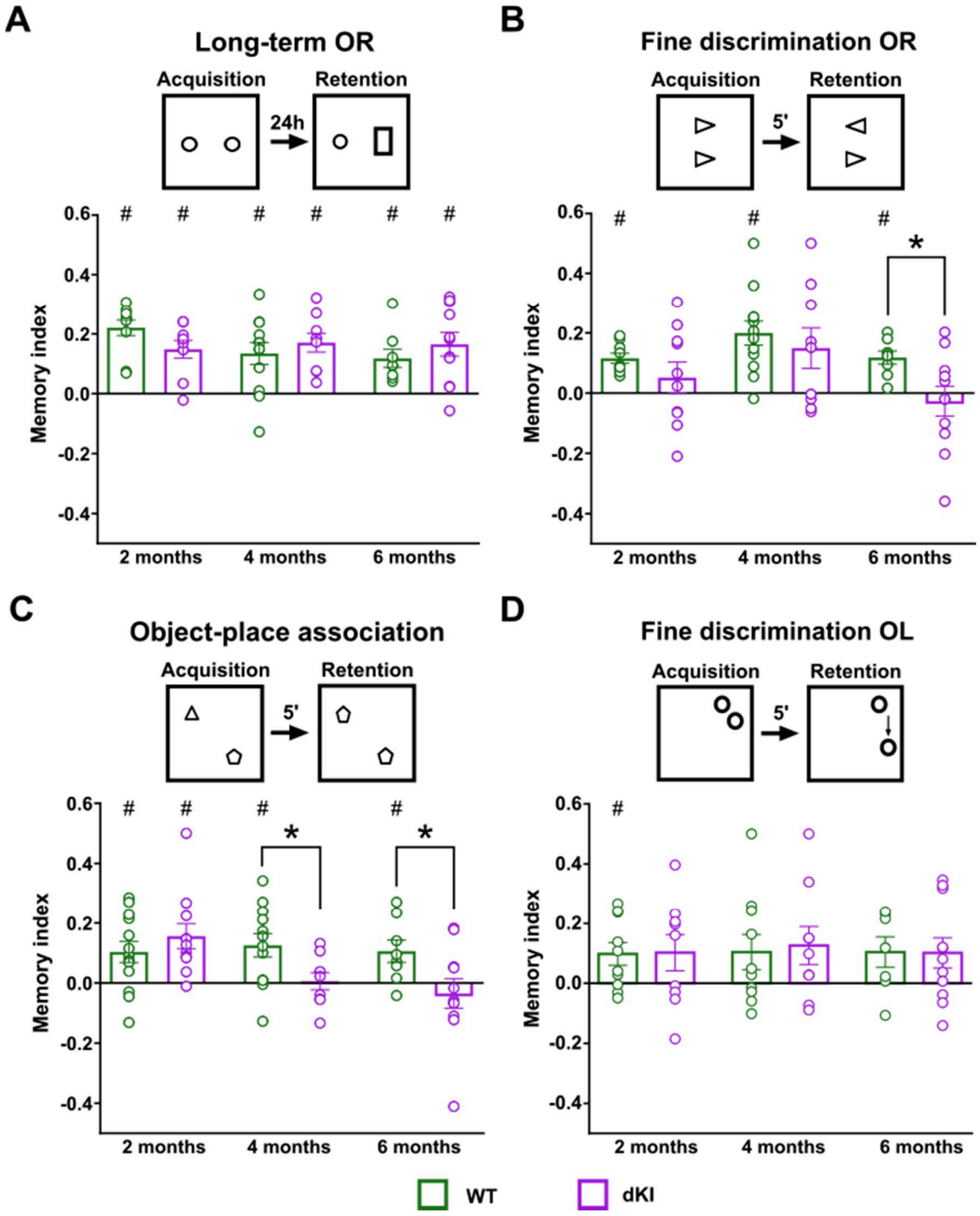

*Figure 32. Preliminary phenotyping of young dKI mice in the (A) long-term object recognition (OR24), (B) fine discrimination object recognition (FDOR5'),(C) the object place association (OP5'), and the fine discrimination object location (FDOL5') tasks at 2 months (WT n = 11, dKI n = 10), 4 months (WT n = 12, dKI n = 9) and at 6 months (WT n = 8, dKI n = 11). Mice were removed from the analysis if they explored both objects less than 2 seconds. Bar graphs represent the mean density (± SEM). difference between genotypes *p<.05 (two sample t-test); difference from chance, #p<.05 (one sample t-test). No multiple comparisons corrections were performed for these preliminary comparisons.*

C. Validating the OP5' deficit for c-Fos analysis, in tandem with OR5' and OL5'

A second cohort of young dKI mice (WT n = 11, dKI n = 11) was tested in the object-place association task (OP5') task at 4 months of age to validate the potential deficit seen during preliminary phenotyping and for evaluation of OP5' dependent c-Fos expression. Short-term object recognition (OR5') and object location (OL5') tasks were evaluated in parallel. We confirmed that dKI mice were unable to detect a new OP association at 4 months of age (***Figure 33A***) (two sample t-test, WT vs. dKI: $t(20) = 2.85$, $P = 0.0098$; one sample t-test, against chance: dKI $t(10)=0.3095$, $p = 0.763$). On the other hand, 4-month-old mice did not show any deficits in OR5' (***Figure 33B***) (two sample t-test, WT vs. dKI: $t(19) = .0934$, $P = 0.9265$; one sample t-test, against chance: all $ts>3.94$, $ps<0.003$) or OL5' (***Figure 33C***) (two sample t-test, WT vs. dKI: $t(20) = 1.052$, $P = 0.9173$; one sample t-test, against chance: all $ts>3.03$, $ps<0.013$). These results confirmed that the OP deficit was due to specific perturbations in associative memory rather than any separate impairments in the object recognition or spatial recognition.

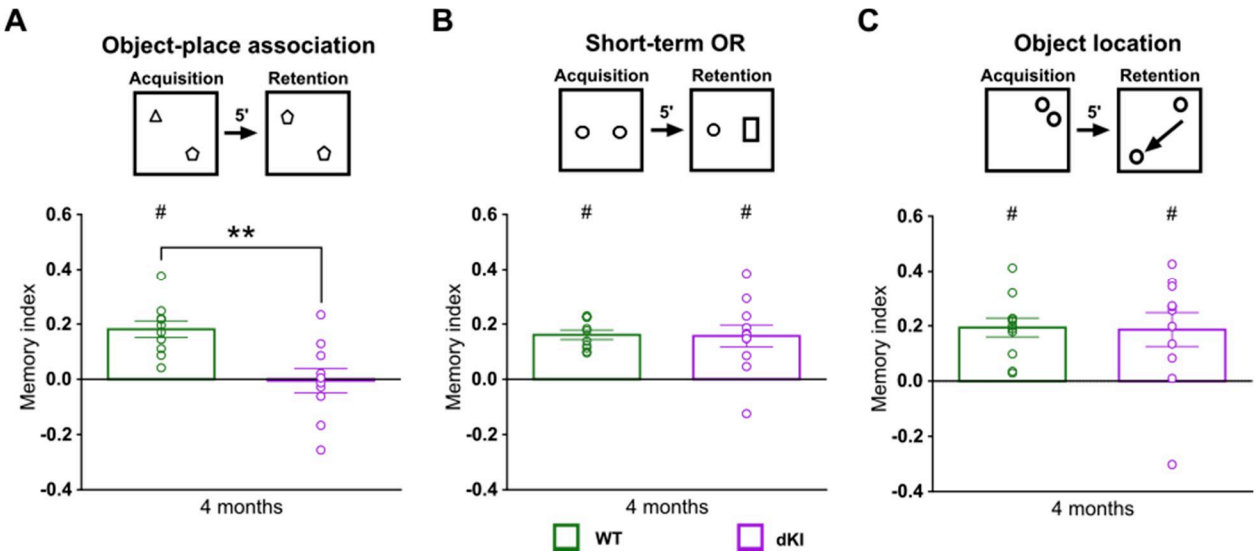

Figure 33. *Behavioral results of the second cohort (WT n = 11, dKI n = 11) tested in the (A) object-place association (OP5'), (B) object recognition (OR5') and (C) object location (OL5') tasks. Bar graphs represent the mean (± SEM). difference between genotypes *p<.01 (two sample t-test); difference from chance, #p<.05 (one sample t-test).*

D. Validating an OP3h deficit for c-Fos analysis, in tandem with OL3h

A final cohort of young dKI mice were tested in the object-place association task with a 3 hour ITI task (OP3h) to conduct a more careful assessment of OP dependent c-Fos expression during each test-phase, acquisition (WT n = 12, dKI n = 12) and retention (WT n = 14, dKI n = 14). The object location task with a 3 hour ITI (OL3h) was evaluated in parallel, and worked as a pre-OP3h habituation to both test-phase groups (OP3h acquisition and retention combined, WT n = 26, dKI n = 26). As with a 5-min ITI, dKI mice that underwent the retention phase after a 3-h ITI were likewise unable to detect the novel OP association (***Figure 4A***) (two sample t-test, WT vs. dKI: t(26) = 3.14, P = 0.004; one sample t-test, against chance: WT t(13) = 3.93, P = 0.002; dKI t(13) = 0.139, P = 0.891). The dKI group did not have any deficit in the OL3h task, indicating that spatial recognition memory after a 3 hour ITI was still intact (***Figure 4B***) (two sample t-test, WT vs. dKI: t(49) = .0882, P = 0.9297; one sample t-test, against chance: all ts>3.24, ps<0.002).

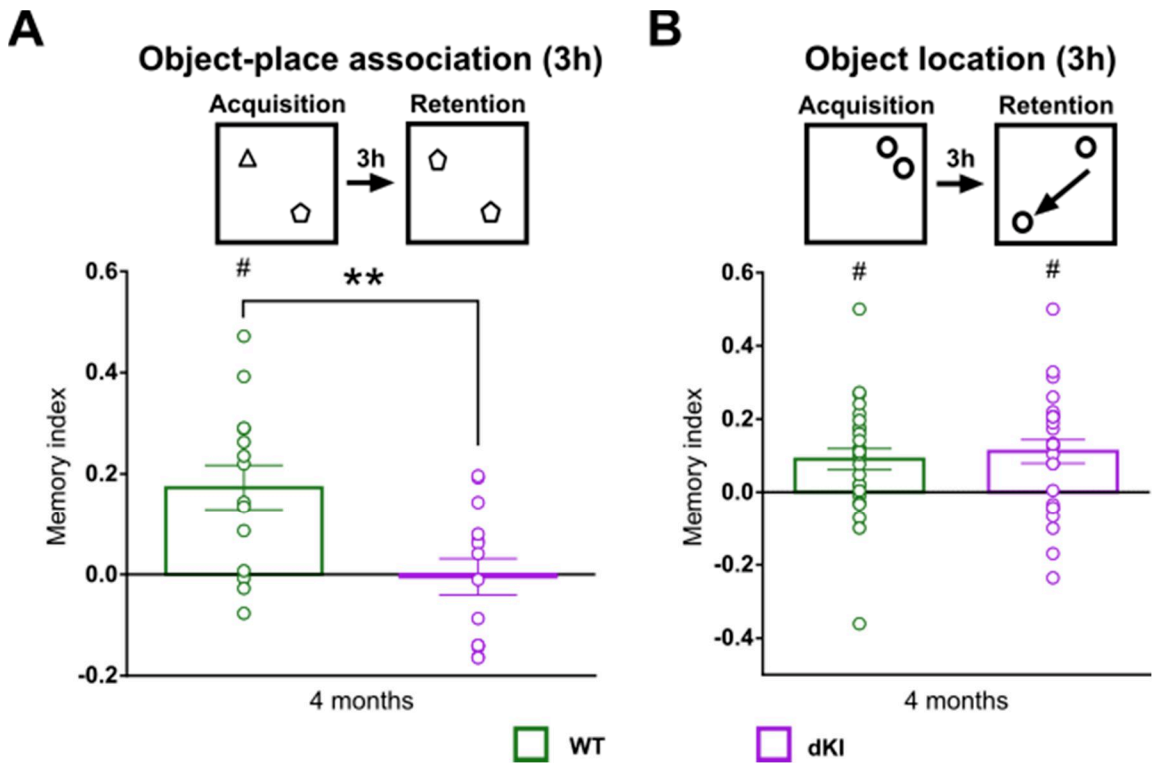

Figure 34. *Behavioral results of the third cohort tested in the object-place association with a 3 hour ITI (OP3h) (WT n = 14, dKI n = 14) and object location with a 3 hour ITI (OL3h) (WT n = 26, dKI n = 26) tasks. Bar graphs represent the mean (± SEM). difference between genotypes **p<.01 (two sample t-test); difference from chance, #p<.05 (one sample t-test).*

E. Actigraphy

A common symptom AD is sleep disturbance (Wang and Holtzman, 2020). We evaluated the sleep wake cycle and general locomotor activity in male WT (n = 8) and dKI (n = 8) mice using actigraphy. No differences were seen in male dKI mice compared to WT mice in any aspect of the sleep wake cycle (***Figure 35A***). The closest change that could be noted is the very slight tendency of increased locomotor activity during the night cycle (***Figure 35B,C***), though this is not significant.

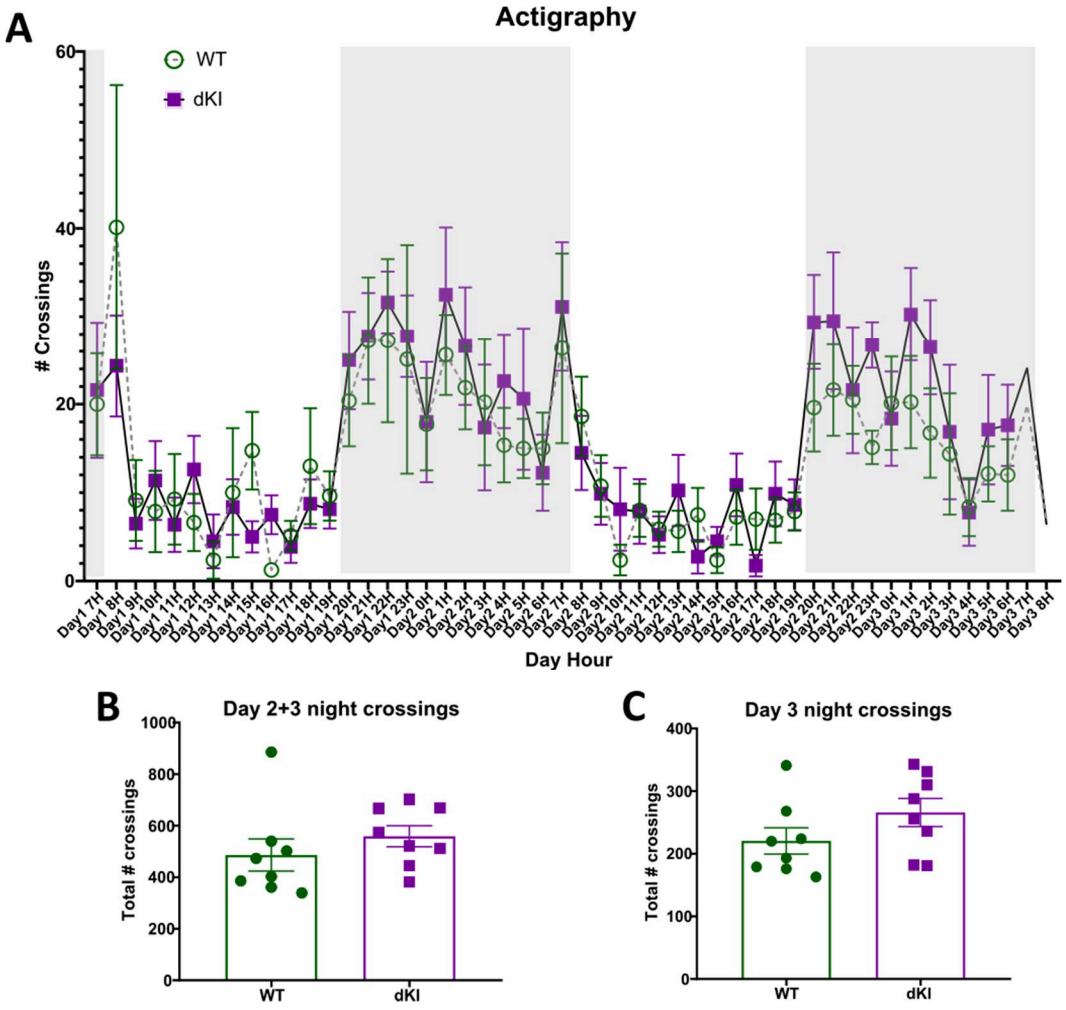

Figure 35. *Actigraphy of 4 month old male WT (n = 8) and dKI (n = 8) mice to evaluate locomotor activity. (A) The line plot depicts the average number of crossing per hour during 2 light cycles (white background) and 2 night cycles (grey background). A crossing was counted every time a mouse crossed both lasers consecutively (located at each end of the cage). An initial examination reveals a potential increase in locomotion in dKI mice during the night cycle. The total number of crossings was compared (B) during both night cycles combined and (C) during only the second night cycle. No significant difference was found in either case (two sample t-test). Bar graphs represent the mean (± SEM).*

F. Light-dark test

Anxiety like behaviors were evaluated in male and female WT (n = 8 for each gender) and dKI (n = 8 for each gender) mice using the light-dark box. Data were analyzed using two way ANOVAs for genotype and gender effects. Simple effects were considered if an interaction was significant. Transitions were evaluated as a measure of locomotion. A transition was counted every time the mouse transitioned between boxes. There was no change in transitions between genotypes or genders (***Figure 36A***). Time in the light box was used a measure of anxiety (or lack of). The dKI mice spent more time in the light box regardless of gender, indicating an anxiolytic phenotype (***Figure 36B***) (two way ANOVA, genotype effect: F (1, 32) = 6.484, P=0.0159; gender effect: F (1, 32) = 3.818, P=0.0595; interaction genotype x gender effect: F (1, 32) = 0.8035, P=0.3768). Latency to enter the light box was used as another measure of anxiety, or as a measure of impulsivity. There as a significantly lower latency in female mice regardless of genotype (***Figure 36C***) (two way ANOVA , genotype effect: F (1, 32) = 0.2357, P=0.6306; gender effect: F (1, 32) = 6.037, P=0.0196; interaction genotype x gender effect: F (1, 32) = 0.8774, P=0.3559).

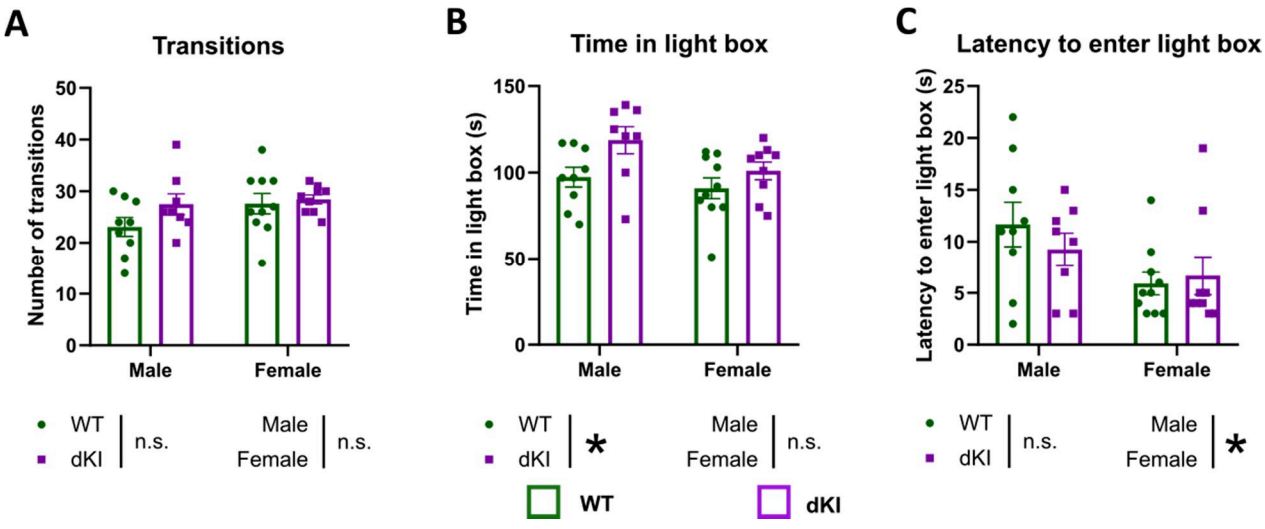

Figure 36. *Anxiety like behaviors were evaluated in male and female WT (n = 8 for each gender) and dKI (n = 8 for each gender) mice using the light-dark box. (A) Transitions were evaluated as a measure of locomotion. A transition was counted every time the mouse transitioned between boxes. There was no change between genotypes or genders. (B) Time in the light box was used a measure of anxiety (or lack of). The dKI mice spent more time in the light box regardless of gender (C) Latency to enter the light box was used as another measure of anxiety, or as a measure of impulsivity. There as a significantly lower latency in female mice across both genotypes. Bar graphs represent the mean (± SEM). * p<0.05, (two way ANOVA major effects, F)*

G. Object in context

Another task that evaluates associative memory is the object-in-context task (OiC). This task is shown to rely on similar structures to the object-place task, including the LEC and mPFC (Wilson et al. 2013a, 2013b; Chao et al., 2016). There are a few papers that have utilized this task, with varying protocols (Spanswick and Dyck, 2012; Lesburguères et al., 2017; Wilson et al. 2013a, 2013b; Chao et al., 2016). There is no real consensus as to the optimal "inter acquisition phase interval" or the "before retrieval interval" length to use. The main consideration for this is the aspect of temporal novelty, since one of the objects will appear before the other in time, in the acquisition phase order. This object will be more interesting to the mouse in terms of temporal novelty. In our preliminary study we wanted to reduce the effect of temporal novelty as much as possible. For this reason, a large disparity between the inter acquisition phase interval (5 minutes) and the before retrieval interval (24 hours) was chosen. This would also allow us to assess more long-term associative memory retention. Regardless, we wanted to verify that there was indeed a negligible effect of temporality. To this end, the group of ten mice was split into two subgroups. Half of the mice (n = 5) were exposed to a "novel object" that was also novel in time; exhibiting *cumulative* novelty of context and temporality. The other half (n = 5) were exposed to a "novel object" that was competing against the other object that itself was novel in time; what is termed here as *competitive* novelty.

In general, WT mice (n = 10) had robust performances, and the group as a whole explored the "novel object" linked to the novel object-context association comfortably above chance level (***Figure 37A***) (one sample t-test, against chance (0): WT $t(9)=4.749$, $P = 0.001$). When the group was split in half into *cumulative* and *competitive* novelty subgroups, the *cumulative* novelty group was revealed to explore significantly above chance level, but not the *competitive* novelty group (***Figure 37B***) (one sample t-test, against chance (0): *cumulative* $t(4)=4.45$, $P = 0.0112$; *competitive* $t(4)=2.589$, $P = 0.0608$). This could reflect the small n = 5. Neither group was significant against chance with the non-parametric Wilcoxon signed-rank test, due to the insufficiently large n = 5. There was no significance between subgroups as evaluated with the two sample t-test or the Mann Whitney U test.

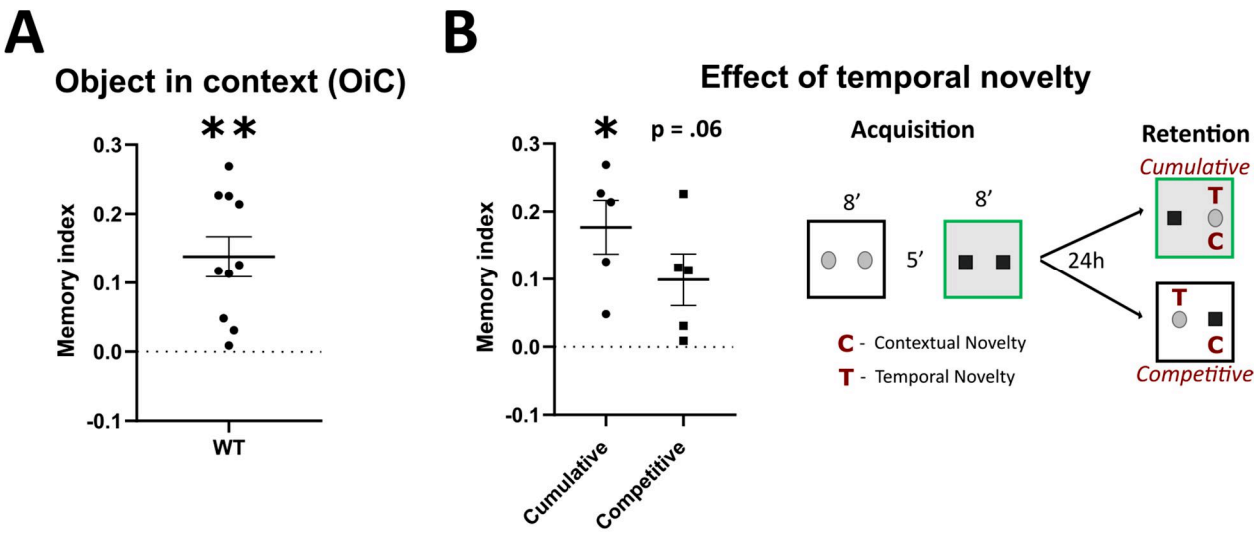

Figure 37. *The object in context (OiC24) was mise en place on WT mice (n = 10) in preparation for testing with dKI mice. (A) WT mice had generally strong memory performances, exploring the "novel object" linked to the novel object-context association comfortably above chance level. The group of ten mice was split into two conditions. (B) Half of the mice (n = 5) were exposed to a "novel object" that was also novel in time; the object had cumulative novelty in context and temporality. The other half (n = 5) were exposed to a "novel object" that was competing against the other object that itself was novel in time, what is termed here as competitive novelty. According to the on sample t-test against 0, the cumulative group explored significantly above chance level, but not the competitive group. This lack of significance could be a reflection of the small n = 5. Neither group was significant against chance with the non-parametric Wilcoxon signed-rank test, due to the insufficiently large n = 5. There was no significance between groups when evaluated with the two sample t-test or the Mann Whitney U test. Scatter plots represent the mean (± SEM). * p<0.05, ** p<0,01 (one sample t-test against 0).*

2. Discussion

Single KI mice did not have any deficits in the FDOR5' and OP5' tasks at 6 months, suggesting that the deficits of these tasks in young dKI mice is likely due to the combination of amyloid and tau pathologies. The FDOL5' task may be the most sensitive to early AD memory loss, but unfortunately the task is highly variable making it difficult to make any robust statistical inferences in comparison to the WT.

The App^{NL-F} mice did not explore above chance level for any task at 10 months of age. This follows previous results reporting that 12 month old App^{NL-F} were deficient in the OR24 task (Izumi et al., 2018). This is also around the age that the $A\beta_{42}/A\beta_{40}$ ratio starts to increase substantially from basal levels (Saito et al., 2014). The more severe memory loss in the App^{NL-F} compared to the *MAPT* is expected, as the *MAPT* are not shown to have any significant physiological disturbances, even compared to WT mice. All effects of the *MAPT* mouse line thus far have been reported in conjunction with other pathological changes (e.g. cross with App^{NL-F} *or* $App^{NLG—F}$, introduction of tau protein seeds) (Saito et al., 2019). This pathological phenotype is almost negligible when compared to the App^{NL-F} that already displays sparse plaques throughout the cortex at this age.

The dKI mice show specific deficits in the OP task at 5-minute and 3-hour ITIs as soon as 4 months of age. The FDOR5' task showed high variability, which may indicate that affected processes, such as DG pattern separation computation or neurogenesis (Cès et al., 2019), may be more individually dependent. The deficit in OP was specifically due to a reduced capacity for binding/associating object and place modalities and not due to reduced processing of the modalities themselves, as the dKI showed good performances in the uni-modal OR5' and OL5' tasks. At the age of 4 months, single KI App^{NL-F} already present similar functional perturbations to those seen in preclinical AD, hyper-activity in the MTL (Petrache et al., 2019) and resting state functional hyper-connectivity in the MTL-DMN (Shah et al., 2018), which may contribute to associative memory dysfunction (Wilson et al., 2013a; Chao et al., 2016; Yeung et al., 2018; Cooper and Ritchey, 2019). However, our rough evaluation of the App^{NL-F} in the OP5' task did

not reveal any deficits, suggesting that an addition of tau/ptau pathology to these functional perturbations is needed to induce memory loss.

The increase in light box exploration in the light-dark box task resembles the results of multiple studies that that have assessed anxiety like behaviors in 6 to 8 month old App^{NL-G-F} single knock in mice. These studies have consistently reported that App^{NL-G-F} mice spend significantly more time in the open arms during the elevated plus maze (EPM) task (Pervolaraki et al., 2019; Latif-Hernandez et al., 2017; Sakakibara et al., 2018), indicating an anxiolytic phenotype similar to ours. However evaluations of anxiety through the open field exploration task are largely inconclusive. One study found that 8 month old App^{NL-G-F} mice spent significantly less center time during an open field (OF) exploration task, indicating a paradoxically anxiogenic phenotype (Pervolaraki et al., 2019). In 6 month old App^{NL-G-F} mice, other studies have reported an increase in OF center time (Latif-Hernandez et al., 2017) or no difference(Whyte et al., 2018) , suggesting that age or the OF set up (e.g. luminosity) play a large role in mediating anxiety like behaviors of these mice. Pervolaraki et al., 2019 found that this anxiolytic profile was accompanied by reductions in white matter integrity in the hippocampus and in the PFC, as measured through diffusion tensor imaging (DTI) fractional anisotropy. They also found concurrent perturbations in NMDA dependent gamma oscillations in the PFC. No physiological disturbances were detected in the amygdala. Both the amygdala and the PFC play a role in anxiety (Davidson, 2002; Davis, 1992; Davis et al., 1994; Etkin et al., 2011), but the PFC has a specific role in decision making (Dias et al., 1996), which could potentially explain the anxiolytic behavior of these mice. The authors hypothesized that the paradoxical phenotype of these mice was thus more likely related to “disinhibition” of decision making, which is manifested as a failure to inhibit the choice to enter the open arm of the elevated plus maze. The fact that our dKI mice exhibit a similar anxiolytic profile in the light dark task, indicates a potential perturbation of the mPFC and resulting disinhibition as reported by Pervolaraki et al., 2019.

We have shown that the OiC24 task can be used to robustly evaluate long-term associative memory in WT mice. The task has since been used by others for the successful evaluation of dKI mice. However, our results also suggest a potential effect of temporal novelty even with a large disparity between the length of the “inter acquisition phase interval” and the “before

retrieval interval". Future experimenters will have to take this into account when using and analyzing this task. For example, if mostly the *competitive novelty* condition is used, a condition (e.g. WT or dKI) may have a worse performance simply because they react more to temporal novelty (and not because they respond less to contextual novelty). The inverse is true in using predominantly the *cumulative novelty* condition. I suggest using the protocol as tested here, splitting each condition into equal parts *competitive novelty* and *cumulative novelty* subgroups. First, the two conditions will cancel each other out in terms of the final result and its representation of object-context association detection. Second, one may even evaluate temporal novelty detection by comparing the *cumulative novelty* and *competitive novelty* subgroups within each condition. If the subgroups are significantly different, then we can say that temporal novelty is significantly detected, and if there is no difference then there is no significant effect of temporal novelty (e.g. "in the WT there was a significant difference in *competitive* vs. *cumulative* subgroups indicating that they detected temporal novelty; in the dKI no significant effect of temporal novelty was detected"). Of course, a sufficiently large sample size would be needed for this kind of analysis, ideally at least n = 14 per condition (to give n = 7 per subgroup). In conclusion, this OiC24 test as set up here may be used to evaluate object-context associative memory, and even perhaps object-temporal associative memory.

Study n°2

Using c-Fos expression to evaluate neural activation and functional connectivity in spontaneous object exploration paradigms with 5' ITIs. Trials and tribulations.

Christopher Borcuk[1], Céline Héraud[1], Karine Herbeaux[1], Anais Robert[1], Julien Caillette[1], Saito T[2], Hashimoto S[2], Saido T[2], Romain Goutagny[1], Chantal Mathis[1]

1 - Laboratoire de Neurosciences Cognitives et Adaptatives (LNCA), Université de Strasbourg, Faculté de Psychologie, 12 rue Goethe, F-67000 Strasbourg, France.

2 - Laboratory for Proteolytic Neuroscience, RIKEN Center for Brain Science, 2-1 Hirosawa, Wako-city, Saitama 351-0198, Japan

Preliminary analyses

1. Scientific context and objectives

In the previous study, we detected an OP5' task deficit in 4 month old dKI mice, similar to associative memory loss seen in preclinical and prodromal stages of AD. Yeung et al. (2019) showed that anterolateral EC and parahippocampal volume predicted OP memory performance in older adults. Cognitively healthy elderly are also commonly affected by sensitive recognition memory loss, including fine mnemonic discrimination (Reagh et al., 2016) and associative memory (Naveh-Benjamin, 2000). As reported in our introduction section, both forms of recognition memory were shown to rely on activity of regions in the MTL, mPFC and PMC, and perturbation of their activity may explain memory dysfunction. Thus, our next goal was to determine neuronal activity in a large set of 22 regions of interest (including the MTL, the mPFC and the RSC) in 4 month old dKI mice tested in the OP5' task. In mice undergoing spontaneous object exploration tasks, task-dependent activity of brain regions can be assessed through the marking of c-Fos, an activity regulated immediate early gene (Kinnavane et al., 2015).

The following section will present two experiments. The first experiment looks at c-Fos expression in young (3 month) and old (18 month) mice that underwent the OR5', OL5', and OP5' tasks. The second experiment looks at c-Fos expression in 4 month old WT and dKI mice that underwent the OP5' task (behavior presented in Study n°1). Our initial goal was to simply detect regionally specific changes in neural activity in order to identify which region(s) was (were) the most affected in dKI mice. I soon found an interest in pushing the analyses further to evaluate functional connectivity between regions of interest. Functional connectivity can be assessed in c-Fos studies through across-mice inter-regional correlations of c-Fos expression. The functional connectivity analyses presented here were based on the study of Tanimizu et al., 2017 (***Figure 38***), and were developed by me without outside guidance. These analyses are not without their problems, as was made understood to me with the arrival and help of Demian Battaglia. In the end, the most important aspect of these experiments was what I learned about the optimizations and considerations needed to best carry out the OP3h c-Fos experiment presented in Study n°3. These optimizations and considerations will be discussed in depth at the end of the section. Methodological optimizations were also identified and have already been described in the Materials and Methods.

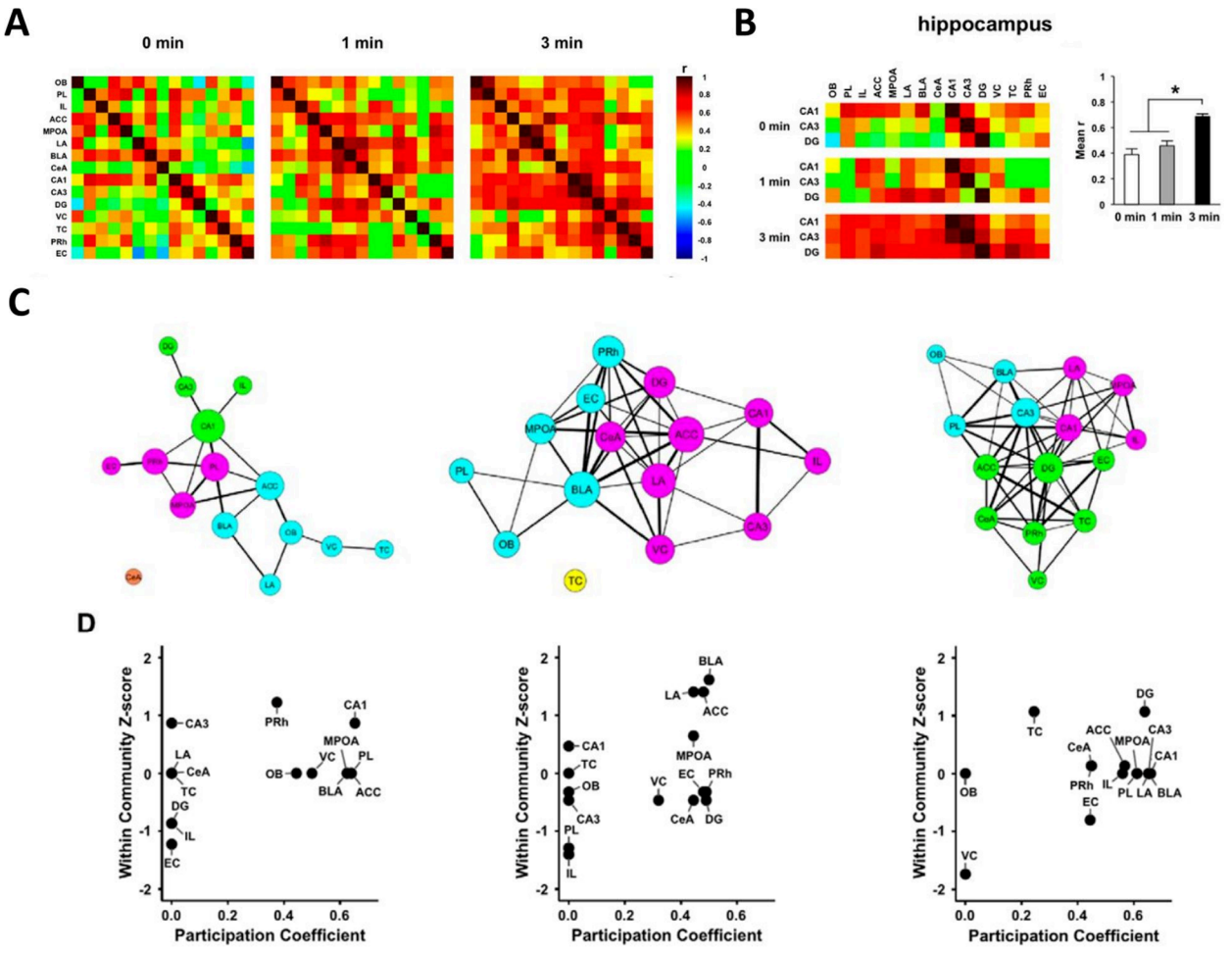

Figure 38. *Example functional connectivity analyses from Tanimizu et al, 2017. (A) Correlation matrices depict all possible pairwise inter-regional correlations in three group conditions. The color code indicates correlation strength (Pearson's r), red is a positive correlation, blue is a negative correlation. (B) The authors compared hippocampal functional connectivity strength, by computing the mean correlation strength (Mean r) of the hippocampus with the rest of the network. This was compared between group conditions where the statistical variance arises from the relevant r values of each matrix. This type of analysis was carried out on both experiments and is explained more in depth there. (C) Finally, a functional network was generated by removing "non-significant" connections with a pre-defined threshold. Communities and community hubs of the network were then assessed using graph theory. This final technique was carried out on my OP5' experiment and will be explained more in depth there.*

A. Aging experiment

Several groups of young (3 month) and old (18 month) old mice were tested in a series of object recognition tasks by Anais Robert (M1 student, 2017), and were later evaluated for c-Fos expression by me. For the sake of brevity, only c-Fos data from the OR5' (***Figure 39A***) (young n = 8, old n = 7), OL5' (***Figure 39B***) (young n = 8, old n = 7), and OP5' (***Figure 39C***) (young n = 7, old n = 7) tasks will be presented and discussed here. These tasks gave the most cohesive results due to their larger sample sizes and are closer tied to my main study, evaluating object-place association in the dKI. No groups presented memory deficits in any of the three tasks. We decided to focus our evaluation on regions of the medial temporal lobe (MTL) , including regions of the dorsal hippocampus (DH; CA1,CA3, DG_ub "upper blade" and DG_lb "lower blade") and regions of the medial temporal cortex (MTC; LEC layers 2,3 5, dorsal and ventral PRC, MEC, POC). No significant differences were found between ages in any region for any task (***Figure 39***). This gave us a first hint that the sample size of around 7 was not sufficient enough to evaluate c-Fos derived neural activity in spontaneous object exploration paradigms, as would be the case for more *intense* experiments (e.g. MWM).

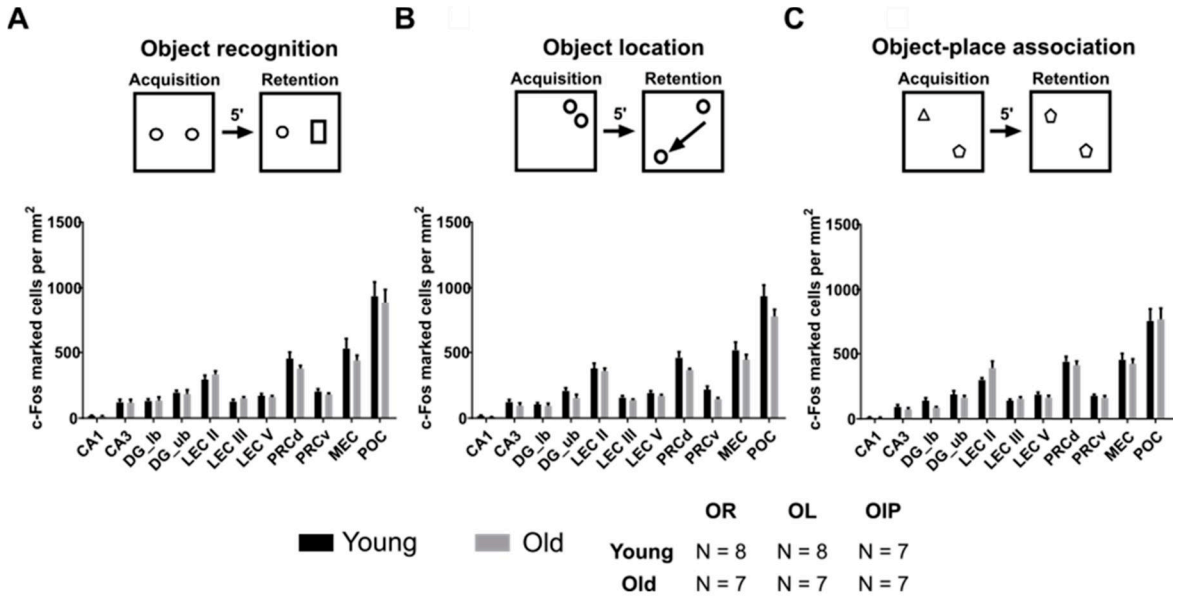

Figure 39. *Young (3 months) and old (18 months) mice were tested in 3 separate cohorts in the (A) object recognition, (B) object location, and (C) object-place tasks. Young and old mice performed all tasks sufficiently well (figure not shown). The mice were perfused 90 minutes after the retention phase of each task, and the brains were later sectioned and immunostained for c-Fos. There were no age dependent differences in any region or task. Bar plots represent the mean (± SEM).*

I was then interested in evaluating age and task dependent changes in functional connectivity within the MTL. Object-place associative memory should require strong communication between groups of structures processing spatial information (DH, MEC), processing object information (PRC, LEC) and associating the two modalities (LEC, POC). A simple hypothesis was put forth that the OP task would illicit stronger communication between DH and the MTC subfields for the efficient association of object and place modalities. We may also evaluate age-dependent changes in DH-MTL functional connectivity in parallel. Functional connectivity was assessed through the computation of across mice interregional Pearson's correlations (Pearson's r). Correlation matrices are used to visualize all possible pairwise correlations for each task-age group (***Figure 40A***). The functional connectivity strength between the DH and the MTC was assessed through taking the mean correlation strength (mean r) between the two subfields (see the green dotted boxes of ***Figure 40A***). The mean r was calculated from absolute values; we chose to consider negative correlations as equal to positive ones. Two-way ANOVA was used to evaluate task- and age-dependent changes in DH-MTC functional connectivity. Young mice were shown to have significantly stronger DH-MTC connectivity than older mice irrespective of the task. The OP task exhibited stronger DH-MTC functional connectivity compared to the OR and OL tasks regardless of age (***Figure 40B***) (two way ANOVA, age effect: $F(1, 162) = 7.924$, $P = 0.006$; task effect: $F(2, 162) = 17.25$, $P<0.0001$; interaction task x age effect: $F(2, 162) = 0.1957$, $P = 0.82$; Tukey post hoc: OR vs. OL $P = 0.13$, OR vs. OP $P = 0.0005$, OL vs. OP $p = 0.0001$).

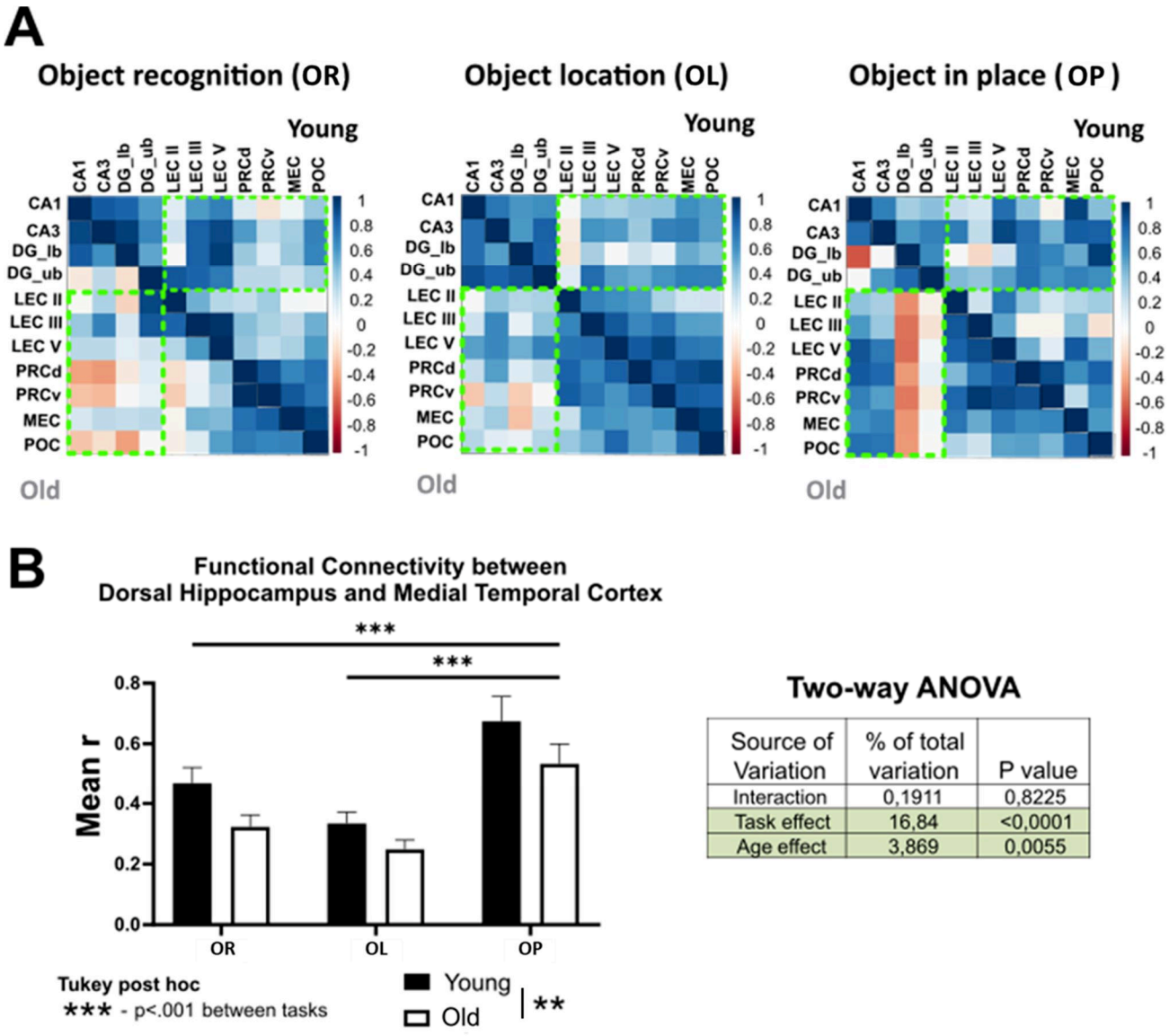

Figure 40. *(A) Functional connectivity is depicted in correlation matrices showing across subjects inter-regional Pearson correlations of c-Fos expression for the object recognition (OR), object location (OL) and object- place (OP) tasks. Colors reflect correlation strength. Please note that here blue represents positive correlations and red represents negative correlations. We were interested in evaluating functional connectivity between the dorsal hippocampus (DH; CA1, CA3, DG_lb, DG_ub) and the medial temporal cortex (MTC; LEC layers, PRCd, PRCv, MEC,POC). We thus calculated the functional connectivity strength of this cross subfield communication by taking the mean r of areas depicted by the green dotted boxes. The mean r was calculated from absolute values; we chose to consider negative correlations as equal to positive ones(B) Two-way ANOVA was used to evaluate task and age dependent changes in DH-MTC functional connectivity. Young mice were shown to have significantly stronger DH-MTC connectivity than older mice across all tasks. ** p<0.01 (two way ANOVA major effect, F). The OP task exhibited stronger DH-MTC functional connectivity compared to both the OR and OL tasks regardless of age. Bar plots represent the mean r (± SEM). *** p<0.0001 (Tukey post hoc).*

B. OP 5' experiment

The object-place association task with a 5' delay was carried out on WT (n = 11) and dKI mice (n = 11). Reproducing the preliminary phenotyping results, the dKI mice did not explore the novel object above chance and had a memory index significantly reduced compared to the wild type (see Study n°1, ***Figure 33C***) (two sample *t*-test, WT vs. dKI: t(20) = 2.85, P = 0.01; against chance: WT t(10)=5.489, P = 0.0003; dKI t(10)=0.3095, P = 0.76) . ### p<0,001 (one sample *t*-test against 0); ** p<0,01 (two sample *t*-test). The caudal claustrum (cCLA) was significantly hyperactive in the dKI (***Figure 41***) (two tample *t*-test Bonferroni corrected: WT vs. dKI: t(20) = -4.3313, P = 0.004), and the caudal perirhinal cortex (cPRC) showed a tendency for hyper-activity (two tample *t*-test Bonferroni corrected , WT vs. dKI: t(20) = -3.15, P = 0.06).

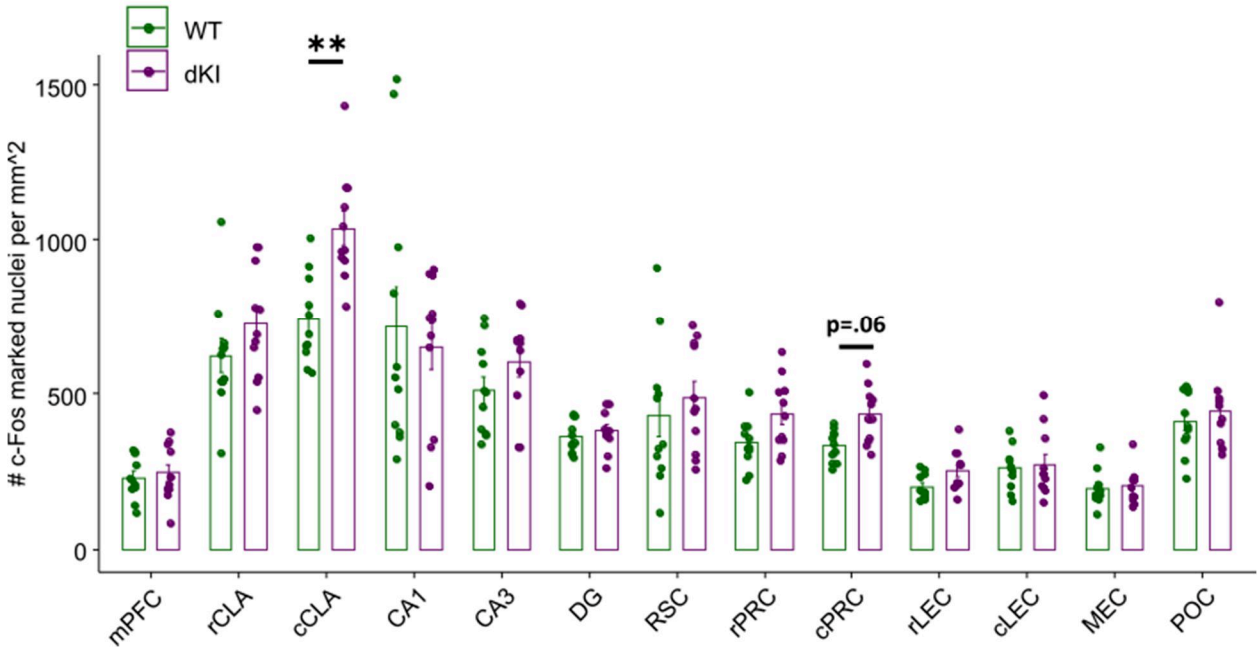

Figure 41. *The object-place task with a 5-minute ITI was carried out on WT (n = 11) and dKI mice (n = 11). Mice were perfused 90 minutes after the retention phase, and the brains were later processed for c-Fos analysis. The dKI mice did not explore the novel object above chance and had a memory index significantly reduced compared to the wild type. (C) The caudal claustrum (cCLA) was significantly hyperactive in the dKI, and the caudal perirhinal cortex (cPRC) showed a tendency for hyper-activity. Bar plots represent the mean (± SEM). ** p<0.01 (two sample t-test, Bonferroni corrected).*

Functional connectivity was calculated by computing the inter-regional Pearson correlations of c-Fos expression. All possible pairwise correlations are depicted in the color coded correlation matrix (***Figure 42A***). Possitive correlations are in red, and negative correlations are in blue. We assessed functional connectivity strength of a region subfield with the rest of the network by computing the mean absolute r value (***Figure 42B***). Absolute r values were used as negative correlations were considered as contributing equally to the network. There was a significant increase in functional connectivity of the mPFC (Mann-Whitney test Bonferroni corrected, U = 1252, p=0.0008) and of the PRC (Mann-Whitney test Bonferroni corrected , U = 1302, p=0.002) with the rest of the network in dKI mice.

Functional networks were computed by removing all correlations that were not significant to a $p < .05$ (for n= 11 mice this is equivalent to $r > .60$). From this, a functional network was created as a graph with regions as nodes (circles) and significant correlations as edges (***Figure 43A***). Communities were detected through modularity optimization, which finds communities of regions that are more connected with each other compared to the rest of the network. Community hubs were analyzed through Within community Z score and Partition coefficient metrics. The Within community Z score evaluates how strongly a region is connected with other regions of its community. Partition coefficient evaluates how well a region is connected to other communities (***Figure 43B***). Strong putative community hubs regions that facilitate communication within and between communities are expected to exhibit both strong intra-community and inter-community hub strength. This can be visualized in a scatter plot with the within community Z score on the y axis and the partition coefficient on the x axis. Regions that have high values in both measures will be found in the top right of the plot and can be considered as candidate community hub regions. In the dKI, the top right corner appears to be mostly populated by the mPFC and PRC subregions, revealing these regions as candidate community hubs.

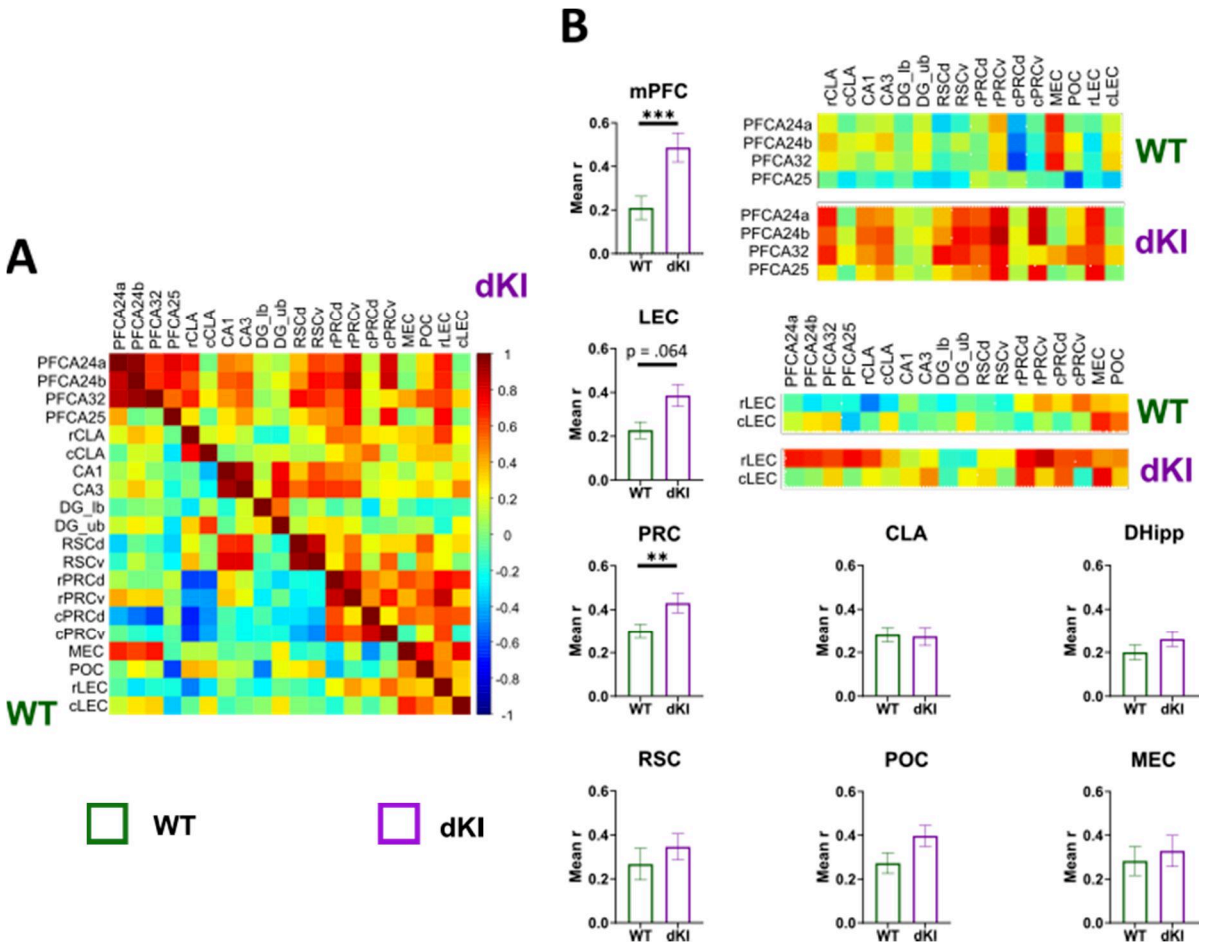

Figure 42. *(A) Functional connectivity is depicted in a correlation matrix showing across subjects inter-regional Pearson correlations of c-Fos expression. Colors reflect correlation strength. (B) We assessed functional connectivity strength of a region subfield with the rest of the network by computing the mean absolute r value. Absolute r values were used as negative correlations were considered as contributing equally to the network. Example values used to compute the mean r are depicted for the mPFC subfield (PFCA24a, PFCA24b, PFCA32, PFCA25) and LEC subfield (rLEC,cLEC). There was a significant increase in functional connectivity of the mPFC and PRC with the rest of the network. Subfields; the mPFC (PFCA24a, PFCA24b, PFCA32, PFCA25), LEC (rLEC,cLEC), PRC (rPRCd,cPRCd, rPRCv,cPRCv), CLA(rCLA,cCLA), DHipp(CA1,CA3, DG_lb, DG_ub), RSC(RSCd,RSCv). Bar plots represent the mean (± SEM). ** p<0.01, *** p<0.001 (Mann-Whitney test, Bonferroni corrected).*

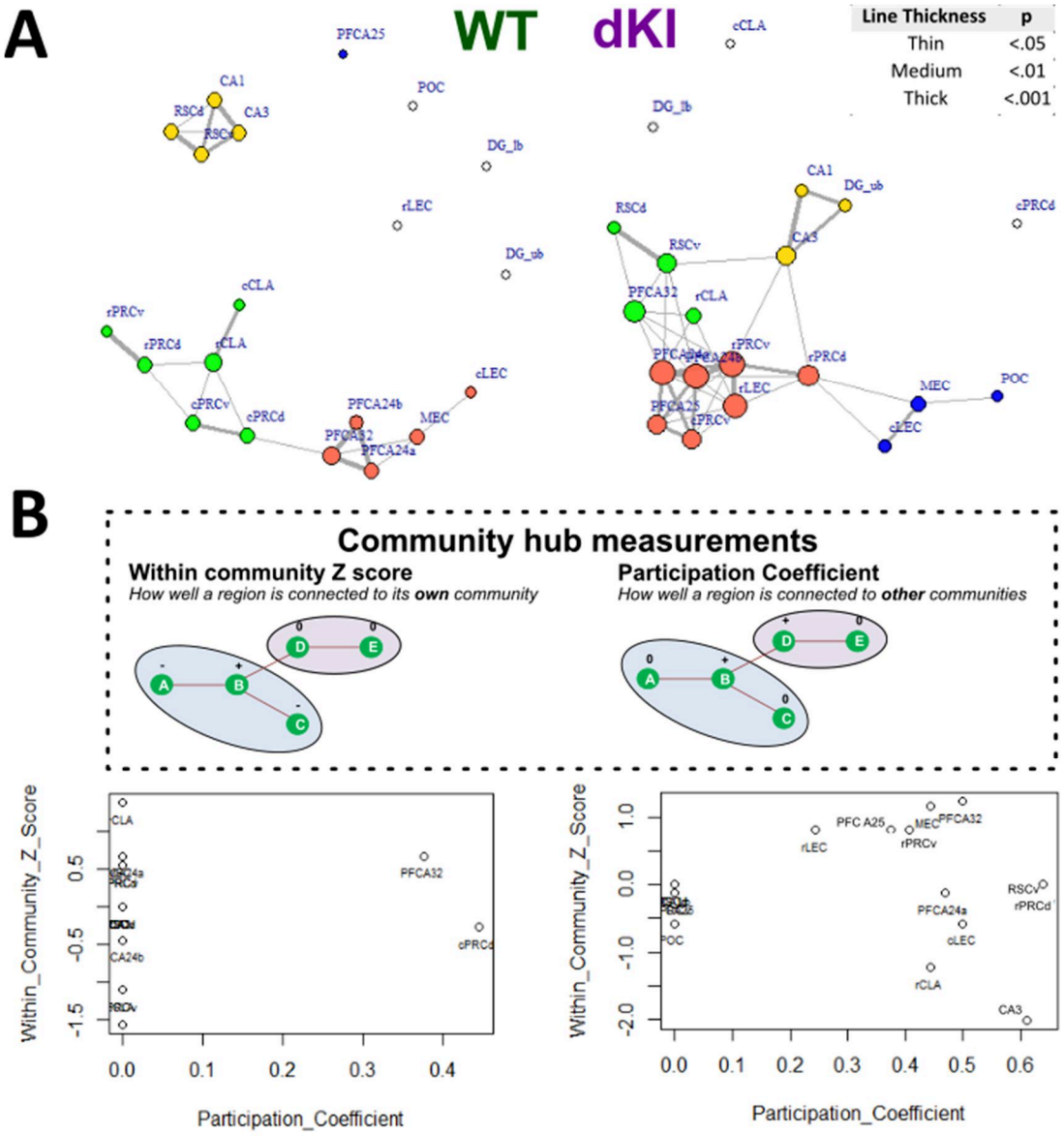

Figure 43. *(A) Functional networks were computed by removing all correlations that were not significant to a P < .05 (for n= 11 mice this is equivalent to r >.60). From this, a functional network was created as a graph with regions as nodes (circles) and significant correlations as edges (lines). The circle width is proportional to a regions degree (the number of significant connections it has). Line thickness indicates the significance strength of each correlation (see top right table). However, line thickness is only for visualization purposes and plays no role in any of the analyses. Communities were detected through modularity optimization, which finds communities of regions that are more connected with each other compared to the rest of the network. For community detection all edges were considered to have equal weights (no effect of line thickness). (B) Community hubs were analyzed through Within community Z score and Partition coefficient metrics. The Within community Z score evaluates how strongly a region is connected with other regions of its community (strong for region B in the blue community). Partition coefficient evaluates how well a region is connected to other communities (strong for regions B and D). Regions that are found in the top right of the scatter plot can thus be said to exhibit strong intra-community and inter-community hub strength. In the dKI these appear to be mostly populated by the mPFC and PRC subregions.*

2. Discussion

Older mice were shown have decreased DH-MTC functional connectivity strength compared to young ones. A similar phenomenon was seen in humans during fMRI evaluations of mnemonic discrimination tasks (Reagh et al., 2018). In our mice we can see this generalizes across many different tasks. Despite this reduced DH-MTC connectivity, the performance of old mice was comparable to those of young mice in all three tasks. This suggests that their ability to express good performance may rely on a shift of connectivity efficiency to compensatory networks. When looking carefully at the functional connectivity matrices, one might propose the following scenario. The reduced DH-MTL connectivity seems to be related to the disconnection of the DG which receives its main inputs from the MTC (particularly obvious in the OP5' task). There seems to be a compensatory increase in connectivity within the MTC and within the DH. This is in agreement with studies showing that alteration in the integrity of the perforant path (which conveys EC inputs to the DG) predicts age-related changes in memory functions in humans (Yassa et al., 2011).

The OP task was shown to have stronger DH-MTC functional connectivity strength than the more uni-modal tasks. This may indicate that object place associative memory needs a stronger interaction between the MTC and the DH in a task that requires the binding of place and object identity information. Some interaction do exist in the MTC between the PRC-LEC axis processing nonspatial (e.g., object identity) aspect of memories and the POC-MEC axis processing spatial aspects of memories. However, both information processing streams converge mainly into the hippocampus in charge of building a multimodal representation of the memorized event. An OP task run in a complex/oriented environment like the one we used requires the binding of object identity and spatial location information which is thought to take place in the hippocampus (see Langston and Wood, 2010).

The cCLA was shown to be hyperactive, and the caudal PRC showed a tendency for hyper-activity in the dKI mice. Both the mPFC and the PRC showed significantly increased functional connectivity strength in the dKI mice. They also appeared as candidate community hubs. Both these regions receive very strong connections from the claustrum. Their increase in functional connectivity strength may therefore be induced by action from the hyperactive caudal claustrum.

Due to its vast cortical connections, initial hyper-activity of the claustrum may play a general role of inducing global network hyper-connectivity as seen in prodromal AD. It is interesting to note that the hyper-activity of the claustrum was reproduced in the following OP 3h c-Fos study. The conservation of the hyperactive claustrum across in both OP c-Fos studies confirms a few histopathological and regional glucose metabolism studies suggesting that the claustrum merit additional attention as a potential contributor to early AD (Ogomori et al., 1989; Morys et al., 1996; Seo et al, 2015).

3. Considerations and optimizations for future c-Fos experiments

Across these two c-Fos studies, the aging study and the OP 5' study, I have detailed analysis techniques that I integrated independently, based mostly on indications from the paper of Tanimizu et al., 2017. These studies played an important role in getting me comfortable with analyzing c-Fos, understanding analyses related to functional connectivity and developing code in R to carry out these analyses. However, in the end a few problematic considerations were identified and were later addressed for the OP 3h study.

A major problem with these studies is experimental in nature, and has to do with the 5-minute ITI. The c-Fos expression curve peaks from 60 to 90 minutes, and will thus take into account both acquisition- and retention-dependent activity. In terms of regional activity, at worst this will add more noise and make it more difficult to detect phase dependent changes. In terms of functional connectivity the consequences may be more drastic. The c-Fos staining represents the culmination of activity that has occurred throughout the task. If two regions are constantly activating together, and do so for each mouse, then this functional relationship can be detected through correlation testing across mice. However, if each phase has different functional networks contributing to it, then the strength of either functional network may be severely reduced in the evaluation of c-Fos. Take for instance a functional relationship between region A and region B, which activate together during the acquisition phase. During the retention phase there is separate functional relationship between region A and another region C, and no longer region B. In the end, because region A if influenced separately by both regions B and C, the overall functional

connectivity of A to either region will be reduced according to c-Fos. This poses a problem in that more dynamic networks will be punished. For example if some hypothetical WT mice have very different but very strong functional networks contributing to each test phase, the final result according to c-Fos may be reduced compared to hypothetical dKI mice who have more consistent but weaker functional networks. Once this aspect of 5-minute ITI c-Fos derived functional connectivity is understood, it makes it difficult to interpret and be confident in the results. Of course they may still be used as preliminary data to be confirmed and added to by future experiments. Regardless, we felt that it was necessary to evaluate the c-Fos expression during an OP3h task with a 3 hour ITI, which would separate the acquisition and retention phases with respect to the c-Fos expression curve.

Other caveats are analytical in nature. Simply put, the analysis techniques as detailed here are not as rigorous as they could be. These considerations were mostly understood with the arrival and invaluable aid of Demian Battaglia, an expert in the field of computational and network neuroscience. The primary fault in these analysis was that we did not take into account the variance across mice when making statistical inferences about functional networks (i.e. the error bars depict variance across interregional correlation coefficients and not variance across mice). A technique for incorporating variance across mice is through bootstrapping (Epskamp et al., 2018), as detailed in the Material and Methods. This method with extrapolate different network estimates from different combinations of the original population of mice, in the end generating a confidence interval reflecting the variance across these combinations, and thus the variance across mice. Bootstrapping is more rigorous than the statistical techniques detailed in these preliminary studies, and was used extensively in the evaluation of OP3h derived functional connectivity. Another problem arises from the thresholding of connections when constructing functional networks. The cutoff is more or less arbitrary and different results could have been obtained with harsher or more lenient thresholds. To remedy this, in the OP3h study no threshold was introduced. Instead, fully connected weighted networks were computed and assessed based solely on the distribution of connection weights.

Study n°3

Early memory deficits and extensive brain network disorganization in the *App^{NL-F}xMAPT* double knock in mouse model of Alzheimer's disease

Christopher Borcuk[1], Céline Héraud[1], Karine Herbeaux[1], Margot Diringer[1], Élodie Panzer[1], Jil Scuto[1], Saito T[2], Hashimoto S[2], Saido T[2], Romain Goutagny[1], Demian Battaglia[1,3,4], Chantal Mathis[1]

1 - Laboratoire de Neurosciences Cognitives et Adaptatives (LNCA), Université de Strasbourg, Faculté de Psychologie, 12 rue Goethe, F-67000 Strasbourg, France.

2 - Laboratory for Proteolytic Neuroscience, RIKEN Center for Brain Science, 2-1 Hirosawa, Wako-city, Saitama 351-0198, Japan

3 University of Strasbourg Institute for Advanced Studies (USIAS), F-67000 Strasbourg, France

4 Université d'Aix-Marseille, Inserm, Institut de Neurosciences des Systèmes (INS) UMR_S 1106, F-13005 Marseille, France

Article submitted to Drs. T Saito, S Hashimoto, and T Saido for review according to the material transfer agreement before submission to BioRiv and e-Life.

1. Scientific context and objectives

In Study n°1, we showed that dKI mice present OP5'deficits as soon as 4 months of age, without any additional clear cut deficits in other sensitive recognition memory tasks. In Study n°2, we evaluated c-Fos expression related to OP5' in two experiments; comparing young and old mice, and comparing 4 month old WT and dKI mice. With a 5-minute ITI, c-Fos expression represents activity during both phases, which should increase the noise of the signal, and may explain why no regional changes in neural activity was seen in the aging study with the relatively small sample sizes. Despite this, with a larger sample size significant regional increases in neural activity (in the caudal CLA) could be detected in dKI mice that underwent the OP5'task.

Regardless, we were interested in understanding if the OP deficit arises from test-phase specific perturbations in neural activity. Moreover, understanding functional connectivity arising from the mixture of acquisition and retention activities is problematic, and using a 5-minute ITI for evaluating c-Fos derived functional connectivity is best avoided. With all this in mind, we decided to evaluate c-Fos expression in the OP3h task with a 3-hour ITI (behavioral results are presented in Study n°1), enough to separate both test-phases in respect to the c-Fos expression curve. Thus, c-Fos expression was analysed in a cohort of mice that underwent only the acquisition phase and a separate cohort that underwent the whole OP3h task until the retention phase. Regional c-Fos expression was assessed to see if we could detect local changes in hyper or hypo-activity associated to early AD. Functional networks were analyzed to determine if associative memory loss could be linked to disruptions to network efficiency or hub strength, as is seen in the DMN of early AD.

This c-Fos analysis is presented with Behavioral results from Study n°1 in the form of an article. This article has been submitted to Drs T Saito and T Saido in accordance to our Material transfer agreement for the *App*$^{NL\ F}$ KI and *MAPT* KI mouse lines. Then, it will be submitted to BioRiv and eLife.

Early memory deficits and extensive brain network disorganization in the *App*$^{NL-F}$/*MAPT* double knock-in mouse model of familial Alzheimer's disease

Christopher Borcuk[1], Céline Héraud[1], Karine Herbeaux[1], Margot Diringer[1], Élodie Panzer[1], Jil Scuto[1], Hashimoto S[2], Saido T[2], Saito T[2], Romain Goutagny[1], Demian Battaglia[1,3,4], Chantal Mathis[1]

[1] Université de Strasbourg, CNRS, Laboratoire de Neurosciences Cognitives et Adaptatives (LNCA) UMR 7364, F-67000 Strasbourg, France

[2] Laboratory for Proteolytic Neuroscience, RIKEN Center for Brain Science, 2-1 Hirosawa, Wako-city, Saitama 351-0198, Japan

[3] University of Strasbourg Institute for Advanced Studies (USIAS), F-67000 Strasbourg, France

[4] Université d'Aix-Marseille, Inserm, Institut de Neurosciences des Systèmes (INS) UMR_S 1106, F-13005 Marseille, France

Corresponding Author

Chantal Mathis, PhD

LNCA UMR 7364, Université de Strasbourg, 12 rue Goethe F-67000 Strasbourg, France.

E-mail: chantal.mathis@unistra.fr

Phone: (33) 368 85 18 76

Fax: (33) 368 85 19 58

Key words: preclinical Alzheimer's disease, functional connectivity, associative memory

Conflict of interest: none

Acknowledgement: Université de Strasbourg, Centre National ,de la Recherche Scientifique, complementary thesis support from the FRM-ALZ201912009643, Anne Pereira de Vasconcelos for advices on experimental design, Laura Durieux for analysis discussion, Dominique Massotte for the nanozoomer, Aminé Isik for mouse genotyping and breeding, Olivier Bildstein for care to our mice.

Abstract:

A critical challenge in current research on AD is to clarify the relationship between early neuropathology and network dysfunction associated to the emergence of subtle memory alterations which announce disease onset. In the present work, the new generation *App*$^{NL-F}$*/MAPT* double knock in (dKI) model was used to evaluate early stages of AD. The initial step of tau pathology was restricted to the perirhinal-entorhinal region, sparing the hippocampus. This discrete neuropathological sign was associated with deficits in the object-place associative memory, one of the earliest recognition memories affected in individuals at risk for developing AD. Analyses of task-dependent c-Fos activation was carried out in 22 brain regions across the medial prefrontal cortex, claustrum, retrosplenial cortex, and medial temporal lobe. Initial hyperactivity was detected in the entorhinal cortex and the claustrum of dKI mice. The retention phase was associated to reduced network efficiency especially across cingulate cortical regions, which may be caused by a disruption of information flow through the retrosplenial cortex. Moreover, the relationship between network global efficiency and memory performance in the WT could predict memory loss in the dKI, further linking reduced network efficiency to memory dysfunction. Our results suggest that early perirhinal-entorhinal pathology is associated with local hyperactivity which spreads towards connected regions such as the claustrum, the medial prefrontal cortex and ultimately the key retrosplenial hub which is needed to relay information flow from frontal to temporal lobes. The similarity between our findings and those reported in the earliest stages of AD suggests that the *App*$^{NL-F}$*/MAPT* dKI model has a high potential for generating key information on the initial stage of the disease.

Abbreviations

AD – Alzheimer's disease

CLA – claustrum

DH – dorsal hippocampus

dKI - *App*$^{NL-F}$*/MAPT* double knock-in mouse

FC – functional connectivity

mPFC – medial prefontal cortex

MTC – medial temporal cortex

MTL – medial temporal lobe

OP – object-place association

PS – Pattern Separation

RSC – retrosplenial cortex

Introduction

Current diagnosis and treatment for Alzheimer's disease (AD) occurs too late, when physiological symptoms such as overt neurodegeneration have already reached an irreversible state (Selkoe, 2012). Hallmark pathologies of AD include insoluble amyloid plaques, initially formed in the medial prefrontal and posterior medial cortices indicative of the default mode network (DMN), and neurofibrillary tangles, initially formed in the medial temporal lobe (MTL). Combining functional neuroimaging with amyloid or tau PET reveals that spatial patterns of deposition induce functional network perturbations (Myers et al., 2014; Jones et al., 2017), and accompany cognitive decline (Sepulcre et al., 2017; Pereira et al., 2019). However, soluble amyloid peptide (Aβ) and hyperphosphorylated tau precursors are generally more toxic and accumulate in the brain decades prior to the onset of typical symptoms (Chen et al., 2017; Hill et al., 2020). This highlights the importance of focusing on the earliest stages to understand the origin of this devastating disease and to develop more proactive detection methods and therapies.

Amnestic mild cognitive impairment (aMCI) indicates a higher risk of progressing to AD and has been extensively studied over the last decade as a potential prodromal stage of AD (Petersen et al., 2009). Resting state functional connectivity (FC) has been evaluated in aMCI patients through the temporal correlation of signal fluctuations in fMRI, EEG, or MEG. In order to achieve a more rigorous understanding of FC disruption, graph theory has been used to evaluate the topology of functional networks. Healthy cognition likely requires efficient small world topology, combining local segregation between anatomically and functionally similar regions, and good integration between distant regions with the help of strongly connected hubs (Filippi et al., 2013, Bassett and Bullmore., 2006). In regards to aMCI, many studies have reported functional network perturbations within and between the DMN and the MTL, with reduced network integration along with reduced strength of cortical hubs (Drzezga et al., 2011; Wang et al., 2013a; Bai et al., 2013, Lin et al., 2019). However, these results are not entirely conclusive, as others have reported opposing or null results (Gardini et al., 2015; Grajski and Bressler, 2019; Liang et al., 2020, Liu et al., 2012). This inconsistency may be indicative of the heterogeneity of aMCI staging, where the sense of perturbation (hyperconnectivity vs hypoconnectivity) is shown to change depending on the severity of the pathological state (Pusil et al., 2019; Jones et al., 2016). This highlights the importance of identifying earlier biomarkers to more precisely detect preclinical stages of AD, even preceding aMCI. Recent progress has led to the development of sensitive recognition memory paradigms, such as pattern separation and associative memory tasks, which can detect slight cognitive defects in subjective cognitive impairment and cognitively healthy elderly (Naveh-Benjamin, 2000, Sinha et al., 2018; Reagh et al., 2018). These tasks depend on specific interactions across DMN and MTL structures sensitive to early AD (Reagh and Yassa., 2014; Miller et al., 2014; Hales and Brewer, 2011; Caviezel et al., 2020; Ritchey et al., 2020), and have be implemented to detect the earliest "asymptomatic" stages of preclinical AD (Rentz et al., 2011; Maass et al., 2019). By evaluating functional networks directly responsible for the earliest subtle memory deficits, we may achieve a clearer understanding of the neural networks first affected in the initial stages of AD.

Initial stages of AD are inevitably linked to discrete physiological and neuroanatomical perturbations, which should be more easily investigated in mouse models of AD (Scearce-Levie et al, 2020). Using fMRI on young AD transgenic mice, increased soluble Aβ (Shah et al, 2016; Shah et al., 2018), and regionally specific increases in neuroinflammation and phospho-tau (Degiorgis et al., 2020) have been linked to disruptions in resting state functional networks. As fMRI/EEG/MEG methods are currently

difficult to implement in freely moving mice, ex-vivo imaging based on quantification of activity regulated expression of immediate early genes (IEG; c-fos, Egr1 and arc) may be used to evaluate memory related neural activation (Kinnavane et al, 2015). Using this technique, early-stage pathophysiology has been linked to individual changes in memory driven regional activity (Hamm et al., 2017), but not to functional networks. However, outside of AD, across-subjects correlations of activity regulated IEG levels have been used to assess functional networks directly related to memory (Tanimizu et al., 2017; Wheeler et al., 2013; Vetere et al., 2017). This approach can prove useful for evaluating memory driven FC in mouse models of AD.

Recently, knock-in mouse models have been created to express AD-related genes under endogenous mouse promotors (Saito et al., 2014). This removes gene overexpression and resulting potential artificial phenotypes, allowing for a more careful assessment of the initial stages of AD (Sasaguri et al., 2017). In the current study, we detected object-place (OP) associative memory deficits as the earliest sign of cognitive decline in the humanized $App^{NL-F}/MAPT$ double knock-in (dKI) mouse model. This model specifically expresses all six isoforms of tau and overexpresses $A\beta_{42}$ which leads to marked amyloid deposition and typical pathological hyperphosphorylation of tau at an advanced age of 24 months (Saito et al., 2019). Given our specific interest in the early stages of AD, this model was chosen rather than the $App^{NL-G-F}xMAPT$ dKIs because of the slower development of its neuropathology. This option seemed fortunate as the first memory deficits detected in the OP task coincided with the emergence of the earliest stages of abnormal tau phosphorylation within the entorhinal-perirhinal region and not in the hippocampus, indicative of an early pathological state. Task-dependent activity was then measured in regions implicated with this form of associative memory, including primarily the DMN/MTL, and FC was assessed using graph theory techniques. Our results show that initial memory decline in AD could be linked to specific topological changes in memory dependent functional networks.

Results

Behavioural phenotyping reveals early alterations in object-place associative memory

Pattern separation (PS) and OP associative memory performances are commonly affected in prodromal stages of AD and cognitively normal elderly (Yeung et al., 2018, Hampstead et al., 2018, Reagh et al., 2018, Reagh and Yassa, 2014), and in mouse models at pre-plaque deposition stages (Zhu et al., 2017; Hamm et al., 2017). In order to detect earliest sensitive recognition memory deficits, a preliminary study was made to evaluate OP and PS performance, as well as long term object recognition performance at 2, 4, and 6 months of age (Figure 1—figure supplement 1). For OP and PS tasks, a short inter-trial-interval (ITI) of 5 minutes was chosen to ensure that deficits did not arise from a confounding perturbation of long-term memory consolidation. Given the high number of ages being tested and the difficult nature of the tasks, no results were significant in this preliminary experiment with multiple comparisons corrections. All groups succeeded in the long-term object recognition task and the PS task remained inconclusive because dKI's performances were highly variable (Figure 1—figure supplement 1A and 1B, respectively). On the other hand, a robust potential deficit could be seen at 4 months in the OP task, and persisted at 6 months of age (Figure 1—figure supplement 1C).

With a second independent cohort of mice, we confirmed that dKI mice were unable to detect a new OP association at 4 months of age (Figure 1A) (two sample t-test, WT vs. dKI: $t(20) = 2.85$, $P = 0.0098$; one sample t-test, against chance: dKI $t(10)=0.3095$, $p = 0.763$). On the other hand, 4-month-old mice did not show any deficits in short term novel object recognition (Figure 1B) (two sample t-test, WT vs. dKI: $t(19) = .0934$, $P = 0.9265$; one sample t-test, against chance: all $ts>3.94$, $ps<0.003$) and object location tasks (Figure 1C) (two sample t-test, WT vs. dKI: $t(20) = 1.052$, $P = 0.9173$; one sample t-test, against chance: all $ts>3.03$, $ps<0.013$). These results confirmed that the OP deficit was due to specific perturbations in associative memory rather than any separate impairments in the object recognition or spatial recognition.

We then evaluated early AD pathophysiological changes in 4-month-old mice using western blotting (Figure 1—figure supplement 2A). Antibodies targeting the amyloid precursor protein, APP-cleaved carboxy terminal fragments, phosphorylated tau (Thr181) and total tau proteins were used. Wild-type mice expressed mainly APP α-CTF fragments whereas dKI expressed mainly APP β-CTF fragments. Moreover, an increase in β-CTF/α-CTF ratio was seen in both the hippocampus (Figure 1—figure supplement 2B) and the medial temporal cortex (MTC; including entorhinal, perirhinal, postrhinal cortices) (Figure 1—figure supplement 2C), indicating upregulated amyloidogenic APP processing. In addition, an increase of the tau phosphorylation degree on Thr181 was only seen in the MTC of dKI mice compared to wild-type mice while both models expressed similar levels of total tau proteins. This is consistent with general consensus of the MTC as the initial area of tau staging (Braak and Braak, 1995). These results highlight that OP deficits occur in conjunction with considerably light pathophysiological changes, akin to an early preclinical AD stage.

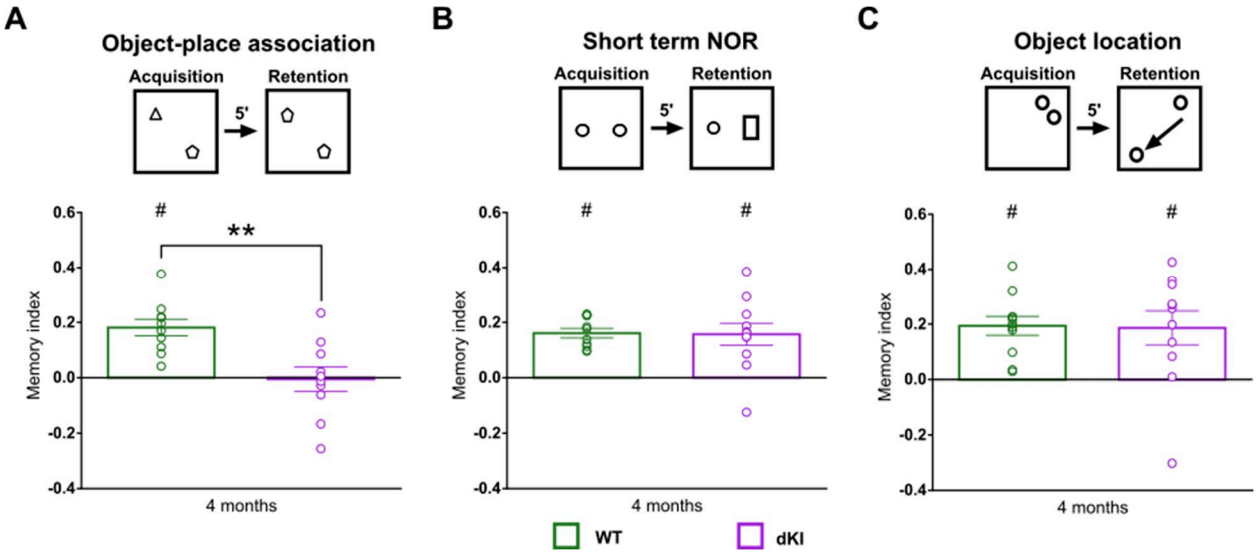

Figure 1. Behavioral characterization of young dKI mice (WT n = 11, dKI n = 11). (A) At 4 months of age, dKI mice reproduced the potential deficit seen in the object-place association task during preliminary phenotyping (two sample t-test, WT vs. dKI: $t(20) = 2.85$, $P = 0.0098$; one sample t-test, against chance: dKI $t(10)=0.3095$, $p = 0.763$). At the same age, dKI mice were normal in (B) object recognition (two sample t-test, WT vs. dKI: $t(19) = .0934$, $P = 0.9265$; one sample t-test, against chance: all $ts>3.94$, $ps<0.003$) (one WT mouse was removed due to being dropped before testing) and (C) spatial recognition (two sample t-test, WT vs. dKI: $t(20) = 1.052$, $P = 0.9173$; one sample t-test, against chance: all $ts>3.03$, $ps<0.013$), indicating that the loss in associative memory was not due to any singular loss in the short term object recognition or object location memory domains. Bar graphs represent the mean density (± SEM) * difference between genotypes **p<.01 (two sample t-test); #, difference from chance, #p<.05 (one sample t-test).

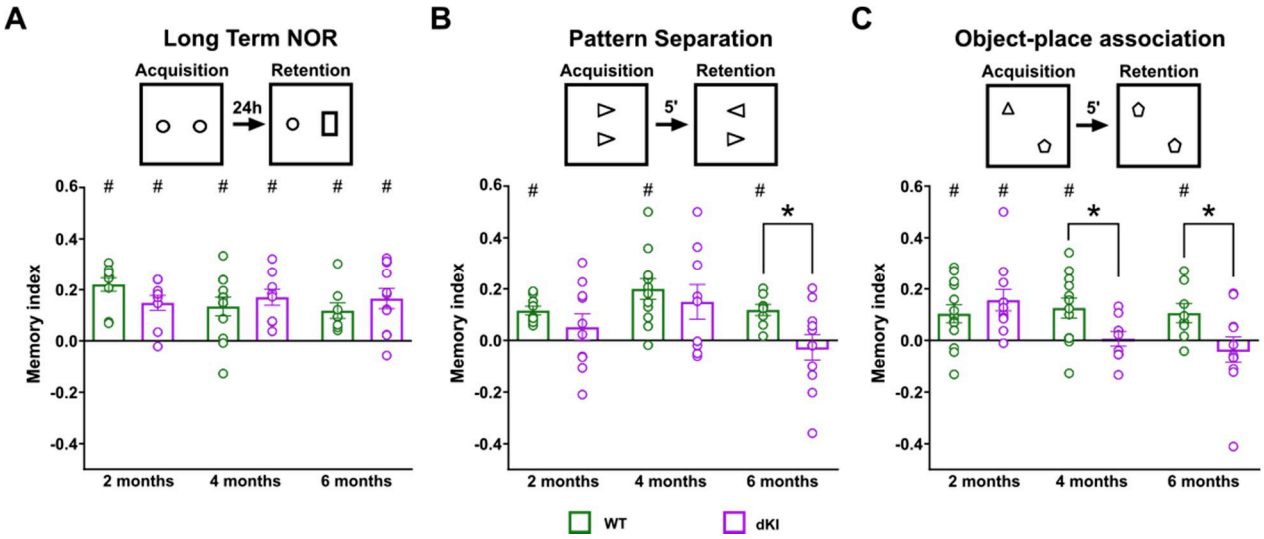

Figure 1 - figure supplement 1. Preliminary phenotyping of young dKI mice with sensitive recognition memory paradigms. Mice were tested at 2 months (WT n = 10, dKI n = 10), 4 months (WT n = 12, dKI n = 9) and at 6 months (WT n = 8, dKI n = 11). An additional cohort of (WT n = 3, dKI n = 1) was tested at 2 months in object-place association as the initial group did not reach significance above 0. (A) In the long term object recognition task, dKI mice were completely unaffected. (B) In the pattern separation task the dKI mice were highly variable making it so that they were not significant against chance at any age (one sample t-test, against chance: all dKI ts<.996, ps>0.055). However, between group significance was only obtained at 6 months of age (WT vs. dKI: t(17) = 2.364, P = 0.030). This variability may represent a variety of factors including perhaps affected DG neurogenesis (Scopa et al., 2020). (C) The earliest significant deficit in dKI mice appeared at 4 months in the object-place association task, a deficit which was conserved at 6 months (two sample t-test, WT_4mo vs. dKI_4mo: t(20) = 2.325, P = 0.0313; one sample t-test, against chance: dKI t(8) = 0.2086, P = 0.8399; two sample t-test, WT_6mo vs. dKI_6mo: t(17) = 2.132, P = 0.0479; one sample t-test, against chance: dKI t(10) = 0.7196, P = 0.4883). Although the variability seen during pattern separation may be interesting, we chose to continue our study with the more robust object-place deficit. Bar graphs represent the mean density (± SEM). difference between genotypes *p<.05 (two sample t-test); difference from chance, #p<.05 (one sample t-test). No multiple comparisons corrections were performed for these preliminary comparisons.

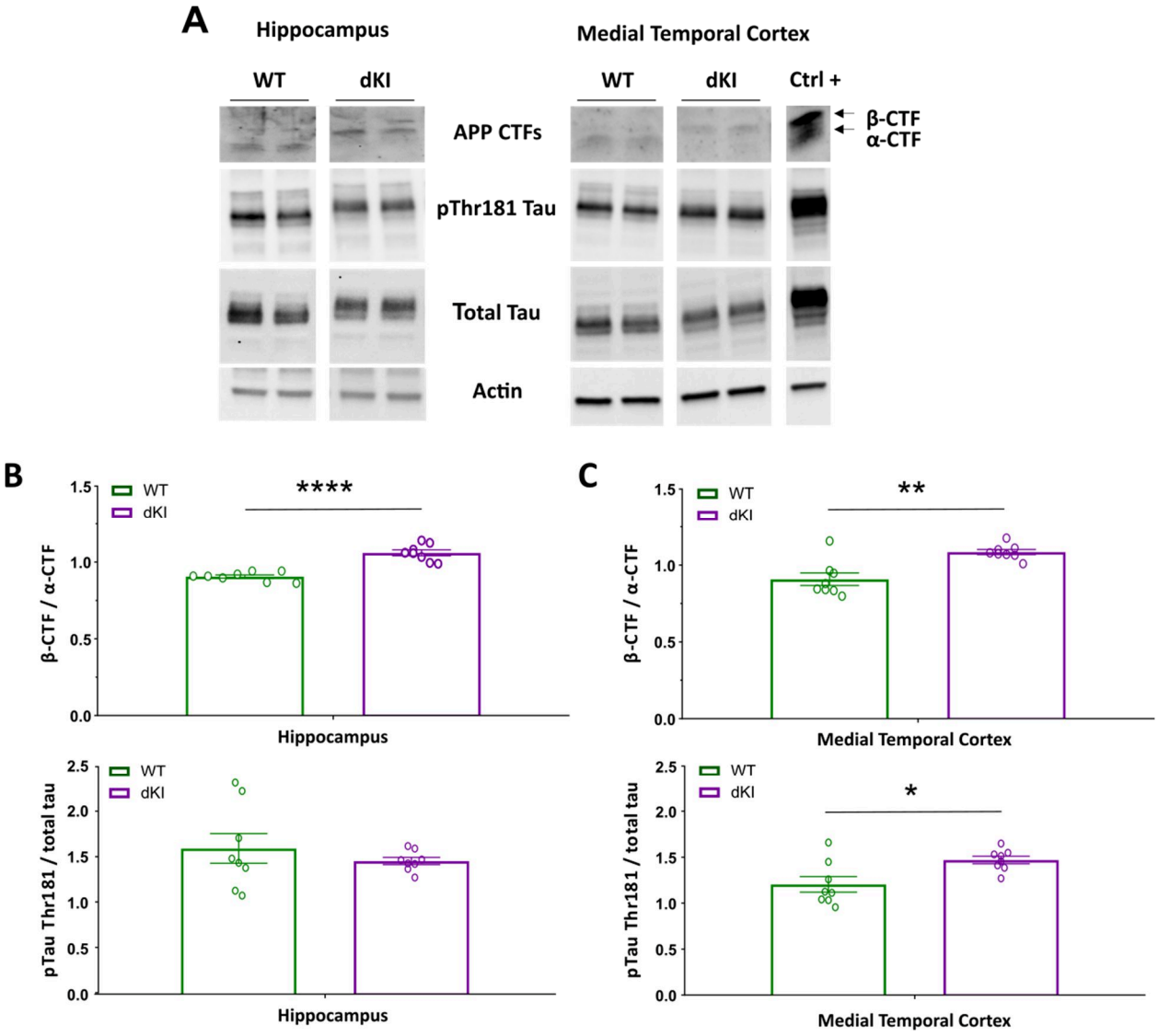

Figure 1 - figure supplement 2. Early stage of Alzheimer-like disease in 4 month old male dKI mice. (A) Representative blots of APP-cleaved fragments, phosphorylated tau proteins on the threonine 181 site and of total tau proteins in the hippocampus and medial temporal cortex from WT and dKI mice. Analysis of the ratio of the β-CTF on α-CTF fragments and the degree of tau phosphorylation on Thr181 in the (B) hippocampus and in the (C) medial temporal cortex. Results showed that dKI mice expressed mainly the β-CTF whereas the WT mice expressed mainly the α-CTF and the β-CTF/α-CTF ratio increased in both brain regions. Only the MTC displayed an increase of phosphorylated tau proteins. Bar graphs represent the mean density (± SEM). * p<0.05, ** p<0,01, *** p<0,001 and **** p<0,0001 (two sample t-test).

Assessing OP dependent changes in brain activity

While encoding processes are known to be perturbed in AD patients (Granholm and Butters, 1988), recent studies in animal models also find dysfunctional retrieval of engrams as a mechanism for memory loss in early stages of AD-like pathology (Roy et al., 2016; Etter et al., 2019). We thus aimed to evaluate encoding versus recall dependent changes in brain activity in relation to the OP deficit, through independent evaluation of the two test-phases. Thus c-Fos activation was quantified in brains of mice that had underwent either the acquisition phase (*encoding*) (Figure 2A) or the retention phase (*recall*) (Figure 2B) of the OP task. In order to account for the c-Fos protein expression curve, the ITI was extended to 3 hours, the shortest delay that could permit definite isolation between test-phases. As with a 5-min ITI, dKI mice that underwent the retention phase after a 3-h ITI were likewise unable to detect the novel OP association (two sample t-test, WT vs. dKI: $t(26) = 3.14$, $P = 0.004$; one sample t-test, against chance: WT $t(13) = 3.93$, $P = 0.002$; dKI $t(13) = 0.139$, $P = 0.891$). (Figure 2C). We then chose to evaluate 22 regions of interest (ROIs) encompassing subregions of the medial prefrontal cortex (mPFC), claustrum (CLA), retrosplenial cortex (RSC), dorsal hippocampus (DH) and medial temporal cortex (MTC) (Figure 2D-J). Neuronal hyperactivity is common feature in early AD and in young pre-plaque mice (Zott et al., 2019). We therefore first assessed test-phase and genotype dependent changes in regional activity.

Acquisition induces higher regional activity than retention

All regions except the DH (phase effect: DH $F(1, 192) = 1.85$, $P = 0.175$; subregion x phase effect: $F(3, 192) = 5.32$, $p = 0.002$; post-hoc Tukey: Acq vs Ret: CA1 $P = .052$, CA3 $P = .383$, DG_ip $P = .597$, DG_sp $P = .513$) showed higher levels of activity in the acquisition phase, although in the LEC this increase in activity was noticeably less drastic (phase effect: LEC $F(1, 96) = 5.22$, $P = 0.025$; all other Fs > 25.6, Ps < 0.001). This can be expected in the initial phase as the mice are subjected to stronger changes with two new objects in previously unoccupied locations in respect to the retention phase, where the only change is a new OP association. During acquisition, the mice are actively encoding several new features, new objects and their unique location in the open-field. Moreover, this helps confirm the absence of residual c-Fos in the retention groups. If residual c-Fos lingered from encoding until perfusion after the retention phase, one would expect similar or increased c-Fos density during the retention phase, not a decrease.

Hyperactivity in the claustrum and entorhinal cortex of dKI mice

The CLA and LEC showed increased activation in dKI mice regardless of the test phase (genotype effect: CLA $F(1, 96) = 8.29$, $P = 0.005$; LEC $F(1, 96) = 10.36$, $P = 0.001$). The MEC revealed increased activation in dKI mice specifically during the acquisition phase (MEC: genotype effect: $F(1, 96) = 25.64$, $P < 0.001$; genotype x phase effect: $F(1, 96) = 7.46$, $P = 0.007$; post-hoc Tukey: WT vs dKI during acquisition $P < .001$, WT vs dKI during retention $P = 0.252$).

Region	Acronym
Prelimbic cortex	PRL
Cingulate cortex	CG1
Infralimbic cortex	IL
Rostral claustrum	rCLA
Caudal claustrum	cCLA
Corpus ammoniss 1	CA1
Corpus ammoniss 3	CA3
Dentate gyrus suprapyramidal blade	DG_sp
Dentate gyrus infrapyramidal blade	DG_ip
Rostral retrosplenial cortex dysgranular (RSD)	rRSCd
Rostral retrosplenial cortex granular (RSG)	rRSCg
Caudal retrosplenial cortex dysgranular (RSD)	cRSCd
Caudal retrosplenial cortex granular (RSG)	cRSCg
Rostral perirhinal cortex dorsal (Ect)	rPRCd
Rostral perirhinal cortex ventral (PRh)	rPRCv
Caudal perirhinal cortex dorsal (Ect)	cPRCd
Caudal perirhinal cortex ventral (PRh)	cPRCv
Rostral lateral entorhinal cortex (DLEnt,DIEnt,VIent)	rLEC
Caudal lateral entorhinal cortex (DLEnt,DIEnt,VIent)	cLEC
Medial entorhinal cortex (MEnt)	MEC
Caudal medial entorhinal cortex (CEnt)	CMEC
Postrhinal cortex (Ect,PRh)	POC

Table 1. List of evaluated regions. Regions were chosen a priori based on their relevance to early AD pathology and to associative memory processing. In parentheses are region identifications according to the third edition Franklin and Paxinos Mouse Brain Atlas.

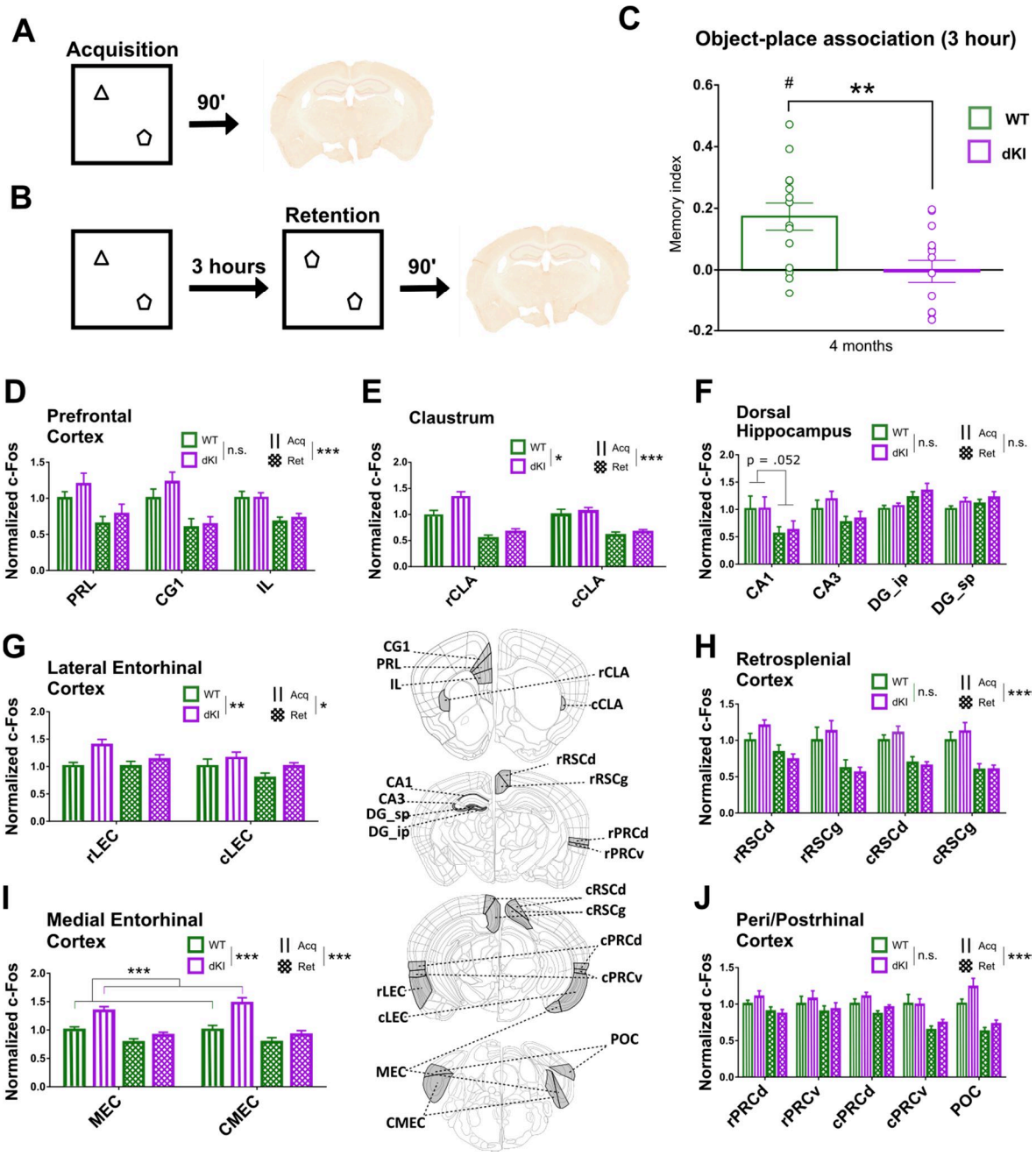

Figure 2. Regional activity during both phases of OP. Separate cohorts of WT and dKI mice were tested in either the (A) acquisition phase only or (B) the entire OP3h task, i.e., acquisition and retention phases. Ninety minutes following one test phase, brains were perfused and expression of the activity-regulated-gene, c-Fos, was evaluated immunohistochemically. (C) The dKI mice that underwent the whole OP3h task reproduced a deficit in object- place associative memory. difference between genotypes, **p<.01 (two sample t-test); difference from chance, #p<.05 (one sample t-test).(D-J) Graphs that illustrate c-Fos counts normalized to the WT-Acquisition group. For each region group a 3-factor ANOVA was performed for test-phase (Acquisition-Lines, Retention-Grid), genotype (WT-green, dKI-purple) and subregion effects. Significance for test-phase and genotype effects are depicted above each region graph; *p<.05, **p<.01, ***p<.001. (D-E,G-J) There was an increase in activity during the acquisition phase across all regions, except the (F) dorsal hippocampus. The (E) claustrum and (G) lateral entorhinal cortex presented increases in activity in dKI mice regardless of the test-phase. The (I) medial entorhinal cortex however, was hyperactive specifically during the acquisition phase ***p<.001 (Tukey post hoc). Bar graphs represent the mean density (± SEM). Subregion prefixes – r,rostral;c,caudal; suffixes – RSCd,dysgranular; RSCg, granular; PRCd, dorsal; PRCv, ventral; ip, infrapyramidal; sp, suprapyramidal. Error bars indicate the SEM. Schematics indicating the general locations of brain regions were adapted from Allen Mouse Brain Atlas derived vector images (Lein et al., 2007).

Computing functional coupling

Brain regions with correlated activity can be said to exhibit functional connectivity (FC), as co-modulations of activity can be a marker of inter-regional information sharing. In humans or head-restrained/anesthetized rodents recorded with EEG, MEG (for electrical signals) or fMRI (for metabolic rate), FC is computed from the covariance across time. In methods using regional expression of c-Fos, FC can be modeled by the covariance of regional activity across subjects to study memory driven networks in mice (Wheeler et al., 2013; Tanimizu et al., 2017). The validity of this approach has been confirmed using chemo-genetic techniques (Vetere et al., 2017).

From the c-Fos signal, we assessed FC by computing the inter-regional Spearman correlation coefficients (r) for each Genotype-Phase group. Correlation matrices were used to visualize all possible correlations within each group (Figure 3A-B). We first assessed global FC strength by taking the mean r value of each matrix. Most FC couplings were positive, however we found a few weakly anti-correlated pairs of regions. In evaluating FC, there were 3 ways to consider these negative correlations; as disruptive, as very-weak or as contributing equally to positive correlations. All three cases were evaluated by taking the mean r with retained, near-zeroed, and absolute valued negative correlations respectively. In the near-zeroed case, negative correlations were reduced to a value of .006, the smallest positive correlation observed.

During acquisition, we found no significant change in global FC strength between WT and dKI groups, for any of the three ways to treat negative correlations in FC (Figure 3C). However, during retention, there was a decrease in global FC strength in dKI mice with respect to WT. This decrease could be proved significant when considering negative correlations as disruptive or as very weak, but not when their absolute value was taken (Figure 3D). This indicates that two phenomena coexist: first, a reduction of positive inter-regional correlations, corresponding to decreased “cooperation” between some regions; second, an increase in absolute strength of inter-regional negative correlations, corresponding to increased “conflict” between some regions.

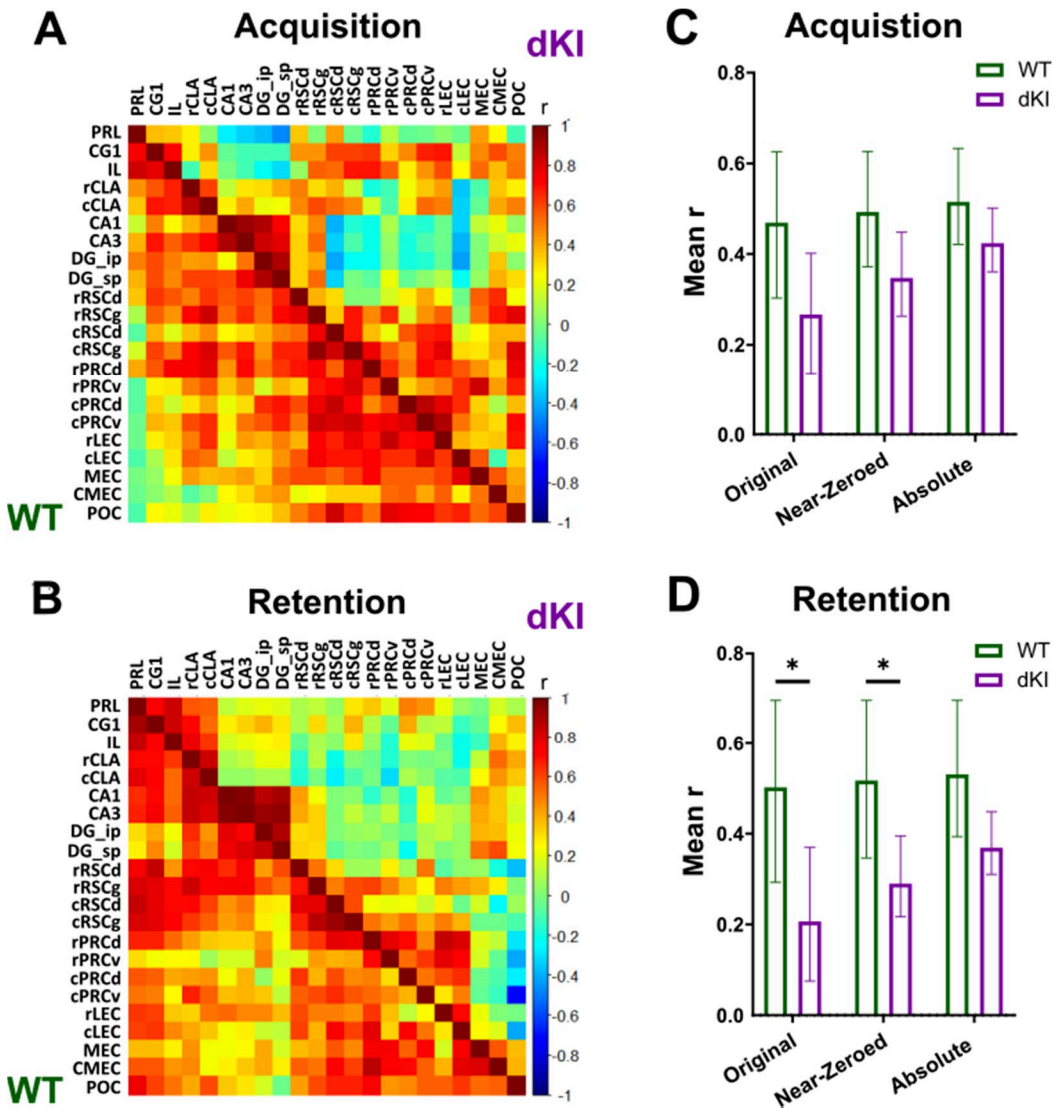

Figure 3. Functional connectivity is depicted with matrices showing across subjects inter-regional spearman correlations for c-Fos expression during (A) retention and (B) acquisition. Colors reflect correlation strength (scale, right). We assessed global FC strength by taking the mean r value of each matrix with retained, near-zeroed, and absolute valued negative correlations. In the near-zeroed case, negative correlations were reduced to a value of .006, the smallest positive correlation observed. (C) We found no change in global FC strength for any of the three cases during acquisition. (D) During retention however, there was a significant decrease in global FC strength with the original and near-zeroed correlations, but not when they are absolute valued. Bar graphs represent the mean bootstrap value, and the error bars represent the bootstrapped 95% confidence interval. * -the 95% CI for the difference ≥ 0

Generating functional networks

Each functional connectivity matrix can be considered as the adjacency matrix of a weighted undirected network (Rubinov and Sporns, 2010), and, as such, its organization can be assessed through the analysis of functional networks, using techniques arising from graph theory. From each matrix a functional network was generated as a fully connected weighted graph. In these graphs, the regions are represented as nodes and the functional connections between regions are represented by edges. The strength of a connection between two regions, as represented by the edge weight, is determined by their inter-regional correlation strength. As negative correlations are weak and pose difficulties of interpretation when dealing with many graph theory techniques, we decided for all following analyses to replace them with near-zeroed values when constructing our functional networks, in line with other studies of c-Fos derived functional networks in-vivo (Vetere et al., 2017). It has been shown that community organization of structural networks can change between healthy individuals and different stages of MCI (Pereira et al., 2016). We decided to evaluate community organization of each functional network to see if any consistent or phase specific changes could be detected between genotypes. This could also aid us in obtaining a qualitative understanding of organization of information flow in each network. Network communities were detected through a modularity maximization procedure (see Materials and Methods). This unsupervised algorithm separates the nodes into distinct groups (the communities), such that nodes within a community are more strongly interacting between them than with nodes in other communities. The separation in communities will partly stochastically vary for different runs of the algorithm and different bootstrap instances of the FC matrix. To extract a robust consensus set of communities we then computed allegiance matrices (Bassett et al., 2015), which depict the percentage of times that any given pair of regions is attributed to the same community among bootstraps (Figure 4).

WT networks differentially engage the DH and mPFC

A stable community is found in both task phases encompassing most of the MTC and the cRSC (Figure 4A,B; red area at the bottom right of each WT allegiance matrix). The main difference between the WT-Acquisition and WT-Retention groups was the differential involvement of the DH or mPFC with this MTC community. During acquisition, the DH shared a community primarily with the mPFC (Figure 4A; red area at top left the allegiance matrix). During retention, the mPFC shared allegiance across the network (Figure 4B; red area along the mPFC rows across the top of the allegiance matrix). This more global incorporation of the mPFC appeared to be driven largely through the RSC (Figure 4B; darker red square area located at the middle of the top three mPFC rows).

dKI networks reveal consistent departures from WT community structure

During acquisition, the DH community largely disengaged with the mPFC as compared to the WT-acquisition group (Figure 4C; green square at the top left of the allegiance matrix). Moreover, the DH appeared to be more strongly aligned to the CMEC, MEC, and POC as compared to the rest of the MTC (Figure 4C; the more red/orange area at the right of the DH rows).

During retention, both the mPFC and the DH disengaged with the MTC. This led to distinct communities containing mPFC/CLA, DH and the MTC (Figure 4D; three separate red squares of the allegiance matrix). Similarly to the acquisition phase, the MEC/CMEC/POC regions were heavily recruited by the mPFC and DH communities (Figure 4D; red area at top right), at the cost of disengagement with the MTC

community (Figure 4D; green area at bottom right of the allegiance matrix). The consistent recruitment of the MEC/CMEC/POC in both dKI groups elucidates a possible role for these regions as compensatory hubs in this mouse model.

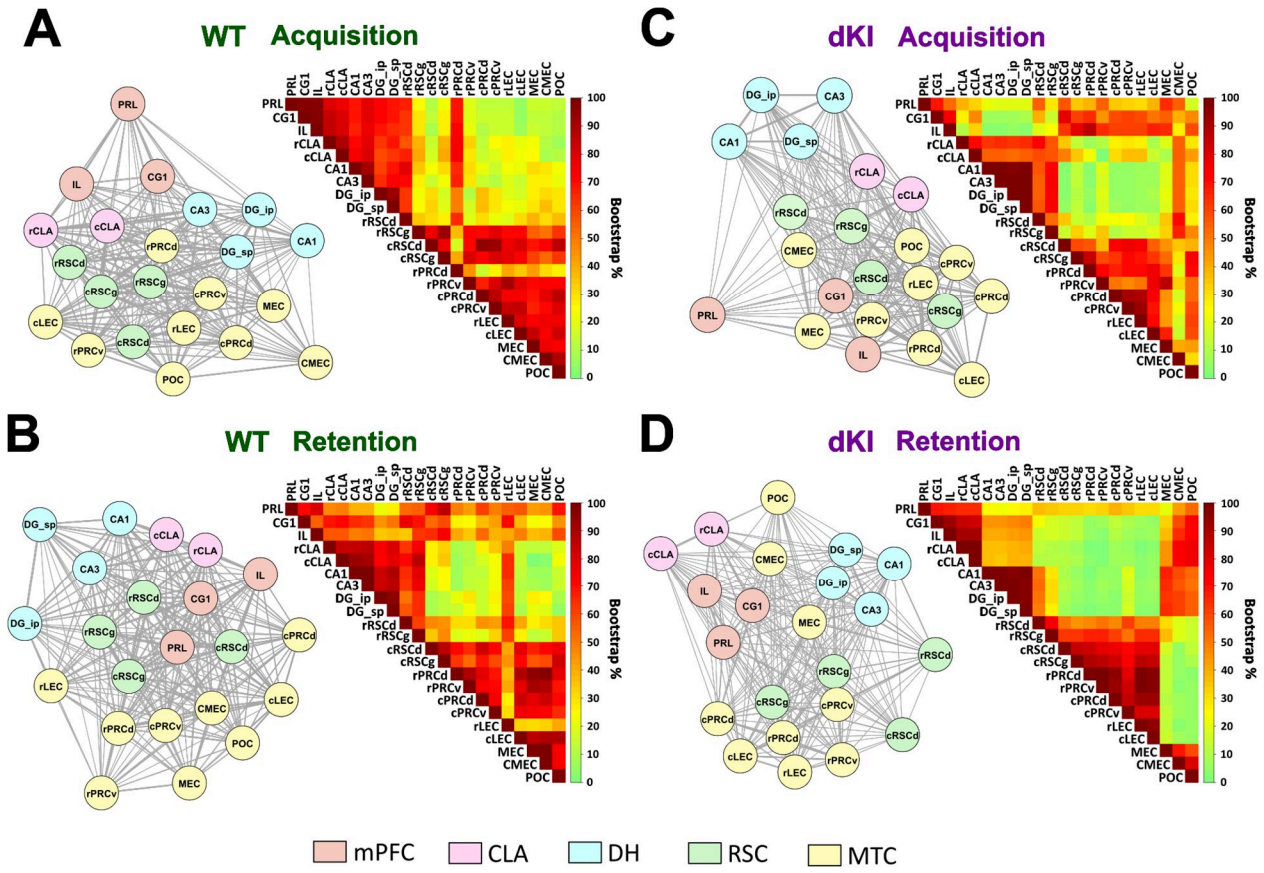

Figure 4. Functional networks were computed as fully connected weighted graphs, with regions as nodes (circles) and inter-regional correlation strengths as edge weights (line thickness). For visual examination of networks, nodes were placed so that they lie closer to nodes with which they are strongly connected, and were color coded according to a priori region subfields. Communities were detected through modularity maximization, which finds communities of regions that have stronger connections with each other relative to the rest of the network. Communities were detected across bootstrapped networks, and allegiance matrices were utilized to depict community stability as the percentage of bootstraps that contain any given pair of regions in the same community. (A,B) In both WT groups there is a stable MTC/cRSC community (red area at the bottom right of each WT allegiance matrix). (A) In the WT-Acq there is a stable DH/mPFC community (red area at the top left of the allegiance matrix). (B) In the WT-Ret the mPFC shares community allegiance with all of the network (red area along the mPFC rows across the top of the allegiance matrix) as mediated through the RSC (darker red square in the middle of the top three mPFC rows). (C,D) Across both dKI groups, the MEC/CMEC/POC regions appear to display a consistently modified community allegiance in respect to the WT, associating more with the DH/mPFC and sometimes less with the rest of the MTC (red area at top right of each dKI allegiance matrix, some green areas at bottom right).

Information flow in functional networks

Efficient integration of information flow across functional networks is shown to aid in cognitive function (Wang et al., 2013a; Martinez et al., 2018). Interpreting network links as "pipes", how well can a network allow information to flow will depend not only on how wide individual pipes are, but also on how pipes are disposed and aligned to form pipelines between the nodes that must communicate, without too many steps and bottlenecks. The general capacity for a network to sustain efficient flows is quantified in graph theory by metrics such as *global efficiency* (see Materials and Methods; Latora and Marchiori, 2001). It is important to note that even if a network has reduced global FC strength, its global efficiency may rest un-affected if there are well placed "hub" regions to facilitate indirect communication. To evaluate information flow at the regional level, *nodal strength* and *nodal efficienc*y metrics are used. Nodal strength measures the degree to which each specific region can exchange information directly with all other regions of the network. A region with low strength may still be able to communicate with its network indirectly, again likely through hub regions. This indirect communication can be measured using nodal efficiency. Organization of information flow in a network can be examined through strength and efficiency distributions. Regions with higher strength and efficiency can be considered to contribute more to their network. High direct connectivity of a region, such as high strength, is also shown to describe potential hub regions (Vetere et al., 2017) which, as we have described, are needed to facilitate indirect information flow and maintain global efficiency.

We compared information flow between WT and dKI networks within each test-phase. Organization of information flow was first evaluated through a qualitative examination of node strength and nodal efficiency distributions. To best visualize distributions, the strength/efficiency values were squared and normalized to the highest value within each network, and were displayed as necklace diagrams (acquisition - Figure 5A,B) (retention – Figure 5F,G). We then directly compared global efficiency and nodal strength/efficiency between genotypes in subsequent analyses (acquisition - Figure 5C,D,E) (retention - Figure 5H,I,J).

Acquisition– the DG_sp maintains efficiency despite a drop in strength

During acquisition, strength and efficiency distributions were largely conserved between genotypes with strong emphasis on RSC and MTC regions. Although, in the dKI there appeared to be additional involvement of mPFC, MEC and POC (Figure 5A,B). Nevertheless, global efficiency was not severely affected in the dKI network (Figure 5C). The unique significant drop in nodal strength was seen in the DG_sp (Figure 5D), but as there was no drop in nodal efficiency (Figure 5E), it could still effectively communicate with the rest of the network indirectly. This maintenance of indirect communication, despite drops in direct communication, reflects the potential importance of the rRSC or MEC/CMEC/POC compensatory hubs.

Retention – severe losses in network efficiency, especially across the cingulate cortex

During retention, heavy emphasis was placed on mPFC and RSC regions in the WT network. In the dKI network this emphasis was largely lost and the distributions take on a more homogenous structure, though the rRSCg and mPFC subregions still appeared to be among the most involved (Figure 5F,G). Global efficiency was significantly reduced in the dKI network (Figure 5H), with sharp drops in strength seen in the PRL and the POC, but most severely in both subregions of the RSCd (Figure 5I). Loss in nodal

efficiency was even more prevalent, with additional reductions in the CG1 and the cRSCg (Figure 5J). These results suggest that retention dependent functional integration across the cingulate cortex is severely disrupted in the dKI, and may be linked to reduced hub strength of the RSCd.

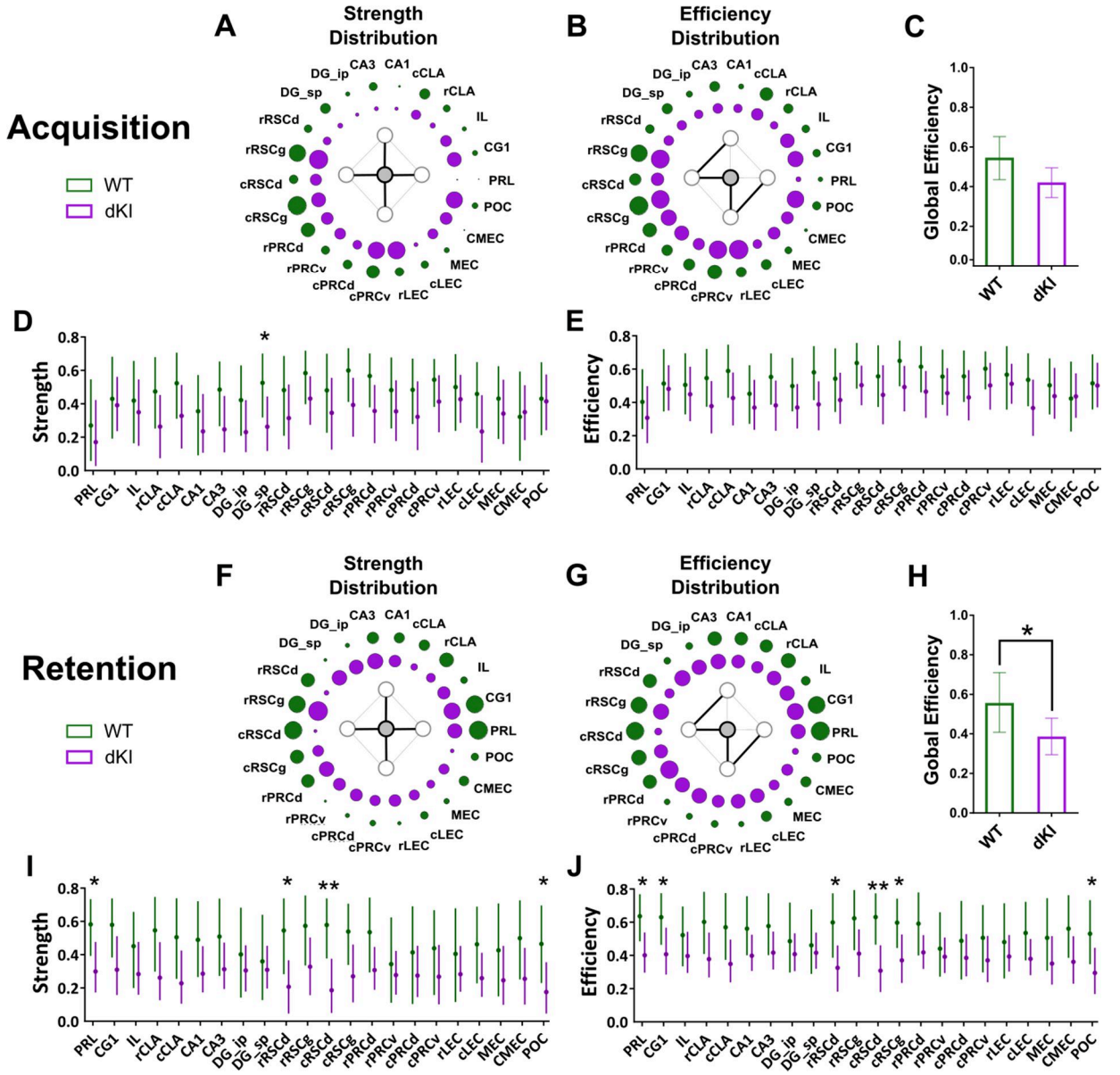

Figure 5. Network organization of information flow was assessed through examination of node strength and nodal efficiency distributions in both test-phases (acquisiton,retention). These distributions were visualized using necklace diagrams, where circle size reflects the within network normalized (A,G) strength[2] and (B,H) efficiency[2]. Global efficiency was then compared directly between genotypes to assess (C,F) network integration. (D,I) Nodal strength and (E,J) nodal efficiency were compared between genotypes to assess region dependent changes in direct and indirect information flow, respectively. (A,B) During acquisition, strength and efficiency distributions were roughly conserved between genotypes, with strong emphasis on the RSC and MTC regions, although in the dKI, mPFC, MEC and POC subregions were much more involved. (C) Global efficiency was not severely affected in dKI mice. (D) A drop in region strength was seen in the DGsp, (E) but its efficiency was unaffected. (G,H) During retention, heavy emphasis was placed on mPFC and RSC regions in the WT network. In the dKI, this emphasis is largely lost. (F) Global efficiency of the dKI network was significantly reduced as compared to the WT network. (I) Reductions in region strength were seen in the POC, PRL, and most severely in both subregions of the RSCd. (J) Reductions in efficiency was retained among these regions, with additional losses in the CG1 and the cRSCg. Bar graphs and dot graphs represent the mean bootstrap value, and the error bars represent the bootstrapped 95% confidence interval. * -the 95% CI for the difference ≥ 0 ; ** -the 99% CI for the difference ≥ 0

Relating network efficiency and memory

Finally, we addressed the question of whether the reduction of OP memory performance in dKI mice could be accounted for by the reduction in network efficiency observed during retention. Our aim was thus to determine if a relationship could be found between global efficiency and memory index in the WT and be used to predict dKI memory loss. This was assessed through correlation testing across sub-sampled WT populations, where each sub-sample corresponded to the removal of one mouse. From each sub-sample the average memory index and resulting global efficiency were calculated, and correlation significance was tested with Pearson and Spearman correlation coefficients.

Global efficiency positively correlates with an exploration adjusted memory index, and predicts memory deficiency in the dKI

No significant correlation was found between global efficiency and memory index across WT sub-samples (Figure 6 - figure supplement 1A). However, we noticed that of the mice with high memory index, those with greater exploration times (total time exploring both objects) appeared to have a weaker contribution to global efficiency. This hinted a potential dampening effect of general object exploration on memory driven FC. Note that increases in exploration time themselves may be interpreted as a further sign of memory function alteration, beyond reductions in the previously defined memory index MI. We thus defined an exploration index EI, quantifying the exploration time of the mouse normalized to the group and used it to compute as well an exploration adjusted memory index as the memory index divided by the exploration index (MI/EI). Decrease of such an exploration adjusted memory index may reflect both MI decrease and EI increase, thus summarizing both probed facets of memory-related behavior alteration. As in the case of MI alone, we did not find a significant correlation between global efficiency and EI index (Figure 6 - figure supplement 1B). A significant positive correlation was found however between global efficiency and the adjusted memory index MI/EI across the WT sub-sampled networks (Figure 6).

Moreover, we could show that extrapolating the best fit line for the WT ensemble to drops in global efficiency as large as the ones observed in the dKI ensemble also predicted the observed dKI decrease of the MI/EI behavioral performance index. This is illustrated in Figure 6 where the dashed continuation of the green line (the extrapolation of the best fit line to the WT ensemble) intersects the cloud of purple points (the ensemble of dKI sub-samples). The prediction of dKI sub-samples MI/EI index based on extrapolating the law fitted on WT sub-samples yielded errors way smaller than what expected at chance level, as we could verify via comparison with a null distribution of prediction errors constructed from 1000 randomly fit models to the WT ensemble. This is shown in the inset histogram of Figure 6, where the green vertical line (prediction error of best fit to WT) lies to the left of the leftmost red vertical line (lower end of the null distribution 95% CI).

This suggests that subjects with a high memory index but low total exploration time are thus more likely to have higher global efficiency. Contrary to memory index, there is no detectable significant difference in total object exploration time between the WT and dKI groups (Figure 6 - figure supplement 1C). Memory index is thus a more sensitive metric of subtle and complex behavioral changes, which are tracked by a decrease of global efficiency from WT to dKI. These results support reduced network integration as a potential factor for impairment of OP memory recall in the dKI.

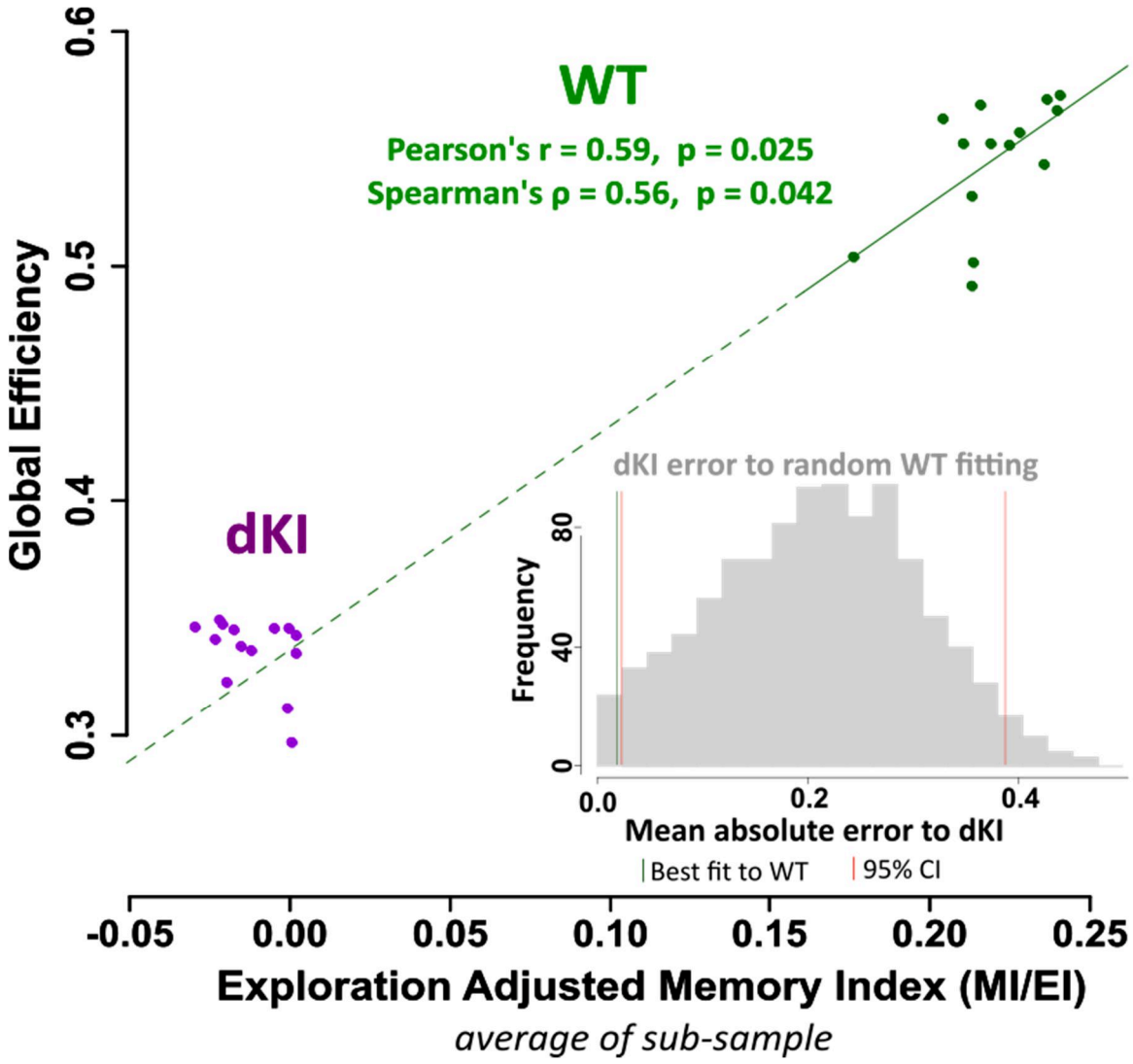

Figure 6. Association between network efficiency and exploration adjusted memory index "MI/EI". Sub-samples were generated from each retention group by resampling n-1 mice without replacement. From each sub-sample, the average MI/EI and the network global efficiency were computed, where each sub-sample is depicted as point on the plot. The relationship between global efficiency and MI/EI was evaluated across only the WT sub-samples (solid green line), and a significant positive linear relationship was found. Interestingly, when this linear law across WT sub-samples was extrapolated down (dashed green line) to the reduced global efficiency of the dKI sub-samples, it could predict their reduction in MI/EI (the intersection of the dashed green line to the cloud of purple points). The prediction of dKI sub-samples MI/EI index based on extrapolating the law fitted on WT sub-samples yielded errors way smaller than what expected at chance level, as we could verify via comparison with a null distribution of prediction errors constructed from 1000 randomly fit models. See inset histogram: the green vertical line (error of best linear fit to WT) lies to the left of the leftmost red vertical line (lower end of the null distribution 95% CI).

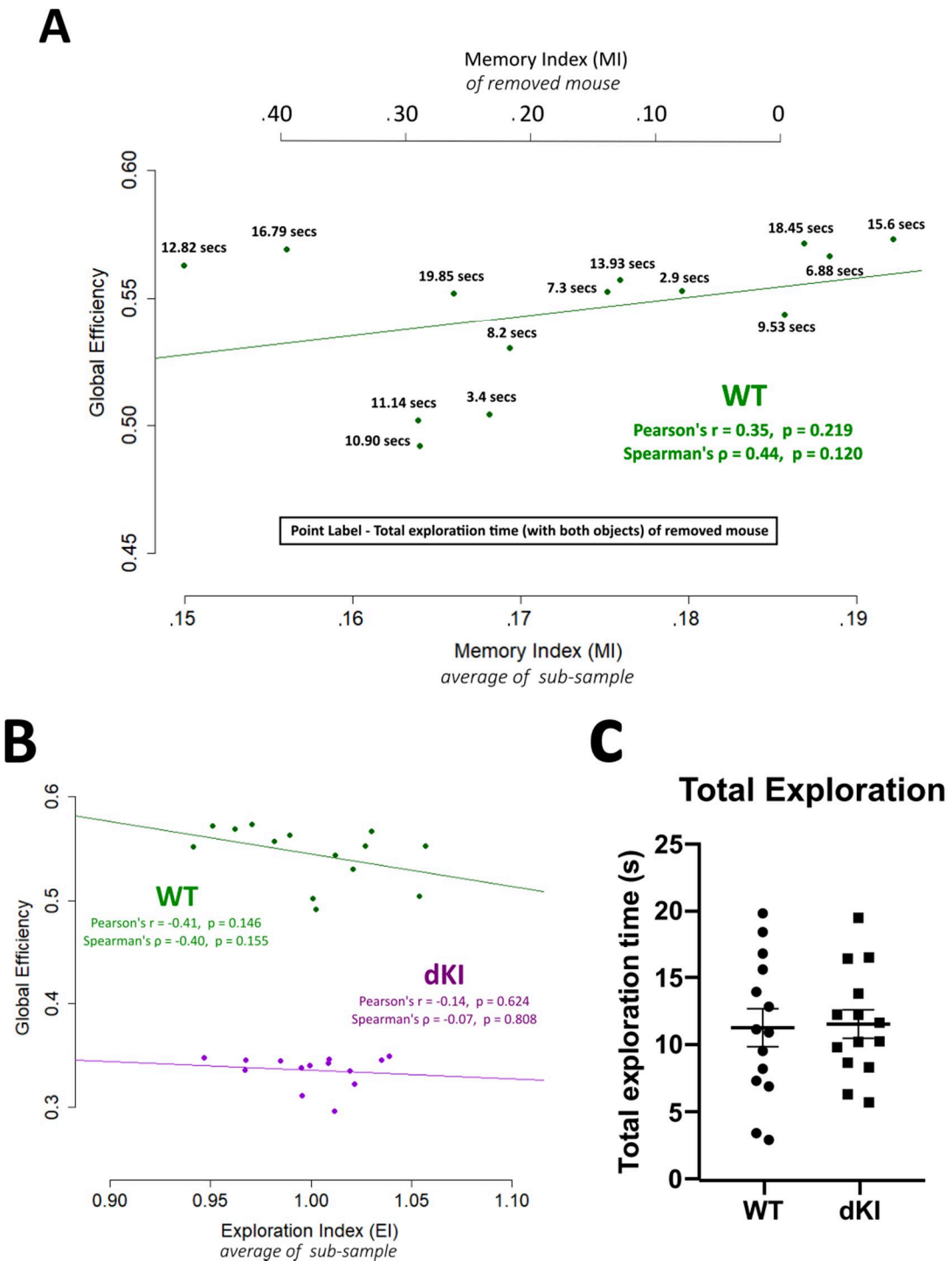

Figure 6-figure supplement 1 (A) There was no relationship found between global efficiency and memory index. However, we noticed that of the mice with high memory index, those with greater exploration times (total time exploring both objects) appeared to have a weaker contribution to global efficiency. To take into account an exploration disruption effect on memory related FC, an exploration adjusted memory index was computed as the memory index divided by the exploration index (MI/EI), where the exploration index (EI) is the exploration time of the mouse normalized to the group. (B) We verified that there was no direct relationship found between global efficiency and EI. (C) There was also no difference in total exploration between WT and dKI mice.

Discussion

The current necessity to learn more about initial steps of AD pathology prompted us to investigate brain network alterations associated to the encoding and retrieval phases of the first recognition memory paradigm affected in the late-onset *App*$^{NL\ F}$*/MAPT* dKI mouse model of the disease (Saito et al, 2019). Here we show that the neuropathology expressed by 4-month-old dKI mice at the time of their earliest recognition deficit is reminiscent of an early preclinical stage. Quantification of c-Fos activation highlighted an abnormally increased activity in the entorhinal cortex and the claustrum, two entities known to be vulnerable to AD pathology. Finally, extensive analyses of network connectivity point to a disorganization of internal communication between and within the MTL and interconnected regions where the RSC seems to play a pivotal "hub" role which could be disrupted in dKI mice.

Object-place recognition deficit as an early marker of emerging AD neuropathology

In the battery of five recognition memory tasks, the object-place associative memory task was the first to detect a deficit in dKI mice at 4 months of age. This recognition deficit occurred 2 months before spatial pattern separation deficits and with intact long term object recognition memory up to 6 months of age. The object-place task seems to be highly sensitive to early amyloid pathology because it was also impaired at pre-plaque stages in more aggressive models of AD (Bonardi et al, 2016; Hamm et al., 2017). In TgCRND8 mice it was specifically associated with increased levels of β-CTF in the hippocampus (Bonardi et al, 2016; Hamm et al., 2017). Aβ levels of *App*$^{NL\ F}$*/MAPT* dKI were not evaluated in this study, but the seminal work characterizing the parental single KI *App*$^{NL\ F}$ mice already showed increased cortical levels of the neurotoxic species $A\beta_{42}$ at the age of 2 months (Saito et al, 2014). This early accumulation of Aβ in 2-month *App*$^{NL\ F}$ mice was associated with significant cell loss and hyperexcitation in the LEC, whereas the same alterations appeared several months later in the CA1 (Petrache et al., 2019). Here, we show for the first time evidence for early onset of AD pathology in 4-month-old dKI mice with specific increases in levels of β-CTF and phosphorylated tau labeled with AT270 antibodies in the MTC, but not in the dorsal hippocampus. These results suggest that early abnormal levels of tau phosphorylation are still restricted to the MTC at the age of 4 months. This is of particular importance because the PRC-EC pathway has long been seen as a primary site of neurodegenerative event and dysfunction that characterizes the earliest preclinical Braak stage I of AD tau deposition (Kahn et al, 2013: Braak and Braak, 1995; Hyman et al, 1984). Interestingly, significant worsening of neuropsychological markers of PRC and EC functionality were detected more than 10 years before AD diagnosis (Hirni et al, 2016). More recently, Yeung et al., 2018, showed that object-place recognition performance was predicted by anterolateral EC volume in the elderly. This result is in agreement with studies attributing a key role of the equivalent rodent LEC in the network supporting association of an object with a place or a scene (Deshmukh et al, 2012; Wilson et al, 2013a,b; Chao et al 2016). It must be noted that deficits in the pattern separation task in 6-month-old dKIs suggest subsequent development of functional alterations within the DG-CA3 region which is in agreement with studies in aMCI patients and transgenic mouse models of AD (Yassa et al, 2010; Zhu et al, 2017). All these findings strongly suggest that 4-month-old dKI mice recapitulate early impairment in recognition memory and specific vulnerability of the PRH-EC region to both amyloid and tau pathologies as found in preclinical stages of AD (Kahn et al, 2014).

Distributed increase in c-Fos activation possibly reflecting spreading of pathological hyperactivity

We detected high level of c-Fos expression in the CLA and the LEC of dKI mice regardless of the test-phase suggesting that both structures would be hyperactivated during memory encoding and recall. On the other hand, the hyperactivation of the MEC restricted to the acquisition phase could be have been triggered by active encoding of the new environment. Well documented in mouse models of AD, early hyperactivity within the LEC appears as a consequence of local increase in amyloid pathology and it is considered as a major factor driving propagation of both Aβ and tau pathology to its main outputs especially the hippocampus (Xu et al., 2015; Nuriel et al., 2017; Rodriquez et al., 2020). The CLA has been less extensively studied, but a few studies show evidence of Aβ accumulation and neurodegeneration in this region (Qin et al, 2013; Ogomori et al., 1989; Gustafson et al., 1998). Interestingly, an early study in Alzheimer's patients found neuronal loss only within a CLA subregion strongly connected with the EC (Morys et al., 1996). Thus, EC may also propagate hyperactivity, exporting amyloid and tau pathology to the CLA as well as other limbic cortices in preclinical stages of AD (Bonthius et al., 2005). Note that an alternative hypothesis has been proposed with a central role of the CLA in the spreading of AD pathology in the brain (Avila and Perry, 2021). Being largely interconnected with most cortical areas (Wang et al, 2017), hyperactivity of CLA may initiate or aggravate spontaneous the cortical network hypersynchrony and task-induced hyperactivation found in elderly at risk and in early MCI (Mueller and Weiner, 2017; Corriveau-Lecavalier et al., 2020).

Early-stage hyperactivity has also been proposed to reflect compensatory mechanisms which would first help maintaining and then worsen cognitive function through the spreading of neuropathological processes and a deleterious impact on cognitive-related network organization and functioning (Corriveau-Lecavalier et al., 2020). There is some indication for a reorganization of network information flow in the dKI mice. We saw through the community organization of dKI functional networks during both phases, that the MEC and POC are more integrated with mPFC and DH communities (Figure 4C,D). This change in community allegiance may be a consequence of an initial hyperactive state within the EC, much like artificial stimulation of brain structures can enforce specific functional networks (Warren et al., 2019). In certain cases, this shift towards stronger outbound allegiance may help facilitate alternative communication between the MTC and interconnected regions, as seen with the maintenance of indirect information flow of the DG_sp during acquisition (Figure 5D,E). The apparition of compensatory hubs may be one way through which hyperactivity could initially help memory processing during the preclinical AD.

mPFC and RSC are disrupted during object-place associative memory retention

The mPFC and RSC were the most heavily utilized regions in WT mice during retention phase, and direct and indirect information flow through these regions was significantly reduced in dKI mice (Figure 5F). The specificity of this dysfunction to the retention phase is not surprising as the mPFC and RSC are shown to be more involved in the retrieval and/or editing of memory traces rather than encoding *per se* (Mitchell et al., 2018). Lesioning the RSC disrupts object-place associative memory in rodents (Parron and Save., 2004), and communication between the mPFC-MTC is also shown to be essential (Chao et al., 2016; Hernandez et al., 2017). The RSC is proposed to play a pivotal “hub” role in facilitating this communication as it exhibits strong structural connections with both the mPFC and the MTC (Sugar et al., 2011, Vann et al., 2009). In humans, the posterior cingulate cortex (PCC) and RSC, close equivalents to the rodent RSC (Lu et al., 2012, Stafford et al., 2014, Vogt and Paxinos, 2014), are shown to support structural connectivity between the mPFC and MTL, essential to associative memory networks and the

DMN (Greicius et al., 2009, Miller et al., 2014). The hubness of the RSC during retrieval is clearly supported by the community organization of our functional networks, where it is well positioned to facilitate communication between the mPFC and MTL communities (Figure 4B). The severe loss in strength seen in the dysgranular RSC may therefore indicate an object-place recall-dependent roadblock for mPFC-MTL communication.

One question lies as to why the dysgranular RSC was more severely disrupted than the granular part. The dysgranular cortex is comparatively more connected to visual and sensory processing areas, making it ideal for processing and identifying local and distal cues for allocentric orientation. Lesioning the dysgranular RSC alone is enough to have rats shift from allocentric to egocentric strategies in a spatial memory task (Vann and Aggleton., 2005). The dysgranular RSC contains landmark dependent head direction cells, which may help orient the mice in the open field with respect to the objects (Jacob et al., 2016), and decreased strength of the dysgranular RSC may contribute to their dysfunction.

Our findings also corroborate those of human studies showing that the mPFC and the PCC/RSC are often disrupted in evaluations of functional and structural connectivity in aMCI (Catheline et al., 2010; Wang et al., 2013c). The especially severe disruption of the RSC reflects clinical observations of the human PCC as one of the most, if not the most, consistently disrupted regions in evaluations of resting state FC of aMCI (Badhwar et al., 2017; Eyler et al., 2019). The mPFC and the PCC/RSC are also the first regions to display amyloid deposition (Palmqvist et al., 2017). The PCC/RSC shows reduced connectivity in pre-plaque APOE ε4 carriers at risk for developing AD (Wang et al., 2013b; Jones et al., 2016), and very early increases in PCC amyloid deposition correlate with face-name associative memory deficits in subjective cognitive decline (Sanabria et al., 2017). Initial pathologies of amyloid in the mPFC/PCC/RSC and tau in the MTC may thus have a combined negative effect on associative memory through reducing memory-recall dependent FC.

Decreased global efficiency during retention predicts memory deficits in dKI mice

In WT mice, we detected a positive relationship between global efficiency of the retention network and memory performance when taking into account a disruptive effect of total object exploration. The exploration disruption on memory driven FC can perhaps be explained by increased focus and a more conscious exploration of objects for mice with a low exploration index, in contrast to a more haphazard exploration of objects for mice with high exploration index. This may also indicate a disruptive effect of simultaneous sensory or motor network activation. Regardless, dKI mice presented no difference in object exploration as compared to the WT mice, making it an unlikely behavioral link to reduced global efficiency in these mice.

Global efficiency of c-Fos derived fear memory networks has already been shown as a reliable measure for predicting memory performance in mice (Vetere et al., 2017). Such findings are consistent with clinical observations linking increased global efficiency to better cognitive function (Li et al., 2009; Stanley et al., 2015). The relationship across the WT group can be extrapolated down to predict memory performance in the dKI. This provides further evidence that their drop in memory performance is directly linked to deficient information transfer of the memory retention network. There is increasing evidence that memory loss in AD pathology is related to dysfunctional recall, as it can be rescued by aiding retrieval processes (i.e., activating the “silent” engram; Roy et al., 2016, Perusini et al., 2017). Perhaps

early associative memory deficits of dKI mice could be rescued by activating "silent" inefficient functional networks. In humans, noninvasive brain stimulation has been extensively studied as a potential therapeutic tool for AD on regions such as the dorsolateral mPFC with mixed results (Weiler et al., 2020). However, electromagnetic stimulation of the parietal cortex was shown to support associative memory by increasing memory-retrieval dependent FC strength of an associated parietal-RSC-hippocampal network (Wang et al., 2014; Warren et al., 2019). Taken together with our study, these results suggest that the PCC/RSC, or more laterally accessible and functionally similar regions such as the parietal cortex, may be more effective targets for improving associative memory in AD.

Contrast with resting state fMRI in other mouse models of AD

Contrary to our results, studies that evaluate resting state networks in pre-plaque or early-NFT mouse models of AD predominantly find cortical and hippocampal-cortical hyperconnectivity, while hypoconnectivity appears at later stages (Asaad and Lee, 2018). This suggests that perturbations in resting state FC may predict memory FC perturbations, but do not directly mirror them. Moreover, the mouse models used to evaluate pre-aggregate resting state FC presented either amyloid pathology (Shah et al., 2016; Shah et al., 2018) or tau pathology (Degiorgis et al., 2020) but not both concurrently. It has been shown with combined resting state fMRI and PET imaging in humans that increased Aβ alone is associated with hyperconnectivity of the DMN while combined Aβ and Tau pathologies reveal hypoconnectivity (Schultz et al., 2017). Whether these contrasting results reflect differences between "resting state vs memory driven FC" or differences in "amyloid/tau pathological staging" will be more thoroughly understood once resting state fMRI is directly measured in young dKI mice.

In conclusion, our results suggest that the present dKI model was caught at the very beginning of its neuropathology as it was restricted to the MTC region, leaving the dorsal hippocampus quite preserved. The local MTC pathology of these mice was associated with EC and CLA hyperactivity which would most likely spread towards densely interconnected regions such as the mPFC, the DH and the RSC. Retrieval dependent communication between cingulate areas and the MTL was disrupted, and can be potentially linked to reduced dysgranular RSC hub strength. The similarity between our findings in the dKI model and those reported in the earliest stages of the disease suggests that the App^{NL-F} version of the dKI model has a high potential for generating new discoveries on the earliest stage of AD.

Methods

Animals

The *App*$^{NL-F}$/*MAPT* double knock-in (dKI) mice were produced through crossing homozygotes of two single knock-in (KI) mouse lines for the humanized *App*$^{NL-F}$ and *MAPT* genes, and then through the crossing of the resulting doubly heterozygote mice to obtain dKI and non-knock-in WT line founders. After three generation of homozygous breeding, the dKI mouse line was backcrossed with C57BL/6J mice (Janvier Laboratories, Le Genest Saint Isle, France) in order to limit genetic drift between dKI mice and their WT controls. The *App*$^{NL-F}$ gene contains a humanized Aβ fragment with Beyreuther/Iberian and Swedish FAD mutations, and the human *MAPT* gene expresses all 6 isoforms of tau found in humans. Both single KI mouse lines were produced by T Saido and T Saito (RIKEN Brain Science Institute, JAPAN) and sent to us by the RIKEN BioResource Center. Mice were group-housed with food and water ad libitum, nesting material, and additional food pellets on bedding to promote natural behavioral patterns. The animal room was under controlled temperature (23 °C ± 1°C) and a 12/12-hour light/dark cycle (lights on at 8.00 AM). Procedures were in compliance with rules of the European Community Council Directive 2010-63 and French Department of Agriculture Directive 2013-118 and approved by the local review board (CREMEAS: APAFIS#9848). Animal facilities were approved for animal experimentation (H 67-482-13).

Behavioral Testing

Behavioral testing took place during the light phase. Mice were single-housed for 1 week before testing. Spontaneous object exploration tests were carried out in an open field (100cmx100cmx50cm, Ugo Basile, Italy) with dark grey acrylic walls and a grey metal floor. The open field was evenly illuminated by three indirect halogen lights (open field center, 15 lux), and a radio gave background noise from 1.5m away (open field center, 45 ± 5 dB). Nine different sets of objects were used: two for the habituation phases, two for the long-term novel object recognition task, two for the OP task, two for the short-term novel object recognition task, and one for the object location task. These objects differed in size (10 to 20 cm), material (metal, glass, or plastic), shape, and color. Each object was available in duplicate or triplicate. Ethanol (30%) was used to clean the objects and the open field between each trial. Object exploration time was recorded and defined as the nose pointing toward the object within 2 cm. Gnawing and climbing of objects were not counted as exploration time.

Habituation

Before testing, all mice received two days of habituation. On the first day, they were given a habituation trial of 10 min with two identical objects placed in the open field. On the second day they were given two 10 min trials with a different set of two identical objects, with the trials separated by an inter trial interval (ITI) of 5' that the mice spent in their home cage. For the OP task with a 3-hour ITI, the second day habituation procedure was applied with an ITI of 3 hours.

Preliminary testing cohorts

Mice were tested at 2 months (WT n = 10, dKI n = 10), 4 months (WT n = 12, dKI n = 9) and at 6 months (WT n = 8, dKI n = 11). An additional cohort of (WT n = 3, dKI n = 1) was tested at 2 months in object-place association as the initial WT group did not reach significance above 0. For pattern separation one

two month old WT mouse was removed due to the wrong objects accidentally being placed during the retention phase.

Short term, pattern separation and long-term novel object recognition

Mice were tested at 4 months (WT n = 11, dKI n = 11) in the short term OR task. One WT mouse was removed from the analysis due to being dropped before the task. Mice explored two identical objects during a 10-min acquisition trial, and were returned to their home cage for an ITI of 5 min (short term, pattern separation) or 24 hours (long term). Thereafter, mice were given a 10-min retention trial, where one of the familiar objects was replaced by an unfamiliar new one. For the pattern separation task, objects were made of legos, the novel object had the same composition of colored lego blocks but a different pattern. Exploration of the objects was recorded during the 6 minutes (4 minutes for pattern separation) following the initial exploration of object for each mouse. The memory index was calculated as:

$$\text{Memory index} = \frac{\text{Time at replaced object} - \text{Time at unchanged object}}{\text{Time at both objects}}$$

Short term object-place association

To validate the potential deficit seen during preliminary phenotyping, an additional cohort (WT n = 11, dKI n = 11) was tested in the object-place association task. Mice explored two different objects during a 10-min acquisition trial, and were returned to their home cage for an ITI of 5 minutes. During the 10-min retention trial, one of the objects was replaced by a copy of the other. The mice had to detect the mismatch between one object and its actual location in the open field. Exploration of the objects was recorded during the 4 minutes following initiation of object exploration episode for each mouse. The memory index was calculated as with the long-term object recognition task.

Short term novel object location

Mice were tested at 4 months (WT n = 11, dKI n =11). Mice explored two identical objects during a 10-min acquisition trial, and were returned to their home cage for an ITI of 5 minutes. During a 10-min retention trial, one of the objects was moved 55 cm from its original position for the object location task. Exploration of the objects was evaluated during the 6 minutes following the initiation of object exploration for each mouse. During both phases, all objects were placed equidistant from the walls. The memory index was calculated as:

$$\text{Memory index} = \frac{\text{Time at moved object} - \text{Time at unmoved object}}{\text{Time at both objects}}$$

Western Blotting

Four-month-old male mice were sacrificed by cervical dislocation (n=8 per group), and their brains were carefully dissected on ice. Hippocampi and medial temporal cortex were quickly removed, frozen in liquid nitrogen and then stored at −80°C until their use. Tissues were homogenized in 10 volumes of ice-cold radioimmunoprecipitation assay buffer containing protease inhibitor cocktail (Sigma-Aldrich), phosphatase inhibitor cocktail (PhosStop, Roche Life Science), and 1 mM phenylmethylsulfonyl fluoride (Sigma-Aldrich). After centrifugation at 20,000g for 20 min at 4°C, supernatants were aliquoted for immunoblot analysis. Brains extracts of Tg2576 and Thy-tau22 mice were homogeneized and separated in parallel to our samples as a positive control for APP proteins and cleaved fragments and for tau

proteins, respectively. Protein concentration was measured using the Bio-Rad Protein Assay (Bio-Rad). Thirty or 20 microgramms were respectively loaded on 4-20% precast gel (Mini-Protean TGX precast gels, Bio-Rad) for APP and tau proteins. After electrophoresis and transfer to nitrocellulose membranes using the Trans-Blot Turbo System (Bio-Rad), membranes were incubated with 5% skimmed milk for 1 hour at room temperature and then with primary antibodies diluted in 2% bovine serum albumin (Sigma) in tris-buffered saline 0.05% Tween 20 (Sigma-Aldrich) overnight at 4°C. After washes, membranes were incubated with anti-mouse or anti-rabbit immunoglobulins conjugated to horseradish peroxidase (Jackson Immunoresearch) for development with enhanced ECL chemiluminescence detection kit (Thermo Fisher Scientific). After detection, all membranes were re-probed with anti-actin antibody for normalization of total protein. The primary antibodies used were the rabbit polyclonal anti-APP, C terminus (Sigma-Aldrich), the rabbit polyclonal anti-tau (B19, generously gifted by JP Brion, ULB, Belgium), the mouse monoclonal anti-phopho-Tau Thr181 (AT270, ThermoScientific), the mouse monoclonal anti-actin (Sigma-Aldrich) and the rabbit polyclonal anti-actin (Sigma-Aldrich). The secondary antibodies used were the peroxidase-conjugated AffiniPure goat anti-mouse and goat anti-rabbit (Jackson Immunoresearch). The quantification of the band intensity acquired with the ChemiDoc Imaging system (Bio-Rad) was performed by densitometry analysis using the ImageJ program. For each mouse, the phosphorylation degree was calculated as the ratio of total phosphorylated Thr181 tau proteins on total tau proteins. The ratio of APP-cleaved fragments was calculated as the total of APP β-CTF on α-CTF fragments.

Object-place association with a 3-hour ITI for ex-vivo imaging

The same protocol as with the short-term object-place task was followed, except with an ITI of 3-hours. The "Acquisition" set of WT (N=12) and dKI (N=12) mice were only tested in the acquisition phase. The "Retention" set of WT (N=14) and dKI (N=14) mice were tested for the entire task, acquisition and retention phases included. At the end of testing mice were left in their home cage in a quiet dim room (9 lux, 35 ± 5 dB) next to the testing room for 90 minutes, after which they were taken for brain perfusion and removal.

Perfusion and tissue preparation.

Mice were killed with an overdose of sodium pentobarbital (105 mg/kg intraperitoneally) and transcardially perfused in 0.1% heparin phosphate-buffered saline (PBS) and 4% paraformaldehyde [PFA; in phosphate buffer (PB) pH7.4; 4°C]. Brains were removed, postfixed in a 4% PFA solution for 24h, and cryoprotected in a saccharose solution (20% in PB, 0.1 M; pH 7.4; 4°C) for 48 hours before being frozen with isopentane (−40°C) and subsequently stored at −80°C. Forty µm coronal cryostat sections were cut from the anterior to the posterior of the brain. For the medial prefrontal cortex (mPFC), claustrum (CLA), dorsal hippocampus (DH), medial entorhinal cortex (MEC), and postrhinal cortex (POC) every 4th section created a set (escapement of 160 µm), and for the retrosplenial cortex (RSC), lateral entorhinal cortex (LEC), and perirhinal cortex (PRC) every 6th section (escapement of 240 µm).

Immunohistochemistry

Brain sections were given three 10 min washes in 0.1 M phosphate-buffered saline (PBS), followed by a 30 min incubation in 1% H_2O_2. They were washed for 5 min with ultra-pure water and again three times for 10 min in 0.1 M PBS. This was followed by a 45 min blocking incubation in a 5% natal goat serum (NGS) diluted in a "diluent" solution consisting of 0.1 M PBS, and 0.5% triton. The sections were

incubated at room temperature for 2 days in a 1/15000 dilution of rabbit-anti-cFos (Synaptic Systems) primary antibody in diluent containing 2% NGS. After 2 days the sections were first given two 10 min washes in 0.1 M PBS, and then incubated for 2 hours at room temperature in a 1/500 dilution of biotinylated mouse-anti-rabbit (Vector Laboratories) secondary antibody in diluent containing 2% NGS. The sections were given two 10 min washes in PBS, followed by a 45 min incubation in the avidin/biotin (Vector Laboratories) solution. This was followed by three 10 min washes in 0.1 M PBS and a 10 min wash in phosphate buffer. The sections were finally revealed with a 10 min incubation in 3,3-diaminobenzidine (Vector Laboratories). Images of whole brain sections were taken at 20x magnification using a Hamamatsu NanoZoomer S60 digital slide scanner (Hamamatsu Photonics K.K., Hamamatsu City, Japan) for offline quantification of c-Fos expression.

c-Fos Imaging

Neuronal activation is associated with increases in intracellular calcium levels, which in turn leads to the rapid up-regulation of immediate early genes such as c-fos. The quantification of c-Fos protein levels can thus be used to derive a measure of neuronal activity (Tischmeyer and Grimm, 1999). c-Fos expression was analyzed in 22 regions of interest (ROIs) (see Table S1), including sub-regions of the PFC, CLA, DH, RSC, PRC, POC and EC. Image processing was done using ImageJ (National Institute of Health, Bethesda, MD). ROIs were anatomically defined according to the atlas of Franklin and Paxinos (2008). For c-Fos quantification, the images were transformed into 8-bit grayscale. A grayscale threshold was set at a consistent level for each region by an experimenter blind to group condition. Only c-Fos positive nuclei with a grayscale intensity below the threshold and an area between 25–300 μm^2 were counted. At least three brain sections were processed per ROI. Mean c-Fos density was calculated for each ROI as the quantity of c-Fos marked nuclei per mm^2, normalized to the WT-Acquisition group. ROIs were grouped into region subfields whenever anatomically and functionally justified. These groupings reduce the number of comparisons and, thereby, restrict Type 1 errors. Three-way ANOVAs compared test-phases (acquisition or retention), genotypes (WT or dKI) and subregions for each subfield. When an interaction was significant, the simple effects were examined.

Functional Connectivity

From the c-Fos signals, functional connectivity (FC) was assessed by computing the between subject inter-regional spearman correlations for each Genotype-Phase group. Spearman correlations, rather than Pearson correlations, were used to account for potential outlier effects and the relatively small sample sizes. Correlation matrices were used to visualize all possible pairwise inter-regional correlations within each group. To assess global FC strength the mean r was calculated with retained, near-zeroed, and absolute valued negative correlations respectively. In the near-zeroed case, negative correlations were reduced to a value of .006, the smallest positive correlation observed.

Generating functional networks as fully connected weighted graphs

From each correlation matrix, a functional network was generated as a fully connected weighted graph. The edges weights of the graph reflect inter-regional spearman correlation strengths and the nodes reflect regions. Negative correlations can be interesting, but complicate considerably graph analyses as various algorithm variants exist to handle them (e.g. in community detection) and there is no obvious criterion to choose one variant over others. For the sake of clarity, we thus treated negative correlations in most analyses (unless explicitly mentioned) as near-zero positive value of correlation (minimum edge weight

of 0.006, see above). In efficiency analyses, this corresponds to interpreting negative correlations as open but difficult paths for information transfer. All graph construction and graph analysis were done through the igraph (Csardi G and Nepusz T, 2006) package on R (R Core Team, 2017).

Bootstrapping confidence intervals

For all network metrics, confidence intervals were computed through bootstrapping. This involves resampling subjects with replacement 1000 times, each time regenerating a functional network, then recalculating the estimate of interest. The 95% quartile of the bootstrap distribution was taken as the 95% confidence interval. Confidence intervals for the difference were used to test for differences between genotype groups (Wright et al., 2011). Groups were considered different to a P<.05 if the 95 % confidence interval for the difference ≥ 0, and to a P<.01 if the 99 % confidence interval for the difference ≥ 0.

Community Analysis

Networks with high modularity, $\boldsymbol{Q}$, have strong connections between the nodes within communities and relatively weaker connections between nodes of different communities.

$$Q = \frac{1}{2m} \sum_{i \neq j \in N} \left[w_{ij} - \frac{s_i s_j}{2m} \right] \delta(c_i, c_j)$$

where *N* denotes the set of all nodes in the network, m denotes the total number of edges in the network, $w(i,j)$ denotes the edge weight between a node i and another node j, s denotes the sum of a node's edge weights, c denotes the community to which a node belongs, and $\delta(c_i, c_j)$ indicates if the compared nodes are in the same community ($\delta(c_i, c_j)$ is 1 if $c_i = c_j$, and 0 otherwise). Communities were detected in each bootstrap through finding the maximum modularity across all possible community partitions. This modularity maximization computation was done through the *cluster_optimal* function of the igraph package. This transforms modularity maximization into an integer programming problem, and calls the GNU Linear Programming Kit (GLPK) to solve that. See Brandes et al, 2008 for more details. This computationally expensive detection method of evaluating all possible community partitions for modularity maximization (in contrast to less expensive methods that infer modularity, as through greedy optimization, i.e. the Louvain method), could be permitted due to the relatively small number of nodes in our network. Allegiance matrices were used to assess community stability across bootstraps, by depicting the percentage of bootstraps (n = 1000) that contain any given pair of regions within the same community.

Information flow

Nodal strength, $\boldsymbol{s}$, is traditionally calculated as the sum of a node's edge weights. In a fully connected network this is directly proportional to the average of a node's edge weights. The average, $\boldsymbol{s_{average}}$, was used in our case for better comparison with nodal efficiency.

$$s_{average}(i) = \frac{1}{n-1} \sum_{j \in N} w_{ij}$$

where *N* denotes the set of all nodes in the network, n denotes the total number of nodes in the network, and w_{ij} denotes the edge weight between a node i and another node j.

For efficiency metrics, edge lengths were first computed as inverted edge weights. Nodal efficiency, $\boldsymbol{E}_{nodal}$, was calculated as the average inverse shortest path length between a region and all other regions of the network.

$$E_{nodal}(i) = \frac{1}{n-1} \sum_{j \in N} \frac{1}{d_{ij}}$$

where d_{ij} denotes the length of the shortest path (lowest sum of edge lengths) between a node i and another node j. Global efficiency, $\boldsymbol{E}_{global}$, was calculated as the average inverse shortest path length of the network.

$$E_{global} = \frac{1}{n(n-1)} \sum_{i \neq j \in N} \frac{1}{d_{ij}}$$

Assessing the impact of global efficiency on memory deficits

Subsamples were generated from each retention group by resampling n-1 mice without replacement. This procedure generates a set of subsamples of size n-1, where the number of subsamples is the number of mice, n. From each subsample, the average memory index and the resulting network global efficiency were computed. Correlation significance between memory index and global efficiency was computed through both Pearson and Spearman correlation coefficients. To compute the exploration adjusted memory index, first the exploration index was defined for each mouse as total time exploring both objects normalized to the group average:

$$\text{Exploration Index (EI)} = \frac{\text{Time exploring both objects of mouse}}{\text{Average time exploring both objects across the group}}$$

The exploration adjusted memory index was then defined as the memory index divided by the exploration index.

$$\text{Exploration adjusted memory index (MI/EI)} = \frac{\text{Memory Index (MI)}}{\text{Exploration Index (EI)}}$$

To assess the significance of the intersection of the WT linear fit with the dKI subsample population, 1000 randomly fit linear models to the WT were generated by permuting the y labels of the WT subsample population and recalculating the best fit line each time. The mean absolute error to the dKI subsamples was calculated for each random model and their distribution is presented as a histogram. The 95% confidence interval was considered as the 95% quartile of the distribution, and compared to the dKI mean absolute error to the original WT fit.

References

Asaad M, Lee JH. 2018. A guide to using functional magnetic resonance imaging to study Alzheimer's disease in animal models. *Dis Model Mech* **11**. doi:10.1242/dmm.031724

Avila J, Perry G. 2021. A Multilevel View of the Development of Alzheimer's Disease. *Neuroscience* **457**:283–293. doi:10.1016/j.neuroscience.2020.11.015

Bai L, Zhang M, Chen S, Ai L, Xu M, Wang D, Wang Fei, Liu L, Wang Fang, Lao L. 2013. Characterizing acupuncture de qi in mild cognitive impairment: relations with small-world efficiency of functional brain networks. *Evid Based Complement Alternat Med* **2013**:304804. doi:10.1155/2013/304804

Bassett DS, Bullmore E. 2006. Small-world brain networks. *Neuroscientist* **12**:512–523. doi:10.1177/1073858406293182

Bergmann E, Zur G, Bershadsky G, Kahn I. 2016. The Organization of Mouse and Human Cortico-Hippocampal Networks Estimated by Intrinsic Functional Connectivity. *Cereb Cortex* **26**:4497–4512. doi:10.1093/cercor/bhw327

Bonardi C, Pardon M-C, Armstrong P. 2016. Deficits in object-in-place but not relative recency performance in the APPswe/PS1dE9 mouse model of Alzheimer's disease: Implications for object recognition. *Behavioral Brain Research* **313**:71–81. doi:10.1016/j.bbr.2016.07.008

Braak H, Braak E. 1995. Staging of Alzheimer's disease-related neurofibrillary changes. *Neurobiol Aging* **16**:271–278; discussion 278-284. doi:10.1016/0197-4580(95)00021-6

Catheline G, Periot O, Amirault M, Braun M, Dartigues J-F, Auriacombe S, Allard M. 2010. Distinctive alterations of the cingulum bundle during aging and Alzheimer's disease. *Neurobiology of Aging* **31**:1582–1592. doi:10.1016/j.neurobiolaging.2008.08.012

Caviezel MP, Reichert CF, Sadeghi Bahmani D, Linnemann C, Liechti C, Bieri O, Borgwardt S, Leyhe T, Melcher T. 2020. The Neural Mechanisms of Associative Memory Revisited: fMRI Evidence from Implicit Contingency Learning. *Front Psychiatry* **10**. doi:10.3389/fpsyt.2019.01002

Chao OY, Huston JP, Li J-S, Wang A-L, Silva MA de S. 2016. The medial prefrontal cortex—lateral entorhinal cortex circuit is essential for episodic-like memory and associative object-recognition. *Hippocampus* **26**:633–645. doi:10.1002/hipo.22547

Corriveau-Lecavalier N, Duchesne S, Gauthier S, Hudon C, Kergoat M, Mellah S, Belleville S, for the Consortium for the Early Identification of Alzheimer's Disease-Quebec (CIMA-Q). 2020. A quadratic function of activation in individuals at risk of Alzheimer's disease. *Alzheimer's & Dementia: Diagnosis, Assessment & Disease Monitoring* **12**. doi:10.1002/dad2.12139

Degiorgis L, Karatas M, Sourty M, Faivre E, Lamy J, Noblet V, Bienert T, Reisert M, von Elverfeldt D, Buée L, Blum D, Boutillier A-L, Armspach J-P, Blanc F, Harsan L-A. 2020. Brain network remodelling reflects tau-related pathology prior to memory deficits in Thy-Tau22 mice. *Brain*. doi:10.1093/brain/awaa312

Deshmukh SS, Johnson JL, Knierim JJ. 2012. Perirhinal cortex represents nonspatial, but not spatial, information in rats foraging in the presence of objects: Comparison with lateral entorhinal cortex. *Hippocampus* **22**:2045–2058. doi:10.1002/hipo.22046

Drzezga A, Becker JA, Van Dijk KRA, Sreenivasan A, Talukdar T, Sullivan C, Schultz AP, Sepulcre J, Putcha D, Greve D, Johnson KA, Sperling RA. 2011. Neuronal dysfunction and disconnection of cortical hubs in non-demented subjects with elevated amyloid burden. *Brain* **134**:1635–1646. doi:10.1093/brain/awr066

Etter G, van der Veldt S, Manseau F, Zarrinkoub I, Trillaud-Doppia E, Williams S. 2019. Optogenetic gamma stimulation rescues memory impairments in an Alzheimer's disease mouse model. *Nature Communications* **10**:5322. doi:10.1038/s41467-019-13260-9

Eyler LT, Elman JA, Hatton SN, Gough S, Mischel AK, Hagler DJ, Franz CE, Docherty A, Fennema-Notestine C, Gillespie N, Gustavson D, Lyons MJ, Neale MC, Panizzon MS, Dale AM, Kremen WS. 2019. Resting State Abnormalities of the Default Mode Network in Mild Cognitive Impairment: A Systematic Review and Meta-Analysis. *J Alzheimers Dis* **70**:107–120. doi:10.3233/JAD-180847

Filippi M, van den Heuvel MP, Fornito A, He Y, Hulshoff Pol HE, Agosta F, Comi G, Rocca MA. 2013. Assessment of system dysfunction in the brain through MRI-based connectomics. *The Lancet Neurology* **12**:1189–1199. doi:10.1016/S1474-4422(13)70144-3

Gardini S, Venneri A, Sambataro F, Cuetos F, Fasano F, Marchi M, Crisi G, Caffarra P. 2015. Increased functional connectivity in the default mode network in mild cognitive impairment: a maladaptive compensatory mechanism associated with poor semantic memory performance. *J Alzheimers Dis* **45**:457–470. doi:10.3233/JAD-142547

Grajski KA, Bressler SL. 2019. Differential medial temporal lobe and default-mode network functional connectivity and morphometric changes in Alzheimer's disease. *NeuroImage: Clinical* **23**:101860. doi:10.1016/j.nicl.2019.101860

Granholm E, Butters N. 1988. Associative encoding and retrieval in Alzheimer's and Huntington's disease. *Brain Cogn* **7**:335–347. doi:10.1016/0278-2626(88)90007-3

Greicius MD, Supekar K, Menon V, Dougherty RF. 2009. Resting-State Functional Connectivity Reflects Structural Connectivity in the Default Mode Network. *Cereb Cortex* **19**:72–78. doi:10.1093/cercor/bhn059

Guo Q, Li H, Cole AL, Hur J-Y, Li Y, Zheng H. 2013. Modeling Alzheimer's Disease in Mouse without Mutant Protein Overexpression: Cooperative and Independent Effects of Aβ and Tau. *PLOS ONE* **8**:e80706. doi:10.1371/journal.pone.0080706

Gustafson L, Brun A, Englund E, Hagnell O, Nilsson K, Stensmyr M, Öhlin A-K, Abrahamson M. 1998. A 50-year perspective of a family with chromosome-14-linked Alzheimer's disease. *Hum Genet* **102**:253–257. doi:10.1007/s004390050688

Hales JB, Brewer JB. 2011. The timing of associative memory formation: frontal lobe and anterior medial temporal lobe activity at associative binding predicts memory. *J Neurophysiol* **105**:1454–1463. doi:10.1152/jn.00902.2010

Hamm V, Héraud C, Bott J-B, Herbeaux K, Strittmatter C, Mathis C, Goutagny R. 2017. Differential contribution of APP metabolites to early cognitive deficits in a TgCRND8 mouse model of Alzheimer's disease. *Sci Adv* **3**:e1601068. doi:10.1126/sciadv.1601068

Hampstead BM, Stringer AY, Stilla RF, Amaraneni A, Sathian K. 2011. Where did I put that? Patients with amnestic mild cognitive impairment demonstrate widespread reductions in activity during the encoding of ecologically relevant object-location associations. *Neuropsychologia* **49**:2349–2361. doi:10.1016/j.neuropsychologia.2011.04.008

Hampstead BM, Towler S, Stringer AY, Sathian K. 2018. Continuous measurement of object location memory is sensitive to effects of age and mild cognitive impairment and related to medial temporal lobe volume. *Alzheimers Dement (Amst)* **10**:76–85. doi:10.1016/j.dadm.2017.10.007

Hernandez AR, Reasor JE, Truckenbrod LM, Lubke KN, Johnson SA, Bizon JL, Maurer AP, Burke SN. 2017. Medial prefrontal-perirhinal cortical communication is necessary for flexible response selection. *Neurobiology of Learning and Memory* **137**:36–47. doi:10.1016/j.nlm.2016.10.012

Hirni DI, Kivisaari SL, Krumm S, Monsch AU, Berres M, Oeksuez F, Reinhardt J, Ulmer S, Kressig RW, Stippich C, Taylor KI. 2016. Neuropsychological Markers of Medial Perirhinal and Entorhinal Cortex Functioning are Impaired Twelve Years Preceding Diagnosis of Alzheimer's Dementia. *JAD* **52**:573–580. doi:10.3233/JAD-150158

Hyman B, Van Hoesen G, Damasio A, Barnes C. 1984. Alzheimer's disease: cell-specific pathology isolates the hippocampal formation. *Science* **225**:1168–1170. doi:10.1126/science.6474172

Jacob P-Y, Casali G, Spieser L, Page H, Overington D, Jeffery K. 2017. An independent, landmark-dominated head-direction signal in dysgranular retrosplenial cortex. *Nature Neuroscience* **20**:173–175. doi:10.1038/nn.4465

Jones DT, Graff-Radford J, Lowe VJ, Wiste HJ, Gunter JL, Senjem ML, Botha H, Kantarci K, Boeve BF, Knopman DS, Petersen RC, Jack CR. 2017. Tau, amyloid, and cascading network failure across the Alzheimer's disease spectrum. *Cortex*, Special Section dedicated to the temporal and parietal lobes **97**:143–159. doi:10.1016/j.cortex.2017.09.018

Jones DT, Knopman DS, Gunter JL, Graff-Radford J, Vemuri P, Boeve BF, Petersen RC, Weiner MW, Jack CR Jr, on behalf of the Alzheimer's Disease Neuroimaging Initiative. 2016. Cascading network failure across the Alzheimer's disease spectrum. *Brain* **139**:547–562. doi:10.1093/brain/awv338

Khan UA, Liu L, Provenzano FA, Berman DE, Profaci CP, Sloan R, Mayeux R, Duff KE, Small SA. 2014. Molecular drivers and cortical spread of lateral entorhinal cortex dysfunction in preclinical Alzheimer's disease. *Nat Neurosci* **17**:304–311. doi:10.1038/nn.3606

Kinnavane L, Albasser MM, Aggleton JP. 2015. Advances in the Behavioral testing and network imaging of rodent recognition memory. *Behavioral Brain Research*, SI: Object Recognition Memory in Rats and Mice **285**:67–78. doi:10.1016/j.bbr.2014.07.049

Liang J, Li Y, Liu H, Zhang S, Wang M, Chu Y, Ye J, Xi Q, Zhao X. 2020. Increased intrinsic default-mode network activity as a compensatory mechanism in aMCI: a resting-state functional connectivity MRI study. *Aging (Albany NY)* **12**:5907–5919. doi:10.18632/aging.102986

Lin S-Y, Lin C-P, Hsieh T-J, Lin C-F, Chen S-H, Chao Y-P, Chen Y-S, Hsu C-C, Kuo L-W. 2019. Multiparametric graph theoretical analysis reveals altered structural and functional network topology in Alzheimer's disease. *NeuroImage: Clinical* **22**:101680. doi:10.1016/j.nicl.2019.101680

Liu Z, Zhang Y, Yan H, Bai L, Dai R, Wei W, Zhong C, Xue T, Wang H, Feng Y, You Y, Zhang X, Tian J. 2012. Altered topological patterns of brain networks in mild cognitive impairment and Alzheimer's disease: A resting-state fMRI study. *Psychiatry Research: Neuroimaging* **202**:118–125. doi:10.1016/j.pscychresns.2012.03.002

Lu H, Zou Q, Gu H, Raichle ME, Stein EA, Yang Y. 2012. Rat brains also have a default mode network. *PNAS* **109**:3979–3984. doi:10.1073/pnas.1200506109

McAvoy K, Besnard A, Sahay A. 2015. Adult hippocampal neurogenesis and pattern separation in DG: a role for feedback inhibition in modulating sparseness to govern population-based coding. *Front Syst Neurosci* **9**. doi:10.3389/fnsys.2015.00120

Miller AMP, Vedder LC, Law LM, Smith DM. 2014. Cues, context, and long-term memory: the role of the retrosplenial cortex in spatial cognition. *Front Hum Neurosci* **8**. doi:10.3389/fnhum.2014.00586

Mitchell AS, Czajkowski R, Zhang N, Jeffery K, Nelson AJD. 2018. Retrosplenial cortex and its role in spatial cognition. *Brain Neurosci Adv* **2**. doi:10.1177/2398212818757098

Morys J, Bobinski M, Wegiel J, Wisniewski HM, Narkiewicz O. 1996. Alzheimer's disease severely affects areas of the claustrum connected with the entorhinal cortex. *J Hirnforsch* **37**:173–180.

Myers N, Pasquini L, Göttler J, Grimmer T, Koch K, Ortner M, Neitzel J, Mühlau M, Förster S, Kurz A, Förstl H, Zimmer C, Wohlschläger AM, Riedl V, Drzezga A, Sorg C. 2014. Within-patient correspondence of amyloid-β and intrinsic network connectivity in Alzheimer's disease. *Brain* **137**:2052–2064. doi:10.1093/brain/awu103

Naveh-Benjamin M. 2000. Adult age differences in memory performance: Tests of an associative deficit hypothesis. *Journal of Experimental Psychology: Learning, Memory, and Cognition* **26**:1170–1187. doi:10.1037/0278-7393.26.5.1170

Nuriel T, Angulo SL, Khan U, Ashok A, Chen Q, Figueroa HY, Emrani S, Liu L, Herman M, Barrett G, Savage V, Buitrago L, Cepeda-Prado E, Fung C, Goldberg E, Gross SS, Hussaini SA, Moreno H, Small SA, Duff KE. 2017. Neuronal hyper-activity due to loss of inhibitory tone in APOE4 mice lacking Alzheimer's disease-like pathology. *Nat Commun* **8**:1464. doi:10.1038/s41467-017-01444-0

Ogomori K, Kitamoto T, Tateishi J, Sato Y, Suetsugu M, Abe M. 1989. Beta-protein amyloid is widely distributed in the central nervous system of patients with Alzheimer's disease. *Am J Pathol* **134**:243–251.

Palmqvist S, Schöll M, Strandberg O, Mattsson N, Stomrud E, Zetterberg H, Blennow K, Landau S, Jagust W, Hansson O. 2017. Earliest accumulation of β-amyloid occurs within the default-mode network and concurrently affects brain connectivity. *Nature Communications* **8**:1214. doi:10.1038/s41467-017-01150-x

Parra MA, Abrahams S, Logie RH, Méndez LG, Lopera F, Della Sala S. 2010. Visual short-term memory binding deficits in familial Alzheimer's disease. *Brain* **133**:2702–2713. doi:10.1093/brain/awq148

Parron C, Save E. 2004. Comparison of the effects of entorhinal and retrosplenial cortical lesions on habituation, reaction to spatial and non-spatial changes during object exploration in the rat. *Neurobiology of Learning and Memory* **82**:1–11. doi:10.1016/j.nlm.2004.03.004

Paxinos G, Franklin K. 2019. The mouse brain in stereotaxic coordinates. San Diego: Academic Press.

Pereira JB, Mijalkov M, Kakaei E, Mecocci P, Vellas B, Tsolaki M, Kłoszewska I, Soininen H, Spenger C, Lovestone S, Simmons A, Wahlund L-O, Volpe G, Westman E. 2016. Disrupted Network Topology in Patients with Stable and Progressive Mild Cognitive Impairment and Alzheimer's Disease. *Cereb Cortex* **26**:3476–3493. doi:10.1093/cercor/bhw128

Pereira JB, Ossenkoppele R, Palmqvist S, Strandberg TO, Smith R, Westman E, Hansson O. 2019. Amyloid and tau accumulate across distinct spatial networks and are differentially associated with brain connectivity. *eLife* **8**:e50830. doi:10.7554/eLife.50830

Perusini JN, Cajigas SA, Cohensedgh O, Lim SC, Pavlova IP, Donaldson ZR, Denny CA. 2017. Optogenetic stimulation of dentate gyrus engrams restores memory in Alzheimer's disease mice. *Hippocampus* **27**:1110–1122. doi:10.1002/hipo.22756

Petersen RC. 2011. Mild Cognitive Impairment. *New England Journal of Medicine* **364**:2227–2234. doi:10.1056/NEJMcp0910237

Petrache AL, Rajulawalla A, Shi A, Wetzel A, Saito T, Saido TC, Harvey K, Ali AB. 2019. Aberrant Excitatory–Inhibitory Synaptic Mechanisms in Entorhinal Cortex Microcircuits During the Pathogenesis of Alzheimer's Disease. *Cerebral Cortex* **29**:1834–1850. doi:10.1093/cercor/bhz016

Pusil S, López ME, Cuesta P, Bruña R, Pereda E, Maestú F. 2019. Hypersynchronization in mild cognitive impairment: the 'X' model. *Brain* **142**:3936–3950. doi:10.1093/brain/awz320

Qin Y-Y, Li M-W, Zhang S, Zhang Y, Zhao L-Y, Lei H, Oishi K, Zhu W-Z. 2013. In vivo quantitative whole-brain diffusion tensor imaging analysis of APP/PS1 transgenic mice using voxel-based and atlas-based methods. *Neuroradiology* **55**:1027–1038. doi:10.1007/s00234-013-1195-0

Reagh ZM, Noche JA, Tustison NJ, Delisle D, Murray EA, Yassa MA. 2018. Functional Imbalance of Anterolateral Entorhinal Cortex and Hippocampal Dentate/CA3 Underlies Age-Related Object Pattern Separation Deficits. *Neuron* **97**:1187-1198.e4. doi:10.1016/j.neuron.2018.01.039

Reagh ZM, Yassa MA. 2014. Object and spatial mnemonic interference differentially engage lateral and medial entorhinal cortex in humans. *Proceedings of the National Academy of Sciences* **111**:E4264–E4273. doi:10.1073/pnas.1411250111

Rentz DM, Amariglio RE, Becker JA, Frey M, Olson LE, Frishe K, Carmasin J, Maye JE, Johnson KA, Sperling RA. 2011. Face-name associative memory performance is related to amyloid burden in normal elderly. *Neuropsychologia* **49**:2776–2783. doi:10.1016/j.neuropsychologia.2011.06.006

Ritchey M, Cooper RA. 2020. Deconstructing the Posterior Medial Episodic Network. *Trends in Cognitive Sciences* **24**:451–465. doi:10.1016/j.tics.2020.03.006

Rodriguez GA, Barrett GM, Duff KE, Hussaini SA. 2020. Chemogenetic attenuation of neuronal activity in the entorhinal cortex reduces Aβ and tau pathology in the hippocampus. *PLOS Biology* **18**:e3000851. doi:10.1371/journal.pbio.3000851

Roy DS, Arons A, Mitchell TI, Pignatelli M, Ryan TJ, Tonegawa S. 2016. Memory retrieval by activating engram cells in mouse models of early Alzheimer's disease. *Nature* **531**:508–512. doi:10.1038/nature17172

Saito T, Matsuba Y, Mihira N, Takano J, Nilsson P, Itohara S, Iwata N, Saido TC. 2014. Single App knock-in mouse models of Alzheimer's disease. *Nat Neurosci* **17**:661–663. doi:10.1038/nn.3697

Saito T, Mihira N, Matsuba Y, Sasaguri H, Hashimoto S, Narasimhan S, Zhang B, Murayama S, Higuchi M, Lee VMY, Trojanowski JQ, Saido TC. 2019. Humanization of the entire murine *Mapt* gene provides a murine model of pathological human tau propagation. *J Biol Chem* jbc.RA119.009487. doi:10.1074/jbc.RA119.009487

Salta E, Walgrave H, Balusu S, Vanden Eynden E, Snoeck S, Craessaerts K, Thrupp N, Wolfs L, Horré K, Fourne Y, Ronisz A, Silajdžić E, Callaerts-Vegh Z, D'Hooge R, Rudolf Thal D, Zetterberg H, Thuret S, Fiers M, Sala Frigerio C, De Strooper B. 2020. Impaired adult hippocampal neurogenesis in Alzheimer's disease is mediated by microRNA-132 deficiency and can be restored by microRNA-132 replacement (preprint). Neuroscience. doi:10.1101/2020.03.12.988709

Sanabria A, Alegret M, Rodriguez-Gomez O, Valero S, Sotolongo-Grau O, Monté-Rubio G, Abdelnour C, Espinosa A, Ortega G, Perez-Cordon A, Gailhajanet A, Hernandez I, Rosende-Roca M, Vargas L, Mauleon A, Sanchez D, Martin E, Rentz DM, Lomeña F, Ruiz A, Tarraga L, Boada M. 2018. The Spanish version of Face-Name Associative Memory Exam (S-FNAME) performance is related to amyloid burden in Subjective Cognitive Decline. *Scientific Reports* **8**:3828. doi:10.1038/s41598-018-21644-y

Scearce-Levie K, Sanchez PE, Lewcock JW. 2020. Leveraging preclinical models for the development of Alzheimer disease therapeutics. *Nature Reviews Drug Discovery* **19**:447–462. doi:10.1038/s41573-020-0065-9

Schultz AP, Chhatwal JP, Hedden T, Mormino EC, Hanseeuw BJ, Sepulcre J, Huijbers W, LaPoint M, Buckley RF, Johnson KA, Sperling RA. 2017. Phases of hyper and hypo connectivity in the Default Mode and Salience

networks track with amyloid and Tau in clinically normal individuals. *J Neurosci*. doi:10.1523/JNEUROSCI.3263-16.2017

Selkoe DJ. 2012. Preventing Alzheimer's Disease. *Science* **337**:1488–1492. doi:10.1126/science.1228541

Sepulcre J, Sabuncu MR, Li Q, El Fakhri G, Sperling R, Johnson KA. 2017. Tau and amyloid β proteins distinctively associate to functional network changes in the aging brain. *Alzheimer's & Dementia* **13**:1261–1269. doi:10.1016/j.jalz.2017.02.011

Shah D, Latif-Hernandez A, Strooper B, Saito T, Saido T, Verhoye M, D'Hooge R, Linden A. 2018. Spatial reversal learning defect coincides with hypersynchronous telencephalic BOLD functional connectivity in APP NL-F/NL-F knock-in mice. *Scientific Reports* **8**:6264. doi:10.1038/s41598-018-24657-9

Shah D, Praet J, Latif Hernandez A, Höfling C, Anckaerts C, Bard F, Morawski M, Detrez JR, Prinsen E, Villa A, De Vos WH, Maggi A, D'Hooge R, Balschun D, Rossner S, Verhoye M, Van der Linden A. 2016. Early pathologic amyloid induces hypersynchrony of BOLD resting-state networks in transgenic mice and provides an early therapeutic window before amyloid plaque deposition. *Alzheimer's & Dementia* **12**:964–976. doi:10.1016/j.jalz.2016.03.010

Sinha N, Berg CN, Tustison NJ, Shaw A, Hill D, Yassa MA, Gluck MA. 2018. APOE ε4 Status in Healthy Older African Americans is Associated with Deficits in Pattern Separation and Hippocampal Hyperactivation. *Neurobiol Aging* **69**:221–229. doi:10.1016/j.neurobiolaging.2018.05.023

Stafford JM, Jarrett BR, Miranda-Dominguez O, Mills BD, Cain N, Mihalas S, Lahvis GP, Lattal KM, Mitchell SH, David SV, Fryer JD, Nigg JT, Fair DA. 2014. Large-scale topology and the default mode network in the mouse connectome. *PNAS* **111**:18745–18750. doi:10.1073/pnas.1404346111

Sugar J, Witter MP, van Strien N, Cappaert N. 2011. The Retrosplenial Cortex: Intrinsic Connectivity and Connections with the (Para)Hippocampal Region in the Rat. An Interactive Connectome. *Front Neuroinform* **5**. doi:10.3389/fninf.2011.00007

Tanimizu T, Kenney JW, Okano E, Kadoma K, Frankland PW, Kida S. 2017. Functional Connectivity of Multiple Brain Regions Required for the Consolidation of Social Recognition Memory. *J Neurosci* **37**:4103–4116. doi:10.1523/JNEUROSCI.3451-16.2017

Tischmeyer W, Grimm R. 1999. Activation of immediate early genes and memory formation. *Cell Mol Life Sci* **55**:564–574. doi:10.1007/s000180050315

Vann SD, Aggleton JP. 2005. Selective dysgranular retrosplenial cortex lesions in rats disrupt allocentric performance of the radial-arm maze task. *Behav Neurosci* **119**:1682–1686. doi:10.1037/0735-7044.119.6.1682

Vann SD, Aggleton JP, Maguire EA. 2009. What does the retrosplenial cortex do? *Nature Reviews Neuroscience* **10**:792–802. doi:10.1038/nrn2733

Vetere G, Kenney JW, Tran LM, Xia F, Steadman PE, Parkinson J, Josselyn SA, Frankland PW. 2017. Chemogenetic Interrogation of a Brain-wide Fear Memory Network in Mice. *Neuron* **94**:363-374.e4. doi:10.1016/j.neuron.2017.03.037

Vogt BA, Paxinos G. 2014. Cytoarchitecture of mouse and rat cingulate cortex with human homologies. *Brain Struct Funct* **219**:185–192. doi:10.1007/s00429-012-0493-3

Wang J, Zuo X, Dai Z, Xia M, Zhao Z, Zhao X, Jia J, Han Y, He Y. 2013a. Disrupted Functional Brain Connectome in Individuals at Risk for Alzheimer's Disease. *Biological Psychiatry*, Disturbances in the Connectome and Risk for Alzheimer's Disease **73**:472–481. doi:10.1016/j.biopsych.2012.03.026

Wang JX, Rogers LM, Gross EZ, Ryals AJ, Dokucu ME, Brandstatt KL, Hermiller MS, Voss JL. 2014. Targeted enhancement of cortical-hippocampal brain networks and associative memory. *Science* **345**:1054–1057. doi:10.1126/science.1252900

Wang L, Brier MR, Snyder AZ, Thomas JB, Fagan AM, Xiong C, Benzinger TL, Holtzman DM, Morris JC, Ances BM. 2013b. Cerebrospinal Fluid Aβ42, Phosphorylated Tau181 , and Resting-State Functional Connectivity. *JAMA Neurol*. doi:10.1001/jamaneurol.2013.3253

Wang Q, Ng L, Harris JA, Feng D, Li Y, Royall JJ, Oh SW, Bernard A, Sunkin SM, Koch C, Zeng H. 2017. Organization of the connections between claustrum and cortex in the mouse. *J Comp Neurol* **525**:1317–1346. doi:10.1002/cne.24047

Wang Y, Risacher SL, West JD, McDonald BC, Magee TR, Farlow MR, Gao S, O'Neill DP, Saykin AJ. 2013c. Altered default mode network connectivity in older adults with cognitive complaints and amnestic mild cognitive impairment. *J Alzheimers Dis* **35**:751–760. doi:10.3233/JAD-130080

Warren KN, Hermiller MS, Nilakantan AS, Voss JL. 2019. Stimulating the hippocampal posterior-medial network enhances task-dependent connectivity and memory. *eLife* **8**:e49458. doi:10.7554/eLife.49458

Weiler M, Stieger KC, Long JM, Rapp PR. 2020. Transcranial Magnetic Stimulation in Alzheimer's Disease: Are We Ready? *eNeuro* **7**. doi:10.1523/ENEURO.0235-19.2019

Wheeler AL, Teixeira CM, Wang AH, Xiong X, Kovacevic N, Lerch JP, McIntosh AR, Parkinson J, Frankland PW. 2013. Identification of a Functional Connectome for Long-Term Fear Memory in Mice. *PLOS Computational Biology* **9**:e1002853. doi:10.1371/journal.pcbi.1002853

Wilson DIG, Langston RF, Schlesiger MI, Wagner M, Watanabe S, Ainge JA. 2013a. Lateral entorhinal cortex is critical for novel object-context recognition. *Hippocampus* **23**:352–366. doi:10.1002/hipo.22095

Wilson DIG, Watanabe S, Milner H, Ainge JA. 2013b. Lateral entorhinal cortex is necessary for associative but not nonassociative recognition memory. *Hippocampus* **23**:1280–1290. doi:10.1002/hipo.22165

Wright DB, London K, Field AP. 2011. Using Bootstrap Estimation and the Plug-in Principle for Clinical Psychology Data. *Journal of Experimental Psychopathology* **2**:252–270. doi:10.5127/jep.013611

Xu W, Fitzgerald S, Nixon RA, Levy E, Wilson DA. 2015. Early hyper-activity in lateral entorhinal cortex is associated with elevated levels of AβPP metabolites in the Tg2576 mouse model of Alzheimer's disease. *Exp Neurol* **264**:82–91. doi:10.1016/j.expneurol.2014.12.008

Yassa MA, Stark SM, Bakker A, Albert MS, Gallagher M, Stark CEL. 2010. High-resolution structural and functional MRI of hippocampal CA3 and dentate gyrus in patients with amnestic Mild Cognitive Impairment. *NeuroImage* **51**:1242–1252. doi:10.1016/j.neuroimage.2010.03.040

Yeung L-K, Olsen RK, Hong B, Mihajlovic V, D'Angelo MC, Kacollja A, Ryan JD, Barense MD. 2018. Object-in-Place Memory Predicted by Anterolateral Entorhinal Cortex and Parahippocampal Cortex Volume in Older Adults. *bioRxiv* 409607. doi:10.1101/409607

Zhu H, Yan H, Tang N, Li X, Pang P, Li H, Chen W, Guo Y, Shu S, Cai Y, Pei L, Liu D, Luo M-H, Man H, Tian Q, Mu Y, Zhu L-Q, Lu Y. 2017. Impairments of spatial memory in an Alzheimer's disease model via degeneration of hippocampal cholinergic synapses. *Nature Communications* **8**:1676. doi:10.1038/s41467-017-01943-0

Zott B, Simon MM, Hong W, Unger F, Chen-Engerer H-J, Frosch MP, Sakmann B, Walsh DM, Konnerth A. 2019. A vicious cycle of β amyloid–dependent neuronal hyperactivation. *Science* **365**:559–565. doi:10.1126/science.aay0198

Study n°4

Electrophysiological evaluation of the CLA->PFC connection in the *App^{NL-F}xMAPT* double knock in mouse model of Alzheimer's disease

Christopher Borcuk[1],

Saito T[2], Hashimoto S[2], Saido T[2],

Romain Goutagny[1], Chantal Mathis[1]

1 - Laboratoire de Neurosciences Cognitives et Adaptatives (LNCA), Université de Strasbourg, Faculté de Psychologie, 12 rue Goethe, F-67000 Strasbourg, France.

2 - Laboratory for Proteolytic Neuroscience, RIKEN Center for Brain Science, 2-1 Hirosawa, Wako-city, Saitama 351-0198, Japan

Complementary study

1. Scientific context and objectives

Across both OP c-Fos studies, Study n°2 with the 5-minute ITI and Study n°3 and 3-hour ITI, we detected hyper-activity in the CLA. Another consistent result across the two OP c-Fos studies is the functional perturbation of the mPFC (hyperconnective in OP5', hypoconnective in the OP3h retention phase). The consistent functional perturbation of this region pair led us to consider evaluating the CLA->mPFC connection more closely. The team of Jackson et al, 2017 targeted the CLA-mPFC circuit directly through a double viral injection technique. A retrograde CRE virus was injected into the PFC and a CRE-dependent excitatory channel rhodopsin was injected into the CLA (***Figure 44A***). As a result, only CLA->mPFC projections would be activated by optical stimulation of the CLA. They found that optical stimulation of the CLA->mPFC induced feed forward inhibition of the PFC through direct action of glutamatergic claustral projections on PFC inhibitory interneurons (***Figure 44B***).

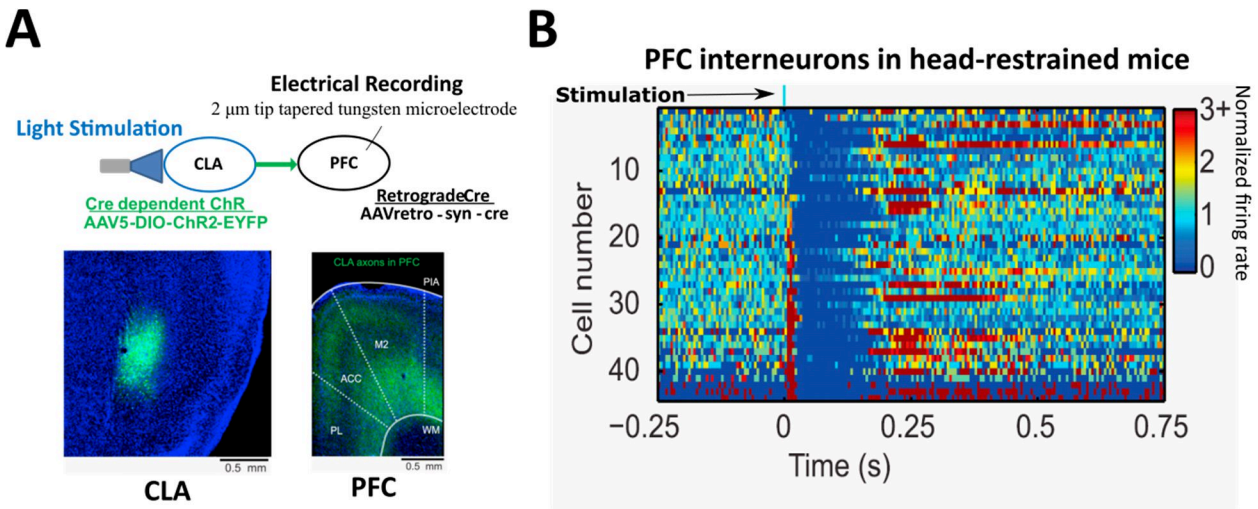

Figure 44. *(A) A retrograde CRE virus was injected in the PFC and a CRE-dependent channel rhodopsin 2 linked to a fluorescent EYFP (green) was injected in the CLA. Here we see the expression of EYFP linked channel rhodopsin 2 in cell bodies of the CLA (blue is DAPI marking of cell bodies and in axons of the PFC. (B) Optical stimulation of the CLA is immediately followed by a rapid activation of PFC interneurons for several micro-seconds, followed then by silence. Pyramidal cells are also inhibited (not shown). Adapted from Jackson et al, 2017.*

Later, this same inhibitory circuit was shown to regulate impulsive behaviors in mice (Liu et al., 2020). An interruption of this circuit may thus also explain the moderate "disinhibition" phenotype hinted to by low level of anxiety behaviors seen in the light-dark test in Study n°1,

and in the elevated plus maze in other studies evaluating the single KI $App^{NL\text{-}G\text{-}F}$ (Pervolaraki et al., 2019; Latif-Hernandez et al., 2017; Sakakibara et al., 2018). Moreover, Pervolaraki and colleagues found an accompanying reduced power of the mPFC gamma oscillations, another indication of interneuron dysfunction. Indeed interneuron dysfunction is a common feature of AD, but has been evaluated most commonly in relation to disrupted homeostatic regulation, leading to functional perturbations such as reduced gamma power and hyper-activity (Palop and Mucke., 2016). Few studies have assessed how interneuron dysfunction could directly contribute to the perturbation of inter-regional circuits. We were thus interested in evaluating this CLA-PFC circuit to better understand the role interneuron dysfunction plays in perturbing interregional communication in early AD.

To this end, we decided to interrogate the CLA-mPFC circuit using the same experimental approach as Jackson et al, 2019. Our hypothesis was that interregional communication between the CLA and mPFC would be affected, perhaps by a reduced response of the mPFC to CLA stimulation or even an opposing excitatory response, which would directly implicate interneuron dysfunction.

A. Electrophysiological interrogation of CLA->PFC projections

A group of WT (male n = 4, female n = 4) and dKI (male n = 4, female n = 4) mice were injected with a virus expressing CRE (AAVretro-syn-Cre) in the mPFC and a virus expressing a CRE-dependent channel rhodopsin linked to the fluorescent protein EYFP (pAAV5-Ef1a-DIO-ChETA-EYFP) in the CLA (***Figure 45A***). After 4 weeks they were recorded as in Jackson et al, 2019, but with a different CRE-dependent channel rhodopsin virus and a different 4 shank silicon probe (based on availability in the lab), and on anesthesized rather than head restrained mice. Unfortunately, our viral expression of ChETA-EYFP was much weaker, fewer cell bodies were marked in the CLA, and areas with marked axons in the mmPFC were difficult to find (***Figure 45B***). The inhibitory response of the PFC was also weak, with many neurons remaining unaffected by CLA stimulation (***Figure 45C***). Regardless, a few inhibited neurons could be found in both the WT and the dKI.

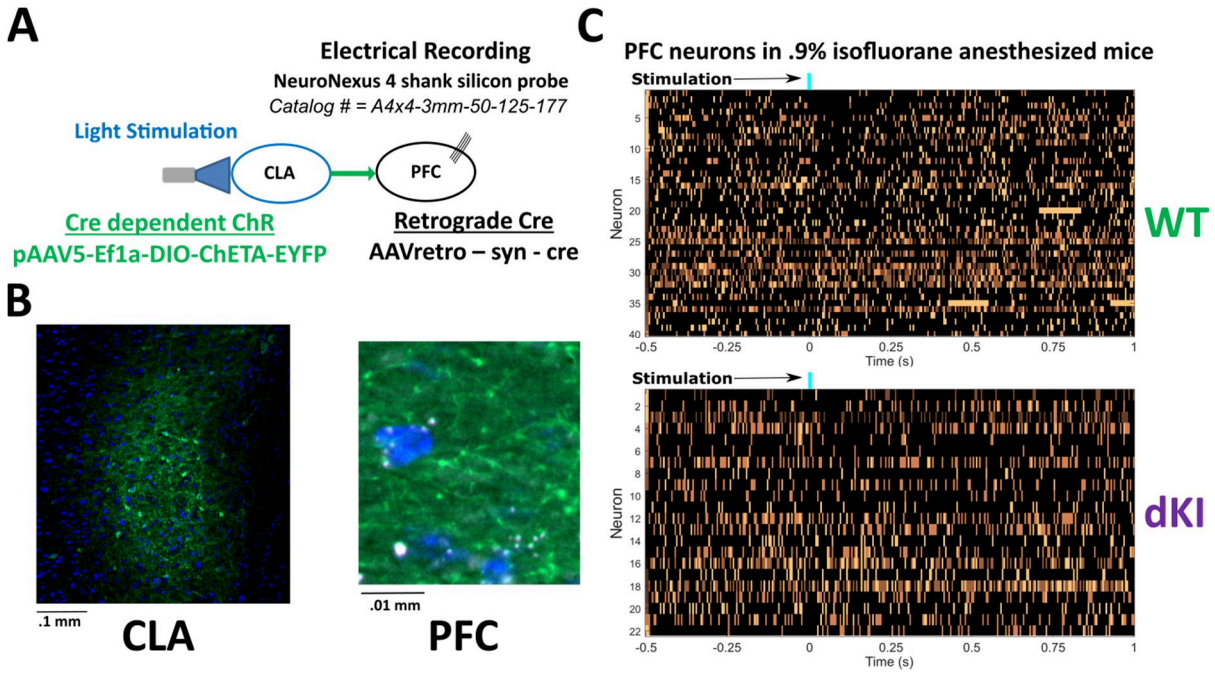

Figure 45. *(A) A similar protocol was used to Jackson et al, except a different CRE-dependent ChETA virus and a larger 4 shank silicon probe (each shank has 55µm width, from shank tip to shank tip 375 µm) were used. (B) In evaluating ChETA-EYFP marking (green), fewer cell bodies were marked in the CLA (blue is DAPI marking of cell bodies), and axonal marking in the PFC was less dense as compared to Jackson et al. 2017. Images ChETA-EYFP and DAPI staining were acquired using the Zeiss Apotome fluorescence microscope. (B) Optical stimulation of the CLA in anesthetized mice led to a much weaker inhibitory response in the PFC as compared to Jackson et al, 2017. Neurons are sorted by most inhibited to least inhibited from top to bottom. Nonetheless, some inhibited neurons were detected in both genotypes.*

2. Discussion

Many experimental drawbacks contributed to the reduced efficacy of this experiment. First, the viral expression was low compared Jackson et al. I may have poorly injected the viruses, or one of the viruses may have degraded. Second, the 4 shank silicon probe was 375 um wide from shank to shank, making it so that a much more dura needed to be removed in order to access the brain. This often led to some cortex being destroyed in the process. Jackson et al showed that the mPFC is most impacted by CLA projections at the dorsal end. My unintended removal of dorsal cortex made it so I had to descend deeper to detect intact neurons, leading to a higher chance of recording those that were CLA independent. This is admittedly a problem that would be fixed with experience, but having a single, thinner shank probe would have enabled me to have it inserted using a much smaller hole, reducing risk of damaging dorsal tissue. Finally, recordings were done on anesthetized mice on .9% isofluorane, where brain activity was much reduced as compared to head restrained mice (in Jackson's work). It was thus difficult to find active neurons, and those that were active had low firing rates and evaluating an inhibitory response was difficult. Regardless, I did find a few inhibited neurons in both the WT and the dKI. As they were found in both genotypes, no direct genotypic difference could be inferred with the data as it stands. However, perhaps with a more in depth sorting of neurons, based on waveform shape or cortical depth, we could reveal some genotypic differences. Unfortunately, the first and second wave of the COVID-19 interrupted twice these experiments, so I could not explore further this very interesting issue. With the little time left I preferred to concentrate on the c-Fos study to refine the analyses and write the corresponding manuscript (Study n°3) and the present thesis report.

Concluding remarks

1. Discussion

A. Why object-place association?

In Study n°1 we found deficits in the OP task at the earliest age of 4 months. These are followed by deficits in the mnemonic discrimination FDOR task at 6 months of age, though these results displayed high variability. These deficits appear without accompanying deficits in easier object recognition and object location tasks. These specific perturbations in associative and mnemonic discrimination memories are consistent with early deficits found in evaluations of preclinical AD, in asymptomatic individuals with FAD and APOE4, and in relation to increased amyloid or tau through PET or CSF (Parra et al., 2010; Wesnes et al., 2014). Interestingly, we found that the OP task was affected earlier than the FDOR task. The FDOR is shown to depend on pattern separation computation in the DG and CA3 of the DH (Bakker et al., 2008; Leutgeb et al., 2007), regions that were not found to be especially perturbed, functionally or pathologically, in 4 month old dKI mice. The LEC on the other hand was hyperactive in dKI mice and is part of the MTC that displays a specific increase in ptau (no increases are seen in the DH). Communication of the LEC with the DH is shown to be required for object pattern separation (Reagh and Yassa; 2014; Leal and Yassa, 2018), whereas communication with the mPFC is required for completion of the OP task in rats (Wilson et al., 2013a; Chao et al., 2016). In normal rodents, lateral perforant path projections from the EC to the dentate gyrus show both structural and functional alterations as early as 8 month of age (Amani et al, 2021), which may contribute to age related pattern separation deficits (Cès et al., 2018). A similarly disconnected DH-MTC in aged mice is detailed in the aging c-Fos experiment of Study n°2. However, the specific OP deficit in the dKI suggests that initial memory loss in AD could be more likely tied to disrupted connectivity between the LEC and the mPFC rather than the DH. This highlights a potential discrepancy between age related and AD related memory decline.

The RSC is another region shown to be essential for performing the OP tasks in rats (Vann and Aggleton, 2002), and amyloid burden in the PMC/RSC and mPFC predicts face-name associative memory loss in humans (Sanabria et al., 2018; Rentz et al., 2011). Moreover, contextual/scene processing, which is taxed in OP but not in FDOR, requires rich communication between the PMC/RSC and the MTL (Ritchey and Cooper; 2020) and is perturbed by initial amyloid burden in the PMC/RSC (Maass et al., 2019). The hypothesis that

OP dysfunction is linked to disconnection between the mPFC-LEC and between the RSC-MTL, is supported by the functional disconnection of the mPFC/RSC from the MTL during the retention phase of OP3h in dKI mice. In respect to neuropathological staging, increased amyloidosis (increased $A\beta_{42}$, oligomeric Aβ, β-CTF) should be first seen in the mPFC and PMC/RSC, but initial OP deficits probably occur only when significant tau pathology (increased ptau) occurs in the MTC and ruptures the link between amyloid and tau affected regions. This required combination of amyloid and tau effects is supported by the finding that single KI mice display no deficits in the OP5' task at 6 months, as detailed in Study n°1.

B. The mystery of the claustrum

We found accompanying hyper-activity in the MTL (PRC in OP5', EC in OP3h), in concordance with the task, again mirroring results seen in preclinical AD (Berron et al., 2019, Quiroz et al., 2010, Reiman et al., 2012). There was also a consistent hyperactivation of the claustrum across both OP c-Fos studies, a functional perturbation that has not yet been documented in humans. This lesser known region has not been a large focus in the evaluation of AD. However, given its ubiquitous connections to regions exhibiting early AD pathology, including both amyloid susceptible regions (mPFC, PMC), and tau susceptible ones (PRC, EC) (Wang et al., 2017), it may be particularly prone to the combined progression of these proteinopathies (Morys et al., 1996; Qin et al, 2013). Given our results, the CLA should merit additional attention in clinical evaluations of preclinical AD. One "attractive" hypothesis could be that the hyperactive CLA, influenced by tau progression from the MTL, drives DMN hyper-connectivity through its strong connectivity to the PMC and the mPFC. Following this hypothesis, fMRI in preclinical patients should reveal at the same time a hyperactive CLA like the MTL, and a hyperconnective CLA with the midline DMN. However, until recently, targeting the CLA through fMRI has not been trivial, given its small size (***Figure 46A***). This problem was highlighted in a recent study by Krimmel et al, 2019. They evaluated resting state functional connectivity of the CLA in cognitively normal individuals using both a high resolution 7 Tesla (7T) MRI scanner and a more traditional lower resolution 3 Tesla (3T) scanner. With the 7T scanner, the high functional coherence of the CLA with the midline DMN is clear, but not with the lower resolution 3T

(***Figure 46B***). Using higher resolution fMRI, future studies may more precisely target the CLA and assess its contribution to functional perturbations of early stages of AD.

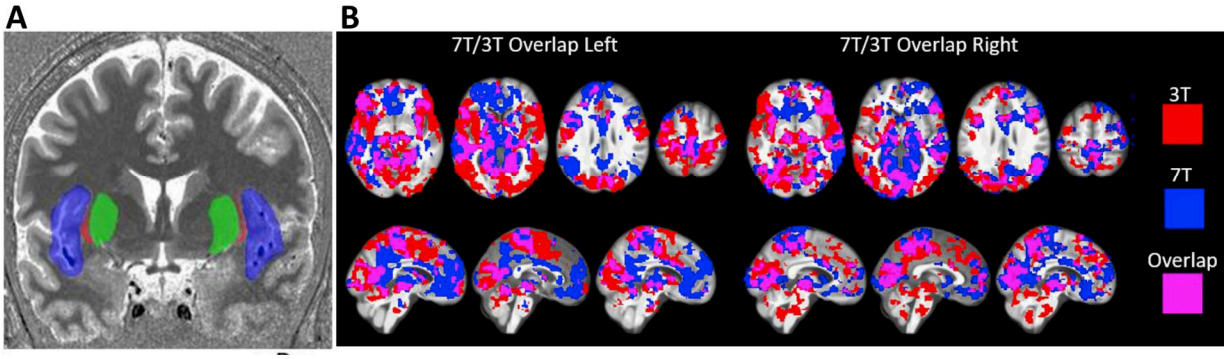

Figure 46. *(A) In humans, the CLA (red) is a thin sheet of gray matter whose fMRI signal is normally confounded by neighboring structures, including the insula (blue) and putamen (green). These regions were hand-drawn for each subject on their anatomical image. (B) Significant resting state connectivity of the left and right CLA at 7T and 3T showing widespread connectivity to cortical and subcortical regions. Notice that the blue (high resolution 7T) heavily overlaps with the midline DMN but not the red (low resolution 3T). Adapted from Krimmel et al, 2019.*

C. Network dysfunction during associative memory retrieval

During the retention phase of the OP3h task we found significantly reduced network efficiency in the dKI, especially in regions of the cingulate cortex. This reduced network efficiency could predict the reduced memory performance, similar to evaluations of network efficiency and reduced cognition in aMCI (Wang et al., 2013c). A strong reduction in hub strength was seen in the RSC, which could contribute to the reduction in network efficiency by also disrupting mPFC-MTL communication. This especially strong perturbation of the RSC is consistent with evaluations of resting state networks in preclinical AD, where communication between the PMC and MTL or mPFC is consistently reported (Hedden et al., 2009; Sheline et al., 2010; Wang et al., 2013a). Very early light increases in amyloid burden in SCD and the cognitively normal also induce PMC specific decreases in resting state DMN connectivity (Jones et al., 2016), and reductions in PMC hub strength to the DMN (Drzezga et al., 2011). Our results thus highlight a similar mechanism of reduced PMC functional connectivity and hub strength in dKI mice, except in relation to an associative memory retrieval network, resulting in associative memory loss.

D. Neuropathological staging

No aggregate formation was detected in 4 month old dKI mice (***Figure 47***). Initial associative memory deficits therefore likely follow staging of soluble proteins. In a preliminary study, mice were dissected before my OP c-Fos results were finalized, and thus only the DH and MTC were taken. We found an increase in β-CTF/α-CTF ratio in both the DH and MTC, but an increase in ptau only in the MTC. Although anatomical staging of soluble protein forms cannot be evaluated in humans, staging of aggregate formation using postmortem brains and tau-PET have robustly identified the MTC at the initial area of tau accumulation (Braak and Braak, 1995; Schwarz et al., 2016; Schöll et al., 2016), consistent with our results. For future evaluations of soluble protein staging, samples of the mPFC and RSC should also be taken. One caveat is the small size of these regions, which may not be sufficient for evaluations through ELISA or western blot. To remedy this, both regions can be pooled and the anterior/posterior cingulate cortex midline DMN can be evaluated as a whole. We would thus be able to determine if there if a larger increase in $A\beta_{42}$ or other amyloidogenic metabolites is seen only in these cingulate areas, as would be expected based on amyloid-PET staging (Palmqvist et al., 2017), and amyloid staging in relation to face-name associative memory loss (Sanabria et al., 2018; Rentz et al., 2011).

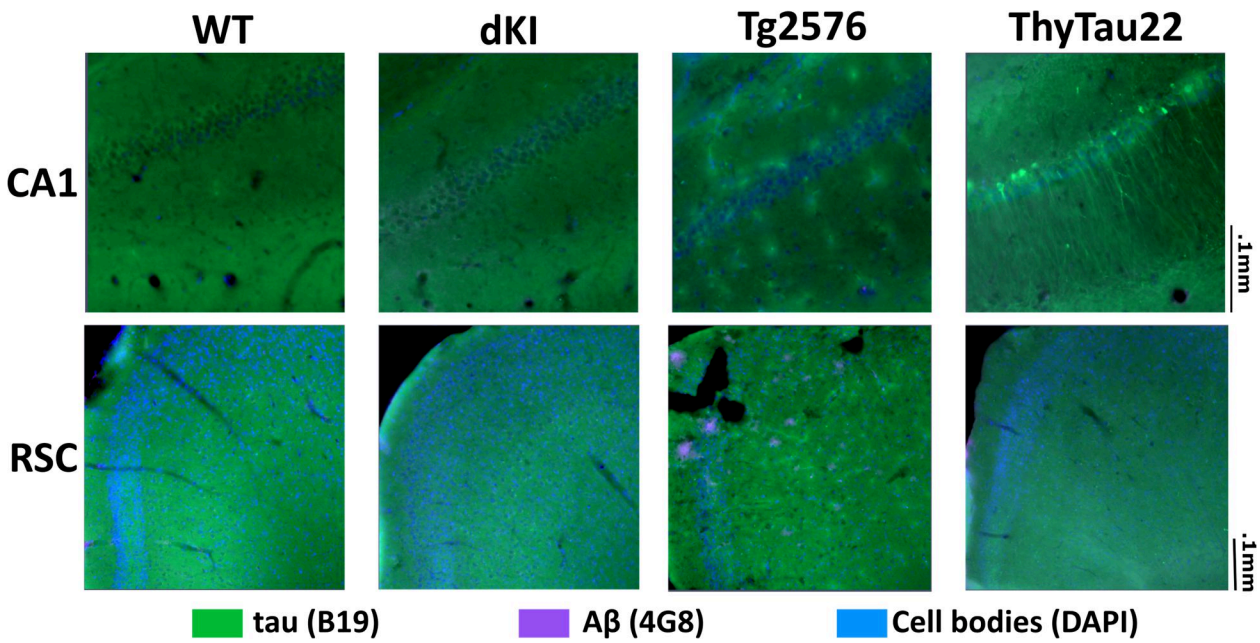

Figure 47. *Immunofluorescent staining of tau (B19 antibody) and Aβ (4G8 antibody) staining in 4 month old WT, dKI, and transgenic Tg2576 (13 months) and ThyTau22 (10 months) mouse models. Extracellular amyloid plaques can be seen in the RSC of the Tg2576 (green blurs are likely non-specific marking to capillaries). Intracellular NFTs are seen in the CA1 of the ThyTau22. Images were acquired using the Zeiss Apotome fluorescent microscope.*

E. Comparison to females

One limit of my study is that I only used male mice. With a three-year duration of a thesis this seemed to be more adapted to be sure to detect, more readily and at least in males, some precocious behavioral and physiological perturbations in the dKI model. As evoked in the introduction section, women seem to have a particular vulnerability to AD pathology in the early stage of the disease (Mosconi et al., 2017; Ferretti et al, 2018). To assess gender discrepancies in dKI mice, my colleague, Cristiana Pistono, behaviorally phenotyped female dKI mice at 2, 4, and 6 months of age. Female dKI mice presented associative memory deficits in the OP5' task at 4 months of age, identical to male dKI phenotype. However, as soon as 2 months of age the female dKI mice were also impaired in long-term recognition memory in the OR24 task, a deficit which remained at 4 and 6 months. This is a stark contrast to male dKI mice that present no deficits at these ages in the OR24 task. This potentially indicates a more severe disruption to mPFC-hippocampal in addition to mPFC-MTC function in female dKI mice. Indeed, mPFC-hippocampal interactions are known to be essential for long-term memory consolidation and retrieval (Simons and Spiers, 2003). Alternatively, the rostral part of the RSC shown to be essential for long-term object recognition (de Landeta et al., 2020) could be more affected in the female dKI, whereas the male dKI show stronger functional disruption at its caudal end (cRSC) which may be more important for contextual scene processing. In Study n°1, I had described and validated an OiC24 task in WT mice for evaluating another long term form of associative memory. Since then, this task was used to evaluate 4 month old male and female dKI mice. The OiC24 task also detected gender discrepancies, where female mice performed poorly but not male mice. This suggests that males could remember associations of other contextual features to the object (such as environmental smell, touch) that they would not be able to access in the OP task with only a spatial location association to the object in an oriented environment (based on distal visual and auditory cues). Females on the other hand may not have the ability to use these other cues to aid in object-context associative remembering. This is another hint of mPFC involvement. The mPFC is shown to be necessary for OiC remembering (Spanswick and Dyck, 2012), is involved in olfactory and tactile processing (Takahashi, 2014; Peters et al., 2013, Higaki et al., 2016; Kida and Shinohara, 2013), and moreover would be heavily tasked by the 24-hour long term ITI (Simons and Spiers, 2003).

F. Contrast with resting state fMRI

Studies that evaluate resting state fMRI in pre-plaque stages of mouse models of AD predominantly find cortical and hippocampal-cortical hyper-connectivity (Shah et al., 2016; Shah et al., 2018), while hypo-connectivity appears at later stages (Asaad and Lee, 2018). This has been reported in 3 month old single KI App^{NL-F} mice, which display increased functional connectivity strength between the hippocampus and the PFC and between the hippocampus and the RSC (Shah et al., 2018). Young 5 month old Thy-Tau22 mice displaying NFTs and gliosis also show resting state hyper-connectivity of the hippocampus with the somatosensory cortex (Degiorgis et al., 2019). Interestingly, these Thy-Tau22 mice are still able to perform the OP task efficiently at this age. The consistent hyperconnective profile of young AD mice lies in contrast to our results in dKI mice, where the mPFC and RSC are hypoconnective in the PFC-RSC-MTL network. These contrasting results may reflect a general reduced control of resting state DMN and related associative memory networks, where varying effects may arise based on testing condition, from resting state *hyper-connectivity* to associative memory dependent *hypo-connectivity*. It may also reflect methodological differences between evaluating across-time functional connectivity in fMRI vs across-subjects functional connectivity with c-Fos. Regardless, increased task dependent functional connectivity of the PMC-MTL is shown to correlate with improved object-place association in fMRI recordings of humans (Warren et al., 2019), making our c-Fos derived hypoconnective network easier to reconcile with associative memory loss in early AD. Moreover, the mouse models used to evaluate early resting state functional connectivity presented either amyloid pathology (Tg2576, PDAPP, App^{NL-F} at 3 months; Shah et al., 2016; Shah et al., 2018) or tau pathology (Thy-Tau22 at 5 months; Degiorgis et al., 2020) but not both concurrently. It has been shown in clinically normal individuals that increased amyloid-PET alone associates with hyper-connectivity of the DMN while the following onset of tau-PET associates with hypo-connectivity (Schultz et al., 2017). The dKI mice may thus have a hypoconnective resting state DMN due to its combined amyloid and tau pathologies. Whether the contrast between studies using resting state fMRI and my task dependent c-Fos analyses reflect differences between “resting state vs associative memory” or “isolated vs combined amyloid and tau pathologies” can be more thoroughly understood once resting state fMRI will be directly measured in young dKI mice.

2. Perspectives

A. Resting state fMRI on dKI

I had previously described the contrast of my task dependent c-Fos analysis finding a general hippocampal-cortical hypo-connectivity and studies of resting state fMRI finding hippocampal – cortical hyper-connectivity. This discrepancy may be better understood through evaluating 4 month old dKI mice with resting state fMRI.

As it stands, evaluating the dKIs with resting state fMRI is the theme of a project that our team is undergoing in collaboration with Dr. Laura Harsan (IMIS, ICube, Strasbourg) with PhD student Ines Ben Aballah. They will evaluate resting state fMRI in 4 month old male and female dKI mice. These mice will undergo the OP task to see if resting state fMRI signatures can be correlated to task performance. Moreover, the mice will also undergo the OR24 task to see if genotype/sex-dependent differences in resting state fMRI (one hypothesis may be that females have a more severe disruption of DH-mPFC connectivity) can explain the diverging performance in OR24 and OiC24 in females compared to males. Studies have shown that amyloid-PET load or decreased $A\beta_{42}$ has minimal effect on structural integrity without accompanying neurodegeneration (Kantarci et al., 2014; Pereira et al., 2018). However, increases in CSF tau appear to have a strong consistent effect on disrupting structural integrity (Alm and Bakker, 2019). This makes sense given the importance of tau in maintaining and preserving cytoskeletal structure as a microtubule binding protein. Since the increase in ptau was specifically seen in the MTC of 4 month old dKI mice, we should expect to see decreases in structural integrity around this region. One might expect reduced integrity of local fiber bundles such as the ventral cingulum bundle, which would explain a decreased connectivity of the RSC with the MTC.

B. Task-dependent EEG on dKI

A current experiment that the team is undergoing is the analysis of task dependent functional connectivity in mice performing the OP5' and OR24 tasks while being recorded with a state-of-the-art approach of high densisty EEG similar to that used in humans. This project is headed by Dr. Romain Goutagny and PhD candidate Matthieu Aguilera, in collaboration with Dr. Demian Battaglia. We could expect to see a similarly hypoconnected mPFC and RSC during the retention phase, in line with our c-Fos results. It would also be interesting to compare task dependent results to resting state activity and sleep, to see if stronger perturbations are elicited by the task demand as is seen in some human studies (Wang et al., 2013d), or if memory loss can be attributed to perturbed consolidation processes during sleep (Boyce et al., 2016). Moreover, using the especially high temporal resolution of EEG (even higher than fMRI), the team plans on looking at the dynamics of so called temporal networks. Here, different networks can be identified at different time intervals, where a new functional network is computed within each time window. One could look at the organization and composition of these networks and how they associate with different task behaviors or to different test-phases. They may also be interested in how quickly mice switch between network states. For example, our collaborator Demian Battaglia et al, 2020, showed that slower switching states predicts worse cognitive performance on the Montreal Cognitive Assessment test, an exam commonly used for detecting aMCI (Battaglia et al., 2019; Lombardo et al., 2020). A similar profile of slowed switching could be expected in the dKI mice who perform poorly on the OP task, perhaps between networks focused around mPFC or RSC as seen in our c-Fos analysis. Again it is difficult to say how these across-time EEG results could translate to those of the across-subjects c-Fos. However, if a specific perturbation is found around similar regions (such as the mPFC or RSC), then it would speak to the predictive power of c-Fos imaging as an efficient and cheap first step to have a general idea of where functional abnormalities may lie.

3. Final conclusion

We have shown that initial memory decline affects associative memory then pattern separation memory in dKI mice, starting at 4 months of age. These are accompanied by functional alterations, including hyper-activity in the MTC, and reduced network efficiency and hypo-connectivity of the mPFC and RSC during the object-place associative memory retrieval. We also detected a consistent hyperactivation of the CLA, a region that merits additional focus in future investigations of preclinical AD. Finally, these cognitive and functional alterations were accompanied by a specific increase of ptau in the MTC, without any aggregate formation. Up to now, our investigations on the behavioral, functional, and neuropathological changes of the dKI model fit well with the preclinical stage of AD. The fact that the initial step of its AD-like pathology develops at an early age, before age-related structural and functional alterations, makes it an extremely valuable model of FAD.

Thèse Abrégée en Français

1. Démence et la maladie d'Alzheimer

A. Le 18e pays le plus riche du monde

La démence est un syndrome causé par une grande variété de maladies du cerveau et qui estcaractérisé par un déclin de la mémoire, du langage et/ou d'autres capacités cognitives qui affectent la capacité d'une personne à effectuer des tâches quotidiennes. Elle toucherait plus de 45 millions de personnes dans le monde (Nichols et al., 2019) et devrait tripler d'ici 2050 avec l'augmentation de l'espérance de vie (An Aging World : 2015, NIH, 2016), notamment dans les pays en en voie de développement (World Alzheimer Report 2010). En 2015, le coût mondial de la démence était estimé à 818 milliards de dollars, dépassant le produit intérieur brut de pays tels que l'Indonésie et les Pays-Bas et faisant de la démence le "18ème pays le plus riche" du monde (World Alzheimer Report 2015). Compte tenu de son impact mondial écrasant et en constante augmentation, il est vital de jouer un rôle actif dans la lutte contre la démence et de promouvoir la recherche de thérapies contre les maladies qui en sont la cause. Sans avancées significatives, la démence constituera un défi croissant pour les systèmes de santé du monde entier.

B. La maladie d'Alzheimer

La cause prédominante de démence est la maladie d'Alzheimer (MA), qui représente environ 70 % des cas de démence dans le monde (Nichols et al., 2019). La maladie porte le nom d'un psychiatre allemand, Alois Alzheimer. En 1907, Alzheimer a publié une étude de cas détaillant les symptômes d'une patiente de 55 ans décrite comme étant "complètementdésorientée dans le temps et l'espace", et qui "avait complètement perdu la capacité de retenir des informations" (Alzheimer, 1895; Strassig et Ganguli, 2005). En utilisant une technique d'histologie à coloration argentique, la biopsie cérébrale de cette patiente a présenté des "neurofibrilles" colorées de façon inhabituelle et intense au sein des cellules corticales. Ces lésions sont maintenant appelées " dégénérescences neurofibrillaires " (DNF), la marque de la pathologie tau. Alzheimer a également découvert des lésions protéiques ressemblant à des grains dispersés dans le cortex, bien que celles-ci aient déjà été décrites des années auparavant par le contemplatif tchèque Oskar Fischer. Ces lésions sont maintenant appelées "plaques amyloïdes", la marque de la pathologie amyloïde. Au cours des deux années suivantes, il décrira d'autres cas présentant une pathologie

neuronale et des troubles cognitifs similaires. En 1910, ces cas seront détaillés dans un manuel de psychiatrie par un collègue d'Alzheimer, et seront désignés sous le nom de "maladie d'Alzheimer" (MA).

2. Symptomatologie de la MA

Les premiers symptômes de la maladie d'Alzheimer se traduisent principalement par de brefs trous de mémoire de reconnaissance où la personne atteinte peut parfois oublier des événements récents, ce qui relève de la mémoire épisodique. La mémoire épisodique est nécessaire pour se souvenir d'événements pertinents sur le plan personnel, avec des détails complexes et pleinement contextualisés (processus de remémoration). Cette forme de mémoire est souvent évaluée dans des paradigmes de reconnaissance utilisant la procédure "se souvenir/savoir" (Tulving, 1985). Les instructions sont adaptées pour différencier le processus épisodique de remémoration (se souvenir) du processus non épisodique de familiarité (savoir; voir Yonelinas, 2002; Rugg et Yonelinas, 2003; Vilberg et Rugg, 2008 pour une discussion sur le double processus de la mémoire de reconnaissance). Les patients présenteront également des défaillances de la mémoire spatiale où ils auront d'abord du mal à se souvenir de l'endroit où ils ont placé des objets et des difficultés d'orientation spatiale, notamment lors de l'apprentissage d'un nouvel itinéraire. À un stade avancé, les patients atteints de la MA perdront progressivement leur capacité à se diriger vers des lieux familiers et à en revenir. En outre, la fonction exécutive est affectée, car la personne atteinte aura plus de mal à prendre des décisions (déficits de prise de décision), à changer ses habitudes (perte de flexibilité cognitive) ou montrera des difficultés à retenir des informations simples nécessaires à des tâches routinières à plusieurs étapes, comme suivre une nouvelle recette. Cette dernière tâche dépend généralement de la mémoire de travail. Le stade prodromique de la MA se caractérise par des troubles cognitifs légers qui n'affectent pas gravement les fonctions quotidiennes, et correspond à un état cognitif appelé trouble cognitif léger (*Mild Cognitive Impairment* : MCI ; Petersen et al., 2001). Au fur et à mesure que la maladie se développe, les problèmes de mémoire et de fonctions exécutives s'aggravent. Finalement, les symptômes évoluent au point de nécessiter une aide quotidienne, signalant ainsi la transition du MCI à la démence. La personne aura du mal à reconnaître sa famille et ses amis. Leur personnalité peut également changer avec une anxiété et une agitation croissantes. De plus

en plus désorientées, elles commenceront à errer, surtout pendant la période de sommeil, et oublieront la date du jour et le lieu où elles se trouvent. Leur anxiété peut se manifester davantage, certains patients développant une grave dépression. Nombre d'entre eux souffriront de délires et de paranoïa. De nouveaux symptômes commenceront à se développer, tels que la perturbation de l'architecture du sommeil et l'aphasie (perte du langage parlé). Les troubles du sommeil sont fréquents dans la MA, touchant jusqu'à 45 % des patients atteints de cette maladie (Moran et al., 2005 ; McCurry et al., 2000). Les troubles du sommeil sont particulièrement importants au regard de la symptomatologie de la MA car ils jouent un rôle crucial dans la formation de la mémoire et dans d'autres fonctions cognitives (Mander et al., 2016). Au stade final de la maladie, le patient peut développer des symptômes physiques, notamment une perte de poids importante et des difficultés à se déplacer ou à manger.

Le diagnostic de la MA repose d'abord sur un examen clinique par un médecin. Celui-ci consiste en un entretien avec le patient et ses proches. Les troubles cognitifs sont ensuite évalués de manière quantitative grâce à l'aide des tests cognitifs. Le plus courant d'entre eux est le Mini Mental State Examination (MMSE) de Folstein (Folstein et Whitehouse, 1983). Ce test fournit une exploration cognitive globale du patient à l'aide de trente questions. Il renseigne sur l'orientation spatio-temporelle, la mémoire à court et moyen terme, le calcul mental, l'attention, le langage, la compréhension et la praxie constructive du patient. Des examens biologiques complémentaires évaluant l'état neuropathologique sont toujours nécessaires pour confirmer le diagnostic. Dans le passé, le diagnostic définitif de la MA ne pouvait être posé qu'après un examen post-mortem du cerveau confirmant la présence des deux lésions caractéristiques de la MA, à savoir les plaques amyloïdes et les DNF.

A. Les agrégats caractéristiques

Les plaques amyloïdes, lésions protéiques en forme de grains décrites par Alzheimer et Fischer, sont formées par l'accumulation extracellulaire d'un peptide amyloïde (Aβ). L'Aβ résulte de la transformation de la protéine précurseur de l'amyloïde (APP). L'accumulation dans le cerveau peut résulter d'une perturbation de l'équilibre entre les voies de production et de clairance de l'Aβ dans le cas de la MA sporadique, ou d'une surproduction d'Aβ due à des mutations génétiques dans la forme familiale de la MA (Familial Alzheimer's Disease : FAD) (Selkoe et

Hardy, 2016). Les peptides Aβ se replient en structures de feuillets bêta hautement fibrillogènes, et s'agrègent pour former des oligomères, puis des filaments et enfin des plaques amyloïdes (Rozemuller et al., 1989). Il existe deux principaux sous-types d'Aβ, l'Aβ40 et l'Aβ42. L'Aβ42 s'agrège plus facilement et est la plus abondante dans les plaques amyloïdes. L'évaluation de la diminution des taux d'Aβ42 dans le liquide céphalo-rachidien (LCR) est un moyen fiable de prédire l'augmentation des dépôts amyloïdes dans le cerveau et elle est systématiquement effectuée pour confirmer le diagnostic de la MA. Il faut noter que dans des conditions saines, la voie amyloïdogénique de l'APP qui implique les β et γ sécretases est secondaire par rapport à la voie non amyloïdogénique qui implique une α-sécrétase agissant au sein de la séquence Aβ, libérant ainsi la forme sécrétée hautement neurotrophique et neuroprotectrice de l'APP (Dodart et al., 2000).

Il existe deux formes principales de plaques : les plaques diffuses et les plaques à noyau dense (***figure 1***). Les plaques diffuses, le sous-type le plus précoce, ont une structure amorphe (Yamaguchi et al., 1988) et sont faiblement colorées par la thioflavine S (un composé utilisé pour colorer les agrégats de protéines) et les colorants de liaison amyloïde tels que le rouge Congo. Les plaques à noyau dense ont un noyau compact constitué de fibrilles amyloïdes densément tassées (Kidd, 1964), et sont intensément positifs à la thioflavine S et au rouge Congo (Dickson et al., 1997). Un sous-ensemble de plaques à noyau dense, appelé plaques neuritiques, contient des processus neuronaux dégénératifs (neurites) entourés de glie réactive et de perte synaptique (Thal et al., 2006 ; Yasuhara et al, 1997).

Les DNF, les neurofibrilles décrites par Alzheimer, sont des agrégats filamenteux de protéine tau (Goedert et al., 1988). La protéine tau a normalement pour fonction de stabiliser et d'organiser les microtubules axonaux (Weingarten et al., 1975). Une phosphorylation anormale de tau entraîne une perte de fonction et son agrégation ultérieure, d'abord en oligomères (Maeda et al., 2006), puis en filaments (Goedert et al., 2018), et enfin en DNF. Les filaments de tau les plus courants ont une structure hélicoïdale double torsadée et sont donc appelés filaments hélicoïdaux appariés (PHF), bien que des filaments hélicoïdaux droits (SH) existent également.

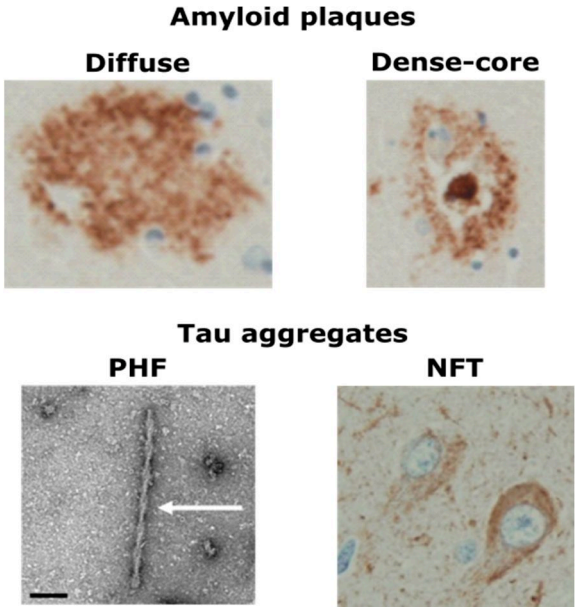

Figure 3. *Les deux caractéristiques de la MA. DNF : dégénérescence neurofibrillaire. PHF : fragment hélicoïdal apparié. Adapté de Deture et Dickson 2019*

B. Du traitement à la prévention

La méthode la plus courante pour diagnostiquer la MA comporte en un examen qualitatif de l'état mental du patient tel qu'il a été évoqué précédemment. Aujourd'hui, les examens biologiques se font grâce à tests de LCR et éventuellement des examens de neuro-imagerie pour vérifier la présence des pathologies amyloïde et tau. En l'état actuel des choses, cette filière de diagnostic est capable de détecter de facon efficace les stades légers à modérés de la MA. Les essais cliniques ont surtout été menés à ces stades de la MA, notamment ceux qui ont testé les anticorps ciblant l'Aβ (solanezumab, bapineuzumab) et les inhibiteurs des sécrétases β (verubecestat) et γ (semagacestat). Malheureusement, jusqu'à présent, ces traitements n'ont pas réussi à ralentir significativement le déclin cognitif et fonctionnel (Doody et al., 2013, 2014). Cela est largement dû au fait que ces traitements interviennent trop tard, après que les changements physiologiques tels que l'atrophie cérébrale ont atteint un état potentiellement irréversible. Il est essentiel d'approfondir les connaissances actuelles sur les stades les plus précoces, afin de pouvoir établir des thérapies ou des méthodes de détection plus proactives. Dans la suite de ce texte, je me concentrerai sur les perturbations physiologiques et cognitives qui sous-tendent les tout premiers stades de la MA.

3. Facteurs génétiques et facteurs de risque de la MA

A. La MA sporadique et ses facteurs de risque

La grande majorité des patients atteints de la maladie d'Alzheimer (95 %) présentent la forme sporadique tardive de la maladie. Parmi les principaux facteurs de risque non modifiables, il y a l'âge , le plus fondamental et le plus connu. Environ 2/3 des patients atteints de la MA aux États-Unis ou en France sont des femmes, ainsi que dans la plupart des pays européens. Ce phénomène a d'abord été attribué au fait que les femmes vieillissaient mieux que les hommes, de sorte que cette proportion déséquilibrée ne reflétait qu'un biais de survie lié au sexe. Cependant, le sexe a été plus récemment identifié comme un important facteur de risque en soi dans la MA (Ferretti et al, 2018). Le risque plus élevé de développer la MA a été en partie lié à une vulnérabilité accrue du cerveau féminin pendant et après la ménopause (Mosconi et al, 2017). En outre, de nombreux autres facteurs de risque modifiables de la MA ont un impact plus élevé sur le sexe féminin et le genre, comme la dépression, les troubles du sommeil et le fardeau des aidants (Rahman et al., 2019). D'autre part, les recherches sur les facteurs de risque environnementaux spécifiques ont rassemblé des preuves relativement faibles concernant la plupart des métaux et l'exposition professionnelle (plomb, peintures, carburants). Cependant, l'examen systématique publié par Killin et al. (2016) se termine tout de même par une courte liste qui inclut la pollution atmosphérique, l'aluminium et les pesticides comme présentant des preuves modérées en tant que facteurs de risque de démence et qui méritent une étude plus approfondie.

Dans la MA sporadique, il existe plusieurs polymorphismes génétiques communs avec une faible taille d'effet qui représentent une part importante de l'héritabilité de la MA. Plutôt que d'augmenter directement la production d'Aβ, la plupart de ces gènes de risque augmentent indirectement la présence ou le métabolisme de l'APP ou de la tau et/ou affectent négativement la clairance de l'Aβ. L'un des principaux facteurs de risque génétique est lié au gène *APOE*, qui code pour l'apoliprotéine E (apoE), une protéine impliquée dans le transport des lipides. Il existe trois allèles *APOE*, ε2, ε3 et ε4, donnant respectivement naissance aux isoformes apoE2, apoE3 et apoE4. L'*APOE ε4* entraîne un risque plus élevé de développer la MA, sa présence hétérozygote entraînant un risque multiplié par 3, et homozygote par 12. On estime qu'il est présent chez 15 à 20% de la population et chez plus de 50% des patients atteints de MCI (Silva et al., 2019). Les porteurs asymptomatiques d'*APOE ε4 font* partie des représentations les plus

couramment évaluées de la MA préclinique, et seront mentionnés tout au long de ce texte. L'impact de l'*APOE ε4* dans le développement de la MA a été lié à ses effets délétères à plusieurs niveaux de la pathologie induite par l'Aβ, ainsi qu'à ses effets indépendants sur la plasticité synaptique, la réparation neuronale ou les fonctions cérébrovasculaires (Yamazaki et al., 2019). En outre, une étude récente suggère également que cet allèle augmente la pathologie tau (Therriault et al., 2020). Il existe de nombreux autres facteurs de risque génétiques en plus du gène *APOE ε4*. De récentes études d'association à l'échelle du génome (*Genome Wide Association* : GWA) ont permis de passer au crible des centaines de milliers de cas de MA afin d'identifier de nouveaux variants génétiques qui augmentent les riques. Ces méta-analyses ont identifié plus de 40 loci génomiques associés à la maladie, qui pourraient impliquer plus de 200 gènes (Lambert et al., 2013 ; Jansen et al,. 2019).

B. La maladie d'Alzheimer familiale (FAD)

Environ 1 % des cas de MA sont de la forme familiale autosomique dominante (FAD), ce qui signifie qu'ils sont liés à une ou plusieurs mutations génétiques au sein d'un gène qui entraînent un risque de 100 % de développer une forme précoce de la MA. Ces mutations se trouvent dans trois gènes, *App*, *PSEN1* et *PSEN2*. *App* code pour la protéine précurseur amyloïde (APP), la protéine qui est clivée pour former l'Aβ. *PSEN1* et *PSEN2* codent respectivement pour les présénilines 1 et 2, les sous-unités catalytiques du complexe γ-secrétase qui clive l'APP et contribue à la formation d'Aβ. Les mutations de ces gènes favorisent donc la production d'Aβ en augmentant le clivage spécifique dee la voie amyloïdogène de l'APP, ou en augmentant le rapport Aβ42/Aβ40. Les individus asymptomatiques atteints de FAD représentent le moyen le plus robuste de suivre les trajectoires pathologiques des patients atteints de la MA, et ils ont contribué à définir pour la première fois la progression préclinique des stades de la MA.

Les changements neuropathologiques dans la MA se produisent des décennies avant le déclin cognitif (Selkoe, 2012). L'évaluation des patients atteints de la MA montre que les taux d'Aβ42 dans le LCR commencent à diminuer dès 25 ans avant l'apparition prévue des symptômes (Bateman et al., 2012). Ensuite, des dépôts amyloïdes et une atrophie progressive du cerveau sont détectés par des techniques de neuro-imagerie (imagerie par tomographie par émission de positons des plaques amyloïdes (amyloid-PET) et imagerie par résonance magnétique

structurelle (sMRI)), suivis de peu par une augmentation des niveaux de tau total et de tau phosphorylé (ptau) dans le LCR apparaissant environ 15 ans avant l'apparition prévue des symptômes (Bateman et al., 2012; Fleisher et al., 2015). Il faut noter que les déficiences cognitives au MMSE et à l'échelle d'évaluation de la démence clinique ne sont détectées que 5 ans avant le diagnostic de la démence. Les contenus du LCR en tau total et ptau sont maintenant évalués de façon routinière pour confirmer le diagnostic clinique de la MA. Les dépôts de tau sont observés par imagerie TEP 6 ans avant l'apparition prévue des symptômes, et sont bien corrélés avec les performances du MMSE (Quiroz et al., 2018). Cette évolution temporelle est généralement retenue dans l'évaluation transversale complémentaire de la MA sporadique (voir la ***figure 2***, et Jack et al., 2010).

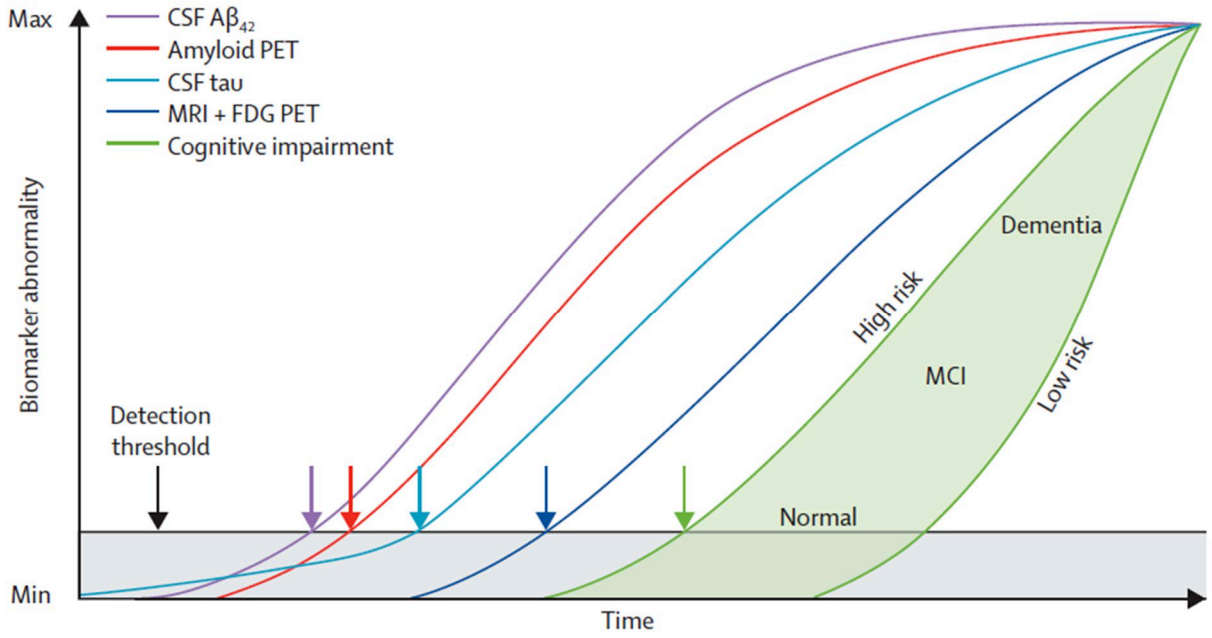

Figure 4. *Progression de la maladie d'Alzheimer. Évolution des biomarqueurs actuellement utilisés pour le diagnostic de la MA en fonction du temps. Reproduit de Jack et al 2013.*

4. Détecter les premiers stades de la maladie d'Alzheimer

A. Trouble cognitif léger (MCI)

Le trouble cognitif léger ou MCI est un syndrome défini par un déclin cognitif supérieur à la normale pour l'âge de l'individu, mais pas assez grave pour interférer sévèrement avec la vie quotidienne (Gauthier et al,. 2006). La prévalence du MCI chez les adultes de plus de 65 ans est de 10 à 20 % (Langa et al., 2014). Le MCI peut être diagnostiqué sur la base de preuves anecdotiques ou par des tests neuropsychologiques tels que le Short Test of Mental Status et le Montreal Cognitive Assessment (Tang-Wai et al., 2003 ; Nasreddine et al., 2005). Il existe deux sous-types de MCI, amnésique et non amnésique. Le MCI amnésique (aMCI) concerne des altérations notables de la mémoire épisodique, les autres capacités telles que les fonctions exécutives restant plus ou moins intactes. Le MCI non amnésique se caractérise au contraire par un déclin subtil de fonctions distinctes telles que les fonctions exécutives, le langage et les aptitudes visuospatiales. Les personnes atteintes d'un aMCI ont plus de chances de passer à la MA, avec un taux de progression d'au moins 10 % par an, contre 2 % chez les personnes âgées normales (Campbell et al., 2013 ; Roberts et al., 2014), de sorte qu'il est considéré comme un stade prodromique de la MA (***figure 3***). Cependant, il est important de garder à l'esprit que le MCI ne décrit qu'un ensemble de symptômes, et non une maladie spécifique. Les patients MCI ne développent pas nécessairement une phase précoce de la MA car la population MCI comprend également d'autres étiologies comme la dépression et d'autres maladies neurodégénératives qui affectent la sphère cognitive.

B. Déclin cognitif préclinique et subjectif

Après trois décennies de recherches intenses, d'échecs d'essais cliniques et de données recueillies chez des patients présymptomatiques atteints de la maladie d'Alzheimer sporadique et de FAD au début des années 2010 (Jack et al. 2010 ; Bateman et al., 2012), la communauté mondiale des chercheurs sur la maladie d'Alzheimer a compris qu'une intervention précoce offrirait un meilleur succès thérapeutique. Par conséquent, le développement d'une prévention et d'un traitement efficaces dépendrait de l'accroissement des connaissances sur les étapes initiales de la maladie (Selkoe, 2012). Entre-temps, de nombreuses recherches et essais cliniques ont été

menés... or il n'existe à ce jour aucun traitement efficace (Yiannopoulou et Papageorgiou, 2020). Ce manque de progrès dans les approches thérapeutiques a fortement stimulé la recherche sur des stades plus précoces que le MCI, comme l'illustre la forte augmentation des publications sur le déclin cognitif préclinique et subjectif, ainsi que sur les personnes d'âge matures et âgées "cognitivement saines" présentant des dépôts amyloïdes. Le présent travail fait partie de cet effort général visant à se concentrer sur le stade préclinique. Cela nous a conduit à rechercher une définition de ce "stade préclinique". Sperling et ses collègues (2011) ont proposé un cadre en trois étapes pour la MA préclinique, basé sur les biomarqueurs cliniques actuellement utilisés. Le premier stade d'amyloïdose asymptomatique est caractérisé par une rétention élevée du traceur amyloïde sur la TEP et un faible taux d'Aβ42 dans le LCR, le second ajoute la neurodégénérescence avec un dysfonctionnement neuronal sur la TEP au 18F-fluorodésoxyglucose (TEP-FDG) ou l'IRM fonctionnelle (IRMf), un taux élevé de tau/ptau dans le LCR et un amincissement cortical/une atrophie hippocampique dans l'IRMs, et enfin la troisième étape ajoute un déclin cognitif subtil avec des preuves de changements par rapport au niveau de base de la cognition, des performances médiocres dans des tests cognitifs plus difficiles sans répondre aux critères du MCI (selon Dubois et al., 2016, " la *MA préclinique s'étendrait théoriquement des premières lésions cérébrales neuropathologiques à l'apparition des premiers symptômes cliniques de la MA* "). Cependant, Ces auteurs évoquent la difficulté de fixer les limites entre ce qui doit être considéré comme le premier signe neuropathologique et ce qui doit être considéré comme le premier symptôme clinique de la MA. En effet, un nouveau stade de la MA préclinique appelé déclin cognitif subjectif (Subjective Cognitive Decline : SCD) a récemment été considéré comme la première manifestation clinique de la MA. Le SCD est basé sur un déclin auto-rapporté des fonctions cognitives sans aucune altération dans la batterie diagnostique classique. Les études de neuro-imagerie du SCD ont révélé des agrégats amyloïdes et tau anormaux, une atrophie régionale et des altérations de la substance blanche (Wang et al, 2020). Ces caractéristiques sont relativement proches de celles énumérées pour le troisième stade proposé par Sperling et al. (2011). Une vue d'ensemble des différents stades de la MA est présentée dans la ***figure 3***.

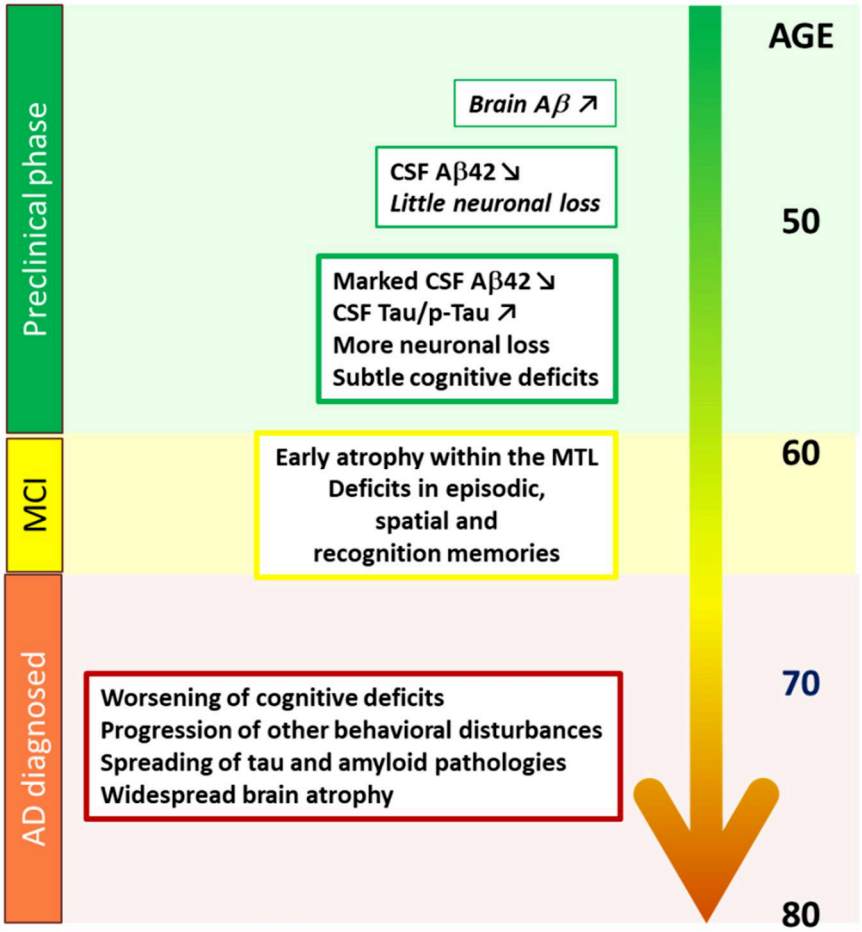

Figure 3. *Stadification de la MA avec des marqueurs cognitifs et biologiques. Inspiré de Selkoe, 2012 et Bateman et al., 2012.*

C. Stades neuropathologiques de la maladie d'Alzheimer

L'accumulation de protéines affecte différentes régions du cerveau à différents stades, ce qui permet de caractériser le dépôt dans un système de classification des stades de la MA. Les premiers systèmes de classificationont été mis au point à partir d'études neuropathologiques post-mortem du cerveau, détaillées dans les recherches fondamentales des équipes de Heiko Braak et de son étudiant Dietmar Thal. Braak et Thal ont décrit une progression descendante du dépôt amyloïde, décrite dans les "stades Thal" : stade 1 dans le néocortex, stades 2 et 3 dans l'allocortex (cortex temporal médian et insulaire) et le système limbique, et stades 4 et 5 dans la région sous-corticale. Braak a décrit la progression des tau avec les "stades de Braak", les stades 1 et 2 commençant dans le lobe temporal médian, les stades 3 et 4 dans le système limbique, et

enfin les stades 5 et 6 dans le néocortex. Ces stades de Braak et de Thal sont illustrés dans la ***figure 4A***.

Grâce au développement récent des techniques d'imagerie fonctionnelle, nous avons un regard plus précis sur les dépôts caractérisant la MA et les changements concomitants dans la physiologie du cerveau (Jagust et al., 2018) (***figure 4B***). La tomographie par émission de positrons (TEP) est une technique qui utilise des substances radioactives appelées radiotraceurs pour visualiser les modifications de la physiologie cérébrale (Ametamey et al., 2008). Certains radiotraceurs ont été vérifiés dans des cerveaux post-mortem pour marquer les plaques et fibrilles amyloïdes (Klunk et al., 2004 ; Clark et al., 2012 ; Sabri et al., 2015 ; Curtis et al., 2015) ainsi que les PHF et DNF de tau (Xia et al., 2013 ; Marquié et al., 2015 ; Schonhaut et al., 2017). Elles peuvent être couplées à d'autres techniques de neuro-imagerie pour évaluer les changements concomitants dans la physiologie du cerveau. Le radiotraceur analogue du glucose 18F-fluorodésoxyglucose utilisé en FDG-PET peut cartographier le métabolisme du glucose dans le cerveau. La pertinence cellulaire de cette technique est quelque peu ambiguë, mais le signal enregistré est variasemblablement lié à un dysfonctionnement synaptique et/ou glial. Les techniques d'imagerie par résonance magnétique telles que l'IRMs et l'IRMf mesurent respectivement le volume du cerveau (par la détection des mouvements aléatoires de l'eau dans les tissus) et l'activité cérébrale (par la détection des niveaux d'oxygène dans le sang). Enfin, les mesures physiologiques ont été évaluées en tandem avec des évaluations standardisées de la fonction cognitive, quantifiées à l'aide de protocoles de tests tels que le Mini-Mental State Examination (MMSE) et le Clinical Dementia Rating Scale Sum of Boxes (CDR).

La TEP-amyloïde révèle plus de détails sur ce qui est essentiellement le stade 1 de Thal. Les dépôts amyloïdes les plus précoces sont observés dans le cortex préfrontal médian (mPFC) et le cortex médian postérieur (PMC) (y compris le cingulaire postérieur, le rétrosplénial, le précuneus) (Palmqvist et al., 2017). Le dépôt amyloïde progresse ensuite vers les autres zones néocorticales décrites dans le stade 1 de Thal (Mattson et al., 2019). La correspondance entre la TEP amyloïde et l'hypométabolisme ou l'atrophie n'est pas claire. De nombreuses études ne signalent aucune correspondance (Furst et al., 2012, Lehmann et al., 2013). Dans le MCI, l'augmentation des dépôts amyloïdes dans le PMC est associée à l'atrophie des régions temporales médianes, ce qui pourrait refléter une association indirecte avec le premier stade de

pathologie tau (Tosun et al., 2011). D'autres ont rapporté une association entre l'amyloïde et l'atrophie uniquement pendant le stade préclinique de la MCS, ce qui suggère que l'Aβ initial peut induire une atrophie subtile à un stade précoce avant que cette dépendance ne soit brouillée par l'apparition d'autres processus atrophiques (Chételat et al., 2010). La pathologie amyloïde se profile des décennies avant la démence, et se retrouve même en abondance chez les personnes âgées en bonne santé cognitive (Villeneuve et al. 2015). La plupart des personnes en bonne santé cognitive présentent une moindre association de l'atrophie et de l'hypométabolisme avec l'Aβ, ce qui indique une résistance à l'Aβ comme mécanisme potentiel de maintien de la cognition (Ewers et al., 2012).

La TEP-Tau récapitule largement la classification de Braak (Schwarz et al., 2016 ; Schöll et al., 2016). Le dépôt de tau apparaît après le dépôt d'amyloïde, mais une augmentation de tau est associée à une augmentation d'amyloïde (Johnson et al., 2016 ; Tosun et al., 2017). Même chez les personnes cognitivement normales, de très légères augmentations de l'amyloïde corticale, quelle que soit sa localisation, s'associent à des augmentations de tau dans le lobe temporal médian (Medial Temporal Lobe : MTL ; Tosun et al., 2017, Leal et al., 2018). Il existe une forte corrélation entre la topographie du dépôt de tau et l'atrophie (Wang et Mandelkow, 2016). Le dépôt de tau et l'atrophie qui l'accompagne dans le MTL sont fortement corrélés à une diminution de la fonction cognitive mesurée par le MMSE et le REC (Brier et al., 2016 ; Pontecorvo et al., 2017 ; Quiroz et al., 2018).

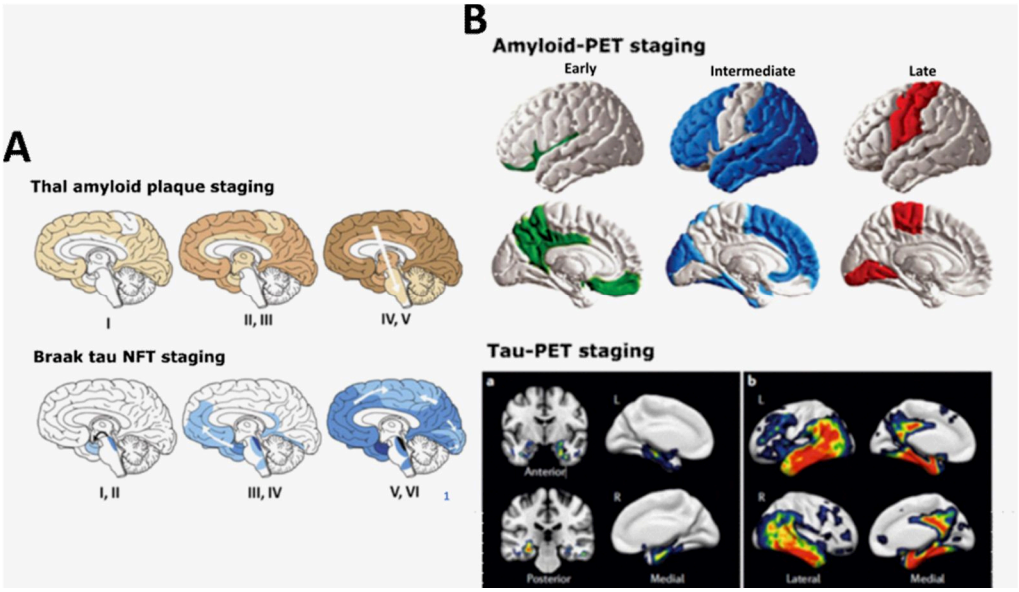

Figure 4. *Stadification de la formation d'agrégats basée sur (A) l'évaluation de cerveaux post mortem et (B) la TEP. Adapté de Jouanne et al., 2017 ; Mattson et al., 2019 ; Maass et al., 2017.*

5. Perturbations fonctionnelles de la MA précoce

A. Hyperactivité dans le MTL

En utilisant l'IRMf et la TEP-FDG chez des patients atteints de MCI, plusieurs études ont signalé une hyperactivité dans le cerveau antérieur basal (Kim et al., 2012) et plus particulièrement dans le MTL (Johnson et al., 2006a ; Hämäläinen et al., 2007 ; Huijbers et al., 2015). L'hyperactivité du MTL est également observée chez les personnes asymptomatiques précliniques présentant un risque génétique de développer la MA, notamment les porteurs de mutations FAD (Quiroz et al., 2010 ; 2015 ; Reiman et al., 2012) et chez les porteurs de l'APOE ε4 présentant un risque accru de MA sporadique (Bookheimer et al., 2000 ; Johnson et al., 2006b ; Tran et al., 2017). La réduction de l'hyperactivité du MTL améliore la cognition dans le cadre de l'aMCI (Bakker et al., 2012). Il existe un lien clair entre l'augmentation de tau et l'hyperactivité des MTL chez les personnes en bonne santé cognitive, évaluée par Tau-PET (Marks et al., 2017 ; Huijbers et al., 2019), et les niveaux de tau dans le LCR (Berron et al., 2019). L'hyperactivité est également bien corrélée avec l'atrophie et l'amincissement cortical (Putcha et al., 2011, Hämäläinen et al., 2007). Étant donné sa proéminence chez les individus asymptomatiques, l'hypothèse a été émise que l'hyperactivité faisait partie d'un mécanisme de compensation contrebalançant les premières altérations neuropathologiques associées à la MA. En effet, des études ont montré que l'hyperactivité hippocampique pendant l'encodage (Kircher et al., 2007) peut être corrélée positivement de manière transitoire avec de meilleures performances lors d'une tâche de mémoire. Cependant, nous verrons plus loin que l'hyperactivité du MTL peut avoir un effet négatif sur certaines formes subtiles de mémoire, qui restent pour l'instant largement non détectées chez les individus précliniques.

B. Mode par défaut Réseau

i. Vue d'ensemble

Le réseau du mode par défaut (Default Mode Network : DMN) est décrit plus simplement comme un ensemble de régions cérébrales coactivé dans le temps (en d'autres termes, elles présentent une connectivité fonctionnelle) au cours des états de repos ou de tâche passive (Buckner et al., 2008). Il s'agit principalement de régions du mPFC, du PMC et du lobe temporal. Cependant, le DMN peut être décrit de manière plus appropriée comme un ensemble de sous-systèmes qui convergent vers les centres de la ligne médiane. Il existe deux principaux sous-systèmes qui convergent vers les hubs du mPFC antérieur (amPFC) et du PMC : le "sous-système temporal médian" contenant la formation hippocampique/MTL, le cortex rétrosplénial (RSC) et le mPFC ventral (vmPFC), et un "sous-système médian dorsal" contenant le mPFC dorsal (dmPFC), le lobe pariétal inférieur et le cortex temporal latéral (Andrews-Hanna et al., 2010). Ces sous-systèmes sont fonctionnellement divergents, chacun soutenant des processus distincts favorisant la pensée autobiographique. Le sous-système temporal médial est plus impliqué dans la récupération de la mémoire épisodique, tandis que le sous-système médial dorsal est plus impliqué dans la mentalisation (capacité à représenter le sentiment et les émotions de soi et des autres) (Andrews-Hanna et al., 2014) (***Figure 8***). Grâce à des techniques d'analyse plus avancées, de nombreux autres sous-systèmes et réseaux individuels contribuant au DMN global ont été identifiés, tels que le DMN postérieur (pDMN) et le DMN antérieur (aDMN), qui présentent respectivement une plus grande implication du PMC et du mPFC. (Jones et al., 2012 ; Buckner et DiNicola, 2019)

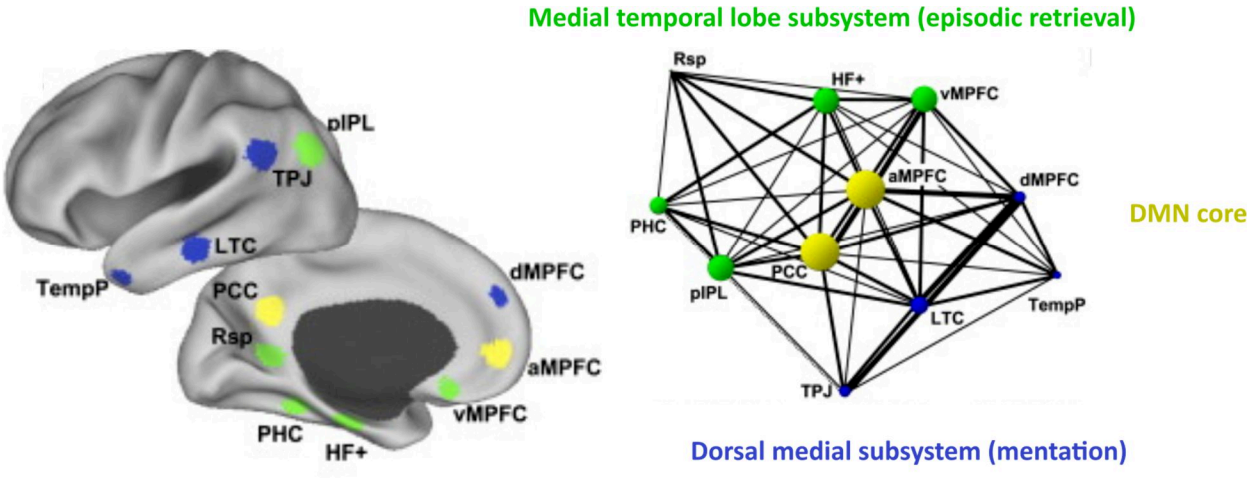

Figure 8. *Le réseau du mode par défaut et ses principaux sous-systèmes qui contribuent aux différents aspects de la mémoire autobiographique. Le sous-système dorsal médial est nécessaire à la mentalisation et comprend le cortex préfrontal dorsal médial (dMPFC), la jonction temporo-pariétale (TPJ), le cortex temporal latéral (LTC) et le pôle temporal (TempP). Le sous-système du lobe temporal médian (MTL) est nécessaire à la récupération épisodique et comprend le cotrex préfrontal médian ventral (vMPFC), le lobule pariétal inférieur postérieur (pIPL), le cortex rétrosplénial (Rsp), le cortex parahippocampique (PHC) et la formation hippocampique (HF+). Ces sous-systèmes se chevauchent dans le DMN par le biais des régions centrales de la ligne médiane du cortex cingulaire postérieur (PCC) et du cortex préfrontal médian antérieur (amPFC). Adapté de Andrews-Hanna et al. 2010.*

ii. Au début de la MA

On a pu remarquer que les principales plaques tournantes soutenant le DMN sont celles qui sont initialement affectées par le dépôt amyloïde précoce, le mPFC et le PMC. Même avant le développement de la TEP-amyloïde, il a été noté par la TEP-FTG que le mPFC et le PMC présentaient un métabolisme du glucose réduit au repos et une hypo-activité chez les porteurs asymptomatiques de l'APOE ε4 (Reiman et al., 1996, 2004). On peut donc émettre l'hypothèse que le réseau du mode par défaut pourrait être particulièrement sensible à la MA préclinique.

La force/intégrité d'un réseau fonctionnel, ou entre réseaux ou sous-systèmes fonctionnels, peut être définie par la force de la co-activation de leurs régions dans le temps. Les évaluations de personnes asymptomatiques établissent systématiquement un lien entre les biomarqueurs précoces de la MA (augmentation de l'amyloïde-PET, diminution de l'Aβ42 et augmentation du ptau181 dans le LCR) et la connectivité réduite du DMN au PMC (Hedden et al., 2009 ; Sheline et al., 2010 ; Wang et al., 2013a). Jones et ses collègues ont montré que chez les porteurs asymptomatiques de l'APOE ε4, le sous-système DMN impliquant principalement le PMC, le pDMN, présente une connectivité fonctionnelle intra-système réduite avant l'apparition des

plaques (Jones et al., 2016). Cette étude a été couplée à une analyse transversale, qui a révélé qu'avec une charge amyloïde élevée et une atrophie hippocampique sévère dans le MCI tardif et la MA précoce, la connectivité de ce sous-système PMC continue de diminuer de manière substantielle, tandis que la connectivité entre le pDMN et les autres sous-systèmes DMN augmente. Dans les stades de la MA où la charge amyloïde est absente ou faible (en CN, SCD ou MCI précoce), la relation entre la charge amyloïde et la force de connectivité n'est pas aussi claire. Cela pourrait indiquer que ce point intermédiaire de la pathologie de la MA, généralement entre les stades pré-plaque et post-plaque, s'accompagne d'un mélange dynamique de profils de connectivité (de l'*hypo-connectivité du* PMC à l'*hyper-connectivité* globale du DMN) qui ne peut être facilement caractérisé. La nature dynamique de la perturbation du DMN dans la MA prodromique pose un problème pour les évaluations d'une forme avancée duMCI (amnesic MCI : aMCI), qui devrait englober un mélange d'états protéopathiques de la MA. Une analyse des évaluations de la connectivité fonctionnelle au repos dans la maladie de Creutzfeldt-Jakob, réalisée à partir de 22 études, montre que la connectivité du réseau DMN au PMC est systématiquement affectée, mais que la direction de la perturbation (hyper ou hypoconnectivité) varie. Cependant, ils constatent une tendance à l'hyperconnectivité PMC-DMN (Badhwar et al., 2017), ce qui suggère une plus grande représentation du MCI au stade avancé, avec un niveau déjà élevé de charge amyloïde et d'atrophie hippocampique. Dans le cas du SCD, une incohérence similaire est constatée ; certaines études rapportent une connectivité accrue au sein du DMN (Wang et al., 2013b), ou entre le PMC et le reste du DMN (Verfaillie et al. ; 2018). En revanche, d'autres ont signalé une diminution de la connectivité entre le pDMN et d'autres sous-systèmes du DMN (Dillen et al., 2017 ; Yasuno et al., 2015).

iii. Analyses théoriques des graphes

Pour une compréhension plus approfondie du flux d'informations dans un réseau fonctionnel, nous pouvons évaluer sa topologie en utilisant la théorie des graphes. Avec la théorie des graphes, un réseau fonctionnel peut être représenté comme un *graphe* avec des *nœuds* (régions) qui sont interconnectés par des *arêtes* (connexions), qui existent si deux régions co-activent significativement ensemble dans le temps (***Figure 9A***). Les réseaux efficaces sont ceux qui sont capables de transférer efficacement des informations entre régions. Cela est généralement mesuré

comme l'*efficacité globale* d'un réseau. Il a été démontré que l'efficacité globale du réseau varie avec la performance cognitive et dépend fortement de la présence de régions centrales (telles que la PMC dans le DMN) pour servir de relais d'information (Toussaint et al., 2014). Les régions pivots sont le plus souvent détectées comme les régions ayant le plus grand nombre de connexions. Le nombre de connexions d'une région est mesuré comme son *degré* de connectivité, et on peut dire que les régions avec un degré élevé sont considérées comme des hubs (***Figure 9B***). Enfin, on peut également évaluer dans quelle mesure le réseau se sépare en clusters ou communautés/modules distincts (***figure 9C***), comme le montre le *coefficient de clustering* ou la *modularité*. La théorie actuelle des réseaux neuronaux postule qu'une cognition normale nécessite une topologie de petit monde, combinant une ségrégation locale entre des régions anatomiquement et fonctionnellement similaires (par exemple pour le traitement de modalités spécifiques), et une bonne intégration entre des régions distantes (par exemple pour l'association de différentes modalités), comme le facilitent les hubs.

Les paramètres du petit monde ont été évalués dans les réseaux au repos liés à l'aMCI. Drzezga et ses collègues ont établi un lien direct entre la diminution de la force du hub de l'état de repos du PCC/RSC et l'augmentation de la charge amyloïde chez les personnes cognitivement normale (Drzezga et al., 2011). Les études évaluant l'aMCI ont souvent signalé une diminution de l'efficacité et de la ségrégation des réseaux à l'état de repos (Wang et al., 2013c ; Bai et al., 2013 ; Lin et al., 2017). En théorie, l'efficacité du réseau est une mesure plus représentative du transfert d'informations que la force de connectivité fonctionnelle du réseau global, car elle prend en compte l'importance des hubs pour relayer les informations entre des régions autrement déconnectées. En effet, Wang et ses collègues ont montré que la réduction de l'efficacité du réseau à l'état de repos, ainsi que la diminution de la force des hubs pariétaux et temporaux, mais pas la réduction de la force du réseau global, étaient corrélées au déclin de la mémoire de reconnaissance (mais pas à d'autres mesures cognitives) dans le cadre du MCI (Wang et al., 2013c). Pourtant, la théorie des graphes ne supprime pas l'incohérence de l'évaluation du DMN dans l'aMCI. Par exemple, une autre étude sur le SCD a rapporté une augmentation de la force du hub du lobe temporal dans l'aMCI (Liang et al., 2020), ce qui a un effet néfaste sur les performances du MMSE. L'incohérence de ces résultats reflète l'hétérogénéité du SCD et du MCI par rapport à leur diagnostic, aux pathologies sous-jacentes ou au stade protéopathique de la MA.

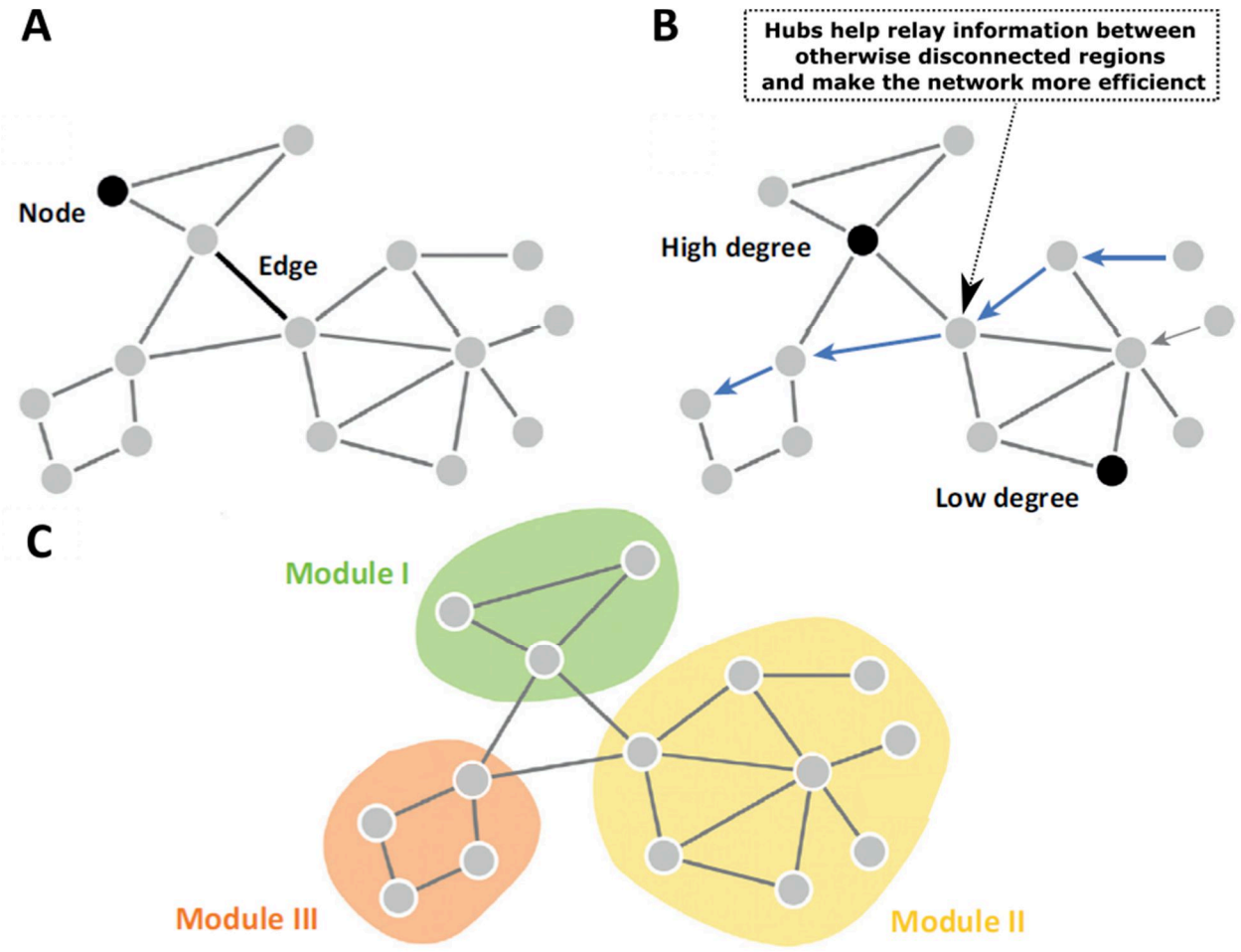

Figure 9. *Propriétés de base de la théorie des graphes. (A) Les nœuds représentent des régions et les arêtes des connexions fonctionnelles significatives. (B) Les régions pivots ou hubs ont généralement un degré élevé (nombre de connexions), et aident à relayer l'information entre les régions périphériques. Un réseau comportant un plus grand nombre de hubs (régions centrales) devrait être plus efficace pour intégrer des régions éloignées. (C) Les réseaux peuvent souvent être subdivisés en communautés (modules) de régions qui sont plus fortement connectées entre elles que le reste du réseau. Adapté de van den Heuvel et Sporns, 2013.*

6. Perte de mémoire subtile dans la MA préclinique

Jusqu'à présent, j'ai souligné l'hétérogénéité problématique du SCD et du MCI, qui représentent respectivement les stades précliniques et prodromiques de la MA. Les méthodes standard d'évaluation du déclin cognitif (MMSE) sont utiles pour évaluer l'installation de la démence/du MCI, mais elles sont trop grossières et les déficits mis à jour reflète souvent un mélange de pathologies sous-jacentes et de stades protéomiques de la MA. De plus, ces stades représentent principalement le stade prodromique de la MA qui présente déjà des déficits potentiellement irréversibles tels que des perturbations de la connectivité aberrante ou une atrophie de l'hippocampe. Pour y remédier, nous avons besoin d'évaluations comportementales plus spécifiques pour cibler les perturbations régionales liées aux stades précliniques les plus précoces. Les perturbations fonctionnelles les plus connues pour leur association à la MA préclinique sont l'hyperactivité du MTL et l'hypo-activité/hypo-connectivité du PMC-DMN. Les tâches cognitives qui nécessitent un fonctionnement précis de ces zones cérébrales sont plus susceptibles de révéler un déclin préclinique spécifique à la MA. Ces tâches comprennent des paradigmes de reconnaissance ou de mémoire spatiale très sensible qui nécessitent un fonctionnement précis au sein des régions MTL, ou des paradigmes de mémoire associative qui font appel aux cortex d'association du PMC et du mPFC. Dans la section suivante, je discuterai des tâches potentielles permettant d'évaluer les déficits cognitifs subtils dans la MA préclinique.

A. Discrimination mnémonique (séparation de motifs)

Dans la tâche mnésique de discrimination fine, également appelée tâche comportementale de séparation des motifs, il faut détecter de très légers changements dans l'identité ou l'emplacement des objets. On considère que ce type de mémoire dépend du processus computationnel de séparation des motifs nécessaire pour séparer les motifs qui se chevauchent, et dans le cas de la mémoire, des assemblées de cellules avec recouvrement partiel qui codent pour des représentations d'évènements similaires mis en mémoire. Il est démontré que cette tâche de mémoire sollicite fortement l'hippocampe, en particulier le gyrus denté (DG) et l'aire CA3, dans l'évaluation de la tâche par IRMf (Bakker et al., 2008). Chez les souris, il a été démontré que le DG présente des assemblées cellulaires distinctes pour chaque évènement et que le CA3 présente

des profils d'activité neuronales variables en réaction à de très légers changements d'environnement, ce qui illustre un mécanisme physiologique clair de séparation des motifs (Leutgeb et al., 2007). Un phénomène similaire a été identifié ultérieurement chez l'homme en utilisant l'IRMf à haute résolution (Berron et al., 2016). Les tâches de séparation de motifs impliquent également une communication entre toutes les régions du MTL, bien que des interactions distinctes soient impliquées si les modalités objet ou spatiale sont testées. La séparation de motifs d'objets implique une communication entre l'hippocampe et le MTL antérieur (LEC, PRC), tandis que la spatialité requiert préférentiellement une communication hippocampique avec le MTL postérieur (MEC, POC) (Reagh et Yassa ; 2014 ; Leal et Yassa, 2018).

La nature précise du processus de calcul de la séparation des motifs devrait le rendre sensible à l'hyperactivité de l'hippocampe présente dans les stades précliniques de la MA. Cette hyperactivité pourrait théoriquement brouiller les lignes entre les "motifs" physiologiquement représentés dans l'hippocampe. Il a été démontré que la séparation des motifs est affectée dans l'aMCI (Yassa et al., 2010) et même chez les personnes âgées cognitivement normales (Reagh et al., 2016). Dans cette population âgée, la communication intra-MTL est largement réduite, et accompagnée d'une hypo-activité dans le LEC et d'une hyperactivité dans le DG et CA3. Les porteurs asymptomatiques de l'APOE ε4 ont également montré des déficits significatifs dans la séparation des motifs avec une hyperactivité hippocampique (Sinha et al., 2018). Une autre étude a révélé que la séparation des motifs d'objets était accompagnée d'une augmentation de la pTau dans le LCR et d'une hyperactivité dans le MTL (Berron et al., 2019). Il est toutefois intéressant de noter que les déficits de séparation des motifs spatiaux s'accompagnaient d'une diminution de l'Aβ42 dans le LCR (Wesnes et al., 2014), mais pas d'une augmentation de la pTau dans le LCR. Les déficits de la séparation spatiale des motifs sont également corrélés à une augmentation de la charge amyloïde en TEP (Webb et al., 2020). Cette dichotomie entre la séparation des objets et des motifs spatiaux par rapport à tau et à l'Aβ respectivement peut refléter l'impact distinct de ces protéinopathies sur différentes régions du cerveau. Conformément à cette hypothèse, la perte de séparation spécifique à l'objet a été associée à la TEP de la protéine tau dans le lobe temporal, mais la perte de séparation des motifs basés sur la scène/le contexte a été associée à la TEP de l'amyloïde dans le PMC (Maass et al., 2019). Cela reflète le rôle important du PMC dans

l'association de caractéristiques pour la construction de scènes liées à la mémoire épisodique, une fonction qui est évaluée dans la prochaine tâche de mémoire.

B. Mémoire associative

Nous avons précédemment mis en évidence le sous-système temporal médian du DMN impliquant le mPFC, le PMC et le MTL, et son implication dans la remémoration de la mémoire épisodique (Andrews-Hanna et al., 2014 ; Bellana et al., 2016). En examinant ce réseau, il est utile de considérer les opérations cognitives qui constituent la pensée épisodique. Au cœur de la pensée épisodique se trouve l'ensemble des caractéristiques définissant un événement unique, qui comprend les personnes, les objets, les lieux et autres détails contextuels associés à l'événement. Ces caractéristiques de l'événement doivent être intégrées dans un cadre relationnel cohérent qui représente les associations entre elles, produisant ainsi une expérience personnelle unifiée. Comme nous l'avons vu précédemment, et en relation avec la séparation des motifs, les régions du lobe temporal médian sont nécessaires pour fournir des détails précis sur les caractéristiques des objets (HIP/LEC/PRC) ou des espaces (HIP/MEC/POC). En revanche, l'intégration de ces caractéristiques des représentations reflétant la multidimensionnalité des événements semblent dépendre des interactions complexes entre le MTL, le lobe pariétal et le mPFC, où le PMC, en particulier le RSC, joue le rôle de plaque tournante anatomique et fonctionnelle importante (***figure 10***) (Andrews-Hanna et al., 2010 ; Rugg et Vilberg, 2013 ; Kaboodvand et al., 2018 ; Cooper et Ritchey, 2019 ; Ritchey et Cooper ; 2020).

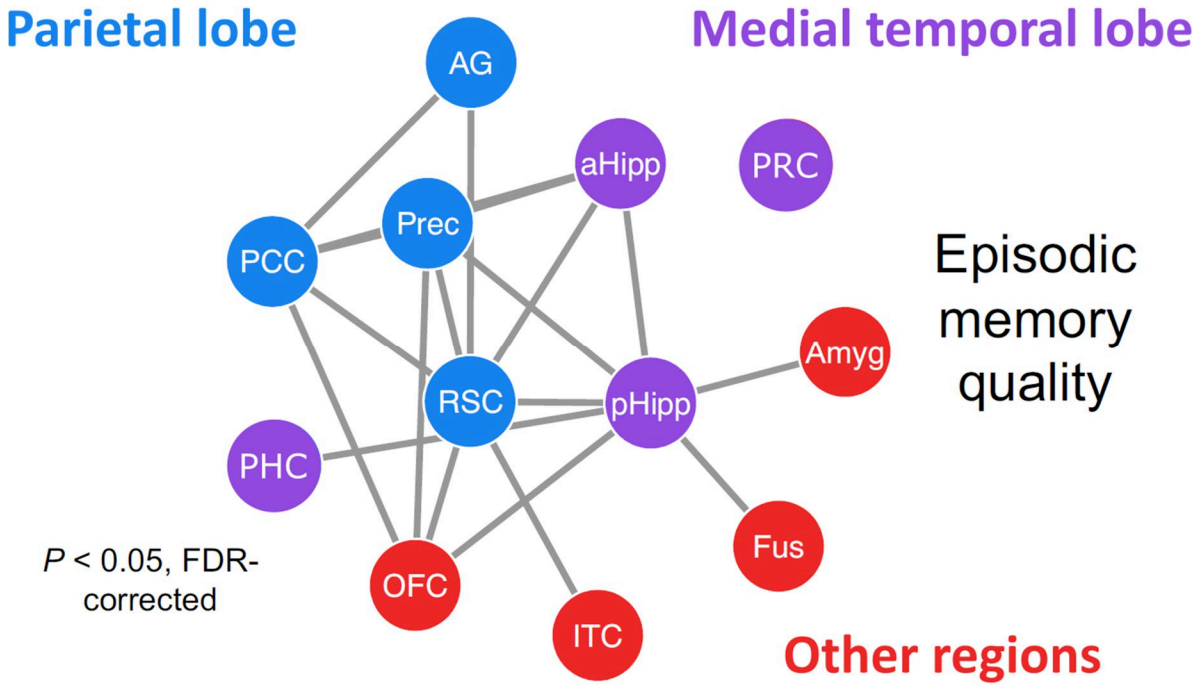

Figure 10. *Connexions fonctionnelles interrégionales dont la force de connectivité suit positivement la qualité (quantité totale et précision des détails) de la récupération épisodique. Ceci a été déterminé par une série d'analyses indépendantes d'interactions psychophysiologiques (IPP) entre graines et cibles dans une analyse de Cooper et Ritchey, 2019. AG : gyrus angulaire ; prec : précuneus ; PCC : cortex cingulaire postérieur ; RSC : cortex rétrosplénial ; pHipp : hippocampe postérieur ; aHipp : hippocampe antérieur ; PRC : cortex périrhinal ; PHC : cortex parahippocampique ; fus : gyrus fusiforme ; ITC : cortex temporal inférieur ; OFC : cortex frontal orbital ; amyg : amygdale. Adapté de Ritchey et Cooper, 2020.*

Ainsi, les paradigmes qui mettent à l'épreuve la capacité d'associer des caractéristiques indépendantes peuvent être sensibles à la connectivité réduite de la CMP, comme on le constate dans les évaluations de l'état de repos de la MA préclinique. Cette susceptibilité spécifique de la mémoire associative a été solidement identifiée par une étude basée sur une batterie neuropsychologique testant la mémoire associative et non associative, l'attention, le langage, les fonctions visuospatiales et exécutives. Ils ont montré que les porteurs asymptomatiques de mutations de la FAD avaient des résultats significativement moins bons que les témoins sains dans la condition de liaison des caractéristiques uniquement (Parra et al., 2010).

Une tâche courante et simple de mémoire associative est le "rappel de mots par le visage", où une personne doit se souvenir de l'association d'un visage à un mot aléatoire (comme "crayon" ou "plage"). Il est démontré que cette tâche dépend fortement de la communication PMC-MTL, car la stimulation transcrânienne du lobe pariétal augmente la connectivité fonctionnelle de ces

régions, ce qui est corrélé à une meilleure performance de la tâche (Wang et al., 2014, Warren et al., 2019). Une tâche similaire à la tâche de " rappel de mots par le visage " est la tâche " visage-nom ", où la personne doit associer un visage à un nom plutôt que n'importe quel mot aléatoire. Cette tâche est privilégiée car elle est moins sensible aux augmentations de la réserve cognitive. En effet, un nom s'accompagne de moins de connexions a priori qu'un mot pris au hasard (***crayon*** - bois, école, écriture vs. ***Tanya*** - qui ?), ce qui peut contribuer à renforcer la mémorisation chez ceux qui ont une plus grande connaissance sémantique. Cette théorie est soutenue par une recherche qui a montré qu'il est plus facile de se souvenir de "Baker" lorsqu'il est présenté comme une profession que lorsqu'il est présenté comme un nom propre (James et al., 2008). En effet, la diminution de la performance dans la tâche de nom de visage est corrélée à une augmentation de la charge amyloïde dans le PCC et le cortex frontal chez les personnes en bonne santé cognitive (Rentz et al., 2011) et corrélée spécifiquement à une augmentation de l'amyloïde dans le PCC chez les personnes atteintes de SCD (Sanabria et al., 2018). Dans les deux cas, la tâche visage-nom a donné de meilleurs résultats que la tâche visage-occupation (associant un visage à une profession, par exemple " professeur "), et mieux que les paradigmes d'apprentissage de listes de mots (tâches de mémoire verbale sémantique et reposant davantage sur la communication préfrontale et temporale latérale) pour prédire la charge amyloïde. Ces études mettent en évidence la perte de mémoire associative comme un marqueur cognitif efficace pour la MA préclinique et la pathologie associée sous-jacente.

7. Modèles animaux de la MA

A. Avant les souris transgéniques

Les premiers modèles murins de la maladie d'Alzheimer ont été mis au point au début des années 1980. Avant que les techniques d'édition de gènes ne soient courantes, les modèles de rongeurs étaient produits pharmacologiquement par la modulation des systèmes de neurotransmetteurs ou par la lésion stéréotaxique des structures cérébrales. Les premiers modèles de la MA chez les rongeurs reposaient principalement sur l'hypothèse cholinergique et ont été développés par la réduction pharmacologique de l'activité du système cholinergique (Bartus et al. 1982). Ces modèles ont joué un rôle essentiel dans la mise au point de médicaments à base d'inhibiteurs d'acétylcholine esterase, qui sont encore utilisés aujourd'hui pour traiter les symptômes de la MA. Ces premiers modèles de la maladie d'Alzheimer se sont révélés inestimables pour poser les fondements des changements symptomatiques observés dans cette maladie. Néanmoins, de nouvelles percées étaient nécessaires pour démêler l'origine de la maladie et comprendre l'impact des protéinopathies amyloïde et tau.

Entre-temps, en 1982, il a été démontré pour la première fois que, grâce à l'injection pronucléaire d'ADN modifié dans des zygotes fécondés, on pouvait développer des souris capables d'exprimer spécifiquement des protéines d'intérêt (Palmiter et al., 1982, Gurumurthy et Lloyd, 2019). Ce serait la première apparition de la souris transgénique, une innovation technologique qui révolutionnerait la recherche animale.

B. Modèles de souris transgéniques

i. APP transgénique unique

Plus d'une décennie plus tard, les premiers modèles de souris transgéniques pour la MA ont vu le jour. Cette première série de souris transgéniques surexprime l'APP humanisé avec une ou plusieurs mutations FAD trouvées dans la MA précoce. Les deux mutations FAD les plus couramment utilisées sont la mutation d'Indiana (V717F) et la double mutation suédoise (KM670/671NL). La mutation d'Indiana se trouve au niveau du site de clivage γ de l'APP et entraîne un rapport Aβ42/Aβ40 élevé (Suzuki et al., 1994 ; Tamaoka et al., 1994). La mutation

suédoise se trouve au niveau du site de clivage β et conduit à une production globalement accrue d'Aβ (Citron et al., 1992).

Le premier modèle transgénique de la MA est la souris PDAPP, qui exprime l'APP humanisé avec la mutation Indiana (V717F). Elle présente un dépôt amyloïde dès l'âge de 6 mois dans le néocortex et l'hippocampe, ainsi qu'une gliose associée (Games et al., 1995). Il existe deux modèles transgéniques précoces qui expriment l'APP humanisé avec la double mutation suédoise (KM670/671NL), mais sous des promoteurs différents et dans des contextes différents. Il s'agit des lignées APP23 (sous le promoteur Thy-1.2 sur le fond C57BL/6) et Tg2576 (sous le promoteur prion de hamster sur le fond mixte B6;SJL). Les souris APP23 présentent une chronologie neuropathologique similaire à celle des souris PDAPP, développant des dépôts amyloïdes néocorticaux et hippocampiques dès l'âge de 6 mois (Sturchler-Pierrat et al., 1997 ; Dodart et al., 2000). Les souris Tg2576, le modèle le plus couramment utilisé, présentent un phénotype moins sévère avec un dépôt amyloïde qui débute seulement vers 9 mois, précédé d'une gliose à 8 mois (Hsiao et al., 1996). Cette apparition tardive de la pathologie amyloïde et l'absence de certaines caractéristiques essentielles de la MA telles que la perte neuronale étendue et l'absence de DNF ont conduit à la création de nouveaux modèles de souris cumulant différentes mutations FAD.

ii. APP transgénique multiple

Des mutations multiples de la FAD ont été combinées pour obtenir un phénotype plus agressif. Le modèle TgCRND8 combine l'expression des mutations suédoise et indienne sur un APP humanisé. Cela conduit naturellement à une neuropathologie accélérée, avec des dépôts amyloïdes apparaissant dès 3 mois dans le subiculum, l'amygdale et le cortex frontal, et s'accompagnant d'une gliose réactive (Chishti et al. 2001). Ces souris présentent également une hyperphosphorylation de la protéine tau et la formation d'oligomères de tau dans l'hippocampe et le néocortex, mais pas de DNF (Belluci et al., 2007).

Les mutations FAD trouvées dans les gènes *PSEN1* ou *PSEN2* affectent l'activité γ-secrétase et augmentent le rapport Aβ42/Aβ40. Lorsqu'elles sont exprimées seules chez la souris, elles augmentent les niveaux d'Aβ42 mais n'entraînent pas de dépôt amyloïde et le phénotype est assez subtil (Duff et al., 1996 ; Borchelt et al. 1996). Le modèle de souris APPSWE/PS1dE9 combine la mutation suédoise sur l'APP avec PSEN1 muté et présente une pathologie amyloïde à l'âge de

6 mois (Jankowsky et al., 2004). Parmi les modèles d'apparition précoce, cette lignée de souris est désormais au moins aussi populaire que le modèle Tg2576. Dans le modèle de souris 5xFAD, de nombreuses mutations FAD différentes sont combinées, avec 3 mutations distinctes sur APP et 2 mutations sur PSEN1. Il présente une neuropathologie très agressive avec des dépôts amyloïdes apparaissant dans le subiculum et le cortex dès l'âge de 2 mois (Oakley et al., 2006).

iii. Tau transgénique

Contrairement à la condition humaine, les modèles de souris exprimant uniquement des mutations FAD ne développent pas de DNF, bien qu'ils présentent parfois des niveaux accrus de ptau. Cela est probablement dû à l'expression limitée des trois isoformes 4R de tau chez la souris plutôt qu'à un ensemble complet de six isoformes (trois 3R et trois 4R) que l'on trouve chez l'homme. Afin d'induire la formation de DNF, de nouvelles souris transgéniques exprimant des formes mutées de tau humanisées ont été développées. La mutation de tau la plus répandue utilisée pour induire la formation de DNF est la mutation tauP301L que l'on trouve dans la démence du lobe temporal frontal, mais pas dans la MA. Les souris Tau P301L exprimant cette mutation présentent une évolution des dépots denchevêtrements anatomiquement différente des stades de Braak observés dans la MA, les DNF apparaissant d'abord dans le cerveau postérieur et la moelle épinière à 8 mois au lieu de la région entorhinale, précédés par une gliose à 7 mois (Lewis et al., 2000). Plusieurs années plus tard, le modèle de souris Thy-Tau22 a été conçu pour exprimer la protéine tau humaine à 4 répétitions mutée aux sites G272V et P301S sous un promoteur Thy1.2, sans dysfonctionnement moteur (Schindowski et al, 2005). Il présente une hyperphosphorylation au niveau d'épitopes pertinents pour la MA (notamment Ser396, Ser202/Thr205 et Thr212/Ser214) et des DNF à un stade précoce, vers 3-6 mois, ainsi qu'une diminution de la transmission synaptique et une neurodégénérescence dans l'hippocampe vers 10 mois, lorsque les souris Thy-Tau22 présentent des déficits de mémoire spatiale dans la tâche du labyrinthe aquatique de Morris. Il est intéressant de noter que les souris Thy-Tau22 présentent une perte importante de neurones cholinergiques du septum médian, une caractéristique de la MA rarement observée dans les modèles murins de la MA (Belarbi et al., 2011).

La souris transgénique hTau, qui surexprime les 6 isoformes de tau non mutées sans la présence de tau endogène de la souris, est beaucoup moins courante mais néanmoins intéressante. Comme elle ne contient pas de mutations de tau, elle présente un profil neuropathologique plus proche de

la MA. Les souris hTau présentent des ptau positifs CP13 dans le soma des cellules pyramidales de l'hippocampe à 3 mois, suivis de DNF à 8 mois, ce qui correspond au développement du stade de Braak (Andorfer et al., 2003). Cela contraste néanmoins avec la situation humaine, où les DNF ne se forment normalement pas en l'absence de mutations tau ou de pathologie amyloïde. Cela peut s'expliquer en grande partie par la surexpression de tau et par le rapport déséquilibré des isoformes de tau, les niveaux de protéines des isoformes 3R commune aux deux espèces dépassant largement ceux des isoformes 4R humaines chez les souris hTau. Lorsque le rapport entre les isoformes 3R et 4R est rectifié au moyen d'un trans-épissage in-vivo du transgène, le nombre de cellules pyramidales présentant des DNF est considérablement réduit (Espindola et al., 2018). De plus, les souris hTau qui co-expriment la tau endogène de la souris, et donc surexpriment de grandes quantités de tau 4R et inversent le rapport 3R/4R, ne forment pas de DNFs (Duff et al., 2000).

iv. Combinaison d'APP et de Tau transgéniques

Afin de produire un modèle plus complet de la MA, avec des pathologies amyloïdes et tau simultanées, des lignées de souris ont été développées pour surexprimer l'APP humanisé avec des mutations FAD ainsi que le tau humanisé muté. Le modèle de souris 3xTg est l'un des modèles de souris de la MA les plus couramment utilisés, et combine la mutation suédoise de l'APP, les mutations PS1M146V et tauP301L. Les souris 3xTg présentent des dépôts amyloïdes à 6 mois dans le cortex frontal et une formation d'enchevêtrement plus similaire au développement du stade de Braak, avec des agrégats de tau hyperphosphorylés apparaissant dès 6 mois dans l'hippocampe (Oddo et al., 2004) suivis de DNF à 12 mois (Oddo et al., 2003) .

8. Évaluation de la mémoire chez les rongeurs

Dans la section suivante, j'aborderai diverses formes de mémoire évaluées chez les rongeurs. Chacune d'entre elles sera abordée en deux parties. La première partie donnera un aperçu des réseaux structurels nécessaires à la tâche. La seconde fera état des déficits observés chez les souris atteintes de la MA et de la façon dont ils peuvent être liés aux changements physiopathologiques mentionnés précédemment. La plupart des tâches de mémoire présentées sont dérivées du paradigme d'exploration spontanée d'objets. Ces tâches sont représentées à la ***figure 11***, à laquelle nous ferons référence tout au long de cette section.

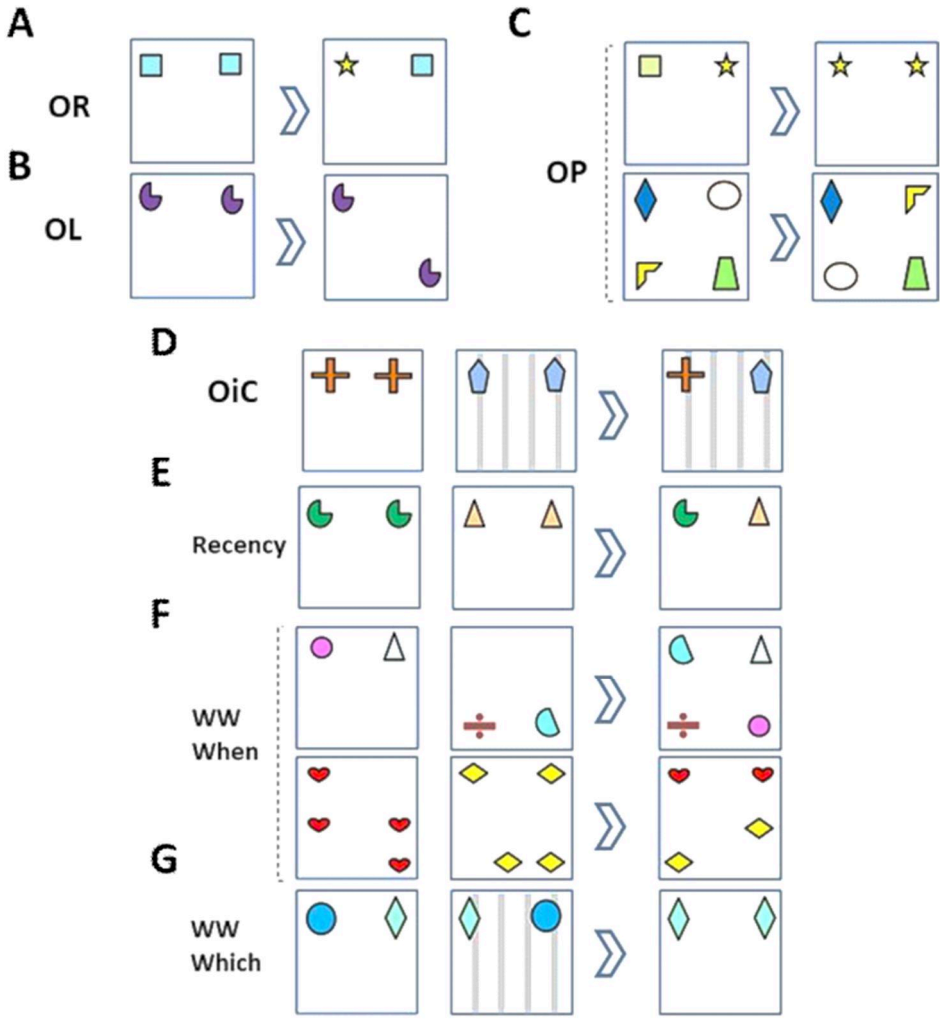

Figure 11. *Tâches d'exploration spontanée d'objets. OR : reconnaissance d'objet, OL : localisation d'objet, OP : objet-en-place, OiC : objet-en-contexte, WWWhen : what where when, WWWhich : what where which. Adapté de Chantal Mathis.*

A. Mémoire de reconnaissance

i. Contexte et anatomie

Les souris ont une curiosité innée. Le paradigme de reconnaissance spontanée d'objets, décrit pour la première fois par Ennaceur et Delacour en 1988, exploite ce trait en utilisant l'augmentation de l'exploration de la nouveauté comme mesure de la rétention de la mémoire. Il consiste d'abord en une phase d'acquisition, au cours de laquelle une souris est placée dans un champ ouvert pour explorer un ensemble de deux objets identiques. Cette phase est suivie d'une phase d'intervalle inter-essai (ITI), au cours de laquelle la souris est laissée pendant une durée déterminée dans sa cage d'origine, loin des objets et du champ ouvert. Enfin, le test se termine par la phase de rétention, au cours de laquelle on montre à la souris un nouvel ensemble d'objets, une copie de l'objet familier et un nouvel objet (***figure 11A***). L'expérimentateur peut alors évaluer la reconnaissance du nouvel objet à travers une augmentation de l'exploration du nouvel objet par rapport à l'objet inchangé. La mémoire de reconnaissance à court et à long terme peut être évaluée en faisant varier la durée de l'ITI de quelques minutes à plusieurs heures, voire plusieurs jours.

La région la plus régulièrement impliquée dans la RO, quelle que soit la durée de l'ITI, est le cortex périrhinal (PRC). Il a été démontré que la PRC, en particulier sa partie la plus caudale, joue un rôle clé dans la performance de la RO pour des ITI de 5 min à 24 h en utilisant diverses approches expérimentales (Ennaceur et al. 1996 ; Wan et al. 1999 ; Norman et Eacott, 2004 ; Winters et al. 2004 ; Barker et al. 2007 ; Albasser at al, 2010). Il faut noter que la contribution de la PRC peut également être influencée par la complexité de l'objet étant donné son implication dans le traitement des propriétés perceptives des objets (Norman et Eacott, 2005 ; Bartko et al. 2007).

De nombreuses études ont fait état d'une RO épargnée dans un large éventail de délais de rétention chez des rats et des souris ayant subi une lésion de l'hippocampe (Mumby et al. 2002 ; Save et al. 1992 ; Winters et al. 2004 ; Oliveira et al. 2010 ; Barker et Warburton, 2011 ; Sannino et al. 2012). Dans certains cas, il a été démontré que l'implication de l'hippocampe dépendait de la taille de la lésion, de l'accès à des repères spatiaux (par exemple, des murs transparents), de plusieurs essais pour l'habituation à l'arène ou l'échantillonnage, ou d'un grand nombre d'objets

(Broadbent et al. 2004 ; Ainge et al. 2006 ; Oliveira et al. 2010 ; Dees et Kesner, 2013 ; Sannino et al. 2012). Moduler l'activité de l'hippocampe par la perfusion locale de traitements pharmacologiques pourrait améliorer ou réduire la mémoire OR à long terme (Hammond et al. 2004 ; Oliveira et al. 2010 ; Melichercik et al. 2012 ; Cohen et al. 2013). Par conséquent, on pourrait proposer que la contribution de l'hippocampe peut dépendre du fait que l'efficacité de la performance dans une tâche donnée nécessite l'établissement et le rappel de représentations spatiales spécifiques ou la liaison d'éléments complexes, et/ou la formation d'une trace mnésique durable. Cette contribution à la mémoire OR à long terme est connue pour dépendre de manière cruciale de l'interaction entre le PFC et l'hippocampe (Preston et Eichenbaum, 2013).

Le mPFC et le RSC semblent être importants pour soutenir la consolidation à long terme de la mémoire de la RO (Warburton et Brown, 2015), car il a été démontré que la perturbation de l'un ou l'autre perturbe spécifiquement la performance de la RO après une ITI de 24 heures (Akirav et Maroun, 2006, de Landeta et al., 2020). L'implication du LEC et du MEC ne semble pas être essentielle pour la mémoire de la RO (Wilson et al., 2013a ; Rodo et al., 2017).

ii. Dans les modèles de souris de la MA

Les souris transgéniques simples APP-Tg (PDAPP, APP23 et Tg2576) et APPSWE/PS1dE9 présentent des déficits initiaux de la RO vers 6 mois avec des ITI allant de 1h à 48h (Dodart et al., 1999 ; Huang et al., 2006 ; Mouri et al., 2007 ; Frye et Walf., 2008). De multiples souris transgéniques APP-Tg (TgCRND8, 5xFAD) présentent une progression accélérée avec des déficits initiaux apparaissant vers 4 mois avec des ITI plus courts allant de 5 minutes à 24 heures (Tohda et al., 2012 ; Richter et al., 2008). Lorsque plusieurs ITI sont testés dans la même étude, les performances sur des délais de rétention plus longs ont tendance à être affectées avant celles sur des délais plus courts (Kubota et al., 2016 ; Sierksma et al., 2014). En d'autres termes, la mémoire à long terme semble très sensible à la pathologie de la MA.

L'induction de la tauopathie semble avoir un impact moins grave sur la mémoire de reconnaissance. Les souris hTau présentent des déficits avec un ITI de 24 heures à 12 mois mais pas à 4 mois (Polydoro et al., 2009), et elles sont cognitivement normales lorsque le déséquilibre 3R/4R est rectifié (Espindola et al., 2018). Les souris Tau P301L ne présentent aucun déficit OR même à 17 mois (Kent et al., 2017). En fait, les souris Tau P301L âgées de 9 semaines présentent une meilleure performance OR avec un ITI de 3,5h, ce qui a été attribué à une meilleure

potentialisation à long terme dans l'hippocampe excluant l'hyperphosphorylation tau (Boekhoorn et al., 2006). Les souris 3xTg-AD présentent une déficience dans la tâche de RO à partir de l'âge de 6 mois avec des ITI allant de 15 min à 24 h.

L'interprétation des déficits de la RO chez les souris App-Tg est assez compliquée par le fait que l'une des régions clés impliquées dans l'encodage de l'identité des objets est la PRC qui n'est presque jamais explorée pour la neuropathologie ou l'activité neuronale. Lorsque les performances de la RO à long terme sont affectées de manière sélective, il est possible qu'une perturbation fonctionnelle dans l'hippocampe ait pu être impliquée dans ce déficit étant donné son rôle dans la consolidation de la RO.

B. Discrimination mnémonique fine (séparation des motifs)

i. Contexte et anatomie

Les tâches de discrimination mnémonique fine utilisées chez l'homme ont été traduites dans le paradigme d'exploration spontanée d'objets chez la souris (Bolz et al., 2015 ; Cès et al., 2018). Dans la tâche de discrimination fine de reconnaissance d'objets, de petits changements dans l'identité des objets peuvent être contrôlés par l'utilisation d'objets lego, où le seul changement est le motif des legos utilisés pour construire l'objet modifié (seul le motif des blocs change, pas la forme ou la composition). Dans la tâche de discrimination fine de localisation d'objet, de petits changements dans la localisation de l'objet sont induits en déplaçant l'objet sur une plus petite distance (20 cm vs 50 cm). Ces deux tâches permettent de détecter des déficits chez les souris âgées mais pas chez les souris jeunes, et en l'absence de déficits des tâches traditionnelles OR et OL (Cès et al., 2018). Ce déficit a pu être bloqué par un traitement à la D-sérine, qui a augmenté la neurogenèse dans le DG, illustrant un lien possible d'une réduction de la neurogenèse du DG en fonction de l'âge avec la perturbation de la séparation des motifs. Ces résultats confirment l'hypothèse d'une implication de la neurogenèse du DG dans la fonction de séparation des motifs (Bolz et al., 2015 ; Clelland et al., 2009).

ii. Dans les modèles de souris de la MA

De manière très surprenante, malgré les nombreux rapports sur les déficits de discrimination fine chez les patients MCI et AD, peu de choses ont été faites dans les modèles de souris AD. Il existe une étude élégante de Zhu et ses collègues (2017) montrant des déficits de discrimination spatiale fine chez les souris Tg2576. Ce déficit était lié à la dégénérescence de l'entrée cholinergique dans le DG et à la réduction associée de la neurogenèse locale (Zhu et al., 2017). Au sein de notre équipe, nous avons montré que ce déficit apparaît dès l'âge de 4 mois chez cette lignée de souris, en l'absence de déficits dans d'autres tâches de reconnaissance (manuscrit en préparation).

C. Mémoire associative

i. Contexte et anatomie

Plusieurs variantes du paradigme d'exploration d'objets ont été conçues pour évaluer différentes formes de mémoire associative. La première variante, souvent appelée tâche d'objet en place (OP) (***Figure 16C***), teste la capacité de l'animal à détecter l'intrusion d'un objet *familier* dans la *position* précédemment occupée par un objet *familier* différent (Dix et Aggleton, 1999). En d'autres termes, cette tâche sonde l'association spécifique de l'identité de l'objet et du lieu. Des PRC, mPFC, RSC, noyau thalamique antérieur et hippocampe intacts ainsi que les interactions doubles PRC-hippocampe, PRC- mPFC sont nécessaires pour réaliser la version 4 objets de la tâche OP (Nelson et Vann., 2014 ; Parron et Save., 2004 ; Barker et al. , 2007 ; Barker et Warburton, 2015 ; DeVito et Eichenbaum, 2010). Seules quelques études ont évalué la version simple à deux objets de la tâche, et ont montré l'implication du LEC et de la voie LEC-mPFC jusqu'à présent (Wilson et al., 2013a ; Chao et al. , 2016). Le réseau sous-jacent à la détection de la nouveauté dans la tâche OP peut varier avec le nombre d'objets et/ou l'accès à un cadre spatial allocentrique (versus égocentrique). En effet, les tâches de PO à 2 objets " allocentriques " semblent reposer principalement sur le LEC et l'hippocampe, mais pas sur le PRC et le POC (Eacott et Norman, 2004 ; Langston et Wood, 2010 ; Wilson et al., 2013a).

La tâche d'objet en contexte (OiC) a été conçue pour tester la capacité de l'animal à détecter un objet *familier qui* n'a jamais été présenté dans un *contexte spécifique et familier* (Dix et

Aggleton, 1999). L'intégrité du POC et son interaction avec le PRC sont obligatoires pour maintenir la performance de reconnaissance d'objets guidée par le contexte dans la tâche OiC (*Figure 16D*) (Norman et Eacott, 2005 ; Heimer-McGinn et al., 2017). Il a été proposé qu'une disposition spatiale des objets soit d'abord intégrée dans le POC par le biais de ses connexions réciproques avec le PRC (Furtak et al. , 2012). En aval, un LEC intact et son interaction avec le mPFC sont également nécessaires à la performance OiC (Wilson et al. , 2013b ; Chao et al., 2016). De plus, le LEC étend son implication à la détection des incohérence entre le lieu et le contexte et entre les combinaisons OP et contexte (tâches non montrées), ce qui suggère que cette structure est nécessaire pour une intégration plus poussée des emplacements des objets et/ou pour ajouter des associations OP à la disposition contextuelle (Wilson et al. , 2013b). Il est à noter que l'un ou l'autre rôle pourrait être tenu par une ou plusieurs autres régions, comme l'hippocampe (Hunsaker et al. , 2013 ; mais voir Langston et Wood, 2010).

Alors que l'existence d'une mémoire épisodique chez les animaux reste une question ouverte, les tâches de reconnaissance basées sur le paradigme d'exploration d'objets sont fréquemment considérées comme évaluant une mémoire "épisodique" chez les rongeurs. Ceci est très probablement lié à la faible connaissance de la différence critique entre la reconnaissance guidée par la familiarité ("sentiment non contextuel que") et la reconnaissance guidée par la remémoration (se souvenir contextuellement de l'événement entier) (voir Ennaceur, 2010). Dans la plupart des tâches évoquées ci-dessus, l'animal peut simplement détecter qu'un objet lui est plus familier qu'un autre (tâches OR) ou qu'une position a été précédemment occupée ou non (tâches OL). Les tâches OP et OiC sollicitent la mémoire associative en liant deux stimuli environnementaux, mais une performance réussie ne garantit pas que le rongeur ait procédé par remémoration complète de l'événement passé où il a rencontré les objets pour la première fois. En d'autres termes, il peut exprimer une certaine familiarité mais pas nécessairement se souvenir de ce qui s'est passé où et quand. Ce débat souvenir/familiarité est toujours une question importante dans le domaine de la recherche sur la mémoire de reconnaissance. Ainsi, deux tâches ont été conçues pour évaluer une certaine forme de souvenir de l'expérience passée qui est basée sur une mémoire associative de i) *ce qui* s'est passé, *où* et *quand* (***Figure 11F***) (tâche WWWhere ; Dere et al., 2005) ou ii) *ce qui* s'est passé, *où* et dans *quel* contexte (***Figure 11G***) (WWWhich ; Eacott et Norman, 2004). Comme on pouvait s'y attendre au vu du rôle de l'hippocampe dans les souvenirs riches en contexte, la capacité à réaliser avec succès les tâches WWWhen et

WWWhich sur les trois composantes nécessite un hippocampe intact, mais pas nécessairement l'intégrité d'autres régions individuelles du lobe temporal médian telles que le PRC ou le POC (Eacott et Norman, 2004 ; Langston et Wood, 2010 ; De Vito et Eichenbaum, 2010). Comme pour les tâches OP et OiC, une interaction intacte entre le LEC et le mPFC est nécessaire pour réussir la tâche WWWhen (Chao et al., 2016). Lorsque l'on considère la mémoire de l'ordre temporel séparément dans le cadre de ces tâches ou dans une tâche dédiée, il convient de noter que l'hippocampe, le PRC, le RSC et le mPFC ont tous été signalés comme jouant un rôle dans la détection de la récence des objets (***figure 16E***) (Mitchell et Laiacona, 1998 ; Barker et al., 2007 ; DeVito et Eichenbaum, 2010 ; Powell et al., 2017).

ii. Dans les modèles de souris de la MA

Les souris Tg2576 présentent un déficit profond de la composante OL d'une tâche WWWhere dès l'âge de 4 mois (Lanté et al., 2013). Ce déficit dans un seul domaine peut remettre en question la nature épisodique de leurs déficits. Les souris APPSWE/PS1dE9 présentent des déficits dans la tâche WWWhere dès l'âge de 3 mois, en l'absence de plaques marquées à la thioflavine (Ramos-Rodriguez et al., 2013). Une autre étude a trouvé des déficits dans la version 4 objets de la tâche OP à l'âge de 5 mois, sans déficits concomitants en OR ou en récence d'objets, mais avec formation simultanée de plaques colorées en Aβ42 (Bonardi et al., 2016). Des souris TgCRND8 âgées de deux mois ont également présenté des déficits dans la version allocentrique à deux objets de la tâche OP, ainsi que des déficits dans la tâche OL mais pas dans la tâche OR, et en l'absence de plaques (Hamm et al., 2017). Leur déficit précoce dans l'OP a été bloqué en inhibant ae β- mais pas la γ-secrétase, ce qui indique qu'il n'était pas causé par une augmentation de l'Aβ, mais plutôt par une augmentation du β-CTF toxique ou une diminution du sAPPα neuroprotecteur.

Toutes ces tâches associatives à 2 ou 3 domaines dépendent de l'intégrité de l'hippocampe. Ainsi, comme cela a été suggéré pour la mémoire spatiale, il n'est pas surprenant que presque tous les modèles classiques aient été testés dans ces tâches et aient montré des déficits de performance. Ceci est également en accord avec le rôle crucial de l'hippocampe dans la mémoire épisodique humaine. La mémoire associative nécessite également une communication entre le LEC et le PFC (Wilson et al., 2013a ; Chao et al., 2016). Ceci est particulièrement intéressant car il existe

de plus en plus de preuves d'altérations pathologiques spécifiques et précoces du cortex frontal et du LEC dans nombre de ces modèles de souris (Zhuo et al., 2008 ; Xu et al., 2015).

9. Inconvénients des modèles de souris transgéniques

Au cours des 20 dernières années, les modèles de souris transgéniques nous ont permis de comprendre l'impact physiologique des pathologies amyloïdes et tau de manière plus précise que ce qui aurait pu être réalisé en clinique. Cependant, ces modèles présentent une série d'inconvénients qui contribuent à l'apparition de phénotypes artificiels et limitent la capacité de ces modèles à représenter la maladie.

Tout d'abord, les transgènes sont surexprimés, car ils sont contrôlés par des promoteurs artificiels et possèdent souvent de multiples sites d'insertion (***Figure 12A)***. La surexpression est particulièrement critique pour l'APP, avec ses nombreux fragments protéolytiques englobant un vaste éventail de fonctions biologiques (Muller et al., 2017), comme l'APP dans le développement du SNC (Nicolas et al., 2014), la sAPP dans la signalisation cellulaire (Rice et al., 2019), l'AICD dans la régulation de la transcription (Konietzko et al., 2012) pour n'en citer que quelques-unes. Il n'est pas surprenant que plusieurs études indiquent que les fragments APP et non-Aβ APP surproduits altèrent le développement des régions du cerveau (Dodart et al., 2000) et peuvent fonctionner de manière non physiologique au sein des processus cellulaires (Willem et al., 2015 ; Kerridge et al., 2015 ; Nahn et al., 2015). Il est donc difficile de déterminer si l'origine des déficits observés chez les souris APP-Tg est uniquement liée à l'accumulation d'Aβ ou à une augmentation du traitement amyloïdogénique.

Deuxièmement, les souris transgéniques co-expriment la version murine du transgène (***Figure 12B***), sauf si elles sont croisées avec un modèle knock-out. Notez que même dans ce cas, le promoteur endogène du gène homologue ne contrôle pas le gène inséré (par exemple, *App* ou *MAPT*). Les protéines endogènes co-exprimées peuvent interférer avec les processus pathologiques induits par les protéines MA. Ceci est illustré par l'impact de la co-expression de tau endogène chez les souris hTau, qui stoppe complètement la formation d'écheveaux (Andorfer et al., 2003). Certains fragments d'APP ont un effet bénéfique sur la plasticité synaptique et la cognition, notamment le sAPPα (Meziane et al., 1998, Ishida et al., 1997) qui serait dérégulé par

une augmentation du clivage β. Les effets de perte de fonction pouvant résulter d'une élévation du clivage amyloïdogène pourraient donc être compensés par une co-expression endogène.

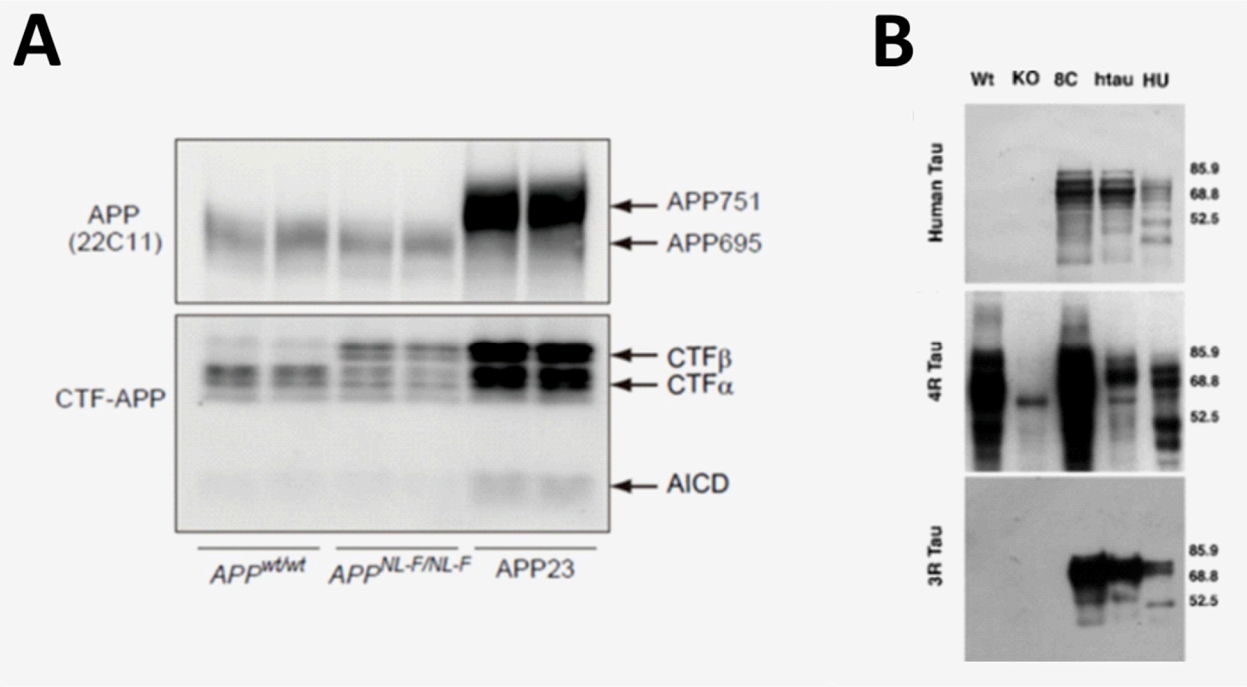

Figure 12. *Exemples de co-expression ou de surexpression de protéines chez les souris transgéniques. (A) Surexpression de fragments dérivés de l'APP chez les souris transgéniques (APP23) par rapport aux souris wt et knock-in. (B) Co-expression de la protéine tau 4R endogène chez la souris WT et le modèle transgénique 8C (hTau sans le gène MAPT endogène éliminé). Adapté de Andorfer et al. 2003 et Saito et al. 2014.*

Troisièmement, la variabilité découle de la nature aléatoire dans laquelle les transgènes sont insérés, et de l'utilisation de différents promoteurs artificiels. Ceci est souligné par une étude récente qui présente des différences dans le niveau d'expression et la configuration régionale du cerveau de l'APP exogène parmi différentes lignées de souris APP-Tg (Höfling et al., 2016). Selon l'emplacement d'insertion du transgène, les loci endogènes peuvent être gravement perturbés ou détruits (Verret et al., 2012 ; Saito et al., 2016). Les promoteurs artificiels entrent en compétition avec les promoteurs endogènes pour les facteurs de transcription, et peuvent conduire à l'expression du transgène dans des types de cellules qui ne l'expriment pas normalement.

10. Modèles de souris Knock In

Les inconvénients des souris transgéniques peuvent être largement compensés par l'utilisation de la technologie knock-in (KI). Les gènes in sont alors directement insérés sous le locus de la souris, remplaçant l'expression du gène endogène. Par conséquent, le gène inséré n'est pas surexprimé et il n'y a pas de co-expression du gène endogène de la souris. L'insertion du gène étant ciblée, il ne devrait pas y avoir de perturbation des autres loci endogènes. Tous les problèmes liés à l'insertion d'un promoteur artificiel, comme l'expression erronée d'un type de cellule, sont contournés.

En 2014, Saito et ses collègues ont présenté un nouvel ensemble de souris KI homozygotes exprimant l'Aβ humanisée avec des mutations FAD (Saito et al., 2014). Trois modèles KI ont été créés : l'*App*^{NL} avec la mutation suédoise (KM670/671**NL**), l'*App*$^{NL-F}$ avec la mutation suédoise et la mutation Beyreuther/Iberian (I716**F**), et l'*App*$^{NL-G-F}$ avec la mutation suédoise, la mutation Beyreuther/Iberian et la mutation Arctic (E693**G**) (***figure 13A***). La mutation suédoise a été décrite précédemment, elle affecte le clivage β de l'APP augmentant la production globale d'Aβ. La mutation Beyreuther/Iberian fonctionne comme la mutation Indiana, elle affecte le clivage γ augmentant le ratio Aβ42/Aβ40 (***Figure 13B***) (Guardia-Laguarta et al., 2010). La mutation Arctic se trouve au milieu de la séquence Aβ et il est démontré qu'elle augmente le taux d'agrégation Aβ et la quantité de grands oligomères Aβ (Nilsberth et al., 2001).

Les souris *App*^{NL} n'accumulent pas de dépôts amyloïdes, mais présentent une microgliose mineure dans l'hippocampe (Masuda et al., 2016). Les souris *App*$^{NL-F}$ présentent des dépôts amyloïdes hippocampiques et corticaux initiaux épars à 6 mois, ainsi qu'une gliose réactive. Chez les souris *App*$^{NL-G-F}$, le dépôt amyloïde est accéléré, les premiers dépôts apparaissant à 2 mois dans le cortex. Comme prévu, aucun des modèles KI ne forme de DNF, mais les souris *App*$^{NL-F}$ et *App*$^{NL-G-F}$ présentent des niveaux élevés de ptau dans les dendrites dystrophiques entourant les plaques (Saito et al., 2014).

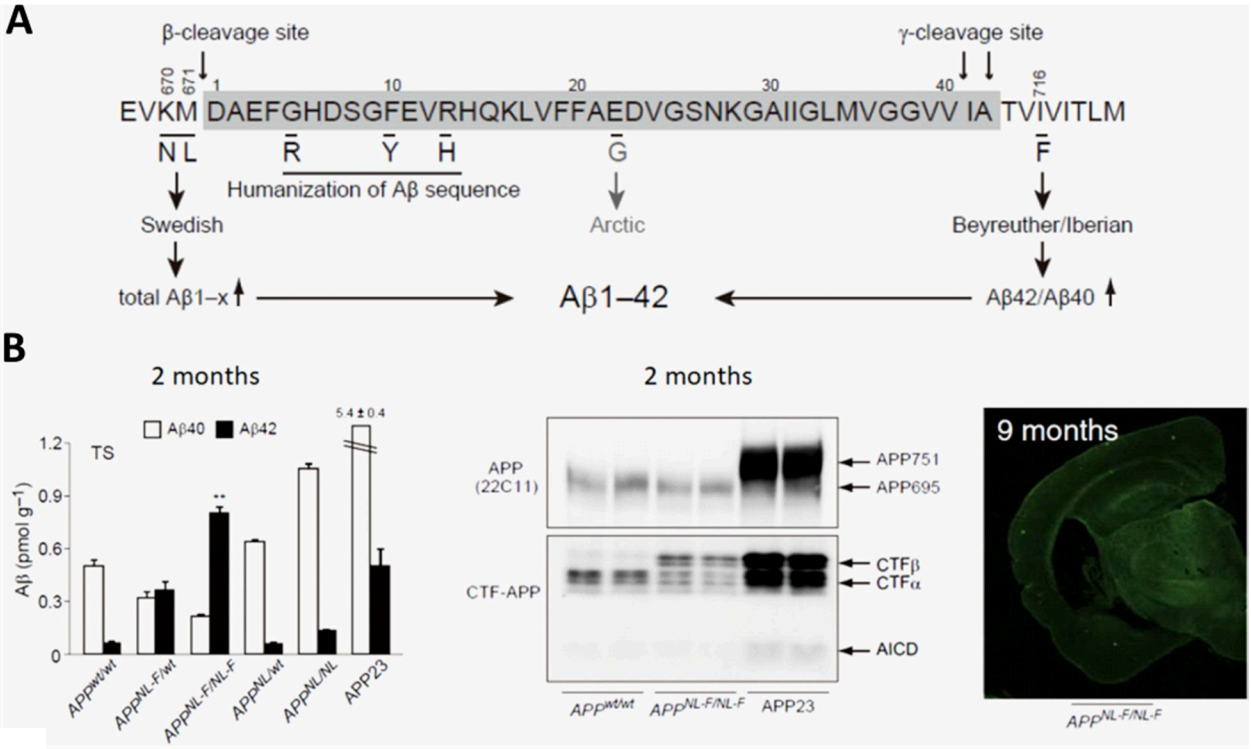

Figure 13. *Souris Knock in créées par Saito et ses collègues (2014). (A) Séquence Aβ humanisée avec des mutations FAD insérées. (B) Focus sur la souris App^{NL-F}. À gauche : par rapport aux autres modèles, la souris homozygote App^{NL-F} présente une augmentation de l'Aβ42/Aβ40 comme marqueur neuropathologique primaire induit par la mutation F. Au milieu : Elle présente également une augmentation du β-CTF, et une diminution de l'α-CTF, en raison de l'augmentation du clivage β induit par la mutation NL. Les deux figures soulignent l'absence de surexpression par rapport au modèle de souris transgénique APP23. À droite : la formation initiale des plaques commencerait à 6 mois, bien que même à 9 mois, les plaques soient encore très éparses. Adapté de Saito et al. 2014.*

À partir de maintenant, je me concentrerai principalement sur la souris homozygote *App*$^{NL-F}$ car elle a été utilisée comme lignée de souris parentale pour produire le modèle de mon travail de thèse. Les souris *App*$^{NL-F}$ ont montré des performances altérées à l'âge de 18 mois dans la tâche d'alternance spontanée du labyrinthe en Y, mais pas dans la tâche de mémoire spatiale du labyrinthe aquatique de Morris (Saito et al., 2014). Dans une autre étude (Shah et al., 2018), l'apprentissage intact de la navigation spatiale a été confirmé à des âges plus précoces (3 et 7 mois). De manière intéressante, les souris âgées de 3 mois ont démontré une flexibilité cognitive altérée dans l'apprentissage par inversion qui accompagnait des altérations de la connectivité fonctionnelle hippocampe-PFC et hippocampe-RSC à l'état de repos. Parallèlement, une étude pharmacologique a révélé que les souris *App*$^{NL-F}$ présentent des déficits à 12 mois, mais pas à 9 mois, dans une tâche de RO à long terme (Izumi et al., 2018). Cela rappelle également une

altération du dialogue entre l'hippocampe et le PFC. Ces résultats nous ont incités à intégrer la tâche de RO à délai de rétention de 24h dans notre batterie de tâches de reconnaissance.

Saito et son équipe ont également développé un nouveau modèle de souris KI pour *MAPT* humanisé, le gène qui exprime la tau (Saito et al., 2019 ; Hashimoto et al., 2019). Les souris *MAPT* KI expriment les 6 isoformes de tau (***figure 14A***), le niveau d'ARNm 4R étant environ 70 % de celui de l'ARNm 3R (***figure 14B***). Elles ne forment pas de DNF, mais ont montré une propagation accélérée des espèces de tau pathologiques (immunoréactives à l'AT8) après l'injection de tau dérivée de la MA dans le cerveau de la souris. La souris *MAPT* KI a été croisée avec les souris App^{NL-F} et App^{NL-G-F} pour créer les lignées de souris $App^{NL-F}xMAPT$ et $App^{NL-G-F}xMAPT$ double knock in (dKI) respectivement. Ces souris dKI ne montrent pas de changements manifestes par rapport aux souris KI originales. Aucune des dKI ne présente de DNF mais elles montrent des niveaux accrus de ptau par rapport aux *MAPT* KI simples (Saito et al., 2019) (***Figure 14C***). À notre connaissance, la lignée de souris $App^{NL-F}xMAPT$ dKI n'a jamais été évaluée dans des tâches comportementales.

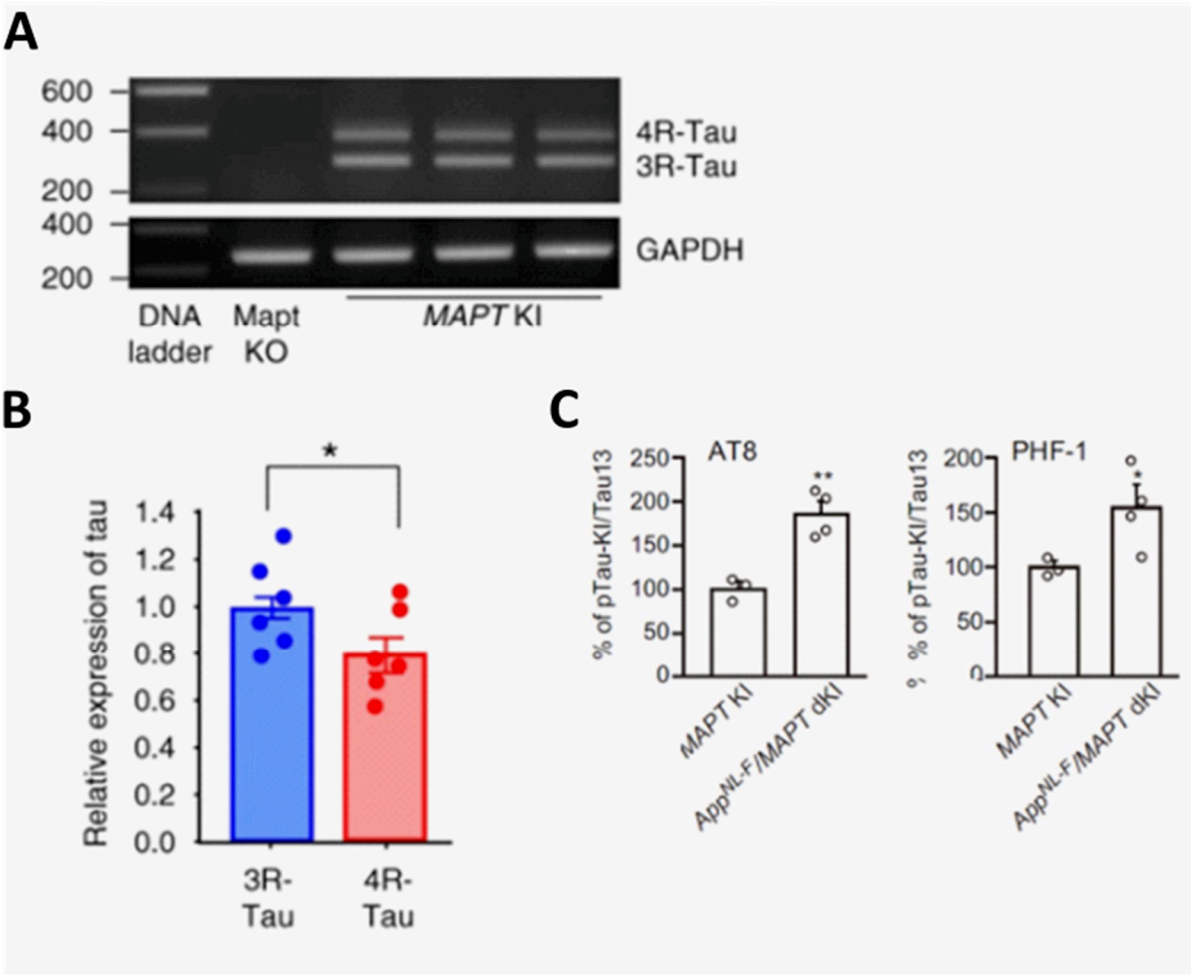

Figure 14 : *Pathologie Tau chez les souris MAPT et App^{NL-F}xMAPT dKI. A) Gel d'électrophorèse PCR représentatif réalisé pour B) comparer les niveaux de 4R-tau et 3R-tau chez les souris MAPT KI. C) Le croisement de la MAPT KI avec l'App^{NL-F} KI augmente la quantité de ptau à l'âge de 24 mois. Adapté de Hashimoto et al., 2019 et Saito et al., 2019.*

11.Mon projet

Le butde mon projet était de détecter les premiers troubles de la mémoire de reconnaissance chez les souris dKI, puis d'élucider l'origine de ce trouble précoce de la mémoire dans le modèle dKI. Mon premier objectif était de caractériser de manière extensive les performances de la mémoire de reconnaissance à la recherche du déficit le plus précoce en utilisant une batterie de tâches basées sur le paradigme d'exploration d'objets (Etude n°1). Le second objectif était de réaliser une imagerie ex vivo de l'activation neuronale liée à la tâche chez des souris WT et dKI afin d'identifier la région la plus précoce affectée chez les souris dKI (Etude n°2). Avec l'aide de Demian Battaglia, les niveaux d'activité régionale et les réseaux fonctionnels ont été évalués afin d'évaluer les perturbations bien décrites dans les études humaines sur la MA préclinique (Etude n°3). Le troisième objectif était de déchiffrer l'origine des perturbations fonctionnelles dans cette région cérébrale. Pour atteindre cet objectif, nous avons prévu d'utiliser deux approches. En collaboration avec Céline Héraud, je déterminerai d'abord l'importance relative des pathologies amyloïde et tau par western blot en me concentrant sur un ensemble de régions cérébrales potentiellement impliquées dans la tâche de mémoire altérée, dont la région d'intérêt. On s'attendait à ce que cette région présente une pathologie exacerbée. Enfin, les perturbations fonctionnelles des régions affectées seront évaluées plus précisément par des techniques électrophysiologiques avec l'aide de Romain Goutagny (Etude n°4). Dans ce texte abrégé en français, seulement l’étude 3 sera traduite. Cela couvrera les résultats et les méthodes les plus pertinents.

Etude n°3

Déficits précoces de la mémoire et désorganisation étendue du réseau cérébral dans le modèle de souris de la maladie d'Alzheimer *AppNL-FxMAPT* double knock-in

Christopher Borcuk[1], Céline Héraud[1], Karine Herbeaux[1],

Margot Diringer[1], Élodie Panzer[1], Jil Scuto[1], Saito[2], Hashimoto[2], Saido[2],

Romain Goutagny[1], Demian Battaglia[1,3,4], Chantal Mathis[1]

1 - Laboratoire de Neurosciences Cognitives et Adaptatives (LNCA), Université de Strasbourg, Faculté de Psychologie, 12 rue Goethe, F-67000 Strasbourg, France.

2 - Laboratoire de neuroscience protéolytique, RIKEN Center for Brain Science, 2-1 Hirosawa, Wako-city, Saitama 351-0198, Japon.

3 Institut d'études avancées de l'Université de Strasbourg (USIAS), F-67000 Strasbourg, France

4 Université d'Aix-Marseille, Inserm, Institut de Neurosciences des Systèmes (INS) UMR_S 1106, F-13005 Marseille, France

Article soumis aux Drs T Saito, S Hashimoto et T Saido pour révision selon l'accord de transfert de matériel avant soumission à BioRiv et e-Life.

Contexte et objectifs scientifiques

Dans l'étude n°1, nous avons montré que les souris dKI présentent des déficits d'OP5' dès l'âge de 4 mois, sans aucun autre déficit marqué dans d'autres tâches de mémoire de reconnaissance sensible. Dans l'étude n°2, nous avons évalué l'expression de c-Fos liée à OP5' dans deux expériences : en comparant des souris jeunes et âgées, et en comparant des souris WT et dKI âgées de 4 mois. Avec un ITI de 5 minutes, l'expression de c-Fos représente l'activité cérébrale pendant les deux phases, ce qui devrait augmenter le bruit du signal, et peut expliquer pourquoi aucun changement régional dans l'activité neuronale n'a été observé dans l'étude sur le vieillissement avec les tailles d'échantillon relativement petites. Malgré cela, avec une taille d'échantillon plus importante, des augmentations régionales significatives de l'activité neuronale (dans le CLA caudale) ont pu être détectées chez les souris dKI qui ont subi la tâche OP5'.

Quoi qu'il en soit, nous avons cherché à comprendre si le déficit d'OP résulte de perturbations de l'activité neuronale spécifiques à la phase du test. De plus, la compréhension de la connectivité fonctionnelle découlant du mélange d'activités d'acquisition et de rétention est problématique, et il vaut mieux éviter d'utiliser un ITI de 5 minutes pour évaluer la connectivité fonctionnelle dérivée de c-Fos. Avec tout cela en tête, nous avons décidé d'évaluer l'expression de c-Fos dans la tâche OP3h avec un ITI de 3 heures (les résultats comportementaux sont présentés dans l'étude n°1), suffisant pour séparer les deux phases de test en ce qui concerne la courbe d'expression de c-Fos. Ainsi, l'expression de c-Fos a été analysée dans une cohorte de souris qui n'a subi que la phase d'acquisition et dans une cohorte distincte qui a subi l'ensemble de la tâche OP3h jusqu'à la phase de rétention. L'expression régionale de c-Fos a été évaluée pour voir si nous pouvions détecter des changements locaux d'hyper ou d'hypo-activité associés à la MA précoce. Les réseaux fonctionnels ont été analysés afin de déterminer si la perte de mémoire associative pouvait être liée à des perturbations de l'efficacité du réseau ou de la force du hub, comme on l'observe dans le DMN de la MA précoce.

Cette analyse c-Fos est présentée avec les résultats comportementaux de l'étude n°1 sous la forme d'un article. Cet article a été soumis aux Drs T Saito et T Saido conformément à notre accord de transfert de matériel pour les lignées de souris App^{N-F} KI et *MAPT* KI. Il sera ensuite soumis à BioRiv et eLife.

Déficits de mémoire précoces et désorganisation étendue du réseau cérébral dans le modèle de souris *App*$^{NL-F}$*/MAPT* double knock-in de la maladie d'Alzheimer familiale.

Christopher Borcuk[1], Céline Héraud[1], Karine Herbeaux[1], Margot Diringer[1], Élodie Panzer[1], Jil Scuto[1], Saito[2], Hashimoto[2], Saido[2], Romain Goutagny[1], Demian Battaglia[1,3,4], Chantal Mathis[1]

[1] Université de Strasbourg, CNRS, Laboratoire de Neurosciences Cognitives et Adaptatives (LNCA) UMR 7364, F-67000 Strasbourg, France

[2] Laboratory for Proteolytic Neuroscience, RIKEN Center for Brain Science, 2-1 Hirosawa, Wako-city, Saitama 351-0198, Japon

[3] Institut d'études avancées de l'Université de Strasbourg (USIAS), F-67000 Strasbourg, France

[4] Université d'Aix-Marseille, Inserm, Institut de Neurosciences des Systèmes (INS) UMR_S 1106, F-13005 Marseille, France

Auteur correspondant

Chantal Mathis, PhD

LNCA UMR 7364, Université de Strasbourg, 12 rue Goethe F-67000 Strasbourg, France.

Courriel : chantal.mathis@unistra.fr

Téléphone : (33) 368 85 18 76

Fax : (33) 368 85 19 58

Mots clés : maladie d'Alzheimer préclinique, connectivité fonctionnelle, mémoire associative

Conflit d'intérêts : aucun

Remerciements : Université de Strasbourg, Centre National ,de la Recherche Scientifique, soutien complémentaire de thèse du FRM-ALZ201912009643, Anne Pereira de Vasconcelos pour les conseils sur le plan expérimental, Laura Durieux pour la discussion des analyses, Dominique Massotte pour le nanozoomer, Aminé Isik pour le génotypage et l'élevage des souris, Olivier Bildstein pour les soins à nos souris.

Résumé

Un défi crucial dans la recherche actuelle sur la MA est de clarifier la relation entre la neuropathologie précoce et le dysfonctionnement du réseau associé à l'émergence de subtiles altérations de la mémoire qui annoncent le début de la maladie. Dans le présent travail, le modèle de nouvelle génération *App*$^{NL-F}$*/MAPT à* double knock in (dKI) a été utilisé pour évaluer les premiers stades de la MA. L'étape initiale de la pathologie tau était limitée à la région périrhinale-entorhinale, épargnant l'hippocampe. Ce signe neuropathologique discret était associé à des déficits de la mémoire associative objet-place, l'une des premières mémoires de reconnaissance affectées chez les personnes à risque de développer la MA. Des analyses de l'activation de c-Fos en fonction de la tâche ont été effectuées dans 22 régions du cerveau à travers le cortex préfrontal médian, le claustrum, le cortex rétrosplénial et le lobe temporal médian. Une hyperactivité initiale a été détectée dans le cortex entorhinal et le claustrum des souris dKI. La phase de rétention a été associée à une réduction de l'efficacité du réseau, en particulier dans les régions corticales cingulaires, ce qui pourrait être dû à une perturbation du flux d'informations dans le cortex rétrosplénial. De plus, la relation entre l'efficacité globale du réseau et la performance de la mémoire chez la souris WT pouvait prédire la perte de mémoire chez la souris dKI, ce qui établit un lien supplémentaire entre l'efficacité réduite du réseau et le dysfonctionnement de la mémoire. Nos résultats suggèrent que la pathologie périrhinale-entorhinale précoce est associée à une hyperactivité locale qui se propage vers des régions connectées telles que le claustrum, le cortex préfrontal médian et, finalement, le pivot rétrosplénial clé qui est nécessaire pour relayer le flux d'informations des lobes frontal et temporal. La similitude entre nos résultats et ceux rapportés dans les premiers stades de la MA suggère que le modèle *App*$^{NL-F}$*/MAPT* dKI a un fort potentiel pour générer des informations clés sur le stade initial de la maladie.

Abréviations

MA - Maladie d'Alzheimer

CLA - claustrum

DH - hippocampe dorsal

dKI - Souris *AppNL-F/MAPT* double knock-in

CF - connectivité fonctionnelle

mPFC - cortex préfontal médian

MTC - cortex temporal médian

MTL - lobe temporal médian

OP - association objet-place

PS - Séparation des motifs

RSC - cortex rétrosplénial

Introduction

Le diagnostic et le traitement actuels de la maladie d'Alzheimer (MA) interviennent trop tard, lorsque les symptômes physiologiques tels que la neurodégénérescence manifeste ont déjà atteint un état irréversible (Selkoe, 2012). Les pathologies caractéristiques de la maladie d'Alzheimer sont les plaques amyloïdes insolubles, initialement formées dans les cortex préfrontal et médian postérieur, qui constitue le réseau du mode par défaut (DMN), et les dégénérescences neurofibrillaires, initialement formées dans le lobe temporal médian (MTL). La combinaison de la neuro-imagerie fonctionnelle avec la TEP amyloïde ou tau révèle que les schémas spatiaux de dépôt induisent des perturbations des réseaux fonctionnels (Myers et al., 2014 ; Jones et al., 2017), et accompagnent le déclin cognitif (Sepulcre et al., 2017 ; Pereira et al., 2019). Cependant, le peptide amyloïde (Aβ) soluble et les précurseurs tau hyperphosphorylés sont généralement plus toxiques et s'accumulent dans le cerveau des décennies avant l'apparition des symptômes typiques (Chen et al., 2017 ; Hill et al., 2020). Cela souligne l'importance de se concentrer sur les stades les plus précoces pour comprendre l'origine de cette maladie dévastatrice et pour développer des méthodes de détection et des thérapies plus proactives.

La déficience cognitive légère amnésique (aMCI) indique un risque plus élevé de progression vers la MA et a été largement étudiée au cours de la dernière décennie comme un stade prodromique potentiel de la MA (Petersen et al., 2009). La connectivité fonctionnelle (CF) au repos a été évaluée chez les patients atteints d'aMCI par la corrélation temporelle des fluctuations du signal en IRMf, EEG ou MEG. Afin de parvenir à une compréhension plus rigoureuse de la perturbation de la FC, la théorie des graphes a été utilisée pour évaluer la topologie des réseaux fonctionnels. Une cognition saine nécessite probablement une topologie efficace de petit monde, combinant une ségrégation locale entre des régions anatomiquement et fonctionnellement similaires, et une bonne intégration entre des régions éloignées à l'aide de concentrateurs fortement connectés (Filippi et al., 2013, Bassett et Bullmore., 2006). En ce qui concerne l'aMCI, de nombreuses études ont rapporté des perturbations du réseau fonctionnel au sein et entre le DMN et le MTL, avec une intégration réduite du réseau ainsi qu'une force réduite des hubs corticaux (Drzezga et al., 2011 ; Wang et al., 2013a ; Bai et al., 2013, Lin et al., 2019). Cependant, ces résultats ne sont pas entièrement concluants, car d'autres ont rapporté des résultats opposés ou non concluants (Gardini et al., 2015 ; Grajski et Bressler, 2019 ; Liang et al., 2020, Liu et al., 2012). Cette incohérence peut être révélatrice de l'hétérogénéité des stades aMCI, où il est démontré que le sens de la perturbation (hyperconnectivité vs hypoconnectivité) change en fonction de la gravité de l'état pathologique (Pusil et al., 2019; Jones et al., 2016). Cela souligne l'importance d'identifier des biomarqueurs plus précoces pour détecter plus précisément les stades précliniques de la MA, précédant même l'aMCI. Des progrès récents ont permis de développer des paradigmes sensibles de mémoire de reconnaissance, tels que des tâches de séparation de motifs et de mémoire associative, qui peuvent détecter de légers défauts cognitifs chez les personnes atteintes de troubles cognitifs subjectifs et les personnes âgées avec une cognition normale (Naveh-Benjamin, 2000, Sinha et al., 2018 ; Reagh et al., 2018). Ces tâches dépendent d'interactions spécifiques entre les structures DMN et MTL sensibles à la MA précoce (Reagh et Yassa., 2014 ; Miller et al., 2014 ; Hales et Brewer, 2011 ; Caviezel et al., 2020 ; Ritchey et al., 2020), et ont été mises en œuvre pour détecter les premiers stades "asymptomatiques" de la MA préclinique (Rentz et al., 2011 ; Maass et al., 2019). En évaluant les réseaux fonctionnels directement responsables des premiers déficits de mémoire subtils, nous pourrions parvenir à une compréhension plus claire des réseaux neuronaux affectés en premier lieu dans les premiers stades de la MA.

Les stades initiaux de la MA sont inévitablement liés à des perturbations physiologiques et neuroanatomiques discrètes, qui devraient être plus facilement étudiées dans les modèles murins de la MA (Scearce-Levie et al, 2020). En utilisant l'IRMf sur de jeunes souris transgéniques de la MA, une augmentation de l'Aβ soluble (Shah et al, 2016 ; Shah et al, 2018), et des augmentations spécifiques à une région de la neuroinflammation et du phospho-tau (Degiorgis et al, 2020) ont été liées à des perturbations des réseaux fonctionnels à l'état de repos. Les méthodes d'IRMf/EEG/MEG étant actuellement difficiles à mettre en œuvre chez des souris se déplaçant librement, l'imagerie ex-vivo basée sur la quantification de l'expression régulée par l'activité des gènes précoces immédiats (IEG ; c-fos, Egr1 et arc) peut être utilisée pour évaluer l'activation neuronale liée à la mémoire (Kinnavane et al, 2015). Grâce à cette technique, la physiopathologie des premiers stades a été liée à des changements individuels dans l'activité régionale liée à la mémoire (Hamm et al., 2017), mais pas aux réseaux fonctionnels. Cependant, en dehors de la maladie d'Alzheimer, les corrélations entre sujets des niveaux d'IEG régulés par l'activité ont été utilisées pour évaluer les réseaux fonctionnels directement liés à la mémoire (Tanimizu et al., 2017 ; Wheeler et al., 2013 ; Vetere et al., 2017). Cette approche peut s'avérer utile pour évaluer la FC liée à la mémoire dans les modèles murins de la MA.

Récemment, des modèles de souris knock-in ont été créés pour exprimer des gènes liés à la MA sous des promoteurs endogènes de la souris (Saito et al., 2014). Cela supprime la surexpression des gènes et les phénotypes artificiels potentiels qui en résultent, ce qui permet une évaluation plus attentive des stades initiaux de la MA (Sasaguri et al., 2017). Dans la présente étude, nous avons détecté des déficits de mémoire associative objet-place (OP) comme le signe le plus précoce de déclin cognitif dans le modèle de souris humanisé *AppNL-F/MAPT* double knock-in (dKI). Ce modèle exprime spécifiquement les six isoformes de tau et surexprime l'Aβ42, ce qui entraîne un dépôt amyloïde marqué et une hyperphosphorylation pathologique typique de tau à un âge avancé de 24 mois (Saito et al., 2019). Étant donné notre intérêt spécifique pour les premiers stades de la MA, ce modèle a été choisi plutôt que les dKI *AppNL-G-FxMAPT en raison du* développement plus lent de sa neuropathologie. Cette option a semblé heureuse car les premiers déficits de mémoire détectés dans la tâche OP ont coïncidé avec l'émergence des premiers stades de phosphorylation tau anormale dans la région entorhinal-perirhinal et non dans l'hippocampe, ce qui indique un état pathologique précoce. L'activité dépendante de la tâche a ensuite été mesurée dans les régions impliquées dans cette forme de mémoire associative, dont principalement le DMN/MTL, et la FC a été évaluée à l'aide de techniques de théorie des graphes. Nos résultats montrent que le déclin initial de la mémoire dans la MA pourrait être lié à des changements topologiques spécifiques dans les réseaux fonctionnels dépendant de la mémoire.

Résultats

Le phénotypage comportemental révèle des altérations précoces de la mémoire associative objet-place.

Les performances de la mémoire associative de la séparation de motifs (PS) et de l'OP sont couramment affectées dans les stades prodromiques de la MA et chez les personnes âgées cognitivement normales (Yeung et al., 2018, Hampstead et al., 2018, Reagh et al., 2018, Reagh et Yassa, 2014), et dans les modèles murins aux stades de dépôt préplaque (Zhu et al., 2017 ; Hamm et al., 2017). Afin de détecter les déficits de mémoire de reconnaissance les plus précocement sensibles, une étude préliminaire a été réalisée pour évaluer les performances OP et PS, ainsi que les performances de reconnaissance d'objets à long terme à l'âge de 2, 4 et 6 mois (Figure 1-supplément figuré 1). Pour les tâches OP et PS, un court intervalle inter-trial (ITI) de 5 minutes a été choisi pour s'assurer que les déficits ne résultent pas d'une perturbation de la consolidation de la mémoire à long terme. Étant donné le nombre élevé d'âges testés et la nature difficile des tâches, aucun résultat n'était significatif dans cette expérience préliminaire avec corrections pour comparaisons multiples. Tous les groupes ont réussi la tâche de reconnaissance d'objets à long terme et la tâche PS est restée non concluante car les performances de dKI étaient très variables (Figure 1-figure supplément 1A et 1B, respectivement). En revanche, un déficit potentiel robuste a pu être observé à 4 mois dans la tâche OP, et a persisté à 6 mois (figure 1-figure supplément 1C).

Avec une deuxième cohorte indépendante de souris, nous avons confirmé que les souris dKI étaient incapables de détecter une nouvelle association d'OP à l'âge de 4 mois (figure 1A). D'autre part, les souris âgées de 4 mois n'ont pas montré de déficits dans la reconnaissance à court terme de nouveaux objets (Figure 1B). Ces résultats ont confirmé que le déficit PO était dû à des perturbations spécifiques de la mémoire associative plutôt qu'à des déficiences distinctes de la reconnaissance d'objets ou de la reconnaissance spatiale.

Nous avons ensuite évalué les changements physiopathologiques précoces de la MA chez les souris âgées de 4 mois en utilisant le western blotting (Figure 1-figure supplément 2A). Des anticorps ciblant l'APP, les fragments carboxy terminaux clivés de l'APP, la protéine tau phosphorylée (Thr181) et les protéines tau totales ont été utilisés. Les souris de type sauvage ont exprimé principalement des fragments α-CTF d'APP, tandis que les souris dKI ont exprimé principalement des fragments β-CTF d'APP. De plus, une augmentation du rapport β-CTF/α-CTF a été observée à la fois dans l'hippocampe (figure 1-figure supplément 2B) et dans le cortex temporal médian (medial temporal cortex - MTC ; comprenant les cortex entorhinal, périrhinal, postrhinal) (figure 1-figure supplément 2C), indiquant une transformation amyloïdogène régulée de l'APP. En outre, une augmentation du degré de phosphorylation de la protéine tau sur Thr181 a été observée uniquement dans le MTC des souris dKI par rapport aux souris de type sauvage, alors que les deux modèles exprimaient des niveaux similaires de protéines tau totales. Cela correspond au consensus général selon lequel la CTM est la zone initiale de la mise en scène de la protéine tau (Braak et Braak, 1995). Ces résultats soulignent que les déficits OP se produisent en conjonction avec des changements physiopathologiques considérablement légers, ce qui s'apparente à un stade précoce préclinique de la MA.

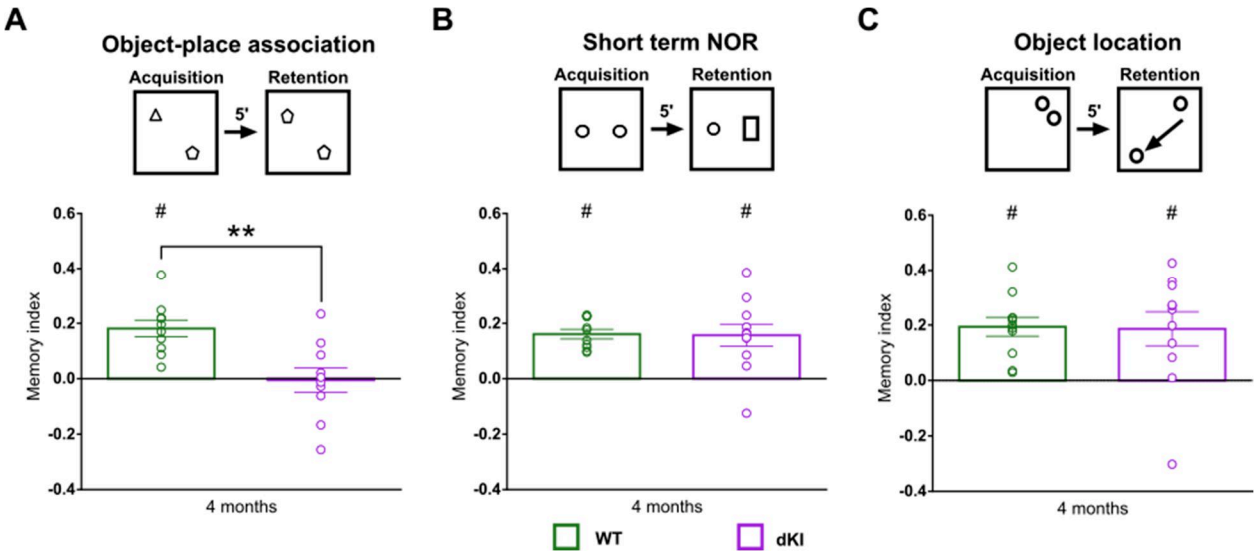

Figure 1. Caractérisation comportementale de jeunes souris dKI (WT n = 11, dKI n = 11). (A) À l'âge de 4 mois, les souris dKI ont reproduit le déficit potentiel observé dans la tâche d'association objet-place lors du phénotypage préliminaire (test t à deux échantillons, WT vs. dKI : t(20) = 2,85, P = 0,0098 ; test t à un échantillon, contre le hasard : dKI t(10)=0,3095, p = 0,763). Au même âge, les souris dKI étaient normales pour (B) la reconnaissance d'objets (test t à deux échantillons, WT vs. dKI : t(19) = .0934, P = 0.9265 ; test t à un échantillon, contre le hasard : tous les ts>3.94, ps<0.003) (une souris WT a été retirée parce qu'elle est tombée avant le test) et (C) la reconnaissance spatiale (test t à deux échantillons, WT vs. dKI : t(20) = 1,052, P = 0,9173 ; test t à un échantillon, contre le hasard : tous les ts>3,03, ps<0,013), indiquant que la perte de mémoire associative n'était pas due à une perte singulière dans les domaines de la reconnaissance d'objet à court terme ou de la mémoire de localisation d'objet. Les graphiques à barres représentent la densité moyenne (± SEM) * différence entre les génotypes **p<.01 (test t à deux échantillons) ; #, différence par rapport au hasard, #p<.05 (test t à un échantillon).

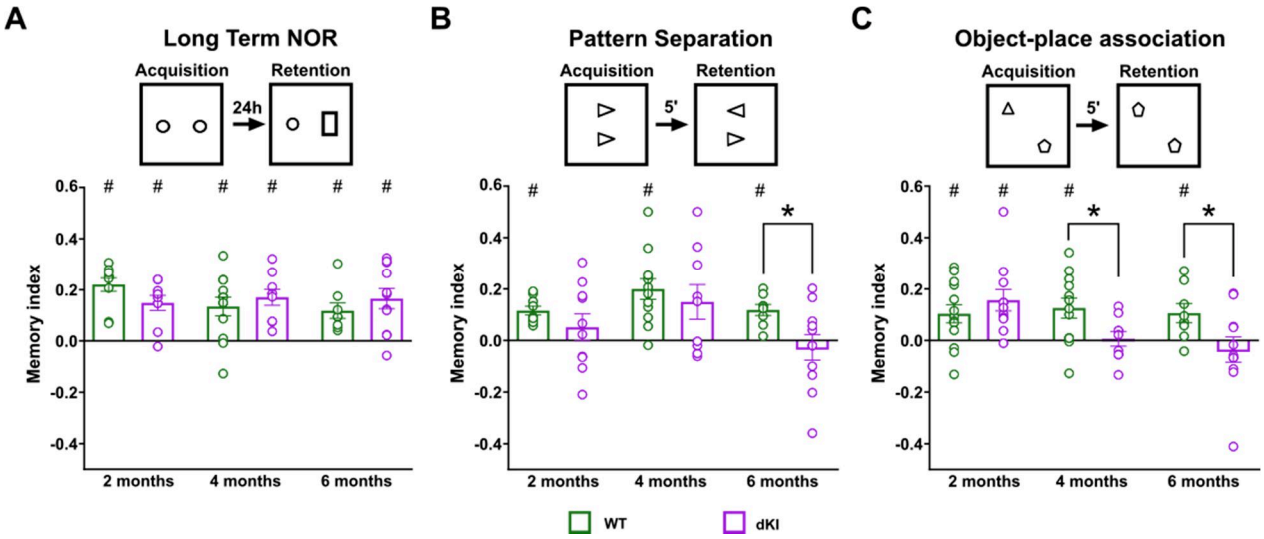

Figure 1 - supplément à la figure 1. Phénotypage préliminaire de jeunes souris dKI avec des paradigmes de mémoire de reconnaissance sensibles. Les souris ont été testées à 2 mois (WT n = 10, dKI n = 10), à 4 mois (WT n = 12, dKI n = 9) et à 6 mois (WT n = 8, dKI n = 11). Une cohorte supplémentaire de (WT n = 3, dKI n = 1) a été testée à 2 mois dans l'association objet-place car le groupe initial n'a pas atteint une signification supérieure à 0. (A) Dans la tâche de reconnaissance d'objet à long terme, les souris dKI n'étaient pas du tout affectées. (B) Dans la tâche de séparation des formes, les souris dKI étaient très variables, de sorte qu'elles n'étaient pas significatives par rapport au hasard, quel que soit l'âge (test t à un échantillon, par rapport au hasard : tous les ts dKI<.996, ps>0.055). Cependant, la signification entre les groupes n'a été obtenue qu'à l'âge de 6 mois (WT vs. dKI : t(17) = 2,364, P = 0,030). Cette variabilité peut représenter une variété de facteurs, y compris peut-être une neurogenèse DG affectée (Scopa et al., 2020). (C) Le déficit significatif le plus précoce chez les souris dKI est apparu à 4 mois dans la tâche d'association objet-place, un déficit qui a été conservé à 6 mois (test t à deux échantillons, WT_4mo vs. dKI_4mo : t(20) = 2,325, P = 0.0313 ; test t à un échantillon, contre le hasard : dKI t(8) = 0,2086, P = 0,8399 ; test t à deux échantillons, WT_6mo vs. dKI_6mo : t(17) = 2,132, P = 0,0479 ; test t à un échantillon, contre le hasard : dKI t(10) = 0,7196, P = 0,4883). Bien que la variabilité observée lors de la séparation des motifs puisse être intéressante, nous avons choisi de poursuivre notre étude avec le déficit objet-place, plus robuste. Les graphiques à barres représentent la densité moyenne (± SEM). Différence entre les génotypes *p<.05 (test t à deux échantillons) ; différence par rapport au hasard, #p<.05 (test t à un échantillon). Aucune correction pour comparaisons multiples n'a été effectuée pour ces comparaisons préliminaires.

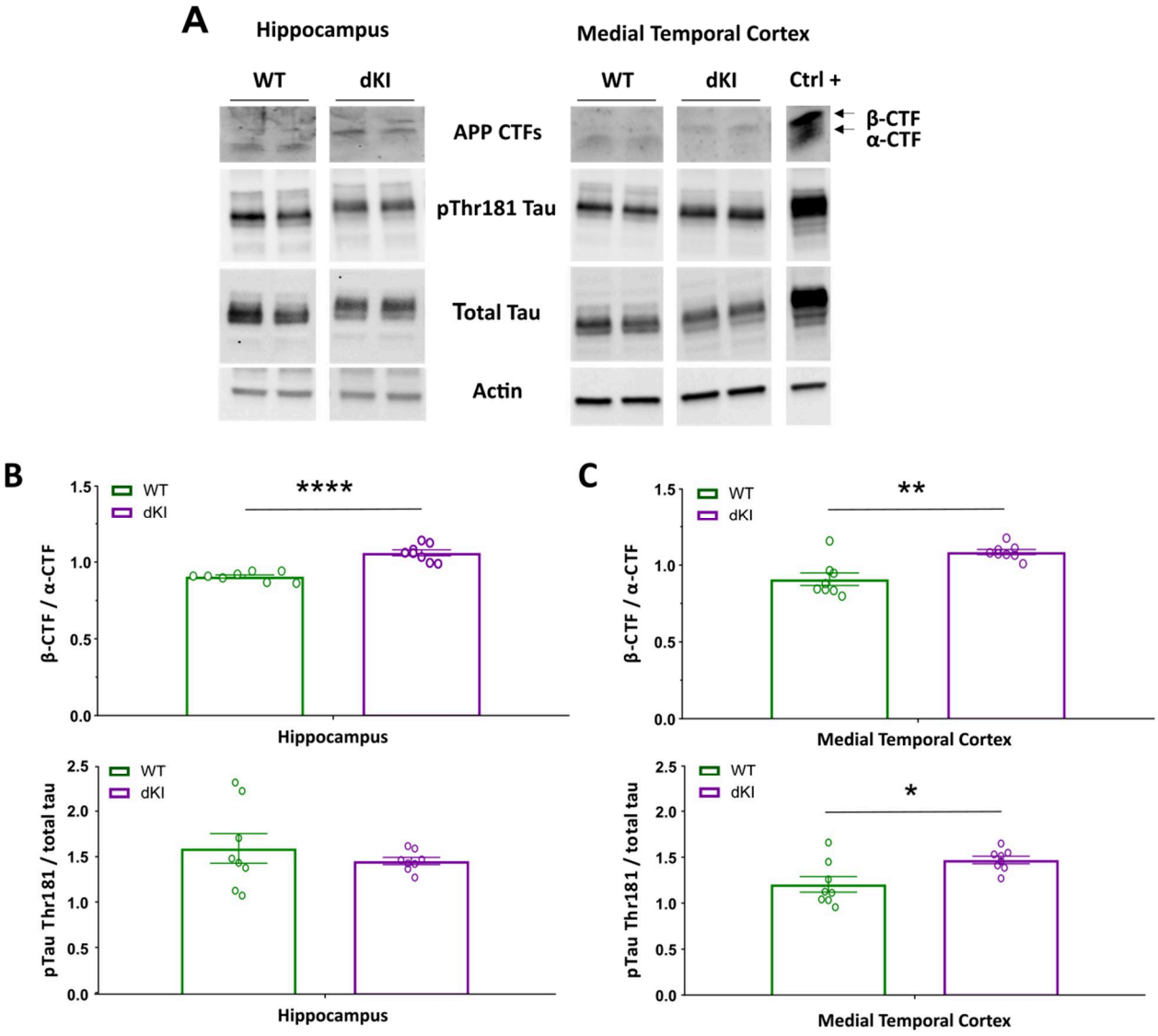

Figure 1 - supplément 2 à la figure. Stade précoce de la maladie de type Alzheimer chez des souris mâles dKI âgées de 4 mois. (A) Blots représentatifs des fragments APP clivés, des protéines tau phosphorylées sur le site thréonine 181 et des protéines tau totales dans l'hippocampe et le cortex temporal médian de souris WT et dKI. Analyse du rapport des fragments β-CTF sur α-CTF et du degré de phosphorylation de tau sur Thr181 dans l'hippocampe (B) et dans le cortex temporal médian (C). Les résultats ont montré que les souris dKI exprimaient principalement le β-CTF alors que les souris WT exprimaient principalement le α-CTF et que le rapport β-CTF/α-CTF augmentait dans les deux régions du cerveau. Seul le MTC a présenté une augmentation des protéines tau phosphorylées. Les graphiques à barres représentent la densité moyenne (± SEM). * p<0,05, ** p<0,01, *** p<0,001 et **** p<0,0001 (test t à deux échantillons).

Évaluation des changements de l'activité cérébrale dépendant de l'OP

Alors que les processus d'encodage sont connus pour être perturbés chez les patients atteints de la MA (Granholm et Butters, 1988), des études récentes sur des modèles animaux trouvent également un dysfonctionnement de la récupération des engrammes comme mécanisme de perte de mémoire dans les premiers stades de la pathologie de MA (Roy et al., 2016 ; Etter et al., 2019). Nous avons donc cherché à évaluer les modifications de l'activité cérébrale dépendantes de l'encodage versus le rappel en lien avec le déficit OP, par une évaluation indépendante des deux phases de test. Ainsi, l'activation de c-Fos a été quantifiée dans le cerveau de souris ayant subi soit la phase d'acquisition (*encodage*) (figure 2A), soit la phase de rétention (*rappel*) (figure 2B) de la tâche OP. Afin de tenir compte de la courbe d'expression de la protéine c-Fos, l'ITI a été prolongé jusqu'à 3 heures, le délai le plus court permettant d'isoler définitivement les phases de test. Comme pour l'ITI de 5 minutes, les souris dKI qui ont subi la phase de rétention après un ITI de 3 heures étaient également incapables de détecter la nouvelle association OP (Figure 2C). Nous avons ensuite choisi d'évaluer 22 régions d'intérêt (ROI) englobant des sous-régions du cortex préfrontal médian (mPFC), du claustrum (CLA), du cortex rétrosplénial (RSC), de l'hippocampe dorsal (DH) et du cortex temporal médian (MTC) (Figure 2D-J). L'hyperactivité neuronale est une caractéristique commune au début de la MA et chez les jeunes souris pré-plaques (Zott et al., 2019). Nous avons donc d'abord évalué les changements de l'activité régionale en fonction de la phase de test et du génotype.

L'acquisition induit une activité régionale plus importante que la rétention

Toutes les régions sauf le DH présentaient des niveaux d'activité plus élevés dans la phase d'acquisition, bien que dans le LEC cette augmentation de l'activité ait été nettement moins radicale. On peut s'attendre à cela dans la phase initiale, car les souris sont soumises à des changements plus forts avec deux nouveaux objets dans des emplacements précédemment inoccupés par rapport à la phase de rétention, où le seul changement est une nouvelle association OP. Pendant l'acquisition, les souris encodent activement plusieurs nouvelles caractéristiques, de nouveaux objets et leur emplacement unique dans le champ ouvert. De plus, cela permet de confirmer l'absence de c-Fos résiduel dans les groupes de rétention. Si le c-Fos résiduel persistait entre l'encodage et la perfusion après la phase de rétention, on s'attendrait à une densité de c-Fos similaire ou accrue pendant la phase de rétention, et non à une diminution.

Hyperactivité dans le claustrum et le cortex entorhinal des souris dKI

Le CLA et le LEC ont montré une activation accrue chez les souris dKI, quelle que soit la phase de test . La MEC a révélé une activation accrue chez les souris dKI, spécifiquement pendant la phase d'acquisition .

Région	Acronyme
Cortex prélimbique	PRL
Cortex cingulaire	CG1
Cortex infralimbique	IL
Claustrum rostral	rCLA
Claustrum caudal	cCLA
Corpus ammoniss 1	CA1
Corpus ammoniss 3	CA3
Gyrus denté lame suprapyramidale	DG_sp
Gyrus denté lame infrapyramidale	DG_ip
Dysgranularité du cortex rétrosplénial rostral (RSD)	rRSCd
Cortex rostral rétrosplénial granulaire (RSG)	rRSCg
Dysgranularité du cortex rétrosplénial caudal (RSD)	cRSCd
Cortex rétrosplénial caudal granulaire (RSG)	cRSCg
Cortex périrhinal rostral dorsal (Ect)	rPRCd
Cortex rostral perirhinal ventral (PRh)	rPRCv
Cortex périrhinal caudal dorsal (Ect)	cPRCd
Cortex périrhinal caudal ventral (PRh)	cPRCv
Cortex entorhinal latéral rostral (DLEnt,DIEnt,VIent)	rLEC
Cortex entorhinal latéral caudal (DLEnt,DIEnt,VIent)	cLEC
Cortex entorhinal médian (MEnt)	MEC
Cortex entorhinal médian caudal (CEnt)	CMEC
Cortex postrinal (Ect,PRh)	POC

Tableau 1. Liste des régions évaluées. Les régions ont été choisies a priori en fonction de leur pertinence dans la pathologie précoce de la MA et dans le traitement de la mémoire associative. Entre parenthèses figurent les identifications des régions selon la troisième édition du Franklin and Paxinos Mouse Brain Atlas.

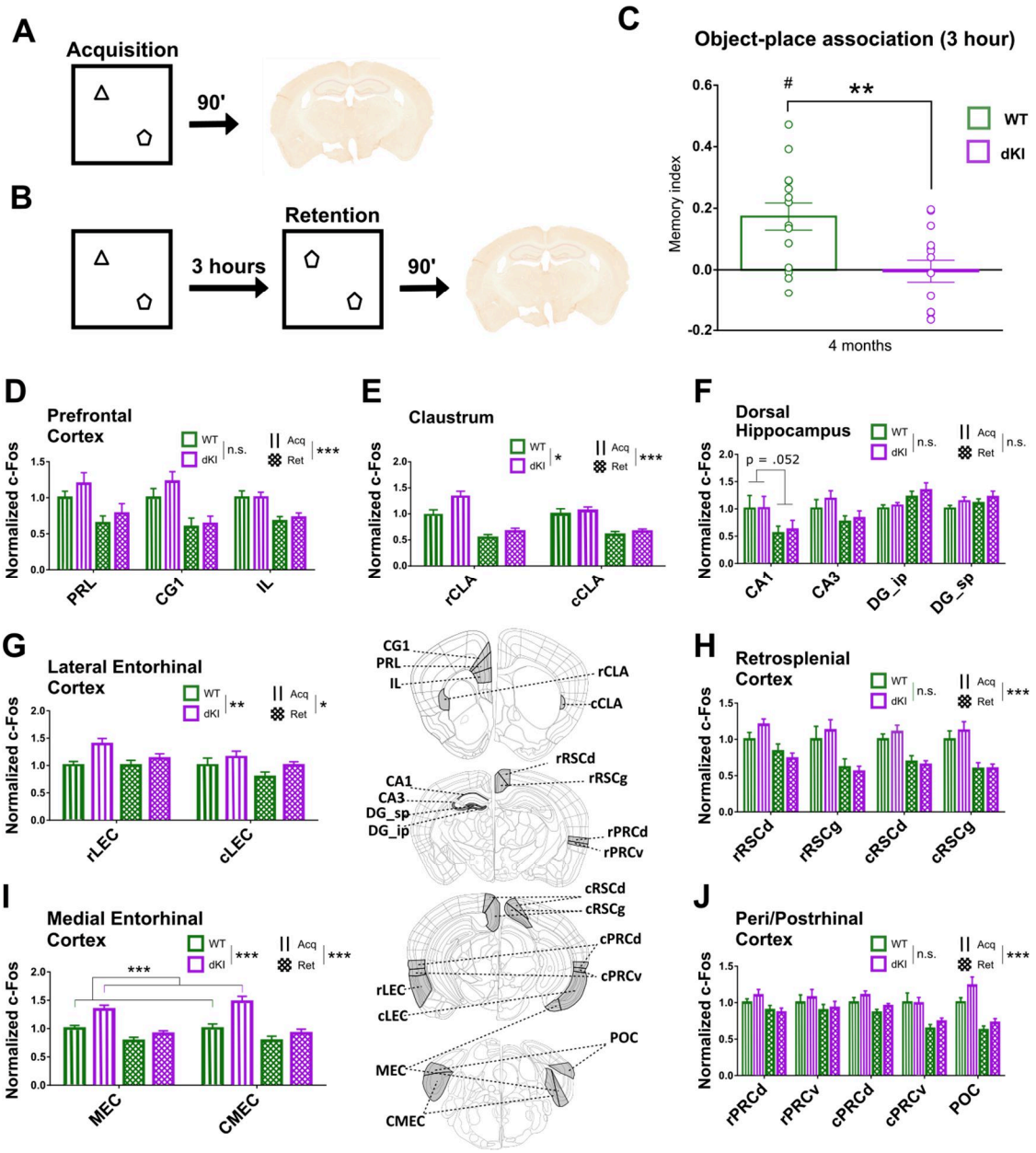

Figure 2. Activité régionale pendant les deux phases de l'OP. Des cohortes distinctes de souris WT et dKI ont été testées soit (A) dans la phase d'acquisition uniquement, soit (B) dans la totalité de la tâche OP3h, c'est-à-dire les phases d'acquisition et de rétention. Quatre-vingt-dix minutes après une phase de test, les cerveaux ont été perfusés et l'expression du gène régulé par l'activité, c-Fos, a été évaluée par immunohistochimie. (C) Les souris dKI qui ont subi l'ensemble de la tâche OP3h ont reproduit un déficit de la mémoire associative objet-place. différence entre les génotypes, **p<.01 (test t à deux échantillons) ; différence par rapport au hasard, #p<.05 (test t à un échantillon).(D-J) Graphiques illustrant le nombre de c-Fos normalisé par rapport au groupe WT-Acquisition. Pour chaque groupe de régions, une ANOVA à 3 facteurs a été réalisée pour les effets de la phase de test (lignes d'acquisition, grille de rétention), du génotype (WT-vert, dKI-violet) et de la sous-région. La signification des effets de la phase de test et du génotype est indiquée au-dessus de chaque graphique de région ; *p<.05, **p<.01, ***p<.001. (D-E,G-J) On a constaté une augmentation de l'activité pendant la phase d'acquisition dans toutes les régions, à l'exception de l'hippocampe dorsal (F). Le claustrum (E) et le cortex entorhinal latéral (G) ont présenté une augmentation de l'activité chez les souris dKI, quelle que soit la phase de test. Le cortex entorhinal médian (I) était toutefois hyperactif spécifiquement pendant la phase d'acquisition ***p<.001 (Tukey post hoc). Les graphiques à barres représentent la densité moyenne (± SEM). Préfixes des sous-régions - r, rostral ; c, caudal ; suffixes - RSCd, dysgranulaire ; RSCg, granulaire ; PRCd, dorsal ; PRCv, ventral ; ip, infrapyramidal ; sp, suprapyramidal. Les barres d'erreur indiquent le SEM. Les schémas indiquant l'emplacement général des régions cérébrales ont été adaptés des images vectorielles dérivées du Mouse Brain Atlas d'Allen (Lein et al., 2007).

Calcul des couplages fonctionnels

On peut dire que les régions du cerveau dont l'activité est corrélée présentent une CF, car les co-modulations de l'activité peuvent être un marqueur du partage d'informations entre les régions. Chez l'homme ou chez les rongeurs anesthésiés ou tête-fixe, les enregistrements sont effectués par EEG, MEG (pour les signaux électriques) ou IRMf (pour le taux métabolique), et la FC est calculée à partir de la covariance dans le temps. Dans les méthodes utilisant l'expression régionale de c-Fos, la FC peut être modélisée par la covariance de l'activité régionale entre les sujets afin d'étudier les réseaux mobilisés par la mémoire chez la souris (Wheeler et al., 2013 ; Tanimizu et al., 2017). La validité de cette approche a été confirmée à l'aide de techniques pharmaco-génétiques (Vetere et al., 2017).

À partir du signal c-Fos, nous avons évalué la CF en calculant les coefficients de corrélation interrégionale de Spearman (r) pour chaque groupe Génotype-Phase. Des matrices de corrélation ont été utilisées pour visualiser toutes les corrélations possibles au sein de chaque groupe (Figure 3A-B). Nous avons d'abord évalué la force globale des CF en prenant la valeur r moyenne de chaque matrice. La plupart des couplages CF étaient positifs, cependant nous avons trouvé quelques paires de régions faiblement anti-corrélées. Lors de l'évaluation de la CF, il y avait 3 façons de considérer ces corrélations négatives : comme perturbatrices, comme très faibles ou comme contribuant de manière égale aux corrélations positives. Les trois cas ont été évalués en prenant le r moyen avec des corrélations négatives conservées, quasi nulles et à valeur absolue respectivement. Dans le cas d'une valeur proche de zéro, les corrélations négatives ont été réduites à une valeur de 0,006, la plus petite corrélation positive observée.

Pendant l'acquisition, nous n'avons constaté aucun changement significatif de la force globale de la CF entre les groupes WT et dKI, pour aucune des trois façons de traiter les corrélations négatives de la CF (figure 3C). Cependant, pendant la rétention, il y avait une diminution de la force globale de la CF chez les souris dKI par rapport au groupe WT. Cette diminution est significative lorsqu'on considère les corrélations négatives comme perturbatrices ou comme très faibles, mais pas lorsqu'on prend leur valeur absolue (figure 3D). Cela indique que deux phénomènes coexistent : premièrement, une réduction des corrélations interrégionales positives, correspondant à une diminution de la " coopération " entre certaines régions ; deuxièmement, une augmentation de la force absolue des corrélations négatives interrégionales, correspondant à une augmentation du " conflit " entre certaines régions.

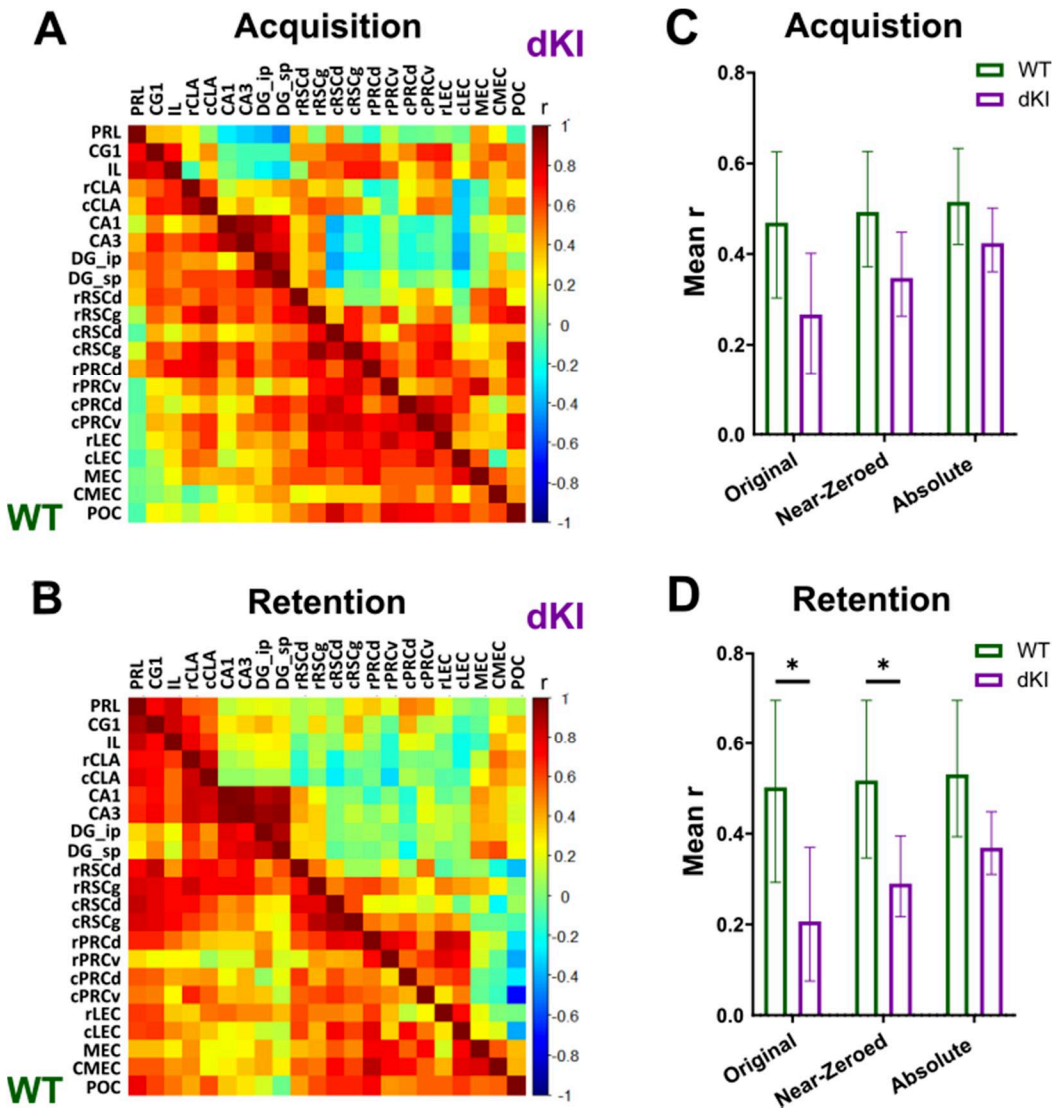

Figure 3. La connectivité fonctionnelle est représentée par des matrices montrant les corrélations de Spearman interrégionales entre les sujets pour l'expression de c-Fos pendant (A) la rétention et (B) l'acquisition. Les couleurs reflètent la force de la corrélation (échelle, à droite). Nous avons évalué la force globale de la CF en prenant la valeur r moyenne de chaque matrice avec les corrélations conservées, presque nulles et négatives à valeur absolue. Dans le cas des corrélations quasi-nulles, les corrélations négatives ont été réduites à une valeur de 0,006, la plus petite corrélation positive observée. (C) Nous n'avons trouvé aucun changement dans la force globale de la CF pour aucun des trois cas pendant l'acquisition. (D) Pendant la rétention, cependant, il y avait une diminution significative de la force globale de la FC avec les corrélations originales et proches de zéro, mais pas lorsqu'elles ont une valeur absolue. Les graphiques à barres représentent la valeur bootstrap moyenne, et les barres d'erreur représentent l'intervalle de confiance bootstrap de 95 %. * -l'IC de 95% pour la différence ≥ 0

Génération de réseaux fonctionnels

Chaque matrice de connectivité fonctionnelle peut être considérée comme la matrice d'adjacence d'un réseau non dirigé pondéré (Rubinov et Sporns, 2010) et, en tant que telle, son organisation peut être évaluée par l'analyse des réseaux fonctionnels, en utilisant des techniques issues de la théorie des graphes. À partir de chaque matrice, un réseau fonctionnel a été généré sous la forme d'un graphe pondéré entièrement connecté. Dans ces graphes, les régions sont représentées par des nœuds et les connexions fonctionnelles entre les régions sont représentées par des arêtes. La force d'une connexion entre deux régions, représentée par le poids de l'arête, est déterminée par la force de leur corrélation interrégionale. Comme les corrélations négatives sont faibles et posent des difficultés d'interprétation lors de l'utilisation de nombreuses techniques de théorie des graphes, nous avons décidé pour toutes les analyses suivantes de les remplacer par des valeurs proches de zéro lors de la construction de nos réseaux fonctionnels, en accord avec d'autres études de réseaux fonctionnels dérivés de c-Fos in-vivo (Vetere et al., 2017). Il a été démontré que l'organisation communautaire des réseaux structurels peut changer entre des individus sains et différents stades de MCI (Pereira et al., 2016). Nous avons décidé d'évaluer l'organisation communautaire de chaque réseau fonctionnel pour voir si des changements cohérents ou spécifiques à une phase pouvaient être détectés entre les génotypes. Cela pourrait également nous aider à obtenir une compréhension qualitative de l'organisation du flux d'informations dans chaque réseau. Les communautés de réseaux ont été détectées par une procédure de maximisation de la modularité (voir Matériaux et méthodes). Cet algorithme non supervisé sépare les nœuds en groupes distincts (les communautés), de sorte que les nœuds d'une communauté interagissent plus fortement entre eux qu'avec les nœuds d'autres communautés. La séparation des communautés varie partiellement de façon stochastique pour différentes exécutions de l'algorithme et différentes instances bootstrap de la matrice CF. Pour extraire un ensemble consensuel robuste de communautés, nous avons ensuite calculé des matrices d'allégeance (Bassett et al., 2015), qui représentent le pourcentage de fois qu'une paire donnée de régions est attribuée à la même communauté parmi les bootstraps (Figure 4).

Les réseaux WT engagent de manière différentielle le DH et le mPFC.

Une communauté stable est trouvée dans les deux phases de la tâche, englobant la plupart du MTC et du cRSC (Figure 4A,B ; zone rouge en bas à droite de chaque matrice d'allégeance WT). La principale différence entre les groupes WT-Acquisition et WT-Retention était l'implication différentielle de la DH ou du mPFC dans cette communauté MTC. Pendant l'acquisition, la DH a partagé une communauté principalement avec le mPFC (Figure 4A ; zone rouge en haut à gauche de la matrice d'allégeance). Pendant la rétention, le mPFC a partagé une allégeance à travers le réseau (Figure 4B ; zone rouge le long des lignes du mPFC en haut de la matrice d'allégeance). Cette incorporation plus globale du mPFC semblait être dirigée en grande partie par le RSC (figure 4B ; zone carrée rouge plus foncée située au milieu des trois rangées supérieures du mPFC).

Les réseaux de dKI révèlent des écarts constants par rapport à la structure communautaire du WT.

Pendant l'acquisition, la communauté DH s'est largement désengagée du mPFC par rapport au groupe WT-acquisition (Figure 4C ; carré vert en haut à gauche de la matrice d'allégeance). De plus, la communauté DH semble être plus fortement alignée avec le CMEC, le MEC et le POC par rapport au reste du MTC (Figure 4C ; la zone plus rouge/orange à droite des rangées DH).

Pendant la rétention, le mPFC et la DH se sont désengagés du MTC. Cela a conduit à des communautés distinctes contenant le mPFC/CLA, la DH et le MTC (figure 4D ; trois carrés rouges distincts de la matrice d'allégeance). Comme pour la phase d'acquisition, les régions MEC/CMEC/POC ont été fortement recrutées par les communautés mPFC et DH (figure 4D ; zone rouge en haut à droite), au prix d'un désengagement avec la communauté MTC (figure 4D ; zone verte en bas à droite de la matrice d'allégeance). Le recrutement cohérent de la MEC/CMEC/POC dans les deux groupes dKI élucide un rôle possible de ces régions comme plaques tournantes compensatoires dans ce modèle de souris.

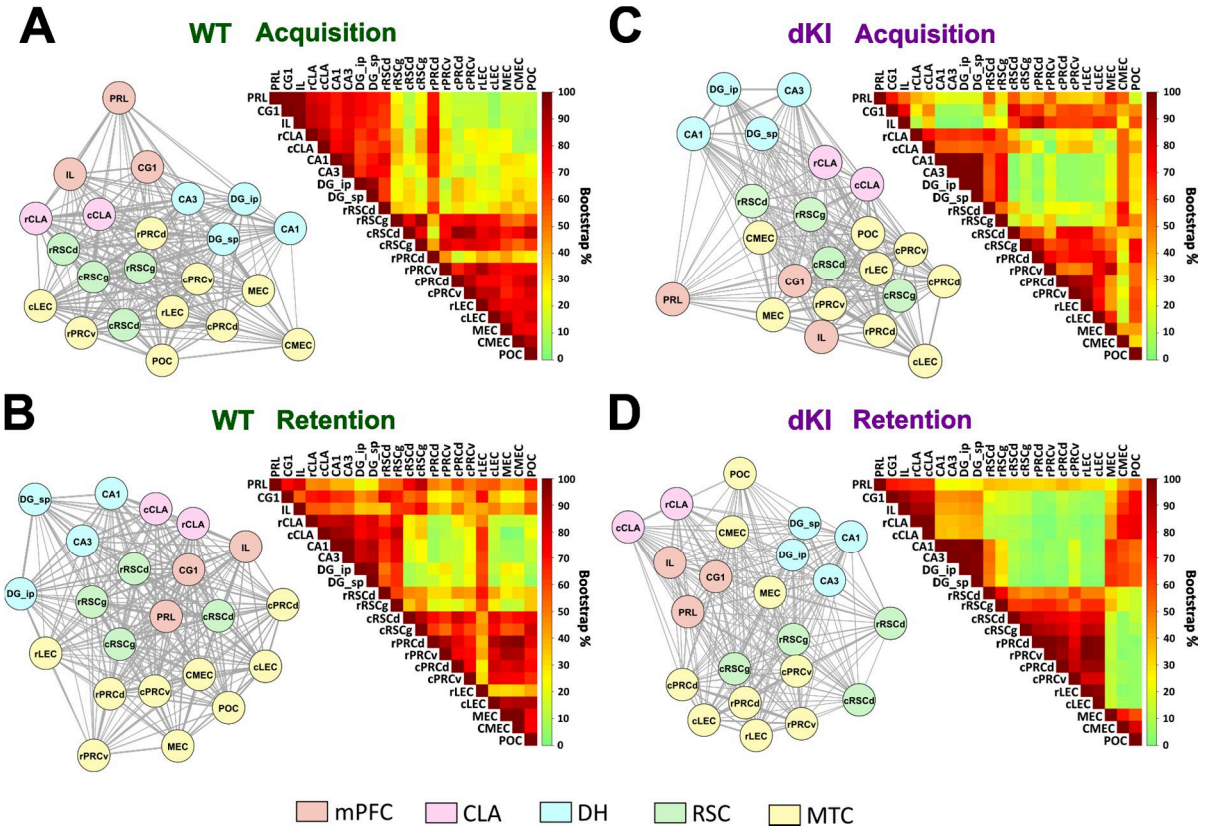

Figure 4. Les réseaux fonctionnels ont été calculés sous forme de graphes pondérés entièrement connectés, les régions étant les nœuds (cercles) et les forces de corrélation interrégionales les poids des bords (épaisseur des lignes). Pour l'examen visuel des réseaux, les nœuds ont été placés de manière à ce qu'ils soient plus proches des nœuds avec lesquels ils sont fortement connectés, et ont été codés par couleur en fonction des sous-domaines de la région a priori. Les communautés ont été détectées par maximisation de la modularité, ce qui permet de trouver des communautés de régions qui ont des connexions plus fortes les unes avec les autres par rapport au reste du réseau. Les communautés ont été détectées à travers des réseaux bootstraps, et des matrices d'allégeance ont été utilisées pour décrire la stabilité de la communauté comme le pourcentage de bootstraps qui contiennent une paire donnée de régions dans la même communauté. (A,B) Dans les deux groupes WT, il existe une communauté MTC/cRSC stable (zone rouge en bas à droite de chaque matrice d'allégeance WT). (A) Dans le groupe WT-Acq, il existe une communauté DH/mPFC stable (zone rouge en haut à gauche de la matrice d'allégeance). (B) Dans le WT-Ret, le mPFC partage l'allégeance communautaire avec l'ensemble du réseau (zone rouge le long des rangées du mPFC en haut de la matrice d'allégeance) par l'intermédiaire du RSC (carré rouge plus foncé au milieu des trois rangées supérieures du mPFC). (C,D) Dans les deux groupes de dKI, les régions MEC/CMEC/POC semblent présenter une allégeance communautaire constamment modifiée par rapport au WT, s'associant davantage avec le DH/mPFC et parfois moins avec le reste du MTC (zone rouge en haut à droite de chaque matrice d'allégeance de dKI, quelques zones vertes en bas à droite).

Flux d'informations dans les réseaux fonctionnels

Il est démontré qu'une intégration efficace du flux d'informations à travers des réseaux fonctionnels favorise la fonction cognitive (Wang et al., 2013a ; Martinez et al., 2018). Si l'on interprète les liens du réseau comme des "tuyaux", l'efficacité avec laquelle un réseau permet à l'information de circuler ne dépend pas seulement de la largeur des tuyaux individuels, mais aussi de la façon dont les tuyaux sont disposés et alignés pour former des conduites entre les nœuds qui doivent communiquer, sans trop d'étapes et de goulots d'étranglement. La capacité générale d'un réseau à soutenir des flux efficaces est quantifiée en théorie des graphes par des mesures telles que l'*efficacité globale* (voir Matériaux et méthodes ; Latora et Marchiori, 2001). Il est important de noter que même si la force globale de la CFMTC d'un réseau est réduite, son efficacité globale peut rester inchangée s'il existe des régions "pivots" bien placées pour faciliter la communication indirecte. Pour évaluer le flux d'informations au niveau régional, on utilise les mesures de la *force nodale* et de l'*efficacité nodale*. La force nodale mesure le degré auquel chaque région spécifique peut échanger des informations directement avec toutes les autres régions du réseau. Une région dont la force nodale est faible peut néanmoins être en mesure de communiquer avec son réseau de manière indirecte, probablement par l'intermédiaire de régions pivots. Cette communication indirecte peut être mesurée à l'aide de l'efficacité nodale. L'organisation du flux d'informations dans un réseau peut être examinée à travers les distributions de force et d'efficacité. On peut considérer que les régions dont la force et l'efficacité sont plus élevées contribuent davantage à leur réseau. Il est également démontré qu'une connectivité directe élevée d'une région, telle qu'une force élevée, décrit des régions pivots potentielles (Vetere et al., 2017) qui, comme nous l'avons décrit, sont nécessaires pour faciliter le flux d'information indirect et maintenir l'efficacité globale.

Nous avons comparé le flux d'information entre les réseaux WT et dKI dans chaque phase de test. L'organisation du flux d'information a d'abord été évaluée par un examen qualitatif des distributions de la force des nœuds et de l'efficacité des nœuds. Pour mieux visualiser les distributions, les valeurs de force/efficacité ont été élevées au carré et normalisées à la valeur la plus élevée au sein de chaque réseau, et ont été affichées sous forme de diagrammes en collier (acquisition - Figure 5A,B) (rétention - Figure 5F,G). Nous avons ensuite comparé directement l'efficacité globale et la force/efficacité nodale entre les génotypes dans des analyses ultérieures (acquisition - Figure 5C,D,E) (rétention - Figure 5H,I,J).

Acquisition- la DG_sp maintient son efficacité malgré une baisse de force

Au cours de l'acquisition, les distributions de la force et de l'efficacité étaient largement conservées entre les génotypes, avec un fort accent sur les régions RSC et MTC. Pourtant, chez les dKIs il semble y avoir une implication supplémentaire des mPFC, MEC et POC (Figure 5A,B). Néanmoins, l'efficacité globale n'a pas été gravement affectée dans le réseau dKI (figure 5C). La seule baisse significative de la force nodale a été observée dans le DG_sp (figure 5D), mais comme il n'y avait pas de baisse de l'efficacité nodale (figure 5E), il pouvait encore communiquer efficacement avec le reste du réseau de manière indirecte. Ce maintien de la communication indirecte, malgré les baisses de la communication directe, reflète l'importance potentielle des nœuds compensatoires rRSC ou MEC/CMEC/POC.

Rétention - pertes sévères de l'efficacité du réseau, en particulier dans le cortex cingulaire.

Pendant la rétention, l'accent était mis sur les régions mPFC et RSC dans le réseau WT. Dans le réseau dKI, cette emphase a été largement perdue et les distributions prennent une structure plus homogène, bien

que les sous-régions rRSCg et mPFC semblent toujours être parmi les plus impliquées (Figure 5F,G). L'efficacité globale a été considérablement réduite dans le réseau dKI (figure 5H), avec de fortes baisses de force observées dans le PRL et le POC, mais plus sévèrement dans les deux sous-régions du RSCd (figure 5I). La perte d'efficacité nodale était encore plus étendue, avec des réductions supplémentaires dans le CG1 et le cRSCg (Figure 5J). Ces résultats suggèrent que l'intégration fonctionnelle dépendante de la rétention dans le cortex cingulaire est gravement perturbée dans le dKI, et peut être liée à la réduction de la force du hub du RSCd.

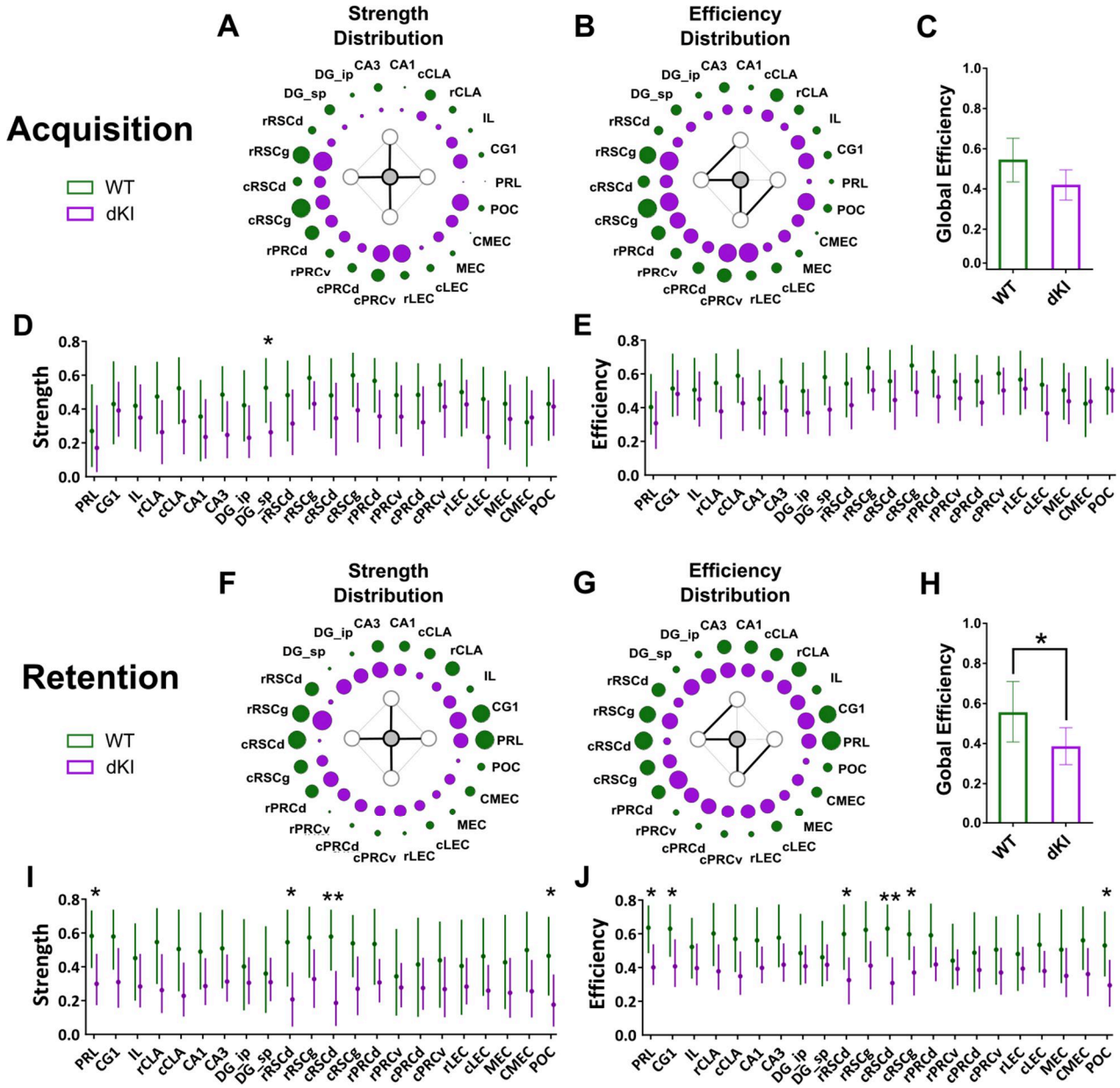

Figure 5. L'organisation en réseau du flux d'informations a été évaluée par l'examen des distributions de la force des nœuds et de l'efficacité nodale dans les deux phases de test (acquisition, rétention). Ces distributions ont été visualisées à l'aide de diagrammes en collier, où la taille des cercles reflète la force[2] (strength) et l'efficacité[2] (effiency) normalisées au sein du réseau (A,G). L'efficacité globale a ensuite été comparée directement entre les génotypes pour évaluer (C,F) l'intégration du réseau. (D,I) La force nodale (strength) et (E,J) l'efficacité nodale (efficiency) ont été comparées entre génotypes pour évaluer les changements dépendants de la région dans le flux d'information direct et indirect, respectivement. (A,B) Pendant l'acquisition, les distributions de la force et de l'efficacité étaient à peu près conservées entre les génotypes, avec un fort accent sur les régions RSC et MTC, bien que dans le dKI, les sous-régions mPFC, MEC et POC étaient beaucoup plus impliquées. (C) L'efficacité globale n'était pas sévèrement affectée chez les souris dKI. (D) Une baisse de la force de la région a été observée dans la DGsp, (E) mais son efficacité n'a pas été affectée. (G,H) Pendant la rétention, l'accent était mis sur les régions du mPFC et du RSC dans le réseau WT. Dans le dKI, cette emphase est largement perdue. (F) L'efficacité globale du réseau dKI était significativement réduite par rapport au réseau WT. (I) Des réductions de la force des régions ont été observées dans le POC, le PRL, et plus sévèrement dans les deux sous-régions du RSCd. (J) Les réductions de l'efficacité ont été conservées parmi ces régions, avec des pertes supplémentaires dans le CG1 et le cRSCg. Les graphiques à barres et les graphiques à points représentent la valeur bootstrap moyenne, et les barres d'erreur représentent l'intervalle de confiance bootstrap de 95 %. * -l'IC à 95 % pour la différence ≥ 0 ; ** -l'IC à 99 % pour la différence ≥ 0.

Relation entre l'efficacité du réseau et la mémoire

Enfin, nous avons abordé la question de savoir si la réduction des performances de la mémoire OP chez les souris dKI pouvait être expliquée par la réduction de l'efficacité du réseau observée pendant la rétention. Notre objectif était donc de déterminer si une relation pouvait être trouvée entre l'efficacité globale et l'indice de mémoire chez les WT et être utilisée pour prédire la perte de mémoire des dKI. Cette relation a été évaluée par des tests de corrélation sur des populations WT sous-échantillonnées, chaque sous-échantillon correspondant à l'élimination d'une souris. À partir de chaque sous-échantillon, l'indice de mémoire moyen et l'efficacité globale résultante ont été calculés, et la signification de la corrélation a été testée avec les coefficients de corrélation de Pearson et de Spearman.

L'efficacité globale présente une corrélation positive avec un indice de mémoire ajusté à l'exploration et permet de prédire les déficiences de mémoire dans le dKI.

Aucune corrélation significative n'a été trouvée entre l'efficacité globale et l'indice de mémoire dans les sous-échantillons WT (figure 6 - supplément 1A à la figure). Cependant, nous avons remarqué que, parmi les souris présentant un indice de mémoire élevé, celles dont le temps d'exploration était plus long (temps total d'exploration des deux objets) semblaient contribuer plus faiblement à l'efficacité globale. Cela laisse supposer un effet d'amortissement potentiel de l'exploration générale de l'objet sur l'indice de mémoire. Il convient de noter que l'augmentation du temps d'exploration peut être interprétée comme un signe supplémentaire d'altération de la fonction de mémoire, au-delà des réductions de l'indice de mémoire MI défini précédemment. Nous avons donc défini un indice d'exploration EI, quantifiant le temps d'exploration de la souris normalisé par rapport au groupe et l'avons utilisé pour calculer également un indice de mémoire ajusté à l'exploration comme l'indice de mémoire divisé par l'indice d'exploration (MI/EI). La diminution d'un tel indice de mémoire ajusté à l'exploration peut refléter à la fois la diminution de l'IM et l'augmentation de l'IE, résumant ainsi les deux facettes étudiées de l'altération du comportement lié à la mémoire. Comme dans le cas de la MI seule, nous n'avons pas trouvé de corrélation significative entre l'efficacité globale et l'indice EI (figure 6 - supplément de figure 1B). Une corrélation positive significative a toutefois été trouvée entre l'efficacité globale et l'indice de mémoire ajusté MI/EI dans les réseaux du sous-échantillon WT (figure 6).

De plus, nous avons pu montrer que l'extrapolation de la ligne de meilleur ajustement pour l'ensemble WT à des baisses d'efficacité globale aussi importantes que celles observées dans l'ensemble dKI prédisait également la baisse dKI observée de l'indice de performance comportementale MI/EI. Ceci est illustré dans la figure 6 où la continuation en pointillés de la ligne verte (l'extrapolation de la ligne de meilleur ajustement à l'ensemble WT) croise le nuage de points violets (l'ensemble des sous-échantillons dKI). La prédiction de l'indice MI/EI des sous-échantillons dKI basée sur l'extrapolation de la loi ajustée sur les sous-échantillons WT a donné des erreurs bien plus petites que celles attendues au niveau de chance, comme nous avons pu le vérifier par comparaison avec une distribution nulle d'erreurs de prédiction construite à partir de 1000 modèles ajustés aléatoirement à l'ensemble WT. Ceci est illustré dans l'histogramme de la figure 6, où la ligne verticale verte (erreur de prédiction du meilleur ajustement à l'ensemble WT) se trouve à gauche de la ligne verticale rouge la plus à gauche (extrémité inférieure de la distribution nulle, IC à 95%).

Cela suggère que les sujets ayant un indice de mémoire élevé mais un temps d'exploration total faible sont donc plus susceptibles d'avoir une efficacité globale plus élevée. Contrairement à l'indice de mémoire, il n'y a pas de différence significative détectable dans le temps total d'exploration des objets entre les groupes WT et dKI (figure 6 - supplément de figure 1C). L'indice de mémoire est donc une mesure plus sensible des changements comportementaux subtils et complexes, qui sont suivis par une diminution de l'efficacité globale entre le groupe WT et le groupe dKI. Ces résultats soutiennent la réduction de l'intégration du réseau comme facteur potentiel de l'altération du rappel de la mémoire OP chez le dKI.

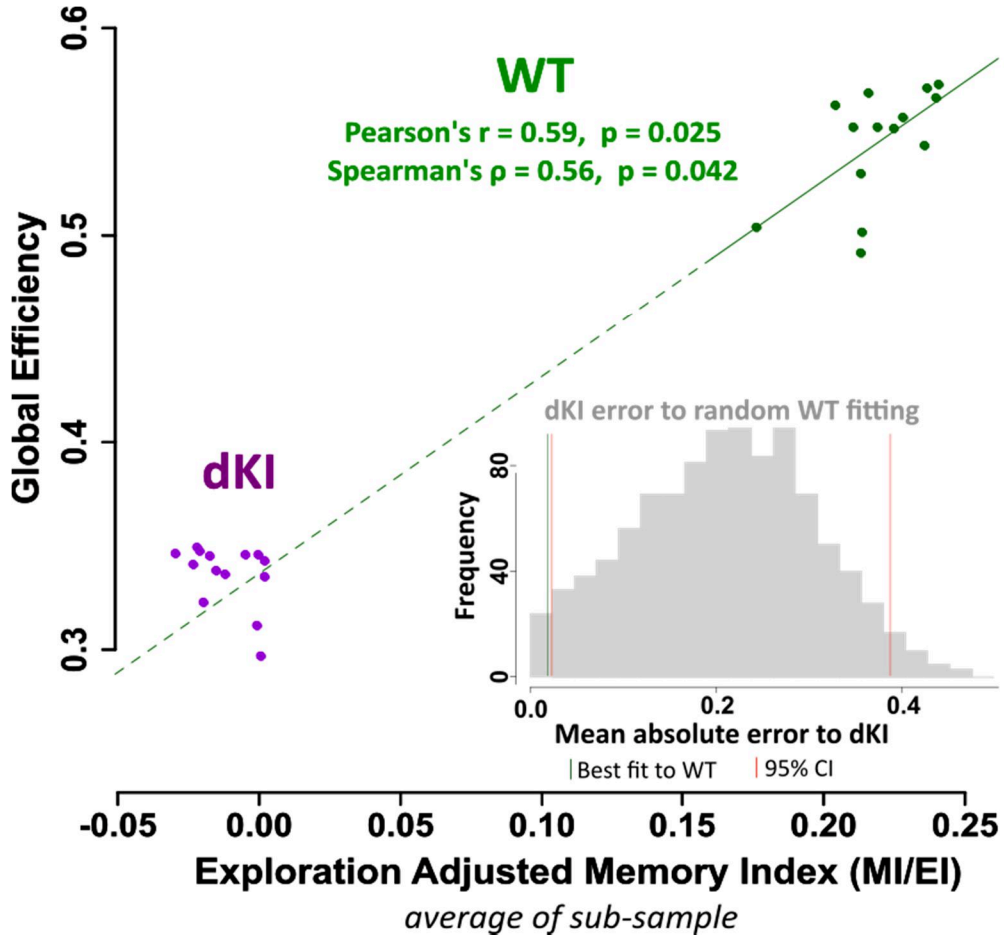

Figure 6. Association entre l'efficacité du réseau et l'indice de mémoire ajusté à l'exploration "MI/EI". Des sous-échantillons ont été générés à partir de chaque groupe de rétention en rééchantillonnant n-1 souris sans remplacement. À partir de chaque sous-échantillon, l'indice MI/EI moyen et l'efficacité globale du réseau ont été calculés, chaque sous-échantillon étant représenté par un point sur le graphique. La relation entre l'efficacité globale et le MI/EI a été évaluée uniquement sur les sous-échantillons WT (ligne verte pleine), et une relation linéaire positive significative a été trouvée. Il est intéressant de noter que lorsque cette loi linéaire sur les sous-échantillons WT a été extrapolée vers le bas (ligne verte pointillée) à l'efficacité globale réduite des sous-échantillons dKI, elle a pu prédire leur réduction de MI/EI (l'intersection de la ligne verte pointillée au nuage de points violets). La prédiction de l'indice MI/EI des sous-échantillons dKI basée sur l'extrapolation de la loi ajustée sur les sous-échantillons WT a donné des erreurs bien plus petites que celles attendues au niveau du hasard, comme nous avons pu le vérifier par comparaison avec une distribution nulle des erreurs de prédiction construite à partir de 1000 modèles ajustés au hasard. Voir l'histogramme en médaillon : la ligne verticale verte (erreur du meilleur ajustement linéaire à WT) se trouve à gauche de la ligne verticale rouge la plus à gauche (extrémité inférieure de la distribution nulle, IC à 95%).

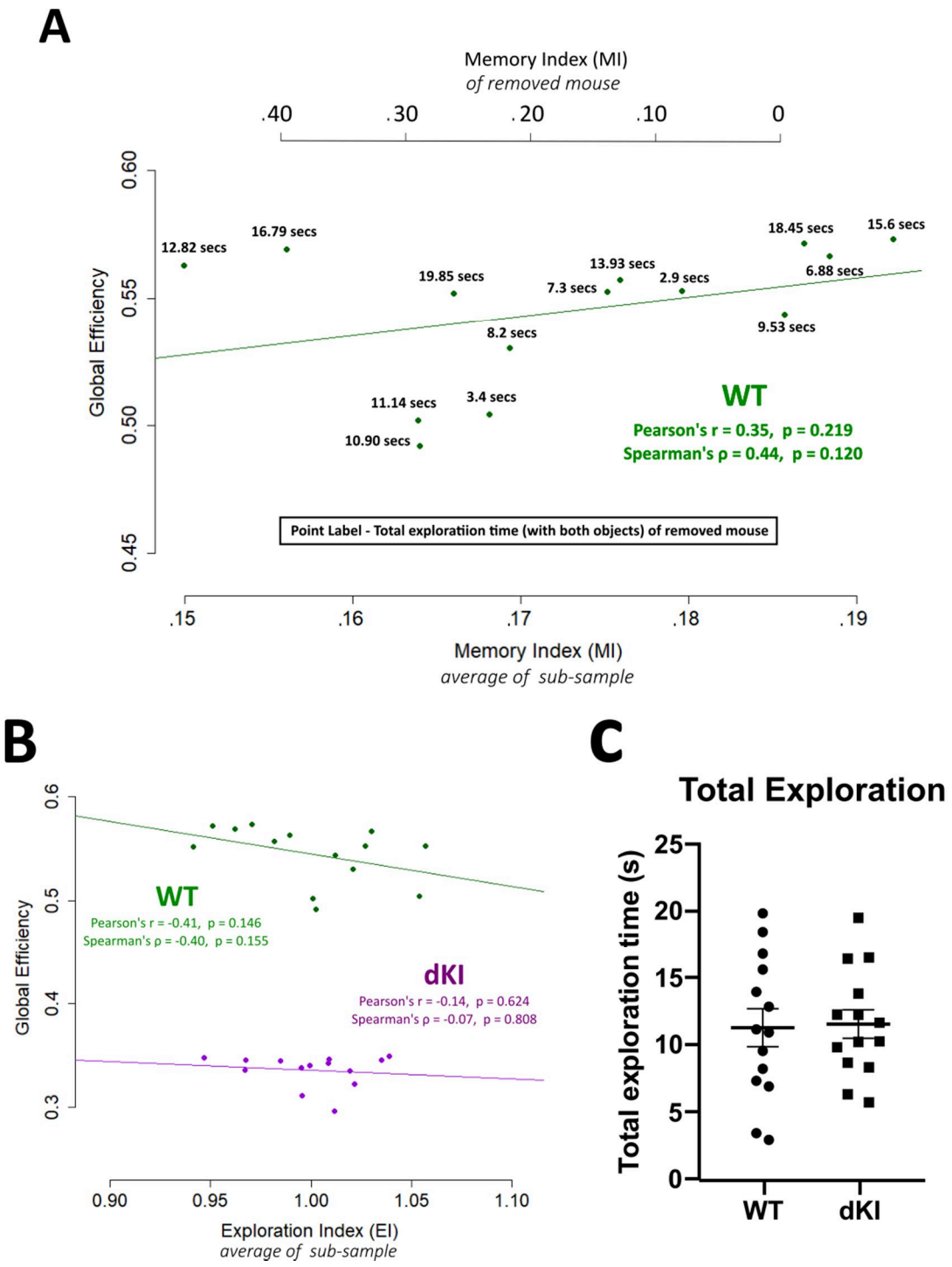

Figure 6-figure supplement 1 (A) Aucune relation n'a été trouvée entre l'efficacité globale et l'indice de mémoire. Cependant, nous avons remarqué que parmi les souris présentant un indice de mémoire élevé, celles dont le temps d'exploration était plus long (temps total d'exploration des deux objets) semblaient contribuer plus faiblement à l'efficacité globale. Pour prendre en compte un effet de perturbation de l'exploration sur la FC liée à la mémoire, un indice de mémoire ajusté à l'exploration a été calculé comme l'indice de mémoire divisé par l'indice d'exploration (MI/EI), où l'indice d'exploration (EI) est le temps d'exploration de la souris normalisé au groupe. (B) Nous avons vérifié qu'il n'y avait pas de relation directe entre l'efficacité globale et l'IE. (C) Il n'y avait également aucune différence dans l'exploration totale entre les souris WT et dKI.

Conclusion finale

Nous avons montré que le déclin initial de la mémoire affecte la mémoire associative dès l'âge de 4 mois puis la mémoire de séparation de motifs chez les souris dKI à partir de 6 mois. Ce déclin cognitif s'accompagne d'altérations fonctionnelles, notamment une hyperactivité du MTC, une réduction de l'efficacité du réseau et une hypo-connectivité du mPFC et du RSC pendant le rappel de la mémoire associative objet-place. Nous avons également détecté une hyperactivation d'une structure connectée au MTC, le CLA, une région qui mérite d'être étudiée de plus près dans le cadre de futures recherches sur la MA préclinique. Enfin, ces altérations cognitives et fonctionnelles étaient accompagnées d'une augmentation du ptau encore circonscrite au MTC, sans formation d'agrégats de tau. Jusqu'à présent, nos études sur les changements comportementaux, fonctionnels et neuropathologiques du modèle dKI correspondent remarquablement bien au stade préclinique de la MA. Le fait que l'étape initiale de la pathologie des souris dKI est semblable à celle de la MA à un stade précoce, avant les altérations structurelles et fonctionnelles liées à l'âge, en fait un modèle extrêmement précieux pour mieux comprendre les tout premiers stades de développement d'une MA.

References

Abramov E, Dolev I, Fogel H, Ciccotosto GD, Ruff E, Slutsky I. 2009. Amyloid-beta as a positive endogenous regulator of release probability at hippocampal synapses. *Nat Neurosci* **12**:1567–1576. doi:10.1038/nn.2433

Aggleton JP, Nelson AJD. 2015. Why do lesions in the rodent anterior thalamic nuclei cause such severe spatial deficits? *Neurosci Biobehav Rev* **54**:131–144. doi:10.1016/j.neubiorev.2014.08.013

Agster KL, Burwell RD. 2009. Cortical efferents of the perirhinal, postrhinal, and entorhinal cortices of the rat. *Hippocampus* **19**:1159–1186. doi:10.1002/hipo.20578

Ainge JA, Heron-Maxwell C, Theofilas P, Wright P, de Hoz L, Wood ER. 2006. The role of the hippocampus in object recognition in rats: Examination of the influence of task parameters and lesion size. *Behavioural Brain Research* **167**:183–195. doi:10.1016/j.bbr.2005.09.005

Akirav I, Maroun M. 2006. Ventromedial prefrontal cortex is obligatory for consolidation and reconsolidation of object recognition memory. *Cereb Cortex* **16**:1759–1765. doi:10.1093/cercor/bhj114

Albasser MM, Poirier GL, Aggleton JP. 2010. Qualitatively different modes of perirhinal–hippocampal engagement when rats explore novel vs. familiar objects as revealed by c-Fos imaging. *European Journal of Neuroscience* **31**:134–147. doi:10.1111/j.1460-9568.2009.07042.x

Alm KH, Bakker A. 2019. Relationships Between Diffusion Tensor Imaging and Cerebrospinal Fluid Metrics in Early Stages of the Alzheimer's Disease Continuum. *J Alzheimers Dis* **70**:965–981. doi:10.3233/JAD-181210

Alvarez A, Muñoz JP, Maccioni RB. 2001. A Cdk5–p35 Stable Complex Is Involved in the β-Amyloid-Induced Deregulation of Cdk5 Activity in Hippocampal Neurons. *Experimental Cell Research* **264**:266–274. doi:10.1006/excr.2001.5152

Alzheimer A. Über einen eigenartigen schweren Erkrankungsprozeβ der Hirnrincle. *Neurol Central.* 1906;25:1134. [Google Scholar]

Amani M, Lauterborn JC, Le AA, Cox BM, Wang W, Quintanilla J, Cox CD, Gall CM, Lynch G. 2021. Rapid Aging in the Perforant Path Projections to the Rodent Dentate Gyrus. *J Neurosci* **41**:2301–2312. doi:10.1523/JNEUROSCI.2376-20.2021

Amaral D, Lavenex P. 2007. Hippocampal neuroanatomyThe Hippocampus Book. New York, NY, US: Oxford University Press. pp. 37–114.

Ametamey SM, Honer M, Schubiger PA. 2008. Molecular Imaging with PET. *Chem Rev* **108**:1501–1516. doi:10.1021/cr0782426

Aminoff EM, Kveraga K, Bar M. 2013. The role of the parahippocampal cortex in cognition. *Trends Cogn Sci* **17**:379–390. doi:10.1016/j.tics.2013.06.009

Andorfer C, Kress Y, Espinoza M, Silva RD, Tucker KL, Barde Y-A, Duff K, Davies P. 2003. Hyperphosphorylation and aggregation of tau in mice expressing normal human tau isoforms. *Journal of Neurochemistry* **86**:582–590. doi:10.1046/j.1471-4159.2003.01879.x

Andrews-Hanna JR, Reidler JS, Sepulcre J, Poulin R, Buckner RL. 2010. Functional-anatomic fractionation of the brain's default network. *Neuron* **65**:550–562. doi:10.1016/j.neuron.2010.02.005

Andrews-Hanna JR, Saxe R, Yarkoni T. 2014. Contributions of episodic retrieval and mentalizing to autobiographical thought: evidence from functional neuroimaging, resting-state connectivity, and fMRI meta-analyses. *Neuroimage* **91**:324–335. doi:10.1016/j.neuroimage.2014.01.032

Asaad M, Lee JH. 2018. A guide to using functional magnetic resonance imaging to study Alzheimer's disease in animal models. *Dis Model Mech* **11**. doi:10.1242/dmm.031724

Assini FL, Duzzioni M, Takahashi RN. 2009. Object location memory in mice: pharmacological validation and further evidence of hippocampal CA1 participation. *Behav Brain Res* **204**:206–211. doi:10.1016/j.bbr.2009.06.005

Avila J, Perry G. 2021. A Multilevel View of the Development of Alzheimer's Disease. *Neuroscience* **457**:283–293. doi:10.1016/j.neuroscience.2020.11.015

Badhwar A, Tam A, Dansereau C, Orban P, Hoffstaedter F, Bellec P. 2017. Resting-state network dysfunction in Alzheimer's disease: A systematic review and meta-analysis. *Alzheimer's & Dementia: Diagnosis, Assessment & Disease Monitoring* **8**:73–85. doi:10.1016/j.dadm.2017.03.007

Bai L, Zhang M, Chen S, Ai L, Xu M, Wang D, Wang Fei, Liu L, Wang Fang, Lao L. 2013. Characterizing acupuncture de qi in mild cognitive impairment: relations with small-world efficiency of functional brain networks. *Evid Based Complement Alternat Med* **2013**:304804. doi:10.1155/2013/304804

Bakker A, Kirwan CB, Miller M, Stark CEL. 2008. Pattern Separation in the Human Hippocampal CA3 and Dentate Gyrus. *Science* **319**:1640–1642. doi:10.1126/science.1152882

Bakker A, Krauss GL, Albert MS, Speck CL, Jones LR, Stark CE, Yassa MA, Bassett SS, Shelton AL, Gallagher M. 2012. Reduction of hippocampal hyperactivity improves cognition in amnestic mild cognitive impairment. *Neuron* **74**:467–474. doi:10.1016/j.neuron.2012.03.023

Barger SW, Harmon AD. 1997. Microglial activation by Alzheimer amyloid precursor protein and modulation by apolipoprotein E. *Nature* **388**:878–881. doi:10.1038/42257

Barker GRI, Bird F, Alexander V, Warburton EC. 2007. Recognition memory for objects, place, and temporal order: a disconnection analysis of the role of the medial prefrontal cortex and perirhinal cortex. *J Neurosci* **27**:2948–2957. doi:10.1523/JNEUROSCI.5289-06.2007

Barker GRI, Warburton EC. 2015. Object-in-Place Associative Recognition Memory Depends on Glutamate Receptor Neurotransmission Within Two Defined Hippocampal-Cortical Circuits: A Critical Role for AMPA and NMDA Receptors in the Hippocampus, Perirhinal, and Prefrontal Cortices. *Cereb Cortex* **25**:472–481. doi:10.1093/cercor/bht245

Barker GRI, Warburton EC. 2011. When Is the Hippocampus Involved in Recognition Memory? *Journal of Neuroscience* **31**:10721–10731. doi:10.1523/JNEUROSCI.6413-10.2011

Bartko SJ, Winters BD, Cowell RA, Saksida LM, Bussey TJ. 2007. Perirhinal cortex resolves feature ambiguity in configural object recognition and perceptual oddity tasks. *Learn Mem* **14**:821–832. doi:10.1101/lm.749207

Bartus RT, Dean RL, Beer B, Lippa AS. 1982. The cholinergic hypothesis of geriatric memory dysfunction. *Science* **217**:408–414. doi:10.1126/science.7046051

Bassett DS, Bullmore E. 2006. Small-world brain networks. *Neuroscientist* **12**:512–523. doi:10.1177/1073858406293182

Bateman RJ, Xiong C, Benzinger TLS, Fagan AM, Goate A, Fox NC, Marcus DS, Cairns NJ, Xie X, Blazey TM, Holtzman DM, Santacruz A, Buckles V, Oliver A, Moulder K, Aisen PS, Ghetti B, Klunk WE, McDade E, Martins RN, Masters CL, Mayeux R, Ringman JM, Rossor MN, Schofield PR, Sperling RA, Salloway S, Morris JC, Dominantly Inherited Alzheimer Network. 2012. Clinical and biomarker changes in dominantly inherited Alzheimer's disease. *N Engl J Med* **367**:795–804. doi:10.1056/NEJMoa1202753

Bates KA, Verdile G, Li Q-X, Ames D, Hudson P, Masters CL, Martins RN. 2009. Clearance mechanisms of Alzheimer's amyloid-beta peptide: implications for therapeutic design and diagnostic tests. *Mol Psychiatry* **14**:469–486. doi:10.1038/mp.2008.96

Battaglia D, Boudou T, Hansen ECA, Lombardo D, Chettouf S, Daffertshofer A, McIntosh AR, Zimmermann J, Ritter P, Jirsa V. 2020. Dynamic Functional Connectivity between order and randomness and its evolution across the human adult lifespan. *NeuroImage* **222**:117156. doi:10.1016/j.neuroimage.2020.117156

Beaudin SA, Singh T, Agster KL, Burwell RD. 2013. Borders and Comparative Cytoarchitecture of the Perirhinal and Postrhinal Cortices in an F1 Hybrid Mouse. *Cereb Cortex* **23**:460–476. doi:10.1093/cercor/bhs038

Beher D, Hesse L, Masters CL, Multhaup G. 1996. Regulation of Amyloid Protein Precursor (APP) Binding to Collagen and Mapping of the Binding Sites on APP and Collagen Type I (∗). *Journal of Biological Chemistry* **271**:1613–1620. doi:10.1074/jbc.271.3.1613

Belarbi K, Burnouf S, Fernandez-Gomez F-J, Desmercières J, Troquier L, Brouillette J, Tsambou L, Grosjean M-E, Caillierez R, Demeyer D, Hamdane M, Schindowski K, Blum D, Buée L. 2011. Loss of medial septum cholinergic neurons in THY-Tau22 mouse model: what links with tau pathology? *Curr Alzheimer Res* **8**:633–638. doi:10.2174/156720511796717230

Belblidia H, Leger M, Abdelmalek A, Quiedeville A, Calocer F, Boulouard M, Jozet-Alves C, Freret T, Schumann-Bard P. 2018. Characterizing age-related decline of recognition memory and brain activation profile in mice. *Exp Gerontol* **106**:222–231. doi:10.1016/j.exger.2018.03.006

Bellana B, Liu Z -X., Diamond NB, Grady CL, Moscovitch M. 2016. Similarities and differences in the default mode network across rest, retrieval, and future imagining. *Hum Brain Mapp* **38**:1155–1171. doi:10.1002/hbm.23445

Bellucci A, Rosi MC, Grossi C, Fiorentini A, Luccarini I, Casamenti F. 2007. Abnormal processing of tau in the brain of aged TgCRND8 mice. *Neurobiol Dis* **27**:328–338. doi:10.1016/j.nbd.2007.06.008

Bergmann E, Zur G, Bershadsky G, Kahn I. 2016. The Organization of Mouse and Human Cortico-Hippocampal Networks Estimated by Intrinsic Functional Connectivity. *Cereb Cortex* **26**:4497–4512. doi:10.1093/cercor/bhw327

Berron D, Cardenas-Blanco A, Bittner D, Metzger CD, Spottke A, Heneka MT, Fliessbach K, Schneider A, Teipel SJ, Wagner M, Speck O, Jessen F, Düzel E. 2019. Higher CSF Tau Levels Are Related to Hippocampal Hyper-activity and Object Mnemonic Discrimination in Older Adults. *J Neurosci* **39**:8788–8797. doi:10.1523/JNEUROSCI.1279-19.2019

Berron D, Schütze H, Maass A, Cardenas-Blanco A, Kuijf HJ, Kumaran D, Düzel E. 2016. Strong Evidence for Pattern Separation in Human Dentate Gyrus. *J Neurosci* **36**:7569–7579. doi:10.1523/JNEUROSCI.0518-16.2016

Billings LM, Oddo S, Green KN, McGaugh JL, LaFerla FM. 2005. Intraneuronal Aβ Causes the Onset of Early Alzheimer's Disease-Related Cognitive Deficits in Transgenic Mice. *Neuron* **45**:675–688. doi:10.1016/j.neuron.2005.01.040

Boekhoorn K, Terwel D, Biemans B, Borghgraef P, Wiegert O, Ramakers GJA, de Vos K, Krugers H, Tomiyama T, Mori H, Joels M, van Leuven F, Lucassen PJ. 2006. Improved long-term potentiation and memory in young tau-P301L transgenic mice before onset of hyperphosphorylation and tauopathy. *J Neurosci* **26**:3514–3523. doi:10.1523/JNEUROSCI.5425-05.2006

Bolmont T, Haiss F, Eicke D, Radde R, Mathis CA, Klunk WE, Kohsaka S, Jucker M, Calhoun ME. 2008. Dynamics of the microglial/amyloid interaction indicate a role in plaque maintenance. *J Neurosci* **28**:4283–4292. doi:10.1523/JNEUROSCI.4814-07.2008

Bolz L, Heigele S, Bischofberger J. 2015. Running Improves Pattern Separation during Novel Object Recognition. *Brain Plast* **1**:129–141. doi:10.3233/BPL-150010

Bonardi C, Pardon M-C, Armstrong P. 2016. Deficits in object-in-place but not relative recency performance in the APPswe/PS1dE9 mouse model of Alzheimer's disease: Implications for object recognition. *Behavioural Brain Research* **313**:71–81. doi:10.1016/j.bbr.2016.07.008

Bookheimer SY, Strojwas MH, Cohen MS, Saunders AM, Pericak-Vance MA, Mazziotta JC, Small GW. 2000. Patterns of Brain Activation in People at Risk for Alzheimer's Disease. *New England Journal of Medicine* **343**:450–456. doi:10.1056/NEJM200008173430701

Borchelt DR, Thinakaran G, Eckman CB, Lee MK, Davenport F, Ratovitsky T, Prada CM, Kim G, Seekins S, Yager D, Slunt HH, Wang R, Seeger M, Levey AI, Gandy SE, Copeland NG, Jenkins NA, Price DL, Younkin SG, Sisodia SS. 1996. Familial Alzheimer's disease-linked presenilin 1 variants elevate Abeta1-42/1-40 ratio in vitro and in vivo. *Neuron* **17**:1005–1013. doi:10.1016/s0896-6273(00)80230-5

Bour A, Little S, Dodart J-C, Kelche C, Mathis C. 2004. A secreted form of the β-amyloid precursor protein (sAPP695) improves spatial recognition memory in OF1 mice. *Neurobiology of Learning and Memory* **81**:27–38. doi:10.1016/S1074-7427(03)00071-6

Bourin M, Hascoët M. 2003. The mouse light/dark box test. *Eur J Pharmacol* **463**:55–65. doi:10.1016/s0014-2999(03)01274-3

Boyce R, Glasgow SD, Williams S, Adamantidis A. 2016. Causal evidence for the role of REM sleep theta rhythm in contextual memory consolidation. *Science* **352**:812–816. doi:10.1126/science.aad5252

Braak H, Braak E. 1995. Staging of Alzheimer's disease-related neurofibrillary changes. *Neurobiol Aging* **16**:271–278; discussion 278-284. doi:10.1016/0197-4580(95)00021-6

Brier MR, Gordon B, Friedrichsen K, McCarthy J, Stern A, Christensen J, Owen C, Aldea P, Su Y, Hassenstab J, Cairns NJ, Holtzman DM, Fagan AM, Morris JC, Benzinger TLS, Ances BM. 2016. Tau and Aβ imaging, CSF measures, and cognition in Alzheimer's disease. *Sci Transl Med* **8**:338ra66. doi:10.1126/scitranslmed.aaf2362

Broadbent NJ, Squire LR, Clark RE. 2004. Spatial memory, recognition memory, and the hippocampus. *Proc Natl Acad Sci U S A* **101**:14515–14520. doi:10.1073/pnas.0406344101

Brown MW, Aggleton JP. 2001. Recognition memory: what are the roles of the perirhinal cortex and hippocampus? *Nat Rev Neurosci* **2**:51–61. doi:10.1038/35049064

Bubb EJ, Kinnavane L, Aggleton JP. 2017. Hippocampal–diencephalic–cingulate networks for memory and emotion: An anatomical guide. *Brain and Neuroscience Advances* **1**:2398212817723443. doi:10.1177/2398212817723443

Buckner RL, Andrews-Hanna JR, Schacter DL. 2008. The brain's default network: anatomy, function, and relevance to disease. *Ann N Y Acad Sci* **1124**:1–38. doi:10.1196/annals.1440.011

Buckner RL, DiNicola LM. 2019. The brain's default network: updated anatomy, physiology and evolving insights. *Nature Reviews Neuroscience* **20**:593–608. doi:10.1038/s41583-019-0212-7

Buée L, Bussière T, Buée-Scherrer V, Delacourte A, Hof PR. 2000. Tau protein isoforms, phosphorylation and role in neurodegenerative disorders11These authors contributed equally to this work. *Brain Research Reviews* **33**:95–130. doi:10.1016/S0165-0173(00)00019-9

Burdick D, Soreghan B, Kwon M, Kosmoski J, Knauer M, Henschen A, Yates J, Cotman C, Glabe C. 1992. Assembly and aggregation properties of synthetic Alzheimer's A4/beta amyloid peptide analogs. *J Biol Chem* **267**:546–554.

Burke SN, Maurer AP, Nematollahi S, Uprety AR, Wallace JL, Barnes CA. 2011. The influence of objects on place field expression and size in distal hippocampal CA1. *Hippocampus* **21**:783–801. doi:https://doi.org/10.1002/hipo.20929

Burwell RD. 2001. Borders and cytoarchitecture of the perirhinal and postrhinal cortices in the rat. *J Comp Neurol* **437**:17–41. doi:10.1002/cne.1267

Cáceres J, Brandan E. 1997. Interaction between Alzheimer's disease βA4 precursor protein (APP) and the extracellular matrix: Evidence for the participation of heparan sulfate proteoglycans. *Journal of Cellular Biochemistry* **65**:145–158. doi:https://doi.org/10.1002/(SICI)1097-4644(199705)65:2<145::AID-JCB2>3.0.CO;2-U

Campbell NL, Unverzagt F, LaMantia MA, Khan BA, Boustani MA. 2013. Risk Factors for the Progression of Mild Cognitive Impairment to Dementia. *Clin Geriatr Med* **29**:873–893. doi:10.1016/j.cger.2013.07.009

Canto C, Wouterlood F, Witter M. 2008. What Does the Anatomical Organization of the Entorhinal Cortex Tell Us? *Neural plasticity* **2008**:381243. doi:10.1155/2008/381243

Castillo-Carranza DL, Gerson JE, Sengupta U, Guerrero-Muñoz MJ, Lasagna-Reeves CA, Kayed R. 2014. Specific targeting of tau oligomers in Htau mice prevents cognitive impairment and tau toxicity following injection with brain-derived tau oligomeric seeds. *J Alzheimers Dis* **40 Suppl 1**:S97–S111. doi:10.3233/JAD-132477

Catheline G, Periot O, Amirault M, Braun M, Dartigues J-F, Auriacombe S, Allard M. 2010. Distinctive alterations of the cingulum bundle during aging and Alzheimer's disease. *Neurobiology of Aging* **31**:1582–1592. doi:10.1016/j.neurobiolaging.2008.08.012

Caviezel MP, Reichert CF, Sadeghi Bahmani D, Linnemann C, Liechti C, Bieri O, Borgwardt S, Leyhe T, Melcher T. 2020. The Neural Mechanisms of Associative Memory Revisited: fMRI Evidence from Implicit Contingency Learning. *Front Psychiatry* **10**. doi:10.3389/fpsyt.2019.01002

Cès A, Burg T, Herbeaux K, Héraud C, Bott J-B, Mensah-Nyagan AG, Mathis C. 2018. Age-related vulnerability of pattern separation in C57BL/6J mice. *Neurobiology of Aging* **62**:120–129. doi:10.1016/j.neurobiolaging.2017.10.013

Chang K-A, Suh Y-H. 2005. Pathophysiological roles of amyloidogenic carboxy-terminal fragments of the beta-amyloid precursor protein in Alzheimer's disease. *J Pharmacol Sci* **97**:461–471. doi:10.1254/jphs.cr0050014

Chao OY, Huston JP, Li J-S, Wang A-L, Silva MA de S. 2016. The medial prefrontal cortex—lateral entorhinal cortex circuit is essential for episodic-like memory and associative object-recognition. *Hippocampus* **26**:633–645. doi:10.1002/hipo.22547

Chasseigneaux S, Allinquant B. 2012. Functions of Aβ, sAPPα and sAPPβ : similarities and differences. *J Neurochem* **120 Suppl 1**:99–108. doi:10.1111/j.1471-4159.2011.07584.x

Chasseigneaux S, Dinc L, Rose C, Chabret C, Coulpier F, Topilko P, Mauger G, Allinquant B. 2011. Secreted amyloid precursor protein β and secreted amyloid precursor protein α induce axon outgrowth in vitro through Egr1 signaling pathway. *PLoS One* **6**:e16301. doi:10.1371/journal.pone.0016301

Chen F, Hasegawa H, Schmitt-Ulms G, Kawarai T, Bohm C, Katayama T, Gu Y, Sanjo N, Glista M, Rogaeva E, Wakutani Y, Pardossi-Piquard R, Ruan X, Tandon A, Checler F, Marambaud P, Hansen K, Westaway D, St George-Hyslop P, Fraser P. 2006. TMP21 is a presenilin complex component that modulates γ-secretase but not ε-secretase activity. *Nature* **440**:1208–1212. doi:10.1038/nature04667

Chen G, Xu T, Yan Y, Zhou Y, Jiang Y, Melcher K, Xu HE. 2017. Amyloid beta: structure, biology and structure-based therapeutic development. *Acta Pharmacol Sin* **38**:1205–1235. doi:10.1038/aps.2017.28

Chen Y, Dong C. 2009. Abeta40 promotes neuronal cell fate in neural progenitor cells. *Cell Death Differ* **16**:386–394. doi:10.1038/cdd.2008.94

Chételat G. 2013. Alzheimer disease: Aβ-independent processes-rethinking preclinical AD. *Nat Rev Neurol* **9**:123–124. doi:10.1038/nrneurol.2013.21

Chételat G, Villemagne VL, Bourgeat P, Pike KE, Jones G, Ames D, Ellis KA, Szoeke C, Martins RN, O'Keefe GJ, Salvado O, Masters CL, Rowe CC, Australian Imaging Biomarkers and Lifestyle Research Group. 2010. Relationship between atrophy and beta-amyloid deposition in Alzheimer disease. *Ann Neurol* **67**:317–324. doi:10.1002/ana.21955

Chishti MA, Yang DS, Janus C, Phinney AL, Horne P, Pearson J, Strome R, Zuker N, Loukides J, French J, Turner S, Lozza G, Grilli M, Kunicki S, Morissette C, Paquette J, Gervais F, Bergeron C, Fraser PE, Carlson GA, George-Hyslop PS, Westaway D. 2001. Early-onset amyloid deposition and cognitive deficits in transgenic mice expressing a double mutant form of amyloid precursor protein 695. *J Biol Chem* **276**:21562–21570. doi:10.1074/jbc.M100710200

Cho J-H, Johnson GVW. 2004. Primed phosphorylation of tau at Thr231 by glycogen synthase kinase 3beta (GSK3beta) plays a critical role in regulating tau's ability to bind and stabilize microtubules. *J Neurochem* **88**:349–358. doi:10.1111/j.1471-4159.2004.02155.x

Chong YH, Sung JH, Shin SA, Chung JH, Suh YH. 2001. Effects of the beta-amyloid and carboxyl-terminal fragment of Alzheimer's amyloid precursor protein on the production of the tumor necrosis factor-alpha and matrix metalloproteinase-9 by human monocytic THP-1. *J Biol Chem* **276**:23511–23517. doi:10.1074/jbc.M009466200

Citron M, Oltersdorf T, Haass C, McConlogue L, Hung AY, Seubert P, Vigo-Pelfrey C, Lieberburg I, Selkoe DJ. 1992. Mutation of the β-amyloid precursor protein in familial Alzheimer's disease increases β-protein production. *Nature* **360**:672–674. doi:10.1038/360672a0

Clark CM, Pontecorvo MJ, Beach TG, Bedell BJ, Coleman RE, Doraiswamy PM, Fleisher AS, Reiman EM, Sabbagh MN, Sadowsky CH, Schneider JA, Arora A, Carpenter AP, Flitter ML, Joshi AD, Krautkramer MJ, Lu M, Mintun MA, Skovronsky DM, AV-45-A16 Study Group. 2012. Cerebral PET with florbetapir compared with neuropathology at autopsy for detection of neuritic amyloid-β plaques: a prospective cohort study. *Lancet Neurol* **11**:669–678. doi:10.1016/S1474-4422(12)70142-4

Clavaguera F, Bolmont T, Crowther RA, Abramowski D, Frank S, Probst A, Fraser G, Stalder AK, Beibel M, Staufenbiel M, Jucker M, Goedert M, Tolnay M. 2009. Transmission and spreading of tauopathy in transgenic mouse brain. *Nature Cell Biology* **11**:909–913. doi:10.1038/ncb1901

Clelland CD, Choi M, Romberg C, Clemenson GD, Fragniere A, Tyers P, Jessberger S, Saksida LM, Barker RA, Gage FH, Bussey TJ. 2009. A functional role for adult hippocampal neurogenesis in spatial pattern separation. *Science* **325**:210–213. doi:10.1126/science.1173215

Cleveland DW, Hwo S-Y, Kirschner MW. 1977. Purification of tau, a microtubule-associated protein that induces assembly of microtubules from purified tubulin. *Journal of Molecular Biology* **116**:207–225. doi:10.1016/0022-2836(77)90213-3

Cohen SJ, Munchow AH, Rios LM, Zhang G, Asgeirsdóttir HN, Stackman RW. 2013. The rodent hippocampus is essential for nonspatial object memory. *Curr Biol* **23**:1685–1690. doi:10.1016/j.cub.2013.07.002

Cook D, Kesner RP. 1988. Caudate nucleus and memory for egocentric localization. *Behav Neural Biol* **49**:332–343. doi:10.1016/s0163-1047(88)90338-x

Cooper RA, Ritchey M. 2019. Cortico-hippocampal network connections support the multidimensional quality of episodic memory. *eLife* **8**:e45591. doi:10.7554/eLife.45591

Copanaki E, Chang S, Vlachos A, Tschäpe J-A, Müller UC, Kögel D, Deller T. 2010. sAPPalpha antagonizes dendritic degeneration and neuron death triggered by proteasomal stress. *Mol Cell Neurosci* **44**:386–393. doi:10.1016/j.mcn.2010.04.007

Corriveau-Lecavalier N, Duchesne S, Gauthier S, Hudon C, Kergoat M, Mellah S, Belleville S, for the Consortium for the Early Identification of Alzheimer's Disease-Quebec (CIMA-Q). 2020. A quadratic function of activation in individuals at risk of Alzheimer's disease. *Alzheimer's & Dementia: Diagnosis, Assessment & Disease Monitoring* **12**. doi:10.1002/dad2.12139

Cowan CM, Bossing T, Page A, Shepherd D, Mudher A. 2010. Soluble hyper-phosphorylated tau causes microtubule breakdown and functionally compromises normal tau in vivo. *Acta Neuropathol* **120**:593–604. doi:10.1007/s00401-010-0716-8

Cullen NC, Mälarstig A nders, Stomrud E, Hansson O, Mattsson-Carlgren N. 2021. Accelerated inflammatory aging in Alzheimer's disease and its relation to amyloid, tau, and cognition. *Scientific Reports* **11**:1965. doi:10.1038/s41598-021-81705-7

Daly T, Houot M, Barberousse A, Agid Y, Epelbaum S. 2020. Amyloid-β in Alzheimer's Disease: A Study of Citation Practices of the Amyloid Cascade Hypothesis Between 1992 and 2019. *J Alzheimers Dis* **74**:1309–1317. doi:10.3233/JAD-191321

Davidson RJ. 2002. Anxiety and affective style: role of prefrontal cortex and amygdala. *Biological Psychiatry* **51**:68–80. doi:10.1016/S0006-3223(01)01328-2

Davis M. 1992. The Role of the Amygdala in Fear and Anxiety. *Annu Rev Neurosci* **15**:353–375. doi:10.1146/annurev.ne.15.030192.002033

de Landeta AB, Pereyra M, Medina JH, Katche C. 2020. Anterior retrosplenial cortex is required for long-term object recognition memory. *Scientific Reports* **10**:4002. doi:10.1038/s41598-020-60937-z

Degiorgis L, Karatas M, Sourty M, Faivre E, Lamy J, Noblet V, Bienert T, Reisert M, von Elverfeldt D, Buée L, Blum D, Boutillier A-L, Armspach J-P, Blanc F, Harsan L-A. 2020. Brain network remodelling reflects tau-related pathology prior to memory deficits in Thy-Tau22 mice. *Brain*. doi:10.1093/brain/awaa312

Demuro A, Mina E, Kayed R, Milton SC, Parker I, Glabe CG. 2005. Calcium dysregulation and membrane disruption as a ubiquitous neurotoxic mechanism of soluble amyloid oligomers. *J Biol Chem* **280**:17294–17300. doi:10.1074/jbc.M500997200

Demuro A, Smith M, Parker I. 2011. Single-channel Ca2+ imaging implicates Aβ1–42 amyloid pores in Alzheimer's disease pathology. *J Cell Biol* **195**:515–524. doi:10.1083/jcb.201104133

Dere E, Huston JP, De Souza Silva MA. 2005. Episodic-like memory in mice: simultaneous assessment of object, place and temporal order memory. *Brain Res Brain Res Protoc* **16**:10–19. doi:10.1016/j.brainresprot.2005.08.001

Deshmukh SS, Johnson JL, Knierim JJ. 2012. Perirhinal cortex represents nonspatial, but not spatial, information in rats foraging in the presence of objects: Comparison with lateral entorhinal cortex. *Hippocampus* **22**:2045–2058. doi:https://doi.org/10.1002/hipo.22046

Deshmukh SS, Knierim JJ. 2011. Representation of non-spatial and spatial information in the lateral entorhinal cortex. *Front Behav Neurosci* **5**:69. doi:10.3389/fnbeh.2011.00069

DeVito LM, Eichenbaum H. 2010. Distinct contributions of the hippocampus and medial prefrontal cortex to the "what-where-when" components of episodic-like memory in mice. *Behav Brain Res* **215**:318–325. doi:10.1016/j.bbr.2009.09.014

Dias R, Robbins TW, Roberts AC. 1996. Dissociation in prefrontal cortex of affective and attentional shifts. *Nature* **380**:69–72. doi:10.1038/380069a0

Dickson DW. 1997. The pathogenesis of senile plaques. *J Neuropathol Exp Neurol* **56**:321–339. doi:10.1097/00005072-199704000-00001

Dillen KNH, Jacobs HIL, Kukolja J, Richter N, von Reutern B, Onur ÖA, Langen K-J, Fink GR. 2017. Functional Disintegration of the Default Mode Network in Prodromal Alzheimer's Disease. *J Alzheimers Dis* **59**:169–187. doi:10.3233/JAD-161120

Diodato A, Ruinart de Brimont M, Yim YS, Derian N, Perrin S, Pouch J, Klatzmann D, Garel S, Choi GB, Fleischmann A. 2016. Molecular signatures of neural connectivity in the olfactory cortex. *Nature Communications* **7**:12238. doi:10.1038/ncomms12238

Dix SL, Aggleton JP. 1999. Extending the spontaneous preference test of recognition: evidence of object-location and object-context recognition. *Behav Brain Res* **99**:191–200. doi:10.1016/s0166-4328(98)00079-5

Dodart JC, Mathis C, Bales KR, Paul SM, Ungerer A. 2000. Behavioral deficits in APP(V717F) transgenic mice deficient for the apolipoprotein E gene. *Neuroreport* **11**:603–607. doi:10.1097/00001756-200002280-00034

Dodart JC, Mathis C, Ungerer A. 1997. Scopolamine-induced deficits in a two-trial object recognition task in mice. *NeuroReport* **8**:1173–1178.

Dodart JC, Meziane H, Mathis C, Bales KR, Paul SM, Ungerer A. 1999. Behavioral disturbances in transgenic mice overexpressing the V717F beta-amyloid precursor protein. *Behav Neurosci* **113**:982–990. doi:10.1037//0735-7044.113.5.982

Doecke JD, Pérez-Grijalba V, Fandos N, Fowler C, Villemagne VL, Masters CL, Pesini P, Sarasa M, for the AIBL Research Group. 2020. Total Aβ $_{42}$ /Aβ $_{40}$ ratio in plasma predicts amyloid-PET status, independent of clinical AD diagnosis. *Neurology* **94**:e1580–e1591. doi:10.1212/WNL.0000000000009240

Doody RS, Raman R, Farlow M, Iwatsubo T, Vellas B, Joffe S, Kieburtz K, He F, Sun X, Thomas RG, Aisen PS, Siemers E, Sethuraman G, Mohs R. 2013. A Phase 3 Trial of Semagacestat for Treatment of Alzheimer's Disease. *New England Journal of Medicine* **369**:341–350. doi:10.1056/NEJMoa1210951

Doody RS, Thomas RG, Farlow M, Iwatsubo T, Vellas B, Joffe S, Kieburtz K, Raman R, Sun X, Aisen PS, Siemers E, Liu-Seifert H, Mohs R, Alzheimer's Disease Cooperative Study Steering Committee, Solanezumab Study Group. 2014. Phase 3 trials of solanezumab for mild-to-moderate Alzheimer's disease. *N Engl J Med* **370**:311–321. doi:10.1056/NEJMoa1312889

Drewes JE, Fox P. 1999. Fate of natural organic matter (NOM) during groundwater recharge using reclaimed water. *Water Science and Technology* **40**:241–248. doi:10.1016/S0273-1223(99)00662-9

Drzezga A, Becker JA, Van Dijk KRA, Sreenivasan A, Talukdar T, Sullivan C, Schultz AP, Sepulcre J, Putcha D, Greve D, Johnson KA, Sperling RA. 2011. Neuronal dysfunction and disconnection of cortical hubs in non-demented subjects with elevated amyloid burden. *Brain* **134**:1635–1646. doi:10.1093/brain/awr066

Dubois B, Hampel H, Feldman HH, Scheltens P, Aisen P, Andrieu S, Bakardjian H, Benali H, Bertram L, Blennow K, Broich K, Cavedo E, Crutch S, Dartigues J-F, Duyckaerts C, Epelbaum S, Frisoni GB, Gauthier S, Genthon R, Gouw AA, Habert M-O, Holtzman DM, Kivipelto M, Lista S, Molinuevo J-L, O'Bryant SE, Rabinovici GD, Rowe C, Salloway S, Schneider LS, Sperling R, Teichmann M, Carrillo MC, Cummings J, Jack CR, Proceedings of the Meeting of the International Working Group (IWG) and the American Alzheimer's Association on "The Preclinical State of AD"; July 23, 2015; Washington DC, USA. 2016. Preclinical Alzheimer's disease: Definition, natural history, and diagnostic criteria. *Alzheimers Dement* **12**:292–323. doi:10.1016/j.jalz.2016.02.002

Duff K, Eckman C, Zehr C, Yu X, Prada CM, Perez-tur J, Hutton M, Buee L, Harigaya Y, Yager D, Morgan D, Gordon MN, Holcomb L, Refolo L, Zenk B, Hardy J, Younkin S. 1996. Increased amyloid-beta42(43) in brains of mice expressing mutant presenilin 1. *Nature* **383**:710–713. doi:10.1038/383710a0

Duff K, Knight H, Refolo LM, Sanders S, Yu X, Picciano M, Malester B, Hutton M, Adamson J, Goedert M, Burki K, Davies P. 2000. Characterization of Pathology in Transgenic Mice Over-Expressing Human Genomic and cDNA Tau Transgenes. *Neurobiology of Disease* **7**:87–98. doi:10.1006/nbdi.1999.0279

Dulin F, Léveillé F, Ortega JB, Mornon J-P, Buisson A, Callebaut I, Colloc'h N. 2008. P3 peptide, a truncated form of A beta devoid of synaptotoxic effect, does not assemble into soluble oligomers. *FEBS Lett* **582**:1865–1870. doi:10.1016/j.febslet.2008.05.002

Eacott MJ, Norman G. 2004. Integrated Memory for Object, Place, and Context in Rats: A Possible Model of Episodic-Like Memory? *J Neurosci* **24**:1948–1953. doi:10.1523/JNEUROSCI.2975-03.2004

Eichenbaum H. 2017. Memory: Organization and Control. *Annual Review of Psychology* **68**:19–45. doi:10.1146/annurev-psych-010416-044131

El-Amouri SS, Zhu H, Yu J, Marr R, Verma IM, Kindy MS. 2008. Neprilysin: An Enzyme Candidate to Slow the Progression of Alzheimer's Disease. *Am J Pathol* **172**:1342–1354. doi:10.2353/ajpath.2008.070620

Engel T, Hernández F, Avila J, Lucas JJ. 2006. Full Reversal of Alzheimer's Disease-Like Phenotype in a Mouse Model with Conditional Overexpression of Glycogen Synthase Kinase-3. *J Neurosci* **26**:5083–5090. doi:10.1523/JNEUROSCI.0604-06.2006

Ennaceur A. 2010. One-trial object recognition in rats and mice: methodological and theoretical issues. *Behav Brain Res* **215**:244–254. doi:10.1016/j.bbr.2009.12.036

Ennaceur A, Delacour J. 1988. A new one-trial test for neurobiological studies of memory in rats. 1: Behavioral data. *Behav Brain Res* **31**:47–59. doi:10.1016/0166-4328(88)90157-x

Ennaceur A, Neave N, Aggleton JP. 1996. Neurotoxic lesions of the perirhinal cortex do not mimic the behavioural effects of fornix transection in the rat. *Behav Brain Res* **80**:9–25. doi:10.1016/0166-4328(96)00006-x

Epskamp S, Borsboom D, Fried EI. 2018. Estimating psychological networks and their accuracy: A tutorial paper. *Behav Res* **50**:195–212. doi:10.3758/s13428-017-0862-1

Espíndola SL, Damianich A, Alvarez RJ, Sartor M, Belforte JE, Ferrario JE, Gallo J-M, Avale ME. 2018. Modulation of Tau Isoforms Imbalance Precludes Tau Pathology and Cognitive Decline in a Mouse Model of Tauopathy. *Cell Rep* **23**:709–715. doi:10.1016/j.celrep.2018.03.079

Etkin A, Egner T, Kalisch R. 2011. Emotional processing in anterior cingulate and medial prefrontal cortex. *Trends in Cognitive Sciences* **15**:85–93. doi:10.1016/j.tics.2010.11.004

Etter G, van der Veldt S, Manseau F, Zarrinkoub I, Trillaud-Doppia E, Williams S. 2019. Optogenetic gamma stimulation rescues memory impairments in an Alzheimer's disease mouse model. *Nature Communications* **10**:5322. doi:10.1038/s41467-019-13260-9

Euston DR, Gruber AJ, McNaughton BL. 2012. The Role of Medial Prefrontal Cortex in Memory and Decision Making. *Neuron* **76**:1057–1070. doi:10.1016/j.neuron.2012.12.002

Ewers M, Insel P, Jagust WJ, Shaw L, Trojanowski JQ, Aisen P, Petersen RC, Schuff N, Weiner MW, Alzheimer's Disease Neuroimaging Initiative (ADNI). 2012. CSF biomarker and PIB-PET-derived beta-amyloid signature predicts metabolic, gray matter, and cognitive changes in nondemented subjects. *Cereb Cortex* **22**:1993–2004. doi:10.1093/cercor/bhr271

Eyler LT, Elman JA, Hatton SN, Gough S, Mischel AK, Hagler DJ, Franz CE, Docherty A, Fennema-Notestine C, Gillespie N, Gustavson D, Lyons MJ, Neale MC, Panizzon MS, Dale AM, Kremen WS. 2019. Resting State Abnormalities of the Default Mode Network in Mild Cognitive Impairment: A Systematic Review and Meta-Analysis. *J Alzheimers Dis* **70**:107–120. doi:10.3233/JAD-180847

Fandos N, Pérez-Grijalba V, Pesini P, Olmos S, Bossa M, Villemagne VL, Doecke J, Fowler C, Masters CL, Sarasa M, AIBL Research Group. 2017. Plasma amyloid β 42/40 ratios as biomarkers for amyloid β cerebral deposition in cognitively normal individuals. *Alzheimers Dement (Amst)* **8**:179–187. doi:10.1016/j.dadm.2017.07.004

Farris W, Mansourian S, Chang Y, Lindsley L, Eckman EA, Frosch MP, Eckman CB, Tanzi RE, Selkoe DJ, Guenette S. 2003. Insulin-degrading enzyme regulates the levels of insulin, amyloid beta-protein, and the beta-amyloid precursor protein intracellular domain in vivo. *Proc Natl Acad Sci U S A* **100**:4162–4167. doi:10.1073/pnas.0230450100

Felgner H, Frank R, Biernat J, Mandelkow E-M, Mandelkow E, Ludin B, Matus A, Schliwa M. 1997. Domains of Neuronal Microtubule-associated Proteins and Flexural Rigidity of Microtubules. *Journal of Cell Biology* **138**:1067–1075. doi:10.1083/jcb.138.5.1067

Ferretti MT, Iulita MF, Cavedo E, Chiesa PA, Dimech AS, Chadha AS, Baracchi F, Girouard H, Misoch S, Giacobini E, Depypere H, Hampel H. 2018. Sex differences in Alzheimer disease — the gateway to precision medicine. *Nat Rev Neurol* **14**:457–469. doi:10.1038/s41582-018-0032-9

Filippi M, van den Heuvel MP, Fornito A, He Y, Hulshoff Pol HE, Agosta F, Comi G, Rocca MA. 2013. Assessment of system dysfunction in the brain through MRI-based connectomics. *The Lancet Neurology* **12**:1189–1199. doi:10.1016/S1474-4422(13)70144-3

Flach K, Hilbrich I, Schiffmann A, Gärtner U, Krüger M, Leonhardt M, Waschipky H, Wick L, Arendt T, Holzer M. 2012. Tau oligomers impair artificial membrane integrity and cellular viability. *J Biol Chem* **287**:43223–43233. doi:10.1074/jbc.M112.396176

Fleisher AS, Chen K, Quiroz YT, Jakimovich LJ, Gutierrez Gomez M, Langois CM, Langbaum JBS, Roontiva A, Thiyyagura P, Lee W, Ayutyanont N, Lopez L, Moreno S, Muñoz C, Tirado V, Acosta-Baena N, Fagan AM, Giraldo M, Garcia G, Huentelman MJ, Tariot PN, Lopera F, Reiman EM. 2015. Associations between biomarkers and age in the presenilin 1 E280A autosomal dominant Alzheimer disease kindred: a cross-sectional study. *JAMA Neurol* **72**:316–324. doi:10.1001/jamaneurol.2014.3314

Folstein MF, Whitehouse PJ. 1983. Cognitive impairment of Alzheimer disease. *Neurobehav Toxicol Teratol* **5**:631–634.

Fournier DI, Monasch RR, Bucci DJ, Todd TP. 2020. Retrosplenial cortex damage impairs unimodal sensory preconditioning. *Behav Neurosci* **134**:198–207. doi:10.1037/bne0000365

Fraser SP, Suh Y-H, Djamgoz MBA. 1997. Ionic effects of the Alzheimer's disease β-amyloid precursor protein and its metabolic fragments. *Trends in Neurosciences* **20**:67–72. doi:10.1016/S0166-2236(96)10079-5

Freude KK, Penjwini M, Davis JL, LaFerla FM, Blurton-Jones M. 2011. Soluble amyloid precursor protein induces rapid neural differentiation of human embryonic stem cells. *J Biol Chem* **286**:24264–24274. doi:10.1074/jbc.M111.227421

Frye CA, Walf AA. 2008. Effects of progesterone administration and APPswe+PSEN1Deltae9 mutation for cognitive performance of mid-aged mice. *Neurobiol Learn Mem* **89**:17–26. doi:10.1016/j.nlm.2007.09.008

Funahashi S. 2017. Working Memory in the Prefrontal Cortex. *Brain Sciences* **7**:49. doi:10.3390/brainsci7050049

Furst AJ, Rabinovici GD, Rostomian AH, Steed T, Alkalay A, Racine C, Miller BL, Jagust WJ. 2012. Cognition, glucose metabolism and amyloid burden in Alzheimer's disease. *Neurobiol Aging* **33**:215–225. doi:10.1016/j.neurobiolaging.2010.03.011

Furtak SC, Ahmed OJ, Burwell RD. 2012. SINGLE NEURON ACTIVITY AND THETA MODULATION IN POSTRHINAL CORTEX DURING VISUAL OBJECT DISCRIMINATION. *Neuron* **76**:976–988. doi:10.1016/j.neuron.2012.10.039

Furukawa K, Sopher BL, Rydel RE, Begley JG, Pham DG, Martin GM, Fox M, Mattson MP. 1996. Increased activity-regulating and neuroprotective efficacy of alpha-secretase-derived secreted amyloid precursor protein conferred by a C-terminal heparin-binding domain. *J Neurochem* **67**:1882–1896. doi:10.1046/j.1471-4159.1996.67051882.x

Gakhar-Koppole N, Hundeshagen P, Mandl C, Weyer SW, Allinquant B, Müller U, Ciccolini F. 2008. Activity requires soluble amyloid precursor protein alpha to promote neurite outgrowth in neural stem cell-derived neurons via activation of the MAPK pathway. *Eur J Neurosci* **28**:871–882. doi:10.1111/j.1460-9568.2008.06398.x

Games D, Adams D, Alessandrini R, Barbour R, Berthelette P, Blackwell C, Carr T, Clemens J, Donaldson T, Gillespie F. 1995. Alzheimer-type neuropathology in transgenic mice overexpressing V717F beta-amyloid precursor protein. *Nature* **373**:523–527. doi:10.1038/373523a0

Gao Y, Pimplikar SW. 2001. The γ-secretase-cleaved C-terminal fragment of amyloid precursor protein mediates signaling to the nucleus. *PNAS* **98**:14979–14984. doi:10.1073/pnas.261463298

Garcia-Osta A, Alberini CM. 2009. Amyloid beta mediates memory formation. *Learn Mem* **16**:267–272. doi:10.1101/lm.1310209

Gardini S, Venneri A, Sambataro F, Cuetos F, Fasano F, Marchi M, Crisi G, Caffarra P. 2015. Increased functional connectivity in the default mode network in mild cognitive impairment: a maladaptive compensatory mechanism associated with poor semantic memory performance. *J Alzheimers Dis* **45**:457–470. doi:10.3233/JAD-142547

Gauthier S, Reisberg B, Zaudig M, Petersen RC, Ritchie K, Broich K, Belleville S, Brodaty H, Bennett D, Chertkow H, Cummings JL, de Leon M, Feldman H, Ganguli M, Hampel H, Scheltens P, Tierney MC, Whitehouse P, Winblad B, International Psychogeriatric Association Expert Conference on mild cognitive impairment. 2006. Mild cognitive impairment. *Lancet* **367**:1262–1270. doi:10.1016/S0140-6736(06)68542-5

Gerson J, Castillo-Carranza DL, Sengupta U, Bodani R, Prough DS, DeWitt DS, Hawkins BE, Kayed R. 2016. Tau Oligomers Derived from Traumatic Brain Injury Cause Cognitive Impairment and Accelerate Onset of Pathology in Htau Mice. *J Neurotrauma* **33**:2034–2043. doi:10.1089/neu.2015.4262

Goedert M. 2018. Tau filaments in neurodegenerative diseases. *FEBS Lett* **592**:2383–2391. doi:10.1002/1873-3468.13108

Goedert M, Jakes R. 1990. Expression of separate isoforms of human tau protein: correlation with the tau pattern in brain and effects on tubulin polymerization. *The EMBO Journal* **9**:4225–4230. doi:10.1002/j.1460-2075.1990.tb07870.x

Goedert M, Wischik CM, Crowther RA, Walker JE, Klug A. 1988. Cloning and sequencing of the cDNA encoding a core protein of the paired helical filament of Alzheimer disease: identification as the microtubule-associated protein tau. *Proc Natl Acad Sci U S A* **85**:4051–4055.

Goldgaber D, Harris HW, Hla T, Maciag T, Donnelly RJ, Jacobsen JS, Vitek MP, Gajdusek DC. 1989. Interleukin 1 regulates synthesis of amyloid beta-protein precursor mRNA in human endothelial cells. *Proc Natl Acad Sci U S A* **86**:7606–7610. doi:10.1073/pnas.86.19.7606

Gómez-Ramos A, Díaz-Hernández M, Cuadros R, Hernández F, Avila J. 2006. Extracellular tau is toxic to neuronal cells. *FEBS Letters* **580**:4842–4850. doi:10.1016/j.febslet.2006.07.078

Gómez-Ramos A, Díaz-Hernández M, Rubio A, Miras-Portugal MT, Avila J. 2008. Extracellular tau promotes intracellular calcium increase through M1 and M3 muscarinic receptors in neuronal cells. *Molecular and Cellular Neuroscience* **37**:673–681. doi:10.1016/j.mcn.2007.12.010

Goodman Y, Mattson MP. 1994. Secreted forms of beta-amyloid precursor protein protect hippocampal neurons against amyloid beta-peptide-induced oxidative injury. *Exp Neurol* **128**:1–12. doi:10.1006/exnr.1994.1107

Götz J, Chen F, van Dorpe J, Nitsch RM. 2001. Formation of neurofibrillary tangles in P301l tau transgenic mice induced by Abeta 42 fibrils. *Science* **293**:1491–1495. doi:10.1126/science.1062097

Gouveia K, Hurst JL. 2013. Reducing Mouse Anxiety during Handling: Effect of Experience with Handling Tunnels. *PLOS ONE* **8**:e66401. doi:10.1371/journal.pone.0066401

Gowing E, Roher AE, Woods AS, Cotter RJ, Chaney M, Little SP, Ball MJ. 1994. Chemical characterization of A beta 17-42 peptide, a component of diffuse amyloid deposits of Alzheimer disease. *Journal of Biological Chemistry* **269**:10987–10990. doi:10.1016/S0021-9258(19)78080-6

Grajski KA, Bressler SL. 2019. Differential medial temporal lobe and default-mode network functional connectivity and morphometric changes in Alzheimer's disease. *NeuroImage: Clinical* **23**:101860. doi:10.1016/j.nicl.2019.101860

Granholm E, Butters N. 1988. Associative encoding and retrieval in Alzheimer's and Huntington's disease. *Brain Cogn* **7**:335–347. doi:10.1016/0278-2626(88)90007-3

Greenberg GD, Howerton CL, Trainor BC. 2014. Fighting in the home cage: Agonistic encounters and effects on neurobiological markers within the social decision-making network of house mice (Mus musculus). *Neuroscience Letters* **566**:151–155. doi:10.1016/j.neulet.2014.02.051

Greicius MD, Supekar K, Menon V, Dougherty RF. 2009. Resting-State Functional Connectivity Reflects Structural Connectivity in the Default Mode Network. *Cereb Cortex* **19**:72–78. doi:10.1093/cercor/bhn059

Guardia-Laguarta C, Pera M, Clarimón J, Molinuevo JL, Sánchez-Valle R, Lladó A, Coma M, Gómez-Isla T, Blesa R, Ferrer I, Lleó A. 2010. Clinical, neuropathologic, and biochemical profile of the amyloid precursor protein I716F mutation. *J Neuropathol Exp Neurol* **69**:53–59. doi:10.1097/NEN.0b013e3181c6b84d

Guillot-Sestier M-V, Sunyach C, Ferreira ST, Marzolo M-P, Bauer C, Thevenet A, Checler F. 2012. α-Secretase-derived Fragment of Cellular Prion, N1, Protects against Monomeric and Oligomeric Amyloid β (Aβ)-associated Cell Death. *J Biol Chem* **287**:5021–5032. doi:10.1074/jbc.M111.323626

Guo Q, Li H, Cole AL, Hur J-Y, Li Y, Zheng H. 2013. Modeling Alzheimer's Disease in Mouse without Mutant Protein Overexpression: Cooperative and Independent Effects of Aβ and Tau. *PLOS ONE* **8**:e80706. doi:10.1371/journal.pone.0080706

Gurumurthy CB, Lloyd KCK. 2019. Generating mouse models for biomedical research: technological advances. *Disease Models & Mechanisms* **12**. doi:10.1242/dmm.029462

Gustafson L, Brun A, Englund E, Hagnell O, Nilsson K, Stensmyr M, Öhlin A-K, Abrahamson M. 1998. A 50-year perspective of a family with chromosome-14-linked Alzheimer's disease. *Human Genetics* **102**:253–257. doi:10.1007/s004390050688

Haass C, Kaether C, Thinakaran G, Sisodia S. 2012. Trafficking and Proteolytic Processing of APP. *Cold Spring Harb Perspect Med* **2**. doi:10.1101/cshperspect.a006270

Hales JB, Brewer JB. 2011. The timing of associative memory formation: frontal lobe and anterior medial temporal lobe activity at associative binding predicts memory. *J Neurophysiol* **105**:1454–1463. doi:10.1152/jn.00902.2010

Hales JB, Schlesiger MI, Leutgeb JK, Squire LR, Leutgeb S, Clark RE. 2014. Medial Entorhinal Cortex Lesions Only Partially Disrupt Hippocampal Place Cells and Hippocampus-Dependent Place Memory. *Cell Reports* **9**:893–901. doi:10.1016/j.celrep.2014.10.009

Hamaguchi T, Eisele YS, Varvel NH, Lamb BT, Walker LC, Jucker M. 2012. The presence of Aβ seeds, and not age per se, is critical to the initiation of Aβ deposition in the brain. *Acta Neuropathol* **123**:31–37. doi:10.1007/s00401-011-0912-1

Hämäläinen A, Pihlajamäki M, Tanila H, Hänninen T, Niskanen E, Tervo S, Karjalainen PA, Vanninen RL, Soininen H. 2007. Increased fMRI responses during encoding in mild cognitive impairment. *Neurobiol Aging* **28**:1889–1903. doi:10.1016/j.neurobiolaging.2006.08.008

Hamm V, Héraud C, Bott J-B, Herbeaux K, Strittmatter C, Mathis C, Goutagny R. 2017. Differential contribution of APP metabolites to early cognitive deficits in a TgCRND8 mouse model of Alzheimer's disease. *Sci Adv* **3**:e1601068. doi:10.1126/sciadv.1601068

Hammond RS, Tull LE, Stackman RW. 2004. On the delay-dependent involvement of the hippocampus in object recognition memory. *Neurobiol Learn Mem* **82**:26–34. doi:10.1016/j.nlm.2004.03.005

Hampstead BM, Stringer AY, Stilla RF, Amaraneni A, Sathian K. 2011. Where did I put that? Patients with amnestic mild cognitive impairment demonstrate widespread reductions in activity during the encoding of ecologically relevant object-location associations. *Neuropsychologia* **49**:2349–2361. doi:10.1016/j.neuropsychologia.2011.04.008

Hampstead BM, Towler S, Stringer AY, Sathian K. 2018. Continuous measurement of object location memory is sensitive to effects of age and mild cognitive impairment and related to medial temporal lobe volume. *Alzheimers Dement (Amst)* **10**:76–85. doi:10.1016/j.dadm.2017.10.007

Han P, Dou F, Li F, Zhang X, Zhang Y-W, Zheng H, Lipton SA, Xu H, Liao F-F. 2005. Suppression of cyclin-dependent kinase 5 activation by amyloid precursor protein: a novel excitoprotective mechanism involving modulation of tau phosphorylation. *J Neurosci* **25**:11542–11552. doi:10.1523/JNEUROSCI.3831-05.2005

Harada A, Oguchi K, Okabe S, Kuno J, Terada S, Ohshima T, Sato-Yoshitake R, Takei Y, Noda T, Hirokawa N. 1994. Altered microtubule organization in small-calibre axons of mice lacking tau protein. *Nature* **369**:488–491. doi:10.1038/369488a0

Hardy J, Allsop D. 1991. Amyloid deposition as the central event in the aetiology of Alzheimer's disease. *Trends Pharmacol Sci* **12**:383–388. doi:10.1016/0165-6147(91)90609-v

Hardy JA, Higgins GA. 1992. Alzheimer's disease: the amyloid cascade hypothesis. *Science* **256**:184–185. doi:10.1126/science.1566067

Hashimoto S, Matsuba Y, Kamano N, Mihira N, Sahara N, Takano J, Muramatsu S, Saido TC, Saito T. 2019. Tau binding protein CAPON induces tau aggregation and neurodegeneration. *Nat Commun* **10**:2394. doi:10.1038/s41467-019-10278-x

He W, Goodkind D, Kowal P. 2016. An Aging World: 2015. doi:10.13140/RG.2.1.1088.9362

Heber S, Herms J, Gajic V, Hainfellner J, Aguzzi A, Rülicke T, von Kretzschmar H, von Koch C, Sisodia S, Tremml P, Lipp HP, Wolfer DP, Müller U. 2000. Mice with combined gene knock-outs reveal essential and partially redundant functions of amyloid precursor protein family members. *J Neurosci* **20**:7951–7963.

Hébert SS, Serneels L, Tolia A, Craessaerts K, Derks C, Filippov MA, Müller U, De Strooper B. 2006. Regulated intramembrane proteolysis of amyloid precursor protein and regulation of expression of putative target genes. *EMBO Rep* **7**:739–745. doi:10.1038/sj.embor.7400704

Hedden T, Dijk KRAV, Becker JA, Mehta A, Sperling RA, Johnson KA, Buckner RL. 2009. Disruption of Functional Connectivity in Clinically Normal Older Adults Harboring Amyloid Burden. *J Neurosci* **29**:12686–12694. doi:10.1523/JNEUROSCI.3189-09.2009

Heimer-McGinn VR, Poeta DL, Aghi K, Udawatta M, Burwell RD. 2017. Disconnection of the Perirhinal and Postrhinal Cortices Impairs Recognition of Objects in Context But Not Contextual Fear Conditioning. *J Neurosci* **37**:4819–4829. doi:10.1523/JNEUROSCI.0254-17.2017

Hernandez AR, Reasor JE, Truckenbrod LM, Lubke KN, Johnson SA, Bizon JL, Maurer AP, Burke SN. 2017. Medial prefrontal-perirhinal cortical communication is necessary for flexible response selection. *Neurobiology of Learning and Memory* **137**:36–47. doi:10.1016/j.nlm.2016.10.012

Herzog V, Kirfel G, Siemes C, Schmitz A. 2004. Biological roles of APP in the epidermis. *Eur J Cell Biol* **83**:613–624. doi:10.1078/0171-9335-00401

Hick M, Herrmann U, Weyer SW, Mallm J-P, Tschäpe J-A, Borgers M, Mercken M, Roth FC, Draguhn A, Slomianka L, Wolfer DP, Korte M, Müller UC. 2015. Acute function of secreted amyloid precursor protein fragment APPsα in synaptic plasticity. *Acta Neuropathol* **129**:21–37. doi:10.1007/s00401-014-1368-x

Hickman SE, Allison EK, El Khoury J. 2008. Microglial dysfunction and defective beta-amyloid clearance pathways in aging Alzheimer's disease mice. *J Neurosci* **28**:8354–8360. doi:10.1523/JNEUROSCI.0616-08.2008

Higaki N, Goto T, Ichikawa T. 2016. Periodontal tactile input activates the prefrontal cortex. *Scientific Reports* **6**:36893. doi:10.1038/srep36893

Hirni DI, Kivisaari SL, Krumm S, Monsch AU, Berres M, Oeksuez F, Reinhardt J, Ulmer S, Kressig RW, Stippich C, Taylor KI. 2016. Neuropsychological Markers of Medial Perirhinal and Entorhinal Cortex Functioning are Impaired Twelve Years Preceding Diagnosis of Alzheimer's Dementia. *JAD* **52**:573–580. doi:10.3233/JAD-150158

Hoe H-S, Lee KJ, Carney RSE, Lee J, Markova A, Lee J-Y, Howell BW, Hyman BT, Pak DTS, Bu G, Rebeck GW. 2009. Interaction of reelin with amyloid precursor protein promotes neurite outgrowth. *J Neurosci* **29**:7459–7473. doi:10.1523/JNEUROSCI.4872-08.2009

Höfling C, Morawski M, Zeitschel U, Zanier ER, Moschke K, Serdaroglu A, Canneva F, von Hörsten S, De Simoni M-G, Forloni G, Jäger C, Kremmer E, Roßner S, Lichtenthaler SF, Kuhn P-H. 2016. Differential transgene expression patterns in Alzheimer mouse models revealed by novel human amyloid precursor protein-specific antibodies. *Aging Cell* **15**:953–963. doi:10.1111/acel.12508

Homolak J, Mudrovčić M, Vukić B, Toljan K. 2018. Circadian Rhythm and Alzheimer's Disease. *Med Sci (Basel)* **6**. doi:10.3390/medsci6030052

Hong X-P, Peng C-X, Wei W, Tian Q, Liu Y-H, Yao X-Q, Zhang Y, Cao F-Y, Wang Q, Wang J-Z. 2010. Essential role of tau phosphorylation in adult hippocampal neurogenesis. *Hippocampus* **20**:1339–1349. doi:https://doi.org/10.1002/hipo.20712

Hsiao K, Chapman P, Nilsen S, Eckman C, Harigaya Y, Younkin S, Yang F, Cole G. 1996. Correlative memory deficits, Abeta elevation, and amyloid plaques in transgenic mice. *Science* **274**:99–102. doi:10.1126/science.274.5284.99

http://fyra.io. n.d. Preclinical, Prodromal, and Dementia Stages of Alzheimer's Disease. *Practical Neurology*. https://practicalneurology.com/articles/2019-june/preclinical-prodromal-and-dementia-stages-ofalzheimers-disease/pdf

Huang S-M, Mouri A, Kokubo H, Nakajima R, Suemoto T, Higuchi M, Staufenbiel M, Noda Y, Yamaguchi H, Nabeshima T, Saido TC, Iwata N. 2006. Neprilysin-sensitive Synapse-associated Amyloid-β Peptide Oligomers Impair Neuronal Plasticity and Cognitive Function*,. *Journal of Biological Chemistry* **281**:17941–17951. doi:10.1074/jbc.M601372200

Huijbers W, Mormino EC, Schultz AP, Wigman S, Ward AM, Larvie M, Amariglio RE, Marshall GA, Rentz DM, Johnson KA, Sperling RA. 2015. Amyloid-β deposition in mild cognitive impairment is associated with increased hippocampal activity, atrophy and clinical progression. *Brain* **138**:1023–1035. doi:10.1093/brain/awv007

Huijbers W, Schultz AP, Papp KV, LaPoint MR, Hanseeuw B, Chhatwal JP, Hedden T, Johnson KA, Sperling RA. 2019. Tau Accumulation in Clinically Normal Older Adults Is Associated with Hippocampal Hyper-activity. *J Neurosci* **39**:548–556. doi:10.1523/JNEUROSCI.1397-18.2018

Hunsaker MR, Chen V, Tran GT, Kesner RP. 2013. The medial and lateral entorhinal cortex both contribute to contextual and item recognition memory: A test of the binding ofitems and context model. *Hippocampus* **23**:380–391. doi:10.1002/hipo.22097

Hunsaker MR, Kesner RP. 2013. The operation of pattern separation and pattern completion processes associated with different attributes or domains of memory. *Neuroscience & Biobehavioral Reviews* **37**:36–58. doi:10.1016/j.neubiorev.2012.09.014

Hyman B, Van Hoesen G, Damasio A, Barnes C. 1984. Alzheimer's disease: cell-specific pathology isolates the hippocampal formation. *Science* **225**:1168–1170. doi:10.1126/science.6474172

International AD, Wimo A, Ali G-C, Guerchet M, Prince M, Prina M, Wu Y-T. 2015. World Alzheimer Report 2015: The global impact of dementia: An analysis of prevalence, incidence, cost and trends.

Ishida A, Furukawa K, Keller JN, Mattson MP. 1997. Secreted form of beta-amyloid precursor protein shifts the frequency dependency for induction of LTD, and enhances LTP in hippocampal slices. *Neuroreport* **8**:2133–2137. doi:10.1097/00001756-199707070-00009

Izumi H, Shinoda Y, Saito T, Saido TC, Sato K, Yabuki Y, Matsumoto Y, Kanemitsu Y, Tomioka Y, Abolhassani N, Nakabeppu Y, Fukunaga K. 2018. The Disease-modifying Drug Candidate, SAK3 Improves Cognitive Impairment and Inhibits Amyloid beta Deposition in App Knock-in Mice. *Neuroscience* **377**:87–97. doi:10.1016/j.neuroscience.2018.02.031

Jack CR, Bennett DA, Blennow K, Carrillo MC, Feldman HH, Frisoni GB, Hampel H, Jagust WJ, Johnson KA, Knopman DS, Petersen RC, Scheltens P, Sperling RA, Dubois B. 2016. A/T/N: An unbiased descriptive classification scheme for Alzheimer disease biomarkers. *Neurology* **87**:539–547. doi:10.1212/WNL.0000000000002923

Jack CR, Knopman DS, Jagust WJ, Petersen RC, Weiner MW, Aisen PS, Shaw LM, Vemuri P, Wiste HJ, Weigand SD, Lesnick TG, Pankratz VS, Donohue MC, Trojanowski JQ. 2013. Tracking pathophysiological processes in Alzheimer's disease: an updated hypothetical model of dynamic biomarkers. *Lancet Neurol* **12**:207–216. doi:10.1016/S1474-4422(12)70291-0

Jack CR, Knopman DS, Jagust WJ, Shaw LM, Aisen PS, Weiner MW, Petersen RC, Trojanowski JQ. 2010. Hypothetical model of dynamic biomarkers of the Alzheimer's pathological cascade. *Lancet Neurol* **9**:119–128. doi:10.1016/S1474-4422(09)70299-6

Jackson J, Karnani MM, Zemelman BV, Burdakov D, Lee AK. 2018. Inhibitory Control of Prefrontal Cortex by the Claustrum. *Neuron* **99**:1029-1039.e4. doi:10.1016/j.neuron.2018.07.031

Jacob P-Y, Casali G, Spieser L, Page H, Overington D, Jeffery K. 2017. An independent, landmark-dominated head-direction signal in dysgranular retrosplenial cortex. *Nature Neuroscience* **20**:173–175. doi:10.1038/nn.4465

Jacob P-Y, Van Cauter T, Poucet B, Sargolini F, Save E. 2020. Medial entorhinal cortex lesions induce degradation of CA1 place cell firing stability when self-motion information is used. *Brain and Neuroscience Advances* **4**:2398212820953004. doi:10.1177/2398212820953004

Jagust W. 2018. Imaging the evolution and pathophysiology of Alzheimer disease. *Nature Reviews Neuroscience* **19**:687–700. doi:10.1038/s41583-018-0067-3

James LE, Fogler KA, Tauber SK. 2008. Recognition Memory Measures Yield Disproportionate Effects of Aging on Learning Face-Name Associations. *Psychol Aging* **23**:657–664. doi:10.1037/a0013008

Jankowsky JL, Slunt HH, Gonzales V, Jenkins NA, Copeland NG, Borchelt DR. 2004. APP processing and amyloid deposition in mice haplo-insufficient for presenilin 1. *Neurobiol Aging* **25**:885–892. doi:10.1016/j.neurobiolaging.2003.09.008

Jansen IE, Savage JE, Watanabe K, Bryois J, Williams DM, Steinberg S, Sealock J, Karlsson IK, Hägg S, Athanasiu L, Voyle N, Proitsi P, Witoelar A, Stringer S, Aarsland D, Almdahl IS, Andersen F, Bergh S, Bettella F, Bjornsson S, Brækhus A, Bråthen G, Leeuw C de, Desikan RS, Djurovic S, Dumitrescu L, Fladby T, Hohman TJ, Jonsson PV, Kiddle SJ, Rongve A, Saltvedt I, Sando SB, Selbæk G, Shoai M, Skene NG, Snaedal J, Stordal E, Ulstein ID, Wang Y, White LR, Hardy J, Hjerling-Leffler J, Sullivan PF, Flier WM van der, Dobson R, Davis LK, Stefansson H, Stefansson K, Pedersen NL, Ripke S, Andreassen OA, Posthuma D. 2019. Genome-wide meta-analysis identifies new loci and functional pathways influencing Alzheimer's disease risk. *Nat Genet* **51**:404–413. doi:10.1038/s41588-018-0311-9

Johnson SC, Schmitz TW, Moritz CH, Meyerand ME, Rowley HA, Alexander AL, Hansen KW, Gleason CE, Carlsson CM, Ries ML, Asthana S, Chen K, Reiman EM, Alexander GE. 2006a. Activation of brain regions vulnerable to Alzheimer's disease: The effect of mild cognitive impairment. *Neurobiology of Aging* **27**:1604–1612. doi:10.1016/j.neurobiolaging.2005.09.017

Johnson SC, Schmitz TW, Trivedi MA, Ries ML, Torgerson BM, Carlsson CM, Asthana S, Hermann BP, Sager MA. 2006b. The Influence of Alzheimer Disease Family History and Apolipoprotein E ε4 on Mesial Temporal Lobe Activation. *J Neurosci* **26**:6069–6076. doi:10.1523/JNEUROSCI.0959-06.2006

Jones DT, Graff-Radford J, Lowe VJ, Wiste HJ, Gunter JL, Senjem ML, Botha H, Kantarci K, Boeve BF, Knopman DS, Petersen RC, Jack CR. 2017. Tau, amyloid, and cascading network failure across the Alzheimer's disease spectrum. *Cortex*, Special Section dedicated to the temporal and parietal lobes **97**:143–159. doi:10.1016/j.cortex.2017.09.018

Jones DT, Knopman DS, Gunter JL, Graff-Radford J, Vemuri P, Boeve BF, Petersen RC, Weiner MW, Jack CR Jr, on behalf of the Alzheimer's Disease Neuroimaging Initiative. 2016. Cascading network failure across the Alzheimer's disease spectrum. *Brain* **139**:547–562. doi:10.1093/brain/awv338

Jones DT, Vemuri P, Murphy MC, Gunter JL, Senjem ML, Machulda MM, Przybelski SA, Gregg BE, Kantarci K, Knopman DS, Boeve BF, Petersen RC, Jr CRJ. 2012. Non-Stationarity in the "Resting Brain's" Modular Architecture. *PLOS ONE* **7**:e39731. doi:10.1371/journal.pone.0039731

Jouanne M, Rault S, Voisin-Chiret A-S. 2017. Tau protein aggregation in Alzheimer's disease: An attractive target for the development of novel therapeutic agents. *European Journal of Medicinal Chemistry* **139**:153–167. doi:10.1016/j.ejmech.2017.07.070

Jucker M, Walker LC. 2013. Self-propagation of pathogenic protein aggregates in neurodegenerative diseases. *Nature* **501**:45–51. doi:10.1038/nature12481

Kaboodvand N, Bäckman L, Nyberg L, Salami A. 2018. The retrosplenial cortex: A memory gateway between the cortical default mode network and the medial temporal lobe. *Hum Brain Mapp* **39**:2020–2034. doi:10.1002/hbm.23983

Kanaan NM, Morfini GA, LaPointe NE, Pigino GF, Patterson KR, Song Y, Andreadis A, Fu Y, Brady ST, Binder LI. 2011. Pathogenic forms of tau inhibit kinesin-dependent axonal transport through a mechanism involving activation of axonal phosphotransferases. *J Neurosci* **31**:9858–9868. doi:10.1523/JNEUROSCI.0560-11.2011

Kane MD, Lipinski WJ, Callahan MJ, Bian F, Durham RA, Schwarz RD, Roher AE, Walker LC. 2000. Evidence for seeding of beta -amyloid by intracerebral infusion of Alzheimer brain extracts in beta -amyloid precursor protein-transgenic mice. *J Neurosci* **20**:3606–3611.

Kantarci K, Schwarz CG, Reid R, Przybelski SA, Lesnick T, Zuk SM, Senjem ML, Gunter JL, Lowe V, Machulda MM, Knopman DS, Petersen RC, Jack CR. 2014. White Matter Integrity on DTI, Amyloid Load, and Neurodegeneration in Non-demented Elderly. *JAMA Neurol* **71**:1547–1554. doi:10.1001/jamaneurol.2014.1482

Kent B, Heath C, Kim C-H, Ahrens R, Fraser P, George-Hyslop P, Bussey T, Saksida L. 2017. Longitudinal evaluation of Tau-P301L transgenic mice reveals no cognitive impairments at 17 months of age. *Brain and Behavior* **8**:e00896. doi:10.1002/brb3.896

Kerr KM, Agster KL, Furtak SC, Burwell RD. 2007. Functional neuroanatomy of the parahippocampal region: the lateral and medial entorhinal areas. *Hippocampus* **17**:697–708. doi:10.1002/hipo.20315

Kerridge C, Kozlova DI, Nalivaeva NN, Turner AJ. 2015. Hypoxia Affects Neprilysin Expression Through Caspase Activation and an APP Intracellular Domain-dependent Mechanism. *Front Neurosci* **9**. doi:10.3389/fnins.2015.00426

Khan UA, Liu L, Provenzano FA, Berman DE, Profaci CP, Sloan R, Mayeux R, Duff KE, Small SA. 2014. Molecular drivers and cortical spread of lateral entorhinal cortex dysfunction in preclinical Alzheimer's disease. *Nat Neurosci* **17**:304–311. doi:10.1038/nn.3606

Kida T, Shinohara K. 2013. Gentle touch activates the anterior prefrontal cortex: An NIRS study. *Neuroscience Research* **76**:76–82. doi:10.1016/j.neures.2013.03.006

Kidd M. 1964. ALZHEIMER'S DISEASE--AN ELECTRON MICROSCOPICAL STUDY. *Brain* **87**:307–320. doi:10.1093/brain/87.2.307

Killin LOJ, Starr JM, Shiue IJ, Russ TC. 2016. Environmental risk factors for dementia: a systematic review. *BMC Geriatrics* **16**:175. doi:10.1186/s12877-016-0342-y

Kim HS, Park CH, Cha SH, Lee JH, Lee S, Kim Y, Rah JC, Jeong SJ, Suh YH. 2000. Carboxyl-terminal fragment of Alzheimer's APP destabilizes calcium homeostasis and renders neuronal cells vulnerable to excitotoxicity. *FASEB J* **14**:1508–1517. doi:10.1096/fj.14.11.1508

Kim J, Onstead L, Randle S, Price R, Smithson L, Zwizinski C, Dickson DW, Golde T, McGowan E. 2007. Abeta40 inhibits amyloid deposition in vivo. *J Neurosci* **27**:627–633. doi:10.1523/JNEUROSCI.4849-06.2007

Kim M-J, Lee K-M, Son Y-D, Jeon H-A, Kim Y-B, Cho Z-H. 2012. Increased basal forebrain metabolism in mild cognitive impairment: an evidence for brain reserve in incipient dementia. *J Alzheimers Dis* **32**:927–938. doi:10.3233/JAD-2012-120133

Kimberly WT, Zheng JB, Guénette SY, Selkoe DJ. 2001. The Intracellular Domain of the β-Amyloid Precursor Protein Is Stabilized by Fe65 and Translocates to the Nucleus in a Notch-like Manner*. *Journal of Biological Chemistry* **276**:40288–40292. doi:10.1074/jbc.C100447200

Kinnavane L, Albasser MM, Aggleton JP. May 15, 2015a. Advances in the behavioural testing and network imaging of rodent recognition memory. *Behavioural Brain Research*, SI: Object Recognition Memory in Rats and Mice **285**:67–78. doi:10.1016/j.bbr.2014.07.049

Kinnavane L, Amin E, Olarte-Sánchez CM, Aggleton JP. 2016. Detecting and discriminating novel objects: The impact of perirhinal cortex disconnection on hippocampal activity patterns. *Hippocampus* **26**:1393–1413. doi:10.1002/hipo.22615

Kinney JW, Bemiller SM, Murtishaw AS, Leisgang AM, Salazar AM, Lamb BT. 2018. Inflammation as a central mechanism in Alzheimer's disease. *Alzheimer's & Dementia: Translational Research & Clinical Interventions* **4**:575–590. doi:https://doi.org/10.1016/j.trci.2018.06.014

Kircher TT, Weis S, Freymann K, Erb M, Jessen F, Grodd W, Heun R, Leube DT. 2007. Hippocampal activation in patients with mild cognitive impairment is necessary for successful memory encoding. *J Neurol Neurosurg Psychiatry* **78**:812–818. doi:10.1136/jnnp.2006.104877

Kitanishi T, Matsuo N. 2017. Organization of the Claustrum-to-Entorhinal Cortical Connection in Mice. *J Neurosci* **37**:269–280. doi:10.1523/JNEUROSCI.1360-16.2016

Klein C, Roussel G, Brun S, Rusu C, Patte-Mensah C, Maitre M, Mensah-Nyagan A-G. 2018. 5-HIAA induces neprilysin to ameliorate pathophysiology and symptoms in a mouse model for Alzheimer's disease. *Acta Neuropathologica Communications* **6**:136. doi:10.1186/s40478-018-0640-z

Klunk WE, Engler H, Nordberg A, Wang Y, Blomqvist G, Holt DP, Bergström M, Savitcheva I, Huang G, Estrada S, Ausén B, Debnath ML, Barletta J, Price JC, Sandell J, Lopresti BJ, Wall A, Koivisto P, Antoni G, Mathis CA, Långström B. 2004. Imaging brain amyloid in Alzheimer's disease with Pittsburgh Compound-B. *Ann Neurol* **55**:306–319. doi:10.1002/ana.20009

Klyubin I, Betts V, Welzel AT, Blennow K, Zetterberg H, Wallin A, Lemere CA, Cullen WK, Peng Y, Wisniewski T, Selkoe DJ, Anwyl R, Walsh DM, Rowan MJ. 2008. Amyloid β Protein Dimer-Containing Human CSF Disrupts Synaptic Plasticity: Prevention by Systemic Passive Immunization. *J Neurosci* **28**:4231–4237. doi:10.1523/JNEUROSCI.5161-07.2008

Kobayashi Y, Amaral DG. 2007. Macaque monkey retrosplenial cortex: III. Cortical efferents. *J Comp Neurol* **502**:810–833. doi:10.1002/cne.21346

Kobayashi Y, Amaral DG. 2003. Macaque monkey retrosplenial cortex: II. Cortical afferents. *Journal of Comparative Neurology* **466**:48–79. doi:https://doi.org/10.1002/cne.10883

Kolata G. 1985. Down syndrome--Alzheimer's linked. *Science* **230**:1152–1153. doi:10.1126/science.2933807

Konietzko U. 2012. AICD nuclear signaling and its possible contribution to Alzheimer's disease. *Curr Alzheimer Res* **9**:200–216. doi:10.2174/156720512799361673

Koo EH, Park L, Selkoe DJ. 1993. Amyloid beta-protein as a substrate interacts with extracellular matrix to promote neurite outgrowth. *Proc Natl Acad Sci U S A* **90**:4748–4752.

Kosik KS, McConlogue L. 1994. Microtubule-associated protein function: lessons from expression in Spodoptera frugiperda cells. *Cell Motil Cytoskeleton* **28**:195–198. doi:10.1002/cm.970280302

Krimmel SR, White MG, Panicker MH, Barrett FS, Mathur BN, Seminowicz DA. 2019. Resting state functional connectivity and cognitive task-related activation of the human claustrum. *NeuroImage* **196**:59–67. doi:10.1016/j.neuroimage.2019.03.075

Kubota T, Matsumoto H, Kirino Y. 2016. Ameliorative effect of membrane-associated estrogen receptor G protein coupled receptor 30 activation on object recognition memory in mouse models of Alzheimer's disease. *Journal of Pharmacological Sciences* **131**:219–222. doi:10.1016/j.jphs.2016.06.005

Kumar S, Rezaei-Ghaleh N, Terwel D, Thal DR, Richard M, Hoch M, Mc Donald JM, Wüllner U, Glebov K, Heneka MT, Walsh DM, Zweckstetter M, Walter J. 2011. Extracellular phosphorylation of the amyloid β-peptide promotes formation of toxic aggregates during the pathogenesis of Alzheimer's disease. *EMBO J* **30**:2255–2265. doi:10.1038/emboj.2011.138

Kummer MP, Hermes M, Delekarte A, Hammerschmidt T, Kumar S, Terwel D, Walter J, Pape H-C, König S, Roeber S, Jessen F, Klockgether T, Korte M, Heneka MT. 2011. Nitration of tyrosine 10 critically enhances amyloid β aggregation and plaque formation. *Neuron* **71**:833–844. doi:10.1016/j.neuron.2011.07.001

Lambert J-C, Ibrahim-Verbaas CA, Harold D, Naj AC, Sims R, Bellenguez C, Jun G, DeStefano AL, Bis JC, Beecham GW, Grenier-Boley B, Russo G, Thornton-Wells TA, Jones N, Smith AV, Chouraki V, Thomas C, Ikram MA, Zelenika D, Vardarajan BN, Kamatani Y, Lin C-F, Gerrish A, Schmidt H, Kunkle B, Dunstan ML, Ruiz A, Bihoreau M-T, Choi S-H, Reitz C, Pasquier F, Hollingworth P, Ramirez A, Hanon O, Fitzpatrick AL, Buxbaum JD, Campion D, Crane PK, Baldwin C, Becker T, Gudnason V, Cruchaga C, Craig D, Amin N, Berr C, Lopez OL, Jager PLD, Deramecourt V, Johnston JA, Evans D, Lovestone S, Letenneur L, Morón FJ, Rubinsztein DC, Eiriksdottir G, Sleegers K, Goate AM, Fiévet N, Huentelman MJ, Gill M, Brown K, Kamboh MI, Keller L, Barberger-Gateau P, McGuinness B, Larson EB, Green R, Myers AJ, Dufouil C, Todd S, Wallon D, Love S, Rogaeva E, Gallacher J, George-Hyslop PS, Clarimon J, Lleo A, Bayer A, Tsuang DW, Yu L, Tsolaki M, Bossù P, Spalletta G, Proitsi P, Collinge J, Sorbi S, Sanchez-Garcia F, Fox NC, Hardy J, Naranjo MCD, Bosco P, Clarke R, Brayne C, Galimberti D, Mancuso M, Matthews F, Moebus S, Mecocci P, Zompo MD, Maier W, Hampel H, Pilotto A, Bullido M, Panza F, Caffarra P, Nacmias B, Gilbert JR, Mayhaus M, Lannfelt L, Hakonarson H, Pichler S, Carrasquillo MM, Ingelsson M, Beekly D, Alvarez V, Zou F, Valladares O, Younkin SG, Coto E, Hamilton-Nelson KL, Gu W, Razquin C, Pastor P, Mateo I, Owen MJ, Faber KM, Jonsson PV, Combarros O, O'Donovan MC, Cantwell LB, Soininen H, Blacker D, Mead S, Mosley TH, Bennett DA, Harris TB, Fratiglioni L, Holmes C, Bruijn RFAG de, Passmore P, Montine TJ, Bettens K, Rotter JI, Brice A, Morgan K, Foroud TM, Kukull WA, Hannequin D, Powell JF, Nalls MA, Ritchie K, Lunetta KL, Kauwe JSK, Boerwinkle E, Riemenschneider M, Boada M, Hiltunen M, Martin ER, Schmidt R, Rujescu D, Wang L-S, Dartigues J-F, Mayeux R, Tzourio C, Hofman A, Nöthen MM, Graff C, Psaty BM, Jones L, Haines JL, Holmans PA, Lathrop M, Pericak-Vance MA, Launer LJ, Farrer LA, Duijn CM van, Broeckhoven CV, Moskvina V, Seshadri S, Williams J, Schellenberg GD, Amouyel P. 2013. Meta-analysis of 74,046 individuals identifies 11 new susceptibility loci for Alzheimer's disease. *Nat Genet* **45**:1452–1458. doi:10.1038/ng.2802

Langa KM, Levine DA. 2014. The Diagnosis and Management of Mild Cognitive Impairment: A Clinical Review. *JAMA* **312**:2551–2561. doi:10.1001/jama.2014.13806

Langston RF, Wood ER. 2010. Associative recognition and the hippocampus: Differential effects of hippocampal lesions on object-place, object-context and object-place-context memory. *Hippocampus* **20**:1139–1153. doi:10.1002/hipo.20714

Lanté F, Chafai M, Raymond E, Salgueiro Peirera AR, Bethus I, Marie H. 2013. Early hippocampal synaptic plasticity and episodic like-memory deficits in a transgenic mouse model of Alzheimer disease - involvment of corticosterone. *Mol Neurodegeneration* **8**:P62. doi:10.1186/1750-1326-8-S1-P62

Lasagna-Reeves CA, Castillo-Carranza DL, Sengupta U, Clos AL, Jackson GR, Kayed R. 2011. Tau oligomers impair memory and induce synaptic and mitochondrial dysfunction in wild-type mice. *Mol Neurodegener* **6**:39. doi:10.1186/1750-1326-6-39

Lasagna-Reeves CA, Castillo-Carranza DL, Sengupta U, Sarmiento J, Troncoso J, Jackson GR, Kayed R. 2012. Identification of oligomers at early stages of tau aggregation in Alzheimer's disease. *FASEB J* **26**:1946–1959. doi:10.1096/fj.11-199851

Latif-Hernandez A, Shah D, Craessaerts K, Saido T, Saito T, De Strooper B, Van der Linden A, D'Hooge R. 2019. Subtle behavioral changes and increased prefrontal-hippocampal network synchronicity in APPNL-G-F mice before prominent plaque deposition. *Behav Brain Res* **364**:431–441. doi:10.1016/j.bbr.2017.11.017

Lauritzen I, Pardossi-Piquard R, Bauer C, Brigham E, Abraham J-D, Ranaldi S, Fraser P, St-George-Hyslop P, Thuc OL, Espin V, Chami L, Dunys J, Checler F. 2012. The β-Secretase-Derived C-Terminal Fragment of βAPP, C99, But Not Aβ, Is a Key Contributor to Early Intraneuronal Lesions in Triple-Transgenic Mouse Hippocampus. *J Neurosci* **32**:16243–16255. doi:10.1523/JNEUROSCI.2775-12.2012

Lauritzen I, Pardossi-Piquard R, Bourgeois A, Pagnotta S, Biferi M-G, Barkats M, Lacor P, Klein W, Bauer C, Checler F. 2016. Intraneuronal aggregation of the β-CTF fragment of APP (C99) induces Aβ-independent lysosomal-autophagic pathology. *Acta Neuropathol* **132**:257–276. doi:10.1007/s00401-016-1577-6

Lazarevic V, Fieńko S, Andres-Alonso M, Anni D, Ivanova D, Montenegro-Venegas C, Gundelfinger ED, Cousin MA, Fejtova A. 2017. Physiological Concentrations of Amyloid Beta Regulate Recycling of Synaptic Vesicles via Alpha7 Acetylcholine Receptor and CDK5/Calcineurin Signaling. *Front Mol Neurosci* **10**. doi:10.3389/fnmol.2017.00221

Leal SL, Lockhart SN, Maass A, Bell RK, Jagust WJ. 2018. Subthreshold Amyloid Predicts Tau Deposition in Aging. *J Neurosci* **38**:4482–4489. doi:10.1523/JNEUROSCI.0485-18.2018

Leal SL, Yassa MA. 2018. Integrating new findings and examining clinical applications of pattern separation. *Nature Neuroscience* **21**:163–173. doi:10.1038/s41593-017-0065-1

Lehmann M, Ghosh PM, Madison C, Laforce R, Corbetta-Rastelli C, Weiner MW, Greicius MD, Seeley WW, Gorno-Tempini ML, Rosen HJ, Miller BL, Jagust WJ, Rabinovici GD. 2013. Diverging patterns of amyloid deposition and hypometabolism in clinical variants of probable Alzheimer's disease. *Brain* **136**:844–858. doi:10.1093/brain/aws327

Lesburguères E, Tsokas P, Sacktor TC, Fenton AA. 2017. The Object Context-place-location Paradigm for Testing Spatial Memory in Mice. *Bio Protoc* **7**. doi:10.21769/BioProtoc.2231

Leutgeb JK, Leutgeb S, Moser M-B, Moser EI. 2007. Pattern separation in the dentate gyrus and CA3 of the hippocampus. *Science* **315**:961–966. doi:10.1126/science.1135801

Lewis J, Dickson DW, Lin WL, Chisholm L, Corral A, Jones G, Yen SH, Sahara N, Skipper L, Yager D, Eckman C, Hardy J, Hutton M, McGowan E. 2001. Enhanced neurofibrillary degeneration in transgenic mice expressing mutant tau and APP. *Science* **293**:1487–1491. doi:10.1126/science.1058189

Liang J, Li Y, Liu H, Zhang S, Wang M, Chu Y, Ye J, Xi Q, Zhao X. 2020. Increased intrinsic default-mode network activity as a compensatory mechanism in aMCI: a resting-state functional connectivity MRI study. *Aging* **12**:5907–5919. doi:10.18632/aging.102986

Lim MM, Gerstner JR, Holtzman DM. 2014. The sleep–wake cycle and Alzheimer's disease: what do we know? *Neurodegener Dis Manag* **4**:351–362. doi:10.2217/nmt.14.33

Lin S-Y, Lin C-P, Hsieh T-J, Lin C-F, Chen S-H, Chao Y-P, Chen Y-S, Hsu C-C, Kuo L-W. 2019. Multiparametric graph theoretical analysis reveals altered structural and functional network topology in Alzheimer's disease. *NeuroImage: Clinical* **22**:101680. doi:10.1016/j.nicl.2019.101680

Liu C, Song X, Nisbet R, Götz J. 2016. Co-immunoprecipitation with Tau Isoform-specific Antibodies Reveals Distinct Protein Interactions and Highlights a Putative Role for 2N Tau in Disease*. *Journal of Biological Chemistry* **291**:8173–8188. doi:10.1074/jbc.M115.641902

Liu J, Wu R, Johnson B, Vu J, Bass C, Li J-X. 2019. The Claustrum-Prefrontal Cortex Pathway Regulates Impulsive-Like Behavior. *J Neurosci* **39**:10071–10080. doi:10.1523/JNEUROSCI.1005-19.2019

Liu L, Drouet V, Wu JW, Witter MP, Small SA, Clelland C, Duff K. 2012. Trans-Synaptic Spread of Tau Pathology In Vivo. *PLOS ONE* **7**:e31302. doi:10.1371/journal.pone.0031302

Liu Z, Zhang Y, Yan H, Bai L, Dai R, Wei W, Zhong C, Xue T, Wang H, Feng Y, You Y, Zhang X, Tian J. 2012. Altered topological patterns of brain networks in mild cognitive impairment and Alzheimer's disease: A resting-state fMRI study. *Psychiatry Research: Neuroimaging* **202**:118–125. doi:10.1016/j.pscychresns.2012.03.002

Llorens-Martin M, Teixeira CM, Fuster-Matanzo A, Jurado-Arjona J, Borrell V, Soriano E, Avila J, Hernández F. 2012. Tau Isoform with Three Microtubule Binding Domains is a Marker of New Axons Generated from the Subgranular Zone in the Hippocampal Dentate Gyrus: Implications for Alzheimer's Disease. *JAD* **29**:921–930. doi:10.3233/JAD-2012-112057

Löffler J, Huber G. 1992. Beta-amyloid precursor protein isoforms in various rat brain regions and during brain development. *J Neurochem* **59**:1316–1324. doi:10.1111/j.1471-4159.1992.tb08443.x

Logan RW, McClung CA. 2019. Rhythms of life: circadian disruption and brain disorders across the lifespan. *Nature Reviews Neuroscience* **20**:49–65. doi:10.1038/s41583-018-0088-y

Lombardo D, Cassé-Perrot C, Ranjeva J-P, Le Troter A, Guye M, Wirsich J, Payoux P, Bartrés-Faz D, Bordet R, Richardson JC, Felician O, Jirsa V, Blin O, Didic M, Battaglia D. 2020. Modular slowing of resting-state dynamic functional connectivity as a marker of cognitive dysfunction induced by sleep deprivation. *NeuroImage* **222**:117155. doi:10.1016/j.neuroimage.2020.117155

Lourenço FC, Galvan V, Fombonne J, Corset V, Llambi F, Müller U, Bredesen DE, Mehlen P. 2009. Netrin-1 interacts with amyloid precursor protein and regulates amyloid-beta production. *Cell Death Differ* **16**:655–663. doi:10.1038/cdd.2008.191

Lu H, Zou Q, Gu H, Raichle ME, Stein EA, Yang Y. 2012. Rat brains also have a default mode network. *PNAS* **109**:3979–3984. doi:10.1073/pnas.1200506109

Lublin AL, Gandy S. 2010. Amyloid-beta oligomers: possible roles as key neurotoxins in Alzheimer's Disease. *Mt Sinai J Med* **77**:43–49. doi:10.1002/msj.20160

Lucey BP, McCullough A, Landsness EC, Toedebusch CD, McLeland JS, Zaza AM, Fagan AM, McCue L, Xiong C, Morris JC, Benzinger TLS, Holtzman DM. 2019. Reduced non-rapid eye movement sleep is associated with tau pathology in early Alzheimer's disease. *Sci Transl Med* **11**. doi:10.1126/scitranslmed.aau6550

Lue LF, Kuo YM, Roher AE, Brachova L, Shen Y, Sue L, Beach T, Kurth JH, Rydel RE, Rogers J. 1999. Soluble amyloid beta peptide concentration as a predictor of synaptic change in Alzheimer's disease. *Am J Pathol* **155**:853–862. doi:10.1016/s0002-9440(10)65184-x

Lue LF, Walker DG, Brachova L, Beach TG, Rogers J, Schmidt AM, Stern DM, Yan SD. 2001. Involvement of microglial receptor for advanced glycation endproducts (RAGE) in Alzheimer's disease: identification of a cellular activation mechanism. *Exp Neurol* **171**:29–45. doi:10.1006/exnr.2001.7732

Maass A, Berron D, Harrison TM, Adams JN, La Joie R, Baker S, Mellinger T, Bell RK, Swinnerton K, Inglis B, Rabinovici GD, Düzel E, Jagust WJ. 2019. Alzheimer's pathology targets distinct memory networks in the ageing brain. *Brain* **142**:2492–2509. doi:10.1093/brain/awz154

Maass A, Landau S, Baker SL, Horng A, Lockhart SN, La Joie R, Rabinovici GD, Jagust WJ. 2017. Comparison of multiple tau-PET measures as biomarkers in aging and Alzheimer's disease. *NeuroImage* **157**:448–463. doi:10.1016/j.neuroimage.2017.05.058

Maccioni RBJ. 2011. Tau protein in Alzheimer's disease. *Curr Alzheimer Res* **8**:607. doi:10.2174/156720511796717159

Maeda S, Sahara N, Saito Y, Murayama S, Ikai A, Takashima A. 2006. Increased levels of granular tau oligomers: an early sign of brain aging and Alzheimer's disease. *Neurosci Res* **54**:197–201. doi:10.1016/j.neures.2005.11.009

Mandelkow E, Mandelkow E-M. 1995. Microtubules and microtubule-associated proteins. *Current Opinion in Cell Biology* **7**:72–81. doi:10.1016/0955-0674(95)80047-6

Mander BA, Winer JR, Jagust WJ, Walker MP. 2016. Sleep: A novel mechanistic pathway, biomarker, and treatment target in the pathology of Alzheimer's disease? *Trends Neurosci* **39**:552–566. doi:10.1016/j.tins.2016.05.002

Manns JR, Eichenbaum H. 2009. A cognitive map for object memory in the hippocampus. *Learn Mem* **16**:616–624. doi:10.1101/lm.1484509

Mao D, Kandler S, McNaughton BL, Bonin V. 2017. Sparse orthogonal population representation of spatial context in the retrosplenial cortex. *Nature Communications* **8**:243. doi:10.1038/s41467-017-00180-9

Mark RJ, Hensley K, Butterfield DA, Mattson MP. 1995. Amyloid beta-peptide impairs ion-motive ATPase activities: evidence for a role in loss of neuronal Ca2+ homeostasis and cell death. *J Neurosci* **15**:6239–6249.

Marks SM, Lockhart SN, Baker SL, Jagust WJ. 2017. Tau and β-Amyloid Are Associated with Medial Temporal Lobe Structure, Function, and Memory Encoding in Normal Aging. *J Neurosci* **37**:3192–3201. doi:10.1523/JNEUROSCI.3769-16.2017

Marquié M, Normandin MD, Vanderburg CR, Costantino IM, Bien EA, Rycyna LG, Klunk WE, Mathis CA, Ikonomovic MD, Debnath ML, Vasdev N, Dickerson BC, Gomperts SN, Growdon JH, Johnson KA, Frosch MP, Hyman BT, Gómez-Isla T. 2015. Validating novel tau positron emission tomography tracer [F-18]-AV-1451 (T807) on postmortem brain tissue. *Ann Neurol* **78**:787–800. doi:10.1002/ana.24517

Marr RA, Guan H, Rockenstein E, Kindy M, Gage FH, Verma I, Masliah E, Hersh LB. 2004. Neprilysin regulates amyloid β peptide levels. *J Mol Neurosci* **22**:5–11. doi:10.1385/JMN:22:1-2:5

Masuda A, Kobayashi Y, Kogo N, Saito T, Saido TC, Itohara S. 2016. Cognitive deficits in single App knock-in mouse models. *Neurobiology of Learning and Memory*, MCCS 2016 **135**:73–82. doi:10.1016/j.nlm.2016.07.001

Mathis C. 2018. Chapter 21 - The Value of the Object Recognition Paradigm in Investigating Animal Models of Alzheimer's Disease: Advances and Future Directions∗∗The author wish to dedicate the present chapter to Professor Howard B. Eichenbaum. In: Ennaceur A, de Souza Silva MA, editors. Handbook of Behavioral Neuroscience, Handbook of Object Novelty Recognition. Elsevier. pp. 307–330. doi:10.1016/B978-0-12-812012-5.00021-5

Mattson MP. 1997. Cellular actions of beta-amyloid precursor protein and its soluble and fibrillogenic derivatives. *Physiol Rev* **77**:1081–1132. doi:10.1152/physrev.1997.77.4.1081

Mattson MP, Barger SW, Cheng B, Lieberburg I, Smith-Swintosky VL, Rydel RE. 1993. beta-Amyloid precursor protein metabolites and loss of neuronal Ca2+ homeostasis in Alzheimer's disease. *Trends Neurosci* **16**:409–414. doi:10.1016/0166-2236(93)90009-b

Mattsson N, Palmqvist S, Stomrud E, Vogel J, Hansson O. 2019. Staging β-Amyloid Pathology With Amyloid Positron Emission Tomography. *JAMA Neurol*. doi:10.1001/jamaneurol.2019.2214

McAvoy K, Besnard A, Sahay A. 2015. Adult hippocampal neurogenesis and pattern separation in DG: a role for feedback inhibition in modulating sparseness to govern population-based coding. *Front Syst Neurosci* **9**. doi:10.3389/fnsys.2015.00120

McCurry SM, Reynolds CF, Ancoli-Israel S, Teri L, Vitiello MV. 2000. Treatment of sleep disturbance in Alzheimer's disease. *Sleep Med Rev* **4**:603–628. doi:10.1053/smrv.2000.0127

McDonald RJ, White NM. 1994. Parallel information processing in the water maze: evidence for independent memory systems involving dorsal striatum and hippocampus. *Behav Neural Biol* **61**:260–270. doi:10.1016/s0163-1047(05)80009-3

McManus RM, Heneka MT. 2017. Role of neuroinflammation in neurodegeneration: new insights. *Alzheimer's Research & Therapy* **9**:14. doi:10.1186/s13195-017-0241-2

Meda L, Cassatella MA, Szendrei GI, Otvos L, Baron P, Villalba M, Ferrari D, Rossi F. 1995. Activation of microglial cells by beta-amyloid protein and interferon-gamma. *Nature* **374**:647–650. doi:10.1038/374647a0

Melichercik AM, Elliott KS, Bianchi C, Ernst SM, Winters BD. 2012. Nicotinic receptor activation in perirhinal cortex and hippocampus enhances object memory in rats. *Neuropharmacology* **62**:2096–2105. doi:10.1016/j.neuropharm.2012.01.008

Meyer-Luehmann M, Coomaraswamy J, Bolmont T, Kaeser S, Schaefer C, Kilger E, Neuenschwander A, Abramowski D, Frey P, Jaton AL, Vigouret J-M, Paganetti P, Walsh DM, Mathews PM, Ghiso J, Staufenbiel M, Walker LC, Jucker M. 2006. Exogenous induction of cerebral beta-amyloidogenesis is governed by agent and host. *Science* **313**:1781–1784. doi:10.1126/science.1131864

Meziane H, Dodart JC, Mathis C, Little S, Clemens J, Paul SM, Ungerer A. 1998. Memory-enhancing effects of secreted forms of the beta-amyloid precursor protein in normal and amnestic mice. *Proc Natl Acad Sci U S A* **95**:12683–12688. doi:10.1073/pnas.95.21.12683

Middei S, Daniele S, Caprioli A, Ghirardi O, Ammassari-Teule M. 2006. Progressive cognitive decline in a transgenic mouse model of Alzheimer's disease overexpressing mutant hAPPswe. *Genes, brain, and behavior* **5**:249–56. doi:10.1111/j.1601-183X.2005.00160.x

Miller AMP, Vedder LC, Law LM, Smith DM. 2014. Cues, context, and long-term memory: the role of the retrosplenial cortex in spatial cognition. *Front Hum Neurosci* **8**. doi:10.3389/fnhum.2014.00586

Miller EK, Cohen JD. 2001. An Integrative Theory of Prefrontal Cortex Function. *Annu Rev Neurosci* **24**:167–202. doi:10.1146/annurev.neuro.24.1.167

Milward EA, Papadopoulos R, Fuller SJ, Moir RD, Small D, Beyreuther K, Masters CL. 1992. The amyloid protein precursor of Alzheimer's disease is a mediator of the effects of nerve growth factor on neurite outgrowth. *Neuron* **9**:129–137. doi:10.1016/0896-6273(92)90228-6

Minopoli G, Stante M, Napolitano F, Telese F, Aloia L, De Felice M, Di Lauro R, Pacelli R, Brunetti A, Zambrano N, Russo T. 2007. Essential Roles for Fe65, Alzheimer Amyloid Precursor-binding Protein, in the Cellular Response to DNA Damage*. *Journal of Biological Chemistry* **282**:831–835. doi:10.1074/jbc.C600276200

Mitani Y, Yarimizu J, Saita K, Uchino H, Akashiba H, Shitaka Y, Ni K, Matsuoka N. 2012. Differential effects between γ-secretase inhibitors and modulators on cognitive function in amyloid precursor protein-transgenic and nontransgenic mice. *J Neurosci* **32**:2037–2050. doi:10.1523/JNEUROSCI.4264-11.2012

Mitchell AS, Czajkowski R, Zhang N, Jeffery K, Nelson AJD. 2018. Retrosplenial cortex and its role in spatial cognition. *Brain Neurosci Adv* **2**. doi:10.1177/2398212818757098

Mitchell JB, Laiacona J. 1998. The medial frontal cortex and temporal memory: tests using spontaneous exploratory behaviour in the rat. *Behav Brain Res* **97**:107–113. doi:10.1016/s0166-4328(98)00032-1

Mohamed N-V, Herrou T, Plouffe V, Piperno N, Leclerc N. 2013. Spreading of tau pathology in Alzheimer's disease by cell-to-cell transmission. *Eur J Neurosci* **37**:1939–1948. doi:10.1111/ejn.12229

Mondragón-Rodríguez S, Perry G, Zhu X, Boehm J. 2012. Amyloid Beta and tau proteins as therapeutic targets for Alzheimer's disease treatment: rethinking the current strategy. *Int J Alzheimers Dis* **2012**:630182. doi:10.1155/2012/630182

Mondragón-Rodríguez S, Salgado-Burgos H, Peña-Ortega F. 2020. Circuitry and Synaptic Dysfunction in Alzheimer's Disease: A New Tau Hypothesis. *Neural Plast* **2020**:2960343. doi:10.1155/2020/2960343

Monro OR, Mackic JB, Yamada S, Segal MB, Ghiso J, Maurer C, Calero M, Frangione B, Zlokovic BV. 2002. Substitution at codon 22 reduces clearance of Alzheimer's amyloid-β peptide from the cerebrospinal fluid and prevents its transport from the central nervous system into blood. *Neurobiology of Aging* **23**:405–412. doi:10.1016/S0197-4580(01)00317-7

Moran M, Lynch CA, Walsh C, Coen R, Coakley D, Lawlor BA. 2005. Sleep disturbance in mild to moderate Alzheimer's disease. *Sleep Med* **6**:347–352. doi:10.1016/j.sleep.2004.12.005

Morris RGM. 1981. Spatial localization does not require the presence of local cues. *Learning and Motivation* **12**:239–260. doi:10.1016/0023-9690(81)90020-5

Morris RGM, Garrud P, Rawlins JNP, O'Keefe J. 1982. Place navigation impaired in rats with hippocampal lesions. *Nature* **297**:681–683. doi:10.1038/297681a0

Morris RGM, Schenk F, Tweedie F, Jarrard LE. 1990. Ibotenate Lesions of Hippocampus and/or Subiculum: Dissociating Components of Allocentric Spatial Learning. *Eur J Neurosci* **2**:1016–1028. doi:10.1111/j.1460-9568.1990.tb00014.x

Morys J, Bobinski M, Wegiel J, Wisniewski HM, Narkiewicz O. 1996. Alzheimer's disease severely affects areas of the claustrum connected with the entorhinal cortex. *J Hirnforsch* **37**:173–180.

Mosconi L, Berti V, Guyara-Quinn C, McHugh P, Petrongolo G, Osorio RS, Connaughty C, Pupi A, Vallabhajosula S, Isaacson RS, Leon MJ de, Swerdlow RH, Brinton RD. 2017. Perimenopause and emergence of an Alzheimer's bioenergetic phenotype in brain and periphery. *PLOS ONE* **12**:e0185926. doi:10.1371/journal.pone.0185926

Mouri A, Noda Y, Hara H, Mizoguchi H, Tabira T, Nabeshima T. 2007. Oral vaccination with a viral vector containing Abeta cDNA attenuates age-related Abeta accumulation and memory deficits without causing inflammation in a mouse Alzheimer model. *FASEB J* **21**:2135–2148. doi:10.1096/fj.06-7685com

Müller UC, Deller T, Korte M. 2017. Not just amyloid: physiological functions of the amyloid precursor protein family. *Nat Rev Neurosci* **18**:281–298. doi:10.1038/nrn.2017.29

Mumby DG, Gaskin S, Glenn MJ, Schramek TE, Lehmann H. 2002. Hippocampal damage and exploratory preferences in rats: memory for objects, places, and contexts. *Learn Mem* **9**:49–57. doi:10.1101/lm.41302

Muñoz M, Insausti R. 2005. Cortical efferents of the entorhinal cortex and the adjacent parahippocampal region in the monkey (Macaca fascicularis). *Eur J Neurosci* **22**:1368–1388. doi:10.1111/j.1460-9568.2005.04299.x

Murray EA, Richmond BJ. 2001. Role of perirhinal cortex in object perception, memory, and associations. *Curr Opin Neurobiol* **11**:188–193. doi:10.1016/s0959-4388(00)00195-1

Murray M, Bernstein S, Nyugen V, Condron M, Teplow D, Bowers M. 2009. Amyloid β Protein: Aβ40 Inhibits Aβ42 Oligomerization. *Journal of the American Chemical Society* **131**:6316–7. doi:10.1021/ja8092604

Myers N, Pasquini L, Göttler J, Grimmer T, Koch K, Ortner M, Neitzel J, Mühlau M, Förster S, Kurz A, Förstl H, Zimmer C, Wohlschläger AM, Riedl V, Drzezga A, Sorg C. 2014. Within-patient correspondence of amyloid-β and intrinsic network connectivity in Alzheimer's disease. *Brain* **137**:2052–2064. doi:10.1093/brain/awu103

Nakayama K, Ohkawara T, Hiratochi M, Koh C-S, Nagase H. 2008. The intracellular domain of amyloid precursor protein induces neuron-specific apoptosis. *Neurosci Lett* **444**:127–131. doi:10.1016/j.neulet.2008.08.034

Nasreddine ZS, Phillips NA, Bédirian V, Charbonneau S, Whitehead V, Collin I, Cummings JL, Chertkow H. 2005. The Montreal Cognitive Assessment, MoCA: a brief screening tool for mild cognitive impairment. *J Am Geriatr Soc* **53**:695–699. doi:10.1111/j.1532-5415.2005.53221.x

Naveh-Benjamin M. 2000. Adult age differences in memory performance: Tests of an associative deficit hypothesis. *Journal of Experimental Psychology: Learning, Memory, and Cognition* **26**:1170–1187. doi:10.1037/0278-7393.26.5.1170

Nelson AJD, Hindley EL, Pearce JM, Vann SD, Aggleton JP. 2015. The effect of retrosplenial cortex lesions in rats on incidental and active spatial learning. *Front Behav Neurosci* **9**. doi:10.3389/fnbeh.2015.00011

Nelson AJD, Vann SD. 20140623. Mammilliothalamic tract lesions disrupt tests of visuo-spatial memory. *Behavioral Neuroscience* **128**:494. doi:10.1037/bne0000001

Nhan HS, Chiang K, Koo EH. 2015. The multifaceted nature of amyloid precursor protein and its proteolytic fragments: friends and foes. *Acta Neuropathol* **129**:1–19. doi:10.1007/s00401-014-1347-2

Nichols E, Szoeke CEI, Vollset SE, Abbasi N, Abd-Allah F, Abdela J, Aichour MTE, Akinyemi RO, Alahdab F, Asgedom SW, Awasthi A, Barker-Collo SL, Baune BT, Béjot Y, Belachew AB, Bennett DA, Biadgo B, Bijani A, Bin Sayeed MS, Brayne C, Carpenter DO, Carvalho F, Catalá-López F, Cerin E, Choi J-YJ, Dang AK, Degefa MG, Djalalinia S, Dubey M, Duken EE, Edvardsson D, Endres M, Eskandarieh S, Faro A, Farzadfar F, Fereshtehnejad S-M, Fernandes E, Filip I, Fischer F, Gebre AK, Geremew D, Ghasemi-Kasman M, Gnedovskaya EV, Gupta R, Hachinski V, Hagos TB, Hamidi S, Hankey GJ, Haro JM, Hay SI, Irvani SSN, Jha RP, Jonas JB, Kalani R, Karch A, Kasaeian A, Khader YS, Khalil IA, Khan EA, Khanna T, Khoja TAM, Khubchandani J, Kisa A, Kissimova-Skarbek K, Kivimäki M, Koyanagi A, Krohn KJ, Logroscino G, Lorkowski S, Majdan M, Malekzadeh R, März W, Massano J, Mengistu G, Meretoja A, Mohammadi M, Mohammadi-Khanaposhtani M, Mokdad AH, Mondello S, Moradi G, Nagel G, Naghavi M, Naik G, Nguyen LH, Nguyen TH, Nirayo YL, Nixon MR, Ofori-Asenso R, Ogbo FA, Olagunju AT, Owolabi MO, Panda-Jonas S, Passos VM de A, Pereira DM, Pinilla-Monsalve GD, Piradov MA, Pond CD, Poustchi H, Qorbani M, Radfar A, Reiner RC, Robinson SR, Roshandel G, Rostami A, Russ TC, Sachdev PS, Safari H, Safiri S, Sahathevan R, Salimi Y, Satpathy M, Sawhney M, Saylan M, Sepanlou SG, Shafieesabet A, Shaikh MA, Sahraian MA, Shigematsu M, Shiri R, Shiue I, Silva JP, Smith M, Sobhani S, Stein DJ, Tabarés-Seisdedos R, Tovani-Palone MR, Tran BX, Tran TT, Tsegay AT, Ullah I, Venketasubramanian N, Vlassov V, Wang Y-P, Weiss J, Westerman R, Wijeratne T, Wyper GMA, Yano Y, Yimer EM, Yonemoto N, Yousefifard M, Zaidi Z, Zare Z, Vos T, Feigin VL, Murray CJL. 2019. Global, regional, and national burden of Alzheimer's disease and other dementias, 1990–2016: a systematic analysis for the Global Burden of Disease Study 2016. *The Lancet Neurology* **18**:88–106. doi:10.1016/S1474-4422(18)30403-4

Nicolas M, Hassan BA. 2014. Amyloid precursor protein and neural development. *Development* **141**:2543–2548. doi:10.1242/dev.108712

Nikolaev A, McLaughlin T, O'Leary DDM, Tessier-Lavigne M. 2009. APP binds DR6 to trigger axon pruning and neuron death via distinct caspases. *Nature* **457**:981–989. doi:10.1038/nature07767

Nilsberth C, Westlind-Danielsson A, Eckman CB, Condron MM, Axelman K, Forsell C, Stenh C, Luthman J, Teplow DB, Younkin SG, Näslund J, Lannfelt L. 2001. The "Arctic" APP mutation (E693G) causes Alzheimer's disease by enhanced Aβ protofibril formation. *Nat Neurosci* **4**:887–893. doi:10.1038/nn0901-887

Norman G, Eacott MJ. 2005. Dissociable effects of lesions to the perirhinal cortex and the postrhinal cortex on memory for context and objects in rats. *Behav Neurosci* **119**:557–566. doi:10.1037/0735-7044.119.2.557

Norman G, Eacott MJ. 2004. Impaired object recognition with increasing levels of feature ambiguity in rats with perirhinal cortex lesions. *Behavioural Brain Research* **148**:79–91. doi:10.1016/S0166-4328(03)00176-1

Nortley R, Korte N, Izquierdo P, Hirunpattarasilp C, Mishra A, Jaunmuktane Z, Kyrargyri V, Pfeiffer T, Khennouf L, Madry C, Gong H, Richard-Loendt A, Huang W, Saito T, Saido TC, Brandner S, Sethi H, Attwell D. 2019. Amyloid β oligomers constrict human capillaries in Alzheimer's disease via signaling to pericytes. *Science* **365**:eaav9518. doi:10.1126/science.aav9518

Novo M, Freire S, Al-Soufi W. 2018. Critical aggregation concentration for the formation of early Amyloid-β (1–42) oligomers. *Scientific Reports* **8**:1783. doi:10.1038/s41598-018-19961-3

Nuriel T, Angulo SL, Khan U, Ashok A, Chen Q, Figueroa HY, Emrani S, Liu L, Herman M, Barrett G, Savage V, Buitrago L, Cepeda-Prado E, Fung C, Goldberg E, Gross SS, Hussaini SA, Moreno H, Small SA, Duff KE. 2017. Neuronal hyper-activity due to loss of inhibitory tone in APOE4 mice lacking Alzheimer's disease-like pathology. *Nat Commun* **8**:1464. doi:10.1038/s41467-017-01444-0

Oakley H, Cole SL, Logan S, Maus E, Shao P, Craft J, Guillozet-Bongaarts A, Ohno M, Disterhoft J, Eldik LV, Berry R, Vassar R. 2006. Intraneuronal β-Amyloid Aggregates, Neurodegeneration, and Neuron Loss in Transgenic Mice with Five Familial Alzheimer's Disease Mutations: Potential Factors in Amyloid Plaque Formation. *J Neurosci* **26**:10129–10140. doi:10.1523/JNEUROSCI.1202-06.2006

Obregon D, Hou H, Deng J, Giunta B, Tian J, Darlington D, Shahaduzzaman M, Zhu Y, Mori T, Mattson MP, Tan J. 2012. Soluble amyloid precursor protein-α modulates β-secretase activity and amyloid-β generation. *Nat Commun* **3**:777. doi:10.1038/ncomms1781

Oddo S, Billings L, Kesslak JP, Cribbs DH, LaFerla FM. 2004. Aβ Immunotherapy Leads to Clearance of Early, but Not Late, Hyperphosphorylated Tau Aggregates via the Proteasome. *Neuron* **43**:321–332. doi:10.1016/j.neuron.2004.07.003

Oddo S, Caccamo A, Shepherd JD, Murphy MP, Golde TE, Kayed R, Metherate R, Mattson MP, Akbari Y, LaFerla FM. 2003. Triple-transgenic model of Alzheimer's disease with plaques and tangles: intracellular Abeta and synaptic dysfunction. *Neuron* **39**:409–421. doi:10.1016/s0896-6273(03)00434-3

Ognibene E, Middei S, Daniele S, Adriani W, Ghirardi O, Caprioli A, Laviola G. 2005. Aspects of spatial memory and behavioral disinhibition in Tg2576 transgenic mice as a model of Alzheimer's disease. *Behavioural Brain Research* **156**:225–232. doi:10.1016/j.bbr.2004.05.028

Ogomori K, Kitamoto T, Tateishi J, Sato Y, Suetsugu M, Abe M. 1989. Beta-protein amyloid is widely distributed in the central nervous system of patients with Alzheimer's disease. *Am J Pathol* **134**:243–251.

Ohkawara T, Nagase H, Koh C-S, Nakayama K. 2011. The amyloid precursor protein intracellular domain alters gene expression and induces neuron-specific apoptosis. *Gene* **475**:1–9. doi:10.1016/j.gene.2010.11.014

Oliveira AMM, Hawk JD, Abel T, Havekes R. 2010. Post-training reversible inactivation of the hippocampus enhances novel object recognition memory. *Learn Mem* **17**:155–160. doi:10.1101/lm.1625310

Palmiter RD, Brinster RL, Hammer RE, Trumbauer ME, Rosenfeld MG, Birnberg NC, Evans RM. 1982. Dramatic growth of mice that develop from eggs microinjected with metallothionein–growth hormone fusion genes. *Nature* **300**:611–615. doi:10.1038/300611a0

Palmqvist S, Schöll M, Strandberg O, Mattsson N, Stomrud E, Zetterberg H, Blennow K, Landau S, Jagust W, Hansson O. 2017. Earliest accumulation of β-amyloid occurs within the default-mode network and concurrently affects brain connectivity. *Nature Communications* **8**:1214. doi:10.1038/s41467-017-01150-x

Pardossi-Piquard R, Checler F. 2012. The physiology of the β-amyloid precursor protein intracellular domain AICD. *Journal of Neurochemistry* **120**:109–124. doi:https://doi.org/10.1111/j.1471-4159.2011.07475.x

Park J, Jang M, Chang S. 2013. Deleterious effects of soluble amyloid-β oligomers on multiple steps of synaptic vesicle trafficking. *Neurobiol Dis* **55**:129–139. doi:10.1016/j.nbd.2013.03.004

Park J-C, Ma J, Jeon WK, Han J-S. 2016. Fructus mume extracts alleviate cognitive impairments in 5XFAD transgenic mice. *BMC Complement Altern Med* **16**. doi:10.1186/s12906-016-1033-0

Parra MA, Abrahams S, Logie RH, Méndez LG, Lopera F, Della Sala S. 2010. Visual short-term memory binding deficits in familial Alzheimer's disease. *Brain* **133**:2702–2713. doi:10.1093/brain/awq148

Parron C, Save E. 2004. Comparison of the effects of entorhinal and retrosplenial cortical lesions on habituation, reaction to spatial and non-spatial changes during object exploration in the rat. *Neurobiology of Learning and Memory* **82**:1–11. doi:10.1016/j.nlm.2004.03.004

Patterson KR, Ward SM, Combs B, Voss K, Kanaan NM, Morfini G, Brady ST, Gamblin TC, Binder LI. 2011. Heat shock protein 70 prevents both tau aggregation and the inhibitory effects of preexisting tau aggregates on fast axonal transport. *Biochemistry* **50**:10300–10310. doi:10.1021/bi2009147

Paxinos G, Franklin F. 2019. The mouse brain in stereotaxic coordinates. San Diego: Academic Press.

Pereira IT, Agster KL, Burwell RD. 2016. SUBCORTICAL CONNECTIONS OF THE PERIRHINAL, POSTRHINAL, AND ENTORHINAL CORTICES OF THE RAT. I. AFFERENTS. *Hippocampus* **26**:1189–1212. doi:10.1002/hipo.22603

Pereira JB, Mijalkov M, Kakaei E, Mecocci P, Vellas B, Tsolaki M, Kłoszewska I, Soininen H, Spenger C, Lovestone S, Simmons A, Wahlund L-O, Volpe G, Westman E. 2016. Disrupted Network Topology in Patients with Stable and Progressive Mild Cognitive Impairment and Alzheimer's Disease. *Cereb Cortex* **26**:3476–3493. doi:10.1093/cercor/bhw128

Pereira JB, Ossenkoppele R, Palmqvist S, Strandberg TO, Smith R, Westman E, Hansson O. 2019. Amyloid and tau accumulate across distinct spatial networks and are differentially associated with brain connectivity. *eLife* **8**:e50830. doi:10.7554/eLife.50830

Pereira JB, van Westen D, Stomrud E, Strandberg TO, Volpe G, Westman E, Hansson O. 2018. Abnormal Structural Brain Connectome in Individuals with Preclinical Alzheimer's Disease. *Cerebral Cortex* **28**:3638–3649. doi:10.1093/cercor/bhx236

Perini G, Della-Bianca V, Politi V, Della Valle G, Dal-Pra I, Rossi F, Armato U. 2002. Role of p75 neurotrophin receptor in the neurotoxicity by beta-amyloid peptides and synergistic effect of inflammatory cytokines. *J Exp Med* **195**:907–918. doi:10.1084/jem.20011797

Perusini JN, Cajigas SA, Cohensedgh O, Lim SC, Pavlova IP, Donaldson ZR, Denny CA. 2017. Optogenetic stimulation of dentate gyrus engrams restores memory in Alzheimer's disease mice. *Hippocampus* **27**:1110–1122. doi:10.1002/hipo.22756

Pervolaraki E, Hall SP, Foresteire D, Saito T, Saido TC, Whittington MA, Lever C, Dachtler J. 2019. Insoluble Aβ overexpression in an App knock-in mouse model alters microstructure and gamma oscillations in the prefrontal cortex, affecting anxiety-related behaviours. *Dis Model Mech* **12**. doi:10.1242/dmm.040550

Peters GJ, David CN, Marcus MD, Smith DM. 2013. The medial prefrontal cortex is critical for memory retrieval and resolving interference. *Learn Mem* **20**:201–209. doi:10.1101/lm.029249.112

Petersen RC. 2011. Mild Cognitive Impairment. *New England Journal of Medicine* **364**:2227–2234. doi:10.1056/NEJMcp0910237

Petersen RC, Doody R, Kurz A, Mohs RC, Morris JC, Rabins PV, Ritchie K, Rossor M, Thal L, Winblad B. 2001. Current concepts in mild cognitive impairment. *Arch Neurol* **58**:1985–1992. doi:10.1001/archneur.58.12.1985

Peters-Libeu C, Campagna J, Mitsumori M, Poksay KS, Spilman P, Sabogal A, Bredesen DE, John V. 2015. sAβPPα is a Potent Endogenous Inhibitor of BACE1. *J Alzheimers Dis* **47**:545–555. doi:10.3233/JAD-150282

Petrache AL, Rajulawalla A, Shi A, Wetzel A, Saito T, Saido TC, Harvey K, Ali AB. 2019. Aberrant Excitatory–Inhibitory Synaptic Mechanisms in Entorhinal Cortex Microcircuits During the Pathogenesis of Alzheimer's Disease. *Cerebral Cortex* **29**:1834–1850. doi:10.1093/cercor/bhz016

Pike CJ, Overman MJ, Cotman CW. 1995. Amino-terminal deletions enhance aggregation of beta-amyloid peptides in vitro. *J Biol Chem* **270**:23895–23898. doi:10.1074/jbc.270.41.23895

Poirier GL, Amin E, Good MA, Aggleton JP. 2011. Early-onset dysfunction of retrosplenial cortex precedes overt amyloid plaque formation in Tg2576 mice. *Neuroscience* **174**:71–83. doi:10.1016/j.neuroscience.2010.11.025

Polydoro M, Acker CM, Duff K, Castillo PE, Davies P. 2009. Age-Dependent Impairment of Cognitive and Synaptic Function in the htau Mouse Model of Tau Pathology. *J Neurosci* **29**:10741–10749. doi:10.1523/JNEUROSCI.1065-09.2009

Pontecorvo MJ, Devous MD, Navitsky M, Lu M, Salloway S, Schaerf FW, Jennings D, Arora AK, McGeehan A, Lim NC, Xiong H, Joshi AD, Siderowf A, Mintun MA, 18F-AV-1451-A05 investigators. 2017. Relationships between flortaucipir PET tau binding and amyloid burden, clinical diagnosis, age and cognition. *Brain* **140**:748–763. doi:10.1093/brain/aww334

Powell AL, Vann SD, Olarte-Sánchez CM, Kinnavane L, Davies M, Amin E, Aggleton JP, Nelson AJD. 2017. The retrosplenial cortex and object recency memory in the rat. *European Journal of Neuroscience* **45**:1451–1464. doi:https://doi.org/10.1111/ejn.13577

Preston AR, Eichenbaum H. 2013. Interplay of hippocampus and prefrontal cortex in memory. *Curr Biol* **23**:R764–R773. doi:10.1016/j.cub.2013.05.041

Pusil S, López ME, Cuesta P, Bruña R, Pereda E, Maestú F. 2019. Hypersynchronization in mild cognitive impairment: the 'X' model. *Brain* **142**:3936–3950. doi:10.1093/brain/awz320

Putcha D, Brickhouse M, O'Keefe K, Sullivan C, Rentz D, Marshall G, Dickerson B, Sperling R. 2011. Hippocampal hyperactivation associated with cortical thinning in Alzheimer's disease signature regions in non-demented elderly adults. *J Neurosci* **31**:17680–17688. doi:10.1523/JNEUROSCI.4740-11.2011

Puzzo D, Privitera L, Fa' M, Staniszewski A, Hashimoto G, Aziz F, Sakurai M, Ribe EM, Troy CM, Mercken M, Jung SS, Palmeri A, Arancio O. 2011. Endogenous amyloid-β is necessary for hippocampal synaptic plasticity and memory. *Ann Neurol* **69**:819–830. doi:10.1002/ana.22313

Puzzo D, Privitera L, Leznik E, Fa M, Staniszewski A, Palmeri A, Arancio O. 2008. Picomolar Amyloid- Positively Modulates Synaptic Plasticity and Memory in Hippocampus. *Journal of Neuroscience* **28**:14537–14545. doi:10.1523/JNEUROSCI.2692-08.2008

Qin Y-Y, Li M-W, Zhang S, Zhang Y, Zhao L-Y, Lei H, Oishi K, Zhu W-Z. 2013. In vivo quantitative whole-brain diffusion tensor imaging analysis of APP/PS1 transgenic mice using voxel-based and atlas-based methods. *Neuroradiology* **55**:1027–1038. doi:10.1007/s00234-013-1195-0

Quintanilla RA, Orellana DI, González-Billault C, Maccioni RB. 2004. Interleukin-6 induces Alzheimer-type phosphorylation of tau protein by deregulating the cdk5/p35 pathway. *Exp Cell Res* **295**:245–257. doi:10.1016/j.yexcr.2004.01.002

Quiroz YT, Budson AE, Celone K, Ruiz A, Newmark R, Castrillón G, Lopera F, Stern CE. 2010. Hippocampal hyperactivation in presymptomatic familial Alzheimer's disease. *Ann Neurol* **68**:865–875. doi:10.1002/ana.22105

Quiroz YT, Schultz AP, Chen K, Protas HD, Brickhouse M, Fleisher AS, Langbaum JB, Thiyyagura P, Fagan AM, Shah AR, Muniz M, Arboleda-Velasquez JF, Munoz C, Garcia G, Acosta-Baena N, Giraldo M, Tirado V, Ramírez DL, Tariot PN, Dickerson BC, Sperling RA, Lopera F, Reiman EM. 2015. Brain Imaging and Blood Biomarker Abnormalities in Children With Autosomal Dominant Alzheimer Disease: A Cross-Sectional Study. *JAMA Neurol* **72**:912–919. doi:10.1001/jamaneurol.2015.1099

Quiroz YT, Sperling RA, Norton DJ, Baena A, Arboleda-Velasquez JF, Cosio D, Schultz A, Lapoint M, Guzman-Velez E, Miller JB, Kim LA, Chen K, Tariot PN, Lopera F, Reiman EM, Johnson KA. 2018. Association Between Amyloid and Tau Accumulation in Young Adults With Autosomal Dominant Alzheimer Disease. *JAMA Neurol* **75**:548–556. doi:10.1001/jamaneurol.2017.4907

R Core Team. 2017. R: A language and environment for statistical computing.

Rahman ML, Zhang C, Smarr MM, Lee S, Honda M, Kannan K, Tekola-Ayele F, Buck Louis GM. 2019. Persistent organic pollutants and gestational diabetes: A multi-center prospective cohort study of healthy US women. *Environ Int* **124**:249–258. doi:10.1016/j.envint.2019.01.027

Ramos-Rodriguez JJ, Pacheco-Herrero M, Thyssen D, Murillo-Carretero MI, Berrocoso E, Spires-Jones TL, Bacskai BJ, Garcia-Alloza M. 2013. Rapid β-amyloid deposition and cognitive impairment after cholinergic denervation in APP/PS1 mice. *J Neuropathol Exp Neurol* **72**:272–285. doi:10.1097/NEN.0b013e318288a8dd

Reagh ZM, Ho HD, Leal SL, Noche JA, Chun A, Murray EA, Yassa MA. 2016. Greater loss of object than spatial mnemonic discrimination in aged adults. *Hippocampus* **26**:417–422. doi:10.1002/hipo.22562

Reagh ZM, Noche JA, Tustison NJ, Delisle D, Murray EA, Yassa MA. 2018. Functional Imbalance of Anterolateral Entorhinal Cortex and Hippocampal Dentate/CA3 Underlies Age-Related Object Pattern Separation Deficits. *Neuron* **97**:1187-1198.e4. doi:10.1016/j.neuron.2018.01.039

Reagh ZM, Yassa MA. 2014. Object and spatial mnemonic interference differentially engage lateral and medial entorhinal cortex in humans. *Proceedings of the National Academy of Sciences* **111**:E4264–E4273. doi:10.1073/pnas.1411250111

Reed MN, Liu P, Kotilinek LA, Ashe KH. 2010. Effect size of reference memory deficits in the Morris water maze in Tg2576 mice. *Behavioural Brain Research* **212**:115–120. doi:10.1016/j.bbr.2010.03.037

Reiman EM, Chen K, Alexander GE, Caselli RJ, Bandy D, Osborne D, Saunders AM, Hardy J. 2004. Functional brain abnormalities in young adults at genetic risk for late-onset Alzheimer's dementia. *Proc Natl Acad Sci U S A* **101**:284–289. doi:10.1073/pnas.2635903100

Reiman EM, Quiroz YT, Fleisher AS, Chen K, Velez-Pardo C, Jimenez-Del-Rio M, Fagan AM, Shah AR, Alvarez S, Arbelaez A, Giraldo M, Acosta-Baena N, Sperling RA, Dickerson B, Stern CE, Tirado V, Munoz C, Reiman RA, Huentelman MJ, Alexander GE, Langbaum JBS, Kosik KS, Tariot PN, Lopera F. 2012. Brain imaging and fluid biomarker analysis in young adults at genetic risk for autosomal dominant Alzheimer's disease in the presenilin 1 E280A kindred: a case-control study. *Lancet Neurol* **11**:1048–1056. doi:10.1016/S1474-4422(12)70228-4

Rentz DM, Amariglio RE, Becker JA, Frey M, Olson LE, Frishe K, Carmasin J, Maye JE, Johnson KA, Sperling RA. 2011. Face-name associative memory performance is related to amyloid burden in normal elderly. *Neuropsychologia* **49**:2776–2783. doi:10.1016/j.neuropsychologia.2011.06.006

Rice HC, Malmazet D de, Schreurs A, Frere S, Molle IV, Volkov AN, Creemers E, Vertkin I, Nys J, Ranaivoson FM, Comoletti D, Savas JN, Remaut H, Balschun D, Wierda KD, Slutsky I, Farrow K, Strooper BD, Wit J de. 2019. Secreted amyloid-β precursor protein functions as a GABABR1a ligand to modulate synaptic transmission. *Science* **363**:eaao4827. doi:10.1126/science.aao4827

Richter H, Ambrée O, Lewejohann L, Herring A, Keyvani K, Paulus W, Palme R, Touma C, Schäbitz W-R, Sachser N. 2008. Wheel-running in a transgenic mouse model of Alzheimer's disease: protection or symptom? *Behav Brain Res* **190**:74–84. doi:10.1016/j.bbr.2008.02.005

Ring S, Weyer SW, Kilian SB, Waldron E, Pietrzik CU, Filippov MA, Herms J, Buchholz C, Eckman CB, Korte M, Wolfer DP, Müller UC. 2007. The secreted beta-amyloid precursor protein ectodomain APPs alpha is sufficient to rescue the anatomical, behavioral, and electrophysiological abnormalities of APP-deficient mice. *J Neurosci* **27**:7817–7826. doi:10.1523/JNEUROSCI.1026-07.2007

Ritchey M, Cooper RA. 2020. Deconstructing the Posterior Medial Episodic Network. *Trends in Cognitive Sciences* **24**:451–465. doi:10.1016/j.tics.2020.03.006

Roberts RO, Knopman DS, Mielke MM, Cha RH, Pankratz VS, Christianson TJH, Geda YE, Boeve BF, Ivnik RJ, Tangalos EG, Rocca WA, Petersen RC. 2014. Higher risk of progression to dementia in mild cognitive impairment cases who revert to normal. *Neurology* **82**:317–325. doi:10.1212/WNL.0000000000000055

Rodo C, Sargolini F, Save E. 2017. Processing of spatial and non-spatial information in rats with lesions of the medial and lateral entorhinal cortex: Environmental complexity matters. *Behavioural Brain Research* **320**:200–209. doi:10.1016/j.bbr.2016.12.009

Rodriguez GA, Barrett GM, Duff KE, Hussaini SA. 2020. Chemogenetic attenuation of neuronal activity in the entorhinal cortex reduces Aβ and tau pathology in the hippocampus. *PLOS Biology* **18**:e3000851. doi:10.1371/journal.pbio.3000851

Roy DS, Arons A, Mitchell TI, Pignatelli M, Ryan TJ, Tonegawa S. 2016. Memory retrieval by activating engram cells in mouse models of early Alzheimer's disease. *Nature* **531**:508–512. doi:10.1038/nature17172

Rozemuller JM, Eikelenboom P, Stam FC, Beyreuther K, Masters CL. 1989. A4 Protein in Alzheimer's Disease: Primary and Secondary Cellular Events in Extracellular Amyloid Deposition. *Journal of Neuropathology & Experimental Neurology* **48**:674–691. doi:10.1097/00005072-198911000-00009

Rugg MD, Vilberg KL. 2013. Brain networks underlying episodic memory retrieval. *Curr Opin Neurobiol* **23**:255–260. doi:10.1016/j.conb.2012.11.005

Rugg MD, Yonelinas AP. 2003. Human recognition memory: a cognitive neuroscience perspective. *Trends Cogn Sci* **7**:313–319. doi:10.1016/s1364-6613(03)00131-1

Sabri O, Sabbagh MN, Seibyl J, Barthel H, Akatsu H, Ouchi Y, Senda K, Murayama S, Ishii K, Takao M, Beach TG, Rowe CC, Leverenz JB, Ghetti B, Ironside JW, Catafau AM, Stephens AW, Mueller A, Koglin N, Hoffmann A, Roth K, Reininger C, Schulz-Schaeffer WJ, Florbetaben Phase 3 Study Group. 2015. Florbetaben PET imaging to detect amyloid beta plaques in Alzheimer's disease: phase 3 study. *Alzheimers Dement* **11**:964–974. doi:10.1016/j.jalz.2015.02.004

Saito T, Matsuba Y, Mihira N, Takano J, Nilsson P, Itohara S, Iwata N, Saido TC. 2014. Single App knock-in mouse models of Alzheimer's disease. *Nature Neuroscience* **17**:661–663. doi:10.1038/nn.3697

Saito T, Matsuba Y, Yamazaki N, Hashimoto S, Saido TC. 2016. Calpain Activation in Alzheimer's Model Mice Is an Artifact of APP and Presenilin Overexpression. *J Neurosci* **36**:9933–9936. doi:10.1523/JNEUROSCI.1907-16.2016

Saito T, Mihira N, Matsuba Y, Sasaguri H, Hashimoto S, Narasimhan S, Zhang B, Murayama S, Higuchi M, Lee VMY, Trojanowski JQ, Saido TC. 2019. Humanization of the entire murine *Mapt* gene provides a murine model of pathological human tau propagation. *J Biol Chem* jbc.RA119.009487. doi:10.1074/jbc.RA119.009487

Sakakibara Y, Sekiya M, Saito T, Saido TC, Iijima KM. 2018. Cognitive and emotional alterations in App knock-in mouse models of Aβ amyloidosis. *BMC Neuroscience* **19**:46. doi:10.1186/s12868-018-0446-8

Salta E, Walgrave H, Balusu S, Vanden Eynden E, Snoeck S, Craessaerts K, Thrupp N, Wolfs L, Horré K, Fourne Y, Ronisz A, Silajdžić E, Callaerts-Vegh Z, D'Hooge R, Rudolf Thal D, Zetterberg H, Thuret S, Fiers M, Sala Frigerio C, De Strooper B. 2020. Impaired adult hippocampal neurogenesis in Alzheimer's disease is mediated by microRNA-132 deficiency and can be restored by microRNA-132 replacement (preprint). Neuroscience. doi:10.1101/2020.03.12.988709

Sanabria A, Alegret M, Rodriguez-Gomez O, Valero S, Sotolongo-Grau O, Monté-Rubio G, Abdelnour C, Espinosa A, Ortega G, Perez-Cordon A, Gailhajanet A, Hernandez I, Rosende-Roca M, Vargas L, Mauleon A, Sanchez D, Martin E, Rentz DM, Lomeña F, Ruiz A, Tarraga L, Boada M. 2018. The Spanish version of Face-Name Associative Memory Exam (S-FNAME) performance is related to amyloid burden in Subjective Cognitive Decline. *Scientific Reports* **8**:3828. doi:10.1038/s41598-018-21644-y

Sannino S, Russo F, Torromino G, Pendolino V, Calabresi P, De Leonibus E. 2012. Role of the dorsal hippocampus in object memory load. *Learn Mem* **19**:211–218. doi:10.1101/lm.025213.111

Sasaguri H, Nilsson P, Hashimoto S, Nagata K, Saito T, De Strooper B, Hardy J, Vassar R, Winblad B, Saido TC. 2017. APP mouse models for Alzheimer's disease preclinical studies. *The EMBO Journal* **36**:2473–2487. doi:10.15252/embj.201797397

Sato C, Barthélemy NR, Mawuenyega KG, Patterson BW, Gordon BA, Jockel-Balsarotti J, Sullivan M, Crisp MJ, Kasten T, Kirmess KM, Kanaan NM, Yarasheski KE, Baker-Nigh A, Benzinger TLS, Miller TM, Karch CM, Bateman RJ. 2018. Tau Kinetics in Neurons and the Human Central Nervous System. *Neuron* **97**:1284-1298.e7. doi:10.1016/j.neuron.2018.02.015

Sauvage MM, Beer Z, Ekovich M, Ho L, Eichenbaum H. 2010. The Caudal Medial Entorhinal Cortex: a Selective Role in Recollection-Based Recognition Memory. *J Neurosci* **30**:15695–15699. doi:10.1523/JNEUROSCI.4301-10.2010

Save E, Poucet B, Foreman N, Buhot M-C. 1992. Object exploration and reactions to spatial and nonspatial changes in hooded rats following damage to parietal cortex or hippocampal formation. *Behavioral Neuroscience* **106**:447–456. doi:10.1037/0735-7044.106.3.447

Scearce-Levie K, Sanchez PE, Lewcock JW. 2020. Leveraging preclinical models for the development of Alzheimer disease therapeutics. *Nature Reviews Drug Discovery* **19**:447–462. doi:10.1038/s41573-020-0065-9

Schindelin J, Arganda-Carreras I, Frise E, Kaynig V, Longair M, Pietzsch T, Preibisch S, Rueden C, Saalfeld S, Schmid B, Tinevez J-Y, White DJ, Hartenstein V, Eliceiri K, Tomancak P, Cardona A. 2012. Fiji: an open-source platform for biological-image analysis. *Nature Methods* **9**:676–682. doi:10.1038/nmeth.2019

Schindowski K, Bretteville A, Leroy K, Bégard S, Brion J-P, Hamdane M, Buée L. 2006. Alzheimer's disease-like tau neuropathology leads to memory deficits and loss of functional synapses in a novel mutated tau transgenic mouse without any motor deficits. *Am J Pathol* **169**:599–616. doi:10.2353/ajpath.2006.060002

Schöll M, Lockhart SN, Schonhaut DR, O'Neil JP, Janabi M, Ossenkoppele R, Baker SL, Vogel JW, Faria J, Schwimmer HD, Rabinovici GD, Jagust WJ. 2016. PET Imaging of Tau Deposition in the Aging Human Brain. *Neuron* **89**:971–982. doi:10.1016/j.neuron.2016.01.028

Schonhaut DR, McMillan CT, Spina S, Dickerson BC, Siderowf A, Devous MD, Tsai R, Winer J, Russell DS, Litvan I, Roberson ED, Seeley WW, Grinberg LT, Kramer JH, Miller BL, Pressman P, Nasrallah I, Baker SL, Gomperts SN, Johnson KA, Grossman M, Jagust WJ, Boxer AL, Rabinovici GD. 2017. 18 F-flortaucipir tau positron emission tomography distinguishes established progressive supranuclear palsy from controls and Parkinson disease: A multicenter study. *Ann Neurol* **82**:622–634. doi:10.1002/ana.25060

Schultz AP, Chhatwal JP, Hedden T, Mormino EC, Hanseeuw BJ, Sepulcre J, Huijbers W, LaPoint M, Buckley RF, Johnson KA, Sperling RA. 2017. Phases of hyper and hypo connectivity in the Default Mode and Salience networks track with amyloid and Tau in clinically normal individuals. *J Neurosci*. doi:10.1523/JNEUROSCI.3263-16.2017

Schwarz AJ, Yu P, Miller BB, Shcherbinin S, Dickson J, Navitsky M, Joshi AD, Devous MD, Mintun MS. 2016. Regional profiles of the candidate tau PET ligand 18F-AV-1451 recapitulate key features of Braak histopathological stages. *Brain* **139**:1539–1550. doi:10.1093/brain/aww023

Selkoe DJ. 2012. Preventing Alzheimer's Disease. *Science* **337**:1488–1492. doi:10.1126/science.1228541

Selkoe DJ. 2001. Alzheimer's disease results from the cerebral accumulation and cytotoxicity of amyloid beta-protein. *J Alzheimers Dis* **3**:75–80. doi:10.3233/jad-2001-3111

Selkoe DJ, Hardy J. 2016. The amyloid hypothesis of Alzheimer's disease at 25 years. *EMBO Molecular Medicine* **8**:595–608. doi:10.15252/emmm.201606210

Sengupta A, Kabat J, Novak M, Wu Q, Grundke-Iqbal I, Iqbal K. 1998. Phosphorylation of tau at both Thr 231 and Ser 262 is required for maximal inhibition of its binding to microtubules. *Arch Biochem Biophys* **357**:299–309. doi:10.1006/abbi.1998.0813

Sepulcre J, Sabuncu MR, Li Q, El Fakhri G, Sperling R, Johnson KA. 2017. Tau and amyloid β proteins distinctively associate to functional network changes in the aging brain. *Alzheimer's & Dementia* **13**:1261–1269. doi:10.1016/j.jalz.2017.02.011

Seubert P, Oltersdorf T, Lee MG, Barbour R, Blomquist C, Davis DL, Bryant K, Fritz LC, Galasko D, Thal LJ. 1993. Secretion of beta-amyloid precursor protein cleaved at the amino terminus of the beta-amyloid peptide. *Nature* **361**:260–263. doi:10.1038/361260a0

Shah D, Latif-Hernandez A, Strooper B, Saito T, Saido T, Verhoye M, D'Hooge R, Linden A. 2018. Spatial reversal learning defect coincides with hypersynchronous telencephalic BOLD functional connectivity in APP NL-F/NL-F knock-in mice. *Scientific Reports* **8**:6264. doi:10.1038/s41598-018-24657-9

Shah D, Praet J, Latif Hernandez A, Höfling C, Anckaerts C, Bard F, Morawski M, Detrez JR, Prinsen E, Villa A, De Vos WH, Maggi A, D'Hooge R, Balschun D, Rossner S, Verhoye M, Van der Linden A. 2016. Early pathologic amyloid induces hypersynchrony of BOLD resting-state networks in transgenic mice and provides an early therapeutic window before amyloid plaque deposition. *Alzheimer's & Dementia* **12**:964–976. doi:10.1016/j.jalz.2016.03.010

Shankar GM, Li S, Mehta TH, Garcia-Munoz A, Shepardson NE, Smith I, Brett FM, Farrell MA, Rowan MJ, Lemere CA, Regan CM, Walsh DM, Sabatini BL, Selkoe DJ. 2008. Amyloid-β protein dimers isolated directly from Alzheimer's brains impair synaptic plasticity and memory. *Nature Medicine* **14**:837–842. doi:10.1038/nm1782

Shariati SAM, De Strooper B. 2013. Redundancy and divergence in the amyloid precursor protein family. *FEBS Lett* **587**:2036–2045. doi:10.1016/j.febslet.2013.05.026

Sheline YI, Raichle ME, Snyder AZ, Morris JC, Head D, Wang S, Mintun MA. 2010. Amyloid plaques disrupt resting state default mode network connectivity in cognitively normal elderly. *Biol Psychiatry* **67**:584–587. doi:10.1016/j.biopsych.2009.08.024

Shibata M, Yamada S, Kumar SR, Calero M, Bading J, Frangione B, Holtzman DM, Miller CA, Strickland DK, Ghiso J, Zlokovic BV. 2000. Clearance of Alzheimer's amyloid-ss(1-40) peptide from brain by LDL receptor-related protein-1 at the blood-brain barrier. *J Clin Invest* **106**:1489–1499. doi:10.1172/JCI10498

Sierksma ASR, van den Hove DLA, Pfau F, Philippens M, Bruno O, Fedele E, Ricciarelli R, Steinbusch HWM, Vanmierlo T, Prickaerts J. 2014. Improvement of spatial memory function in APPswe/PS1dE9 mice after chronic inhibition of phosphodiesterase type 4D. *Neuropharmacology* **77**:120–130. doi:10.1016/j.neuropharm.2013.09.015

Silva MVF, Loures C de MG, Alves LCV, de Souza LC, Borges KBG, Carvalho M das G. 2019. Alzheimer's disease: risk factors and potentially protective measures. *Journal of Biomedical Science* **26**:33. doi:10.1186/s12929-019-0524-y

Simons JS, Spiers HJ. 2003. Prefrontal and medial temporal lobe interactions in long-term memory. *Nature Reviews Neuroscience* **4**:637–648. doi:10.1038/nrn1178

Sinha N, Berg CN, Tustison NJ, Shaw A, Hill D, Yassa MA, Gluck MA. 2018. APOE ε4 status in healthy older African Americans is associated with deficits in pattern separation and hippocampal hyperactivation. *Neurobiol Aging* **69**:221–229. doi:10.1016/j.neurobiolaging.2018.05.023

Smith-Swintosky VL, Pettigrew LC, Craddock SD, Culwell AR, Rydel RE, Mattson MP. 1994. Secreted forms of beta-amyloid precursor protein protect against ischemic brain injury. *J Neurochem* **63**:781–784. doi:10.1046/j.1471-4159.1994.63020781.x

Spanswick SC, Dyck RH. 2012. Object/context specific memory deficits following medial frontal cortex damage in mice. *PLoS One* **7**:e43698. doi:10.1371/journal.pone.0043698

Sperling RA, Aisen PS, Beckett LA, Bennett DA, Craft S, Fagan AM, Iwatsubo T, Jack CR, Kaye J, Montine TJ, Park DC, Reiman EM, Rowe CC, Siemers E, Stern Y, Yaffe K, Carrillo MC, Thies B, Morrison-Bogorad M, Wagster MV, Phelps CH. 2011. Toward defining the preclinical stages of Alzheimer's disease: recommendations from the National Institute on Aging-Alzheimer's Association workgroups on diagnostic guidelines for Alzheimer's disease. *Alzheimers Dement* **7**:280–292. doi:10.1016/j.jalz.2011.03.003

Stafford JM, Jarrett BR, Miranda-Dominguez O, Mills BD, Cain N, Mihalas S, Lahvis GP, Lattal KM, Mitchell SH, David SV, Fryer JD, Nigg JT, Fair DA. 2014. Large-scale topology and the default mode network in the mouse connectome. *PNAS* **111**:18745–18750. doi:10.1073/pnas.1404346111

Stark SM, Yassa MA, Lacy JW, Stark CEL. 2013. A task to assess behavioral pattern separation (BPS) in humans: Data from healthy aging and mild cognitive impairment. *Neuropsychologia* **51**:2442–2449. doi:10.1016/j.neuropsychologia.2012.12.014

Strange BA, Witter MP, Lein ES, Moser EI. 2014. Functional organization of the hippocampal longitudinal axis. *Nature Reviews Neuroscience* **15**:655–669. doi:10.1038/nrn3785

Strassnig M, Ganguli M. 2005. About a Peculiar Disease of the Cerebral Cortex. *Psychiatry (Edgmont)* **2**:30–33.

Sturchler-Pierrat C, Abramowski D, Duke M, Wiederhold KH, Mistl C, Rothacher S, Ledermann B, Bürki K, Frey P, Paganetti PA, Waridel C, Calhoun ME, Jucker M, Probst A, Staufenbiel M, Sommer B. 1997. Two amyloid precursor protein transgenic mouse models with Alzheimer disease-like pathology. *Proc Natl Acad Sci U S A* **94**:13287–13292. doi:10.1073/pnas.94.24.13287

Sugar J, Moser M-B. 2019. Episodic memory: Neuronal codes for what, where, and when. *Hippocampus* **29**:1190–1205. doi:https://doi.org/10.1002/hipo.23132

Sugar J, Witter MP, van Strien N, Cappaert N. 2011. The Retrosplenial Cortex: Intrinsic Connectivity and Connections with the (Para)Hippocampal Region in the Rat. An Interactive Connectome. *Front Neuroinform* **5**. doi:10.3389/fninf.2011.00007

Sutherland RJ, Whishaw IQ, Kolb B. 1988. Contributions of cingulate cortex to two forms of spatial learning and memory. *J Neurosci* **8**:1863–1872. doi:10.1523/JNEUROSCI.08-06-01863.1988

Suzuki N, Cheung TT, Cai XD, Odaka A, Otvos L, Eckman C, Golde TE, Younkin SG. 1994. An increased percentage of long amyloid beta protein secreted by familial amyloid beta protein precursor (beta APP717) mutants. *Science* **264**:1336–1340. doi:10.1126/science.8191290

Svedružić ŽM, Popović K, Šendula-Jengić V. 2015. Decrease in catalytic capacity of γ-secretase can facilitate pathogenesis in sporadic and Familial Alzheimer's disease. *Molecular and Cellular Neuroscience* **67**:55–65. doi:10.1016/j.mcn.2015.06.002

Szczepanik AM, Rampe D, Ringheim GE. 2001. Amyloid-beta peptide fragments p3 and p4 induce pro-inflammatory cytokine and chemokine production in vitro and in vivo. *J Neurochem* **77**:304–317. doi:10.1046/j.1471-4159.2001.t01-1-00240.x

Takahashi LK. 2014. Olfactory systems and neural circuits that modulate predator odor fear. *Front Behav Neurosci* **8**. doi:10.3389/fnbeh.2014.00072

Tamaoka A, Fukushima T, Sawamura N, Ishikawa K, Oguni E, Komatsuzaki Y, Shoji S. 1996. Amyloid β protein in plasma from patients with sporadic Alzheimer's disease. *Journal of the Neurological Sciences* **141**:65–68. doi:10.1016/0022-510X(96)00143-8

Tamayev R, D'Adamio L. 2012. Inhibition of γ-secretase worsens memory deficits in a genetically congruous mouse model of Danish dementia. *Molecular Neurodegeneration* **7**:19. doi:10.1186/1750-1326-7-19

Tamayev R, Zhou D, D'Adamio L. 2009. The interactome of the amyloid β precursor protein family members is shaped by phosphorylation of their intracellular domains. *Molecular Neurodegeneration* **4**:28. doi:10.1186/1750-1326-4-28

Tang-Wai DF, Knopman DS, Geda YE, Edland SD, Smith GE, Ivnik RJ, Tangalos EG, Boeve BF, Petersen RC. 2003. Comparison of the short test of mental status and the mini-mental state examination in mild cognitive impairment. *Arch Neurol* **60**:1777–1781. doi:10.1001/archneur.60.12.1777

Tanimizu T, Kenney JW, Okano E, Kadoma K, Frankland PW, Kida S. 2017. Functional Connectivity of Multiple Brain Regions Required for the Consolidation of Social Recognition Memory. *J Neurosci* **37**:4103–4116. doi:10.1523/JNEUROSCI.3451-16.2017

Taylor CJ, Ireland DR, Ballagh I, Bourne K, Marechal NM, Turner PR, Bilkey DK, Tate WP, Abraham WC. 2008. Endogenous secreted amyloid precursor protein-alpha regulates hippocampal NMDA receptor function, long-term potentiation and spatial memory. *Neurobiol Dis* **31**:250–260. doi:10.1016/j.nbd.2008.04.011

Thal DR, Capetillo-Zarate E, Del Tredici K, Braak H. 2006. The development of amyloid beta protein deposits in the aged brain. *Sci Aging Knowledge Environ* **2006**:re1. doi:10.1126/sageke.2006.6.re1

Therriault J, Benedet AL, Pascoal TA, Mathotaarachchi S, Savard M, Chamoun M, Thomas E, Kang MS, Lussier F, Tissot C, Soucy J-P, Massarweh G, Rej S, Saha-Chaudhuri P, Poirier J, Gauthier S, Rosa-Neto P. 2020. APOEε4 potentiates the relationship between amyloid-β and tau pathologies. *Molecular Psychiatry* 1–12. doi:10.1038/s41380-020-0688-6

Tischmeyer W, Grimm R. 1999. Activation of immediate early genes and memory formation. *Cell Mol Life Sci* **55**:564–574. doi:10.1007/s000180050315

Tohda C, Nakada R, Urano T, Okonogi A, Kuboyama T. 2011. Kamikihi-to (KKT) Rescues Axonal and Synaptic Degeneration Associated with Memory Impairment in a Mouse Model of Alzheimer's Disease, 5XFAD. *International Journal of Neuroscience* **121**:641–648. doi:10.3109/00207454.2011.602809

Tosun D, Schuff N, Mathis CA, Jagust W, Weiner MW, Alzheimer's Disease NeuroImaging Initiative. 2011. Spatial patterns of brain amyloid-beta burden and atrophy rate associations in mild cognitive impairment. *Brain* **134**:1077–1088. doi:10.1093/brain/awr044

Tran TT, Speck CL, Pisupati A, Gallagher M, Bakker A. 2016. Increased hippocampal activation in ApoE-4 carriers and non-carriers with amnestic mild cognitive impairment. *Neuroimage Clin* **13**:237–245. doi:10.1016/j.nicl.2016.12.002

Trojanowski JQ, Lee VM. 1995. Phosphorylation of paired helical filament tau in Alzheimer's disease neurofibrillary lesions: focusing on phosphatases. *FASEB J* **9**:1570–1576. doi:10.1096/fasebj.9.15.8529836

Tsao A, Moser M-B, Moser EI. 2013. Traces of experience in the lateral entorhinal cortex. *Curr Biol* **23**:399–405. doi:10.1016/j.cub.2013.01.036

Tulving E. 1985. Memory and consciousness. *Canadian Psychology/Psychologie canadienne* **26**:1–12. doi:10.1037/h0080017

Tulving E, Markowitsch HJ. 1998. Episodic and declarative memory: role of the hippocampus. *Hippocampus* **8**:198–204. doi:10.1002/(SICI)1098-1063(1998)8:3<198::AID-HIPO2>3.0.CO;2-G

Tyan S-H, Shih AY-J, Walsh JJ, Maruyama H, Sarsoza F, Ku L, Eggert S, Hof PR, Koo EH, Dickstein DL. 2012. Amyloid precursor protein (APP) regulates synaptic structure and function. *Molecular and Cellular Neuroscience* **51**:43–52. doi:10.1016/j.mcn.2012.07.009

Van Cauter T, Camon J, Alvernhe A, Elduayen C, Sargolini F, Save E. 2013. Distinct Roles of Medial and Lateral Entorhinal Cortex in Spatial Cognition. *Cerebral Cortex* **23**:451–459. doi:10.1093/cercor/bhs033

van den Heuvel MP, Sporns O. 2013. Network hubs in the human brain. *Trends Cogn Sci* **17**:683–696. doi:10.1016/j.tics.2013.09.012

van der Kant R, Goldstein LSB. 2015. Cellular functions of the amyloid precursor protein from development to dementia. *Dev Cell* **32**:502–515. doi:10.1016/j.devcel.2015.01.022

van Strien NM, Cappaert NLM, Witter MP. 2009. The anatomy of memory: an interactive overview of the parahippocampal-hippocampal network. *Nat Rev Neurosci* **10**:272–282. doi:10.1038/nrn2614

Vann SD, Aggleton JP. 2005. Selective dysgranular retrosplenial cortex lesions in rats disrupt allocentric performance of the radial-arm maze task. *Behav Neurosci* **119**:1682–1686. doi:10.1037/0735-7044.119.6.1682

Vann SD, Aggleton JP. 2002. Extensive cytotoxic lesions of the rat retrosplenial cortex reveal consistent deficits on tasks that tax allocentric spatial memory. *Behav Neurosci* **116**:85–94.

Vann SD, Aggleton JP, Maguire EA. 2009. What does the retrosplenial cortex do? *Nature Reviews Neuroscience* **10**:792–802. doi:10.1038/nrn2733

Vasconcelos B, Stancu I-C, Buist A, Bird M, Wang P, Vanoosthuyse A, Van Kolen K, Verheyen A, Kienlen-Campard P, Octave J-N, Baatsen P, Moechars D, Dewachter I. 2016. Heterotypic seeding of Tau fibrillization by pre-aggregated Abeta provides potent seeds for prion-like seeding and propagation of Tau-pathology in vivo. *Acta Neuropathol* **131**:549–569. doi:10.1007/s00401-015-1525-x

Verfaillie SCJ, Pichet Binette A, Vachon-Presseau E, Tabrizi S, Savard M, Bellec P, Ossenkoppele R, Scheltens P, van der Flier WM, Breitner JCS, Villeneuve S, PREVENT-AD Research Group. 2018. Subjective Cognitive Decline Is Associated With Altered Default Mode Network Connectivity in Individuals With a Family History of Alzheimer's Disease. *Biol Psychiatry Cogn Neurosci Neuroimaging* **3**:463–472. doi:10.1016/j.bpsc.2017.11.012

Verret L, Mann EO, Hang GB, Barth AMI, Cobos I, Ho K, Devidze N, Masliah E, Kreitzer AC, Mody I, Mucke L, Palop JJ. 2012. Inhibitory interneuron deficit links altered network activity and cognitive dysfunction in Alzheimer model. *Cell* **149**:708–721. doi:10.1016/j.cell.2012.02.046

Vetere G, Kenney JW, Tran LM, Xia F, Steadman PE, Parkinson J, Josselyn SA, Frankland PW. 2017. Chemogenetic Interrogation of a Brain-wide Fear Memory Network in Mice. *Neuron* **94**:363-374.e4. doi:10.1016/j.neuron.2017.03.037

Vilberg KL, Rugg MD. 2008. Memory retrieval and the parietal cortex: a review of evidence from a dual-process perspective. *Neuropsychologia* **46**:1787–1799. doi:10.1016/j.neuropsychologia.2008.01.004

Villeneuve S, Rabinovici GD, Cohn-Sheehy BI, Madison C, Ayakta N, Ghosh PM, La Joie R, Arthur-Bentil SK, Vogel JW, Marks SM, Lehmann M, Rosen HJ, Reed B, Olichney J, Boxer AL, Miller BL, Borys E, Jin L-W, Huang EJ, Grinberg LT, DeCarli C, Seeley WW, Jagust W. 2015. Existing Pittsburgh Compound-B positron emission tomography thresholds are too high: statistical and pathological evaluation. *Brain* **138**:2020–2033. doi:10.1093/brain/awv112

Vogt BA, Paxinos G. 2014. Cytoarchitecture of mouse and rat cingulate cortex with human homologies. *Brain Struct Funct* **219**:185–192. doi:10.1007/s00429-012-0493-3

Walsh DM, Klyubin I, Fadeeva JV, Cullen WK, Anwyl R, Wolfe MS, Rowan MJ, Selkoe DJ. 2002. Naturally secreted oligomers of amyloid beta protein potently inhibit hippocampal long-term potentiation in vivo. *Nature* **416**:535–539. doi:10.1038/416535a

Walsh DM, Selkoe DJ. 2007. A beta oligomers - a decade of discovery. *J Neurochem* **101**:1172–1184. doi:10.1111/j.1471-4159.2006.04426.x

Wan H, Aggleton JP, Brown MW. 1999. Different contributions of the hippocampus and perirhinal cortex to recognition memory. *J Neurosci* **19**:1142–1148.

Wang C, Holtzman DM. 2020. Bidirectional relationship between sleep and Alzheimer's disease: role of amyloid, tau, and other factors. *Neuropsychopharmacology* **45**:104–120. doi:10.1038/s41386-019-0478-5

Wang HY, Lee DH, D'Andrea MR, Peterson PA, Shank RP, Reitz AB. 2000. beta-Amyloid(1-42) binds to alpha7 nicotinic acetylcholine receptor with high affinity. Implications for Alzheimer's disease pathology. *J Biol Chem* **275**:5626–5632. doi:10.1074/jbc.275.8.5626

Wang J, Zuo X, Dai Z, Xia M, Zhao Z, Zhao X, Jia J, Han Y, He Y. 2013c. Disrupted Functional Brain Connectome in Individuals at Risk for Alzheimer's Disease. *Biological Psychiatry*, Disturbances in the Connectome and Risk for Alzheimer's Disease **73**:472–481. doi:10.1016/j.biopsych.2012.03.026

Wang JX, Rogers LM, Gross EZ, Ryals AJ, Dokucu ME, Brandstatt KL, Hermiller MS, Voss JL. 2014. Targeted enhancement of cortical-hippocampal brain networks and associative memory. *Science* **345**:1054–1057. doi:10.1126/science.1252900

Wang L, Brier MR, Snyder AZ, Thomas JB, Fagan AM, Xiong C, Benzinger TL, Holtzman DM, Morris JC, Ances BM. 2013a. Cerebrospinal Fluid Aβ42, Phosphorylated Tau $_{181}$, and Resting-State Functional Connectivity. *JAMA Neurol*. doi:10.1001/jamaneurol.2013.3253

Wang L, Li H, Liang Y, Zhang J, Li X, Shu N, Wang YY, Zhang Z. 2013d. Amnestic mild cognitive impairment: topological reorganization of the default-mode network. *Radiology* **268**:501–514. doi:10.1148/radiol.13121573

Wang Q, Ng L, Harris JA, Feng D, Li Y, Royall JJ, Oh SW, Bernard A, Sunkin SM, Koch C, Zeng H. 2017. Organization of the connections between claustrum and cortex in the mouse. *J Comp Neurol* **525**:1317–1346. doi:10.1002/cne.24047

Wang X, Huang W, Su L, Xing Y, Jessen F, Sun Y, Shu N, Han Y. 2020. Neuroimaging advances regarding subjective cognitive decline in preclinical Alzheimer's disease. *Mol Neurodegener* **15**:55. doi:10.1186/s13024-020-00395-3

Wang Y, Risacher SL, West JD, McDonald BC, Magee TR, Farlow MR, Gao S, O'Neill DP, Saykin AJ. 2013b. Altered default mode network connectivity in older adults with cognitive complaints and amnestic mild cognitive impairment. *J Alzheimers Dis* **35**:751–760. doi:10.3233/JAD-130080

Warburton EC, Brown MW. 2015. Neural circuitry for rat recognition memory. *Behav Brain Res* **285**:131–139. doi:10.1016/j.bbr.2014.09.050

Warren KN, Hermiller MS, Nilakantan AS, Voss JL. 2019. Stimulating the hippocampal posterior-medial network enhances task-dependent connectivity and memory. *eLife* **8**:e49458. doi:10.7554/eLife.49458

Webb CE, Foster CM, Horn MM, Kennedy KM, Rodrigue KM. 2020. Beta-amyloid burden predicts poorer mnemonic discrimination in cognitively normal older adults. *Neuroimage* **221**:117199. doi:10.1016/j.neuroimage.2020.117199

Weber SN, Sprekeler H. 2018. Learning place cells, grid cells and invariances with excitatory and inhibitory plasticity. *eLife* **7**:e34560. doi:10.7554/eLife.34560

Wei W, Norton DD, Wang X, Kusiak JW. 2002. Aβ 17–42 in Alzheimer's disease activates JNK and caspase-8 leading to neuronal apoptosis. *Brain* **125**:2036–2043. doi:10.1093/brain/awf205

Weiler M, Stieger KC, Long JM, Rapp PR. 2020. Transcranial Magnetic Stimulation in Alzheimer's Disease: Are We Ready? *eNeuro* **7**. doi:10.1523/ENEURO.0235-19.2019

Weingarten MD, Lockwood AH, Hwo SY, Kirschner MW. 1975. A protein factor essential for microtubule assembly. *PNAS* **72**:1858–1862. doi:10.1073/pnas.72.5.1858

Wesnes KA, Annas P, Basun H, Edgar C, Blennow K. 2014. Performance on a pattern separation task by Alzheimer's patients shows possible links between disrupted dentate gyrus activity and apolipoprotein E ∈4 status and cerebrospinal fluid amyloid-β42 levels. *Alzheimers Res Ther* **6**:20. doi:10.1186/alzrt250

Weyer SW, Zagrebelsky M, Herrmann U, Hick M, Ganss L, Gobbert J, Gruber M, Altmann C, Korte M, Deller T, Müller UC. 2014. Comparative analysis of single and combined APP/APLP knockouts reveals reduced spine density in APP-KO mice that is prevented by APPsα expression. *Acta Neuropathol Commun* **2**:36. doi:10.1186/2051-5960-2-36

Wheeler AL, Teixeira CM, Wang AH, Xiong X, Kovacevic N, Lerch JP, McIntosh AR, Parkinson J, Frankland PW. 2013. Identification of a Functional Connectome for Long-Term Fear Memory in Mice. *PLOS Computational Biology* **9**:e1002853. doi:10.1371/journal.pcbi.1002853

Whishaw IQ, Maaswinkel H, Gonzalez CL, Kolb B. 2001. Deficits in allothetic and idiothetic spatial behavior in rats with posterior cingulate cortex lesions. *Behav Brain Res* **118**:67–76. doi:10.1016/s0166-4328(00)00312-0

White JA, Manelli AM, Holmberg KH, Van Eldik LJ, Ladu MJ. 2005. Differential effects of oligomeric and fibrillar amyloid-beta 1-42 on astrocyte-mediated inflammation. *Neurobiol Dis* **18**:459–465. doi:10.1016/j.nbd.2004.12.013

Whyte LS, Hemsley KM, Lau AA, Hassiotis S, Saito T, Saido TC, Hopwood JJ, Sargeant TJ. 2018. Reduction in open field activity in the absence of memory deficits in the AppNL-G-F knock-in mouse model of Alzheimer's disease. *Behav Brain Res* **336**:177–181. doi:10.1016/j.bbr.2017.09.006

Willem M, Tahirovic S, Busche MA, Ovsepian SV, Chafai M, Kootar S, Hornburg D, Evans LDB, Moore S, Daria A, Hampel H, Müller V, Giudici C, Nuscher B, Wenninger-Weinzierl A, Kremmer E, Heneka MT, Thal DR, Giedraitis V, Lannfelt L, Müller U, Livesey FJ, Meissner F, Herms J, Konnerth A, Marie H, Haass C. 2015. η-Secretase processing of APP inhibits neuronal activity in the hippocampus. *Nature* **526**:443–447. doi:10.1038/nature14864

Wilson DI, Langston RF, Schlesiger MI, Wagner M, Watanabe S, Ainge JA. 2013b. Lateral Entorhinal Cortex is Critical for Novel Object-Context Recognition. *Hippocampus* **23**:352–366. doi:10.1002/hipo.22095

Wilson DIG, Watanabe S, Milner H, Ainge JA. 2013a. Lateral entorhinal cortex is necessary for associative but not nonassociative recognition memory. *Hippocampus* **23**:1280–1290. doi:https://doi.org/10.1002/hipo.22165

Wimo A, Prince M. 2010. Alzheimer's Disease International World Alzheimer Report 2010 The Global Economic Impact of Dementia 56.

Winters BD, Forwood SE, Cowell RA, Saksida LM, Bussey TJ. 2004. Double Dissociation between the Effects of Peri-Postrhinal Cortex and Hippocampal Lesions on Tests of Object Recognition and Spatial Memory: Heterogeneity of Function within the Temporal Lobe. *J Neurosci* **24**:5901–5908. doi:10.1523/JNEUROSCI.1346-04.2004

Witter Menno P., Naber PA, Haeften T van, Machielsen WCM, Rombouts SARB, Barkhof F, Scheltens P, Silva FHL da. 2000. Cortico-hippocampal communication by way of parallel parahippocampal-subicular pathways. *Hippocampus* **10**:398–410. doi:https://doi.org/10.1002/1098-1063(2000)10:4<398::AID-HIPO6>3.0.CO;2-K

Witter M. P., Wouterlood FG, Naber PA, Van Haeften T. 2000. Anatomical organization of the parahippocampal-hippocampal network. *Ann N Y Acad Sci* **911**:1–24. doi:10.1111/j.1749-6632.2000.tb06716.x

Wittmann CW, Wszolek MF, Shulman JM, Salvaterra PM, Lewis J, Hutton M, Feany MB. 2001. Tauopathy in Drosophila: neurodegeneration without neurofibrillary tangles. *Science* **293**:711–714. doi:10.1126/science.1062382

Wolfe MS. 2010. Structure, Mechanism and Inhibition of γ-Secretase and Presenilin-Like Proteases. *Biol Chem* **391**:839–847. doi:10.1515/BC.2010.086

Wright DB, London K, Field AP. 2011. Using Bootstrap Estimation and the Plug-in Principle for Clinical Psychology Data. *Journal of Experimental Psychopathology* **2**:252–270. doi:10.5127/jep.013611

Xia C-F, Arteaga J, Chen G, Gangadharmath U, Gomez LF, Kasi D, Lam C, Liang Q, Liu C, Mocharla VP, Mu F, Sinha A, Su H, Szardenings AK, Walsh JC, Wang E, Yu C, Zhang W, Zhao T, Kolb HC. 2013. [(18)F]T807, a novel tau positron emission tomography imaging agent for Alzheimer's disease. *Alzheimers Dement* **9**:666–676. doi:10.1016/j.jalz.2012.11.008

Xiong M, Jones OD, Peppercorn K, Ohline SM, Tate WP, Abraham WC. 2017. Secreted amyloid precursor protein-alpha can restore novel object location memory and hippocampal LTP in aged rats. *Neurobiology of Learning and Memory*, MCCS 2017 **138**:291–299. doi:10.1016/j.nlm.2016.08.002

Xu W, Fitzgerald S, Nixon RA, Levy E, Wilson DA. 2015. Early hyper-activity in lateral entorhinal cortex is associated with elevated levels of AβPP metabolites in the Tg2576 mouse model of Alzheimer's disease. *Experimental Neurology* **264**:82–91. doi:10.1016/j.expneurol.2014.12.008

Yamaguchi H, Hirai S, Morimatsu M, Shoji M, Harigaya Y. 1988. Diffuse type of senile plaques in the brains of Alzheimer-type dementia. *Acta Neuropathol* **77**:113–119. doi:10.1007/BF00687420

Yamazaki Y, Zhao N, Caulfield TR, Liu C-C, Bu G. 2019. Apolipoprotein E and Alzheimer disease: pathobiology and targeting strategies. *Nat Rev Neurol* **15**:501–518. doi:10.1038/s41582-019-0228-7

Yassa MA, Stark SM, Bakker A, Albert MS, Gallagher M, Stark CEL. 2010. High-resolution structural and functional MRI of hippocampal CA3 and dentate gyrus in patients with amnestic Mild Cognitive Impairment. *NeuroImage* **51**:1242–1252. doi:10.1016/j.neuroimage.2010.03.040

Yassine N, Lazaris A, Dorner-Ciossek C, Després O, Meyer L, Maitre M, Mensah-Nyagan AG, Cassel J-C, Mathis C. 2013. Detecting spatial memory deficits beyond blindness in tg2576 Alzheimer mice. *Neurobiol Aging* **34**:716–730. doi:10.1016/j.neurobiolaging.2012.06.016

Yasuhara O, Matsuo A, Terai K, Walker DG, Berger AE, Akiguchi I, Kimura J, McGeer PL. 1997. Expression of interleukin-1 receptor antagonist protein in post-mortem human brain tissues of Alzheimer's disease and control cases. *Acta Neuropathol* **93**:414–420. doi:10.1007/s004010050633

Yasuno F, Kazui H, Yamamoto A, Morita N, Kajimoto K, Ihara M, Taguchi A, Matsuoka K, Kosaka J, Tanaka T, Kudo T, Takeda M, Nagatsuka K, Iida H, Kishimoto T. 2015. Resting-state synchrony between the retrosplenial cortex and anterior medial cortical structures relates to memory complaints in subjective cognitive impairment. *Neurobiol Aging* **36**:2145–2152. doi:10.1016/j.neurobiolaging.2015.03.006

Yeung L-K, Olsen RK, Hong B, Mihajlovic V, D'Angelo MC, Kacollja A, Ryan JD, Barense MD. 2019. Object-in-place Memory Predicted by Anterolateral Entorhinal Cortex and Parahippocampal Cortex Volume in Older Adults. *Journal of Cognitive Neuroscience* 1–19. doi:10.1162/jocn_a_01385

Yeung L-K, Olsen RK, Hong B, Mihajlovic V, D'Angelo MC, Kacollja A, Ryan JD, Barense MD. 2018. Object-in-Place Memory Predicted by Anterolateral Entorhinal Cortex and Parahippocampal Cortex Volume in Older Adults. *bioRxiv* 409607. doi:10.1101/409607

Yiannopoulou KG, Papageorgiou SG. 2020. Current and Future Treatments in Alzheimer Disease: An Update. *J Cent Nerv Syst Dis* **12**:1179573520907397. doi:10.1177/1179573520907397

Yonelinas AP. 2002. The nature of recollection and familiarity: A review of 30 years of research. *Journal of Memory and Language* **46**:441–517. doi:10.1006/jmla.2002.2864

Yoon S-S, Jo SA. 2012. Mechanisms of Amyloid-β Peptide Clearance: Potential Therapeutic Targets for Alzheimer's Disease. *Biomol Ther (Seoul)* **20**:245–255. doi:10.4062/biomolther.2012.20.3.245

Young-Pearse TL, Bai J, Chang R, Zheng JB, LoTurco JJ, Selkoe DJ. 2007. A critical function for beta-amyloid precursor protein in neuronal migration revealed by in utero RNA interference. *J Neurosci* **27**:14459–14469. doi:10.1523/JNEUROSCI.4701-07.2007

Zheng H, Koo EH. 2006. The amyloid precursor protein: beyond amyloid. *Mol Neurodegener* **1**:5. doi:10.1186/1750-1326-1-5

Zhu H, Yan H, Tang N, Li X, Pang P, Li H, Chen W, Guo Y, Shu S, Cai Y, Pei L, Liu D, Luo M-H, Man H, Tian Q, Mu Y, Zhu L-Q, Lu Y. 2017. Impairments of spatial memory in an Alzheimer's disease model via degeneration of hippocampal cholinergic synapses. *Nature Communications* **8**:1676. doi:10.1038/s41467-017-01943-0

Zhuo J-M, Prakasam A, Murray ME, Zhang H-Y, Baxter MG, Sambamurti K, Nicolle MM. 2008. An increase in Abeta42 in the prefrontal cortex is associated with a reversal-learning impairment in Alzheimer's disease model Tg2576 APPsw mice. *Curr Alzheimer Res* **5**:385–391. doi:10.2174/156720508785132280

Zlokovic BV, Deane R, Sallstrom J, Chow N, Miano JM. 2005. Neurovascular pathways and Alzheimer amyloid beta-peptide. *Brain Pathol* **15**:78–83. doi:10.1111/j.1750-3639.2005.tb00103.x

Zott B, Simon MM, Hong W, Unger F, Chen-Engerer H-J, Frosch MP, Sakmann B, Walsh DM, Konnerth A. 2019. A vicious cycle of β amyloid–dependent neuronal hyperactivation. *Science* **365**:559–565. doi:10.1126/science.aay0198

Université de Strasbourg

École Doctorale des Sciences de la Vie et de la Santé STRASBOURG

Christopher BORCUK

Déficits précoces de la cognition et de la connectivité cérébrale chez la Souris *App^{NL-F}/MAPT*: modélisation du stade prodromal de la maladie d'Alzheimer

Summary

A critical challenge in current research of Alzheimer's disease (AD) is to clarify the relationship between early neuropathology and network dysfunction associated to the emergence of subtle memory alterations which announce disease onset. In the present work, the new generation *App^{NL-F}xMAPT* double knock in (dKI) model was used to evaluate early stages of AD. The initial step of tau pathology was restricted to the perirhinal-entorhinal region, sparing the hippocampus. This discrete neuropathological sign coincided with deficits in object-place associative memory, one of the earliest recognition memory forms affected in individuals at risk for developing AD. Analyses of task-dependent c-Fos activation were carried out in regions susceptible to early AD pathology. Initial hyper-activity was detected in the entorhinal cortex and the claustrum of dKI mice. Decreased network efficiency during memory recall was directly linked to poor memory performance. This decreased efficiency was especially prevalent in the cingulate cortex, and may be caused by a blockade of information flow through the retrosplenial cortex. Our results suggest that early perirhinal-entorhinal pathology is associated with local hyper-activity which spreads towards connected regions such as the claustrum, the medial prefrontal cortex and ultimately the key retrosplenial hub which is needed to relay information flow from frontal to temporal lobes. The similarity between our findings and those reported in the earliest stages of AD suggests that the *App^{NL-F}* dKI model has a high potential for generating key information on the initial stage of the disease.

Résumé

L'un des défis majeurs de la recherche actuelle sur la maladie d'Alzheimer (MA) est de clarifier la relation entre la neuropathologie précoce et le dysfonctionnement des réseaux associés à l'émergence de subtiles altérations de la mémoire qui annoncent l'apparition de la maladie. Dans ce travail de thèse, le modèle *App^{NL-F}/MAPT* de nouvelle génération double knock-in (dKI) a été utilisé pour évaluer les stades précoces de la maladie d'Alzheimer. A l'âge de 4 mois, l'émergence de de la pathologie tau est limitée à la région périrhinale-entorhinale, en épargnant l'hippocampe. Ce signe neuropathologique discret coïncide avec des déficits de la mémoire associative objet-place, l'une des premières formes de mémoire de reconnaissance affectée chez les personnes à risque de développer la MA. Des analyses de l'activation des c-Fos associée à la tâche ont été effectuées dans des régions susceptibles de présenter une neuropathologie précoce. Une hyperactivité a été détectée dans le cortex entorhinal et le claustrum. La diminution de l'efficacité du réseau pendant le rappel de la mémoire est directement liée à de mauvaises performances dans la tâche. Cette diminution de l'efficacité était particulièrement fréquente dans le cortex cingulaire, et peut être causée par un blocage du flux d'information au niveau du cortex rétrosplénial. Nos résultats suggèrent que la pathologie périrhinale-entorhinale précoce est associée à une hyperactivité locale qui se propage vers des régions connexes telles que le claustrum, le cortex préfrontal médian et finalement le principal hub rétrosplénien qui est nécessaire pour relayer le flux d'information des lobes frontaux vers les lobes temporaux. La similitude entre nos résultats et ceux rapportés dans les premiers stades de la MA suggère que le modèle *App^{NL-F}/MAPT* a un fort potentiel pour générer des informations clés sur le stade initial de la maladie.